The Handbook of Environmental Chemistry 32
Series Editors: Damià Barceló · Andrey G. Kostianoy

Elena Jiménez
Beatriz Cabañas
Gilles Lefebvre *Editors*

Environment, Energy and Climate Change I

Environmental Chemistry of Pollutants and Wastes

Springer

The Handbook of Environmental Chemistry

Founded by Otto Hutzinger

Volume 32

The Handbook of Environmental Chemistry

Recently Published and Forthcoming Volumes

Environment, Energy and Climate Change I: Environmental Chemistry of Pollutants and Wastes
Volume Editors: Elena Jiménez, Beatriz Cabañas, and Gilles Lefebvre
Vol. 32, 2015

The Sava River
Volume Editors: R. Milačič, J. Ščančar, and M. Paunović
Vol. 31, 2014

Potable Water: Emerging Global Problems and Solutions
Volume Editors: T. Younos and C.A. Grady
Vol. 30, 2014

Risk – Informed Management of European River Basins
Volume Editors: J. Brils, W. Brack, D. Müller, P. Négrel, and J.E. Vermaat
Vol. 29, 2014

The Turkmen Lake Altyn Asyr and Water Resources in Turkmenistan
Volume Editors: I.S. Zonn and A.G. Kostianoy
Vol. 28, 2014

Oil Pollution in the Baltic Sea
Volume Editors: A.G. Kostianoy and O.Yu. Lavrova
Vol. 27, 2013

Urban Air Quality in Europe
Volume Editors: M. Viana
Vol. 26, 2013

Climate Change and Water Resources
Volume Editors: T. Younos and C.A. Grady
Vol. 25, 2013

Emerging Organic Contaminants in Sludges: Analysis, Fate and Biological Treatment
Volume Editors: T. Vicent, G. Caminal, E. Eljarrat, and D. Barceló
Vol. 24, 2013

Global Risk-Based Management of Chemical Additives II: Risk-Based Assessment and Management Strategies
Volume Editors: B. Bilitewski, R.M. Darbra, and D. Barceló
Vol. 23, 2013

Chemical Structure of Pelagic Redox Interfaces: Observation and Modeling
Volume Editor: E.V. Yakushev
Vol. 22, 2013

The Llobregat: The Story of a Polluted Mediterranean River
Volume Editors: S. Sabater, A. Ginebreda, and D. Barceló
Vol. 21, 2012

Emerging Organic Contaminants and Human Health
Volume Editor: D. Barceló
Vol. 20, 2012

Emerging and Priority Pollutants in Rivers: Bringing Science into River Management Plans
Volume Editors: H. Guasch, A. Ginebreda, and A. Geiszinger
Vol. 19, 2012

Global Risk-Based Management of Chemical Additives I: Production, Usage and Environmental Occurrence
Volume Editors: B. Bilitewski, R.M. Darbra, and D. Barceló
Vol. 18, 2012

Polyfluorinated Chemicals and Transformation Products
Volume Editors: T.P. Knepper and F.T. Lange
Vol. 17, 2012

Brominated Flame Retardants
Volume Editors: E. Eljarrat and D. Barceló
Vol. 16, 2011

Effect-Directed Analysis of Complex Environmental Contamination
Volume Editor: W. Brack
Vol. 15, 2011

Environment, Energy and Climate Change I

Environmental Chemistry of Pollutants and Wastes

Volume Editors: Elena Jiménez · Beatriz Cabañas · Gilles Lefebvre

With contributions by

R. Álvarez · I. Barnes · F.J.G. Bernardo · A.M. Borreguero · J. Bueno · B. Cabañas · R. Camarillo · P. Cañizares · P. Chelin · I. Colmenar · J. Cuesta · G. Da · J.C. de Haro · A. de la Hoz · A. de Lucas · S. del Reino · Á. Díaz-Ortiz · M. Eremenko · J. M. Esbrí · O. Escolano · N.R. Fariñas · F.J. Fernández · J. L. Fernández · R. Fernández-Martínez · J.-M. Flaud · M.T. García · M.L. García-Lorenzo · E. Géhin · M.-I. González-Sánchez · I. Gracia · C. Gutiérrez · F. Hase · M. Havet · D. Hidalgo · P. Higueras · M-P.G. Iniesta · C. Jiménez · E. Jiménez · J. Lillo · J. Lobato · J. Loredo · P. Martín · E. Martínez · F. Martínez · R.C.R. Martín-Doimeadiós · J.Mª. Martín-Marroquín · R. Millán · A. Moreno · M.J. Moreno · A. Ordóñez · J. Orphal · M.B. Othmane · R. Oyarzun · M.-T. Pérez-Prior · P. Prieto · M. Ray · J. Rincón · M.A. Rodrigo · J.F. Rodríguez · M. Rodríguez-Rastrero · I. Rucandio · S. Salgado · T. Schmid · D. Simón · C. Solliec · A. Tapia · S. Tostón · E. Valero · C. Viatte · J. Villaseñor · L. Welte

Springer

Editors
Elena Jiménez
Beatriz Cabañas
Department of Physical Chemistry
University of Castilla-La Mancha (UCLM)
Ciudad Real
Spain

Gilles Lefebvre
CERTES-IUT
The University Paris-Est Créteil
Paris Créteil
France

The Handbook of Environmental Chemistry
ISSN 1867-979X ISSN 1616-864X (electronic)
ISBN 978-3-319-12906-8 ISBN 978-3-319-12907-5 (eBook)
DOI 10.1007/978-3-319-12907-5
Springer Cham Heidelberg New York Dordrecht London

Library of Congress Control Number: 2015930134

Printed on acid-free paper

Springer is part of Springer Science+Business Media (www.springer.com)

Editors-in-Chief

Prof. Dr. Damià Barceló

Department of Environmental Chemistry
IDAEA-CSIC
C/Jordi Girona 18–26
08034 Barcelona, Spain
and
Catalan Institute for Water Research (ICRA)
H20 Building
Scientific and Technological Park of the
University of Girona
Emili Grahit, 101
17003 Girona, Spain
dbcqam@cid.csic.es

Prof. Dr. Andrey G. Kostianoy

P.P. Shirshov Institute of Oceanology
Russian Academy of Sciences
36, Nakhimovsky Pr.
117997 Moscow, Russia
kostianoy@gmail.com

Advisory Board

The Handbook of Environmental Chemistry Also Available Electronically

The Handbook of Environmental Chemistry is included in Springer's eBook package *Earth and Environmental Science*. If a library does not opt for the whole package, the book series may be bought on a subscription basis.

For all customers who have a standing order to the print version of *The Handbook of Environmental Chemistry,* we offer free access to the electronic volumes of the Series published in the current year via SpringerLink. If you do not have access, you can still view the table of contents of each volume and the abstract of each article on SpringerLink (www.springerlink.com/content/110354/).

You will find information about the

– Editorial Board
– Aims and Scope
– Instructions for Authors
– Sample Contribution

at springer.com (www.springer.com/series/698).

All figures submitted in color are published in full color in the electronic version on SpringerLink.

Aims and Scope

Since 1980, *The Handbook of Environmental Chemistry* has provided sound and solid knowledge about environmental topics from a chemical perspective. Presenting a wide spectrum of viewpoints and approaches, the series now covers topics such as local and global changes of natural environment and climate; anthropogenic impact on the environment; water, air and soil pollution; remediation and waste characterization; environmental contaminants; biogeochemistry; geoecology; chemical reactions and processes; chemical and biological transformations as well as physical transport of chemicals in the environment; or environmental modeling. A particular focus of the series lies on methodological advances in environmental analytical chemistry.

Series Preface

With remarkable vision, Prof. Otto Hutzinger initiated *The Handbook of Environmental Chemistry* in 1980 and became the founding Editor-in-Chief. At that time, environmental chemistry was an emerging field, aiming at a complete description of the Earth's environment, encompassing the physical, chemical, biological, and geological transformations of chemical substances occurring on a local as well as a global scale. Environmental chemistry was intended to provide an account of the impact of man's activities on the natural environment by describing observed changes.

While a considerable amount of knowledge has been accumulated over the last three decades, as reflected in the more than 70 volumes of *The Handbook of Environmental Chemistry,* there are still many scientific and policy challenges ahead due to the complexity and interdisciplinary nature of the field. The series will therefore continue to provide compilations of current knowledge. Contributions are written by leading experts with practical experience in their fields. *The Handbook of Environmental Chemistry* grows with the increases in our scientific understanding, and provides a valuable source not only for scientists but also for environmental managers and decision-makers. Today, the series covers a broad range of environmental topics from a chemical perspective, including methodological advances in environmental analytical chemistry.

In recent years, there has been a growing tendency to include subject matter of societal relevance in the broad view of environmental chemistry. Topics include life cycle analysis, environmental management, sustainable development, and socio-economic, legal and even political problems, among others. While these topics are of great importance for the development and acceptance of *The Handbook of Environmental Chemistry,* the publisher and Editors-in-Chief have decided to keep the handbook essentially a source of information on "hard sciences" with a particular emphasis on chemistry, but also covering biology, geology, hydrology and engineering as applied to environmental sciences.

The volumes of the series are written at an advanced level, addressing the needs of both researchers and graduate students, as well as of people outside the field of "pure" chemistry, including those in industry, business, government, research

establishments, and public interest groups. It would be very satisfying to see these volumes used as a basis for graduate courses in environmental chemistry. With its high standards of scientific quality and clarity, *The Handbook of Environmental Chemistry* provides a solid basis from which scientists can share their knowledge on the different aspects of environmental problems, presenting a wide spectrum of viewpoints and approaches.

The Handbook of Environmental Chemistry is available both in print and online via www.springerlink.com/content/110354/. Articles are published online as soon as they have been approved for publication. Authors, Volume Editors and Editors-in-Chief are rewarded by the broad acceptance of *The Handbook of Environmental Chemistry* by the scientific community, from whom suggestions for new topics to the Editors-in-Chief are always very welcome.

Damià Barceló
Andrey G. Kostianoy
Editors-in-Chief

Preface

This work, which is divided into two volumes, *Environment, Energy and Climate Change I* and *Environment, Energy and Climate Change II*, is a consequence of the *Energy and Environment Knowledge Week* (E2KW) congress that was held in Toledo (Spain) from 20th to 22nd of November 2013 (http//www.congress.e2kw.es). This congress represented an exceptional opportunity for presenting cutting-edge research in the field environmental, energy and climate change and illustrating the wide experience on several interesting topics of the contributing authors. The two volumes aim to address some of the key issues facing the environmental problems through interdisciplinary approaches.

Volume 1 is dedicated to the *Environmental Chemistry of Pollutants and Wastes* and collects a selection of 15 chapters that review several aspects of the environmental chemistry of air, soil and water contaminants as well as treatments of organic wastes. The first two chapters (by G. Da et al. and by P. Chelin et al.) provide an overview on the atmospheric monitoring of indoor (particles) and outdoor (O_3 and CO) pollutants. A revision of the daytime and night-time atmospheric chemistry of oxygenated pollutants is presented in two following chapters by E. Jiménez and I. Barnes and by B. Cabañas et al., respectively. Soil pollution by heavy metals in mining areas is the subject matter of the chapters by P. Higueras et al., by R.C. Rodríguez et al. and by J. Lillo et al., while the chapter by S. del Reino et al. presents a chemical oxidation treatment of hydrocarbon polluted soils. In the subsequent chapters, sustainable and emerging technologies on chemical treatments of organic wastes (chapters by D. Simón et al., by C. Gutiérrez et al., and by F.J. Fernández et al.), wastewaters (chapter by E. Valero et al.) and animal wastes (chapter by J.M. Martín-Marroquín and D. Hidalgo Barrio) are described. Capture and storage of CO_2 is one of the most promising technologies for reducing the levels of this greenhouse gas. The chapter by J. Rincón et al. is devoted to mitigation of the greenhouse effect by using photocatalytic conversion methods. The use of non-conventional

methods in green chemistry synthesis is also highlighted in the last chapter (by A. de la Hoz et al.).

We sincerely thank all authors for their involvement and efforts in preparing their chapters.

Ciudad Real, Spain — Elena Jiménez and Beatriz Cabañas
Paris, France — Gilles Lefebvre

Contents

Preventing Indoor Bioaerosol Contamination in Food Processing Environments and HVAC Systems: Assessment of Particle Deposition for Hygienic Design Purposes

Guillaume Da, Evelyne Géhin, Michel Havet, Mourad Ben Othmane, and Camille Solliec

Abstract This chapter deals with airborne particle contamination in food processing indoor environments and particularly within heating, ventilation, and air-conditioning (HVAC) systems in food factory buildings. The major types of bioaerosols encountered in the food manufacturing sector as well as the bioaerosol sampling methods are firstly introduced. Secondly, some features of air handling systems such as zoning, cleanrooms, localized air handling systems, and HVAC systems are presented. Besides, the study of particle deposition to duct surfaces from turbulent airflow is reviewed and discussed. Substantially, an original work combining industrial diagnosis and experiments at factory scale with experiments at laboratory scale is then proposed through the case study of the CleanAirNet project. The CleanAirNet project (Hygienic Design of Ventilation Duct Networks in Food Factories) aimed at producing new knowledge, models, and techniques to help control the safety of the food products through a better control of aerosol particle transport and deposition in the ventilation networks of the food industry. The different work packages of the project are presented relatively to the state-of-the-art particle deposition on duct surfaces. The methodological findings and relevant applications (e.g., a newly patented particle trapping device for air handling systems) for food industries are exposed. The CleanAirNet project was supported by the French National Research Agency (ANR) from 2008 to 2012; the project

G. Da (✉) and E. Géhin
CERTES—Université Paris Est Créteil, 61 Av. du Général de Gaulle, 94010 Créteil, France
e-mail: guillaume.da@u-pec.fr

M. Havet
UMR GEPEA—ONIRIS, 44322 Nantes, France

M. Ben Othmane
CLAUGER, 69530 Brignais, France

C. Solliec
UMR GEPEA—EMN, 44300 Nantes, France

E. Jiménez et al. (eds.), *Environment, Energy and Climate Change I: Environmental Chemistry of Pollutants and Wastes*, Hdb Env Chem (2015) 32: 1–20,
DOI 10.1007/698_2014_269, © Springer-Verlag Berlin Heidelberg 2014,
Published online: 6 August 2014

consortium was conducted by seven institutes and universities, as well as three industries from the food sector.

Keywords Bioaerosols, Food factories, Heating ventilation and air-conditioning systems (HVAC systems), Hygienic design, Indoor air quality, Particle deposition, Ventilation networks

Contents

1 Introduction

Airborne particle pollution in indoor environments has been identified to be a major concern, and many epidemiologic evidences have emphasized the impacts of particulate matter exposure on a range of health outcomes [1]. In the industrial sector, there are a variety of measures and regulations that manufacturers can follow to improve indoor air quality and therefore reducing the operators' exposure to indoor air pollutants. Usually, the quality of air within buildings is maintained by the introduction of mechanical ventilation, and airborne contaminants are commonly removed by filtration.

In the case of food factories, specified air quality and air change rate are required, not only for the safety of employees but also to contribute to hygienic food manufacture. Indeed, Lopez-Gomez et al. [2] stressed that awareness of the food industry about the importance of the hygienic design is still very low, remarkably for air handling systems. Accordingly, contributions to the development of the recent concept of food safety engineering and hygienic designs are

clearly encouraged in order to ensure the manufacturing of high-quality food products that are both safe and secure.

Despite significant advances that have been made in the last decade, little has been published on the sources and routes of airborne pathogens toward products, during the manufacturing process [3] or after the final lethal processing steps [4, 5]. In order to prevent air contamination from pathogens, different air handling strategies are used, which are zoning, localized systems, and heating, ventilation, and air-conditioning (HVAC) systems. However, Bluyssen et al. [6] reported that the HVAC systems can play a significant role in polluting the air passing through, subsequently leading to a significant pollution of the indoor environment. Lopez-Gomez et al. [2] also stressed the need to understand the pollution mechanisms and more generally the need for a more proactive science-based approach for the management of food safety.

This chapter firstly addresses the issue of indoor air quality and HVAC systems in food factory buildings, with a focus on particles and bioaerosols. Secondly, perspectives for hygienic designs of HVAC systems through the study of particle deposition to duct surfaces from turbulent airflow are presented and discussed. This work follows the findings of the CleanAirNet project (Hygienic Design of Ventilation Duct Networks in Food Factories) which was funded by the French National Research Agency from 2008 to 2012. The project aimed at producing new knowledge, models, and techniques to help control the safety of the food products through a better control of aerosol particle transport and deposition in the ventilation networks of the food industry.

2 Indoor Bioaerosols in Food Processing Environments

2.1 Bioaerosol Hazards

In the food processing industries, air has been established as a significant route for bacterial contamination [3]. Therefore, air contamination is of primary importance for products that use air for food preparation, such as dairy products [7].

Despite that the European Hygienic Engineering and Design Group (EHEDG) emphasizes the importance to clean the air [8], the group indicated that providing clean air will not prevent food contamination if major sources of contamination are present in the food production environment [9]. Hence, high airborne concentrations of particles pose a hygiene risk since particles may include infectious pathogens (such as *Salmonella*, *Listeria*, *Escherichia Coli*, *Yersinia*, and *Campylobacter*), toxigenic pathogens (such as *Staphylococcus aureus* and *Clostridium*) and spoilage organisms (such as yeast, molds, fungi, and fungal spores, e.g., *Aspergillus niger*

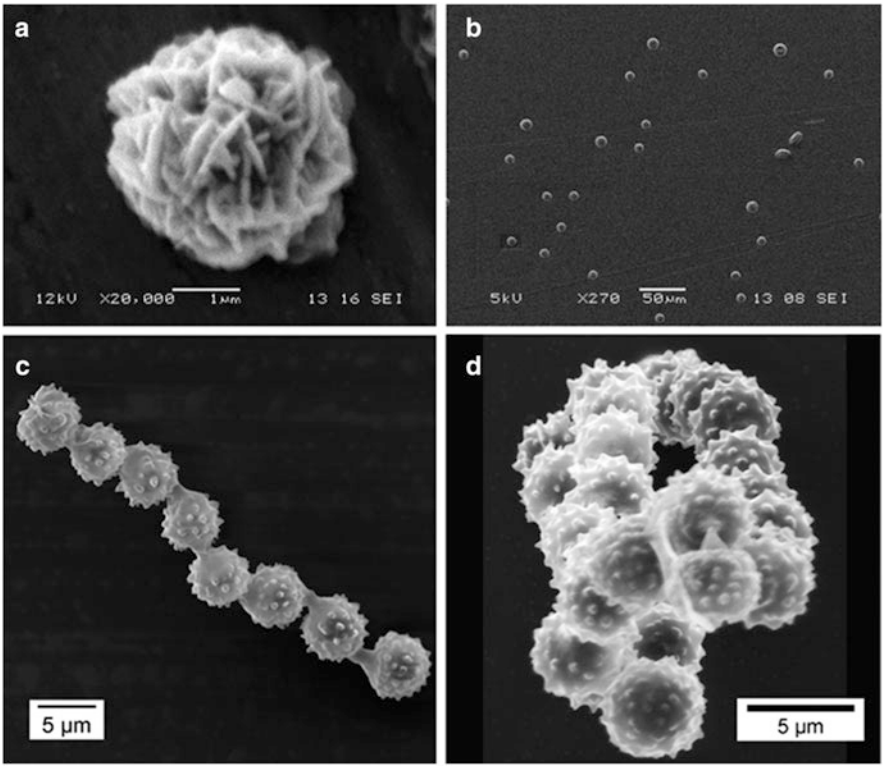

Fig. 1 *Up*: (**a**) dry airborne particle of fluorescein ($C_{20}H_{10}Na_2O$) collected using an impaction method. (**b**) Particles of fluorescein deposited on a galvanized-steel smooth surface. The airborne particles of fluorescein were produced by a means of a monodispersed aerosol generator [16]. *Down*: chain of *A. niger* spores observed in scanning electron microscopy (×10,000 magnification). The spores were produced on Petri dish with agar, prior to aerosolization (using a blowing technique), and ultimately collected on stubs by a means of a sedimentation method [17]

and *Penicillium* spp.) as reported by several authors [5, 8, 10–14]. These airborne particles are classically referred as bioaerosols.

The term "bioaerosols" describes suspended solid airborne particles derived from biological organisms, including microorganisms and fragments of biological materials such as plant debris and animal dander [15]. Within the text of this chapter, the term bioaerosols is restricted to bioaerosols that present a pathogenicity. Figure 1 shows scanning electron microscopy photographs of two different types of airborne particles: abiotic particles (fluorescein) and microbiological particles. The latter were produced from airborne bacterial spores of *A. niger* previously aerosolized from Petri dishes and subsequently deposited on surface using a sedimentation method [17].

2.2 Indoor Bioaerosol Contamination Levels

In food processing environments, the concentrations of airborne microorganisms have been measured in a wide range of locations; however, it is still limited to developed countries [18]. Interestingly, Sheehana and Giranda [19] reported a study where bioaerosol concentrations were investigated for two operating modes in a food processing industry: production alone versus production with concurrent sanitation (using pressure water) of food processing equipment. Total bacterial plate counts ranged from 150 to 325 colony-forming units per cubic meter of air (cfu m^{-3}) for production alone and from 850 to 2,500 cfu m^{-3} for production with concurrent sanitation. Likewise, other published data have shown that dairy products, chilled meals, fish, or meat-processed products were subjected to significant quantities of airborne microorganisms that contributed to food-borne diseases [3, 20–22]. Interestingly, the air-to-food contamination transfer levels reached in some foodstuff (e.g., sandwiches and salads) can be similar to other transfers such as surface-to-food by contact transfer [22]. Moreover, based on data related to aerial concentrations as well as calculations of settling velocities for different types of microorganisms (bacteria, yeasts, molds), Monte Carlo simulations were used to estimate the contamination level (log cfu m^{-3}) of three example food products due to exposure to air in food production facilities. den Aantrekker et al. [23] showed that the type of product and processing conditions strongly influence the contamination level. Lastly, new threats continue to be identified in the food sector, such as noroviruses in particular and aerial mycotoxin spread [4, 24]. Though, the importance of proper sampling and monitoring techniques is no less relevant [25].

2.3 Bioaerosol Sampling

As far as the methods of air system monitoring are concerned, the EHEDG [8] differentiated physical measurements (temperature, humidity, airflow, pressure, dust, and particles) from microbiological measurements. Microbiological measurements consisted in collecting bioaerosols that present sizes which can range from hundreds nanometers such as cell fragments [26] to few hundred micrometers in aerodynamic diameter such as pollen. As far as viruses are concerned, recent studies showed that viral aerosol mode (which is the specific type of aerosol that carries viruses) is for particles smaller than 5 μm in diameter [27].

Widely used bioaerosol sampling methods are based on different physical principles such as impaction, impingement, filtration, and electrostatic precipitation; the latter is known to improve collection efficiency. Interestingly, the use of different sampling methods, reviewed by Reponen et al. [28], leads to different estimates of airborne contamination. Subsequently, these authors indicated that the sample analysis method should be selected as part of the sampling plan. Likewise, traditional sampling analysis such as microscopic counting and cultivation analysis

presents some limitations that could be partly complemented with recent biochemical, immunochemical, and molecular biological assays. So far, Xu et al. [29] pointed out that in the bioaerosol field, the new challenge is now to detect bioaerosols in real time. For example, Qian et al. [30] and Bhangar et al. [31] were the first to report laser-induced fluorescence techniques to characterize bioaerosols at high time and size resolution in common-use indoor environments.

3 Controlling Indoor Air to Prevent Bioaerosol Contamination

3.1 Zoning Concept

According to the EHEDG [8], aerosols may enter food production areas via drains, doorways and hatches, disinfection tunnels, and compressed air supplies or may be generated from dispersed droplets within the food production area during cleaning and washing operations [19, 32, 33]. Furthermore, den Aantrekker et al. [7] specified that recontamination attributed to aerosols via the factory environment can also occur during the packaging of products. As a result, in order to prevent such diverse sources of airborne contamination, food industries used segregation of work areas [34] and hygienic zoning [35]. Within these zones, and as far as air handling is concerned, there are a range of system requirements such as filters, controlled overpressures (from higher to lower risk zones), temperature and humidity control, air changes per hour, fresh air changes per hour, and management of microbiological monitoring (EHEDG, personal communication). Air filter recommendations are F5–F7 secondary filters, F7–F9 secondary filters, and up to E10/H13 efficiency/high-efficiency particulate air filters for low-, moderate-, and high-risk zones, respectively. The management of microbiological risks is based on the principles of Hazard Analysis and Critical Control Points (HACCP) and on Good Manufacturing Practices [4].

3.2 Cleanrooms and Localized Air Delivery Systems

The most widely used solution in food processing industries to maintain the desired cleanliness in particle-controlled volumes of production is cleanrooms. These types of environments correspond to the ISO 14644 classification [36, 37]. As shown on Table 1, ISO cleanrooms are rated according to the number of particles of specific sizes per air cubic meter.

Table 1 Definition of clean room classes based on ISO 14644 standards [37]

	Number of particle size (μm) per cubic meter of air (#.m^{-3})					
Class name	0.1 μm	0.2 μm	0.3 μm	0.5 μm	1 μm	5 μm
ISO1	10	2				
ISO2	100	24	10	4		
ISO3	1,000	237	102	35	8	
ISO4	10,000	2,370	1,020	352	83	
ISO5	100,000	23,700	10,200	3,520	832	29
ISO6	1,000,000	237,000	102,000	35,200	8,320	293
ISO7				352,000	83,200	2,930
ISO8				3,520,000	832,000	29,300
ISO9				35,200,000	8,320,000	293,000

The number of particle size corresponds to the concentration of airborne particles with size equal to or larger than the size shown. For example, one cubic meter of air in an ISO7 environment will not contain more than 352,000 particles of 0.5 μm diameter or larger.

Moreover, a critical factor in cleanroom design is controlling air change rate (ACR in $m^3\ h^{-1}$). This refers to the number of times each hour that filtered outside air replaces the existing volume in a volume chamber. Published studies dealing with removal efficiency or ACR in food processing cleanrooms have been developed [38]. Havet and Hennequin [39] showed that the usual ACRs do not always ensure a cleanliness class 10,000 (according to the Federal Standard 209E) during the food processing and that the machines largely contribute to the particle emission. However, the cleanliness class can be obtained with low ACRs if the process is suited to the cleanroom and if optimal position of working areas and machines inside the room is found. Additionally, Rouaud and Havet [40] showed that the contaminant removal effectiveness and the mean age of air permit to optimize the contaminant source position as well as to determine decontamination time, respectively. In addition, the EHEDG [8] indicated that factors that affect the choice of ACR are as follows: volume of the space, cooling capacity (or the capacity to evacuate heat, like in cold storage of meat), number of people (to estimate the ACR per person), temperature differences with adjoining work areas, humidity and odor control, and overpressure required. Aires et al. [41] concluded that the use of cleanroom technology is an operational alternative to be taken into consideration, provided that the characteristics of the whole system are compatible with the high standards of the clean air.

Alternatively, other specific equipment design systems have been proposed to restrict airborne contamination and maintain low air temperatures. In the chilled food sector, for example, a particular attention was paid to the development of localized air delivery systems. The objective is to blow clean filtered air toward the foodstuff being manufactured (local application) and ultimately to maintain a low level of airborne particle, consistent with the sensitivity of food throughout the duration of operations [3, 42, 43]. Designs of such equipments are based on unidirectional flows, open troughs, and semi-closed and closed tunnels. Fully closed systems present a significant disadvantage for conducting easily cleaned

procedures as compared to open systems. However, they require machines specially designed to operate in a closed sterilized environment.

4 HVAC Systems in Food Processing Environments

4.1 Airborne Contamination

In food factories, most of indoor air is taken from fresh/outdoor air (which contains a wide range of small-size dust particles), which is eventually mixed (0–90%) with recirculating air (air returned to the air handling unit for retreatment), prior to passing through the HVAC systems. As previously modeled by Bluyssen et al. [6], Lopez-Gomez et al. [2] recently indicated that the sources of indoor air pollution in factory buildings are mainly construction materials (odors) and the HVAC-systems components, such as heating/cooling tubes and humidifiers, filters, and ducts. Remarkably, these authors highlighted the lack of hygienic design (which means that equipment must allow easy and effective cleaning and disinfection) of air-conditioning and refrigeration systems in the food manufacturing sector. Therefore, assessing the case study of slicing and packaging of ready-to-eat meat products, they showed the long-term benefits of using hygienic design in the equipment and subsequently the potential for reducing maintenance and operating costs.

Indeed, HVAC systems present fairly right physicochemical conditions (such as temperature, high relative humidity, and source of nutrients) for growth of spores, molds, or other biological agents; prior to these, the latter organisms might be released in large quantities on airborne particles such as bioaerosols [44–46]. Nevertheless, there is no study to evaluate bioaerosol deposition and biofilm development onto duct surfaces of ventilation ducts [47]. Hence, an interesting approach to describe airborne contamination in HVAC systems may be found in microbiology of aquatic systems. den Antrekker et al. [7] described biofilm process (in liquid phase) of industrial pipelines, in which previous and irreversible attachment of bacteria onto the pipeline surfaces, is followed by biofilm growth, cell detachment, and ultimately conducted to product recontamination. Therefore, most biofilm models developed for aquatic systems consist of a set of differential equations describing attachment, growth, and detachment of cells.

4.2 Prevention of Pathogen Growth and Duct Cleaning

Inorganic biocides such as silver and copper active ions embedded in inert matrixes are sometimes used in the ducts and filters of HVAC systems in order to prevent the growth of bacteria and molds, respectively. Yet, Makarian [48] stated a steady

growth for the use of biocides. Nevertheless, because of their limited efficiency in case of fouling, as well as health concerns for people and foodstuff, Lopez-Gomez et al. [2] stated that their use does not match the objectives of hygienic designs for HVAC systems.

As far as cleaning is concerned, a protocol to evaluate the impact of duct cleaning on indoor air quality of office has been proposed recently [47, 49]. Zuraimi [47] demonstrated that it is possible to determine harmful airborne pollutant concentration levels attributed to duct cleaning activities while still maintaining industrial performance standards of surface cleanliness.

So far, in the food processing environment, one unsolved aspect of the HVAC systems is the very complex implementation of an automatic cleaning and disinfection system, using a sort of cleaning-in-place (CIP) system like those for liquids in food factories [2]. To date, different techniques such as dry (mechanical) or humid cleaning are implemented subsequent to duct inspections at specific points, but more attention needs to be paid for improving cleaning efficiencies. Besides, the development of new methods simultaneously to the involvement of professionals might be very useful. The components of the HVAC systems should be designed for service with a minimum of downtime while avoiding ducting and production area contamination. Easy access and suitable filters should be installed and replaced frequently to avoid fouling. Henceforward, innovative ways like hygienic designs could occur only after a sufficient understanding of the pollution mechanisms, starting with the ability to predict where and how fouling might occur.

4.3 Predicting Fouling Rate

Very little information is available on recognized methods for assessing dust buildup in HVAC systems. Still, Lavoie et al. [50] revealed that existing methods applied for nonporous HVAC systems in nonindustrial buildings are roughly based on experts' judgments. Thus, these authors compared three sampling methods using templates as recommended by the Canadian organization Institut de recherche Robert-Sauvé en santé et en sécurité du travail (IRSST), the US organization National Air Duct Cleaner Association (NADCA), and the French organization Association pour la Prévention et l'Étude de la Contamination (ASPEC). Lavoie et al. [50] demonstrated that cleaning initiation criteria under real conditions were found to be 6.0, 2.0, and 23 mg/100 cm^2 using the IRSST method, the NADCA method, and the ASPEC method, respectively. They therefore recommended using the latter method to objectively assess dust accumulation levels in HVAC ductwork. Accordingly, Ben Othmane et al. [51] stated that the control of indoor air quality and the cleaning of HVAC systems in food processing environments could be intensely related to the control of deposits of particles in the ventilation ducts. As a result, based on ASPEC recommendation, a criteria to initiate duct cleaning in food industries could be a dirt accumulation of 400 mg m^{-2}. Finally, a good understanding of the rate of particle deposition in the duct systems may help to

design hygienic duct systems and subsequently may be used to predict dirt accumulation and cleaning procedures if necessary.

5 A Case Study for Particle Deposition Assessment in HVAC Systems

Hygienic design of ventilation ducts has been studied in the frame of the CleanAirNet project. The project consortium was conducted by seven institutes and universities, as well as three industries from the food sector. The main objective was to study the dynamics of airflows in the ducts and air handling units, relatively to the deposition mechanisms of bioaerosols onto surfaces. One of the goals was to finally propose a technique enabling a new particle trapping stage in the air handling systems, able to localize under control the unavoidable particle deposition, with the lowest energy expense possible.

5.1 Diagnosis of HVAC Systems Under Real Industrial Situations

At first, the consortium conducted in situ measurements (such as airflow, temperature, relative humidity, particle number concentrations, particle size and mass distributions, duct surface samplings) and observations on four different industrial sites. Temperature, humidity, air velocity, and flow rates were measured continuously at all sites during 6 months; particle counts and particle samplings were made daily for 1 month on each site. The sites were carefully chosen in order to meet contrasted situations, markedly in terms of foodstuff type (e.g., dairy and seafood), production environment parameters (e.g., temperature, relative humidity), HVAC-systems designs, and characteristics of HVAC component materials. Finally, work-package participants of the project consortium reported the significant and quantitative analysis as well as key findings from this diagnosis undertaken on factories [51–53].

Figure 2 shows schematic diagram of three different ventilation systems that were studied throughout the project. As far as physical parameters were concerned, the obtained results show that ducts were characterized as follows: large diameter (0.3–0.8 m), high Reynolds number ($1.7–6.0 \times 10^5$) and air speed (5–12 m s^{-1}), temperature difference (1–20°C), relative humidity (20–80%), and roughness height (5–60 μm) [55].

Likewise, the diagnosis has produced practical knowledge on the specific conditions peculiar to aerosols and particle deposition in the ventilation networks of the food industry. For example, the concentration of particulate matter of aerodynamic diameters in the size range 0.3–20 μm varied from 0.2 to 1.7 $\mu g.m^{-3}$. Markedly, one

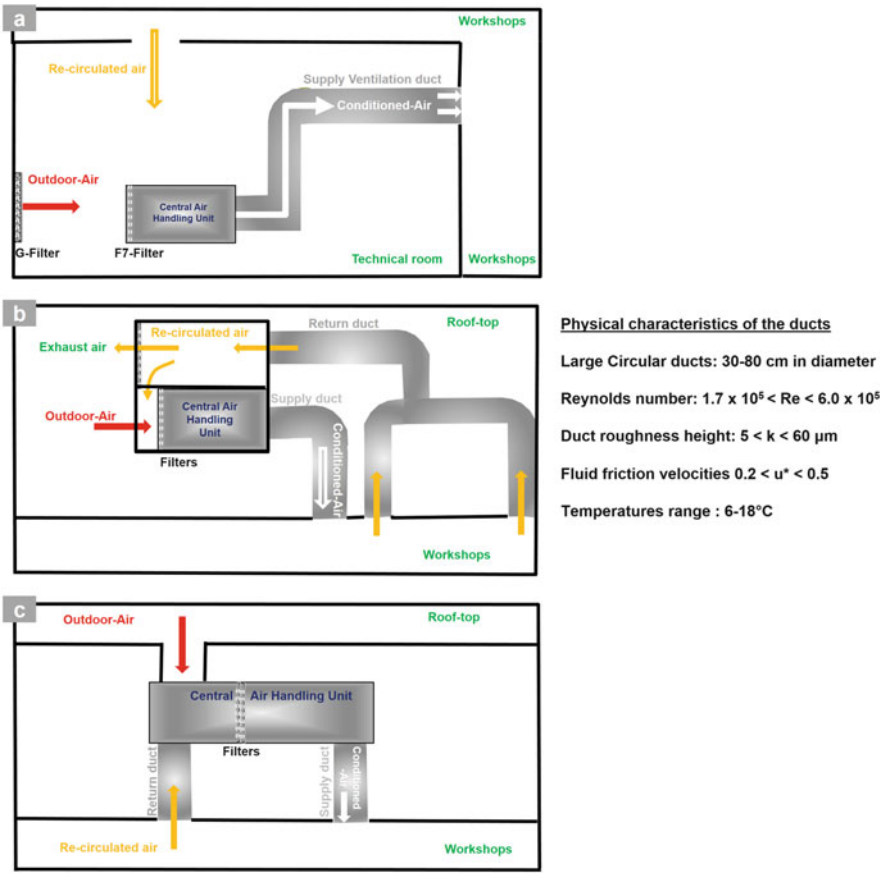

Fig. 2 Schematic diagram of three different industrial ventilation systems (**a**–**c**) studied in the CleanAirNet project. Adapted from Ben Othmane et al. [54]

of the relevant conclusions was the significance of the 2–7 μm particle size for airborne contamination of ventilation ducts with non-fully developed regime [54]. Previous studies have reported comparable observations with these particle sizes but for nonindustrial HVAC systems [47, 56–58].

5.2 Particle Deposition: Definitions and Modeling

There are a wide range of mechanisms (such as gravitational settling, Brownian diffusion, inertial and turbulent diffusion, turbophoresis, and thermophoresis) affecting the transport and deposition of coarse particles in different geometries [58, 59].

The deposition velocity, V_d (m s^{-1}), of a particle to a duct surface is defined as

$$V_d = \frac{J}{C_{ave}} \tag{1}$$

where J is the time-averaged mass flux toward the surface (μg m^{-2} s^{-1}) and C_{ave} (μg m^{-3}) is the time-averaged airborne particle concentration in the air passing through the duct.

The dimensionless deposition velocity, V_d^+, is defined as

$$V_d^+ = \frac{V_d}{u^*} = \frac{V_d}{U_{ave}\sqrt{f/2}} \tag{2}$$

where u^* is the friction velocity of a turbulent duct flow, U_{ave} is the average air speed in the duct (m s^{-1}), and f is the Fanning friction factor [60]. For spherical particles in the Stokes regime, a dimensionless particle relaxation time, τ_p^+, is given by

$$\tau_p^+ = \frac{\rho_p d_p^2 u^{*2}}{18\mu v} \tag{3}$$

where ρ_p is the particle density, d_p is the particle diameter, μ is the dynamic viscosity of air, and v is the kinematic viscosity of air.

Modeling and computer simulation dynamics have been used to apprehend the fates of airborne particles in ventilation ducts with turbulent flow [56, 58, 61–63]. In the frame of the CleanAirNet project and based on the knowledge acquired under real situations, Ben Othmane et al. [54] have proposed improvements to existing Eulerian models that predict particle deposition velocity with turbulent flow in common-used ventilation ducts. Applying this model to typical mechanical ventilation systems cited above, these authors quantified the effects of various factors specific to food industries (nature of the product, thermophoresis, surface roughness) that may contribute to the particle deposition flux to duct surfaces (mg m^{-2} per year). Nevertheless, experimental data were dramatically scarce to validate these models [64, 65]. Thus, for the purpose of studying particle deposition, knowledge on roughness structure, temperature gradient, and flow characteristics is needed for further investigation in the laboratory.

5.3 *Experimental Approaches for Particle Deposition*

Until 2002, most published data related to particle deposition from turbulent flow were collected from tubes or ducts with hydraulic diameters much smaller than ducts in typical HVAC systems. Sippola and Nazaroff [56, 57] substantially

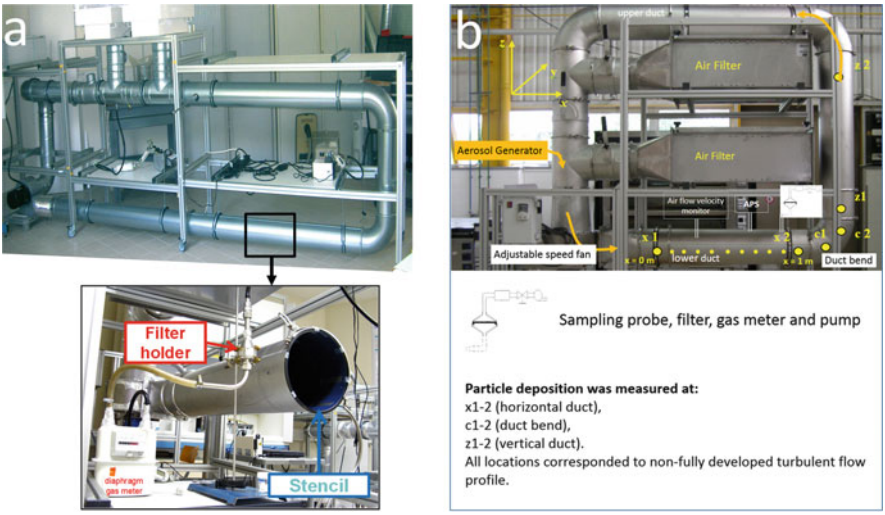

Fig. 3 (**a**) The MIDAS experimental setup to investigate particle deposition velocity for fully developed turbulent flow in a large circular ventilation duct. (**b**) The experimental device (called MECAD) for aeraulic characterization and particle deposition on surfaces with non-fully developed turbulent flow (Reynolds number of 5.3×10^5)

reviewed these data and pointed out widely scattered results. Thus, Sippola and Nazaroff [65, 66] conducted new experiments with steel and internally insulated rectangular ducts at air speeds typically found in ventilation ducts, 2–9 m s^{-1}. Behaviors of monodisperse particles with diameters in the size range 1–16 μm were investigated. These authors showed that deposition rates measured to a given surface (floor, wall, and ceiling) in straight ducts increased with an increase in particle size or air speed. Therefore, measured deposition rates were higher than predicted by published models. Fan and Hua [61] corroborated these assumptions (models underestimate the deposition rates) and encouraged the development of more experiments, as proposed by the CleanAirNet project in the case of large ventilation ducts with turbulent flow.

In the frame of the CleanAirNet project, two experimental setups were developed to investigate particle deposition velocity to duct surface with turbulent flow (Fig. 3). Aerosol particles used in the deposition experiments were monodispersed, residues of fluorescein (Fig. 1a, b), the latter being used as a fluorescent tracer for quantitative analysis of the deposited particles [16]. In order to validate this original experimental approach, the MIDAS setup was designed for fully developed turbulent flow (Fig. 3a). The technique offers a significant advantage to discriminate different orientations for horizontal section of large circular duct. For 2–6 μm particles, deposition rates to floors were 1–2 orders of magnitude higher than rates to the ceiling and greater than rates to the wall. For 1 μm particles, the effect of surface orientation to particle deposition was not apparent. It should be indicated that other experimental studies used similar monodispersed aerosols to describe the

wall deposition rate in mixing conditions [67]. Nevertheless, Cheng produced data for fine particles (in the size range 5 nm to 2 μm). Thus, an interesting work recently published by You et al. [68] and based on Zhao and Wu's model [58] was used to compare the deposition velocity relatively to the particle size and the surface inclinations. This method may be useful for quick particle deposition data comparisons in ventilation ducts.

The second work package of the CleanAirNet project also proposed the development of a setup called MECAD (Fig. 3b). MECAD was design to mimic industrials ducts by using HVAC materials and non-fully developed turbulent flow in large circular ventilation duct. Measurements obtained with MECAD confirmed the great heterogeneity in deposition velocities according to the surface orientation but also showed that particle deposition velocity increases when the flow is not fully developed [55, 69]. Deposition velocities were 2 cm s^{-1} for larger particles (5.82 μm) and less than 0.5 mm s^{-1} for smaller particles (0.95 μm). Ben Othmane also showed that particles tend to migrate toward the wall in the direction of decreasing turbulence level. Remarkably, they revealed high deposition zones due to the flow structure [55]. The effect of temperature on particle deposition was also studied: preliminary experiments conducted on MIDAS and results issued using the modeling approach confirmed that temperature may affect the particle deposition—small particles tend to migrate toward the cold surface [69].

5.4 Recommendations and Innovative Applications for Hygienic Designs

Taking into account the contributions of the deposition mechanisms such as turbophoresis, the experimental approach cited above was completed with a modeling approach. Models might be useful to quantify the total deposited mass flux in real ventilation systems of industrial ventilation networks [55].

An innovative principle of particle trapping was designed and tested in the frame of the CleanAirNet project [70]. The new technique was based on the principle of local turbulence generation used to accelerate the particle deposition on specific collection surfaces. A hygienically designed prototype called PEPITE was developed at lab scale and finally tested on one of the industrial sites selected for the project (Fig. 4). Noticeably, the prototype also contributes to improve the energy consumption efficiency as required for HVAC systems [72]. Finally, the prototype for low-pressure-drop particle trapping was validated in industrial conditions and patented [71].

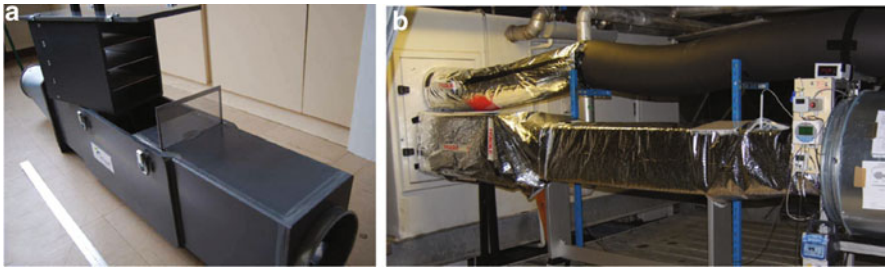

Fig. 4 The CleanAirNet prototype called PEPITE developed in the frame of the CleanAirNet project. PEPITE consisted of a low-pressure-drop particle trapping [71]. The setup was firstly developed at lab scale (**a**), prior to testing and validation at industrial scale (**b**)

6 Conclusion

The prevention to airborne particle pollution in indoor food processing environments has been clearly addressed in this chapter. The main bioaerosol types encountered in the food manufacturing sector, as well as the methodological issues of bioaerosol sampling, have been indicated. It has been highlighted that more work is necessary (at factory scale and at laboratory scale) in order to prevent bioaerosol contamination within HVAC systems, preferably with hygienic design systems. Hence, it is crucial to have a good understanding of the mechanisms of particle deposition (and the subsequent fouling rate) in ventilation ducts in order to achieve these goals in the case of the food factories.

The 4-year project called CleanAirNet, which conducted substantial industrial trials under real conditions and original laboratory experiments (for particle deposition to duct surfaces with developed and undeveloped turbulent airflow) and prior to practical proposals, has been presented as a case study for hygienic design of air handling systems in the food sector. A relevant finding of the project was to propose a low-pressure-drop particle trapping prototype as well as an improvement of energy consumption efficiency. Finally, the prototype was validated in industrial conditions and patented. The CleanAirNet project eventually contributes to supplement information to HVAC systems in nonindustrial or common-used buildings.

Acknowledgments This work was conducted within the framework of the CleanAirNet project, a joint project of research groups from IRSTEA (ACTA-Rennes), GEPEA (Process Engineering Laboratory including ONIRIS and EMN in Nantes), CSTB (Laboratory of Indoor Environment Microbiology-Champs sur Marne), CERTES-Université Paris-Est (Center for Thermal and Environmental Research), ADRIA NORMANDIE (center of technological resources devoted to food industry), and LAVAL MAYENNE TECHNOPOLE (territorial agency for economic development and innovation promotion). Three industries from the food sector were taking part in the consortium. We are thankful for Dr. Amine Metani for supplying the scanning electron photographs of *Aspergillus niger*.

References

1. WHO (2010) WHO guidelines for indoor air quality: selected pollutants. World Health Organization Regional Office for Europe, Copenhagen
2. Lopez-Gomez A, Castano-Villar A, Palop A, Marin-Iniesta F (2013) Hygienic design and microbial control of refrigeration and Air conditioning systems for food processing and packaging plants. Food Eng Rev 5:18–35
3. Burfoot D, Whyte R, Tinker D, Hall K, Allen V (2007) A novel method for assessing the role of air in the microbiological contamination of poultry carcasses. Int J Food Microbiol 115:48–52
4. Havelaar A, Brul S, de Jong A, de Jong R, Zwietering M, ter Kuile B (2010) Future challenges to microbial food safety. Int J Food Microbiol 139:579–594
5. Reij M, den Aantrekker E (2004) Recontamination as a source of pathogens in processed foods. Int J Food Microbiol 91:1–11
6. Bluyssen P, Cox C, Seppanen O, Fernandes E, Clausen G, Muller B, Roulet C (2003) Why, when and how do HVAC-systems pollute the indoor environment and what to do about it? The European AIRLESS project. Build Environ 38:209–225
7. den Aantrekker E, Boom R, Zwietering M, van Schothorst M (2003) Quantifying recontamination through factory environments – a review. Int J Food Microbiol 80:117–130
8. EHEDG (2006) Guidelines on air handling in the food industry. Trends Food Sci Technol 17:331–336
9. Harral B, Burfoot D (2005) A comparison of two models for predicting the movements of airborne particles from cleaning operations. J Food Eng 69:443–451
10. Carrasco E, Morales-Rueda A, Garcia-Gimeno R (2012) Cross-contamination and recontamination by Salmonella in food: a review. Food Res Int 45:545–556
11. Kim K, Kim H, Kim D, Nakajima J, Higuchi T (2009) Distribution characteristics of airborne bacteria and fungi in the feedstuff-manufacturing factories. J Hazard Mater 169:1054–1060
12. Robine E, Dérangère D, Robin D (2000) Survival of a Pseudomonas fluorescens and Enterococcus faecalis aerosol on inert surfaces. Int J Food Microbiol 55:1–3
13. Rostagno M, Callaway T (2012) Pre-harvest risk factors for Salmonella enterica in pork production. Food Res Int 45:634–640
14. Zorzete P, Baquiao A, Atayde D, Reis T, Gonzales E, Correa B (2013) Mycobiota, aflatoxins and cyclopiazonic acid in stored peanut cultivars. Food Res Int 52:380–386
15. Després V, Huffman J, Burrows S, Hoose C, Safatov A, Buryak G, Fröhlich-Nowoisky J, Elbert W, Andreae M, Pöschl U, Jaenicke R (2012) Primary biological aerosol particles in the atmosphere: a review. Tellus B. doi:10.3402/tellusb.v3464i3400.15598
16. Da G, Géhin E, Ben Othmane M, Havet M, Solliec C, Motzkus C (2014) An experimental approach to measure particle deposition in large circular ventilation ducts. Environ Sci Pollut Res Int. http://link.springer.com/article/10.1007/s11356-014-2859-y
17. Metani A (2013) Déposition et Réenvol de Spores Fongiques. Contribution à la Compréhension du Risque Nosocomial Aérotransmis. PhD Thesis, Ecole Normale Supérieure de Lyon – Université de Lyon, Lyon, France
18. Shale K, Lues J (2007) The etiology of bioaerosols in food environments. Food Rev Int 23:73–90
19. Sheehana M, Giranda J (2011) Bioaerosol generation in a food processing plant: a comparison of production and sanitation operations. Appl Occup Environ Hyg 9:346–352
20. Evans J, Russell S, James C, Corry J (2004) Microbial contamination of food refrigeration equipment. J Food Eng 62:225–232
21. Pearce R, Sheridan J, Bolton DJ (2005) Distribution of Airborne microorganisms in commercial pork slaughter processes. Int J Food Microbiol 107:186–191
22. Perez-Rodriguez F, Valero A, Carrasco E, Garcia R, Zurera G (2008) Understanding modelling bacterial transfer to foods : a review. Trends Food Sci Technol 19:131–144

23. den Aantrekker E, Beumer R, van Gerwen S, Zwietering M, van Schothorst M, Boom R (2003) Estimating the probability of recontamination via the air using Monte Carlo simulations. Int J Food Microbiol 87:1–15
24. Koopmans M, Duizer E (2004) Foodborne viruses: an emerging problem. Int J Food Microbiol 90:23–41
25. Skovgaard N (2007) The mycotoxin factbook. Food and feed topics. Int J Food Microbiol 116:301 (Barug D, Bhatnagar D, van Egmond HP, van der Kamp JW, van Osenbruggen WA, Visconti A (eds.), (2006) Book review)
26. Gorny R, Reponen T, Willeke K, Schmechel D, Robine E, Boissier M, Grinshpun S (2002) Fungal fragments as indoor air biocontaminants. Appl Environ Microbiol 68:3522–3531
27. Ge S (2014) Viral aerosol survivability, transmission, and sampling in an environmental chamber. PhD Thesis, University of Minnesota, USA
28. Reponen T, Willeke K, Grinshpun S, Nevalainen A (2011) Biological particle sampling. In: Kulkarni P, Baron P, Willeke K (eds) Aerosol measurement, principles, techniques, and applications, 3rd edn. Wiley, San Francisco, CA, pp 549–570
29. Xu Z, Wu Y, Shen Y, Chen Q, Tan M, Yao M (2011) Bioaerosol science, technology, and engineering: past, present, and future. Aerosol Sci Technol 45:1337–1349
30. Qian J, Hospodsky D, Yamamoto N, Nazaroff W, Peccia J (2012) Size-resolved emission rates of airborne bacteria and fungi in an occupied classroom. Indoor Air 22:339–351
31. Bhangar S, Huffman J, Nazaroff W (2014) Size-resolved fluorescent biological aerosol particle concentrations and occupant emissions in a university classroom. Indoor Air. doi:10.1111/ina.12111
32. Burfoot D, Reavell S, Tuck C, Wilkinson D (2003) Generation and dispersion of droplets from cleaning equipment used in the chilled food industry. J Food Eng 58:343–353
33. Kang Y, Frak J (1990) Characteristics of biological aerosols in dairy processing plants. J Dairy Sci 73:621–626
34. Byrne B, Lyn J, Dunne G, Bolton D (2008) An assessment of the microbial quality of the air within a pork processing plant. Food Contr 19:915–920
35. Lopez-Gomez A, Fernandez P, Palop A, Periago P, Matrinez-Lopez A, Marin-Iniesta F, Barbosa-Canovas G (2009) Food safety engineering : an emergent perspective. Food Eng Rev 1:84–104
36. ASPEC, Alloul-Marmor L (2011) Salles propres et environnements maîtrises apparentés: Etat des lieux de la normalisation. CVC 868:23–28
37. ISO (1999) ISO 14644: cleanrooms and associated controlled environments Part 1: classification of air cleanliness by particle concentration. http://www.iso.org/iso/home/store/catalogue_tc/catalogue_detail.htm?csnumber = 25052
38. Norton T, Sun D (2006) Computational fluid dynamics (CFD) – an effective and efficient design and analysis tool for the food industry: a review. Trends Food Sci Technol 17:600–620
39. Havet M, Hennequin F (1999) Experimental characterization of the ambience in a food-processing clean room. J Food Eng 39:329–335
40. Rouaud O, Havet M (2005) Numerical investigation on the efficiency of transient contaminant removal from a food processing clean room using ventilation effectiveness concepts. J Food Eng 68:163–174
41. Aires G, Walter E, Faria J, Roig S (2010) Restrictions to the use of cleanrooms for packaging pasteurised milk. Int J Dairy Technol 63:266–272
42. Burfoot D, Brown K, Xu Y, Reavell S, Hall K (2000) Localised air delivery systems in the food industry. Trends Food Sci Technol 11:410–418
43. Santa Cruz A, Coste N, Makhloufi R, Guillou S, Delboulbé D, Tiffonnet A, Marion M (2011) Airflow inside an open ventilated system: influence of operator's arms or moving conveyor. J Food Eng 105:197–209
44. Foarde K, Menetrez M (2002) Evaluating the potential efficacy of three antifungal sealants of duct liner and galvanized steel as used in HVAC systems. J Ind Microbiol Biotechnol 29:38–43

45. Li A, Liu Z, Liu Y, Xu X, Pu Y (2012) Experimental study on microorganism ecological distribution and contamination mechanism in supply air ducts. Energy Build 47:497–505
46. Maus R, Goppelsröder A, Umhauer H (2001) Survival of bacterial and mold spores in air filter media. Atmos Environ 35:105–113
47. Zuraimi M (2010) Is ventilation duct cleaning useful? A review of the scientific evidence. Indoor Air 20:445–457
48. Makarian J (2006) Steady growth predicted for biocides. Plastics Addit Comp 8:30–33
49. Zuraimi M, Magee R, Nilsson G (2012) Development and application of a protocol to evaluate impact of duct cleaning on IAQ of office buildings. Build Environ 56:86–94
50. Lavoie J, Bahloul A, Cloutier Y, Gravel R (2007) Cleaning initiation criteria for heating, ventilation and air conditioning (HVAC) systems in non-industrial buildings. Paper presented at the Proceedings of Clima 2007, Helsinki, Finland, June 10–14, 2007
51. Ben Othmane M, Havet M, Géhin E, Solliec C (2010) Mechanisms of particle deposition in ventilation ducts for a food factory. Aerosol Sci Technol 44:775–784
52. Arroyo G, Denis C, Ben Othmane M, Havet M, Géhin E (2010) Hygienic design of ventilation networks in food factories. Paper presented at the Food Factory 2010, 5th International Conference for Food Factory in the future, Gothenburg, Sweden, 30 June–2 July 2010
53. Denis C, Arroyo G (2011) Agroalimentaire : recueil de données microbiologiques dans les réseaux de ventilation. Salles Propres 76:40–46
54. Ben Othmane M, Havet M, Géhin E, Solliec C (2011) Predicting cleaning time of ventilation duct systems in the food industry. J Food Eng 105:400–407
55. Havet M, Ben Othmane M, Géhin E, Solliec C (2012) Experimental study of particle deposition in ventilation duct systems of the food industry. Paper presented at the 10th International Conference on Industrial Ventilation, Paris, France, 17–19 September 2012
56. Sippola M (2002) Particle deposition in ventilation ducts. Unpublished PhD Thesis, University of California, Berkeley, USA
57. Sippola M, Nazaroff W (2002) Particle deposition from turbulent flow: review of published research and its applicability to ventilation ducts in commercial buildings. Lawrence Berkeley National Laboratory Report LBNL-51432
58. Zhao B, Wu J (2006) Modeling particle deposition from fully developed turbulent flow in ventilation duct. Atmos Environ 40:457–466
59. Guha A (1997) A unified Eulerian theory of turbulent deposition to smooth and rough surfaces. J Aerosol Sci 28:1517–1537
60. Montgomery T, Corn M (1970) Aerosol deposition in a pipe with turbulent air flow. J Aerosol Sci 1:185–213
61. Fan H, Hua J (2013) Experimental research and modeling of particle deposition in ventilation ducts. Adv Mech Eng Article ID 208528. http://dx.doi.org/10.1155/2013/208528
62. Tian L, Ahamadi G (2007) Particle deposition in turbulent duct flows - comparisons of different model predictions. J Aerosol Sci 38:377–397
63. Wood N (1981) A simple method for the calculation of turbulent deposition to smooth and rough surfaces. J Aerosol Sci 12:275–290
64. Liu B, Agarwal J (1974) Experimental observation of aerosol deposition in turbulent flow. Aerosol Sci Technol 5:145–155
65. Sippola M, Nazaroff W (2004) Experiments measuring particle deposition from fully developed turbulent flow in ventilation ducts. Aerosol Sci Technol 38:914–925
66. Sippola M, Nazaroff W (2005) Particle deposition in ventilation ducts: connectors, bends and developing turbulent flow. Aerosol Sci Technol 39:139–150
67. Cheng Y (1997) Wall deposition of radon progeny and particles in a spherical chamber. Aerosol Sci Technol 27:131–146
68. You R, Zhao B, Chen C (2012) Developing an empirical equation for modeling particle deposition velocity onto inclined surfaces in indoor environments. Aerosol Sci Technol 46:1090–1099

69. Ben Othmane M (2011) Study of particle deposition mechanism in ventilation ducts of food factory. In French. PhD Thesis, ONIRIS, L'UNAM, Nantes, France
70. Arroyo G, Chomel N (2012) CLEANAIRNET: Conception hygiénique des réseaux de distribution d'air dans les industries agroalimentaires. Compte-rendu de fin de projet. Hygienic design of Ventilation Networks in Food Factories. Final report. In French. Report No. ANR-07-PNRA-0019. French National Research Agency (ANR), France
71. Carlier J, Arroyo G, Georgeault P, Guibert A, Loubat M, Wallian L (2014) Assembly for trapping particles suspended in a fluid (Ensemble de piégeage de particules en suspension dans un fluide). French Patent WO 2014/057221 A1, 17 avril 2014
72. Afram A, Janabi-Sharifi F (2014) Review of modeling methods for HVAC systems. Appl Thermal Eng 67:507–519

The OASIS Observatory Using Ground-Based Solar Absorption Fourier-Transform Infrared Spectroscopy in the Suburbs of Paris (Créteil-France)

P. Chelin, C. Viatte, M. Ray, M. Eremenko, J. Cuesta, F. Hase, J. Orphal, and J.-M. Flaud

Abstract Ground-based Fourier-transform infrared (FTIR) solar absorption spectroscopy has led to a number of significant advances in our understanding of the atmosphere by providing information on the vertical distribution of various trace gases. Previously used to analyse solar absorption spectra measured at high-resolution in unpolluted sites, the retrieval code PROFFIT has been adapted to deal with spectra recorded at medium spectral resolution with a Bruker Optics Vertex 80 FTIR spectrometer. As one of the major instruments of the experimental observatory named OASIS (Observations of the Atmosphere by Solar Infrared Spectroscopy), this instrument is dedicated to the study of air composition in the

P. Chelin (✉), M. Ray, M. Eremenko, J. Cuesta, and J.-M. Flaud
Laboratoire Inter-Universitaire des Systèmes Atmosphériques (LISA) CNRS UMR 7583, Université Paris-Est Créteil, Université Paris Diderot, Institut Pierre-Simon Laplace, 61 Avenue du Général de Gaulle, 94010 Créteil Cedex, France
e-mail: pascale.chelin@lisa.u-pec.fr

C. Viatte
Laboratoire Inter-Universitaire des Systèmes Atmosphériques (LISA) CNRS UMR 7583, Université Paris-Est Créteil, Université Paris Diderot, Institut Pierre-Simon Laplace, 61 Avenue du Général de Gaulle, 94010 Créteil Cedex, France

Division of Geological and Planetary Sciences, California Institute of Technology, Pasadena, CA, USA

F. Hase
Institute for Meteorology and Climate Research (IMK), Karlsruhe Institute of Technology (KIT), Karlsruhe, Germany

J. Orphal
Laboratoire Inter-Universitaire des Systèmes Atmosphériques (LISA) CNRS UMR 7583, Université Paris-Est Créteil, Université Paris Diderot, Institut Pierre-Simon Laplace, 61 Avenue du Général de Gaulle, 94010 Créteil Cedex, France

Institute for Meteorology and Climate Research (IMK), Karlsruhe Institute of Technology (KIT), Karlsruhe, Germany

E. Jiménez et al. (eds.), *Environment, Energy and Climate Change I: Environmental Chemistry of Pollutants and Wastes*, Hdb Env Chem (2015) 32: 21–52,
DOI 10.1007/698_2014_270,
Published online: 29 July 2014

suburbs of Paris. Accurate measurements of the most important atmospheric pollutants are indeed essential to improve the understanding and modelling of urban air pollution processes. Located in an urban region, OASIS enables to monitor key pollutants such as NOx, O_3, CO and VOCs. In this chapter, 5 years intercomparison study with on-ground and satellite measurements for O_3 and CO is reported, demonstrating the performances of a medium-resolution ground-based instrument and especially confirming its capability for tropospheric ozone monitoring.

Keywords Air quality in megacity, Carbon monoxide, IR spectroscopy, Ozone, Remote sensing, Solar occultation

Contents

Abbreviations

DOAS	Differential optical absorption spectroscopy
DOF	Degrees of freedom
DTGS	Deuterated triglycine sulphate
DU	Dobson unit
EOS	Earth observing system
ESA	European Space Agency
FTIR	Fourier-transform infrared
GOME-2	Global Ozone Monitoring Experiment-2
HITRAN	High-resolution transmission molecular absorption database
IASI	Infrared Atmospheric Sounder Interferometer
ILS	Instrumental line shape
IR	Infrared
LAN	Local area network
MetOp	Meteorological operational polar satellite
MIPAS	Michelson Interferometer for Passive Atmospheric Sounding

MOPITT	Measurements of Pollution in the Troposphere
MOZAIC	Measurements of ozone and water vapour by in-service airbus aircraft programme
MRD	Mean relative difference
NASA	National Aeronautics and Space Administration
NCEP	National Centers for Environment Prediction
NDACC	Network for the Detection of Atmospheric Composition Change
OASIS	Observations of the atmosphere by solar infrared spectroscopy
OMI	Ozone Monitoring Instrument
SAOZ	Système d'Analyse par Observation Zénithale
TCCON	Total Carbon Column Observing Network
TOMS	Total Ozone Mapping Spectrometer

1 Introduction

Ozone (O_3) plays an important role in the Earth's atmosphere. In the stratosphere, its presence is vital for life on Earth because it absorbs harmful ultraviolet radiation [1]; in the troposphere, it is involved in photochemical processes, a key parameter for both air quality and climate issues [2]. In the boundary-layer, O_3 is harmful to humans [3], animals and vegetation [4]. In the upper troposphere, O_3 impacts radiative forcing [5–7]. O_3 also controls the oxidizing capacity of the atmosphere [8]. In addition to O_3, carbon monoxide (CO) is also involved in tropospheric photochemical processes: in fact O_3 production takes place when CO and hydrocarbons are photo-oxidized in the presence of nitrogen oxides (NOx). Also CO is an excellent tropospheric air-mass tracer due to its rather long lifetime of 2 months on average.

In the international Network for the Detection of Atmospheric Composition Change (NDACC), around 20 high-quality, remote-sensing IR research stations employ ground-based Fourier-transform infrared (FTIR) solar absorption spectroscopy to observe and to analyse the physical and chemical states of the stratosphere and upper troposphere and to assess the impact of stratospheric changes on the underlying troposphere and on global climate. These high spectral resolution FTIR stations are preferentially operated at remote sites far away from sources of air pollution and often are located at high altitudes (e.g. Izaña, Jungfraujoch, Zugspitze, Table Mountain, etc.) so that measurements of tropospheric ozone are obviously limited at these stations. Hence, in order to perform air quality research in large megacities, we have assessed the capability of a medium-resolution FTIR solar absorption spectrometer for monitoring pollutants, especially O_3 and CO. We have demonstrated that such an observatory, named OASIS (Observations of the Atmosphere by Solar Infrared Spectroscopy) installed in Créteil near Paris (France) since 2008, is able to continuously monitor tropospheric ozone over Créteil with good accuracy as documented by a first analysis of information content in OASIS ozone retrievals [9].

The purpose of the present study is to confirm and expand this preliminary result by incorporating time series of total and tropospheric ozone during 5 years of measurements from February 2009 to July 2013 and by intercomparing satellite observations and in situ measurements. Another new aspect is to complement the O_3 observations with CO total columns (and its seasonal cycle) that are measured simultaneously with O_3 by taking advantage of the wide spectral range covered by the OASIS instrument.

This chapter firstly describes in detail the OASIS instrumentation (Sect. 2) and outlines the radiative transfer equation and the radiative transfer model and retrieval code applied (Sect. 3). In this latter section, a discussion on the separation of tropospheric and stratospheric columns of ozone based on the information content analysis is included. The overall results derived from the OASIS measurements are presented in Sect. 4 for the total columns of O_3 and CO and for the tropospheric ozone column. Also columns derived from OASIS measurements are compared with correlative satellite and ground-based observations. Finally, Sect. 5 is devoted to the conclusions.

2 OASIS Instrumentation

The OASIS observatory (48.79° N, 2.44° E, 56 m above sea level) was established in 2008 with the installation of a medium-resolution, Vertex model Fourier-transform infrared spectrometer manufactured by Bruker Optics (Ettlingen, Germany). This instrument collects infrared atmospheric absorption spectra using the sun as light source (Fig. 1) and monitors continuously the concentrations of important atmospheric constituents, such as H_2O, CO_2, CH_4, N_2O, O_2, NH_3, OCS, O_3 and CO. The observatory comprises an automatized cupola (Sirius 3.5 "School Model" observatory, 3.25 m high and 3.5 m in diameter) in which the upper part, the dome, equipped with a mobile aperture, rotates in order to be aligned with the solar tracker and the sun. The drive engine of the dome is fed by a battery recharged by two solar panels.

2.1 Sun Tracker

The alt-azimutal solar tracker in OASIS is the A547N model manufactured by Bruker Optics. To reach a tracking precision of ± 2 min of arc, the solar tracker uses a quadrant diode to register deviations from the precalculated pointing direction of the tracking system. The diode signal is then fed into the control loop of the tracker under cloudless blue sky conditions. In case of overcast sky, the diode signal drops down, and if it is under a minimal value, the sun tracker sustains tracking according to astronomic calculation.

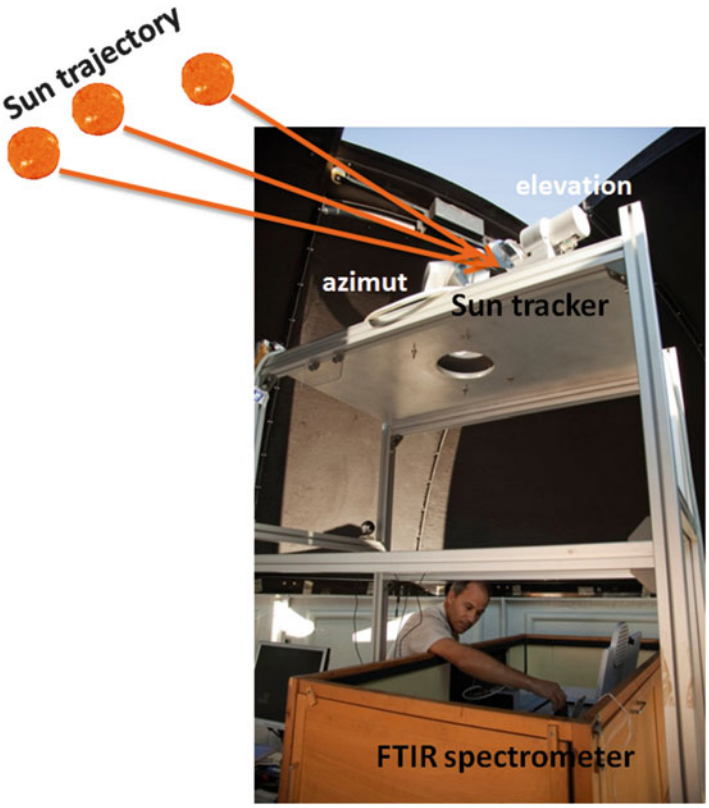

Fig. 1 *Interior view* of the OASIS observatory showing the FTIR spectrometer and the sun tracker

The solar light that is analysed by the quadrant diode is decoupled from the parallel beam a few cm in front of the entrance aperture by a small planar mirror, so that only a small subsection of the full beam diameter is used. Both tracker mirrors are coated with protected aluminium to cover the entire spectral range from 700 to 40,000 cm^{-1}. However, we experienced corrosion problems with the Al mirrors. Visible damage appeared on the mirror's surface like white coatings after several months of use. Likely these problems are due to high humidity levels and large temperature excursions inside the cupola and maybe also to the presence of corrosive pollutants in the urban area. In the near future, the replacement of the current Al mirrors by bare gold-coated mirrors which cover the spectral range from 10 to 15,800 cm^{-1} will be tested. Moreover, two heaters have been installed to generate a less hostile environment during the cold season: one heater diminishes the overall humidity inside the cupola, the other one circulates dry air around the two mirrors. Indeed, relative global humidity dropped from 80 to 30%.

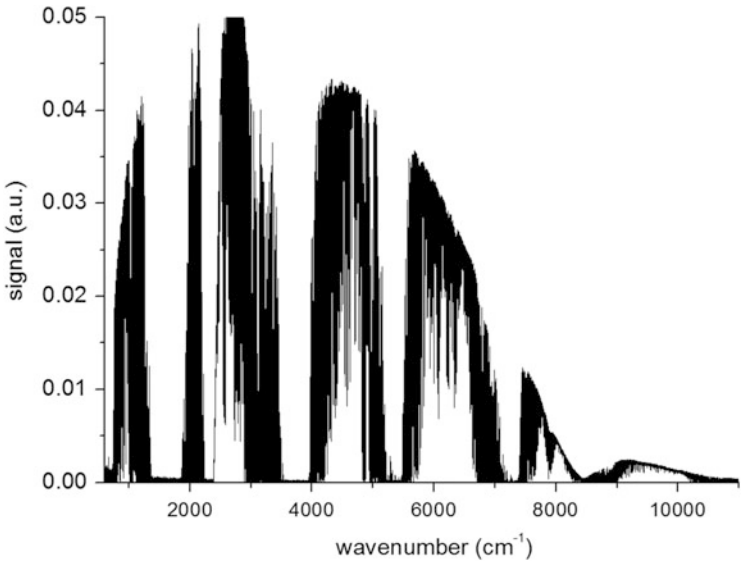

Fig. 2 Ground-based atmospheric solar spectrum recorded with an entrance aperture diameter of 1.5 mm and a maximum nominal spectral resolution of 0.075 cm^{-1}

A software provided by Bruker controls the sun tracker from the OASIS computer. The latter is also controlled by internet connection which permits the remote control of all the instruments from any computer in the university LAN.

2.2 Fourier-Transform Infrared Spectrometer

As one of the major instruments of the OASIS observatory, the Fourier-transform spectrometer is dedicated to the measurement of atmospheric spectra in solar occultation geometry using the infrared spectral region in order to investigate the air composition in the suburbs of Paris. The optical key element of the OASIS spectrometer is a linear Michelson interferometer that records single-sided interferograms with a maximum optical path difference of 12 cm. Infrared solar absorption spectra are nominally recorded on a DTGS (deuterated triglycine sulphate) detector using a potassium bromide (KBr) beam splitter to cover the spectral region from 700 to 11,000 cm^{-1} (0.9–14.3 μm). It is a dry air purged spectrometer to always maintain the humidity in the optical benchmark at values lower than 10%. During low temperature conditions, the spectrometer is placed inside a wood container with an additional heater.

To achieve a sufficiently high signal-to-noise ratio, each spectrum is produced by co-adding 30, 12-cm optical path difference scans, resulting in one interferogram recorded over a period of approximately 10 min (Fig. 2). Each interferogram is Fourier-transformed into a spectrum without further numerical apodization (i.e. unapodized/boxcar apodization).

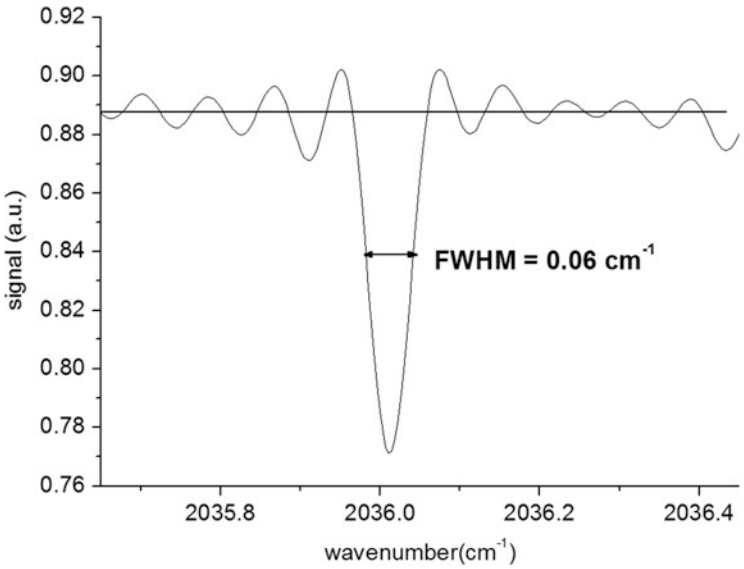

Fig. 3 Gas cell spectra recorded with OCS at low pressure for the determination of the ILS parameters

2.3 Spectrometer Accuracy

Any quantitative trace gas retrieval depends on a proper knowledge of the spectral characteristics of the instrument. For FTIR spectrometers, the Instrumental Line Shape (ILS) is advantageously separated into one part which refers to the inherent self-apodization due to the circular field stop. This contribution can be calculated easily using the spectrometer's field of view and the optical path difference of the interferometer. The second component of the ILS can be described by a complex modulation efficiency (represented by a modulation amplitude and a phase error, both functions of the optical path difference) which result from misalignments and optical aberrations [10]. In our case, the determination of the instrumental line shape (ILS) is made with a 25 cm long gas cell (using CaF_2 windows) filled with OCS (carbonyl sulphide) at very low pressure, which is put in the interferometer's sample compartment (Fig. 3). To analyse the results and to obtain the modulation efficiency and the phase error, the version 12 of the LINEFIT programme [11] is used.

The zero transmittance baseline has also been checked in an atmospheric spectrum on the ν_2 fundamental band of H_2O centred around 1,595 cm^{-1} that is totally saturated as showed in Fig. 4. The accuracy on the zero transmittance is better than 0.15% checked between 1,600 and 1,700 cm^{-1}. This is important since it demonstrates a very low nonlinearity of the detector.

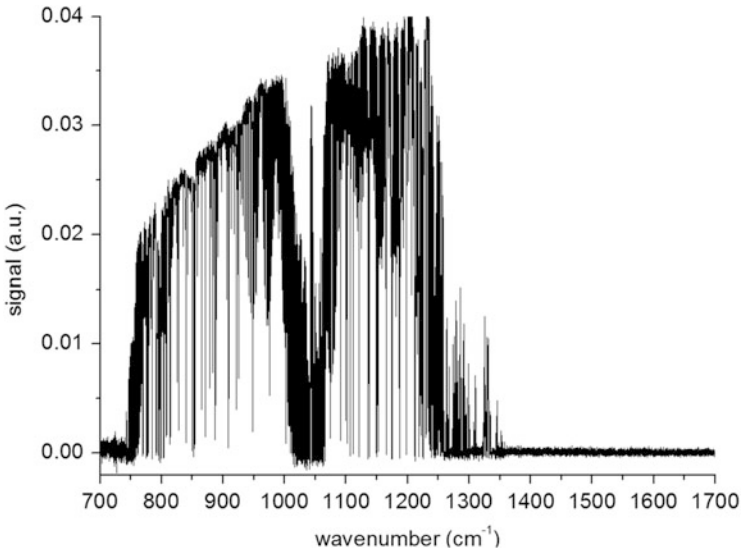

Fig. 4 Atmospheric spectrum with zero transmittance in the ν_2 band of H_2O

3 Radiative Transfer Equation and Retrieval Code

In order to retrieve the concentrations of the target species in the atmosphere, one needs first to calculate a synthetic atmospheric spectrum using a radiative transfer algorithm. This is done using the PROFile ForWarD (PROFFWD) model of the PROFFIT 9.6 code [12] widely used by the NDACC community to retrieve trace gases from high-resolution FTIR measurements.

3.1 Forward Calculation of a Synthetic Spectrum

When the sun is used as the external source, the radiative transfer model is based on the integrated form of the Beer–Lambert law accounting only for absorption [13]:

$$I_{\widetilde{\nu}}(l) = I_{\widetilde{\nu}}(0) \times T_{\widetilde{\nu}}(l, 0) \tag{1}$$

where $I_{\widetilde{\nu}}(0)$ is the incident solar intensity at the top of the atmosphere (typically in W cm^{-2} sr^{-1} $(cm^{-1})^{-1}$ at the wavenumber $\widetilde{\nu}$ (in cm^{-1}), $I_{\widetilde{\nu}}(l)$ is the intensity at the position l (in cm) along the absorption path, and $T_{\widetilde{\nu}}(l, 0)$ is the atmospheric transmittance between the positions l and 0. However, one can note that PROFFWD takes into account (in the long-wave part of the spectrum, below 1,000 cm^{-1}) also the atmospheric emission which becomes a non-negligible correction to the pure absorption spectrum.

The transmittance is given in case of line spectra by the following equation:

$$T_{\tilde{\nu}}(l,0) = \mathrm{e}^{-\tau_{\tilde{\nu}}(l,0)} \tag{2}$$

where the optical depth $\tau_{\tilde{\nu}}(l,0)$ between l and 0 is defined by

$$\tau_{\tilde{\nu}}(l,0) = \sum_i \sum_j \int_0^l S^i_{\tilde{\nu}_j}(T(l')) \times \Phi\left(\tilde{\nu} - \tilde{\nu}_j, p(l'), T(l')\right) \times N_i(l')\mathrm{d}l' \tag{3}$$

where i characterizes the various absorbing species; $N_i(l')$ is the local density of molecules of species (in mol cm^{-3}); $S^i_{\tilde{\nu}_j}$ is the intensity (in cm mol^{-1}) of the line j of the species i, with the line centre at $\tilde{\nu}_j$; and $\Phi\left(\tilde{\nu} - \tilde{\nu}_j, p(l'), T(l')\right)$ is the line profile (in cm) that depends on pressure (Lorentz profile) and temperature (Doppler and Lorentz profiles). For the species under consideration, the Voigt profile (the convolution of a Doppler and a Lorentz profile) is currently used and is commonly calculated in the atmospheric radiative transfer models (however, note that PROFFWD also supports non-Voigt line shapes and line mixing).

For the forward calculation of a theoretical spectrum, the spectroscopic reference data were taken from the HITRAN 2004 data base [14].

3.2 Retrieval Code

PROFFIT (PROFile FIT) [12] is the retrieval tool used to analyse the solar absorption spectra measured with high-resolution ground-based FTIR spectrometers. It is here adapted to the medium spectral resolution of the instrument. Note that to achieve sufficient information content in the retrievals, the micro-windows have to be widened as compared to high-resolution retrievals (as described in Sect. 3.3). The retrieval of trace gas profiles from such spectra is an ill-posed problem and needs a constrained nonlinear least squares fitting technique [15]. For this purpose, an analytical altitude-dependent regularization method with the regularization matrix containing first- and second-order Tikhonov constraints [16] is used, together with altitude-dependent coefficients that are optimized to maximize the information content of the retrievals.

For ozone, the a priori profile is taken from the mean annual McPeters climatology [17] adapted to the location of the observatory (i.e. between 40° and 50° N). It is worth noting that all retrievals are performed with the same a priori data set to ensure that all the variability seen in the retrieved profiles comes from the measurements. Furthermore, it was observed that the retrieved ozone profiles do not significantly depend on the choice of the a priori profile since a change of a priori profiles produced negligible differences on the results. For carbon monoxide and its interfering species, the a priori profiles were taken from the MIPAS project

[18]. They correspond to the mean annual profiles used for the inversion of MIPAS satellite data for latitudes between 30° and 50° N.

The temperature and pressure profiles, interpolated on the same grid as the species a priori profiles, are obtained from the Goddard Space Flight Center (NCEP, National Center for Environment Prediction). For the radiative transfer calculations, all profiles are discretized in 46 levels from the ground up to 85 km.

3.3 Spectral Windows and Analysis

Ozone and carbon monoxide concentrations shown in this chapter are derived from the spectra measured by the OASIS observatory, corresponding to 203 clear-sky days, from 25 February 2009 to 19 July 2013 at Créteil (France). Atmospheric ozone is retrieved using the spectral window from 991 to 1,073 cm^{-1} (where the interfering species are H_2O, SO_2 and NH_3), while CO is retrieved in the spectral region between 2,134 and 2,174 cm^{-1} (where the interfering species are H_2O, CO_2, O_3, N_2O and OCS).

3.3.1 Ozone

Figure 5 shows a measured spectrum, the corresponding simulated spectrum and the difference between observation and simulation for the spectral window used for the ozone retrievals. As the radiance values are small below 1,000 cm^{-1}, a quality filter is introduced selecting only spectra with a signal-to-noise ratio higher than 30 measured between 960 and 990 cm^{-1} where there is a CO_2 band.

Retrievals are characterized by the averaging kernel matrix which represents their sensitivity to the true atmospheric state and also by the degrees of freedom (DOF) which are the trace of this matrix [15]. The DOF of a given atmospheric layer reaches unity when the retrieval contains sufficient information to consider that the partial column in this layer is quasi-independent from the others. Figure 6 shows typical averaging kernels of OASIS retrievals. From the ground up to 8 km (empty square symbols) and from 8 to 17 km (solid square symbols), the DOF reaches 1.03 and 1.08, respectively, showing that these two partial columns can be separated. Typical degrees of freedom obtained through OASIS retrievals reach at least 3, which is a surprisingly good result for a spectrometer of medium resolution, given that an NDACC system (using very high-resolution spectrometers) reaches DOF around 4 [19, 20].

To validate the separation of tropospheric and stratospheric ozone columns, stratospheric and tropospheric ozone column time series are compared and the correlation between these two partial columns is evaluated (Fig. 7). The total uncertainties of tropospheric ozone, including statistical, systematical and smoothing errors, are estimated to about 13–15% (depending on the solar elevation angle and the meteorological conditions), while the uncertainty of the stratospheric ozone column is estimated to about 3%. In Fig. 7, one can see that stratospheric (solid circle symbols) and tropospheric (empty square symbols) ozone time series do not

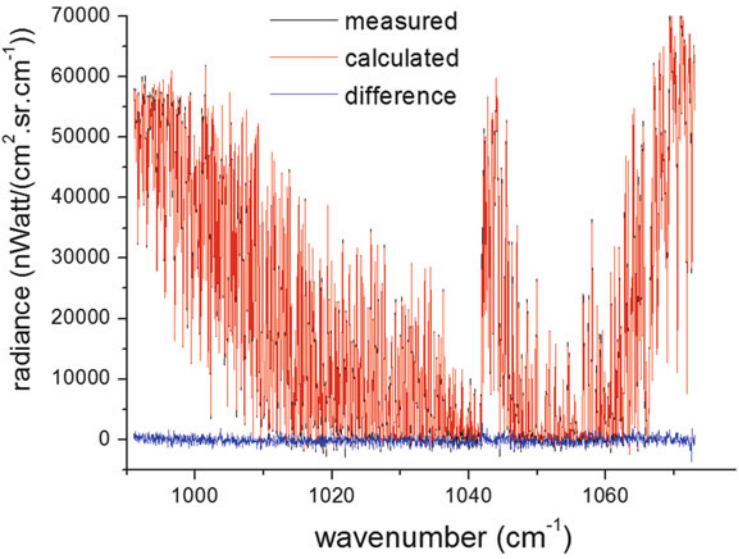

Fig. 5 Spectral window for the ozone retrievals recorded with OASIS on 31 March 2009 at 12:58 p.m. (UT). *Black*: the measured spectrum. *Red*: the calculated spectrum. *Blue*: the difference between the measured and calculated spectra

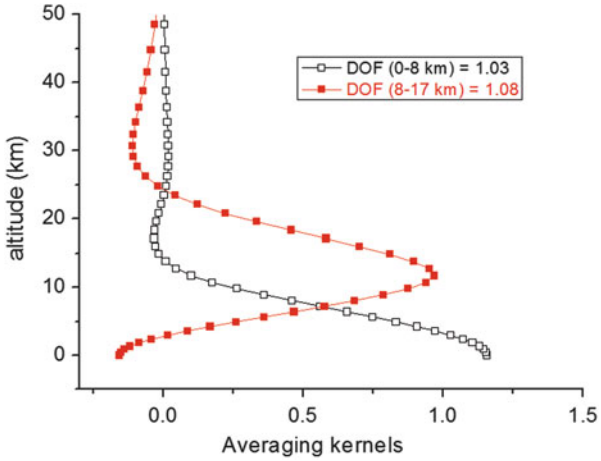

Fig. 6 OASIS typical averaging kernels in partial column from ground to 8 km and 8–17 km in *empty* and *solid square symbols*, respectively, corresponding to the spectra in Fig. 5

present the same structures and that a correlation coefficient of 0.39 is observed for the 203 measurements. The averaging kernels, which reflect the vertical sensitivity of the retrievals, show that the retrieved tropospheric amounts (integrated from the ground to 8 km) have a small stratospheric contribution through vertical transport, and vice versa (Fig. 7). Viatte et al. [9] demonstrated by a first analysis of the

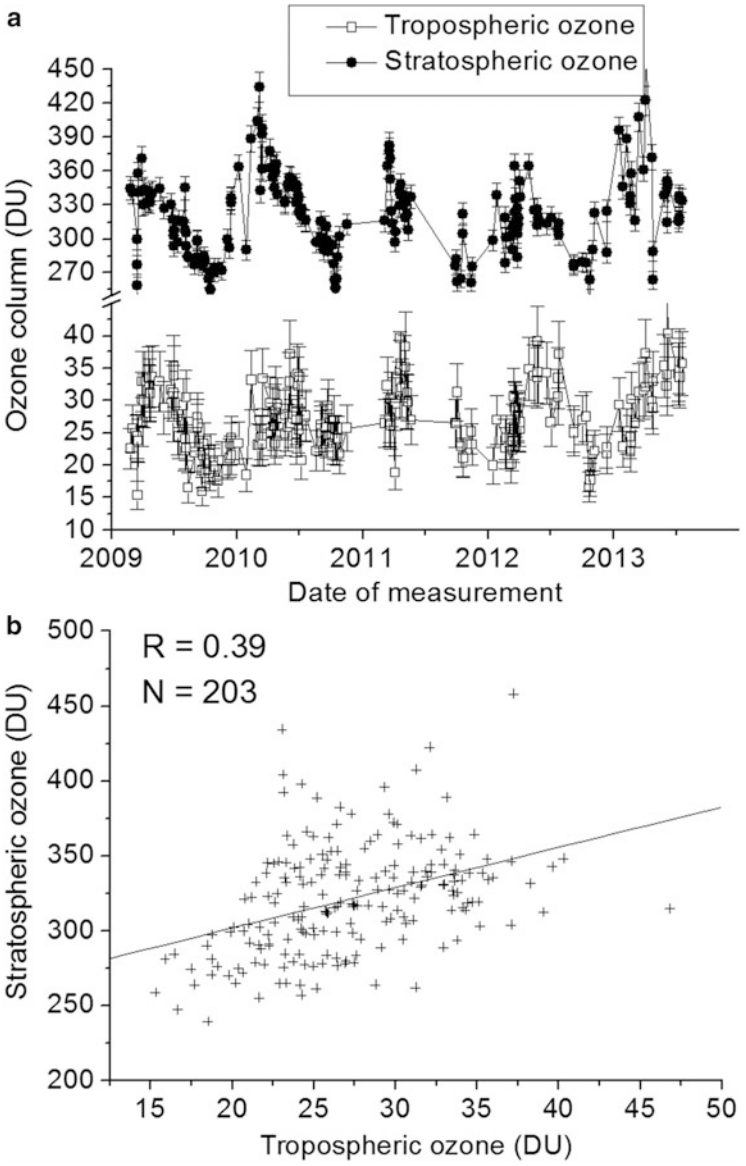

Fig. 7 *Upper plot*: times series of tropospheric (*empty square symbols*) and stratospheric (*solid circle symbols*) ozone columns derived from OASIS measurements from 25 February 2009 to 19 July 2013 at Créteil (France). *Lower plot*: stratospheric ozone related to tropospheric ozone derived from OASIS spectra

information content in OASIS ozone retrievals that using a medium-resolution instrument, tropospheric ozone can be monitored separately from stratospheric ozone since degrees of freedom reach unity in those two partial atmospheric layers.

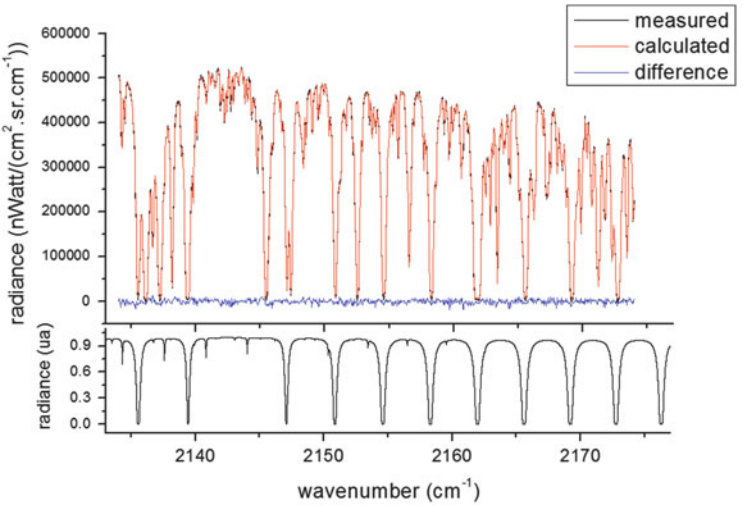

Fig. 8 *Upper plot*: spectral window for the carbon monoxide retrievals recorded with OASIS on 16 December 2009 at 13:28 p.m. (UT). *Black*: the measured atmospheric spectrum. *Red*: the calculated spectrum. *Blue*: the difference between the measured and calculated spectra. *Lower plot*: pure CO absorption spectrum

In this work, the performance for tropospheric ozone monitoring by OASIS is confirmed by 5 years time series.

3.3.2 Carbon Monoxide

Carbon monoxide is simultaneously measured with ozone due to the wide spectral range covered by the DTGS detector from 700 to 11,000 cm^{-1}.

The absorption of carbon monoxide is too weak to justify a retrieval of a vertical profile. Instead, only the CO total column is determined using the spectral window from 2,134 to 2,174 cm^{-1} (Fig. 8). A single parameter, the scaling factor, is retrieved which scales the whole a priori profile for all altitudes. Since in this spectral range, radiance values are roughly twice higher than in the 10 μm window, a quality filter selects spectra only for signal-to-noise ratio larger than 50. The total uncertainty of CO total columns, including statistical, systematical and smoothing errors, is estimated to 4.5%.

4 Results

In this section, the performances of a mid-resolution ground-based instrument are demonstrated to retrieve separately stratospheric and tropospheric ozone and carbon monoxide total columns through 203 measurement days from 25 February

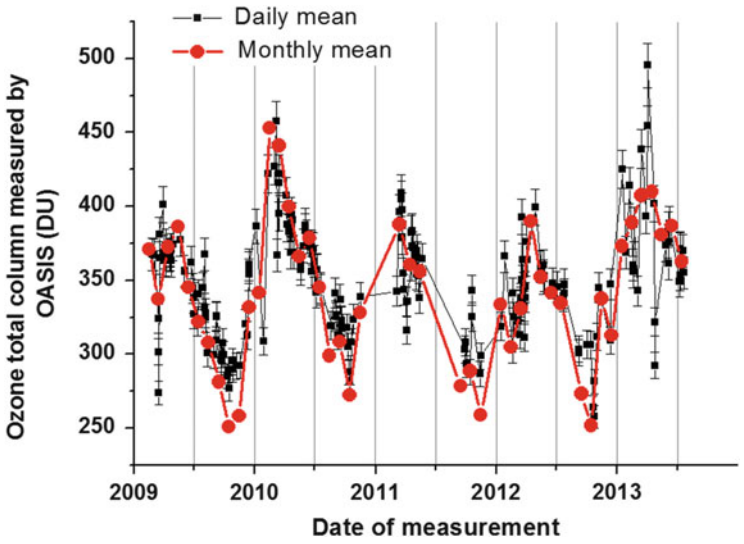

Fig. 9 Daily and monthly means (respectively in *solid square* and *solid circle symbols*) of ozone total columns from OASIS derived from 203 days measurements between 25 February 2009 and 19 July 2013. Error bars of 3% are added for daily means

2009 to 19 July 2013. For each trace species, seasonal variability at mid-latitude was derived. Also comparisons of data from different sources were performed using coincidence criteria based on space and time. More precisely all measurements were referred to a precise location around Creteil: satellite data were selected using a 2° latitude and 2° longitude belt, i.e. between 47.8° and 49.6° N and 1.6° and 3.4° E for GOME-2 and OMI, and between 47.7° and 49.7° N and 1.0° and 4.0° E for IASI for ozone comparisons, and between 47.5° and 49.5° N and 1.5° and 3.5° E for MOPITT for CO comparisons. For the temporal criterion, daily mean total and partial columns were derived from ground-based measurements. A significantly stricter temporal criterion of 1 h would be indeed insufficient for capturing small-scale ozone variations: ozone variability is rather fast and local in urban regions [21], but the number of coincidences with satellite data would decrease too much using this restrictive selection. For this reason, the above-mentioned criteria (spatial and temporal) are typically used for O_3 retrievals at the cost of increased scatter, in agreement with criteria found in the literature [22–25].

4.1 Ozone Total Columns

4.1.1 Seasonal Variability of OASIS Ozone Total Columns

Daily and monthly ozone total columns are given on Fig. 9 derived from the 203 days measurements between 25 February 2009 and 19 July 2013. Note that

the total uncertainty of ozone total columns derived from OASIS measurements, including statistical, systematical and smoothing errors, is estimated to 3%. The existence of a seasonal variability of the total column ozone content is shown with respective maximum values observed in February–March and minimum values observed in October due to the Brewer–Dobson circulation at mid-latitude. This ozone variability is well known [26] and defined as the stratospheric mean meridional circulation due to dynamics in stratosphere coupled with stratosphere–troposphere exchange. The results are also in very good agreement with the climatology from McPeters [17].

4.1.2 Comparison of OASIS Total Ozone Columns with IASI Products

IASI (Infrared Atmospheric Sounding Interferometer, Clerbaux et al. [27, 28]) is a nadir-viewing Fourier-transform spectrometer designed for operation on the meteorological MetOp satellites (ESA/EUMETSAT). The first instrument was launched in orbit aboard the satellite MetOp-A on 19 October 2006 and started operational measurements in June 2007. It measures the thermal infrared radiation emitted by the Earth's surface and the atmosphere. IASI is a Michelson-type Fourier-transform spectrometer, with a spectral resolution of 0.5 cm^{-1} after a Gaussian apodization. The MetOp-A satellite flies in a polar sun-synchronous orbit and covers each geographic region at least twice per day (at 09:30 and 21:30 LT – local time). At the nadir point, the size of one view is 50×50 km. It consists of four individual ground pixels with 12 km diameter each (at the nadir point). The ozone total columns derived from the OASIS instrument are compared with the data obtained from the IASI retrievals which are performed between 980 and 1,073 cm^{-1}, using a physical method regularization (analytical) algorithm [29]. Figure 10 shows the time series of O_3 total columns retrieved by IASI (solid circle symbols) and OASIS (solid square symbols).

Relative differences were calculated as follows:

$$\frac{(\text{X data} - \text{OASIS data})}{\text{OASIS data}} \times 100 \tag{4}$$

The mean relative difference (MRD), for the 173 coincidences, between ozone total columns derived from OASIS and IASI, is -5.9 (± 4.3)% showing a very good agreement between those two sets of data. The correlation coefficient for the regression plot of IASI columns against OASIS measurements (Fig. 11) is 0.92.

4.1.3 Comparison of OASIS Total Ozone Columns with OMI and GOME-2 Observations

In this section, comparisons are performed between OASIS measurements and two satellite observations both derived from the UV spectral region (OMI and

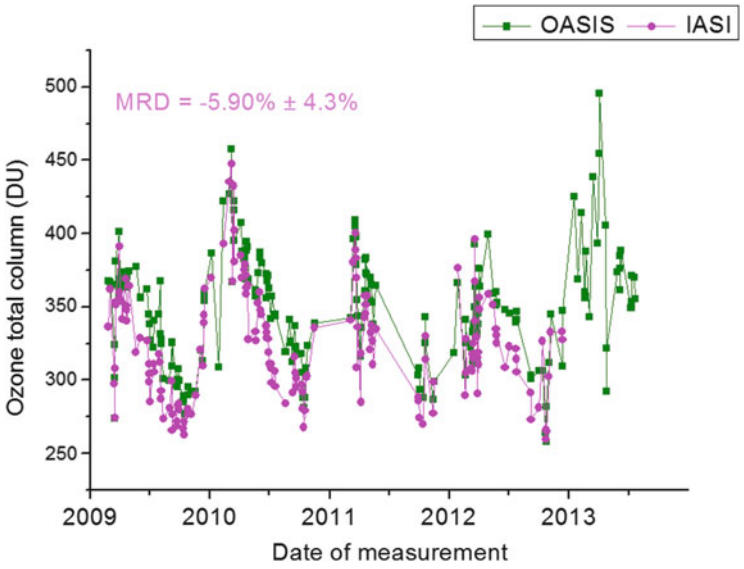

Fig. 10 Time series of O_3 total columns retrieved by IASI (*solid circle symbols*) and OASIS (*solid square symbols*) on 173 days from 25 February 2009 to 12 December 2012

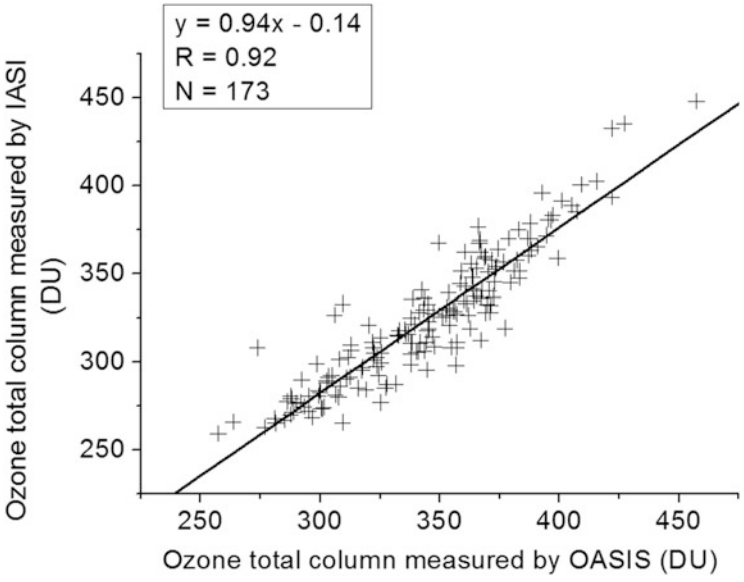

Fig. 11 O_3 total columns derived from IASI measurements as a function of OASIS data

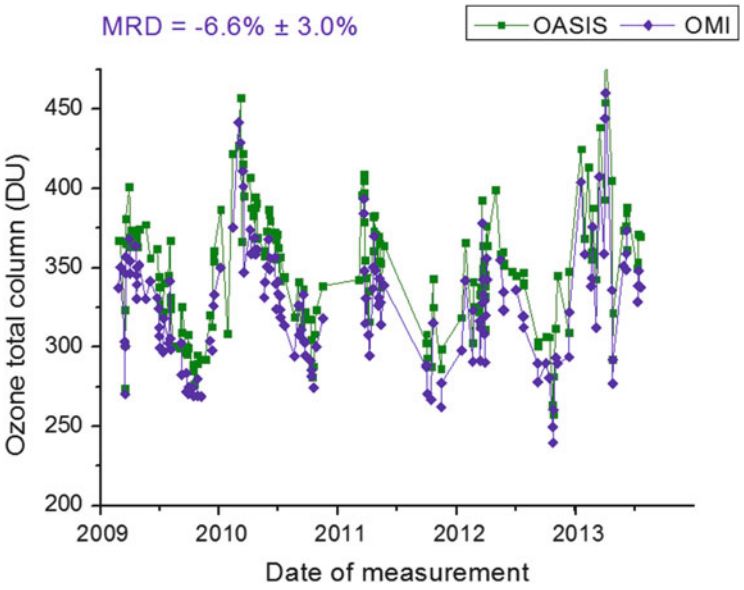

Fig. 12 Time series of O_3 total columns retrieved by OMI (*solid diamond symbols*) and OASIS (*solid square symbols*) on 162 days from 25 February 2009 to 19 July 2013

GOME-2). The Ozone Monitoring Instrument, OMI [30], is one of the four sensors aboard the EOS-Aura satellite (launched in July 2004). It is a nadir-viewing imaging spectrograph that measures the solar radiation backscattered by the Earth's atmosphere and surface between 290 and 340 nm with a spectral resolution of about 0.5 nm. O_3 total column data, measured from ground to approximately 80 km, are retrieved using both the TOMS (Total Ozone Mapping Spectrometer) technique (developed by NASA) [31] and a DOAS (Differential Optical Absorption Spectroscopy) technique developed at KNMI. The OMI O_3 products used in the present study are from the level 3 Aura/OMI data based on the level 2 OMDOA product that uses a DOAS multiwavelength algorithm [32]. The O_3 total column uncertainty from OMI is estimated to 3% [31]. Furthermore, recent validations of OMI O_3 products have been performed [17, 33–35]. In Figure 12, the mean relative difference (MRD), for 162 coincidences, between ozone total columns derived from OASIS (solid square symbols) and OMI (solid diamond symbols), is −6.6 (±3.0)% showing very good agreement between those two sets of data with correlation coefficient of 0.96 (Fig. 13).

The Global Ozone Monitoring Experiment-2 (GOME-2) aboard MetOp-A is a scanning spectrometer that captures light reflected from the Earth's surface and backscattered by aerosols and the atmosphere. The measured spectra are mainly used to derive ozone total columns and vertical profiles in the same UV region (290–340 nm) than OMI, as well as concentrations of nitrogen dioxide, bromine monoxide, water vapour, sulphur dioxide, and other trace gases and also cloud properties and aerosols. The O_3 columns used here are from the level 3 data of

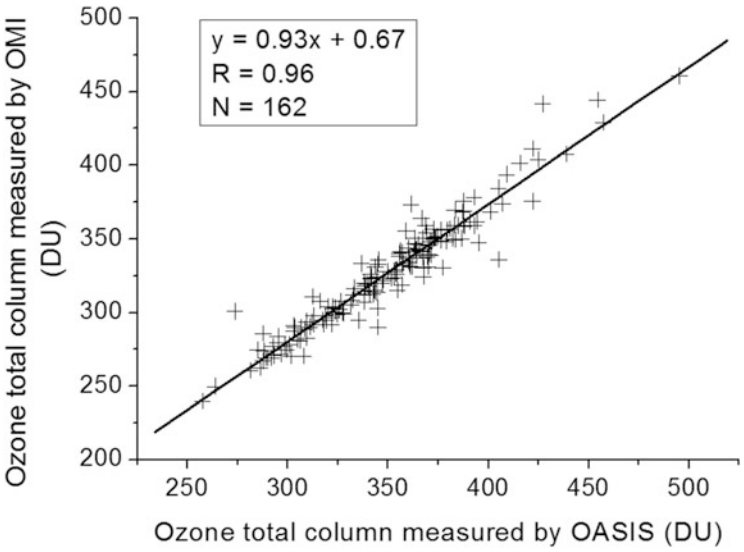

Fig. 13 O_3 total columns derived from OMI observations as a function of OASIS data

GOME-2, i.e. geophysical parameters that have been spatially and/or temporally resampled from level 2 data. The O_3 algorithm retrieval, GOME Data Processor (GPD), version 4.2 has been applied and is based on two methods: the DOAS (Differential Optical Absorption Spectroscopy) method [36] and the iterative AMF/VCD (Air-Mass Factor/Vertical Column Density) computation [37]. Total ozone columns derived from this algorithm have been validated using ground-based networks [38]. Error analysis indicates an accuracy and precision of O_3 total columns of 3.6–4.3% and 2.4–3.3%, respectively [39]. A very good agreement between ozone total columns derived from OASIS (solid square symbols) and GOME-2 (solid triangle symbols) (Fig. 14) was found with a mean relative difference (MRD), for 186 coincidences, of −7.3 (±3.0)% and correlation coefficient of 0.96 (Fig. 15).

The FTIR measures systematically higher O_3 total columns that the UV instruments (OMI and GOME-2), which may be due to inconsistencies in the spectroscopic parameters also observed in laboratory UV/IR intercomparison experiments [40–42]. But also when compared with IASI observations, OASIS measures higher ozone columns, however, with a lower MRD. One can then suspect that the OASIS O_3 total columns may be slightly high biased.

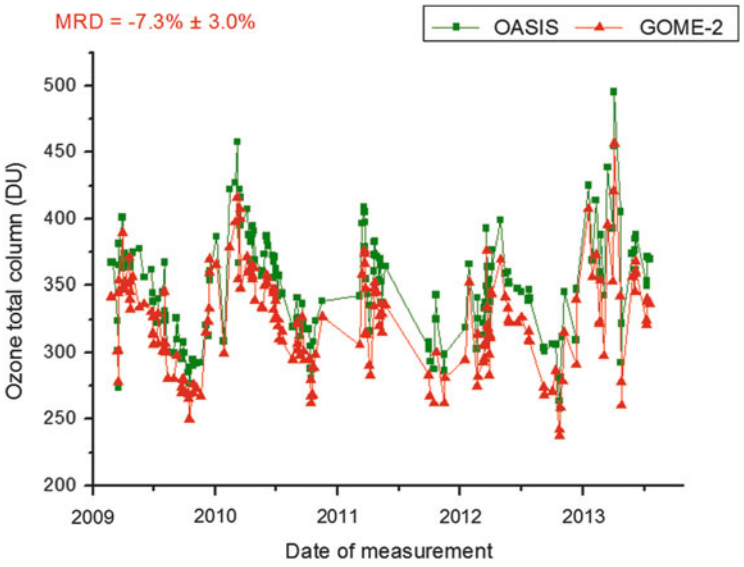

Fig. 14 Time series of O_3 total columns retrieved by GOME-2 (*solid triangle symbols*) and OASIS (*solid square symbols*) on 186 days from 25 February 2009 to 19 July 2013

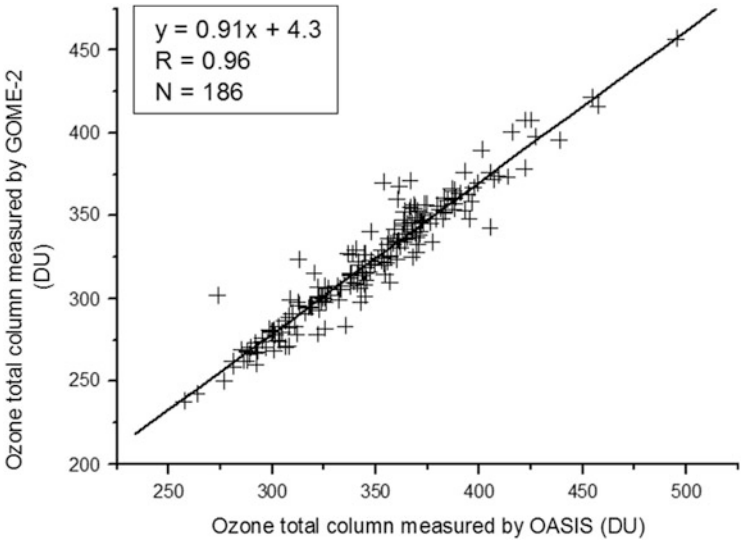

Fig. 15 O_3 total columns derived from GOME-2 observations as a function of OASIS data

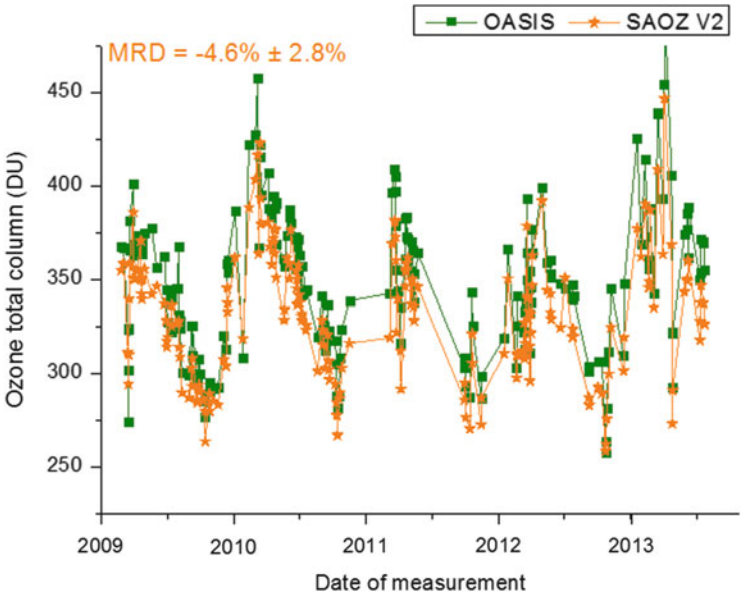

Fig. 16 Time series of O_3 total columns retrieved by SAOZ (*solid star symbols*) and OASIS (*solid square symbols*) on 177 days from 25 February 2009 to 22 July 2013

4.1.4 Comparison Between Two Ground-Based Measurements: OASIS and SAOZ

The SAOZ (Système d'Analyse par Observation Zénithale, Pommereau and Goutail [43]) instrument is part of the NDACC international network. It has been developed at Service d'Astronomie in the late 1980s following the discovery of the ozone hole in Antarctica. The SAOZ, which measures the absorption by the atmosphere of scattered sunlight at the zenith in the visible region (450–600 nm in the Chappuis band for ozone) at 1 nm resolution during twilight using the DOAS technique, allows the continuous monitoring of the daily integrated ozone columns. Data were collected from the SAOZ Paris instrument, located at the University of Pierre and Marie Curie in Paris (48.84° N, 2.35° E), using an improved retrieval, called SAOZ version V2 [44] as recommended by the NDACC. The total accuracy in ozone retrievals from SAOZ V2 is estimated to around 5.9%. The mean relative difference (MRD), for 177 coincidences, between ozone total columns derived from OASIS and SAOZ, is −4.6 (±2.8)% showing a very good agreement between those two sets of ground-based measurements (Fig. 16). The correlation coefficient for the regression plot of SAOZ columns against OASIS ones (Fig. 17) is 0.96.

In order to resume all these results concerning intercomparisons of ozone total columns, Table 1 collects the number of coincidences N, the correlation coefficients of the linear regression R, and the bias between measurements derived from the OASIS observatory and from satellite or local instruments. In addition to very good

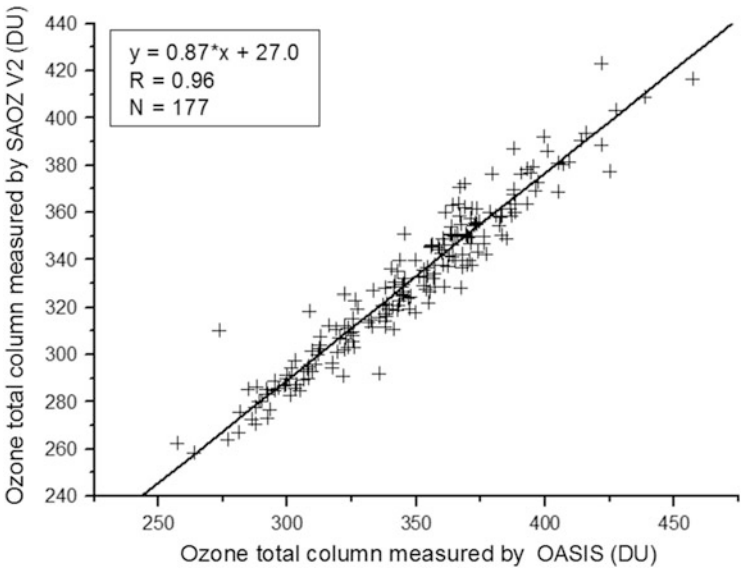

Fig. 17 O_3 total columns derived from SAOZ V2 measurements as a function of OASIS data

Table 1 Summary of the comparison between O_3 total columns derived from OASIS and from various satellites or local data. "*N*" is the number of daily averaged total ozone columns for the coincidences, "MRD" is the mean relative difference (in %) with the relative rms at 1σ, "*R*" is the correlation coefficient of the linear regression and the relative slope of the linear regression is given in the last line

	IASI	OMI	GOME-2	SAOZ
N	173	162	186	177
R	0.92	0.96	0.96	0.96
MRD in % (rms 1σ)	−5.9 (±4.3)	−6.6 (±3.0)	−7.3 (±3.0)	−4.6 (±2.8)
Slope	0.94	0.93	0.91	0.87

correlation coefficients between 0.92 and 0.96, these comparisons show the good quality of the OASIS measurements with mean relative difference always consistent with the data precision of all the independent data.

4.2 Tropospheric Ozone Columns

In Sect. 3.3.1, the performance for tropospheric ozone monitoring using the OASIS instrument was discussed. Indeed the DOF reaches 1.03 for the partial column integrated from ground to 8 km. In this paper, using 5 years of OASIS measurements, we are then capable of studying the seasonal variability of tropospheric ozone.

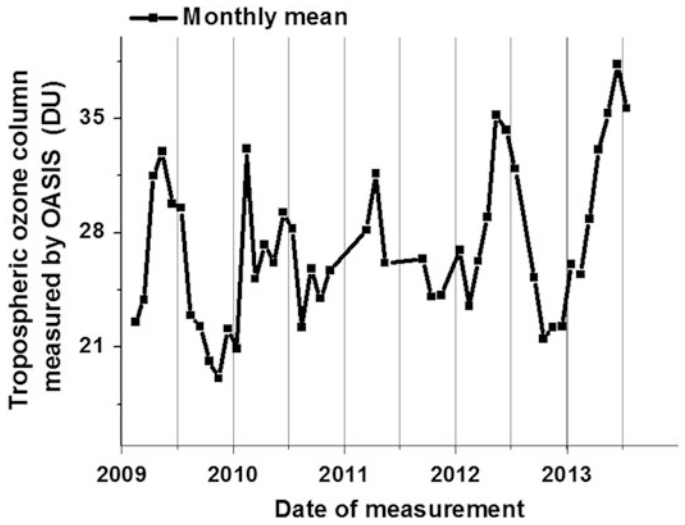

Fig. 18 Monthly means (*solid square symbols*) of the OASIS tropospheric ozone column (integrated from ground to 8 km) derived from 203 days between 25 February 2009 and 19 July 2013

4.2.1 Seasonal Variability of Tropospheric Ozone Columns

Figure 18 shows monthly means of tropospheric ozone measured by the OASIS instrument derived from 203 days between 25 February 2009 and 19 July 2013. In this figure, one can observe a seasonal cycle with a small summer maximum in May/June and a winter minimum in October/November. The summer maximum is well correlated to the maximum of photochemical production of ozone in the lower troposphere. Other part can come from vertical transport from stratosphere as highlighted by the OASIS averaging kernels showing that tropospheric ozone has a small stratospheric contribution. The OASIS variability is in very good agreement with recent results on climatology of pure tropospheric profiles and column contents of ozone and carbon monoxide using the MOZAIC (Measurements of OZone and water vapour by in-service AIrbus airCraft programme, Marenco et al. [45]) results in the mid-northern latitudes from 1994 to 2009 [46]. Indeed the monthly averaged pure tropospheric columns of ozone, based on the ascent and descent phase of MOZAIC flights, strictly from the surface to the altitude of the dynamical tropopause exhibit for Paris and Germany a summer maximum with 35.6 DU and a winter minimum with 24.3 DU.

4.2.2 Comparison of OASIS Tropospheric Ozone Columns with IASI Product

The capabilities of IASI to monitor total and tropospheric ozone have been demonstrated previously [9, 25, 29, 47]. Note that IASI has indeed a good sensitivity to lower atmospheric layers under conditions of higher surface temperatures and

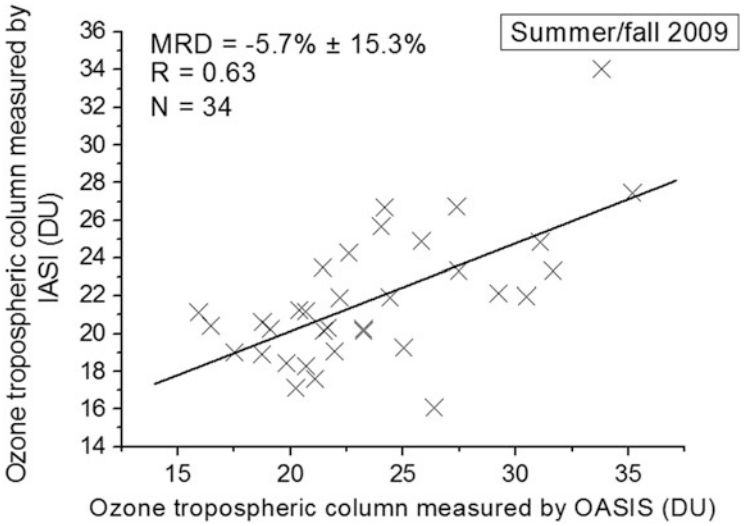

Fig. 19 Tropospheric ozone columns derived from IASI observations as a function of OASIS data for summer/fall 2009

larger thermal contrast conditions [29]. This is why the comparisons in this paper focus on measurements acquired during the summer/fall months in 2009 and 2010. Figures 19 and 20 show rather good correlations between the two sets of data with coefficient of 0.63 for 2009 and 2010 and with mean relative differences of −5.7 (±15.3)% in 2009 for 34 coincidences, and of 1.3 (±11.0)% in 2010 for 25 coincidences. Concerning the other years, results are not shown because comparisons with IASI are not statistically representative. It must be acknowledged that IASI and OASIS have different averaging kernels which reflect differing vertical sensitivities, due to different observation geometries, spectral scenes and analysis methods. OASIS retrievals are slightly more sensitive to tropospheric ozone compared to IASI given values of DOF in the troposphere (1.03 compared to 0.92).

4.2.3 Comparison of OASIS Tropospheric Ozone Columns with Surface Ozone Measurements from Airparif

In order to verify the quality of tropospheric ozone columns derived from OASIS, the OASIS time series are compared with surface ozone data delivered by the Airparif in situ network. Indeed, Fig. 6 shows that OASIS ozone retrievals are strongly sensitive to the variability of the lower atmospheric layers. The AirParif network was created in 1979 and approved by the Ministry of Environment to monitor air quality over Paris by analysing major pollutants (such as ozone, SO_2, CO, NO_x, particles, etc.) in various sites of Ile-de-France. Concerning the comparison with OASIS ozone data, the nearest station in Champigny-sur-Marne, 10 km

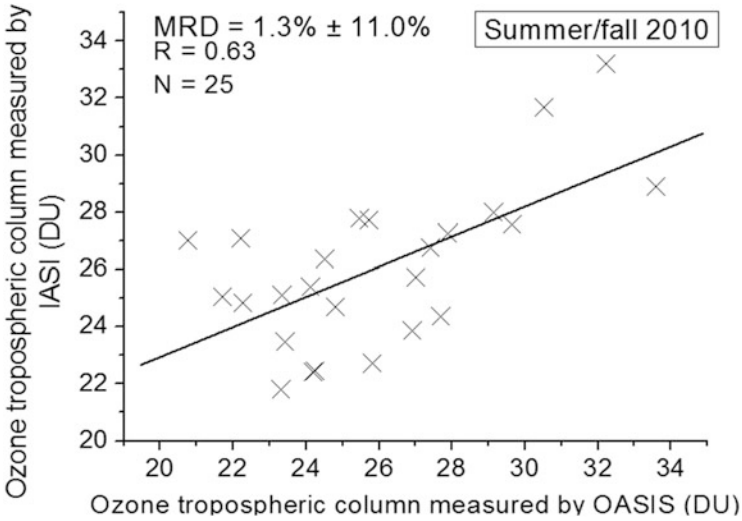

Fig. 20 Tropospheric ozone columns derived from IASI observations as a function of OASIS data for summer/fall 2010

away from the OASIS observatory was selected among the 24 stations monitoring ozone. Time series of daily tropospheric ozone columns derived from OASIS (solid square symbols) and in situ measurements of O_3 provided by Airparif (solid star symbols) for the 198 coincidence days (25 February 2009 to 22 July 2013) are given in Fig. 21.

Although measurements from both sites are not quantitatively comparable, the correlation coefficient calculated for the regression plot of Airparif surface ozone in μg m^{-3} against OASIS measurements in DU is 0.68 (Fig. 22). This result confirms that a large part of the tropospheric ozone columns derived from OASIS is dominated by photochemical production in the lower troposphere. In addition, twelve sharp maxima are observed by OASIS and Airparif showing that OASIS is also able to monitor high-pollution episodes (arrows, Fig. 21).

Future work plans to compare tropospheric ozone measured by OASIS every 10 min to the tropospheric chemistry–transport model CHIMERE [48] to study diurnal variability. Indeed ground-based FTIR measurements made by OASIS are a cost-effective approach for pollutant diurnal variations monitoring compared to satellite observations with their low time dependence, low vertical resolution, cloud screening, etc.

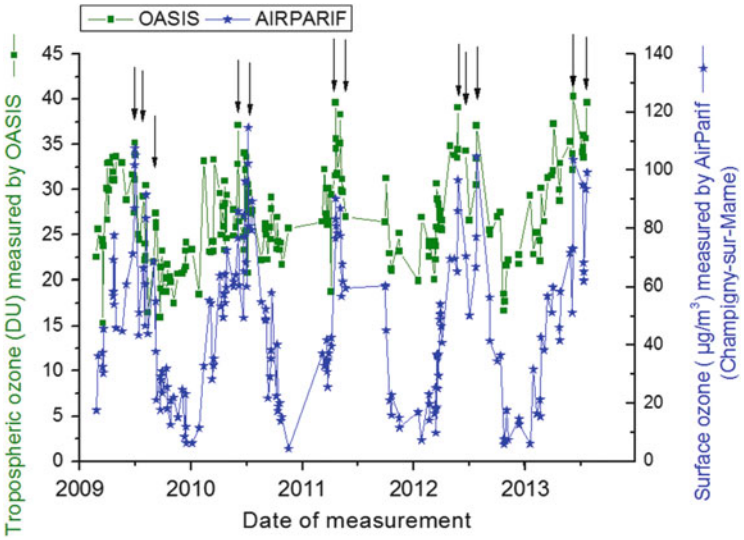

Fig. 21 Time series of tropospheric ozone from OASIS (*solid square symbols*) and ozone surface concentrations from in situ measurements of the Airparif network (*solid star symbols*) on 198 days from 25 February 2009 to 22 July 2013. The Aiparif station location is Champigny-sur-Marne (10 km away from OASIS observatory). *Arrows* represent high pollution episodes measured by OASIS and also observed by Airparif

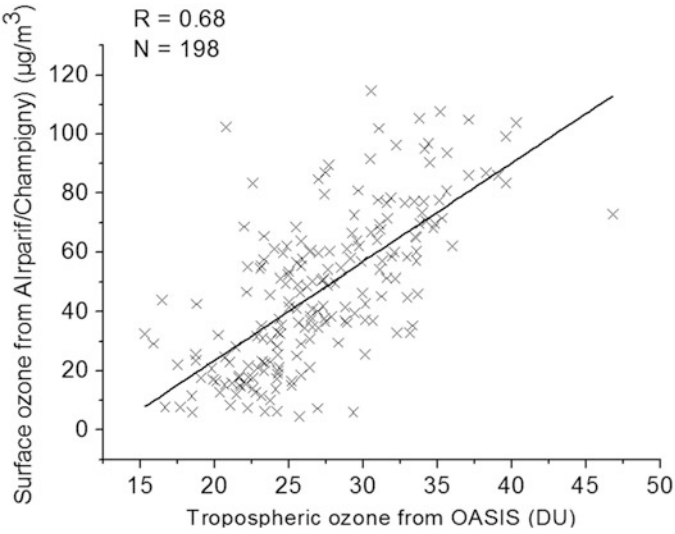

Fig. 22 Surface ozone (µg/m^3) derived from Airparif station as a function of OASIS tropospheric ozone column (DU)

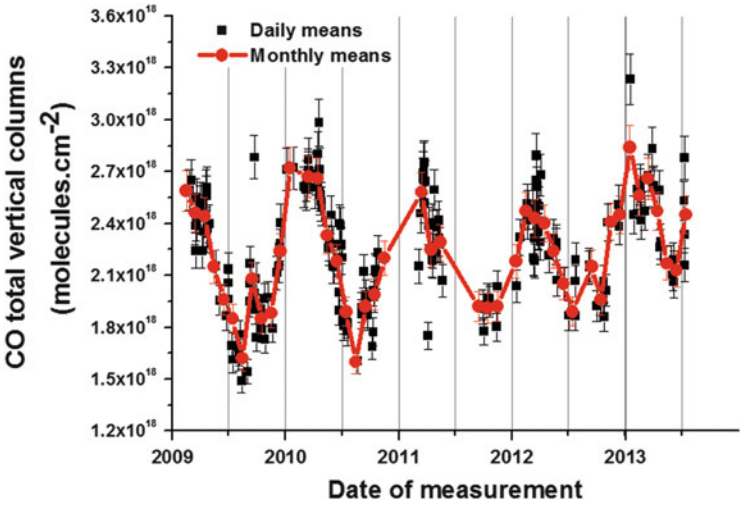

Fig. 23 Daily and monthly means (respectively in *solid square* and *solid circle symbols*) of CO total columns from OASIS derived from 202 days between 25 February 2009 and 12 July 2013. Error bars of 4.5% are added for daily means

4.3 CO Total Columns

In addition to ozone, carbon monoxide (CO) was also retrieved from OASIS measurements. As already mentioned in Sect. 3.3.2, only carbon monoxide total columns were measured by retrieving a scaling factor to scale the whole a priori profile for all altitudes.

4.3.1 Seasonal Variability of CO Total Columns

Figure 23 shows daily and monthly means of CO total columns measured by the OASIS instrument derived from 202 days measurements between 25 February 2009 and 12 July 2013. In this figure, one can observe a seasonal cycle with a winter maximum in February/March and a summer minimum in August/September. This variability and the sharp depletion in May/June also observed by Zbinden et al. [46] for European pure tropospheric CO cycles are evidence of powerful OH cleansing efficiency regulated by NOx [49]. The very good agreement between OASIS and the Zbinden CO climatology is also seen for the quantitative results with a $1.9–2.7 \times 10^{18}$ mol cm^{-2} cycle. This result confirms for the first time the good quality of CO total columns measured by the OASIS medium-resolution instrument.

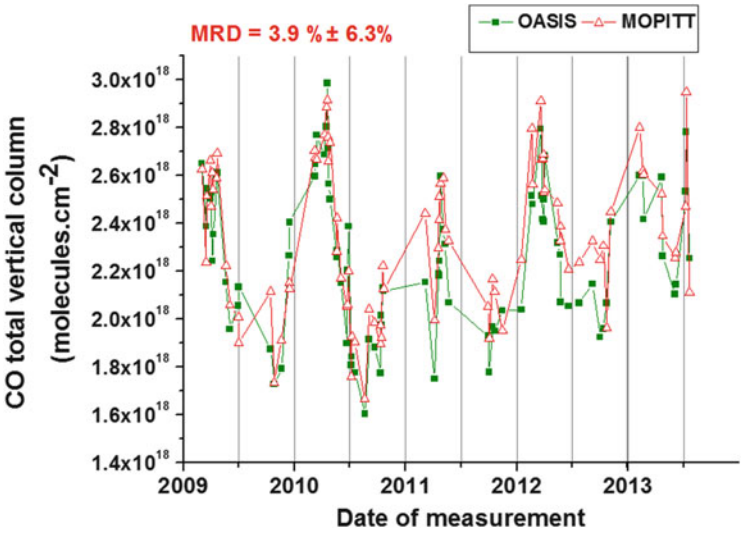

Fig. 24 Time series of CO total columns retrieved by MOPITT (*empty triangle symbols*) and OASIS (*solid square symbols*) on 87 days from 03 March 2009 to 22 July 2013

4.3.2 Comparison of OASIS CO Total Columns with MOPITT Observations

MOPITT (Measurements of Pollution in the Troposphere) is an instrument flying on the NASA's Earth Observing System Terra spacecraft, measuring tropospheric carbon monoxide (CO) on the global scale since 2000. MOPITT measurements enable scientists to analyse the distribution, transport, sources and sinks of CO. MOPITT is a nadir-sounding instrument with a 22 km nadir resolution, 3 km vertical resolution and 640 km swath width which measures upwelling infrared radiation at 4.7 μm and 2.2–2.4 μm. It uses correlation spectroscopy to derive total columns and profiles of carbon monoxide in the lower atmosphere. For the comparison with OASIS, MOPITT data are derived from the inversion code version 3 which has not been yet validated but compared to the Jungfraujoch (Switzerland) station data of the NDACC: error on MOPITT CO total column has been evaluated to about 7.9% [50].

Figure 24 shows time series of daily CO total ozone columns derived from OASIS (solid square symbols) and MOPITT observations (empty triangle symbols) for the 87 coincidence days (03 March 2009 to 22 July 2013). The mean relative difference (MRD), for these 87 coincidences is 3.9 (±6.3)% showing a very good agreement between the two sets of measurements. The correlation coefficient for the regression plot of MOPITT columns against OASIS measurements is 0.90 (Fig. 25).

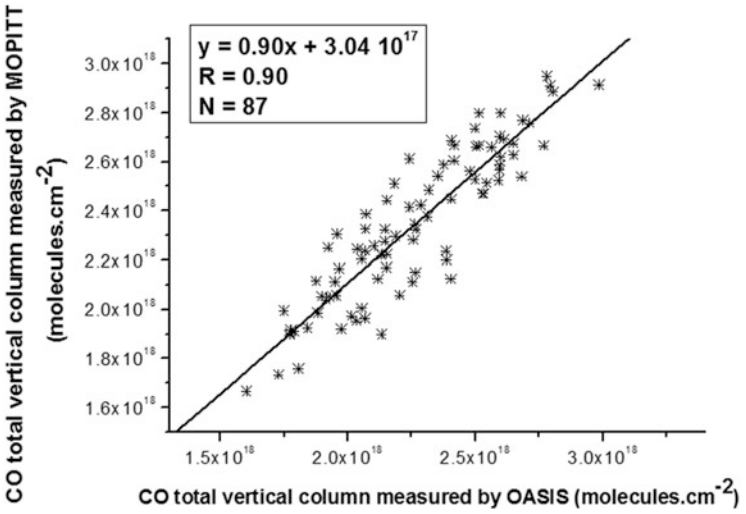

Fig. 25 CO total columns derived from MOPITT observations as a function of OASIS data

5 Conclusions

In this chapter, a new ground-based medium spectral resolution Fourier-transform spectrometer (OASIS) installed in an urban region was presented showing its capabilities of retrieving atmospheric trace gases (particularly ozone and carbon monoxide). A detailed description of the OASIS observatory and its different subsystems has been given. Total columns of ozone and carbon monoxide and also tropospheric ozone columns have been derived from about 200 days of clear-sky OASIS measurements from February 2009 to July 2013 using the PROFFIT retrieval code adapted to the medium spectral resolution of the instrument.

First, ozone total columns over OASIS were compared to satellite and ground-based measurements showing the good quality of the OASIS measurements with mean relative difference always consistent with the data precision and very good correlation coefficients (between 0.92 and 0.96). Furthermore, the performance of OASIS for tropospheric ozone monitoring is demonstrated showing that the retrieved tropospheric amounts (integrated from the ground to 8 km) have a small stratospheric contribution through vertical transport, and vice versa. This latter result is confirmed by the observed seasonal cycle of OASIS tropospheric ozone with a small summer maximum in May/June and a winter minimum in October/November, very well correlated to recent results on climatology of tropospheric ozone profiles using MOZAIC [46]. Moreover, when comparing the OASIS tropospheric ozone with in situ surface data of the Airparif network, a good correlation coefficient of 0.68 indicates that a large part of the tropospheric ozone columns derived from OASIS is dominated by photochemical production in the lower troposphere.

Finally, in addition to ozone, carbon monoxide (CO) total columns were also retrieved from OASIS measurements. The very good agreement between OASIS measurements and a reference CO climatology [46] in the mid-northern latitudes was shown.

Future work has already begun to analyse the diurnal variations of tropospheric ozone and CO and to perform comparisons with atmospheric chemistry–transport models. Also, using the large spectral domain (700–11,000 cm^{-1}) recorded by the OASIS spectrometer, tests will be performed to assess the capability of OASIS to monitor also greenhouse gases such as CH_4 and CO_2. In this case, we will use the wide spectral coverage of the OASIS instrument to record the 1.27 μm O_2 band which is necessary to get accurate results (see TCCON (Total Carbon Column Observing Network) [51]. Finally, given the moderate costs and the compactness of a system such as OASIS, deployment of analogous systems nearby large megacities might be envisaged in support of satellite and air quality studies in many regions of the world.

Acknowledgements The authors wish to thank F. Goutail for SAOZV2 data, AirParif for in situ data, the NASA Goddard Space Flight Center for providing the temperature and pressure profiles of the National Centers for Environmental Prediction (NCEP). The ETHER French atmospheric database (http://ether.ipsl.jussieu.fr) is acknowledged for providing the IASI data. We are also grateful to the European Centre for Medium-Range Weather Forecasts (ECMWF), the Global Monitoring for Environment and Security (GMES) and the Monitoring of the Atmospheric Composition and Climate (MACC) project for supplying data. Acknowledgements are addressed to the University of Paris-Est Créteil for their technical support during all phases of the OASIS observatory installation.

References

1. Brasseur GP, Solomon S (2005) Aeronomy of the middle atmosphere. Springer, Dordrecht
2. Finlayson-Pitts BJ, Pitts JN (1999) Chemistry of the upper and lower atmosphere: theory, experiments, and applications. Academic, San Diego
3. West JJ, Szopa S, Hauglustaine DA (2007) Human mortality effects of future concentrations of tropospheric ozone. C R Geosci 339:775–783
4. Felzer BS, Cronin T, Reilly JM et al (2007) Impacts of ozone on trees and drops. C R Geosci 339:784–798
5. de Forster PM, Shine KP (1997) Radiative forcing and temperature trends from stratospheric ozone changes. J Geophys Res 102:10841–10855
6. Aghedo AM, Bowman KW, Worden HM et al (2011) The vertical distribution of ozone instantaneous radiative forcing from satellite and chemistry climate models. J Geophys Res. doi:10.1029/2010JD014243
7. Riese M, Ploeger F, Rap A et al (2012) Impact of uncertainties in atmospheric mixing on simulated UTLS composition and related radiative effects. J Geophys Res. doi:10.1029/2012JD017751
8. Seinfeld JH, Pandis SN (2006) Atmospheric chemistry and physics: from air pollution to climate change, 2nd edn. Wiley, New York

9. Viatte C, Gaubert B, Eremenko M et al (2011) Tropospheric and total ozone columns over Paris (France) measured using medium-resolution ground-based solar-absorption Fourier-transform infrared spectroscopy. Atmos Measure Tech 4:2323–2331
10. Hase F (2012) Improved instrumental line shape monitoring for the ground-based, high-resolution FTIR spectrometers of the network for the detection of atmospheric composition change. Atmos Measure Tech 5:603–610
11. Hase F, Blumenstock T, Paton-Walsh C (1999) Analysis of the instrumental line shape of high-resolution fourier transform IR spectrometers with gas cell measurements and new retrieval software. Appl Optics 38:3417–3422
12. Hase F, Hannigan JW, Coffey MT et al (2004) Intercomparison of retrieval codes used for the analysis of high-resolution, ground-based FTIR measurements. J Quant Spectrosc Rad Trans 87:25–52
13. Flaud JM, Orphal J (2011) Spectroscopy of the earth's atmosphere. In: Quack M (ed) Handbook of high-resolution spectroscopy. Wiley, London, p 1971
14. Rothman LS, Jacquemart D, Barbe A et al (2005) The HITRAN 2004 molecular spectroscopic database. J Quant Spectrosc Rad Trans 96:139–204
15. Rodgers CD (2000) Inverse methods for atmospheric sounding: theory and practice. World Sci, Hackensack, NJ
16. Tikhonov AN (1963) Solution of incorrectly formulated problems and the regularization method. Soviet Math Dokl 4:1035–1038 English translation of. Dokl Akad Nauk SSSR 151:501–504
17. McPeters RD, Kroon M, Labow G et al (2008) Validation of the aura ozone monitoring instrument total column ozone product. J Geophys Res. doi:10.1029/2007JD008802
18. Remedios JJ, Leigh RJ, Waterfall AM et al (2007) MIPAS reference atmospheres and comparisons to V4.61/V4.62 MIPAS level 2 geophysical data sets. Atmos Chem Phys Discuss 7:9973–10017
19. Schneider M, Hase F, Blumenstock T et al (2008) Quality assessment of O_3 profiles measured by a state-of-the-art ground-based FTIR observing system. Atmos Chem Phys 8:5579–5588
20. Vigouroux C, De Mazière M, Demoulin P et al (2008) Evaluation of tropospheric and stratospheric ozone trends over Western Europe from ground-based FTIR network observations. Atmos Chem Phys 8:6865–6886
21. Antón M, López M, Serrano A et al (2010) Diurnal variability of total ozone column over Madrid (Spain). Atmos Environ 44:2793–2798
22. Cortesi U, Lambert JC, De Clercq C et al (2007) Geophysical validation of MIPAS-ENVISAT ozone data. Atmos Chem Phys 7:1–61
23. Dupuy E, Walker KA, Kar J et al (2009) Validation of ozone measurements from the atmospheric chemistry experiment (ACE). Atmos Chem Phys 9:287–343
24. Nassar R, Logan JA, Worden HM et al (2008) Validation of tropospheric emission spectrometer (TES) nadir ozone profiles using ozone sonde measurements. J Geophys Res. doi:10.1029/2007JD008819
25. Keim C, Eremenko M, Orphal J et al (2009) Tropospheric ozone from IASI: comparison of different inversion algorithms and validation with ozone sondes in the northern middle latitudes. Atmos Chem Phys 9:11441–11479
26. Dobson GMB, Harrison DN, Lawrence J (1929) Measurements of the amount of ozone in the earth's atmosphere and it's relation to other geophysical conditions. Part III Proc R Soc Lond A122:456–486
27. Clerbaux C, Hadji-Lazaro J, Turquety S et al (2007) The IASI/MetOp mission: first observations and highlights of its potential contribution to GMES. Space Res Today (COSPAR Inf Bul) 168:19–24
28. Clerbaux C, Boynard A, Clarisse L et al (2009) Monitoring of atmospheric composition using the thermal infrared IASI/MetOp sounder. Atmos Chem Phys 9:6041–6054

29. Eremenko M, Dufour G, Foret G et al (2008) Tropospheric ozone distributions over Europe during the heat wave in July 2007 observed from infrared nadir spectra recorded by IASI. Geophys Res Lett. doi:10.1029/2008GL034803
30. Levelt PF (2002) OMI algorithm theoretical basis document, vol. I, OMI instrument, Level0–1b processor, calibration and operations. http://eospso.gsfc.nasa.gov/eoshomepage/forscientists/atbd/docs/OMI/ATBD-OMI-01.pdf. Accessed 11 Mar 2011
31. Bhartia PK, Wellemeyer CW (2002) OMI TOMS-V8 total O_3 algorithm, algorithm theoretical baseline document: OMI ozone products, vol. II, ATBD-OMI-02, version 2.0. http://eospso.gsfc.nasa.gov/eoshomepage/forscientists/atbd/docs/OMI/ATBD-OMI-02.pdf. Accessed 11 Mar 2011
32. Veefkind JP, de Haan JF, Brinksma EJ et al (2006) Total ozone from the ozone monitoring instrument (OMI) using the DOAS technique. IEEE T Geosci Remote 44:1239–1244
33. Balis D, Kroon M, Koukouli ME et al (2007) Validation of ozone monitoring instrument total ozone column measurements using brewer and Dobson spectrophotometer ground-based observations. J Geophys Res. doi:10.1029/2007JD008796
34. Liu X, Bhartia PK, Chance K et al (2010) Validation of ozone monitoring instrument (OMI) ozone profiles and stratospheric ozone columns with microwave limb sounder (MLS) measurements. Atmos Chem Phys 10:2539–2549
35. Kroon M, Petropavlovskikh I, Shetter R et al (2008) OMI total ozone column validation with Aura-AVE CAFS observations. J Geophys Res. doi:10.1029/2007JD008795
36. Platt U (1994) Differential optical absorption spectroscopy (DOAS) in: air monitoring by spectroscopic techniques. Wiley, New York, p 8427
37. Van Roozendael M, Loyola D, Spurr RJD et al (2006) Reprocessing the 10-year GOME/ERS-2 total ozone record for trend analysis: the new GOME data processor version 4.0, algorithm description. J Geophys Res. doi:10.1029/2005JD006375
38. Balis D, Lambert JC, Van Roozendael M et al (2007) Ten years of GOME/ERS2 total ozone data the new GOME data processor (GDP) version 4.2: ground-based validation and comparisons with TOMS V7/V8. J Geophys Res. doi:10.1029/2005JD006376
39. Van Roozendael M, Lambert JC, Spurr RJD et al (2004) GOME direct fitting (GODFIT) GDOAS delta validation report. ERS Exploitation AO/1-4235/02/I-LG, Oberpfaffenhofen, Germany
40. Viatte C, Schneider M, Redondas A et al (2011) Comparison of ground-based FTIR and Brewer O_3 total column with data from two different IASI algorithms and from OMI and GOME-2 satellite instruments. Atmos Measure Tech 4:535–546
41. Gratien A, Picquet-Varrault B, Orphal J (2010) New laboratory intercomparison of the ozone absorption coefficients in the mid-infrared (10 μm) and ultraviolet (300–350 nm) spectral regions. J Phys Chem A 14:10045–10048
42. Picquet-Varrault B, Orphal J, Doussin JF et al (2005) Laboratory intercomparison of the ozone absorption coefficients in the mid-infrared (10 μm) and ultraviolet (300–350 nm) spectral regions. J Phys Chem A 109:1008–1014
43. Pommereau JP, Goutail F (1988) O_3 and NO_2 ground-based measurements by visible spectrometry during arctic winter and spring 1988. Geophys Res Lett 15:891–894
44. Hendrick F, Pommereau JP, Goutail F et al (2011) NDACC/SAOZ UV-visible total ozone measurements: improved retrieval and comparison with correlative ground-based and satellite observations. Atmos Chem Phys 11:5975–5995
45. Marenco A, Thouret V, Nédélec P et al (1988) Measurement of ozone and water vapor by Airbus in-service aircraft: the MOZAIC airborne program, an overview. J Geophys Res 103:631–642
46. Zbinden RM, Thouret V, Ricaud P et al (2013) Climatology of pure tropospheric profiles and column contents of ozone and carbon monoxide using MOZAIC in the mid-northern latitudes (24° N to 50° N) from 1994 to 2009. Atmos Chem Phys Discuss 13:14695–14747

47. Dufour G, Eremenko M, Orphal J et al (2010) IASI observations of seasonal and day-to-day variations of tropospheric ozone over three highly populated areas of China: Beijing, Shanghai, and Hong Kong. Atmos Chem Phys 10:3787–3801
48. Schmidt H, Derognat C, Vautard R et al (2001) A comparison of simulated and observed ozone mixing ratios for the summer of 1998 in western Europe. Atmos Environ 35:6277–6297
49. Lamsal LN, Martin RV, Padmanabhan A et al (2011) Application of satellite observations for timely updates to global anthropogenic NOx emission inventories. Geophys Res Lett. doi:10.1029/2010GL046476
50. Barret B, De Mazière M, Mahieu E (2003) Ground-based FTIR measurements of CO from the Jungfraujoch: characterisation and comparison with in situ surface and MOPITT data. Atmos Chem Phys 3:2217–2223
51. Wunch D, Toon GC, Blavier JFL et al (2011) The total carbon column observing network. Phil Trans Roy Soc A 369:2087–2112

Daytime Atmospheric Chemistry of C_4–C_7 Saturated and Unsaturated Carbonyl Compounds

Elena Jiménez and Ian Barnes

Abstract This chapter aims to review the daytime atmospheric chemistry of some carbonyl compounds, crucial intermediates in the autocatalytic production of the main atmospheric oxidant, the hydroxyl radical (OH•). Carbonyl compounds are very important trace gases for the physico-chemistry of the troposphere mainly because they are directly emitted into the atmosphere or formed in situ in the photooxidation of almost all organic compounds. Particularly aldehydes (RCHO, R=alkyl chain) and ketones (RC(O)R′) are important key species in many atmospheric processes, because they undergo a wide variety of reactions, both chemical and photolytic. This chapter presents a synthesis of the studies on the chemistry of C_4–C_7 saturated and unsaturated aldehydes and ketones in the troposphere. A comprehensive revision of the gas-phase rate coefficients for the reactions of these carbonyls with the major diurnal oxidants, photolysis frequencies and chemical mechanisms is also presented. The impact of these species on urban air pollution is also discussed. These kinetic and photochemical data can be included in the chemical modules of atmospheric models which are used by policymakers in formulating and deciding strategies for the improvement of air quality.

E. Jiménez (✉)
Departamento de Química Física, Facultad de Ciencias y Tecnologías Químicas, Universidad de Castilla-La Mancha, Avda. Camilo José Cela s/n, 13071 Ciudad Real, Spain

Instituto de Investigación en Combustión y Contaminación Atmosférica (ICCA), Universidad de Castilla-La Mancha, Camino de Moledores s/n, 13071 Ciudad Real, Spain
e-mail: Elena.Jimenez@uclm.es

I. Barnes
Bergische Universität Wuppertal, Fachbereich C – Physikalische Chemie, Gauss Strasse 20., 42119 Wuppertal, Germany
e-mail: barnes@uni-wuppertal.de

E. Jiménez et al. (eds.), *Environment, Energy and Climate Change I: Environmental Chemistry of Pollutants and Wastes*, Hdb Env Chem (2015) 32: 53–104,
DOI 10.1007/698_2014_286,
Published online: 16 October 2014

Keywords Aldehydes, Atmospheric degradation, Ketones, Kinetics, Photochemistry

Contents

Abbreviations

CL	Chemiluminescence
DF	Discharge flow tube
FID	Flame ionisation detection
FP	Flash photolysis
FT	Flow tube
FTIR	Fourier transform infrared
GC	Gas chromatography
LIF	Laser-induced fluorescence
MCM	Master chemical mechanism
MIR	Maximum incremental reactivity
MS	Mass spectrometry
n.m.	Not measured
OVOC	Oxygenated volatile organic compound
PAN	Peroxyacetyl nitrate
PANs	Peroxyacyl nitrates
PLP	Pulsed laser photolysis
POCP	Photochemical ozone creation potential
ppmv	Parts per million based on volume
RF	Resonance fluorescence
ROG	Reactive organic gas
RR	Relative rate
SAR	Structure activity relationship
SOA	Secondary organic aerosol
UV	Ultraviolet
VOC	Volatile organic compound

1 Introduction

The atmosphere is a chemically complex and dynamic system. The knowledge of the composition and chemistry of the atmosphere is of great importance for several reasons, but primarily because of the interactions between the atmosphere and oceans, land and living organisms. The composition of the atmosphere is not only highly influenced by human activity but also by natural events, such as volcano eruptions, biogenic emissions, etc.

A key process proceeding in the atmosphere is the oxidation of a wide variety of relatively reduced chemical compounds produced largely by the biosphere. Over the last decades, the growth in the knowledge of atmospheric chemical processes (formation and depletion of trace gases) has been considerably extensive [1–5]. Especially, the reactions initiated by the major diurnal atmospheric oxidants – ozone (O_3), hydroxyl radicals (OH•) and chlorine atoms (Cl•) in marine environments – are important in determining the oxidising capacity of the troposphere, which is essentially the global burden of these oxidants. Without this efficient cleansing process, the levels of many emitted gases could become so high that they would radically change the chemical nature of our atmosphere and biosphere and, through the greenhouse effect, our climate.

Gas-phase processes initiated by OH chemistry that affect the oxidising capacity of the atmosphere have been widely studied since the 1970s when the importance of OH• was discovered. More recently, especial attention has been drawn to halogen chemistry in the marine and polar troposphere, where these reactive compounds provide a small but significant additional pathway for oxidation besides OH•. These oxidation processes also dominate in the chemistry of air pollution, where the occurrence of harmful levels of O_3 and acidic aerosols depends on the relative and absolute levels of urban emissions of NO, CO, hydrocarbons and SO_2. Atmospheric oxidation of trace gases initiated by O_3 is quite important for unsaturated compounds, competing in many cases with oxidation by OH• and Cl•. For carbonyl compounds, photochemical processes are also important in the troposphere. Wavelengths shorter than 290 nm are absorbed mainly by stratospheric O_3; therefore, the solar radiation available for driving these photochemical processes in the troposphere is at wavelengths $\lambda > 290$ nm, i.e. the so-called actinic radiation.

Carbonyl compounds are ubiquitous gaseous chemical constituents in the atmosphere and belong to the group of compounds classified as oxygenated volatile organic compounds (OVOCs) and, in environmental chemistry, are frequently referred to simply as oxygenates. In the atmosphere, they are produced by photochemical oxidation of hydrocarbons, emitted from a variety of biogenic and anthropogenic sources. In addition, some carbonyl compounds are also emitted directly from different sources. Keisselmeier and Staudt [6] have compiled the natural sources of atmospherically relevant biogenic carbonyls (such as formaldehyde, acetaldehyde, propanal, acetone, butanal, *i*-butanal, butenal, *i*-butenal, butanone, crotonaldehyde, 2-pentanone, 2-methyl-2-pentenal, hexanal, *trans*-2-hexenal, *cis*-3-hexenal and methyl vinyl ketone, among others) and their atmospheric

concentrations measured outside vegetated urban areas. König et al. [7] have measured the emission rate of a series of aldehydes (such as propanal, butanal, hexanal, *trans*-2-hexenal, heptanal, octanal and nonanal) and ketones (such as butanone, 2-pentanone, 3-pentanone and 6-methyl-5-hepten-2-one) from grassland typical for natural deciduous and agricultural vegetation in Austria. For example, in a remote inland area in Japan, some semi-volatile aldehydes (such as hexanal, heptanal, octanal, nonanal, decanal and undecanal) are ubiquitous [8]. In urban areas, motor vehicle exhaust is an important source of aldehydes in air both through direct emission of aldehydes and through the emission of hydrocarbons, which in turn are converted to carbonyls through photochemical oxidation reactions (e.g. see [9, 10]).

With the exception of acetone, it is not generally recognised how important atmospheric carbonyls are in the lower stratosphere and upper troposphere. Carbonyl compounds play a central role close to the tropopause, and this is directly relevant to issues such as the assessment of the impact of air traffic and ozone depletion [11].

In the literature, to the best of our knowledge, there are two publications which review the gas-phase atmospheric chemistry of OVOCs [12, 13]. Mellouki et al. [12] have presented a concise, but incomplete, compilation on the kinetics and mechanisms for the reactions of many different oxygenates with the main atmospheric oxidants. In the more recent and extensive review by Calvert et al. [13], apart from discussions on the chemistry, recommendations are given for the room temperature rate coefficients of a great number of oxygenates, including carbonyls, with the main atmospheric oxidants. When possible, Arrhenius expressions describing the temperature dependence of the rate coefficients (k_{Ox}) for the reviewed reactions are also recommended by Calvert et al. [13]:

$$k_{Ox} = A\exp(-E_a/RT), \tag{1}$$

where A is the pre-exponential factor, and E_a is the activation energy of the process (usually expressed as $B = E_a/R$). Since new kinetic and mechanistic data on carbonyls have been published, a more complete and updated review is needed. Inclusion of a review of the kinetics and mechanisms of the reactions of ground state oxygen atoms, $O(^3P)$, and nitrate radicals, $NO_3\bullet$, with the aldehydes and ketones reviewed here is beyond the scope of the present chapter.

A comprehensive review on the gas-phase photochemistry of simple aldehydes and ketones has been made by Lee and Lewis [14], and the review of Calvert et al. [13] contains a revision of the photochemistry of some saturated and unsaturated carbonyls. Lee and Lewis [14] reviewed the photochemistry of the following C_4–C_6 carbonyls: *trans*-2-butenal (*trans*-crotonaldehyde), 3-methylpentanal, *n*-hexanal, 5-hexenal, 2-pentanone and biacetyl ($CH_3C(O)C(O)CH_3$), among others. In the review of Calvert et al. [13], apart from discussions on the photochemistry of some C_1–C_3 carbonyls, an exhaustive compilation of the UV absorption cross sections, photodecomposition quantum yields and photolysis frequencies of C_4 carbonyls (butanal, 2-methylpropanal, *trans*-2-butenal and butanone), C_5 carbonyls

(*n*-pentanal and 3-methylbutanal), C_6 carbonyls (*n*-hexanal, *trans*-2-hexenal, 3-pentanone and 2-hexanone) and C_7 carbonyls (*n*-heptanal and 2-methyl-3-hexanone) is given.

The aim of this chapter is to update previous reviews by compiling all the current kinetic data for the diurnal oxidation of some C_4–C_7 saturated and unsaturated carbonyls initiated by photochemically mediated reactions with O_3, OH• and Cl• and direct photolysis by sunlight. Chemical names, empirical formulae and structures of the C_4–C_7 aldehydes and ketones reviewed are shown in Tables 1 and 2, respectively.

2 Daytime Photooxidation of C_4–C_7 Aldehydes

The diurnal photooxidation of a series of C_4–C_7 saturated and unsaturated aldehydes (listed in Table 1) is reviewed in this section.

2.1 Gas-Phase Reaction with Tropospheric Oxidants

2.1.1 Reactions with Ozone (O_3)

Studies on the gas-phase reactivity of ozone with aldehydes are presently limited to reactions with unsaturated aldehydes of less than six carbon atoms. As can be seen in Table 3, the rate coefficients k_{O_3} are on the order of 10^{-18} cm^3 molecule^{-1} s^{-1} at room temperature and atmospheric pressure [15–19]. Measuring rate coefficients of around 10^{-18} cm^3 molecule^{-1} s^{-1} is experimentally challenging, and in many cases only upper limits of k_{O_3} have been reported. Consequently, k_{O_3} for the saturated aldehydes, i.e. from *n*-butanal to *n*-heptanal, have not been measured, since the reactivity of ozone toward these aldehydes is expected to be even lower than that toward unsaturated aldehydes where the reactions proceed by an addition mechanism.

2.1.2 Reactions Initiated by OH•

The kinetics of saturated and unsaturated aldehydes toward OH• has been widely investigated under different experimental conditions: (a) at atmospheric T and p conditions in *smog* chambers employing relative kinetic methods and (b) as a function of temperature (243–374 K) and pressure (23–760 Torr) using absolute methods [20–35]. Table 4 summarises all available k_{OH} at 298 K and their temperature dependencies. For linear saturated aldehydes from (*n*-butanal to *n*-heptanal), the reported k_{OH}(298 K) are, in general, around (2–3) $\times$ 10^{-11} cm^3 molecule^{-1} s^{-1}. The observed slight positive effect of the hydrocarbon chain length on the OH

Table 1 Name, chemical formula and structure of the reviewed aldehydes

	Name	Formula	Structure
C_4	*n*-Butanal	$CH_3(CH_2)_2CHO$	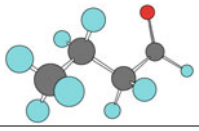
	Trans-2-butenal (crotonaldehyde)	$CH_3CH{=}CHCHO$	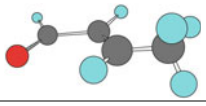
C_5	*n*-Pentanal	$CH_3(CH_2)_3CHO$	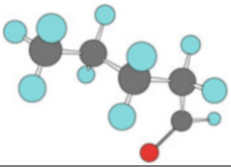
	3-Methylbutanal (*i*-pentanal)	$(CH_3)_2CH_2CHCHO$	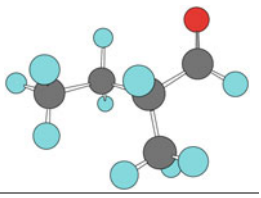
	Trans-2-pentenal	$CH_3CH_2CH{=}CHCHO$	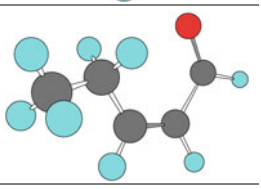
	3-Methyl-2-butenal	$(CH_3)_2C{=}CHCHO$	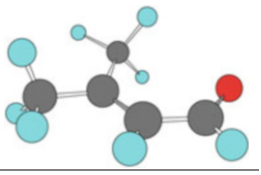
	Trans-2-methyl-2-butenal	$CH_3CH{=}C(CH_3)CHO$	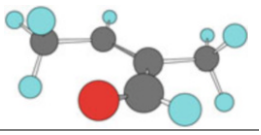

(continued)

Table 1 (continued)

	Name	Formula	Structure
C_6	*n*-Hexanal	$CH_3(CH_2)_4CHO$	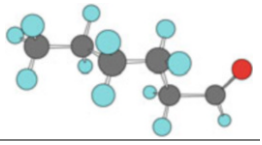
	Trans-2-hexenal	$CH_3(CH_2)_2CH{=}CHCHO$	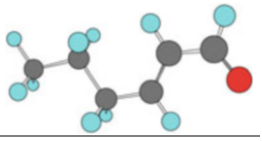
C_7	*n*-Heptanal	$CH_3(CH_2)_5CHO$	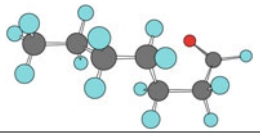
	Trans-2-heptenal	$CH_3(CH_2)_3CH{=}CHCHO$	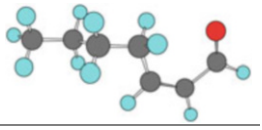

reactivity is indicative of not only H-abstraction at the aldehyde H (which dominates) but also from the alkyl chain. For unsaturated aldehydes, it is difficult to see a definite trend since the k_{OH}(298 K) values are too scattered (ranging from 3 to 5×10^{-11} cm^3 molecule^{-1} s^{-1}). The discrepancies in k_{OH} (298 K) are larger for the unsaturated compounds than for their saturated homologues. It is observed that k_{OH} (298 K) for unsaturated aldehydes slightly increase with respect to that of the corresponding saturated aldehyde. Within the uncertainty limits, no pressure dependence of k_{OH} (298 K) is observed.

It should be noted that the kinetics of the OH• + 3-methylbutanal reaction was reviewed by Calvert et al. [13] only at room temperature. Unfortunately, the *T*-dependence expression for k_{OH} reported by Jiménez et al. [30] in 2009 was omitted in that review. Even though, the recommended value by Calvert et al. [13] for the rate coefficient for the OH• + *trans*-2-butenal reaction at room temperature is correct, we would like to point out that k_{OH} (298 K) reported by Albaladejo et al. [20] was discarded in the Calvert et al. review for "being significantly lower" than the recommended average value of 3.6×10^{-12} cm^3 molecule^{-1} s^{-1}. However, as can be seen in Table 4, the reported k_{OH} (298 K), $(3.51 \pm 0.71) \times 10^{-12}$ cm^3 molecule^{-1} s^{-1}, by Albaladejo et al. [20] is in excellent agreement with the recommended value.

Regarding the branched unsaturated aldehydes, the relatively determined k_{OH} for 3-methyl-2-butenal determined at 740 Torr by Tuazon et al. [33] is 30 % higher than that reported by Jiménez et al. [30] at lower pressures (see Table 4). By comparison with the reviewed linear unsaturated aldehydes, no pressure

Table 2 Name, chemical formula and structure of the reviewed ketones

	Name	Formula	Chemical Structure
C_4	Butanone	$CH_3C(O)CH_2CH_3$	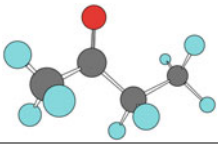
	3-Buten-2-one (methyl vinyl ketone)	$CH_3C(O)CH{=}CH_2$	
C_5	2-Pentanone	$CH_3C(O)(CH_2)_2CH_3$	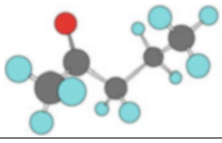
	3-Pentanone	$CH_3CH_2C(O)CH_2CH_3$	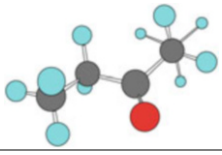
	3-Penten-2-one	$CH_3C(O)CH{=}CHCH_3$	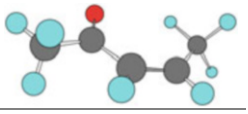
	4-Penten-3-one	$CH_3CH_2C(O)CH{=}CH_2$	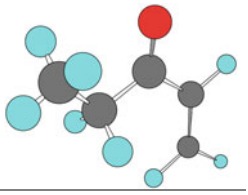
	2,4-Pentanedione (acetylacetone)	$CH_3C(O)CH_2C(O)CH_3$	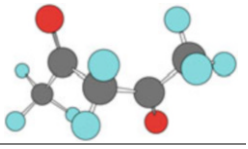
	Enol form of 2,4-pentanedione	$CH_3C(OH){=}CHC(O)CH_3$	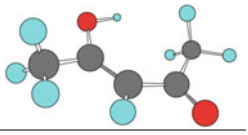
	3-Penten-2-one	$CH_3C(O)CH{=}CHCH_3$	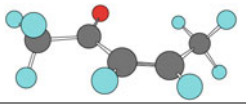

(continued)

Table 2 (continued)

	Name	Formula	Chemical Structure
C_6	2-Hexanone	$CH_3C(O)(CH_2)_3CH_3$	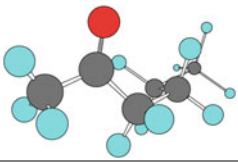
	3-Hexanone	$CH_3CH_2C(O)$ $CH_2CH_2CH_3$	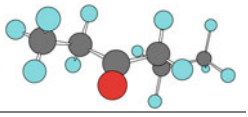
	4-Hexen-3-one	$CH_3CH_2C(O)$ $CH{=}CHCH_3$	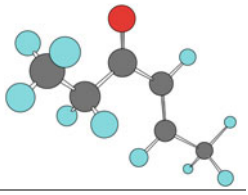
	5-Hexen-2-one	$CH_3C(O)$ $(CH_2)_2CH{=}CH_2$	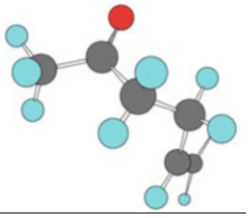
	3-Methyl-2,4-pentanedione	$CH_3C(O)CH(CH_3)C(O)$ CH_3	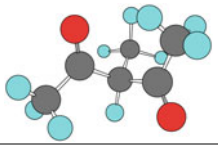
	Enol form of 3-methyl-2,4-pentanedione	$CH_3C(OH){=}C(CH_3)C$ $(O)CH_3$	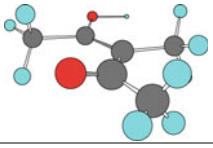
C_7	2-Heptanone	$CH_3C(O)(CH_2)_3CH_3$	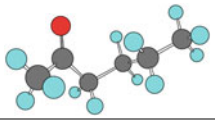

dependence of k_{OH} is expected for this reaction. Additional kinetic data are needed to corroborate the expected pressure independency of k_{OH} for 3-methyl-2-butenal. For *trans*-2-methyl-2-butenal, the only available k_{OH} rate coefficient and its temperature dependence is that reported by Jiménez et al. [30].

The T-dependence of k_{OH} for all these reactions is well described by an Arrhenius expression, and both A and B factors are listed in Table 4. In all cases, the

Table 3 Summary of the reported rate coefficients for the reactions of the reviewed C_4–C_7 aldehydes with O_3 at room temperature (298 ± 2 K) and pressure (740–760 Torr). All k_{O_3} were determined using relative methods

	Name	k_{O_3} (298 K) (10^{-18} cm^3 molecule^{-1} s^{-1})	References
C_4	*n*-Butanal	n.m.	
	Trans-2-butenal (crotonaldehyde)	1.39	Calvert et al. [13]
		1.58 ± 0.23	Sato et al. [15]
		1.74 ± 0.20	Grosjean and Grosjean [16]
		0.90 ± 0.18	Atkinson et al. [17]
C_5	*n*-Pentanal	n.m.	
	3-Methylbutanal (*i*-pentanal)	n.m.	
	Trans-2-pentenal	1.59 ± 0.22	Sato et al. [15]
	3-Methyl-2-butenal	1.82 ± 0.26	Sato et al. [15]
	Trans-2-methyl-2-butenal	5.34 ± 0.73	Sato et al. [15]
C_6	*n*-Hexanal	n.m	
	Trans-2-hexenal	1.28 ± 0.28	Grosjean et al. [18]
		2.1 ± 1.0	Atkinson et al. [19]
C_7	*n*-Heptanal	n.m.	
	Trans-2-heptenal	n.m.	

exponential factors B, and therefore the activation energies, are low and negative (B values range from −306 K to −666 K, i.e. E_a ranges from 2.5 to 5.5 kJ/mol). The negative dependence of k_{OH} with temperature is usually interpreted as a result of the formation of a hydrogen-bonded complex preceding the H-abstraction from the aldehydic C–H bond [36]. The energy of the bond is sufficiently weak that hydrogen atom abstraction from the C–H bonds of the alkyl chain is of minor importance.

2.1.3 Reactions with Cl•

Chlorine atoms are of particular interest because they are around 10^2–10^3 times more reactive than OH• and, therefore, even at low concentrations, have the ability to enhance hydrocarbon oxidation in the atmosphere of marine environments. Due to the recent recognition of the importance of Cl chemistry, the kinetic database for Cl reactions has been progressively extended in the last decades. In Table 5, the rate coefficients for all available reactions of Cl•, k_{Cl}, with C_4–C_7 saturated and unsaturated aldehydes are listed [29, 37–42]. Thévenet et al. [29] were the first to investigate the reaction of Cl atoms with *n*-pentanal at 298 K and atmospheric pressure. No kinetic data are available for *i*-pentanal, 3-methyl-2-butenal and *trans*-2-methyl-2-butenal. The majority of k_{Cl} determinations have been reported for room temperature and 760 Torr. The values of k_{Cl}(298 K) range from approximately 1 to 3 × 10^{-10} cm^3 molecule^{-1} s^{-1}, one order of magnitude higher than the

Table 4 Summary of the reported rate coefficients for the reactions of the reviewed C_4–C_7 aldehydes with OH radicals as a function of temperature and pressure

	Name	p (Torr)	T-range (K)	k_{OH} (298 K) $\times 10^{11}$ (cm^3 molecule^{-1} s^{-1})	$A \times 10^{12}$ (cm^3 molecule^{-1} s^{-1})	B (K)	Technique	References
C_4	*n*-Butanal			2.37	6.2	−411	Recommendation	Calvert et al. [13]
		100–400	298	2.88 ± 0.26			PLP–LIF	Albaladejo et al. [20]
		760	298 ± 2	2.38 ± 0.15			RR–FTIR	D'Anna et al. [21]
		740	296 ± 2	2.47 ± 0.15			RR–GC	Pagagni et al. [22]
		100	258–422	2.06 ± 0.30	5.7 ± 0.3	−411 ± 164	FP–RF	Semmes et al. [23]
		300	298	2.52 ± 0.32			RR–GC	Audley et al. [24]
		760	298 ± 4	2.6 ± 0.4			RR–GC	Kerr and Sheppard [25]
	Trans-2-butenal (crotonaldehyde)			3.6	6	−533	Recommendation	Calvert et al. [13]
		20–300	243–372	3.35 ± 0.3	5.77 ± 1.14	−533 ± 58	PLP–LIF	Magneron et al. [26]
		100–400	298	3.51 ± 0.71			PLP–LIF	Albaladejo et al. [20]
		765	298	4.0 ± 0.3			RR–FTIR	Ullerstam et al. [27]
		735	298	3.5 ± 0.4			RR–GC	Atkinson et al. [28]
		760	298 ± 4	3.3 ± 0.6			RR–GC	Kerr and Sheppard [25]

(continued)

Table 4 (continued)

	Name	p (Torr)	T-range (K)	k_{OH} (298 K) $\times 10^{11}$ (cm^3 molecule^{-1} s^{-1})	$A \times 10^{12}$ (cm^3 molecule^{-1} s^{-1})	B (K)	Technique	References
C_5	*n*-Pentanal			2.66	8.6	−336	Recommendation	Calvert et al. [13]
		100–400	298	2.48 ± 0.24			PLP–LIF	Albaladejo et al.[20]
		760	298 ± 2	2.61 ± 0.14			RR–FTIR	D'Anna et al. [21]
		740	296 ± 2	2.99 ± 0.19			RR–GC	Pagagni et al. [22]
		32–417	243–372	2.8 ± 0.2	9.9 ± 1.9	−306 ± 56	PLP–LIF	Thévenet et al. [29]
		100	253–410	2.69 ± 0.39	6.3 ± 0.2	−451 ± 108	FP–RF	Semmes et al. [23]
		300	298	1.38 ± 0.17			RR–GC	Audley et al. [24]
		760	298 ± 4	2.6 ± 0.4			RR–GC	Kerr and Sheppard [25]
	3-Methylbutanal (*i*-pentanal)	49.5–100	263–353	2.97 ± 0.19	5.8 ± 1.7	−499 ± 94	PLP–LIF	Jiménez et al. [30]
				2.59			Recommendation	Calvert et al. [13]
		760	298 ± 2	2.79 ± 0.07			RR–FTIR	D'Anna et al. [21]
		740	300 ± 5	4.0 ± 0.7			RR–FTIR	Glasius et al. [31]
		100	298	2.58 ± 0.40			FP–RF	Semmes et al. [23]
		300	298	1.84 ± 0.20			RR–GC	Audley et al. [24]

		760	298 ± 4	2.7 ± 0.1			RR–GC	Kerr and Sheppard [25]
	Trans-2-pentenal			4.4	7.9	−510	Recommendation	Calvert et al. [13]
		23–150	244–374	4.3 ± 0.6	7.9 ± 1.2	−510 ± 20	PLP–LIF	Davis et al. [32]
		100–400	298	2.35 ± 0.32			PLP–LIF	Albaladejo et al. [20]
	3-Methyl-2-butenal	46.2–72.0	263–353	4.77 ± 0.53	6.9 ± 0.9	−526 ± 42	PLP–LIF	Jiménez et al. [30]
		740	298	6.21 ± 0.65			RR–FTIR	Tuazon et al. [33]
	Trans-2-methyl-2-butenal	50.6–73	263–353	4.08 ± 0.31	5.6 ± 1.2	−666 ± 54	PLP–LIF	Jiménez et al. [30]
C_6	*n*-Hexanal			2.83	4.3	−565	Recommendation	Calvert et al. [13]
		50	263–353	2.78 ± 0.50	4.2 ± 0.8	−565 ± 65	PLP–LIF	Jiménez et al. [34]
		100–400	298	2.60 ± 0.21			PLP–LIF	Albaladejo et al. [20]
		760	298 ± 2	2.86 ± 0.13			RR–FTIR	D'Anna et al. [21]
		740	296 ± 2	3.17 ± 0.15			RR–GC	Pagagni et al. [22]
	Trans-2-hexenal			4.3	7.5	−520	Recommendation	Calvert et al. [13]
		760	298 ± 2	3.93 ± 0.21			RR–GC	Gao et al. [35]
		23–150	244–374	4.4 ± 0.5	7.5 ± 1.1	−520	PLP–LIF	Davis et al. [32]

(continued)

Table 4 (continued)

	Name	p (Torr)	T-range (K)	k_{OH} (298 K) $\times 10^{11}$ (cm^3 molecule^{-1} s^{-1})	$A \times 10^{12}$ (cm^3 molecule^{-1} s^{-1})	B (K)	Technique	References
		50	263–353	4.68 ± 0.50	9.8 ± 2.4	-455 ± 80	PLP–LIF	Jiménez et al. [34]
		100–400	298	2.95 ± 0.45			PLP–LIF	Albaladejo et al. [20]
C_7	*n*-Heptanal	100–400	298	2.96 ± 0.23			PLP–LIF	Albaladejo et al. [20]
	Trans-2-heptenal			4.4	9.7	−450	Recommendation	Calvert et al. [13]
		23–150	244–374	4.4 ± 0.7	9.7 ± 1.5	−450	PLP–LIF	Davis et al. [32]
		100–400	298	2.45 ± 0.30			PLP–LIF	Albaladejo et al. [20]

Table 5 Summary of the reported rate coefficients for the reactions of the reviewed C_4–C_7 aldehydes with Cl atoms as a function of temperature and pressure

	Name	p (Torr)	T-range (K)	$k_{Cl}(298\ K) \times 10^{10}$ (cm^3 $molecule^{-1}$ s^{-1})	$A \times 10^{11}$ (cm^3 $molecule^{-1}$ s^{-1})	B (K)	Technique	References
C_4	*n*-Butanal	25–800	365–380	1.66	3.8	−446	Recommendation	Calvert et al. [13]
		800 ± 3	298 ± 2	1.63 ± 0.59			RR–FTIR	Singh et al. [37]
		760	298 ± 2	2.04 ± 0.36			RR–GC–MS	Wu and Mu [38]
		25–200	265–380	1.38 ± 0.18	3.09 ± 0.40	−446 ± 77	PLP–RF	Cuevas et al. [39]
		765	297 ± 2	1.5 ± 0.3			RR–FTIR	Ullerstam et al. [27]
	Trans-2-butenal (crotonaldehyde)	760	298	2.65			Recommendation	Calvert et al. [13]
		760	298	3.2 ± 0.9			RR–FTIR	Wang et al. [40]
		760	298	2.2 ± 0.4			RR–FTIR	Ullerstam et al. [27]
C_5	*n*-Pentanal	8–950	265–380	2.4	4.3	−450	Recommendation	Calvert et al. [13]
		800 ± 3	298 ± 2	2.37 ± 0.82			RR–FTIR	Singh et al. [37]
		8	295 ± 2	2.31 ± 0.35			PLP–LIF	Iwasaki et al. [41]
		800–950	295 ± 2	2.24 ± 0.20			PLP–LIF	Iwasaki et al. [41]
		20–200	265–380	1.89 ± 0.24	4.17 ± 0.54	−450 ± 80	PLP–RF	Cuevas et al. [39]
		760	298	2.56 ± 0.27			RR–GC	Rodríguez et al. [42]

(continued)

Table 5 (continued)

	Name	p (Torr)	T-range (K)	$k_{Cl}(298\ K) \times 10^{10}$ (cm^3 $molecule^{-1}$ s^{-1})	$A \times 10^{11}$ (cm^3 $molecule^{-1}$ s^{-1})	B (K)	Technique	References
		760	298 ± 3	2.6 ± 0.3			RR–GC–FID	Thévenet et al. [29]
	3-Methylbutanal (*i*-pentanal)			n.m.				
	Trans-2-pentenal	760	298	1.31 ± 0.19			RR–GC	Rodríguez et al. [42]
	3-Methyl-2-butenal			n.m.				
	Trans-2-methyl-2-butenal			n.m.				
C_6	*n*-Hexanal	20–760	265–380	2.79	8.6	−349	Recommendation	Calvert et al. [13]
		20–200	265–380	2.55 ± 0.21	7.91 ± 0.66	−349 ± 51	PLP–RF	Cuevas et al. [39]
		760	298	2.88 ± 0.37			RR–GC	Rodríguez et al. [42]
	Trans-2-hexenal	760	298	1.92 ± 0.22			RR–GC	Rodríguez et al. [42]
C_7	*n*-Heptanal	20–760	265–380	3.0	11	−306	Recommendation	Calvert et al. [13]
		20–200	265–380	2.96 ± 0.56	10.6 ± 2.0	−306 ± 115	PLP–RF	Cuevas et al. [39]
		760	298	3.00 ± 0.34			RR–GC	Rodríguez et al. [42]
	Trans-2-heptenal	760	298	2.40 ± 0.29			RR–GC	Rodríguez et al. [42]

corresponding OH reactions. The only temperature dependence study of k_{Cl} for linear saturated aldehydes is that of Cuevas et al. [39] which was performed between 20 and 200 Torr of He using the PLP–RF method. The reported activation energies were negative with B values ranging from −306 to −450 K which is of the same order of magnitude observed for the corresponding OH reactions. The temperature dependence of k_{Cl} for linear unsaturated aldehydes and branched saturated aldehydes remains to be investigated.

2.2 General Reaction Mechanisms and Gaseous Oxidation Products

The atmospheric reactivity and mechanisms of saturated and unsaturated aldehydes is slightly different because of differences in their structure. The reactivity of these compounds arises largely through two features of their structures: the polarity of the carbonyl group, the acidity of any α hydrogens that are present and the presence of the *C*–*C* double bond.

2.2.1 Saturated Aldehydes

To our knowledge, no experimental gas-phase studies have been performed to elucidate a reaction mechanism for the reaction of ozone with saturated aldehydes. In any case, the importance of the atmospheric reactions of saturated hydrocarbons with O_3 is negligible since the reaction rates are several orders of magnitude slower than the corresponding reactions with OH• and Cl• [12, 13, 43].

Calvert et al. [13] have discussed quite extensively the H-atom abstraction reaction mechanism (reaction 2) for the OH•- and Cl•-initiated oxidation of the saturated aldehydes reviewed in this chapter and also the atmospheric fate of the resulting products. In general, for saturated aldehydes, H-atom abstraction by OH• or Cl• occurs mainly from the –CHO group, forming acyl radicals (RCO•s) and water or HCl, respectively, as a coproduct [44, 45]:

$$\mathrm{OH}\bullet\,(\mathrm{Cl}\bullet) + \mathrm{RCHO} \rightarrow \mathrm{RCO}\bullet + \mathrm{H_2O(HCl)}. \tag{2}$$

The yield of acyl radicals from the OH and Cl reactions depends on the aldehyde. In a clean atmosphere, i.e. at low-NO_x levels, RCO• reacts with oxygen to form $RC(O)O_2$•:

$$\mathrm{RCO}\bullet + \mathrm{O_2} + \mathrm{M} \rightarrow \mathrm{RC(O)O_2}\bullet + \mathrm{M}, \tag{3a}$$

$$\rightarrow\ \mathrm{OH}\bullet + \mathrm{Products}. \tag{3b}$$

Groß et al. [46] have recently quantified the OH• formation (channel 3b) in the reaction of the most studied acyl radical, acetyl radical (CH_3CO•), with O_2 as a function of total pressure. From this and previous studies, it is known that the yield of OH• in channel 3b decreases with increasing pressure. Therefore, channel 3a for CH_3CO• is the predominant at one atmospheric pressure. In the atmosphere RC(O)O_2• reacts with HO_2• to produce OH• (4a, main reaction pathway) and organic acids (4c):

$$\mathrm{RC(O)O_2\bullet + HO_2 \rightarrow\ RC(O)O\bullet + OH\bullet + O_2}, \quad (4a)$$

$$\rightarrow\ \mathrm{RC(O)O_2H + O_2}, \quad (4b)$$

$$\rightarrow \mathrm{RC(O)OH + O_3}. \quad (4c)$$

Reaction 4a is a radical-propagating reaction, which helps sustain atmospheric oxidation capacity [47]. At room temperature, Groß et al. [47] determined that the branching ratio for channel 4a for R=CH_3 was 61% and 16% for channel 4c.

In a polluted atmosphere, i.e. at high-NO_x levels, the reaction of RC(O)O_2• with NO_2 produces peroxyacyl nitrates (PANs, RC(O)OONO_2) [44, 45]:

$$\mathrm{RC(O)O_2\bullet + NO_2 + M \rightarrow RC(O)OONO_2 + M}. \quad (5)$$

As a consequence, atmospheric degradation of saturated aldehydes contributes to the formation of harmful PANs in polluted environments.

2.2.2 Unsaturated Aldehydes

Mechanistic studies on the reactions of O_3 with unsaturated aldehydes are very limited; only investigations on the reaction mechanisms for the reaction of O_3 with crotonaldehyde and *trans*-2-hexenal have been reported in the literature [16–18]. These reactions proceed almost exclusively via addition to the double bond. In general, when one of the substituents of the double bond is an oxygen-containing substituent (X=–CHO for aldehydes and −C(O)R for ketones), the global reaction can be represented by [16]

$$\mathrm{O_3 + R_1R_2C = CR_3X} \rightarrow \alpha(\mathrm{R_1COR_2 + R_3XCOO}) + (1-\alpha)(\mathrm{R_3COX + R_1R_2COO.}) \quad (6)$$

Products of reaction (6) are the primary carbonyls R_1COR_2 and R_3COX and carbonyl oxide biradicals (R_1R_2COO and R_3XCOO). The further reactions of R_1R_2COO and R_3XCOO also lead to the formation of carbonyls [12, 16, 18]. For example, Grosjean et al. [18] reported the yields of carbonyl formation from the O_3 reaction with *trans*-2-hexenal to be (0.53 ± 0.06) for *n*-butanal and (0.56 ± 0.04) for glyoxal (HC(O)C(O)H). These reactions were investigated at atmospheric pressure, ambient temperature (286–291 K) and a relative humidity of (55 ± 10)%. On the

other hand, reaction (6) for unsaturated oxygenates is also an important source of OH•. For instance, Atkinson et al. [19] reported a yield of ~62 % for OH• in the ozonolysis of *trans*-2-hexenal at room temperature.

The reaction mechanisms for the reactions of OH• with unsaturated aldehydes has been widely studied. Apart from H-atom abstraction from the carbonyl group (and to a lesser extent from the hydrocarbon chain), the addition of OH• to the double bond is an important reaction pathway. The contribution of the OH addition reaction channel with respect to the H-abstraction pathway depends on the unsaturated aldehyde. For instance, Orlando and Tyndall [48] concluded that the contribution of OH• addition to the double bond to the overall k_{OH} at 1 atm increases from 30% for acrolein to 50% for crotonaldehyde and to 55% for methacrolein. Magneron et al. [26] have quantified the reaction products for the reaction of OH• with crotonaldehyde and found that acetaldehyde (CH_3CHO) and HC(O)C(O)H are the major end products with molar yields of $(30 \pm 5)\%$ and $(16 \pm 2)\%$, respectively. Therefore, we present here only the mechanism for the reaction between OH• and some *trans*-2-enals, 3-methyl-2-butenal and *trans*-2-methyl-2-butenal, which have not been reviewed before. To our knowledge, at the moment of this writing, no mechanistic study for the reaction of *trans*-2-methyl-2-butenal with any of the diurnal atmospheric oxidants has been reported. No experimental product studies on the oxidation reaction of OH• with *trans*-2-pentenal, *trans*-2-hexenal and *trans*-2-heptenal (R-CH=CH-CHO, where R=C_2H_5, C_3H_7 and C_4H_9, respectively) presently exist on which a reaction mechanism could be formulated. However, based on the reaction mechanisms proposed for α,β-unsaturated aldehydes, Davis et al. [32] have suggested that the atmospheric oxidation products from the reaction of OH• with R-CH=CH-CHO are most probably HC(O)C(O)H, other aldehydes and alkyl glycolaldehydes (RCH(OH)CHO). For the reaction of OH• with 3-methyl-2-butenal, Tuazon et al. [33] reported that the main reaction products were HC(O)C(O)H and CH_3CHO with molar formation yields of $(40 \pm 3)\%$ and $(74 \pm 6)\%$, respectively. The formation of these products were explained by a reaction mechanism based on those previously formulated for the corresponding reactions of α,β-unsaturated aldehydes such as acrolein, crotonaldehyde and methacrolein with OH•. Tuazon et al. [33] concluded that at room temperature, H-atom abstraction from the −CHO group of 3-methyl-2-butenal accounted for $(40 \pm 6)\%$ of the overall reaction, and OH• radical addition to the double bond accounted for $(53 \pm 4)\%$ of the overall reaction. A similar mechanism is expected for the reaction of OH• with *trans*-2-methyl-2-butenal, with CH_3CHO and $CH_3C(O)CHO$ as the expected reaction products.

To our knowledge, no information has been found in the literature on the mechanisms of the reactions of Cl atoms with the reviewed unsaturated aldehydes; however, an addition mechanism is expected to be the dominant pathway at room temperature and atmospheric pressure.

2.3 Photochemistry of Aldehydes in the Troposphere

As stated in the Introduction, the actinic radiation is capable of initiating photochemical processes in the troposphere at wavelengths greater than 290 nm. Aldehydes exhibit a weak absorption band between roughly 200 and 400 nm due to the forbidden $n \rightarrow \pi^*$ transition of the C=O chromophore. Apart from the $n \rightarrow \pi^*$ transition, unsaturated aldehydes exhibit an additional strong absorption band at wavelengths shorter than ca. 200 nm due to the allowed electronic $\pi \rightarrow \pi^*$ transition from the double bond. From an atmospheric point of view, only absorption by the C=O chromophore is of interest for the compounds under review. The ability to absorb radiation of a certain wavelength for a species is given by the absorption cross section, $\sigma(\lambda)$, and the effectiveness of the absorption process to dissociate the molecule (or to undergo other photochemical processes) is given by the overall primary quantum yield, $\Phi(\lambda)$.

Generally, saturated aldehydes (C_xH_yCHO) undergo UV photolysis by C–C bond scission (7a) or dissociation by a molecular channel (7b and 7c):

$$C_xH_yCHO + h\nu \rightarrow HCO\bullet + C_xH_y\bullet, \quad (7a)$$

$$\rightarrow CO + RH, \quad (7b)$$

$$\rightarrow C_{x-1}H_{y-3} + CH_2 = CHOH. \quad (7c)$$

Ethenol, CH_2=CHOH, formed in channel (7c) tautomerises to acetaldehyde. As a consequence, the assessment and quantification of the yields of each channel is important to better evaluate the atmospheric impact of the photolytic degradation process. The relative importance of the radical and molecular channels depends on the aldehyde. For instance, the relative yields of the radical channel (7a) and the molecular channel (7b) at 700 Torr were reported to be $(68 \pm 3)\%$ and $(32 \pm 3)\%$ for *n*-butanal, $(20 \pm 4)\%$ and $(80 \pm 4)\%$ for *n*-pentanal and 27 and 73% for *n*-hexanal, respectively [49, 50].

The wavelength dependence of $\sigma(\lambda)$ and $\Phi(\lambda)$ of the carbonyl compound has to be known in order to estimate the photolysis frequency, J (or j-value). The photolysis frequency of a compound at a given altitude (z) in the troposphere is defined as

$$J(z,\theta) = \int_{\lambda > 290\ \text{nm}} F(\lambda, z, \theta)\sigma(\lambda)\Phi(\lambda)d\lambda, \quad (8)$$

where $F(\lambda,z,\theta)$ (in photons $cm^{-2}\ nm^{-1}\ s^{-1}$) is the solar spectral actinic flux at z for a specific zenith angle (θ) or location. Under natural sunlight conditions in outdoor chambers, $J(z, \theta)$ values at ground level are determined by measuring the loss of the carbonyl under study using different analytical techniques. In this kind of photochemical study, effective quantum yields, φ_{eff}, are determined by comparison of the

measured photolysis frequencies with the theoretical photolysis rates using the measured actinic fluxes $F(\lambda,z,\theta)$ and assuming a $\Phi(\lambda)$ of unity.

$$J(z,\theta) = \varphi_{\text{eff}} \int_{\lambda > 290\ \text{nm}} F(\lambda,z,\theta)\sigma(\lambda)\mathrm{d}\lambda. \tag{9}$$

In the laboratory, the estimation of the atmospheric $J(z,\theta)$ is based on the measurements of $\sigma(\lambda)$ and $\Phi(\lambda)$. $F(\lambda,z,\theta)$ is usually taken from tabulated data at wavelength intervals, which are usually calculated for cloudless and aerosol-free sky conditions from the radiative transfer model developed by Madronich and Flocke [51]. Therefore, Eq. (8) can be rewritten as follows:

$$J(z,\theta) \approx \sum_{\lambda>290\text{nm}} F(\lambda,z,\theta)\sigma(\lambda)\Phi(\lambda)\Delta\lambda. \tag{10}$$

Up to now, there are only a limited number of direct studies concerning the photolysis of aldehydes under atmospheric conditions. The photochemistry of most of the aldehydes reviewed in this chapter has been described in detail by Calvert et al. in several books [13, 43, 52]. In the most recent revision of the photochemistry of these oxygenated compounds, Calvert et al. [13] updated the recommended $\sigma(\lambda)$, $\Phi(\lambda)$ and j-values. J-values were estimated under cloud-free conditions as a function of the solar zenith angle at several overhead ozone columns.

2.3.1 UV Absorption Cross Sections

As temperature decreases with altitude in the troposphere, the contribution of T-dependent $\sigma(\lambda)$ and $\Phi(\lambda)$ could vary the estimated j-values at high altitudes. For the majority of the aldehydes reviewed here, the T-dependence of $\sigma(\lambda)$ and $\Phi(\lambda)$ has not been reported and $J(z, \theta)$ are usually estimated from room temperature $\sigma(\lambda)$ and $\Phi(\lambda)$. For 3-methylbutanal, *trans*-2-methyl-2-butenal and 3-methyl-2-butenal, Lanza et al. [53] reported that, within the uncertainties, $\sigma(\lambda)$ between 255 and 390 nm did not depend on temperature in the T-range studied (273–305 K). The absorption cross sections for the reviewed aldehydes are compiled in spectral databases by Keller-Rudek et al. [54] and Noelle et al. [55].

New UV absorption cross sections for 3-methylbutanal, *trans*-2-methyl-2-butenal, 3-methyl-2-butenal [53], hexanal and *trans*-2-hexenal [34] were not included in Calvert et al [13]. The values of $\sigma(\lambda)$ for 3-methylbutanal determined by Lanza et al. [53] are in good agreement with those reported by Zhu et al. [56]. However, the values of $\sigma(\lambda)$ for hexanal and *trans*-2-hexenal reported by Jiménez et al. [34] are systematically lower around the maximum absorption than those measured by Tadić et al. [50] and O'Connor et al. [57]. In the case of $\sigma(\lambda)$ for *trans*-2-methyl-2-butenal and 3-methyl-2-butenal, the reason for not including

them in the evaluation of Calvert et al. [13] seems to be that no quantum yields were available that allow J estimations for these oxygenated (see below).

2.3.2 Photolysis Quantum Yields

Literature on quantum yields of aldehydes is extremely limited. In the database of Keller-Rudek et al. [54], $\Phi(\lambda)$ values are only compiled for the lightest saturated aldehydes, formaldehyde (HC(O)H) and CH_3CHO. For larger aldehydes, $\Phi(\lambda)$ are compiled, when available, in other databases such as that of Noelle et al. [55] and book reviews such as those from Calvert et al. [13, 43].

Overall Quantum Yields, $\Phi(\lambda)$

Moortgat [58] and Moortgat et al. [59] have reported the effective quantum yields for most of the carbonyl compounds reviewed here. Values of φ_{eff} were measured under natural sunlight conditions in the outdoor photoreactor EUPHORE in Valencia (Spain). These authors found that the φ_{eff} values were all significantly below unity at atmospheric pressure, ranging from 0.03 (crotonaldehyde) to 0.3 (*n*-pentanal).

Since the gas density in the atmosphere decreases with altitude, the pressure dependence of $\Phi(\lambda)$ is also important for estimating J-values. To our knowledge, the p-dependence of $\Phi(\lambda)$ has been studied for *n*-butanal and *n*-pentanal by Tadić et al. [49]. For *n*-hexanal and *n*-heptanal, the pressure dependence of $\Phi(\lambda)$ between 275 and 380 nm was determined at total pressures between 100 and 700 Torr of air [50, 60]. The absolute quantum yields were found to be only slightly dependent on the total pressure.

The photochemistry of unsaturated carbonyls, in particular α,β-unsaturated carbonyls, mainly proceeds via a photoisomerisation process. For example, Magneron et al. [26] measured at EUPHORE during summer a very low effective quantum yield for *trans*-crotonaldehyde,$\varphi_{eff} \leq (0.030 \pm 0.006)$. These authors speculated that an isomer (*cis*-crotonaldehyde or enol-crotonaldehyde) could be formed during the photolysis. In the same photoreactor, O'Connor et al. [57] observed a fast photoisomerisation of *trans*-2-hexenal, confirming the possibility suggested for crotonaldehyde by Magneron et al. [26]. No quantum yield measurements for *trans*-2-methyl-2-butenal and 3-methyl-2-butenal have been performed.

Primary Quantum Yields, $\phi(\lambda)$

The formation yield of formyl radicals (HCO•) produced in the radical channel (7a) has been quantified by using dye laser photolysis in combination with cavity ring-down spectroscopy in the 280–330 nm wavelength range by Zhu's research group [49, 50, 61]. The pressure dependence of $\phi_{HCO}(\lambda = 280\text{–}330\ \text{nm})$ in the photolysis of *n*-pentanal [61], *i*-pentanal and *t*-pentanal was investigated between 8 and

480 Torr and between 20 and 400 Torr of N_2 [56], respectively. The value of $\phi_{HCO}(\lambda)$ in the photolysis of *n*-pentanal was observed to be independent of pressure and slightly dependent on wavelength, with values around 0.1 at wavelengths between 280 and 330 nm. The peak HCO yields from the photolysis of *t*-pentanal and *i*-pentanal were (0.92 ± 0.11) and (0.40 ± 0.08) at 315 nm, respectively. As can be seen, photodissociation quantum yields for linear-chain aldehydes are relatively low compared to those for branched-chain aldehydes.

2.3.3 Photolysis Frequencies: Measurements and Estimations

The *j*-values for the reviewed aldehydes listed in Table 6 are total photolysis frequencies corresponding to all photodissociation channels (see below) at ground level. In the EUPHORE photoreactor, Moortgat et al. [59] measured *J*-values on

Table 6 Rate coefficients (in cm^3 $molecule^{-1}$ s^{-1}) for the reactions of saturated and unsaturated aldehydes with OH radicals and Cl atoms at 298 K and atmospheric pressure, photolysis frequencies (s^{-1}) and estimated lifetimes due to these atmospheric processes

Aldehyde	$k_{OH} \times 10^{11}$	$k_{Cl} \times 10^{10}$	$j \times 10^5$	τ_{OH}/ hours[a]	τ_{Cl}/ days[b]	τ_{Cl}/ hours[c]	τ_{hv}/ hours[d]
n-Butanal	2.37[e]	1.66[e]	1.5[e], 1.0[f]	12	70	17	22
n-Pentanal	2.66[e]	2.40[e]	3.78[f]	10	48	12	7
3-Methylbutanal	2.76[g]	–	1.26[f], 3[h]	10	–	–	21
n-Hexanal	2.83[e]	2.79[e]	1.65[f], 1.14[h]	10	41	10	21
n-Heptanal	2.96[g]	3.00[e]	–	9	39	9	–
Trans-2-butenal	3.60[e]	2.65[e]	1.2[i]	8	44	10	23
Trans-2-pentenal	4.40[e]	1.31[e]	–	6	88	21	–
3-Methyl-2-butenal	5.50[g]	–	100[j]	5	–	–	0
Trans-2-methyl-2-butenal	4.08[g]	–	30[j]	7	–	–	1
Trans-2-hexenal	4.30[e]	1.92[i]	~0[k]	6	60	14	–
Trans-2-heptenal	4.40[e]	2.40[i]	–	6	48	12	–

[a]Calculated with a global average $[OH] = 10^6$ molecules cm^{-3}
[b]Calculated with global average $[Cl] = 10^3$ atoms cm^{-3}
[c]Calculated with $[Cl] = 10^5$ atoms cm^{-3} for the marine boundary layer and polluted urban regions
[d]Calculated for overhead sun using an average *j*
[e]From of Calvert et al. [13]
[f]Moortgat et al. [59]
[g]Non-weighted average from data in Table 4
[h]Jiménez et al. [34]
[i]Non-weighted average from data in Table 3
[j]Upper limit from Lanza et al. [53]
[k]O'Connor et al. [57]

the order of 10^{-5} s^{-1} for some C_4–C_6 aldehydes. The estimated *j*-values as a function of θ for *n*-butanal by Calvert et al. [13] are in excellent agreement with those from Moortgat [58] at the same zenith angle. For 3-methylbutanal, Calvert et al. [13] used an adjusted quantum yield of 0.13 at 1 atm, based on the zero pressure $\Phi(\lambda)$ reported by Zhu et al. [54], to fit the results from Moortgat et al. [59]. Lanza et al. [53] reported *j*-values for $\theta = 16°$ ranging from 3×10^{-5} s^{-1} at ground level to around 4×10^{-5} s^{-1} at the boundary layer, assuming the quantum yields reported by Zhu et al. [56]. For hexanal, the *j*-values calculated by Calvert et al. [13] are a bit higher than those reported by Moortgat [58]. Jiménez et al. [34] also estimated *j*-values for hexanal as a function of altitude for $\theta = 16°$ under clear-sky conditions, assuming a photolysis quantum yield of 0.28.

Concerning the unsaturated aldehydes, Magneron et al. [26] reported $J \leq 1.2 \times 10^{-5}$ s^{-1} for *trans*-crotonaldehyde, from experiments performed during summer under natural sunlight conditions at EUPHORE. For *trans*-2-hexenal, O'Connor et al. [57] observed the formation of *cis*-2-hexenal with a molar yield of unity at the same facility and $J = 1.02 \times 10^{-4}$ s^{-1}. Their result implies that photoisomerisation is the major photochemical process, and photodissociation can be neglected. Photolysis frequencies for other aldehydes, such as *trans*-2-methyl-2-butenal and 3-methyl-2-butenal, were not evaluated in Calvert et al. [13] because of the lack of $\Phi(\lambda)$ data. However, for *trans*-2-methyl-2-butenal and 3-methyl-2-butenal, Lanza et al. [53] have reported upper limits for *J* as a function of altitude assuming a $\Phi(\lambda)$ of 1 (see Table 6).

3 Daytime Photooxidation of C_4–C_7 Ketones

This section focuses on the daytime photooxidation of a series of C_4–C_7 saturated and unsaturated ketones.

3.1 Gas-Phase Reaction with Tropospheric Oxidants

The chemistry of the smallest possible ketone, i.e. the C_3 compound ($CH_3C(O)CH_3$), is not covered in this review since the atmospheric chemistry of acetone has been the subject of several in-depth reviews [13 and references therein]. Tables 7, 8 and 9 list all of the presently available studies on rate coefficients for the reactions of saturated and unsaturated C_4 to C_7 ketones with O_3, OH• and Cl• [28, 62–105]. Table 10 lists the currently recommended rate coefficients for the reactions taken mainly from [1, 13] or in a few cases from the only literature reference available for that reaction [69, 86, 87, 105].

Although this review is confined to daytime chemistry, it should be noted that the ketones can react with NO_3• radicals during the night. There are not many

Table 7 Summary of the reported rate coefficients for the reactions of the reviewed C_4–C_7 ketones with O_3 at approximately room temperature and atmospheric pressure

Ketone	k_{O_3} (≈298 K) × 10^{18} (cm^3 $molecule^{-1}$ s^{-1})	Technique	References
Butanone	$<10^{-2a}$	Estimate	Atkinson and Arey [1]
3-Butene-2-one (methyl vinyl ketone)	4.77 ± 0.59	O_3, CL	Atkinson et al. [17]
	4.2 ± 0.4	UV abs.	Treacy et al. [62][b]
	4.72 ± 0.09	UV abs.	Grosjean et al. [63]
	5.84 ± 0.39	UV abs	Grosjean and Grosjean [16]
	5.4 ± 0.6	FTIR abs.	Neeb et al. [64]
2-Pentanone	$<10^{-2a}$	Estimate	Atkinson and Arey [1]
3-Pentanone	$<10^{-2a}$	Estimate	Atkinson and Arey [1]
3-Penten-2-one	21.3 ± 3.9	O_3, CL	Atkinson et al. [17]
	34.8 ± 1.5	RR	Greene and Atkinson [65]
	29.5 ± 4.1	RR	Sato et al. [15]
4-Penten-3-one	6.0 ± 0.4	UV abs.	Grosjean et al. [63]
2,4-Pentanedione (keto form)	$<10^{-2a}$	Estimate	Atkinson and Arey [1]
2,4-Pentanedione(enol form)	1.03	RR	Zhou et al. [66]
2-Hexanone	$<10^{-2a}$	Estimate	Atkinson and Arey [1]
3-Hexanone	$<10^{-2a}$	estimate	Atkinson and Arey [1]
4-Hexen-3-one	63.7 ± 9.9	UV abs.	Grosjean and Grosjean [67]
5-Hexen-2-one	9.17 ± 0.15	RR	Wang et al. [68]
3-Methyl-2,4-pentanedione (keto form)	$<10^{-2a}$	Estimate	Atkinson and Arey [1]
3-Methyl-2,4-pentanedione (enol form)	n.m		
2-Heptanone	$<10^{-2a}$	Estimate	Atkinson and Arey [1]

[a]Assumed limit for all alkyl ketones
[b]Report strong positive temperature dependence
$k_{O_3} = 6.9 \times 10^{-16} \exp(-1.521/T)$ cm^3 $molecule^{-1}$ s^{-1} for $240 < T < 324$ K

measurements of the rate coefficients for the reaction of NO_3• with either saturated or unsaturated ketones. The C_4–C_7 saturated ketones will have rate coefficients with NO_3• of around $(1–3) \times 10^{-16}$ $cm^3 molecule^{-1}$ s^{-1} and those of the unsaturated between 5×10^{-16} and 10^{-14} cm^3 $molecule^{-1}$ s^{-1} [13].

Table 8 Summary of the reported rate coefficients for the reactions of the reviewed C_4–C_7 ketones with OH radicals as a function of temperature and pressure

Name	p (Torr)	T-range (K)	k_{OH} (298 K) $\times 10^{12}$ (cm^3 $molecule^{-1}$ s^{-1})	$A \times 10^{12}$ (cm^3 $molecule^{-1}$ s^{-1})	B (K)	Technique	References
Butanone	760	305	3.6 ± 1.0			RR	Winer et al. [69]
	760	300	<2.5			RR	Cox et al. [70]
	760	298	0.88 ± 0.09			RR	Cox et al. [71]
	760	297	0.93 ± 0.17			RR	Edney et al. [72]
	25–50	240–440	1.15 ± 0.10	2.3 ± 1.1	170 ± 120	FP–RF	Wallington and Kurylo[73]
	100–300	243–372	1.19 ± 0.18	1.19 ± 0.18	60 ± 61	PLP–LIF	Le Calvé et al. [74]
	100–600	228–388	1.04 ± 0.07	1.35 ± 0.35	78 ± 52	PLP–LIF	Jiménez et al. [75]
	25–200	213–598	1.06 ± 0.06	3.84 ± 0.12	$-1{,}038 \pm 11$	PLP–LIF	Carr et al. [76]
3-Buten-2-one (methyl vinyl ketone)	760	300	14			RR	Cox et al. [71]
		298–424	17.9 ± 2.8	3.85	-456 ± 73	FT–RF	Kleindienst et al. [77]
	740	299	21.7 ± 1.6			RR	Atkinson et al. [28]
		232–378	20.8 ± 1.2	2.67 ± 0.45	-612 ± 130	FP–LIF	Gierczak et al. [78]
	740	296	22.1 ± 1.2			RR	Aschmann and Atkinson [79]
	2–5	300–422	17.3 ± 2.1			DF–LIF/ RF	Chuong and Stevens [80]
	2–5	300	17.8 ± 0.8			DF–LIF	Chuong and Stevens [81]
	100–300	298	18.6 ± 1.2			PLP–LIF	Holloway et al. [82]

2-Pentanone	740	299	4.37 ± 0.13			RR	Atkinson et al. [83]
	25–50	296	4.00 ± 0.29			FP–RF	Wallington and Kurylo [73]
	740	296	4.74 ± 0.24			RR	Atkinson and Aschmann [84]
	740	298	4.42 ± 0.29			RR	Atkinson et al. [85]
	100–600	248–388	3.14 ± 0.40	6.74×10^{-19} T^2	1,215	PLP–LIF	Jiménez et al. [75]
3-Pentanone	740	299	1.72 ± 0.31			RR	Atkinson et al. [83]
	25–50	240–440	2.74 ± 0.13			FP–RF	Wallington and Kurylo [73]
	740	296	1.95 ± 0.13			RR	Atkinson and Aschmann [84]
3-Penten-2-one	760	298	72.2 ± 17.4			RR	Blanco et al. [86]
4-Penten-3-one (ethyl vinyl ketone)	750	298	29.0 ± 7.9			RR	Blanco and Teruel [87]
	45–100	298	23.6 ± 4.7	4.4 ± 1.4	507 ± 90	PLP–LIF	Jiménez et al. [88]
2,4-Pentanedione	50	298	1.15 ± 0.15			FP–RF	Dagaut et al. [89]
(Acetylacetone) enol	760	298	87.6 ± 57			RR	Holloway et al. [82]
Enol	100–300	298	87.6 ± 57			PLP–LIF	
Enol	760	298	90.5 ± 18.1	3.35	-983 ± 130	RR	Zhou et al. [66]
2-Hexanone	740	299	8.43 ± 0.56			RR	Atkinson et al. [83]
	25–50	296	6.64 ± 0.56			FP–RF	Wallington and Kurylo[73]
	740	296	8.51 ± 0.42			RR	Atkinson and Aschmann[84]
	100–600	263–405	10.2 ± 1.20	2.13×10^{-18} T^2	1,038	PLP–LIF	Jiménez et al. [75]
4-Hexen-3-one	760	298	90.4 ± 21.2			RR	Blanco et al. [86]
5-Hexen-2-one	760	298	44.9 ± 10.2			RR	Wang et al. [68]
	760	298	51.8 ± 12.7			RR	Blanco et al. [86]

(continued)

Table 8 (continued)

Name	p (Torr)	T-range (K)	k_{OH} (298 K) $\times 10^{12}$ (cm^3 $molecule^{-1}$ s^{-1})	$A \times 10^{12}$ (cm^3 $molecule^{-1}$ s^{-1})	B (K)	Technique	References
2,5-Hexanedione	50	298	7.13 ± 0.24	1.49 ± 0.3	-450 ± 90	FT–RF	Dagaut et al. [89]
3-Methyl-2,4-pentanedione							
Keto form		298	11.6 ± 0.9			RR	Holloway et al. [82]
Enol form		298	60.6 ± 5.4			RR	Holloway et al. [82]
2-Heptanone	25–50	296	8.67 ± 0.84			PLP–RF	Wallington and Kurylo[73]
	740	298	11.1 ± 1.10			RR	Atkinson et al. [85]
	100–600	260–405	8.22 ± 1.10	1.54×10^{-18} T^2	1,144	PLP–LIF	Jiménez et al. [75]

Table 9 Summary of the reported rate coefficients for the reactions of the reviewed C_4–C_7 ketones with Cl atoms

Name	p (Torr)	T-range (K)	k_{Cl} (298 K) $\times 10^{12}$ (cm^3 molecule^{-1} s^{-1})	$A \times 10^{12}$ (cm^3 molecule^{-1} s^{-1})	B (K)	Technique	References
Butanone	700	295	42.8 ± 5.9			RR	Wallington et al. [90]
	15–60	298	32.4 ± 3.8			PLP–LIF	Notario et al. [91]
	20–200	298	33.0 ± 2.0			PLP–LIF	Albaladejo et al. [92]
	20–200	270–380	32.3 ± 4.29	73 ± 1.2	239 ± 108	PLP–LIF	Cuevas et al. [93]
3-Buten-2-one	700	296	40.4 ± 3.3			RR	Taketani et al. [94]
	900	296	38 ± 3			RR	Kaiser and Wallington [95]
	6.6	295	40.8 ± 2.1			PLP–LIF	Takahashi et al. [96]
	30–300	210–440	36.6 ± 1.8	27.7	76 ± 33	PLP–RF	Zhao et al. [97]
	800–950	297–475	42 ± 2	40 ± 3	0	RR	Kaiser et al. [98]
		298	210 ± 50			RR	Canosa-Mass et al. [99]
		298	190 ± 20			RR	Finlayson-Pitts et al. [100]
	1.6	298				DF–RF	Canosa-Mass et al. [101]
		298	210 ± 50			RR	Wang et al. [40]
		298				RR	Orlando et al. [102]
2-Pentanone	20–200	298	45.7 ± 2.8			PLP–RF	Albaladejo et al. [92]
	20–200	270–380	46.1 ± 1.2	7.8 ± 2.3	$-1{,}186 \pm 178$	PLP–RF	Cuevas et al. [93]
	700	296	111 ± 10			RR	Taketani et al. [94]
	6.6	295	123 ± 13			PLP–RF	Takahashi et al. [96]

(continued)

Table 9 (continued)

Name	p (Torr)	T-range (K)	k_{Cl} (298 K) $\times 10^{12}$ (cm^3 molecule^{-1} s^{-1})	$A \times 10^{12}$ (cm^3 molecule^{-1} s^{-1})	B (K)	Technique	References
3-Pentanone	20–200	298	45.0 ± 3.2			PLP–RF	Albaladejo et al. [92]
	1	260–333	59 ± 5	150 ± 70	281 ± 138	DF–MS	Aranda et al. [103]
	700	296	81.0 ± 8.5			RR	Taketani et al. [94]
	6.6	295	88.7 ± 9.2			PLP–RF	Takahashi et al. [96]
	30–300	228–436	74.7 ± 3.0	56.6 ± 4.1	-87 ± 22	PLP–RF	Zhao et al. [97]
	700–900	297–490	81.0 ± 8.0		0	RR	Kaiser et al. [104]
3-Penten-2-one	760	298	253 ± 54			RR	Blanco et al. [86]
4-Penten-3-one	760	298	291 ± 110			RR	Teruel et al. [105]
2-Hexanone	20–200	298	65.4 ± 5.8			PLP–RF	Albaladejo et al. [92]
	20–200	298	64.9 ± 3.8	10.0 ± 1.5	-565 ± 92	PLP–RF	Cuevas et al. [93]
	700	296	188 ± 18			RR	Taketani et al. [94]
	6.6	295	208 ± 32			PLP–RF	Takahashi et al. [96]
3-Hexanone	20–200	298	66.9 ± 6.2			PLP–RF	Albaladejo et al. [92]
	1	260–333	83 ± 17	65.4 ± 5.8		DF–MS	Aranda et al. [103]
	700	296	143 ± 19			RR	Taketani et al. [94]
	6.6	295	143 ± 19			PLP–RF	Takahashi et al. [96]
5-Hexen-2-one	760	298	315 ± 50			RR	Blanco et al. [86]
4-Hexen-3-one	760	298	300 ± 58			RR	Blanco et al. [86]
2-Heptanone	760	298	n.m.				

Table 10 Photolysis frequencies (s^{-1}) for straight-chained, saturated and unsaturated, ketones and rate coefficients (in cm^3 $molecule^{-1}$ s^{-1}) for their reactions with OH•, Cl• and O_3 at 298 K and atmospheric pressure

Ketone	$k_{OH} \times 10^{11}$[a]	$k_{Cl} \times 10^{10}$[a]	$k_{O_3} \times 10^{18}$[a]	$j \times 10^{6}$[b]
Butanone	0.11	0.4	$<10^{-2}$	4.68
2-Pentanone	0.41	1.16	$<10^{-2}$	2.67
3-Pentanone	0.20	0.79	$<10^{-2}$	–
2-Hexanone	0.75	2.0	$<10^{-2}$	8.04
3-Hexanone	0.64	1.44	$<10^{-2}$	–
2-Heptanone	0.94	–	$<10^{-2}$	–
2,4-Pentanedione (enol)	9.0	–	–	–
3-Methyl-2,4-pentandione (keto)	1.16	–	$<10^{-2}$	–
3-Methyl-2,4-pentandione (enol)	6.1	–	–	–
3-Buten-2-one	2.0	2.0	5.2	4.73
3-Penten-2-one	7.22[c]	2.53[c]	32	–
4-Penten-3-one	2.9[d]	2.9[e]	6	–
4-Hexen-3-one	9.04[c]	3.00[c]	64	–
5-Hexen-2-one	5.18[c]	3.15[c]	9.2[f]	–

[a]Except where indicated the rate coefficients are from Atkinson and Arey [1] and Calvert et al. [13]
[b]Values for overhead sun taken from Calvert et al. [13]
[c]From Blanco et al. [86]
[d]From Blanco and Teruel [87]
[e]From Teruel et al. [105]
[f]From Wang et al. [69]

3.1.1 Reaction with Ozone (O_3)

Saturated ketones are very unreactive toward O_3, and a universal upper limit of $<10^{-20}$ cm^3 $molecule^{-1}$ s^{-1} is generally assigned to the rate coefficient for their reaction with O_3 at 298 K and atmospheric pressure (Table 7). Unsaturated ketones are more reactive toward O_3, the reactivity arising from addition of O_3 to the double bond in the compounds. For the linear unsaturated ketones listed in Table 7, the rate coefficients for reaction with O_3 vary between approximately 1 and 6×10^{-17} cm^3 $molecule^{-1}$ s^{-1}. There is not a large kinetic database for the reactions of O_3 with unsaturated ketones, and many of the rate coefficients are associated with a large degree of uncertainty which makes it difficult to discern any reactivity trends. It is known that the carbonyl group, when positioned adjacent (α-) to the double bond, will deactivate it toward electrophilic addition of O_3. When further removed from the double, the reactivity of the unsaturated ketone toward O_3 is expected to be similar to that observed for the reactions of O_3 with structurally similar alkenes. Recommended rate coefficients for the reactions of O_3 with unsaturated ketones can be found in Calvert et al. [13].

3.1.2 Reactions Initiated by OH•

Rate coefficients for the reactions of OH• with straight-chain C_4–C_7 saturated (alkanones) and unsaturated ketones (alkenones) are listed in Table 8. The majority of the measurements have been made using relative kinetic techniques, but some absolute measurement techniques have also been applied. Rate coefficients for the reaction of OH• with unsaturated ketones generally exceed those for reactions of OH• with the corresponding alkanes [1]. The carbonyl group is known to deactivate the hydrogen atoms on the carbon directly attached to the carbonyl group, i.e. in the α-position, but activate the hydrogen atoms on the β-carbon atom. The activation has been observed to extend to the γ-carbon atom, and it has been argued that the activation is the result of hydrogen bonding in six- and seven-membered-ring transition states which provides a mechanism for the long-range activation as described in Calvert et al. [13] and Mellouki [12]. For the alkanones, there are significant differences between the room temperature of OH rate coefficients obtained using relative methods and those obtained using absolute techniques with the values from the relative kinetic method being higher. There is presently no plausible explanation for the discrepancies.

The temperature dependence for the reaction of OH• with butanone has been studied quite extensively, and the most recent measurements are in good agreement. The temperature dependence around ambient temperatures is linear and positive, but at higher temperatures, Carr et al. [76] have observed strong nonlinear Arrhenius behaviour and a positive temperature dependence. For alkanones, only one temperature-dependent study of the OH reactions with 2-pentanone, 2-hexanone and 2-heptanone exists by Jiménez et al. [75]. For these compounds, Jiménez et al. found strong nonlinear Arrhenius behaviour with a negative temperature dependence, which was quite pronounced at temperatures below 298 K. This is substantially different to the temperature dependence found for butanone and also to that observed for the reaction of OH• with alkanes.

There is not a large body of kinetic data for the reactions of OH• with unsaturated ketones, and with the exception of 3-buten-2-one, all the measurements have been at room temperature. The temperature-dependent kinetic measurements on the reaction of OH• with 3-buten-2-one all show linear Arrhenius behaviour with a negative temperature dependence. This is to be expected for a reaction which will occur predominantly via reversible addition of OH• to the double bond.

Blanco et al. [86] have noted that the rate coefficients for the reactions of OH• with 3-buten-2-one (methyl vinyl ketone) and 4-penten-3-one (ethyl vinyl ketone) both agree approximately, within the error limits, with those of the corresponding alkenes propene and 1-butene while those of the other unsaturated ketones are higher than those of the corresponding alkenes. Instinctively, one would also expect the OH rate coefficients for all of the unsaturated ketones investigated to be less than those of their analogous alkenes based simply on the deactivating effect of the C(O) group toward electrophilic reactions. The activating effect is especially

difficult to rationalise in the cases of 4-hexen-3-one and 3-penten-2-one where the deactivating carbonyl group is attached directly to the double bond.

The kinetic data suggests that the mechanism of the OH addition to the double bond in the unsaturated ketones is different to that for OH addition to alkenes. As pointed out above, the carbonyl group is known to enhance H-atom abstractions from carbons situated β and γ to itself probably through a mechanism involving a transient ring. To explain the higher than expected rate coefficients, Blanco et al. [86] have speculated that the reactions of OH• with the unsaturated ketones may also proceed via a mechanism involving some form of hydrogen-bonded complex between the OH• and the carbonyl as has been discussed in the literature for reactions of OH radicals with various oxygenated organics [13]. However, at present, this remains a speculation, and further kinetic measurements will be necessary to validate the observations.

The two diketones listed in Table 8, 2,4-pentanedione (acetylacetone) and 3-methyl-2,4-pentanedione, are a special class of ketone since they can exist in both keto and enol tautomeric forms. In the gas phase, 2,4-pentanedione exists predominantly in the enol form ($CH_3C(O)CH=C(OH)CH_3$, >95%), while 3-methyl-2,4-pentanedione is a mixture of the tautomers with a keto contribution of $(60 \pm 5)\%$. Consequently an OH rate coefficient exists only for the keto form of 2,4-pentanedione, whereas rate coefficients exist for both the keto and enol forms of 3-methyl-2,4-pentanedione. The rate coefficients for the reactions of OH• with the enol tautomers of the compounds are similar to those obtained for OH• with the alkenes resulting from substituent of the carbonyl and –OH groups with methyl groups. This has been taken as indication that both the $–CH_2OH$ group and the –OH group attached directly to the double bond enhance the reactivity of OH addition to the enol double bond (Holloway et al. [82]). The negative temperature dependence observed by Zhou et al. [66] is in line with the addition of OH• to the double bond in the enol form being the dominant reaction pathway for the reaction of OH• with 2,4-pentanedione. The rate coefficient for the reaction of OH• with the keto tautomer of 3-methyl-2,4-pentanedione is of the magnitude expected for a mechanism involving only H-atom abstraction from a saturated ketone.

3.1.3 Reactions with Cl•

Reported rate coefficients for the reactions of Cl• with saturated and unsaturated C_4–C_7 ketones are listed in Table 9. There have been issues with Cl rate coefficients determined with absolute kinetic techniques due to problems caused by secondary loss of Cl• through reaction with products and regeneration of Cl• via reaction of radical products with Cl_2. These issues have been addressed in the latest measurements applying absolute methods where good agreement between measurements with absolute and relative techniques has been achieved; see, for example, Takahashi et al. [96]. It has also been postulated that Cl rate coefficients determined with the relative kinetic technique in air may be slightly too high due to a contribution from OH radicals generated via peroxy–peroxy radical reactions. If

it is assumed that the most recent rate coefficient determinations for Cl reactions are the most accurate (from 2006 and higher), a comparison of these values for the reactions of Cl• with saturated ketone with those for Cl• with alkanes [106] shows that the rate coefficients for Cl• with the saturated ketones are significantly lower than those for the corresponding alkane. For example, an averaged value of ~8.2×10^{-11} cm^3 $molecule^{-1}$ s^{-1} for the reaction of Cl• with 3-pentanone can be compared with a value of 19.4×10^{-11} cm^3 $molecule^{-1}$ s^{-1} for the reaction of Cl• with butane [106]. The difference between the reaction of Cl• with 2-pentanone and that of Cl• with butane is slightly smaller. A similar pattern is observed when the rate data for Cl• with 3-hexanone and 2-hexanone are compared with the rate coefficient for Cl• with pentane. The results suggest a strong deactivating effect of the carbonyl group toward H-atom abstraction from the alkyl groups which contrasts very strongly with the activating behaviour observed for the reactions of OH• with the saturated ketones described in Sect. 3.1.2 where activation of H-atoms β and γ to the carbonyl has been observed. Since the reactions are already quite fast, the temperature dependence for Cl reactions is generally small and, in the case of alkyl ketones, positive, although in a few cases, negative temperature dependencies have been reported, suggesting the possibility of complex intermediate transient states.

Apart from 3-buten-2-one, there have been very few determinations of rate coefficients for the reactions of Cl• with unsaturated ketones. The rate coefficients for all unsaturated ketones listed in Table 9 are very similar and, in most cases, agree with one another within the error limits. Since the rate coefficients are approaching the gas kinetic collision limit and the precision of the measurements is not very high, the similarity in the rate coefficients is not surprising. There have not been any temperature dependence studies on the reactions of Cl• with the unsaturated ketones reviewed in this chapter, but again since the reactions are approaching the gas kinetic limit, any temperature dependence is expected to be very small. Here again, one can compare the rate coefficients for the reactions of Cl• with the unsaturated ketones with those of Cl• with the corresponding alkenes [107]. As for the saturated ketones, the rate coefficients for the reactions of Cl• with the unsaturated ketones are generally lower than those of the corresponding alkenes, although the differences are not very pronounced because of the already high values of the rate coefficients [86]. This reduction in reactivity indicates that for the reactions of Cl• with the unsaturated ketones, the expected electron-withdrawing effect of the carbonyl group is operational which was not the case for the reactions with OH radicals described in Sect. 3.1.2.

3.2 General Reaction Mechanisms and Gaseous Oxidation Products

Saturated ketones will react with oxidants such as OH•, NO_3• and Cl• via H-atom abstraction from the alkyl groups attached to the carbonyl group. Whereby, as can be seen from the estimated atmospheric lifetimes (see Table 11), the reaction with OH• will dominate. Reaction with Cl• will only be able to compete in areas with high Cl atom concentrations such as may occur in the marine boundary layer or polluted urban areas with chlorine producing sources such as power stations. The only differences in the mechanisms for the various oxidants will be in the relative contributions of H-atom abstraction from the various primary, secondary and tertiary H-atoms in the ketone, whereby reactions with Cl atoms are much less selective than those with either OH• or NO_3•. Considering the potentially significant importance of saturated ketones in atmospheric chemistry, there have been surprisingly few products studies on their reactions with the major atmospheric oxidants [13, 19, 85, 104].

The main oxidation channels in the reaction of butanone under high-NO_x conditions are shown in Fig. 1. Attack at the CH_2 group positioned α to the carbonyl will result in the formation of the 3-butanoyl radical which through an intermediary oxy radical reacts to form CH_3CHO and CH_3CO•. The acetyl radical will add molecular oxygen to form the $CH_3C(O)OO$• peroxy radical which reacts with NO

Table 11 Estimated lifetimes of ketones with respect to reaction with OH•, Cl•, O_3 and photolysis

Ketone	OH[a]	Cl[b]	Cl[c]	O_3[d]	Photolysis[e]
Butanone	10 days	289 days	2.9 days	<4.5 years	2.5 days
2-Pentanone	2.8 days	100 days	1 day	<4.5 years	4.3 days
3-Pentanone	5.8 days	147 days	1.5 days	<4.5 years	–
2-Hexanone	1.5 days	58 days	14.4 h	<4.5 years	1.5 days
3-Hexanone	1.8 days	80 days	19.2 h	<4.5 years	–
2-Heptanone	1.2 days	–	–	<4.5 years	–
2,4-Pentanedione (enol)	3.1 h	–	–	–	–
3-Methyl-2,4-pentandione (keto)	23 h	–	–	<4.5 years	–
3-Methyl-2,4-pentandione (enol)	4.6 h	–	–	–	–
3-Buten-2-one	13.9 h	58 days	14 h	3.2 days	2.5 days
4-Penten-3-one	9.6 h	40 days	9.6 h	2.8 days	–
3-Penten-2-one	3.8 h	46 days	11 h	12.4 h	–
4-Hexen-3-one	3.1 h	39 days	9.4 h	6.2 h	–
5-Hexen-3-one	5.4 h	37 days	8.9 h	1.8 days	–

[a]Calculated with a global average $[OH] = 10^6$ molecules cm^{-3}
[b]Calculated with global average $[Cl] = 10^3$ atoms cm^{-3}
[c]Calculated with $[Cl] = 10^5$ atoms cm^{-3} for the marine boundary layer and polluted urban regions
[d]Calculated with a 24 h average $[O_3] = 7 \times 10^{11}$ molecules cm^{-3}
[e]Calculated for overhead sun

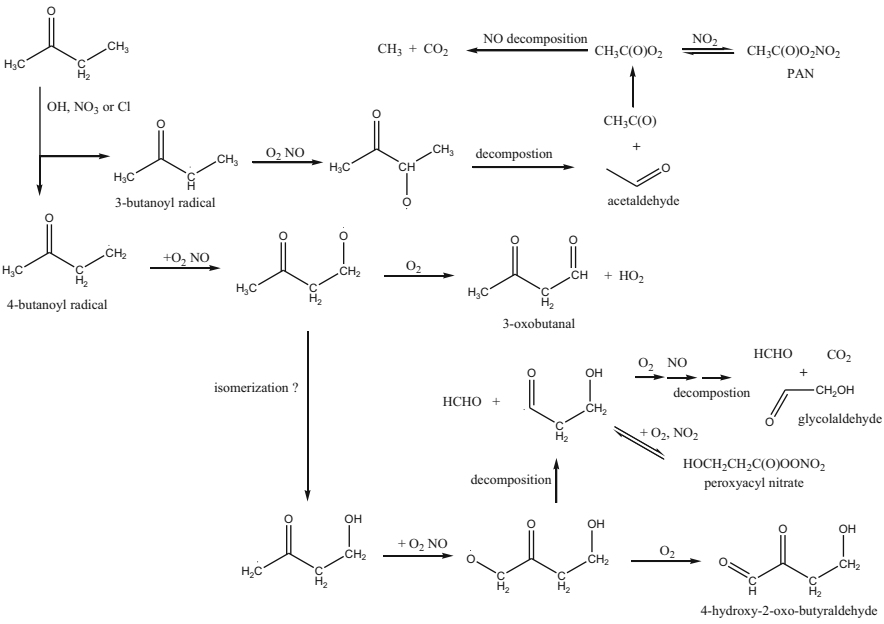

Fig. 1 Main reaction routes in the oxidant-mediated oxidation of butanone which apply to reaction with the oxidants OH and NO_3 radicals and also Cl atoms under high-NO_x conditions

to form CH_3CO_2 which decomposes to give methyl radicals (CH_3•) and CO_2. Further oxidation of CH_3• results in formation of HCHO and HO_2• [1]. Under conditions of high NO_x, the $CH_3C(O)OO$• peroxy radical can add NO_2 in a thermal equilibrium to form the acyl peroxy nitrate "peroxyacetyl nitrate ($CH_3C(O)O_2NO_2$)" also known as PAN. Since peroxyacyl nitrates dissociate slowly in the atmosphere, they are able to transport nitrogen over long distances in the atmosphere and thus influence troposphere chemistry in regions far removed from their point of origin.

Attack at the $-CH_3$ group positioned β to the carbonyl will produce the 4-butanoyl radical which as shown in Fig. 1 forms an oxy radical which can react with O_2 to form 3-oxobutanal and HO_2• radicals. However, isomerisation via an H-atom transfer from the CH_3• group positioned α to the carbonyl group is also possible. Isomerisation will gain importance as a reaction route with increasing chain–chain length of the alkyl group attached to the carbonyl entity. This results in the formation of a difunctional alkyl radical, $•CH_2C(O)CH_2CH_2OH$, which via addition of O_2 and further reaction of the resulting peroxy radicals with NO forms the oxy radical $•OCH_2C(O)CH_2CH_2OH$. The oxy radical can react with O_2 to form 4-hydroxy-2-oxobutyraldehyde or decompose to form HCHO and a $•C(O)CH_2CH_2OH$ radical which will add O_2 to form the $•OOC(O)CH_2CH_2OH$ peroxy radical. This peroxy radical can add NO_2 to form a semi-stable peroxyacyl nitrate or react with NO to form an oxy radical which decomposes to form CO_2, HCHO and glycolaldehyde ($HOCH_2CHO$). Similar reaction sequences can be written for the larger unsaturated ketones; however, since there have been very few product

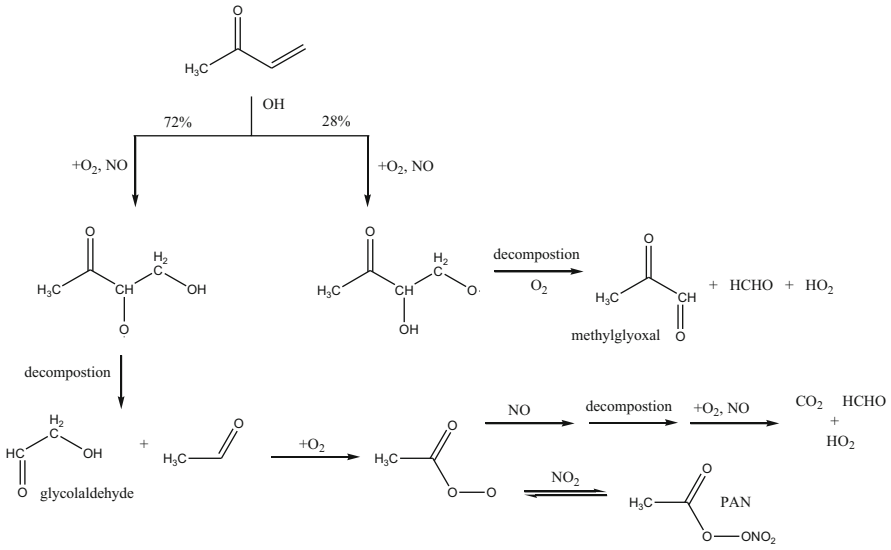

Fig 2 Main reaction routes in the reaction of OH radicals with 3-buten-2-one (methyl vinyl ketone)

studies, which are often incomplete, it is presently not possible to write unique mechanisms for the ketones on the basis of the product observations.

Based on the available limited kinetic data, the major daytime loss mechanism for unsaturated ketone in the atmosphere is probably reaction OH•, although reaction with O_3 may also play a quite significant role in some cases. Reaction with NO_3• radicals during the night may be potentially important for some unsaturated ketones under polluted conditions. The photolytic lifetimes of unsaturated ketones where the double bond is directly attached to the carbonyl are thought to be fairly long and thus are not important atmospheric loss processes [13]. However, for unsaturated ketones where the double bond is remote from the carbonyl group, the photolysis lifetime may be similar to those of the saturated ketones, and photolysis may compete with the reaction of OH• as an atmospheric loss process.

Unsaturated C_4–C_7 ketones will react with OH radicals mainly via the addition of OH• to the double in the ketones. H-atom abstraction will in most cases be fairly negligible. The main reaction routes in the reaction of OH radicals with 3-buten-2-one (methyl vinyl ketone) are shown in Fig. 2. The major pathway is OH addition to the terminal CH_2 group with a contribution of ~72% (route A), the remainder being to the carbon of the double bond directly attached to the carbonyl group (route B). The radicals formed after addition of OH• with the addition of O_2 and under high-NO_x conditions react with NO to form oxy radicals. The oxy radicals formed via route A will decompose to give glycolaldehyde and acetyl radicals the further reactions which can form PAN, CO_2, HCHO and HO_2•. The oxy radical formed in route B will decompose to give methylglyoxal, HCHO and HO_2• radicals.

The reactions of the unsaturated alkenes with O_3 will react via a mechanism involving 1,3-cyclo addition of O_3 to the double bond in the alkene to form an

intermediate primary ozonide which rapidly decomposes to a corresponding carbonyl oxide (Criegee intermediate) and carbonyl [52]. The decomposition of the Criegee intermediate is considered to be the main source of the OH radicals [108] observed in the ozonolysis of unsaturated compounds, and it is only very recently that a Criegee intermediate has been detected directly in the gas phase [109]. The ozonolysis of 3-buten-2-one, for example, in addition to OH radicals would produce HCHO and methylglyoxal as major carbonyl products. The ozonolysis of double bonds is extremely complex, and a detailed explanation of the mechanism is beyond the scope of the present chapter. The reader is, therefore, referred to Calvert et al. [52] and Johnston and Marston [108] for more details of the reaction mechanism.

3.3 *Photochemistry of Ketones in the Troposphere*

Absorption of solar radiation by the C_4–C_7 ketones ($\lambda > 290$ nm) results in the formation of an excited singlet state (S_1) via an $n \rightarrow \pi^*$ transition. The known $n \rightarrow \pi^*$ transition absorption bands for simple ketones are fairly similar with a featureless absorption extending from around 220–340 nm with a maximum between 280 and 290 nm.

Since the absorption features extend into the tropospheric actinic regain, the alkyl C_4–C_7 ketones will be subject to photolysis in the troposphere. The primary photolysis processes of alkyl ketones are all very similar [13, 14, 43]. For example, the following three photodecomposition pathways have been considered for excitation of butanone in its $n \rightarrow \pi^*$ absorption band:

$$CH_3C(O)CH_2CH_3 + hv \rightarrow CH_3CO + CH_3CH_2, \quad (11a)$$

$$\rightarrow CH_3 + CH_3CH_2CO, \quad (11b)$$

$$\rightarrow CH_3CH_2 + (CH_3CO)* \rightarrow CH_3CH_2 + CH_3 + CO. \quad (11c)$$

Photochemical studies performed under atmospherically relevant conditions show that process (11a) dominates process (11b) contributing ≤ 10 %. Evidence was also found for a small contribution from process (11c). When the ketone contains a γ-hydrogen atom in addition to the photodecomposition channels 11a, 11b and 11c above, a photochemical pathway known as a Norrish "type II" process can occur. This is illustrated below for 2-pentanone.

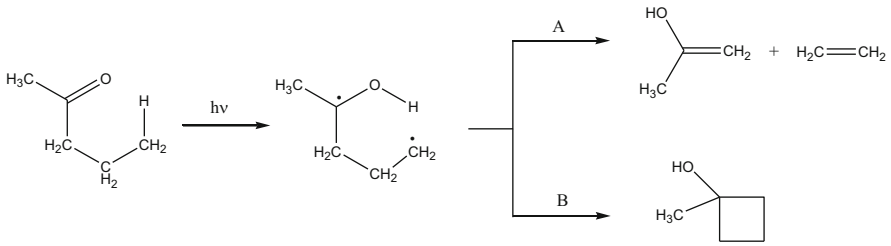

The Norrish type II process involves a six-membered ring transition state whereby intramolecular abstraction of a γ-hydrogen by the excited carbonyl group to produce a 1,4-biradical as a primary photoproduct occurs. This is followed either by fragmentation to form an enol and an alkene (path A) or intramolecular recombination of the two radicals to a cyclobutane derivative (path B). Depending on the stability of the enol, gas-phase keto–enol tautomerisation can occur to form the corresponding ketone; in the case of 2-pentanone, this would be acetone. For 2-pentanone, 2-hexanone, 3-hexanone and 4-heptanone, all of the above processes have been observed to some degree in photolysis product studies [47].

There is limited data on the photodissociation lifetimes of the alkyl C_4–C_7 ketones; however, the available data supports that the lifetimes will be comparable with the lifetimes estimated for the reactions with OH• (see Table 11 in Sect. 3.4.1.1). As indicated in Sect. 3.2, the photolytic lifetimes of unsaturated ketones where the double bond is directly attached to the carbonyl are thought to be long and thus are not of any significance as an atmospheric sink for these compounds [13].

4 Atmospheric Implications

4.1 Lifetimes in the Atmosphere

The environmental implications of the chemistry of the reviewed carbonyl compounds can be at a local, regional or even global scale. The short- or long-term effect in the atmosphere of a species is related to the residence time or lifetime (τ). The main parameter that controls the residence time of a species in the atmosphere and its effect on air quality is the reactivity with the main atmospheric oxidants. Lifetimes due to reaction with a particular oxidant (τ_{Ox}) or due to UV photolysis (τ_{hv}) are defined as follows:

$$\tau_{\text{homog}} = \frac{1}{\sum_i k_{Ox}[Ox]}, \tag{12}$$

$$\tau_{hv} = \frac{1}{J(z,\theta)}, \tag{13}$$

where k_{Ox} is the rate coefficient for the reaction of the compound i with the oxidant Ox, and [Ox] is the averaged atmospheric concentration of the oxidant. τ_{Homog} have been estimated using a 24 h average oxidant concentration in the troposphere of 1×10^6 radical cm^{-3} for OH• [110] and 10^3 atom cm^{-3} for Cl• [111]. In the marine boundary layer and polluted urban regions, the Cl• concentration can reach a peak value of 10^5 atom cm^{-3} [112]. Reactions with O_3 were neglected in the lifetime calculation since they are too slow to compete with OH or Cl reactions.

The estimation, when possible, of the atmospheric lifetimes due to homogeneous gas-phase reactions and UV photolysis is presented in Table 6 for aldehydes and in Table 11 for ketones. Other losses such as heterogeneous reactions and physical wet and dry deposition are not considered here, but in the majority of the aldehydes, they are expected to be negligible. Rate coefficients k_{Ox} listed in Table 6 are those recommended by Calvert et al. [13], the average from data in Tables 3 and 4 or, in some cases, the only available data at this writing. In some cases, inconsistent kinetic data were neglected in the averaging process. For instance, for the rate coefficients, the reactions of OH• with 3-methylbutanal from Audley et al. [24] and Glasius et al. [31] were not considered.

The rate coefficients used in the calculation of the atmospheric lifetimes of the ketones given in Table 11 for reaction the oxidants were taken from [1, 13] and in a few cases from the only study available in the literature for that particular reaction.

Lifetimes of saturated aldehydes due to the OH reaction (τ_{OH}) are typically less than 10 h, while those due to the Cl reaction are similar only at specific conditions of the marine boundary layer. Globally, the atmospheric degradation of these compounds initiated by OH reaction predominates versus Cl reactions in all cases. However, for saturated aldehydes, UV photolysis can compete with OH reaction (lifetimes typically around a day). Photolysis rates in Table 6 are those measured under natural sunlight conditions or estimated at ground level. It should be noted that zenith angle is somewhat different in the cited works.

A bar diagram of the relative contribution (in %) of each removal process for the aldehydes is shown in Fig. 3. The atmospheric degradation of saturated aldehydes is controlled mainly by reaction with OH radicals and by UV photolysis, for which the loss rates are of comparable magnitude. In contrast, reaction with OH radicals is generally the dominant loss process for unsaturated aldehydes, although photolysis could be important in some cases.

The atmospheric lifetimes of the ketones with respect to the different photooxidative degradation pathways mirror quite closely those of the aldehydes with only a few exceptions. As for the aldehydes, reaction with OH• and photolysis is the main daytime sinks for the both unsaturated and saturated ketones. The photolysis database for photolysis is not very extensive for the ketones, but the available data would support that for butanone, photolysis will dominate over reaction with OH• as a sink, whereas for the other ketones, reaction with OH• will probably dominate in most cases. Reaction of the ketones with Cl• will play an important contributory role in the photodegradation initiated in areas with elevated levels of Cl• such as the marine boundary layer and polluted industrial areas. In pollution episodes with high

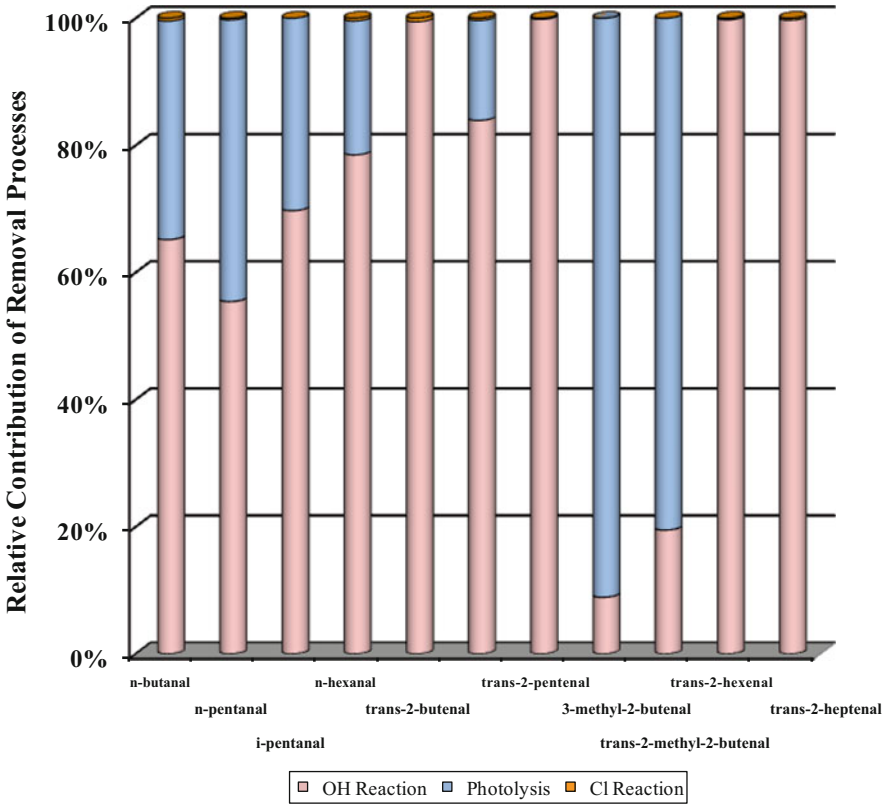

Fig. 3 Bar diagram showing the relative importance of UV photolysis and OH radical-initiated reactions for several aldehydes

levels of O_3 formation, reaction of some of the unsaturated ketones with O_3 will also make a significant contribution to the loss of these types of ketones.

4.2 Formation of Secondary Pollutants

Formation of gaseous products in the reaction of carbonyls with diurnal atmospheric oxidants were discussed in the preceding sections. However, the formation of secondary products, such as ground-level O_3 and secondary organic aerosols (SOAs) as a result of further photodegradation, is also an important contributing factor affecting the quality of urban and rural environments. In this section, a brief overview on the estimation methods for ozone formation from the reviewed homogeneous reactions is given. Moreover, the available laboratory and field studies on SOA formation as a consequence of the oxidation of the reviewed carbonyls are presented.

4.2.1 Ground Ozone Formation: MIR and POCP Indexes

It is well established that ozone is mainly generated in situ in the troposphere from the sunlight-initiated oxidation of volatile organic compounds, VOCs, in the presence of high levels of NO_x. Regional scale photochemical air pollution is a widespread phenomenon and is characterised by the formation of high levels of O_3 and other photooxidants such as PAN. The production of elevated levels of ozone is of particular concern, since it is known to have adverse effects on human health, vegetation and materials. Control of the emissions of the precursor VOCs and NO_x poses is a possible method for the reduction of ozone levels during photochemical pollution episodes. However, the relative contributions of VOCs to ozone formation can vary significantly from one compound to another by virtue of differences in their reactivity and structure. In addition, many hundreds of VOCs are emitted into the atmosphere from a multitude of sources; therefore, a method to classify a particular VOC with respect to its propensity to form O_3 is obviously highly desirable, since it would enable high-O_3-generating VOCs to be preferentially targeted in abatement strategies.

Several methods have been suggested in order to classify organic compounds with respect to their ability to form ozone. To these methods belongs incremental reactivity, which is defined as the change in the amount of ozone formed due to a change in emission of that particular compound [113, 114]. Incremental reactivities have been calculated for various chemical environments and ROG (reactive organic gas)/NO_x ratios using a box model. Estimates of the incremental reactivities are obtained from the maximum amount of ozone formed during the first day after emission into a certain environment. The reactivities are most often reported as Maximum Incremental Reactivities (MIR; gm O_3/ gm VOC). Typical MIRs for C_4, C_5, C_6 and C_7aldehydes are 5.97, 5.08, 3.14 and 3.69, respectively, and for C_4, C_5, C_6 and C_7 ketones are 1.48, 2.81, 3.34 and 2.36, respectively (www.engr.ucr.edu/~carter/SAPRC/MIR10.pdf). These values can be compared to an MIR of 9.0 for ethene. The MIRs for unsaturated C_4–C_7 aldehydes and ketones are similar or somewhat higher than the MIR for ethene.

The photochemical ozone creation potential (POCP) concept is another method which has been used to classify compounds according to their ability to form ozone. The POCP method calculates the total additional ozone formed in a multiday modelling of adding a given amount of VOC relative to adding the same mass of ethene. Therefore, POCP for ethene is defined as 100. POCPs are determined from the calculated formation of ozone in the boundary layer over a period of approximately five days along an idealised straight line trajectory, using a photochemical trajectory model and methodology described by Derwent et al. [115–117]. The chemical development in the boundary layer air parcel is described using the Master Chemical Mechanism (MCM), which includes a detailed, explicit treatment of the degradation of 139 VOCs. A POCP for a specific VOC is not an absolute value but will vary depending upon the model employed and other parameters used in its calculation.

To make POCP values more readily calculable without resource to computer modelling, Derwent et al. [116] and Jenkin [118] have developed a simplified estimation procedure which uses fundamental molecular properties (molecular weight, number of reactive bonds and rate coefficient for reaction with OH radicals) to provide estimated POCPs (ε^{POCP}) using an analytical expression. This analytical expression gives ε^{POCP} values which are in reasonable agreement for a wide range of different compound classes. For aldehydes and ketones, the estimated POCP values are consistently lower than the model POCP values. This is not unexpected since the ε^{POCP} calculation is based exclusively on OH radical-initiated VOC degradation and does not include direct photolysis which competes effectively with the OH-mediated photooxidation. The photolysis of aldehydes and ketones clearly has an influence on the other classes of VOC considered in the present study, since they are invariably formed as degradation products. From the point of view of ozone formation, their photolysis is particularly significant since it leads to secondary radical generation. Although this is not explicitly taken into account in the analytical expression used to calculate ε^{POCP}, such secondary radical formation is clearly common to all VOCs, and its influence can effectively be regarded as cancelling out in a comparative ozone formation index such as ε^{POCP}, at least to a first approximation. The values of ε^{POCP} for the aldehydes reviewed here range from only 51 to 74, while those for the values for ketones cover a much larger range from 17 to 82. The values for the saturated ketones lie in the range 17–40, while those for the unsaturated ketones are in the range 66 to 82. These values were obtained using the estimation method given in Jenkin [118] and the recommended OH rate coefficients for the aldehyde/ketone reactions.

Although the ability of aldehydes and ketones to generate ozone is greater than that implied by the ε^{POCP} scale, the predicted trend of values is very similar to the model POCP scale and is thus a good indicator of the O_3 formation potential of the compounds.

4.2.2 Role of Carbonyl Chemistry in the Formation of Secondary Organic Aerosols (SOAs)

Extensive literature can be found on laboratory studies, field measurements and modelling of SOAs. Studies on SOA formation by gas/particle partitioning have been traditionally focused on laboratory measurements of low volatility reaction products from isoprene and monoterpenes [e.g. 119–121 and references therein] as well as on field campaigns in boreal and urban areas [e.g. 122, 123 and references therein] and over oceans [e.g. 124 and references therein]. Ervens and Kreidenweis [119] have discussed the effects of different parameters on the SOA formation efficiency of biogenic compounds (α-pinene, isoprene) and aliphatic aldehydes (glyoxal, hexanal, octanal, hexadienal).The important role of aldehyde chemistry in SOA formation has been recently highlighted by Chan et al. [125]. The molecular structure of the aldehyde determines the amount of SOA formation, as the SOA mass yields are the highest for aldehydes that are α,β-unsaturated and contain an

additional methyl group on the α-carbon. Chan et al. concluded that NO_2 enhances SOA formation from methacrolein and two other α,β-unsaturated aldehydes, specifically acrolein and crotonaldehyde.

The reactive uptake mechanism for relatively small VOCs (short-chain aldehydes and ketones) is not well understood. Partitioning of VOCs to the particle phase invariably involves hydration as the first step, followed by various (possibly acid-catalysed) reactions such as polymerisation, hemiacetal/acetal formation and aldol condensation [126]. Jang and Kamnes [127] measured the particle growth by the heterogeneous reaction of glyoxal, butanal, hexanal, octanal and decanal in the presence of seed aerosols and 1-decanol investigating the catalytic effect of sulphuric acid. More recently, Ervens and Kreidenweis [119] also found that acid-catalysed reactions can yield >50% more SOA mass than processes under neutral conditions. They concluded that aldehydes can significantly contribute to SOA formation through heterogeneous reactions in the presence of an acid catalyst.

5 Final Remarks

Although not specifically handled in this chapter, apart from experimental methods to measure the rate coefficients for the reactions of atmospheric oxidants with the aldehydes and ketone, many types of method exist to estimate the rate coefficients such as structure activity relationships (SAR) which are particularly advanced for predicting the rate coefficients of OH and NO_3 radicals and O_3 with VOCs [128–130]. They are particularly helpful when data for a particular rate coefficient does not exist, in assessing if a rate coefficient measurement is reasonable and in predicting the relative contributions of reaction channels in a mechanism.

The atmospheric degradation of the carbonyls reviewed in this chapter is controlled to a greater or lesser extent by photolysis and by reaction with OH radicals. In many cases, the loss rates for both processes are of comparable magnitude. The initial step in the degradation of these carbonyls by OH reaction is quite fast (lifetimes of hours to a few days) to generate ground-level ozone and other secondary pollutants. In clean environments, the atmospheric degradation of unsaturated carbonyls can help sustain the oxidation capacity of the atmosphere by recycling OH radicals. Under low-NO_x conditions, oxidation of carbonyls is also a source of organic acids and hydroperoxides in the atmosphere. In contrast, in polluted environments (high-NO_x conditions), the formation of PANs is the main atmospheric fate for carbonyls. As discussed above, the formation of SOAs is enhanced in polluted urban areas by the presence of NO_x; however, in boreal areas and oceans, high levels of SOAs have been detected as a result of the chemistry of biogenic emissions.

The potential detrimental impact of primary gaseous products and SOAs on air quality and, therefore, on health is obvious. Major concerns for human health are focused on the increase of harmful pollutants such as ozone and PANs and the exposure to particulate matter. In addition to health effects, ground-level ozone and

particulate matter can contribute to climate change by modifying the radiation budget of the Earth. Ozone is considered a potent greenhouse gas (global warming), while aerosols reduce the amount of radiation reaching the surface by absorption or scattering thus affecting the surface temperature (global dimming).

References

1. Atkinson R, Arey J (2003) Atmospheric degradation of volatile organic compounds. Chem Rev 103:4605–4638
2. Atkinson R, Baulch DL, Cox RA, Crowley JN, Hampson RF, Hynes RG, Jenkin ME, Rossi MJ, Troe J (2004) Evaluated kinetic and photochemical data for atmospheric chemistry: volume I – gas phase reactions of O_x, HO_x, NO_x and SO_x species. Atmos Chem Phys 4:1461–1738
3. Atkinson R, Baulch DL, Cox RA, Crowley JN, Hampson RF, Hynes RG, Jenkin ME, Rossi MJ, Troe J, Subcommittee IUPAC (2006) Evaluated kinetic and photochemical data for atmospheric chemistry: volume II – gas phase reactions of organic species. Atmos Chem Phys 6:3625–4055
4. Atkinson R, Baulch DL, Cox RA, Crowley JN, Hampson RF, Hynes RG, Jenkin ME, Rossi MJ, Troe J (2007) Evaluated kinetic and photochemical data for atmospheric chemistry: volume III – gas phase reactions of inorganic halogens. Atmos Chem Phys 7:981–1191
5. Atkinson R, Baulch DL, Cox RA, Crowley JN, Hampson RF, Hynes RG, Jenkin ME, Rossi MJ, Troe J, Wallington TJ (2008) Evaluated kinetic and photochemical data for atmospheric chemistry: volume IV – gas phase reactions of organic halogen species. Atmos Chem Phys 8:4141–4496
6. Kesselmeier J, Staudt M (1999) Biogenic volatile organic compounds (VOC): an overview on emission, physiology and ecology. J Atmos Chem 33:23–88
7. König G, Brunda M, Puxbaum H, Hewitt CN, Duckham SC, Rudolph J (1995) Relative contribution of oxygenated hydrocarbons to the total biogenic VOC emissions of selected mid-European agricultural and natural plant species. Atmos Environ 29:861–874
8. Yokouchi Y, Muka H, Nakajima K, Ambe Y (1990) Semi-volatile aldehydes as predominant organic gases in remote areas. Atmos Environ 24A:439–442
9. Grosjean E, Grosjean D, Fraser MP, Cass R (1996) Air quality model evaluation data for organics. 2. C_1-C_{14}carbonyls in Los Angeles air. Environ Sci Tech 30:2687–2703
10. Kawamura K, Steinberg S, Kaplan IR (2000) Homologous series of C_1–C_{10} monocarboxylic acids and C_1–C_6 carbonyls in Los Angeles air and motor vehicle exhausts: North America. Atmos Environ 34:4175–4191
11. Lary DJ, Shallcross DE (2000) Central role of carbonyl compounds in atmospheric chemistry. J Geophys Res 105:19771–19778
12. Mellouki A, Le Bras G, Sidebottom H (2003) Kinetics and mechanisms of the oxidation of oxygenated organic compounds in the gas phase. Chem Rev 103:5077–5096
13. Calvert JG, Mellouki A, Orlando JJ, Pilling MJ, Wallington TJ (2011) The mechanisms of atmospheric oxidation of the oxygenates. Oxford University Press, New York
14. Lee EKC, Lewis RS (1980) Photochemistry of simple aldehydes and ketones in the gas phase. In: Pitts Jr. JN, Hammond GS, Gollnick K (eds) Advances in photochemistry, vol 12. Wiley, New York, pp 1–96
15. Sato K, Klotz B, Taketsugu T, Takayanagi T (2004) Kinetic measurements for the reactions of ozone with crotonaldehyde and its methyl derivatives and calculations of transition-state theory. Phys Chem Chem Phys 6:3969–3976
16. Grosjean D, Grosjean E (1998) Rate constants for the gas-phase reaction of ozone with unsaturated oxygenates. Int J Chem Kinet 30:21–29

17. Atkinson R, Aschmann SM, Winer AM, Pitts JN Jr (1981) Rate constants for the gas-phase reactions of O_3 with a series of carbonyls at 296 K. Int J Chem Kinet 13:1133–1142
18. Grosjean E, Grosjean D, Seinfeld JH (1996) Gas-phase reaction of ozone with *trans*-2-hexenal, *trans*-2-hexenyl acetate, ethylvinyl ketone, and 6-methyl-5-hepten-2-one*Int*. J Chem Kinet 28:373–382
19. Atkinson R, Arey J, Aschamann SM, Corchnoy SB, Shu Y (1995) Rate constants for the gas-phase reactions of *cis*-3-Hexen-1-ol, *cis*-3-Hexenylacetate, *trans*-2-Hexenal, and Linalool with OH and NO_3 radicals and O_3 at 296 ± 2 K, and OH radical formation yields from the O_3 reactions. Int J Chem Kinet 27:941–955
20. Albaladejo J, Ballesteros B, Jiménez E, Martin P, Martínez E (2002) A PLP-LIF kinetic study of the atmospheric reactivity of a series of C_4–C_7 saturated and unsaturated aliphatic aldehydes with OH. Atmos Environ 36:3231–3239
21. D'Anna B, Andresen Ø, Gefen Z, Nielsen CJ (2001) Kinetic study of OH and NO_3 radical reactions with 14 aliphatic aldehydes. Phys Chem Chem Phys 3:3057–3063
22. Pagagni C, Arey J, Atkinson R (2000) Rate constants for the gas phase reactions of a series of C_3–C_6 aldehydes with OH and NO_3 radicals. Int J Chem Kinet 32:79–84
23. Semmes DH, Ravishankara AR, Gump-Perkins CA, Wine PH (1985) Kinetics of the reactions of hydroxyl radical with aliphatic aldehydes. Int J Chem Kinet 17:303–313
24. Audley GJ, Baulch DL, Campbell IM, Breitenbach LP (1981) Gas-phase reactions of hydroxyl radicals with aldehydes in flowing $H_2O_2 + NO_2 + CO$ mixtures. J Chem Soc Faraday Trans 77:2541–2549
25. Kerr JA, Sheppard DW (1981) Kinetics of the reactions of hydroxyl radicals with aldehydes studied under atmospheric conditions. Environ Sci Tech 15:960–963
26. Magneron I, Thévenet R, Mellouki A, Moortgat GK (2002) A study of the photolysis and OH-initiated oxidation of acrolein and trans-crotonaldehyde. J Phys Chem A 106:2526–2537
27. Ullerstam M, Ljungström E, Langer S (2001) Reactions of acrolein, crotonaldehyde and pivalaldehyde with Cl atoms: structure-activity relationship and comparison with OH and NO_3 reactions. Phys Chem Chem Phys 3:986–992
28. Atkinson R, Aschmann SM, Pitts JN Jr (1983) Kinetics of the gas-phase reactions of OH radicals with a series of alpha, beta-unsaturated carbonyls at 299 ± 2 K. Int J Chem Kinet 15:75–81
29. Thévenet R, Mellouki A, Le Bras G (2000) Kinetics of OH and Cl reactions with a series of aldehydes. Int J Chem Kinet 32:676–685
30. Jiménez E, Lanza B, Antiñolo M, Albaladejo J (2009) Influence of temperature on the chemical removal of 3-methylbutanal, *trans*-2-methyl-2-butenal, and 3-methyl-2-butenal by OH radicals in the troposphere. Atmos Environ 43:4043–4049
31. Glasius M, Galogirou A, Jensen NR, Hjorth J, Nielsen CJ (1997) Kinetic study of gas-phase reactions of pinonaldehyde and structurally related compounds. Int J Chem Kinet 29:527–533
32. Davies ME, Gilles MK, Ravishankara AR, Burkholder JB (2007) Rate coefficients for the reaction of OH with (E)-2-pentenal, (E)-2-hexenal, and (E)-2-heptenal. Phys Chem Chem Phys 9:2240–2248
33. Tuazon EC, Aschmann SM, Nishino N, Arey J, Atkinson R (2005) Kinetic and products of the OH radical-initiated reaction of 3-methyl-2-butenal. Phys Chem Chem Phys 7:2298–2304
34. Jiménez E, Lanza B, Martínez E, Albaladejo J (2007) Daytime tropospheric loss of hexanal and trans-2-hexenal/ OH kinetics and UV photolysis. Atmos Chem Phys 7:1565–1574
35. Gao T, Andino JM, Rivera CC, Francisco Márquez M (2009) Rate constants of the gas-phase reactions of OH radicals with trans-2-hexenal, trans-2-octenal and trans-2-nonenal. Int J Chem Kinet 41:483–489
36. Smith IWM, Ravishankara AR (2002) Role of hydrogen-bonded intermediates in the bimolecular reactions of the hydroxyl radical. J Phys Chem A 106:4798–4807
37. Singh S, Hernandez S, Ibarra Y, Hasson AS (2009) Kinetics and mechanism of the reactions of *n*-butanal and *n*-pentanal with chlorine atoms. Int J Chem Kinet 41:133–141

38. Wu H, Mu Y (2007) Rate constants and products for the reaction of Cl atom with n-Butyraldehyde. Int J Chem Kinet 39:168–174
39. Cuevas CA, Notario A, Martínez E, Albaladejo J (2006) Temperature-dependence study of the gas-phase reactions of atmospheric Cl atoms with a series of aliphatic aldehydes. Atmos Environ 40:3845–3854
40. Wang W, Ezell MJ, Ezell AA, Soskin G, Finlayson-Pitts BJ (2002) Rate constants for the reactions of chlorine atoms with a series of unsaturated aldehydes and ketones at 298 K: structure and reactivity. Phys Chem Chem Phys 4:1824–1831
41. Iwasaki E, Nakayama T, Matsumi Y, Takahashi K, Wallington TJ, Hurley MD, Kaiser EW (2008) Kinetics and mechanism of the reaction of chlorine atoms with n-Pentanal. J Phys Chem A 112:1741–1746
42. Rodríguez D, Rodríguez A, Notario A, Aranda A, Diaz de Mera Y, Martínez E (2005) Kinetic study of the gas-phase reaction of atomic chlorine with a series of aldehydes. Atmos Chem Phys 4:3433–3440
43. Calvert JG, Derwent RG, Orlando JJ, Tyndall GS, Wallington TJ (2008) Mechanisms of atmospheric oxidation of the alkanes. Oxford University press, New York
44. Finlayson-Pitts BJ, Pitts Jr. JN (2000) Chemistry of the upper and lower atmosphere. Academic Press, New York
45. Wayne RP (2000) Chemistry of atmospheres, 3rd edn. Oxford University Press, New York
46. Groß CBM, Dillon TJ, Crowley JN (2014) Pressure dependent OH yields in the reactions of CH_3CO and $HOCH_2CO$ with O_2. Phys Chem Chem Phys 16:10990–10998
47. Groß CBM, Dillon TJ, Schuster G, Lelieveld J, Crowley JN (2014) Direct kinetic study of OH and O_3 formation in the reaction of $CH_3C(O)O_2$ with HO_2. J Phys Chem A 118:974–985
48. Orlando JJ, Tyndall GS (2002) Mechanisms for the reactions of OH with two unsaturated aldehydes: crotonaldehyde and acrolein. J Phys Chem A106:12252–12259
49. Tadić J, Juranić I, Moortgat GK (2001) Pressure dependence of the photooxidation of selected carbonyl compounds in air: *n*-butanal and *n*-pentanal. J Photochem Photobiol A Chem 143:169–179
50. Tadić J, Juranić I, Moortgat GK (2001) Photooxidation of *n*-hexanal in air. Molecules 6:287–299
51. Madronich S, Flocke S (1999) The role of solar radiation in atmospheric chemistry. In: Handbook of environmental chemistry/ Springer-Verlag, Heidelberg
52. Calvert JG, Atkinson R, Kerr JA, Madronich S, Moortgat GK, Wallington TJ, Yarwood G (2000) The mechanisms of atmospheric oxidation of the alkenes. Oxford University Press, New York
53. Lanza B, Jiménez E, Ballesteros B, Albaladejo J (2008) Absorption cross section determination of biogenic C_5-aldehydes in the actinic region. Chem Phys Lett 454:184–189
54. Keller-Rudek H, Moortgat GK, Sander R, Sörensen R (2013) The MPI-Mainz UV/VIS spectral atlas of gaseous molecules of atmospheric interest. Earth SystSci Data 5:365–373
55. Noelle A, Hartmann GK, Fahr A, Lary D, Lee Y-P, Limao-Vieira et al (2013) UV/Vis + spectra data base. http://www.science-softcon.de/
56. Zhu L, Cronin T, Narang A (1999) Wavelength-dependent photolysis of *i*-pentanal and *t*-pentanal from 280 to 330 nm. J Phys Chem A 103:7248–7253
57. O'Connor MP, Wenger JC, Mellouki A, Wirtz K, Muñoz A (2006) The atmospheric photolysis of E-2-hexenal, Z-3-hexenal and E, E-2,4-hexadienal. Phys Chem Chem Phys 8:5236–5246
58. Moortgat GK (2001) Important photochemical processes in the atmosphere. Pure Appl Chem 73:487–490
59. Moortgat GK, Wirtz K, Hjorth J, Ljungstroem E, Ruppert L, Hayman G, Mellouki W (2002) Evaluation of radical sources in atmospheric chemistry through chamber and laboratory studies: RADICAL (Final SCA Project Report)

60. Tadić J, Juranić I, Moortgat GK (2002) Photooxidation of *n*-heptanal in air: *Norrish t*ype I and II processes and quantum yield total pressure dependency. J Chem Soc Perkin Trans 2:135–140
61. Cronin TJ, Zhu L (1998) Dye laser photolysis of *n*-pentanal from 280 to 330 nm. J Phys Chem A 102:10274–10279
62. Treacy J, El Hag M, O'Farrell D, Sidebottom H (1992) Reactions of ozone with unsaturated organic compounds. Ber Bunsenges Phys Chem 96:422–4227
63. Grosjean D, Grosjean E, Williams EL II (1993) Rate constants for the gas-phase reactions of ozone with unsaturated alcohols, esters, and carbonyls. Int J Chem Kinet 25:783–794
64. Neeb, P.; Kolloff, A.; Koch, S.; Moortgat, G. K. (1998) Rate constants for the reactions of methyl vinyl ketone, methacrolein, methacrylic acid, and acrylic acid with ozone. *Int. J. Chem. Kinet*.30:769–776
65. Greene CR, Atkinson R (1994) Rate constants for the gas-phase reactions of O_3 with a series of cycloalkenes and α,β-unsaturated ketones at 296 ± 2 K. Int J Chem Kinet 26:37–44
66. Zhou S, Barnes I, Zhu T, Bejan I, Albu M, Benter T (2008) Atmospheric chemistry of acetylacetone. Environ Sci Tech 42:7905–7910
67. Grosjean E, Grosjean D (1999) The reaction of unsaturated aliphatic oxygenates with ozone. J Atmos Chem 32:205–232
68. Wang K, Maofa Ge M, Weigang Wang W (2010) Kinetics of the gas-phase reactions of 5-hexen-2-one with OH and NO_3 radicals and O_3. Chem Phys Lett 490:29–33
69. Winer AM, Lloyd AC, Darnall KR, Atkinson R, Pitts JN Jr (1976) Relative rate constants for the reaction of the hydroxyl radical with selected ketones, chloroethenes and monoterpene hydrocarbons. J Phys Chem 80:1635–1639
70. Cox RA, Derwent RG, Williams MR (1980) Atmospheric photooxidation reactions. Rates reactivity, and mechanisms for reaction of organic compounds with hydroxyl radicals. Environ Sci Tech 14:57–61
71. Cox RA, Patrick KF, Chant SA (1981) Mechanism of atmospheric photooxidation of organic compounds. Reactions of alkoxy radicals in oxidation of n-butane and simple ketones. Environ Sci Tech 15:587–592
72. Edney EO, Kleindienst TE, Corse EW (1986) Room temperature rate constants for the reaction of OH with selected chlorinated and oxygenated hydrocarbons. Int J Chem Kinet 18:1355–1371
73. Wallington TJ, Kurylo MJ (1987) Flash photolysis resonance fluorescence investigation of the gas-phase reactions of OH radicals with a series of aliphatic ketones over the temperature range 240–440 K. J Phys Chem 91:5050–5054
74. Le Calvé S, Hitier D, Le Bras G, Mellouki A (1998) Kinetic studies of OH reactions with a series of ketones. J Phys Chem A 102:4579–4584
75. Jiménez E, Ballesteros B, Martínez E, Albaladejo J (2005) Tropospheric reaction of OH with selected linear ketones: kinetic studies between 228 and 405 K. Environ Sci Tech 39:814–820
76. Carr SA, Baeza-Romeo MT, Blitz MA, Price BJS, Seakins PW (2008) Ketone photolysis in the presence of oxygen: a useful source of OH for flash photolysis kinetics experiments. Int J Chem Kinet 40:504–514
77. Kleindienst TE, Harris GW, Pitts JN Jr (1982) Rates and temperature dependence of the reaction of OH with isoprene, its oxidation products, and selected terpenes. Environ Sci Technol 16:844–846
78. Gierczak T, Burkholder JB, Talukdar RK, Mellouki A, Barone SB, Ravishankara AR (1997) Atmospheric fate of methyl vinyl ketone and methacrolein. J Photochem Photobiol A110:1–10
79. Aschmann SM, Atkinson R (1998) Kinetics of the gas-phase reactions of the OH radical with selected glycol ethers, glycols, and alcohols. Int J Chem Kinet 30:533–540
80. Chuong B, Stevens PS (2003) Kinetics of the OH + methyl vinyl ketone and OH + methacrolein reactions at low pressure. J Phys Chem A 107:2185–2191

81. Chuong B, Stevens PS (2004) Measurements of the kinetics of the OH-initiated oxidation of methyl vinyl ketone and methacrolein. Int J Chem Kinet 36:12–25
82. Holloway AL, Treacy J, Sidebottom H, Mellouki A, Daële V, Le Bras G, Barnes I (2005) Rate coefficients for the reactions of OH radicals with the keto/enol tautomers of 2,4-pentanedione and 3-methyl-2,4-pentanedione, allyl alcohol and methyl vinyl ketone using the enols and methyl nitrite as photolytic sources of OH. J Photochem Photobiol A Chem 176:183–190
83. Atkinson R, Aschmann SM, Carter WPL, Pitts Jr. JN (1982) Rate constants for the gas-phase reaction of OH radicals with a series of ketones at 299 ± 2 K. Int Chem Kinet 14:839–847
84. Atkinson R, Aschmann SM (1988) Comment on "Flash photolysis resonance – fluorescence investigation of the gas-phase reactions of OH radicals with a series of aliphatic ketones over the temperature range 240–440 K. J Phys Chem 92:4008
85. Atkinson R, Tuazon EC, Aschmann SM (2000) Atmospheric chemistry of 2-pentanone and 2-heptanone. Environ Sci Tech 34:623–631
86. Blanco MB, Barnes I, Wiesen P (2012) Kinetic investigation of the OH radical and Cl atom initiated degradation of unsaturated ketones at atmospheric pressure and 298 K. J Phys Chem A 116:6033–6040
87. Blanco MB, Teruel MA (2011) Atmospheric photodegradation of ethyl vinyl ketone and vinyl propionate initiated by OH radicals. Chem Phys Lett 502:159–162
88. Jiménez E, Lanza B, Antiñolo M, Albaladejo J (2009) Photooxidation of leaf-wound oxygenated compounds, 1-penten-3-ol, (*Z*)-3-hexen-1-ol, and 1-penten-3-one, initiated by OH radicals and sunlight. Environ Sci Tech 43:1831–1837
89. Dagaut P, Wallington TJ, Liu R, Kurylo MJ (1988) A kinetic investigation of the gas-phase reactions of OH radicals with cyclic ketones and diones: mechanistic insights. J Phys Chem 92:4375–4377
90. Wallington TJ, Andino JM, Ball JC, Japar SM (1990) Fourier transform infrared studies of the reaction of Cl atoms with PAN, PPN, CH_3OOH, HCOOH, CH_3COCH_3 and $CH_3COC_2H_5$ at 295 ± 2 K. J Atmos Chem 10:301–313
91. Notario A, Mellouki A, Le Bras G (2000) Rate constants for the gas-phase reactions of chlorine atoms with a series of ketones. Int J Chem Kinet 32:62–66
92. Albaladejo J, Notario A, Cuevas CA, Jiménez E, Cabañas B, Martínez E (2003) Gas-phase chemistry of atmospheric Cl atoms: *a PLP-RF* kinetic study with a series of ketones. Atmos Environ 37:455–463
93. Cuevas CA, Notario A, Martínez E, Albaladejo J (2004) A kinetic study of the reaction of Cl with a series of linear and ramified ketone*s as a functio*n of temperature. Phys Chem Chem Phys 6:2230–2236
94. Taketani F, Matsumi Y, Wallington TJ, Hurley MD (2006) Kinetics of the gas phase reactions of chlorine atoms with a series of ketones. Chem Phys Lett 431:257–260
95. Kaiser EW, Wallington TJ (2007) Rate constants for the reaction of Cl with a series of C_4 to C_6 ketones using the relative rate method. J Phys Chem A 111:10667–10670
96. Takahashi K, Iwasaki E, Matsumi Y, Wallington TJ (2007) Pulsed laser photolysis vacuum UV laser-induced fluorescence kinetic study of the gas-phase reactions of $Cl(^2P_{3/2})$ atoms with C_3-C_6 ketones. J Phys Chem A 111:1271–1276
97. Zhao Z, Huskey DT, Nicovich JM, Wine PH (2008) Temperature-dependent kinetics study of the gas-phase reactions of atomic chlorine with acetone, 2-butanone, and 3-pentanone. Int J Chem Kinetic 40:259–267
98. Kaiser EW, Wallington TJ, Hurley MD (2009) Products and Mechanism of the reaction of Cl with butanone in N_2/O_2 diluent at 297−526 K. J Phys Chem A 113:2424–2437
99. Canosa-Mass CE, Hutton-Squire HR, King MD, Stewart DJ, Thompson KC, Wayne RP (1999) J Atmos Chem 34:163–170
100. Finlayson-Pitts BJ, Keoshian CJ, Buehler B, Ezell AA (1999) Kinetics of reaction of chlorine atoms with some biogenic organics. Int J Chem Kinet 31:491–499

101. Canosa-Mas CE, Cotter ESN, Duffy J, Thompson KC, Wayne RP (2001) The reactions of atomic chlorine with acrolein, methacrolein and methyl vinyl ketone. Phys Chem Chem Phys 3:3075–3084
102. Orlando JJ, Tyndall GS, Apel EC, Riemer DD, Paulson SE (2003) Rate coefficients and mechanisms of the reaction of Cl-atoms with a series of unsaturated hydrocarbons under atmospheric conditions. Int J Chem Kinet 35:334–353
103. Aranda A, Díaz de Mera Y, Rodríguez YA, Morales L, Martínez E (2004) Kinetic study of the gas-phase reactions of Cl radicals with 3-pentanone and 3-hexanone. J Phys Chem A 108:7027–7031
104. Kaiser EW, Wallington TJ, Hurley MD (2010) Products and mechanism of the reaction of chlorine atoms with 3-pentanone in 700–950 Torr of N_2/O_2 diluent at 297–515 K. J Phys Chem A 114:343–354
105. Teruel MA, Achad M, Blanco MB (2009) Kinetic study of the reactions of Cl atoms with unsaturated carbonyl compounds at atmospheric pressure and structure activity relations (SARs). Chem Phys Lett 479:25–29
106. Aschmann SM, Atkinson R (1995) Rate constants for the gas-phase reactions of alkanes with Cl atoms at 296 ± 2 K. Int J Chem Kinet 27:613–622
107. Ezell MJ, Wang W, Ezell AA, Soskin G, Finlayson-Pitts BJ (2002) Kinetics of reactions of chlorine atoms with a series of alkenes at 1 atm and 298 K. Phys Chem Chem Phys 4:5813–5820
108. Johnson D, Marston G (2008) The gas-phase ozonolysis of unsaturated volatile organic compounds in the troposphere. Chem Soc Rev 37:699–716
109. Welz O, Savee JD, Osborn DL, Vasu SS, Percival CJ, Shallcross DE, Taatjes CJ (2012) Direct Kinetic measurements of Criegee intermediate (CH_2OO) formed by reaction of CH_2I with O_2. Science 335:204–207
110. Krol M, van Leeuwen PJ, Lelieveld J (1998) Global OH trend inferred from methylchloroform measurements. J Geophys Res Atmos 103:10697–10711
111. Singh HB, Thakur AN, Chen YE, Kanakidou M (1996) Tetrachloroethylene as an indicator of low CI atom concentrations in the troposphere. Geophys Res Lett 23:1529–1532
112. Spicer CW, Chapman EG, Finlayson-Pitts BJ, Plastridge RA, Hubbe JM, Fast JD, Berkowitz CM (1998) Unexpectedly high concentrations of molecular chlorine in coastal air. Nature 394:353–356
113. Carter WPL, Atkinson R (1987) Computer modelling study of incremental hydrocarbon reactivity. Environ Sci Technol 21:670–679
114. Carter WPL (1994) Development of ozone reactivity scales for volatile organic compounds. J Air Waste Manag Assoc 44:881–899
115. Derwent RG, Jenkin ME, Saunders SM (1996) Photochemical ozone creation potentials for a large number of reactive hydrocarbons under European conditions. Atmos Environ 30:181–199
116. Derwent RG, Jenkin ME, Saunders SM, Pilling MJ (1998) Photochemical ozone creation potentials for organic compounds in Northwest Europe calculated with a master chemical mechanism. Atmos Environ 32:2429–2441
117. Derwent RG, Jenkin ME, Passant NR, Pilling MJ (2007) Photochemical ozone creation potentials (POCPs) for different emission sources of organic compounds under European conditions estimated with a Master Chemical Mechanism. Atmos Environ 41:2570–2579
118. Jenkin ME (1998) Photochemical ozone and PAN creation potentials: rationalisation and methods of estimation. AEA Technology plc, Report AEAT-4182/20150/003, AEA Technology plc. National Environmental Technology Centre, Culham
119. Ervens B, Kreidenweis SM (2007) SOA Formation by biogenic and carbonyl compounds: data evaluation and application. Environ Sci Technol 41:3904–3910
120. Carlton AG, Wiedinmyer C, Kroll JH (2009) A review of secondary organic aerosol (SOA) formation from isoprene. Atmos Chem Phys 9:4987–5005

121. Zhao DF, Kaminski M, Schlag P, Fuchs H, Acir I-H, Bohn B, Häseler R, Kiendler-Scharr A, Rohrer F, Tillmann R, Wang MJ, Wegener R, Wildt J, Wahner A, Mentel TF (2014) Secondary Organic Aerosol (SOA) formation from hydroxyl radical oxidation and ozonolysis of monoterpenes. Atmos Chem Phys Discuss 14:12591–12634
122. Kourtchev IS, Fuller J, Giorio C, Healy RM, Wilson E, O'Connor I, Wenger JC, McLeod M, Aalto J, Ruuskanen TM, Maenhaut W, Jones R, Venables DS, Sodeau JR, Kulmala M, Kalberer M (2014) Molecular composition of biogenic secondary organic aerosols using ultrahigh-resolution mass spectrometry: comparing laboratory and field studies. Atmos Chem Phys 14:2155–2167
123. Volkamer R, Jimenez JL, San Martini F, Dzepina K, Zhang Q, Salcedo D, Molina LT, Worsnop DR, Molina MJ (2006) Secondary organic aerosol formation from anthropogenic air pollution: Rapid and higher than expected. Geophys Res Lett 33, L17811
124. Hu Q-H, Xie Z-Q, Wang X-M, Kang H, He Q-F, Zhang P (2013) Secondary organic aerosols over oceans via oxidation of isoprene and monoterpenes from Arctic to Antarctic. Nat Sci Reports 3:2280
125. Chan AWH, Chan MN, Surratt JD, Chhabra PS, Loza CL, Crounse JD, Yee LD, Flagan RC, Wennberg PO, Seinfeld JH (2010) Role of aldehyde chemistry and NO_x concentrations in secondary organic aerosol formation. Atmos Chem Phys 10:7169–7188
126. Barsanti KC, Pankow JF (2004) Thermodynamics of the formation of atmospheric organic particulate matter by accretion reactions – part 1: aldehydes and ketones. Atmos Environ 38:4371–4382
127. Jang M, Kamens RM (2001) Atmospheric Secondary aerosol formation by heterogeneous reactions of aldehydes in the presence of a sulfuric acid aerosol catalyst. Environ Sci Technol 35:4758–4766
128. Kwok ESC, Atkinson R (1995) Estimation of hydroxyl radical reaction rate constants for gas-phase organic compounds using a structure-reactivity relationship: an update. Atmos Environ 29:1685–1695
129. Pfrang C, King MD, Canosa-Mas CE, Mark Flugge M, Wayne RP (2007) Gas-phase rate coefficients for the reactions of NO_3, OH and O3with α, β-unsaturated esters and ketones: structure reactivity relations (SARs). Atmos Environ 41:1792
130. Kerdouci J, Picquet Varrault B, Doussin J-F (2010) prediction of rate constants for gas-phase reactions of nitrate radical with organic compounds: a new structure-activity relationship. Chem Phys Chem 11:3909–3920

Night-Time Atmospheric Reactivity of Some Oxygenated Organic Compounds

B. Cabañas, P. Martín, S. Salgado, I. Colmenar, M-P. Gallego Iniesta, E. Martínez, A. Moreno, and A. Tapia

Abstract The nitrate radical (NO_3) is the most important atmospheric oxidant during the night-time for organic volatile compounds. In the review reported here, the available kinetic and product data for nitrate radical reactions with a series of oxygenated volatile organic compounds (OVOCs) are reviewed. The results cover the reactivity of NO_3 towards unsaturated aldehydes, aliphatic alcohols and acrylate esters. The kinetic results obtained by different research groups on using various experimental techniques are compared and discussed. Trends in reactivity are analyzed, and studies on the primary reaction products, when available, are presented. The reaction mechanisms elucidated from the kinetic and product data are presented and discussed.

Kinetic data for the reactions of the OVOCS reviewed in this chapter with atmospheric oxidants are necessary to obtain a realistic representation of the chemistry of these compounds in tropospheric models, which are used to assess the impact of contaminants on air quality. The rate coefficients for the reactions of the oxidants with the OVOCs can be employed to calculate the tropospheric lifetimes of the OVOCs in the atmosphere with respect to each oxidant. The lifetimes of the reviewed compounds in their reactions with NO_3 are summarized in this chapter, and the atmospheric relevance of the loss processes is analyzed in comparison to losses through reactions with other important atmospheric oxidants.

Keywords Gas-phase reactivity, Night-time reactivity, NO_3 radical, Oxygenated compounds

B. Cabañas, P. Martín (✉), S. Salgado, I. Colmenar, M.-P.G. Iniesta, E. Martínez, A. Moreno, and A. Tapia
Departamento de Química Física, Facultad de Ciencias y Tecnologías Químicas, Universidad de Castilla La Mancha, Avda. Camilo José Cela S/N, 13071 Ciudad Real, Spain

Instituto de Combustión y Contaminación Atmosférica (ICCA), Universidad de Castilla La Mancha, Camino Moledores S/N, 13071 Ciudad Real, Spain
e-mail: mariapilar.martin@uclm.es

E. Jiménez et al. (eds.), *Environment, Energy and Climate Change I: Environmental Chemistry of Pollutants and Wastes*, Hdb Env Chem (2015) 32: 105–134,
DOI 10.1007/698_2014_283,
Published online: 16 September 2014

Contents

1 Introduction

Atmospheric chemistry has been studied since the eighteenth century with the primary aim of identifying the main components of the atmosphere, which include nitrogen, oxygen, water and CO_2. Over the decades, these studies have been extended to other aspects, but atmospheric chemistry has long been associated with daytime phenomena such as the formation of ozone and secondary aerosols. The discovery of the nitrate radical (NO_3) in the nocturnal troposphere and stratosphere [1, 2] clearly showed that chemistry was also taking place at night. Only in the past decade has it been recognized that the nocturnal radical chemistry of NO_3 and related species such as N_2O_5 can have a much more marked effect than previously thought and such chemistry has an impact on a number of key atmospheric phenomena.

The nitrate radical was probably the first radical species to be identified positively, but it was not until 1958 that Schott and Davidson monitored concentrations of NO_3 directly by absorption spectroscopy in kinetics experiments [3]. The first studies on the reactions of NO_3 with organic species were performed by Morris and Niki in the early 1970s [4].

We now know that this radical is mainly produced in the atmosphere by the reaction between O_3 and NO_2. During the day, NO_3 is rapidly photolysed and this leads to low daytime concentrations [5, 6]. However, during the night, NO_3 can accumulate and a rapid equilibrium with N_2O_5 is established through the production of N_2O_5 in the reaction $NO_3 + NO_2$, which is followed by rapid thermal decomposition of N_2O_5 back to NO_3 and NO_2 [5, 6].

The nitrate radical can be consumed by its reaction with NO and NO_2 and by unimolecular decomposition [7]. Tropospheric levels of the nitrate radical have been measured in recent years using a variety of different techniques and in different environments (e.g. urban and forest). In the recent review by Brown and Stutz [6] on night-time radical observation and chemistry, a brief description of the analytical techniques and methods commonly used for their analysis is given and the database of nocturnal radicals is reviewed. The results include field measurements over the last 30 years and estimations based on the measurement of other species. Recently, the mechanisms involved in the atmospheric oxidation of oxygenates have also been reviewed [8].

The NO_3 radical plays an important role in tropospheric chemistry as it can react with hydrocarbons and oxygenated volatile organic compounds (VOCs) such as alcohols, ethers, esters, ketones and aldehydes. The reactions occur by a mechanism that involves either initial abstraction of a hydrogen atom or the addition of NO_3 to a double bond in the compound. For some compounds, both mechanisms may be operative:

$$NO_3 + RH \rightarrow HNO_3 + R \quad (1)$$

$$NO_3 + > C = C < \rightarrow > C(ONO_2)C < \quad (2)$$

The rate coefficients of these reactions cover a very wide range, with values varying from 10^{-12} to 10^{-17} cm^3 $molecule^{-1}$ s^{-1}. Among the fastest reactions are those involving unsaturated aldehydes and vinyl ethers. The reactions of NO_3 with VOCs may lead to the formation of harmful compounds such as peroxyacetyl nitrate (PAN) and other nitrates and oxidized compounds. Furthermore, the products of NO_3 reactions can also act as temporary reservoirs of NO_x in the atmosphere. Moreover, the nitrate radical can contribute significantly to the generation of secondary organic aerosols (SOA) through its reactions with alkenes and terpenes [9]. However, the impact of this chemistry on regional and global aerosol levels is still poorly understood [6].

As a conclusion, nocturnal chemistry is prevalent in many environments in the atmosphere and it has an impact on a number of central chemical systems, such as those concerned with sulphur, nitrogen, halogens and aerosol. In the last few decades, numerous studies on the reactivity of the NO_3 radical with different gas species in the atmosphere have been reported. In this respect, it is worth noting the extensive review by Wayne et al. [5] and the recent review by Brown and Stutz [6].

In the review presented here, the results obtained recently by our research group are summarized along with others related to the reactivity of this important atmospheric radical with a series of oxygenated volatile organic compounds (OVOCs), namely, unsaturated aldehydes, aliphatic alcohols and acrylate esters in order to assess the relevance of these reactions in global atmospheric chemistry.

2 Kinetics and Mechanisms of the NO_3-Initiated Oxidation of Some Oxygenated Compounds

2.1 Alcohols

Alcohols are emitted into the atmosphere by a large number of anthropogenic and natural processes. These compounds are emitted by grassland and agricultural vegetation [10] and by microbiological activity and plants [11]. Anthropogenic emissions of saturated alcohols are mainly due to the use of such compounds as motor vehicle fuels, fuel additives and solvents in various industries [12]. These

volatile organic compounds are also produced in the atmosphere by the photooxidation of hydrocarbons [13, 14].

The oxidation of alcohols leads to the production of aldehydes, ketones and organic nitrates as the major products [15]. Therefore, the release of saturated alcohols is likely to contribute to the formation of ozone and other components of photochemical smog, such as aldehydes, ketones and PANs, in urban areas. The main atmospheric degradation process for saturated alcohols in the troposphere, and for oxygenated organic compounds in general, is the reaction with OH radicals [16–18]. During the night-time, however, reactions with NO_3 radicals are also expected to contribute to the degradation of these compounds, although the gas-phase reactions of NO_3 radicals with saturated alcohols studied to date are generally slow [19, 20]. The reactions of O_3 with saturated alcohols are too slow ($k \leq 10^{-20}$ cm^3 molecule^{-1} s^{-1}; [21]) to make any significant contribution to the degradation of saturated alcohols. Cl atoms react faster with most hydrocarbons than OH radicals, with the rate coefficients for reactions between Cl atoms and organic compounds typically about one or two orders of magnitude higher than the corresponding values for OH reactions [22]. This high reactivity implies that chlorine can play an important role in atmospheric chemistry in areas where its atmospheric concentration is sufficiently high, for example, in the marine boundary layer and some industrial regions.

The largest aliphatic alcohol investigated to date is 2-ethyl-1-hexanol. This alcohol has attracted particular attention because it has been detected in indoor air at relatively high concentrations [23] and is also a potentially significant pollutant in outdoor air as it has been identified as one of the top 20 chemicals in concentration in biodiesel vapours [24].

2.1.1 Rate Coefficients for NO_3 Reactions

A summary of the experimental kinetic information obtained to date for the reactions of NO_3 radicals with aliphatic alcohols is given in Table 1. The rate coefficients determined for the reactions of NO_3 with these alcohols are generally around 10^{-15} cm^3 molecule^{-1} s^{-1}, which shows that these reactions are slow. Absolute rate studies conducted to date have proven to be problematical due to the occurrence of secondary reactions, which lead to erroneously high rate coefficients. This is the case for the rate coefficients determined for methanol and ethanol by absolute techniques at room temperature [25] and also as a function of temperature to give the corresponding Arrhenius expressions [19, 26]. For methanol, the Arrhenius expression preferred by the IUPAC Panel is based on the work of Langer and Ljungström [19], $k = 9.4 \times 10^{-13} \exp(-2{,}650/T)$ over the range 250–370 K and $k = 1.3 \times 10^{-16}$ cm^3 molecule^{-1} s^{-1} at 298 K with an uncertainty of ~50%. However, it is possible that these values are still high due to potential errors related to secondary reactions in slow reaction systems on using absolute rate methods [28].

In the case of ethanol, the IUPAC recommended rate coefficient at 298 K, $k < 2 \times 10^{-15}$ cm^3 molecule^{-1} s^{-1}, is based on the upper limit of Wallington

Table 1 Room-temperature rate coefficients, temperature-dependent parameters and temperature ranges over which these data have been measured for the gas-phase reactions of NO_3 radicals with saturated alcohols

Organic	$A/10^{-12}$ cm^3 molecule^{-1} s^{-1}	$k_{(NO_3)}/10^{-15}$	T/K	–B/K	Temperature range/K	Reference	Technique
Methanol		0.13	298			Calvert et al. [8]	Evaluation
		≤0.6	298			Wallington et al. [25]	FP-A/AR
	1.25	0.21 ± 0.11	294	2,562 ± 241	294–473	Canosa-Mas et al. [26]	DF-A/AR
	0.936	0.13 ± 0.02	295	2,652 ± 312	258–367	Langer and Ljungström [19]	DF-A/AR
Ethanol		≤2	298			Calvert et al. [8]	Evaluation
		≤0.9	298			Wallington et al. [25]	FP-A/AR
	0.69 ± 0.12	0.18 ± 0.02	297	1,815 ± 419	273–367	Langer and Ljungström [19]	DF-A/AR
1-Propanol		≤2.10 ± 0.80	298			Chew et al. [27]	GC-FID/RR
2-Propanol		1.4	298			Calvert et al. [8]	Evaluation
		≤1.70 ± 0.60	298			Chew et al. [27]	GC-FID/RR
		≤2.3	298			Wallington et al. [25]	FP-A/AR
	1.54	3.13 ± 0.64	295	1,743 ± 1,009	273–367	Langer and Ljungström [19]	DF-A/AR
		1.40 ± 0.30	298			Calvert et al. [8]	Evaluation
1-Butanol		≤2.71 ± 0.99	298			Chew et al. [27]	GC-FID/RR
		1.87 ± 014	298			Moreno et al. [20]	FTIR/RR
2-Butanol		2.51 ± 0.42	298			Moreno et al. [20]	FTIR/RR
		≤2.50 ± 0.80	298			Chew et al. [27]	GC-FID/RR
		2	298			Calvert et al. [8]	Evaluation
2-Methyl-1-butanol		2.39 ± 0.20	298			Moreno et al. [20]	FTIR/RR
2-Methyl-2-butanol		1.57 ± 0.16	298			Moreno et al. [20]	FTIR/RR

(continued)

Table 1 (continued)

Organic	A/10^{-12} cm^3 $molecule^{-1}$ s^{-1}	$k_{(NO_3)}/10^{-15}$	T/K	–B/K	Temperature range/K	Reference	Technique
3-Methyl-1-butanol		2.28 ± 0.17	298			Moreno et al. [20]	FTIR/RR
3-Methyl-2-butanol		3.06 ± 0.52	298			Moreno et al. [20]	FTIR/RR
3,3-Dimethyl-1 butanol		1.80 ± 0.13	298			Moreno et al. [20]	FTIR/RR
2,3-Dimethyl-2 butanol		2.67 ± 0.30	298			Moreno et al. [20]	FTIR/RR
3,3-Dimethyl-2 butanol		3.52 ± 0.19	298			Moreno et al. [20]	FTIR/RR
4-Heptanol		$\leq 5.99 \pm 1.99$	298			Chew et al. [27]	GC-FID/ RR
2-Ethyl-1-hexanol		2.93 ± 0.92	298			Gallego-Iniesta et al. [23]	GC-FID/ RR

k in units of cm^3 $molecule^{-1}$ s^{-1}

Technique: *RR* relative rate, *AR* absolute rate, *FP-A* flash photolysis-absorption, *DF-A* discharge flow-optical absorption, *GC-FID* gas-chromatography flame ionization detection, *FTIR* Fourier transform infrared absorption spectroscopy

et al. [25], which is consistent with the rate coefficient at that temperature derived from the Arrhenius expression reported by Langer and Ljungström [19]. A recommendation has not been made for temperature dependence. In any case, and as mentioned above, the proposed values may be too high as a result of the possible occurrence of secondary reactions in the applied absolute rate methods.

The reactions of NO_3 with 1-propanol and 2-propanol were investigated by Chew et al. [27] using a relative kinetic technique to determine the rate coefficients. The experiments were carried out in a 7,500 L Teflon chamber at 298 ± 2 K and 740 Torr total pressure, and reactant concentrations were measured by gas chromatography. Chew et al. [27] also reported rate coefficients for the reactions of NO_3 with 1-butanol, 2-butanol and 4-heptanol. Reported values are considered upper limits because authors recognize possible interferences caused by losses of the alcohols via heterogeneous reaction with N_2O_5. Indicated uncertainties include the estimated overall uncertainties of the rate coefficient of reference compounds. The rate coefficient for the NO_3 + 2-propanol reaction determined by Chew et al. [27] is consistent with the upper limit reported by Wallington et al. [25], but a factor of two lower than the absolute value reported by Langer and Ljungström [19]. It has been suggested that the rate coefficient can be calculated from the acetone yield observed in the experiments by Chew et al. Using this acetone yield, 0.79 ± 0.09, and assuming an actual yield of unity, a rate coefficient of $k = 1.4 \times 10^{-15}$ cm^3 molecule^{-1} s^{-1} has been recommended at 298 K with an estimated uncertainty of $\pm 30\%$ [29]. No recommendation is given for the temperature dependence of k for 2-propanol since the only available temperature dependence study [19] might be affected by secondary chemistry [8]. The IUPAC recommendation for k for 2-butanol is derived from a combination of the rate coefficient and product yield of butanone measured by Chew et al. [27] assuming that the reaction occurs almost exclusively by H-atom abstraction from the tertiary C–H bond. This procedure leads to $k = 2.0 \times 10^{-15}$ cm^3 molecule^{-1} s^{-1} at 298 K [8].

Rate coefficients for the reactions of the NO_3 radical with 2-butanol, 2-methyl-2-butanol, 3-methyl-2-butanol and 2,3-dimethyl-2-butanol have been determined using the relative rate technique in a 50 L glass Pyrex photoreactor at room temperature in the pressure range 350–670 Torr, with monitoring carried out in situ by FTIR spectroscopy [20]. The room-temperature rate coefficients follow the trend $k_{\text{3-methyl-2-butanol}} > k_{\text{2,3-dimethyl-2-butanol}} = k_{\text{2-butanol}} > k_{\text{2-methyl-2-butanol}}$. The value obtained for 2-butanol is in good agreement with the upper limit proposed by Chew et al. [27] and also with the preferred value proposed by IUPAC [29]. The quoted errors in Table 1 are a combination of the 2σ statistical errors from the linear regression analysis and also errors caused by the uncertainty in the reference rate coefficients.

Rate coefficients for the reactions of the NO_3 radical with 1-butanol, 2-methyl-1-butanol, 3-methyl-1-butanol, 3,3-dimethyl-1-butanol and 3,3-dimethyl-2-butanol have recently been determined [30] using the same technique, conditions and experimental system that our previous work [20] the following trend in reactivity: $k_{\text{3,3-dimethyl-2-butanol}} > k_{\text{2-methyl-1-butanol}} \geq k_{\text{3-methyl-1-butanol}} > k_{\text{1-butanol}} \geq k_{\text{3,3-dimethyl-1-butanol}}$.

Concerning the reactivity of 2-ethyl-1-hexanol with NO_3 radicals, Gallego-Iniesta et al. reported that the measured rate coefficient was not as high as one would expect for compounds with such a long hydrocarbon chain [23]. The authors indicated that some steric impediment, i.e. the presence of the ethyl group, leads to some hindrance in the electrophilic attack of the oxidant. This effect is compensated by the increase in reactivity that would be expected on increasing the chain length.

2.1.2 Mechanisms of the NO_3-Initiated Oxidation of Alcohols

The reactions of saturated alcohols with atmospheric oxidants are expected to occur mainly by H-atom abstraction from the C–H groups along with H-atom abstraction from the O–H group to a much lesser extent [14]. This situation is consistent with the bond energies of O–H bonds (104 kcal mol^{-1}), which are much stronger than C–H bonds (94 kcal mol^{-1}).

The reaction of NO_3 with methanol and ethanol is expected to proceed almost totally by H-atom abstraction from the C–H bonds of the -CH_3 group in methanol and the –CH_2– group in ethanol. For higher alcohols, the reactions of 2-propanol and 2-butanol are expected to occur almost entirely by H-abstraction from the tertiary C–H bond [27]. The rate coefficients determined by Chew et al. [27] for a series of alcohols mentioned above increase with the hydrocarbon chain length and it was proposed that H-atom abstraction at the carbon atom to which the –OH group is attached is the initial reaction step, which leads to the formation of, for example, 2-butanone from 2-butanol.

In the most recent investigation of the reaction of NO_3 with 2-butanol and methylated analogues [20], it was also concluded that the reactions mainly occur by H-abstraction from the C–H bonds and that, as expected, the abstraction of a hydrogen atom attached to a tertiary carbon is faster than that of an H atom attached to a methylene or methyl group. These observations are consistent with the results of previous studies on the reactions of OH radicals with alcohols [16–18]. Consequently, the reactivity trend for the reactions of NO_3 with butanols can be explained in terms of the different types of hydrogen bonds in the hydrocarbon chain (>CH–, –CH_2– or –CH_3) [20]. Comparison of the reactivities of the alcohols towards NO_3 with those of the corresponding alkanes [31, 32] shows that the substitution of a –CH_3 group by an OH group enhances the reactivity of the resulting alcohol towards NO_3 by approximately one order of magnitude. This result is expected because oxygen is more electronegative than carbon and its ability to share a pair of electrons far outweighs the electron-withdrawing effect. Thus, the higher rate coefficients for the reactions of NO_3 with alcohols when compared to the corresponding alkanes demonstrate quite clearly the activating effect of the OH group towards electrophilic attack by oxidants [20].

Finally, it is important to emphasize that the trend in reactivity for butanols is similar to that observed for the reactions of other saturated alcohols with OH and NO_3 radicals, a finding that supports the assumption of a similar reaction mechanism [16–18, 20].

As an example of the expected reactivity, the reaction of the NO_3 radical with 3-methyl-2-butanol may involve up to four abstraction pathways [20]:

$$CH_3CH(OH)CH(CH_3)_2 + NO_3 \rightarrow (\cdot CH_2)CH(OH)CH(CH_3)_2 + HNO_3 \quad (3)$$

$$CH_3CH(OH)CH(CH_3)_2 + NO_3 \rightarrow CH_3(\cdot C)(OH)CH(CH_3)_2 + HNO_3 \quad (4)$$

$$CH_3CH(OH)CH(CH_3)_2 + NO_3 \rightarrow CH_3CH(OH)(C\cdot)(CH_3)_2 + HNO_3 \quad (5)$$

$$CH_3CH(OH)CH(CH_3)_2 + NO_3 \rightarrow CH_3CH(OH)CH(\cdot CH_2)(CH_3) + HNO_3 \quad (6)$$

Reaction pathways (4) and (5) are expected to be the most important reaction channels since they involve H-atom abstraction from tertiary C–H bonds.

Relative rate coefficients for the NO_3-radical-initiated oxidation of 1-butanol, 2-methyl-1-butanol, 3-methyl-1-butanol, 3,3-dimethyl-1-butanol and 3,3-dimethyl-2-butanol determined recently [30] in our laboratory also confirm that the reactivity of the NO_3 radical towards saturated alcohols is determined by hydrogen abstraction from the C_α–H position of the OH group and also that the reactivity depends on the types of hydrogens present in the hydrocarbon chain.

2.2 Acrylates

Acrylate esters are α,β-unsaturated esters that contain vinyl groups directly attached to the carbonyl carbon (e.g. $CH_2=CHCOO-$ and $CH_2=C(CH_3)COO-$). These compounds are widely used in industrial applications such as the production of plastics (also called acrylate polymers) and resins. Important acrylate monomers used to form acrylate polymers include butyl and isobutyl acrylate, butyl methacrylate, 2-ethylhexyl acrylate, methyl acrylate, ethyl acrylate and methyl methacrylate. These acrylic polymers have the desirable characteristics of acrylic acid and acrylate esters for the manufacture of dispersants, thickeners, adhesives, binders and vehicle paint [33–36].

The most common sources of acrylate emissions are the manufacture of plastics, aircraft factories and the production of electronic components [37, 38]. For example, the production of 2-ethylhexyl acrylate and its use in the manufacture of plastics, protective coatings, paper treatments and water-based paints may result in the release of this compound into the environment through various waste streams. Acrylate esters also have natural sources. For example, methyl 3-methylacrylate is an aroma-related compound from fruit crops including strawberries [39] and methyl 3,3-dimethylacrylate is emitted from sunflower crops [40]. Acrylates can also be formed in the atmosphere as oxidation products of certain ethers that are used as automobile fuel additives [41, 42].

Once they are in the atmosphere, the atmospheric degradation of acrylates is mainly controlled by chemical reactions with OH and NO_3 radicals and with O_3 and Cl atoms. Removal of acrylate esters by reaction with ozone or night-time reactions with NO_3 are expected to be minor degradation processes compared to removal

through OH or Cl reactions [43–47]. Photolytic degradation of acrylate esters is negligible because these compounds do not absorb sunlight in the atmospheric actinic region [48, 49]. The relevance of the atmospheric degradation processes of these compounds is currently not well understood.

2.2.1 Rate Coefficients for NO_3 Reactions

A summary of all the available kinetic data for the reactions of acrylates with the nitrate radical is presented in Table 2. The reaction of NO_3 with methyl acrylate was studied by Canosa et al. [50] using absolute and relative techniques. However, a significant discrepancy was observed between the measured values and this was attributed to secondary chemistry and fast-reacting impurities in the absolute study. In fact, the rate coefficient was redetermined by the same authors in a subsequent paper [51] in which the relative kinetic technique was used. In that paper, rate coefficients for the reactions of NO_3 with methyl 3-methylacrylate and methyl 3,3-dimethylacrylate were reported for the first time. The relative rate method has also been used by Wang et al. [45] to determine the rate coefficients for the gas-phase reactions of NO_3 with ethyl acrylate, *n*-butyl acrylate, methyl methacrylate and ethyl methacrylate at 298 K and 760 Torr. In a more recent study, Salgado et al. [46] reported rate coefficients for the reactions of NO_3 with three methacrylate esters (methyl methacrylate, ethyl methacrylate and butyl methacrylate) determined in a Teflon static reactor at room temperature and atmospheric pressure. In the same paper, a qualitative product evaluation was carried out using the SPME-GC-MS technique and FTIR spectroscopy. All of the values for the rate coefficients

Table 2 Room-temperature rate coefficients, k, for the reactions of NO_3 radicals with a series of unsaturated esters (acrylates) in units of cm^3 $molecule^{-1}$ s^{-1}

Organic	$k_{(NO_3)}/10^{-15}$	Reference
Methyl acrylate	0.10 ± 0.06	Canosa-Mas et al. [50]
	0.12 ± 0.051	Canosa-Mas et al. [51]
Methyl methacrylate	3.6 ± 1.3	Canosa-Mas et al. [50]
	3.7 ± 0.65	Canosa-Mas et al. [51]
	3.55 ± 0.62	Salgado et al. [46]
	3.60 ± 1.20	Wang et al. [45]
Ethyl acrylate	0.17 ± 0.02	Wang et al. [45]
Ethyl methacrylate	5.42 ± 1.90	Salgado et al. [46]
	4.90 ± 1.70	Wang et al. [45]
Butyl acrylate	0.21 ± 0.03	Wang et al. [45]
Butyl methacrylate	7.87 ± 3.86	Salgado et al. [46]
Methyl 3-methylacrylate	1.85 ± 0.56	Canosa-Mas et al. [51]
Methyl 3,3-dimethylacrylate	14.1 ± 2.3	Canosa-Mas et al. [51]

Experiments developed by Relative Rate Technique and Gas-Chromatography Flame Ionization Detection, Canosa-Mas et al. [51], Salgado et al. [46] and Wang et al. [45]

obtained by the different authors on using the relative kinetic technique for the reactions of NO_3 with methyl methacrylate and ethyl methacrylate are, within experimental error, in excellent agreement.

2.2.2 Mechanisms of the NO_3-Initiated Oxidation of Acrylates

It can be seen in Table 2 that the values of the rate coefficients determined for the reactions of NO_3 with acrylate esters are in the order of 10^{-16}–10^{-15} cm^3 molecule^{-1} s^{-1}. The data show a slight increase in the rate coefficient on increasing the chain length of the alkyl group in –C(O)OR for the acrylates, and this can probably be ascribed to the electron-donating inductive effect of the substituents [46]. The increase is more pronounced for the methacrylates than for the acrylates, i.e. k(methyl methacrylate) < k(ethyl methacrylate) < k(butyl methacrylate).

Comparison of the reactivities of the acrylates and methacrylates shows that the rate coefficients for the methacrylates are higher than those for the analogous acrylates and this is due to the electron-donating inductive effect of the α-substituted methyl group on the double bond in the methacrylates, for example, k(methyl acrylate) < k(methyl methacrylate). β-Substitution also has a positive influence on the reactivity although this is less marked than the effect for the α-position, e.g. methyl-3-methylacrylate is less reactive than methyl methacrylate. The effect, however, is more significant when the number of alkyl substituents in the β-position is two (greater inductive effect), e.g. k(methyl 3-methylacrylate) < k(methyl methacrylate) ≪ k(methyl 3,3-dimethylacrylate). This increase in reactivity with increasing electron-donating substitution is usually indicative of an electrophilic addition mechanism [52]. It is important to note that for the reactions of acrylate esters with OH and Cl, the reactivity also increases with the number of methyl substituents on the double bond and with the chain length of the alkyl group in the –C(O)OR unit [48, 53–57], where electrophilic addition of NO_3 to the double bond is proposed as the dominant reaction pathway [58].

The presence of the carbonyl group attached to the carbon–carbon double bond in acrylates will lower the electron density on the double bond by electron withdrawing and consequently reduce the reactivity in comparison with the corresponding to the parent alkenes (the alkenes from which the carbonyl compounds are derived by substitution of the terminal methyl group, i.e. $–CH_3$ by $–C(O)OCH_3$). For example, we can compare the rate coefficients for 2-butene (the parent alkene) with that of methyl 3-methylacrylate. For NO_3 reaction, k (isobutene) is 3.32×10^{-13} cm^3 molecule^{-1} s^{-1} [59], which is higher than the value obtained for the acrylate, as one would expect (see Table 2).

A qualitative study of products from the reactions of NO_3 with methyl, ethyl and butyl methacrylates by GC-MS [46] showed unequivocally that alkyl pyruvates are the most prevalent products. Nitrated compounds were expected as products in these reactions, but due to the sampling and analysis (very high temperature in the injection port) methods used in the study, these compounds were not identified by the SPME-GC/MS technique. In the same study, FTIR spectroscopy was used to

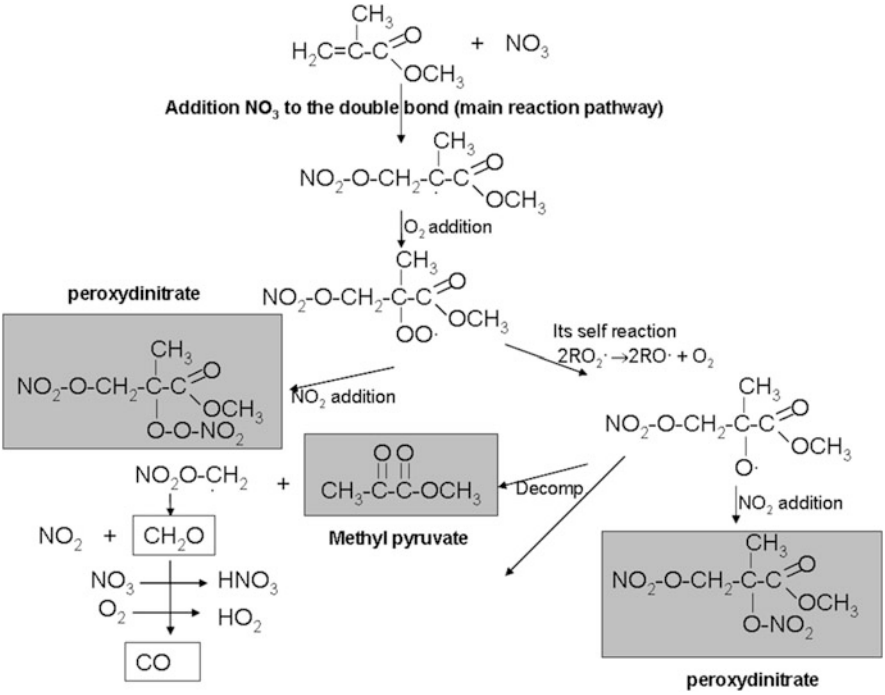

Fig. 1 Mechanism of the main degradation processes proposed for the OH-radical-initiated oxidation of methyl methacrylate (with kind permission from Springer Science + Business Media. Scheme 1. [46])

measure the products, but once again the analysis was qualitative due to the absence of commercially available nitrate standards. Several bands were assigned to nitroperoxy compounds ($OONO_2$), nitrooxy compounds (ONO_2) [60] and unidentified carbonyl compounds. It was concluded from the identified products and the observed trends in reactivity that NO_3 reactions with methacrylates in the presence of oxygen mainly proceed by a mechanism that involves addition of the NO_3 radical to the C=C double bond, in a similar way to OH reactions, to form a nitrooxyalkyl radical – as shown in Scheme 1 (reproduced from Salgado et al. [46]) (Fig. 1). As indicated in that paper, this radical can decompose to an epoxide plus NO_2 or, more probably, can add O_2 to form a nitrooxyalkyl peroxy radical. The nitrooxyalkyl peroxy radical can react via different pathways: (a) it can add NO_2 to form a thermally unstable peroxydinitrate or (b) it can be reduced by self-reaction or reaction with other peroxy radicals to form the nitrooxyalkoxy radical. The nitroalkoxy radical can further react (a) with NO_2 to form a dinitrate or (b) decompose to form a pyruvate, an aldehyde and NO_2.

Apart from the reactions presented above, to our knowledge no other kinetic or mechanistic information is available for reactions of NO_3 with acrylate esters. However, product studies have been reported for the reactions of OH radicals and

Cl atoms with methyl acrylate and methyl methacrylate [61, 62], and their results confirm that for these reactions, the major reaction pathway involves initial addition of OH or Cl to the terminal carbon atom of the C=C bond to give 1,2-hydroxyalkyl or 1,2-chloroalkyl radicals that can decompose by various channels.

2.3 Unsaturated Aldehydes

Unsaturated aldehydes are oxygenated compounds that contain at least one C=C double bond and a carbonyl group (–C(O)H) group. These compounds are also referred to as α,β-unsaturated carbonyl compounds when the unsaturated double bond and the carbonyl group are in adjacent positions. Acrolein and crotonaldehyde are the unsaturated aldehydes that have been most widely studied. These compounds are released into the atmosphere as primary pollutants from different anthropogenic sources such as combustion processes and chemical industries [63, 64], and they can be formed in situ in the atmosphere by the photooxidation of 1,3-dienes [60]. Other α,β-unsaturated aldehydes such as E-2-hexanal and other larger aldehydes have been measured in ambient air in urban and rural areas [65, 66].

Furanaldehydes are also unsaturated aldehydes that are furan derivatives with a –C(O)H group in their structure. These compounds can be present in the atmosphere as primary pollutants released from anthropogenic sources such as emissions from motor vehicles powered by diesel fuel, as products of the incomplete combustion of biomass and from forest fires [67–69] or biogenic sources (emissions from tropical forests [70]). Villanueva et al. [71] detected furanaldehydes as reaction products in the Cl-atom-mediated degradation of alkyl furans. 2-Furanaldehyde (or furfural) is the most important furanaldehyde and it is used as a solvent for the extraction of dienes in petrochemical refining. This compound has also been identified as a component in food and in the emissions of volatile compounds during food processing [72–74]. Another unsaturated aldehyde that has received particular attention over the years is butenedial (OHCCH=CHCHO). Butenedial has been identified as a primary product from the reaction of furan and aromatic compounds, such as toluene and *o*-xylene, with the main atmospheric oxidants [75–79].

Numerous kinetic and mechanistic studies on the reactions of NO_3 with organic compounds such as aldehydes have been carried out and reviewed [13, 28, 80]. In recent years, new studies on the reactivity of linear C3–C8 unsaturated aldehydes with NO_3 have been carried out in an attempt to address uncertainties in some of the previous rate coefficient measurements [66, 81, 82]. In addition, first-time measurements for the reactions of NO_3 with furanaldehydes and butenedial have been reported [83, 84]. All of the studies on unsaturated aldehydes show that these compounds are mainly removed from the atmosphere by photolysis and gas-phase reactions with OH radicals and possibly also Cl atoms in coastal and marine areas during the daytime and by reactions with NO_3 radicals and O_3 during the night [5, 7, 14, 59, 66, 82–86]. Studies have shown that unsaturated aldehydes

play a key role in tropospheric chemistry as a source of HO_x radicals and as possible intermediates in the formation of secondary organic aerosols (SOA) [14, 66, 82, 87].

The data discussed below represent a compilation of the experimental results from our research group's studies on the reactions of the NO_3 radical with unsaturated aldehydes and the results from other research groups that are available in the peer-reviewed literature.

2.3.1 Rate Coefficients for NO_3 Reactions

The kinetic data obtained in our studies on the reactions of the NO_3 radical with unsaturated aldehydes [65, 66, 83, 84] are summarized in Table 3 together with the available literature data [50, 81, 82, 88, 89, 91, 92]. The reported rate coefficients have been measured either by an absolute rate technique by monitoring the disappearance of NO_3 or by relative rate techniques using reference compounds whose rate coefficients with NO_3 are well established. Room-temperature rate coefficients have been reported by several groups for the reactions of NO_3 with acrolein, crotonaldehyde, E-2-pentenal, E-2-hexenal, E-2-heptenal and Z-4-heptenal, although in some cases there are large discrepancies between the reported values. In the study by Cabañas et al. [65], the reason for the disagreement in the results could be due to secondary chemistry, but in the study by Kerdouci et al. [82], the reason is not clear. Only two studies on the temperature dependence of the rate coefficient for the reactions of NO_3 with unsaturated aldehydes have been reported in the literature. In the study by Cabañas et al. [65], the rate coefficients for the compounds mentioned above were determined over the temperature range 298–433 K. Salgado et al. [66] later studied the reactions of acrolein and crotonaldehyde with NO_3 over the temperature range 249–330 K. The temperature-dependent parameters (A and B) are shown in Table 3. The data reported in these studies for acrolein and crotonaldehyde at low and high temperatures show different activation energies depending on the temperature range used for the experiments, and it is possible that the reaction mechanism changes.

The rate coefficients for the reactions of NO_3 with unsaturated aldehydes vary significantly, i.e. from 1.7×10^{-15} cm^3 $molecule^{-1}$ s^{-1} in the case of E-butenedial (an unsaturated compound with two aldehyde groups) to 5.51×10^{-12} cm^3 $molecule^{-1}$ s^{-1} for 5-methylfurfural (an aldehyde with aromatic character). In the case of the linear α,β-unsaturated mono-aldehydes, the rate coefficients appear to increase slightly with the length of the alkyl chain from acrolein to E-2-heptenal, with the exception of E-2-hexenal – for which almost all data reported in the literature have a lower value than for E-2-pentenal. Further studies are required in order to establish a clear trend for the rate coefficient on changing the alkyl chain.

The rate coefficients for the reactions of NO_3 with some alkanes, alkenes and saturated aldehydes are shown in Table 4 in order to evaluate the effect of the carbonyl group on the reactivity. Comparison of the rate coefficients for each unsaturated aldehyde (Table 3) with the rate coefficients for the corresponding

Table 3 Room-temperature rate coefficients, temperature-dependent parameters and temperature ranges over which these data have been measured for the gas-phase reactions of NO_3 radicals with unsaturated aldehydes

Organic	A/cm^3 molecule^{-1} s^{-1}	$k_{(NO_3)}/10^{-15}$	T/K	B/K	Temperature range/K	Reference	Technique
Acrolein		1.1 ± 0.2	298			Atkinson et al. [88]	RR
		1.1 ± 0.4	298			Canosa-Mas et al. [50]	RR
		8.9 ± 2.8					FFD/AR
		1.1 ± 0.2	298			Ullerstam et al. [89]	RR
	$(1.70 \pm 2.3) \times 10^{-11}$	2.5 ± 0.39	298	$-3{,}232 \pm 355$	298–433	Cabañas et al. [65, 90]	FFD/AR
	$(1.72 \pm 0.5) \times 10^{-13}$	3.3 ± 0.39	298	$-1{,}190 \pm 43$	249–330	Salgado et al. [66]	FFD/AR
Crotonaldehyde		5.1 ± 0.2	298			Atkinson et al. [88]	RR
		6 ± 0.8	298			Ullerstam et al. [89]	RR
	$(5.5 \pm 0.8) \times 10^{-11}$	16.1 ± 2.0	298	$-2{,}418 \pm 57$	298–433	Cabañas et al. [65, 90]	FFD/AR
	$(5.2 \pm 0.7) \times 10^{-13}$	13.5 ± 0.6	298	$-1{,}076 \pm 47$	249–330	Salgado et al. [66]	FFD/AR
E-2-pentenal	$(5.4 \pm 0.3) \times 10^{-12}$	28.8 ± 2.9	298	$-1{,}540 \pm 200$	298–433	Cabañas et al. [65, 90]	FFD/AR
		19.3 ± 4.0	295			Zhao et al. [81]	CI-MS/RR
E-2-hexenal		12.1 ± 4.3	298			Atkinson et al. [91]	RR
	$(1.2 \pm 0.3) \times 10^{-11}$	54.9 ± 9.5	298	-926 ± 85	298–433	Cabañas et al. [65, 90]	FFD/AR
		13.6 ± 2.9	295			Zhao et al. [81]	CI-MS/RR
		4.7 ± 1.5	294			Kerdouci et al. [82]	UVS/AR
E-2-heptenal	$(0.8 \pm 0.2) \times 10^{-12}$	95.9 ± 1.9	298	-632 ± 47	298–433	Cabañas et al. [65, 90]	FFD/AR
		23 ± 3.6	295			Zhao et al. [81]	CI-MS/RR
		5.3 ± 1.6	294			Kerdouci et al. [82]	UVS/AR
Z-4-heptenal	$(0.2 \pm 0.1) \times 10^{-11}$	260 ± 4	298	-657 ± 6	298–433	Cabañas et al. [65, 90]	FFD/AR
		403 ± 24	295			Zhao et al. [81]	CI-MS/RR
E-2-octenal		5.6 ± 2.3	294			Kerdouci et al. [82]	UVS/AR

(continued)

Table 3 (continued)

Organic	A/cm^3 molecule^{-1} s^{-1}	$k_{(NO_3)}/10^{-15}$	T/K	B/K	Temperature range/K	Reference	Technique
2-Furanaldehyde		1,280 ± 280	298			Colmenar et al. [83]	FTIR/RR
3-Fuanaldehyde		3,410 ± 790	298			Colmenar et al. [83]	FTIR/RR
5-Methyl-2-furanaldehyde		5,510 ± 1,270	298			Colmenar et al. [83]	FTIR/RR
E-butenedial		1.70 ± 0.83	298			Martín et al. [84]	GC-MS/RR
E,E-2,4-hexadiendial		5.34 ± 0.12	298			Klotz et al. [92]	RR

k in unit of cm^3 molecule^{-1} s^{-1}

Technique: *RR* relative rate, *AR* absolute rate, *FFD* fast flow discharge, *CI-MS* chemical ionization-mass spectrometry, *UV* ultraviolet spectroscopy

Table 4 Rate coefficients for a list of alkanes, alkenes and saturated aldehydes with NO_3

Organic	Structure	$k_{(NO_3)}/10^{-15}$	Reference
Propene		9.54 ± 0.2	Atkinson [85]
Propanal		6.4 ± 0.2	Atkinson et al. [28]
Propane		0.07	IUPAC [93]
E-2-butene		390 ± 0.27	Atkinson [59]
Butanal		11 ± 1.5	Atkinson et al. [28]
		14.6 ± 1.6	Canosa-Mas et al. [94]
Butane	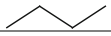	0.046	IUPAC [93]
E-2-pentene	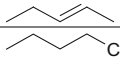	378 ± 45	Pfrang et al. [95]
Pentanal		17.1 ± 0.2	Noda et al. [96]
Pentane		0.081 ± 0.016	Atkinson [59]
E-2-hexene	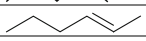	383 ± 47	Pfrang et al. [95]
Hexanal	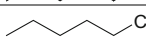	16 ± 2	Noda et al. [96]
		18.3 ± 3.6	Cabañas et al. [90]
Hexane	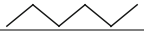	0.105 ± 0.019	Atkinson [59]
E,E-2,4-hexadiene	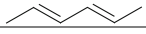	$16{,}000 \pm 2{,}990$	Ellermann et al. [97]
E-2-heptene	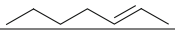	538	Grosjean et al. [98]
Heptane	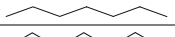	0.137 ± 0.0136	Atkinson [59]
Heptanal	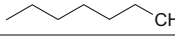	21 ± 3	Noda et al. [96]
E-2-octane	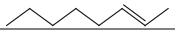	–	
Octanal	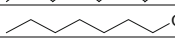	20 ± 3	Noda et al. [96]
Octane	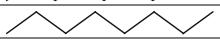	0.183	Atkinson [59]

k in cm^3 $molecule^{-1}$ s^{-1}

alkenes (Table 4) shows that the alkenes are more reactive towards NO_3 by one or two orders of magnitude when compared to the unsaturated aldehydes. This finding suggests that the carbonyl group strongly deactivates the addition of NO_3 to the double bond. This situation is consistent with the electron-withdrawing effect of the carbonyl group located α to the double bond. On the other hand, the rate coefficients for the unsaturated aldehydes (Table 3) are lower than or similar to those of the corresponding saturated aldehydes (Table 4), suggesting that the double bond may slightly deactivate the H-atom abstraction from the aldehyde group [82–84, 89]. This latter effect could explain the low values for the NO_3 rate coefficients obtained for E-butenedial and E,E-2,4-hexadienedial.

The rate coefficients for the reactions of NO_3 with E-butenedial and E,E-2,4-hexadienedial are higher than those of their corresponding alkanes ($k = 4.65 \times 10^{-17}$ cm^3 $molecule^{-1}$ s^{-1} for butane and $k = 1.05 \times 10^{-16}$ cm^3 $molecule^{-1}$ s^{-1} for hexane), which is consistent with an increase in reactivity due to the abstraction of the aldehyde hydrogen versus the alkylic hydrogen or to the presence of a double bond. On the other hand, the rate coefficients are lower than those for the reactions of NO_3 with the corresponding alkenes ($k = 3.90 \times 10^{-13}$ cm^3 $molecule^{-1}$ s^{-1} for E-2-butene and $k = 1.6 \times 10^{-11}$ cm^3 $molecule^{-1}$ s^{-1} for E,E-2,4-hexadiene) and

saturated aldehydes ($k = 1.1 \times 10^{-14}$ cm^3 molecule^{-1} s^{-1} for butanal and 1.6×10^{-14} cm^3 molecule^{-1} s^{-1} for hexanal [96]). These results indicate that both a deactivating effect of the aldehyde groups towards the addition of NO_3 to the double bond and also a deactivating effect of the double bond towards NO_3 abstraction of the aldehyde hydrogen are operative.

The rate coefficients for the reactions of NO_3 with furfural, 3-furanaldehyde and 5-methylfurfural are around 10^{-12} cm^3 molecule^{-1} s^{-1} and are two to three orders of magnitude higher than those for the other compounds listed in Table 3. This high reactivity is attributed mainly to the addition of the NO_3 radical to the double bond in the compounds rather than to H-atom abstraction from the aldehyde group. The reactivity of the three furanaldehydes with NO_3 is in the order $k_{\text{5-methyl-2-furanaldehyde}} > k_{\text{3-furanaldehyde}} > k_{\text{2-furanaldehyde}}$. This trend in reactivity can be understood in terms of the deactivation effect exerted by the –C(O)H group on the aromatic ring. The aldehyde group itself gives rise to a negative inductive (−I) effect, although when it is attached to the furan ring, a negative conjugated effect (−K) also occurs due to conjugation of the electron pairs on the carbonyl with the electron pairs of the aromatic ring. The conjugation results in deactivation of the aromatic ring in the furaldehydes towards electrophilic addition. The effectiveness of the deactivating effect depends on the position occupied by the –C(O)H group in the structure of the furanaldehyde: positions C3 and C5 for 2-furanaldehyde and position C2 in 3-furanaldehyde. A schematic representation of the conjugative effect (−K) for 2-furanaldehyde is shown in Fig. 2 (taken from Cabañas et al. [99]). In the case of 5-methyl-2-furanaldehyde, the presence of a methyl group in the C5 position, which has a positive inductive effect (+I), leads to charge donation to the aromatic ring, thus helping to compensate for the deactivating effect of the aldehyde group and increasing the probability of electrophilic addition by the NO_3 radical [83, 99]. However, Colmenar et al. [83] carried out a kinetic study on the reaction of NO_3 with furanaldehydes and obtained a rate coefficient for 2-furanaldehyde that is very similar to the rate coefficient for the reaction of NO_3 with furan. This finding implies an important contribution of the aldehyde hydrogen abstraction process to the overall rate coefficient.

In conclusion, all of the results discussed above show that the chemical structure of the unsaturated aldehydes has a significant influence on the reactivity of the unsaturated aldehydes towards attack by the NO_3 radical. However, the discrepancies in the data available to date show that further kinetic studies are needed, especially for E-2-hexenal and E-2-heptenal, in order to obtain more reliable rate coefficients and to determine more precisely the effect that the alkyl chain length has on the reactivity.

2.3.2 Mechanisms of the NO_3-Initiated Oxidation of Unsaturated Aldehydes

The values of the activation energies obtained by Cabañas et al. [65] for acrolein (26 kJ/mol), crotonaldehyde (20 kJ/mol) and E-2-pentenal (13 kJ/mol) are higher

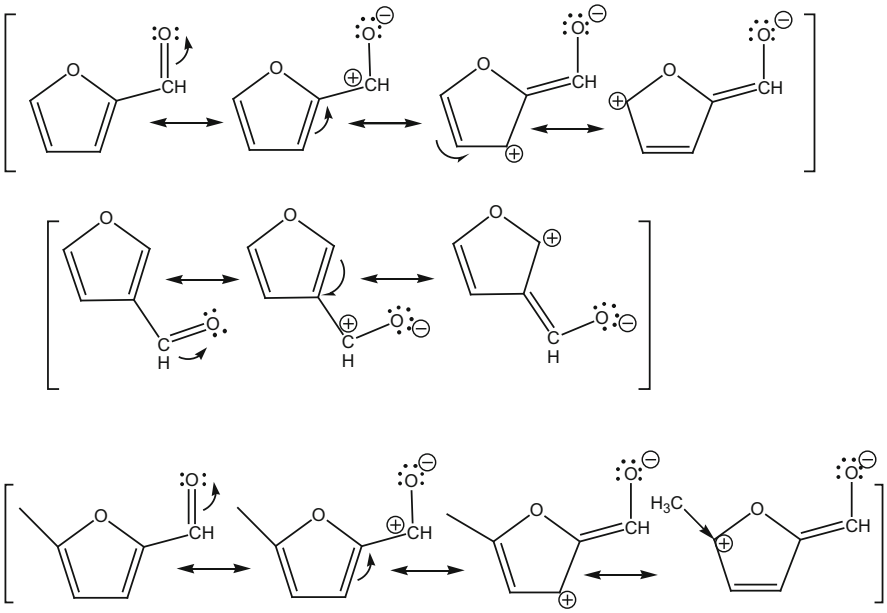

Fig. 2 Scheme of the conjugative charge distribution resonance possibilities, −K, for the –C(O)H substituent in the aromatic ring of furanaldehyde. Extracted with permission from Cabañas et al. [99]. Copyright 2014 Wiley Periodicals, Inc.

than those obtained for the reactions of the NO_3 radical with alkenes, haloalkenes or terpenes, which are only a few kJ/mol or have negative values [5, 80, 100–103]. The values are slightly lower, but are of the same order of magnitude, than the activation energies for the reaction of NO_3 with alkanes, which are above 30 kJ/mol [5, 80]. The values of the activation energies suggest a mechanistic process involving abstraction of the aldehyde H atom. In the cases of E-2-hexenal, E-2-heptenal and Z-4-heptenal, the measured activation energies are around 7–5 kJ/mol, indicating that for these reactions, the addition of the NO_3 radical to the C=C double bond could be occurring in addition to the abstraction of the aldehyde H atom.

From the product study on the reactions of NO_3 with acrolein and crotonaldehyde (C3 and C4 unsaturated aldehydes), Salgado et al. [66] showed that these reactions proceed exclusively via H-atom abstraction from the aldehyde group. Recently, Kerdouci et al. [82] determined the products for the reactions of NO_3 with E-2-hexenal, E-2-heptenal and E-2-octenal, and they also concluded, from the formation of the respective peroxyacylnitrate products, that the main reaction pathway is H-atom abstraction from the aldehyde group. However, they stressed that further studies are necessary to confirm these results. A possible reaction mechanism for the H-atom abstraction pathway in the reaction of the NO_3 radical with acrolein is shown in Fig. 3 (adapted from Salgado et al. [66]). Conclusions of the mechanism can probably be extended to other linear unsaturated aldehydes.

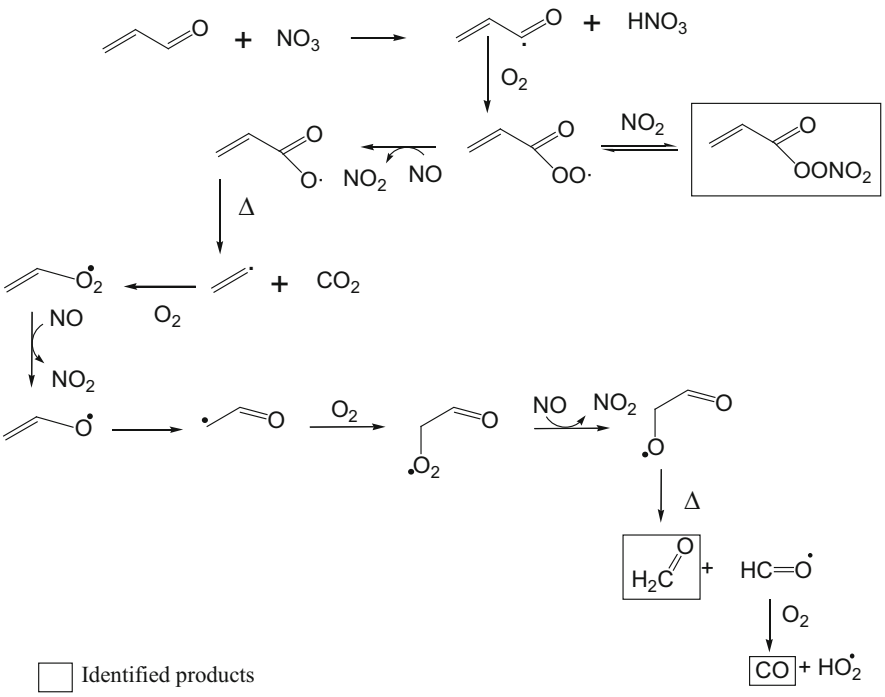

Fig. 3 Schematic reaction mechanism for the reaction of acrolein with NO_3. Adapted with permission from Salgado et al. [66]. Copyright 2014 American Chemical Society

For E-butenedial, the only product study available in the literature is that carried out by Bierbach et al. [104] on the reaction of this compound with OH radicals. The results of the study suggest that slightly less than 50% of the reaction proceeds by H-atom abstraction from the aldehyde functional groups in butenedial. Based on this result, it is highly probable that the reaction of NO_3 with butenedial proceeds to a large extent by H-atom abstraction from the aldehyde groups. In the case of furanaldehydes, there is currently no information on reaction products available in the literature. However, in order to establish the first step in the reaction mechanism, different correlations can be used for compounds for which product data does not exist. There are numerous different types of correlations, but some of the most useful involve correlations based on the relationships between $\log(k_{NO_3})$ and $\log(k_{OH})$ [5] and $\ln(k_{NO_3})$ and the energy of the highest occupied molecular orbital, E_{HOMO} [105]. The results obtained from these correlations in the case of NO_3-furanaldehyde reactions show that the reaction mechanism is different to that for the reactions of NO_3 with alkenes and alkanes, where the initial step is addition of the radical to the C=C double bond and abstraction of a hydrogen atom, respectively. This infers that the furanaldehydes can react either by electrophilic addition, by abstraction of the aldehyde hydrogen or by abstraction of aliphatic hydrogen atoms. The percentage contribution of each process to the overall mechanism is not

well established and further studies are needed to elucidate the importance of the three possible reaction channels [83, 106]. For the NO_3 + E-butenedial reaction, Martín et al. [84] concluded, based on the results of correlations (($\log(k_{NO_3})$ versus $\log(k_{OH})$ and $\ln(k_{NO_3})$ versus E_{HOMO}), that the reaction proceeds mainly by direct abstraction of the aldehydic hydrogen – in contrast to the saturated aldehydes, where the abstraction of the aldehyde hydrogen is proposed to occur through the formation of an intermediate NO_3-aldehyde adduct [90, 107]. It is probable that a reaction mechanism similar to that proposed by Salgado et al. [66] for acrolein occurs for the reaction of E-butenedial and NO_3.

In summary, mechanistic studies have shown that the reaction of NO_3 with unsaturated aldehydes can proceed by two main pathways: H-atom abstraction from the aldehyde group and addition to the double bond [65, 66, 81–84, 89]. The percentage contribution of each pathway could depend on various factors, such as the size of the alkyl chain in the unsaturated aldehyde, the position of the double bond (conjugated or not with respect to the aldehyde group), the number of aldehyde groups and possible conjugation with an aromatic ring.

3 Atmospheric Implications

Kinetic data for the reactions of the compounds reviewed in this chapter with atmospheric oxidants are necessary for the realistic representation of the chemistry of these compounds in tropospheric models, which are used to assess the impact of contaminants on air quality. The rate coefficients summarized in Tables 1, 2 and 3 for the reactions of the NO_3 radical with the reviewed compounds can be used to calculate the atmospheric lifetimes of the compounds due to reaction with NO_3 using the expression $\tau_R = 1/(k_R[Ox])$, where [Ox] is the typical atmospheric concentration of the oxidant (NO_3 in this case) and k_R is the rate coefficient for the reaction of the oxidant with the compound. The estimated atmospheric lifetimes for saturated alcohols, unsaturated esters and unsaturated aldehydes with respect to the reaction with NO_3 radicals are presented in Tables 5, 6 and 7, respectively. A typical tropospheric concentration for NO_3 radicals of $[NO_3] = 5 \times 10^8$ radical cm^{-3} was used in the calculations [108].

Beginning with the saturated alcohols, it can be seen from the data in Table 5 that the lifetimes of the saturated alcohols with respect to NO_3-initiated degradation are in the order of days. Atmospheric lifetimes for OH reactions according to rate coefficients previously available for methanol and ethanol are too low [13], and on increasing the hydrocarbon chain length, the atmospheric lifetimes for the OH reactions are significantly shorter than those for the corresponding NO_3 reactions. For example, 2-butanol, depending on the literature rate coefficient used [17, 18], has an atmospheric lifetime with respect to reaction with OH of between 20 and 77 h, which is clearly shorter than the lifetime listed in Table 5 for the NO_3 reaction. The lifetimes for saturated alcohols in reactions with Cl atoms are over 200 h [22],

Table 5 Preferred room-temperature rate coefficients (in units of cm^3 $molecule^{-1}$ s^{-1}) and calculated atmospheric lifetimes for the reactions of NO_3 radicals with saturated alcohols

Organic	$k_{(NO_3)}/10^{-15}$	τ/days
Methanol	0.14	17
Ethanol	1.81	12
1-Propanol	≤2.10	11
2-Propanol	1.71	14
1-Butanol	≤2.71	9
2-Butanol	2.22	10
2-Methyl-2-butanol	1.57	15
3-Methyl-2-butanol	3.06	8
2,3-Dimethyl-2-butanol	2.67	9
4-Heptanol	≤5.99	4
1-Propanol	≤2.10	11
2-Ethyl-1-hexanol	2.93	8

Table 6 Room-temperature rate coefficients (in units of cm^3 $molecule^{-1}$ s^{-1}) and calculated atmospheric lifetimes for the reactions of NO_3 radicals with a series of acrylates and methacrylates

Organic	$k_{(NO_3)}/10^{-15}$	τ/days
Methyl acrylate	0.12	191
Methyl methacrylate	3.62	6
Ethyl acrylate	0.17	136
Ethyl methacrylate	5.13	5
Butyl acrylate	2.10	110
Butyl methacrylate	7.87	3
Methyl 3-methylacrylate	1.85	13
Methyl 3,3-dimethylacrylate	14.1	2

Table 7 Atmospheric lifetimes estimated for unsaturated aldehydes and rate coefficients obtained in our works

Organic	$k_{(NO_3)}/10^{-15}$	τ/days
Acrolein	2.5 [65, 90]	9
Crotonaldehyde	16.1 [65, 90]	1.4
E-2-pentenal	28.8 [65, 90]	0.8
E-2-hexenal	54.9 [65, 90]	0.4
E-2-heptenal	95.9 [65, 90]	0.2
Z-4-pentenal	260 [65, 90]	2 h
E-2-octenal	56 [82]	0.4
2-Furanaldehyde	1,280 [83]	0.4 h
3-Furanaldehyde	3,410 [83]	0.2 h
5-Methyl-2-furanaldehyde	5,510 [83]	0.1 h
E-butenedial	1.7 [84]	14
E,E-2,4-hexadiendial	5.3 [92]	4

k, in units of cm^3 $molecule^{-1}$ s^{-1}

which indicates that, despite their high reactivity, the Cl-atom concentrations are simply too low to allow effective competition with OH radical reactions. The reactions of saturated alcohols with O_3 [21] are much slower to make a significant contribution to the atmospheric degradation of alcohols.

The values reported here clearly indicate that the atmospheric lifetimes for saturated alcohols due to NO_3 reactions are longer than those for the corresponding OH reactions and are of the same order of magnitude as the corresponding Cl reactions. This finding indicates that for these alcohols, and for saturated alcohols in general, reactions with OH radicals will be the dominant atmospheric loss process. However, the lifetime for alcohols is in the order of 10–40 h in coastal areas and in the marine boundary layer where high Cl-atom levels were observed especially at dawn; e.g. peak concentrations of Cl atoms as high as 1×10^5 atoms cm^{-3} have been reported by Spicer et al. [109]. Under these circumstances, the Cl-atom-initiated degradation of alcohols can be an important homogeneous loss process.

If one considers the NO_3 atmospheric lifetimes τ_R estimated for the acrylates and methacrylates listed in Table 6, the calculated values for methyl acrylate, ethyl acrylate and butyl acrylate are very large. Comparison of the NO_3 lifetimes for these compounds with those for reactions with other atmospheric oxidants again clearly shows that the dominant atmospheric loss process for acrylates in the daytime will be a reaction with the hydroxyl radical, with lifetimes in the range of 2–13 h [48, 49, 53–55, 57]. The short atmospheric lifetimes for reactions with OH imply that these compounds will be removed in the gas phase close to their emission sources. The atmospheric lifetimes for these compounds due to reactions with Cl are on the order of days, making removal of the acrylates by reaction with Cl generally a negligible loss process [56–58, 110]. Considering continental areas, recent observations of nitryl chloride derived from anthropogenic sources [111] and the significant mixing ratios observed over continental Europe [112] are associated with air masses influenced by sea salt and also anthropogenic NOx emissions. Considering that primary fate of ClNO2 is photo dissociation at sunrise to yield NO_2 and Cl atoms, the role of Cl in initiating the oxidation of VOCs may be widespread and significant than previously thought. It's also important to mention the high Cl atoms concentration in industrial zones [113] where acrylic esters concentrations should also be significant.

The calculated lifetimes for acrylates and methacrylates are sufficiently long to allow these compounds to persist into the night, when reactions with NO_3 and ozone could be the most relevant removal processes. The calculated atmospheric lifetimes for most acrylate esters towards NO_3 radicals are much longer than those for the corresponding reactions with O_3 (3–16 days), indicating again that night-time reaction of acrylates with NO_3 radicals is an insignificant degradation process for these compounds. Methacrylate esters have significantly shorter atmospheric lifetimes (between 2 and 4 days) than acrylates, and this indicates that for these compounds reaction with NO_3 could compete with reaction with O_3 as a night-time degradation process. The atmospheric lifetime for methyl 3-methylacrylate is comparable to those for the methacrylates and methyl 3,3-dimethylacrylate

(lifetime 2 days) is the only compound for which NO_3 degradation is the relevant night-time process.

The estimated lifetimes for the reactions of NO_3 with unsaturated aldehydes (Table 7) cover a wide range, with values from 6 to 24 min for furanaldehydes, several hours or days for unsaturated aldehydes with $C > 5$ (depending on data of rate coefficient used), and some days for dialdehydes and acrolein. The very short atmospheric lifetimes estimated for the furaldehydes indicate that these compounds are rapidly degraded in the atmosphere by reaction with NO_3 radicals, thus making it necessary to establish the reaction products in order to evaluate whether the products are more important than furaldehydes themselves. In the case of the other unsaturated aldehydes, it has been shown that reaction with NO_3 is the principal oxidative degradation pathway for these compounds during the night. The main products generated in H-abstraction reactions, namely, HNO_3 and peroxyacylnitrate compounds such as PAN, contribute to important episodes of contamination. HNO_3 is the main contributor to acidity in precipitation and peroxyacylnitrates contribute to photochemical ozone formation and to the oxidizing potential of the atmosphere [85, 114]. The long lifetimes of PANs allow them to transport NO_2 over large distances [115]. With regard to human health, PANs are eye irritants, mutagens, possible skin cancer-causing agents and phytotoxins [116–118]. Another important product detected in the degradation process of unsaturated aldehydes is formaldehyde, which is associated with serious health effects [119].

Acknowledgements The authors acknowledge the financial support provided by the Consejería de Ciencia y Tecnología de la Junta de Comunidades de Castilla-La Mancha and Ministerio de Ciencia e Innovación of Spain.

References

1. Noxon JF, Norton RB, Henderson WR (1978) Observation of atmospheric NO_3. Geophys Res Lett 5:675–678
2. Platt U, Perner D, Winner AM, Harris GW, Pitts JN Jr (1980) Detection of NO_3 in the polluted troposphere by differential optical absorption. Geophys Res Lett 7:89–92
3. Schott G, Davidson N (1958) Shock waves in chemical kinetics: the decomposition of N_2O_5 at high temperatures. J Am Chem Soc 80:1841–1853
4. Morris ED Jr, Niki H (1974) Reaction of the nitrate radical with acetaldehyde and propylene. J Phys Chem 78:1337–1338
5. Wayne RP, Barnes I, Biggs P, Burrows JP, Canosa-Mas CE, Hjorth J, Le Bras G, Moortgat GK, Perner D, Poulet G, Restelli G, Sidebottom H (1991) The nitrate radical: physics, chemistry, and the atmosphere. Atmos Environ 25:1–203
6. Brown SS, Stutz J (2012) Nighttime radical observations and chemistry. Chem Soc Rev 41:6405–6447
7. Finlayson-Pitts BJ, Pitts JN Jr (2000) Chemistry of the upper and lower atmosphere, theory, experiments and applications. Academic, San Diego
8. Calvert JG, Mellouki A, Orlando JJ, Pilling MJ, Wallington TJ (2011) The mechanisms of atmospheric oxidation of the oxygenates. Oxford University Press, New York

9. Hoyle CR, Boy M, Donahue NM, Fry JL, Glasius M, Guenther A, Hallar AG, Huff K, Hartz MD, Petters T, Petaja T, Rosenoern T, Sullivan AP (2011) A review of the anthropogenic influence on biogenic secondary organic aerosol. Atmos Chem Phys 11:321–343
10. König G, Brunda M, Puxbau H, Hewitt CN, Duckham SC, Rudolph J (1995) Relative contribution of oxygenated hydrocarbons to the total biogenic VOC emissions of selected mid-European agricultural and natural plant species. Atmos Environ 29:861–874
11. McDonald RC, Fall R (1993) Detection of substantial emissions of methanol from plants to the atmosphere. Atmos Environ A 27:1709–1713
12. Bilde M, Mogelberg TE, Sehested J, Nielsen OJ, Wallington TJ, Hurley MD, Japar SM, Dill M, Orkin VL, Buckley TJ, Huie RE, Kurylo MJ (1997) Atmospheric chemistry of dimethyl carbonate: reaction with OH radicals, UV spectra of $CH_3OC(O)OCH_2$ and $CH_3OC(O)OCH_2O_2$ radicals, reactions of $CH_3OC(O)OCH_2O_2$ with NO and NO_2, and fate of $CH_3OC(O)OCH_2O$ radicals. Phys Chem 101:3514–3525
13. Atkinson R, Arey J (2003) Atmospheric degradation of volatile organic compounds. Chem Rev 103:4605–4638
14. Mellouki A, Le Bras G, Sidebottom H (2003) Kinetics and mechanisms of the oxidation of oxygenated organic compounds in the gas phase. Chem Rev 103:5077–5096
15. Noda J, Hallquist M, Langer S, Ljungström E (2000) Products from the gas-phase reaction of some unsaturated alcohols with nitrate radicals. Phys Chem Chem Phys 2:2555–2564
16. Baxley JS, Wells JR (1998) The hydroxyl radical reaction rate constant and atmospheric transformation products of 2-butanol and 2-pentanol. Int J Chem Kinet 30:745–752
17. Mellouki A, Oussar F, Lun X, Chakir A (2004) Kinetics of the reactions of the OH radical with 2-methyl-1-propanol, 3-methyl-1-butanol and 3-methyl-2-butanol between 241 and 373 K. Phys Chem Chem Phys 6:2951–2955
18. Jiménez E, Lanza B, Garzón A, Ballesteros B, Albaladejo J (2005) Atmospheric degradation of 2-butanol, 2-methyl-2-butanol and 2,3-dimethyl-2-butanol: OH kinetics and UV absorption cross section. J Phys Chem A 109:10903–10909
19. Langer S, Ljungström E (1995) Rates of reaction between the nitrate radical and some aliphatic alcohols. J Chem Soc Faraday Trans 91:405–410
20. Moreno A, Salgado MS, Martín MP, Martínez E, Cabañas B (2012) Kinetic study of the gas phase reactions of a series of alcohols with the NO_3 radical. J Phys Chem A 116:10383–10389
21. Atkinson R, Carter WP (1984) Kinetics and mechanisms of gas phase reactions of ozone with organic compound under atmospheric conditions. Chem Rev 84:437–470
22. Ballesteros B, Garzón A, Jiménez E, Notario A, Albaladejo J (2007) Relative and absolute kinetic studies of 2-butanol and related alcohols with tropospheric Cl atoms. Phys Chem Chem Phys 9:1210–1218
23. Gallego-Iniesta MP, Moreno A, Martín MP, Tapia A, Cabañas B, Salgado MS (2010) Reactivity of 2-ethyl-1-hexanol in the atmosphere. Phys Chem Chem Phys 12:3294–3300
24. Peng CY, Lan CH, Dai YT (2006) Speciation and quantification of vapor phases in soy biodiesel and waste cooking oil biodiesel. Chemosphere 65:2054–2062
25. Wallington TJ, Atkinson R, Winer AM, Pitts JN Jr (1987) A study of the reaction $NO_3 + NO_2 + M \rightarrow N_2O_5$ ($M = N_2$, O_2). Int J Chem Kinet 19:243–249
26. Canosa-Mas CE, Smith SJ, Toby S, Wayne RP (1989) Laboratory studies of the reactions of the nitrate radical with chloroform, methanol, hydrogen chloride and hydrogen bromide. J Chem Soc Faraday Trans 85:709–725
27. Chew AA, Atkinson R, Aschmann SM (1998) Kinetics of the gas-phase reactions of NO_3 radicals with a series of alcohols, glycol ethers, ethers and chloroalkenes. J Chem Soc Faraday Trans 94:1083–1089
28. Atkinson R, Baulch DL, Cox RA, Crowley JN, Hampson RF, Hynes RG, Jenkin ME, Rossi MJ, Troe J (2006) Evaluated kinetic and photochemical data for atmospheric: volume II-gas phase reactions of organic species. J Atmos Chem Phys 6:3625–4055

29. IUPAC (2008) Subcommitee for gas kinetic data evaluation, evaluated gas kinetic data for atmospheric chemistry, www.iupac-kinetic.ch.cam.ac.uk
30. Moreno A, Salgado MS, Taccone R, Martín MP, Cabañas B (2014) Atmospheric degradation of saturated alcohols: room temperature rate coefficients for NO_3 radical reactions. Atmos Environ 96:229–235
31. Aschmann S, Atkinson R (1995) Rate constants for the reactions of the NO_3 radical with alkanes at 296 ± 2 K. Atmos Environ 29:2311–2316
32. Atkinson R, Aschmann SM, Pitts JN (1988) Rate constants for the gas-phase reactions of the nitrate radical with a series of organic compounds at 296.+−. 2 K. J Phys Chem 92:3454–3457
33. Dittgen M, Durrani M, Lehmann K (1997) Acrylic polymers: a review of pharmaceutical applications. STP Pharma Sci 7:403–437
34. Hervás-García A, Martínez-Lozano MA, Cabanes-Vila J, Barjau-Escribano A, Fos-Galve P (2006) Composite resins. A review of the materials and clinical indications. Med Oral Patol Oral Cir Bucal 11:215–220
35. Ryou M, Thompson CC (2006) Tissue adhesives: a review. Tech Gastrointest Endosc 8:33–37
36. Burns D, Doolan KP (2005) The discrimination of automotive clear coat paints indistinguishable by Fourier transform infrared spectroscopy via pyrolysis–gas chromatography–mass spectrometry. Anal Chim Acta 539:157–164
37. Bauer W Jr (2002) Methacrylic acid and derivatives. Ullmann's encyclopedia of industrial chemistry. Wiley-VCH, Weinheim
38. Pankow JF, Luo W, Bender DA, Isabelle LM, Hollingsworth JS, Chen C, Asher WE, Zogorski JS (2003) Concentration and concurrence correlations of 88 volatile organic compounds (VOCs) in the ambient air of 13 semi-rural to urban locations in the United States. Atmos Environ 37:5023–5046
39. Etievant PX, Azar M, Pham-Delegue H, Masson CJ (1984) Isolation and identification of volatile constituents of sunflowers (Helianthus annuus. L.). J Agric Food Chem 32:503–509
40. Isidorov V, Jdanova M (2002) Volatile organic compounds from leaves litter. Chemosphere 48:975–979
41. Klotz B, Barnes I, Imamura T (2004) Product study of the gas-phase reactions of O_3, OH and NO_3 radicals with methyl-ethyl-ether. Phys Chem Chem Phys 6:1725–1734
42. Smith DF, Melver CD, Kleindienst TE (1995) Kinetics and mechanism of the atmospheric oxidation of tertiary-amyl methyl ether. Int J Chem Kinet 27:453–472
43. Gai Y, Ge M, Wang W (2009) Rate constants for the gas phase reaction of ozone with n-butyl acrylate and ethyl methacrylate. Chem Phys Lett 473:57–60
44. Bernard F, Eyglunent G, Daële V, Mellouki A (2010) Kinetics and products of gas-phase reactions of ozone with methyl methacrylate, methyl acrylate and ethyl acrylate. J Phys Chem A 114:8376–8383
45. Wang K, Ge M, Wang W (2010) Kinetics of the gas-phase reactions of NO_3 radicals with ethyl acrylate, n-butyl acrylate, methyl methacrylate and ethyl methacrylate. Atmos Environ 44:1847–1850
46. Salgado MS, Gallego-Iniesta MP, Martín P, Tapia A, Cabañas B (2011) Night-time atmospheric chemistry of methacrylates. Environ Sci Pollut Res 18:940–948
47. Gaona E, Blanco MB, Barnes I, Teruel MA (2013) Gas phase kinetics for the ozonolysis of n-butyl methacrylate, ethyl crotonate and vinyl propionate under atmospheric conditions. Chem Phys Lett 579:11–15
48. Teruel MA, Lane SI, Mellouki A, Solignac G, Le Bras G (2006) OH reaction rate constants and UV absorption cross-sections of unsaturated esters. Atmos Environ 40:3764–3772
49. Blanco MB, Teruel MA (2008) Photodegradation of butyl acrylate in the troposphere by OH radicals: kinetics and fate of 1,2-hydroxyalcoxy radicals. J Phys Org Chem 21:397–401

50. Canosa-Mas CE, Carr S, King MD, Shallcross DE, Thompson KC, Wayne RP (1999) Kinetic study of the reactions of NO_3 with methyl vinyl ketone, methacrolein, acrolein, methyl acrylate and methyl methacrylate. Phys Chem Chem Phys 1:4195–4202
51. Canosa CE, Flugge ML, King MD, Wayne RP (2005) An experimental study of the gas-phase reaction of the radical NO3 with α, β-unsaturated compounds. Phys Chem Chem Phys 7:643–650
52. Atkinson R (1997) Gas-phase tropospheric chemistry of volatile organic compounds. 1. Alkanes and alkenes. J Phys Chem Ref Data 26:215–290
53. Saunders SM, Baulch DL, Cooke KM, Pilling MJ (1994) Smurthwaite PI. Kinetics and mechanisms of the reactions of OH with some oxygenated compounds of importance in tropospheric chemistry. Int J Chem Kinet 26:113–130
54. Blanco MB, Taccone RA, Lane SI, Teruel MA (2006) On the OH initiated degradation of methacrylates in the troposphere: gas-phase kinetics and formation of pyruvates. Chem Phys Lett 429:389–394
55. Blanco MB, Bejan I, Barnes I, Wiesen P, Teruel MA (2009) OH-initiated degradation of unsaturated esters in the atmosphere: kinetics in the temperature range of 287–313 K. J Phys Chem A 113:5958–5965
56. Blanco MB, Bejan I, Barnes I, Wiesen P, Teruel MA (2009) Temperature-dependent rate coefficients for the reactions of Cl atoms with methyl methacrylate, methyl acrylate and butyl methacrylate at atmospheric pressure. Atmos Environ 43:5996–6002
57. Colomer JP, Blanco MB, Peñéñory AB, Barnes I, Wiesen P, Teruel MA (2013) FTIR gas-phase kinetic study on the reactions of OH radicals and Cl atoms with unsaturated esters: Methyl 3,3-dimethylacrylate, (E)-ethyl tiglate and methyl-3-butenoate. Atmos Environ 79:546–552
58. Martín MP, Gallego-Iniesta MP, Espinosa JL, Tapia A, Cabañas B, Salgado MS (2010) Gas-phase reactions of unsaturated esters with Cl atoms. Environ Sci Pollut Res 17:539–546
59. Atkinson R (1991) Kinetics and mechanisms of the gas-phase reactions of the NO_3 radical with organic compounds. J Phys Chem Ref Data 20:459–507
60. Tuazon EC, Alvarado A, Aschmann SM, Atkinson R, Arey J (1999) Products of the gas-phase reactions of 1,3-butadiene with OH and NO_3 radicals. Environ Sci Technol 33:3586–3595
61. Blanco MB, Bejan I, Barnes I, Wiesen P, Teruel MA (2010) FTIR product distribution study of the Cl and OH initiated degradation of methyl acrylate at atmospheric pressure. Environ Sci Technol 44:7031–7036
62. Blanco MB, Bejan I, Barnes I, Wiesen P, Teruel MA (2014) Products and mechanism of the reactions of OH radicals and Cl atoms with methyl methacrylate ($CH_2 = C(CH_3)C(O)OCH_3$) in the presence of NOx. Environ Sci Technol 48:1692–1699
63. Grosjean D (1990) Atmospheric chemistry of toxic contaminants. Unsaturated aliphatics: acrolein, acrylonitrile, maleic anhydride. J Air Waste Manage Assoc 40:1664–1668
64. Environmental Protection Agency, http://www.epa.gov
65. Cabañas B, Salgado S, Martín P, Baeza MT, Martínez E (2001) Night-time atmospheric loss process for unsaturated aldehydes: reaction with NO_3 radicals. J Phys Chem A 105:4440–4445
66. Salgado MS, Monedero E, Villanueva F, Martín P, Tapia A, Cabañas B (2008) Night time atmospheric fate of acrolein and crotonaldehyde. Environ Sci Technol 42:2394–2400
67. Gertler AW, Bagley ST, Dippel WA (1998) Measurements of dioxin and furan emissions factors from heavy-duty diesel vehicles. J Air Waste Manage Assoc 48:276–278
68. Ciccioli P, Brancaleoni E, Frattoni M, Cecinato A, Pinciarelli L (2001) Determination of volatile organic compounds (VOC) emitted from biomass burning of mediterranean vegetation species by GC-MS. Anal Lett 34:937–955
69. Lev-On M, Le Travec C, Uijlein J, Alleman TL, Lawson DR, Vertin K, Thompson G.H, Gautam M, Wayne S, Okamoto R, Rieger P, Yee G, Ospital J, Zielinska B, Sagebiel J, Chatterjee S, Hallstrom K (2002) Chemical speciation of exhaust emissions from trucks and

buses fuelled on ultra-low sulphur diesel and CNG. Society of Automotive Engineers, SP-2002, SP-1673
70. Yokelson RJ, Karl T, Artaxo P, Blake DR, Christian TJ, Griffith DWT, Guenther A, Hao WM (2007) The tropical forest and fire emissions experiment: overview and airborne fire emission factor measurements. Atmos Chem Phys Discuss 7:5175–5196
71. Villanueva F, Cabañas B, Monedero E, Salgado S, Bejan I, Martín P (2009) Atmospheric degradation of alkylfurans with chlorine atoms: product and mechanistic study. Atmos Environ 43:2804–2813
72. Ameur LA, Rega B, Giampaoli P, Trystam G, Birlouez-Aragon I (2008) The fate of furfurals and other volatile markers during the baking process of a model cookie. Food Chem 111:758–763
73. Bail S, Krist S, Masters E, Unterweger H, Buchbauer G (2009) Volatile compounds of shea butter samples made under different production conditions in western, central and eastern Africa. J Food Compos Anal 22:738–744
74. Moon JK, Shibamoto T (2009) Role of roasting conditions in the profile of volatile flavour chemicals formed from coffee beans. J Agric Food Chem 57:5823–5831
75. Bierbach A, Barnes I, Becker KH (1995) Product and kinetic study of the OH-initiated gas-phase oxidation of furan, 2-methylfuran and furanaldehydes at $\approx$ 300 K. Atmos Environ 29:2651–2660
76. Berndt T, Böge O, Rolle W (1997) Products of gas-phase reactions of NO_3 radicals with furan and tetramethylfuran. Environ Sci Technol 31:1157–1162
77. Villanueva F, Barnes I, Monedero E, Salgado MS, Gómez MV, Martín P (2007) Primary distribution from the Cl-atom initiated atmospheric degradation of furan: environmental implications. Atmos Environ 41:8796–8810
78. Arey A, Obermeyer G, Aschamann SM, Chattopadhyay S, Cusick RD, Atkinson R (2009) Dicarbonyl products of the OH radical-initiated reaction of a series of aromatic hydrocarbons. Environ Sci Technol 43:683–689
79. Gómez-Álvarez E, Borrás E, Viidanoja J, Hjorth J (2009) Unsaturated dicarbonyl products from the OH-initiated photo-oxidation of furan, 2-methylfuran and 3-methylfuran. Atmos Environ 43:1603–1612
80. Atkinson R (1994) Gas phase tropospheric chemistry of organic compounds. J Phys Chem Ref Data Monogr 2:1–216
81. Zhao Z, Husainy S, Smith GD (2011) Kinetics studies of the gas-phase reactions of NO_3 radicals with series of 1-alkenes, dienes, cycloalkenes, alkenols, and alkenals. J Phys Chem A 115:12161–12172
82. Kerdouci J, Picquet-Varrault B, Durand-Jolibois R, Gaimoz C, Doussin JF (2012) An experimental study of the gas-phase reactions of NO3 radicals with a series of unsaturated aldehydes:trans-2-hexenal, trans-2-heptenal, and trans-2-octenal. J Phys Chem A 116:10135–10142
83. Colmenar I, Cabañas B, Martínez E, Salgado MS, Martín P (2012) Atmospheric fate of a series of furanaldehydes by their NO_3 reactions. Atmos Environ 54:177–184
84. Martín P, Cabañas B, Colmenar I, Salgado MS, Villanueva F, Tapia A (2013) Reactivity of E-butenedial with the major atmospheric oxidants. Atmos Environ 70:351–360
85. Atkinson R (2000) Atmospheric chemistry of VOCs and NOx. Atmos Environ 34:2063–2101
86. Atkinson R (2007) Gas-phase tropospheric chemistry of organic compounds: a review. Atmos Environ 41:200–240
87. Kanakidou M, Seinfeld JH, Pandis SN, Barnes I, Dentener FJ, Facchini MC, Van Dingenen R, Ervens B, Nenes A, Nielsen CJ, Swietlicki E, Putaud JP, Balkanski Y, Fuzzi S, Horth J, Moortgat GK, Winterhalter R, Myhre CEL, Tsigaridis K, Vignati E, Stephanou G, Wilson J (2005) Organic aerosols and global climate modelling. A review. Atmos Chem Phys 5:1053–1123

88. Atkinson R, Aschmann SM, Goodman MA (1987) Kinetics of the gas-phase reactions of nitrate radicals with a series of alkynes, haloalkenes, and α, β-unsaturated aldehydes. Int J Chem Kinet 19:299–307
89. Ullerstam M, Ljungstrom E, Langer S (2001) Reactions of acrolein, crotonaldehyde and pivalaldehyde with Cl atoms: structure activity relationship and comparison with OH and NO_3 reactions. Phys Chem Chem Phys 3:986–992
90. Cabañas B, Martín P, Salgado S, Ballesteros B, Martínez E (2001) An experimental study on the temperature dependence for the gas-phase reactions of NO_3 radicals with a series of aliphatic aldehydes. J Atmos Chem 40:23–39
91. Atkinson R, Arey J, Aschmann SM, Corchnoy SB, Shu Y (1995) Rate constants for the gas-phase reactions of cis-3-hexen-1-ol, cis-3-hexenylacetate, trans-2-hexenal, and linalool with OH and NO_3 radicals and O_3 at 296 ± 2 K, and OH radical formation yields from the O_3 reactions. Int J Chem Kinet 27:941–955
92. Klotz B, Bierbach A, Barnes I, Becker KH (1995) Kinetic and mechanistic study of the atmospheric chemistry of muconaldehydes. Environ Sci Technol 29:2322–2332
93. IUPAC (2001) Subcommittee for gas kinetic data evaluation, evaluated gas kinetic data for atmospheric chemistry, www.iupac-kinetic.ch.cam.ac.uk
94. Canosa-Mas CE, Cotter ESN, Duffy J, Thompson KC, Wayne RP (2001) The reactions of atomic chlorine with acrolein, methacrolein and methyl vinyl ketone. Phys Chem Chem Phys 3:3075–3084
95. Pfrang C, Martin RS, Nalty A, Waring R, Canosa-Mas CE, Wayne RP (2005) Gas-phase rate coefficients for the reactions of nitrate radicals with (Z)-pent-2-ene, (E) pent-2-ene, (Z)-hex-2-ene, (E)-hex-2-ene, (Z)-hex-3-ene, (E)-hex-3-ene and (E)-3 methylpent-2-ene at room temperature. Phys Chem Chem Phys 7:2506–2512
96. Noda J, Holm C, Nyman G, Langer S, Ljungstrom E (2003) Kinetics of the gas phase reaction of n-C_6-C_{10} aldehydes with the nitrate radical. Int J Chem Kinet 35:120–129
97. Ellermann T, Nielsen OJ, Skov H (1992) Absolute rate constants for the reaction of NO_3 radicals with a series of dienes at 295 K. Chem Phys Lett 200:224–229
98. Grosjean D, Grosjean E, Williams EL (1992) Environmental persistence of organic compounds estimated from structure-reactivity and linear free energy relationships unsaturated aliphatics. Atmos Environ A 26:1395–1405
99. Cabañas B, Tapia A, Villanueva F, Salgado S, Monedero E, Martín P (2008) Kinetic study of 2-furanaldehyde, 3-furanaldehyde and 5-methyl-2- furanaldehyde reactions initiated by Cl atoms. Int J Chem Kinet 40:670–678
100. Martínez E, Cabañas B, Aranda A, Wayne RP (1996) Kinetic study of the reactions of NO_3 with 3-chloropropene, 3-bromopropene and 3-iodopropene using LIF detection. J Chem Soc Faraday Trans 92:4385–4389
101. Martínez E, Cabañas B, Aranda A, Albaladejo J, Wayne RP (1997) Absolute rate coefficients for the reaction of NO_3 with pent-1-ene and hex-1-ene at $T = 228$ to 433 K determined using LIF detection. J Chem Soc Faraday Trans 93:2043–2057
102. Martínez E, Cabañas B, Aranda A, Martin P, Salgado S (1999) Absolute rate coefficients for the gas-phase reactions of NO_3 radicals with a series of monoterpenes at $T = 298$ to 433K. J Atmos Chem 33:265–282
103. Martínez E, Cabañas B, Aranda A, Martin P, Notario A, Salgado S (1999) Study of the NO_3 radical reactivity: reaction with cyclic alkenes. J Phys Chem 103:5321–5327
104. Bierbach A, Barnes I, Becker KH, Wiesen E (1994) Atmospheric chemistry of unsaturated carbonyls: butenedial, 4-oxo-2-pentenal, 3-hexene-2,5-dione, maleic anhydride, 3H-furan-2-one, and 5-methyl-3H-furan-2-one. Environ Sci Technol 28:715–729
105. Marston G, Monks PS, Canosa-Mas C, Wayne RP (1993) Correlations between rate parameters and calculated molecular properties in the reactions of the nitrate radical with alkenes. J Chem Soc Faraday Trans 89:3899–3905
106. Colmenar Ph Thesis 2013. Degradación e implicaciones atmosféricas de aldehídos insaturados. Estudio cinético y mecanismos de reacción. Universidad de Castilla La Mancha

107. D'Anna B, Nielsen CJ (1997) Kinetic study of the vapour-phase reaction between aliphatic aldehydes and the nitrate radical. J Chem Soc Faraday Trans 93:3479–3483
108. Shu Y, Atkinson R (1995) Atmospheric lifetimes and fates of a series of sesquiterpenes. J Geophys Res Atmos 100:7275–7281
109. Spicer CW, Chapman EG, Finlayson-Pitts BJ, Plastridge RA, Hubbe JM, Fast JD, Berkowitz CM (1998) Unexpected high concentrations of molecular chlorine in coastal air. Nature 394:353–356
110. Blanco MB, Bejan I, Barnes I, Wiesen P, Teruel MA (2009) The Cl-initiated oxidation of CH3C(O)OCH = CH2, CH3C(O)OCH2CH = CH2, and CH2 = CHC(O)O(CH2)3CH3 in the troposphere. Environ Sci Pollut Res 16:641–648
111. Mielke LH, Furgeson A, Osthoff HD (2011) Observation of ClNO2 in a mid-continental urban environment. Environ Sci Technol 45:8889–8896
112. Phillips GJ, Tang MJ, Thieser J, Brickwedde B, Schuster G, Bohn B, Lelieveld J, Crowley JN (2012) Significant concentrations of nitryl chloride observed in rural continental Europe associated with the influence of sea salt chloride and anthropogenic emissions. Geophys Res Lett. doi:10.1029/2012GL051912
113. Galán E, Gonzalez I, Fabbri B (2002) Estimation of fluorine and chlorine emissions from Spanish structural ceramic industries. The case study of Bailén area, Southern Spain. Atmos Environ 9:5289–5298
114. Roberts JM (1995) In: Singh HB (ed) Composition chemistry and climate of the atmosphere. VNR-Verlag, New York
115. Olszyna KJ, Bailey EM, Simonaitis R, Meagher JF (1994) O_3 and NO_x relationships at a rural site. J Geophys Res A 99:14557–14563
116. Peak MJ, Belser WL (1969) Some effects of the air pollutant, peroxyacetyl nitrate, upon deoxyribonucleic acid and upon nucleic acid bases. Atmos Environ 3:385–397
117. Taylor OC (1969) Importance of peroxyacetyl nitrate (PAN) as a phytotoxic air pollutant. J Air Pollut Control Assoc 19:347–351
118. Kleindienst TE, Shepson PB, Smith DF, Hudgens EE, Nero CM, Cupitt LT, Bufalini JJ, Claxton LD (1990) Comparison of mutagenic activities of several peroxyacyl nitrates. Environ Mol Mutagen 16:70–80
119. IARC, International Agency for Research on Cancer (2002) Monographs on the evaluation of carcinogenic risks to humans. World Health Organization, http://monographs.iarc.fr

Mercury Soil Pollution in Spain: A Review

Pablo Higueras, Rodolfo Fernández-Martínez, José María Esbrí, Isabel Rucandio, Jorge Loredo, Almudena Ordóñez, and Rodrigo Álvarez

Abstract Spain has been the main mercury producer worldwide, with mines or mining districts scattered across its geography. In particular, two main areas show generally higher contents of this element in the soils, namely, Asturias (or the Cantabrian Zone in geological terms) and the Almadén area in the Southern Central Iberian Zone. In this review six different aspects are considered: (1) distribution of total concentrations, (2) mercury mobility and availability, (3) soil to plant transfer, (4) mercury transfer to animal biota, (5) soil to atmosphere transfer and (6) possibility of remediation for sites polluted by mercury. The conclusions drawn from the available results highlight significant differences in contents, mobility and transfer processes depending on the different types of mercury pollution and different climatic conditions. A general background level for Spanish soils can be established at 20 μg kg^{-1}, but very different ranges can be found in different areas according to the volumetric importance of each source and depending on other local factors. Mercury mining appears to be the most important source of soil pollution, and studies on the possible mobility and transfer to other environmental compartments demonstrate the highest levels at which mercury affects the population living in the proximity of such sources.

Keywords Availability, Mercury, Plants, Soil pollution, Spain

P. Higueras (✉) and J.M. Esbrí
Instituto de Geología Aplicada, University of Castilla-La Mancha (Spain). E.I.M.I. Almadén, Pl. Manuel Meca 1, 13400 Almadén (Ciudad Real), Spain
e-mail: pablo.higueras@uclm.es

R. Fernández-Martínez and I. Rucandio
Spectroscopy Unit, Chemistry Division, Technology Department, Centro de Investigaciones Energéticas, Medioambientales y Tecnológicas (CIEMAT), Av. Complutense 40, E-28040, Madrid, Spain

J. Loredo, A. Ordóñez, and R. Álvarez
Dep. Explotación y Prospección de Minas, University of Oviedo, Escuela Técnica Superior de Ingenieros de Minas, c/Independencia, 13, 33004, Oviedo, Spain

E. Jiménez et al. (eds.), *Environment, Energy and Climate Change I: Environmental Chemistry of Pollutants and Wastes*, Hdb Env Chem (2015) 32: 135–158,
DOI 10.1007/698_2014_280,
Published online: 9 August 2014

Contents

1 Introduction

Mercury (Hg) is considered to be a 'Global Pollutant' because of its biogeochemical mobility. This element can be emitted to the environment in different chemical forms or as different species, many of which are innocuous per se in terms of availability but are susceptible to transformation into other species that can enter the human food chain, particularly through the consumption of fish. Spain has been the major Hg producer worldwide and, in particular, Almadén (Ciudad Real; South Central Spain) has been the source of almost one third of the total historic production of this heavy metal. Almadén is not just a mine but a district (Almadén Mercury Mining District, AMMD), with cinnabar (HgS, the most important Hg ore) deposits exploited in an area totalling some 125 km^2. Other national Hg-producing regions include Asturias (Northern Spain), which has a number of small to intermediate mines throughout the Cantabrian Mountains; the Alpujarras region (Granada and Almería provinces, SE Spain), which also has a number of small mines; Usagre (Badajoz, SW Spain), with an intermediate-sized mine; and Chóvar (Sierra de Espadán, Castellón province, E Spain). The majority of these mines (all except the AMMD mines) closed in the early 1970s due to ecotoxicological and ecological concerns arising from the catastrophic Minamata (Japan) and Iraq poisoning episodes [1, 2]. The closure of these mines before the general implementation of legislative action to protect the environment in the 1980s led to them being abandoned without any decontamination measures, a situation that has made these sites significant sources of Hg pollution to the surrounding soils over several decades. Besides, Hg in Spain has been used in a number of industrial processes. For example, the chlor-alkali industry has been the main consumer of this metal, with seven national plants using this technology since the opening of the first plant (Flix) in 1899. The explosives and cartridge industries were also

significant consumers of mercury, with the most important ones located outside Oviedo in Asturias and in the outskirts of Toledo. Zn smelters are also potential sources of Hg pollution to their surroundings, and in Spain such plants exist in Avilés (Asturias) and in Cartagena (Murcia province, Eastern Spain). Coal-fired power plants are also important contributors to atmospheric Hg pollution ([3, 4], among others) and, as such, they could also contribute to soil pollution with this metal. The same can be said for incinerators ([5], among others). Other Spanish industries that use Hg to a greater or lesser extent are those related to the fabrication of fluorescent lamps, thermometers and batteries. In terms of soil pollution, the major recognised contributors to this process have been, in our experience, Hg mining and chlor-alkali plants.

2 Descriptions of the Main Sources of Hg Pollution

In this review, we will consider the main Hg pollution sources in Spain with reference to published data concerning soil pollution. These main sources are described below.

Almadén (Ciudad Real province, South Central Spain) is the largest Hg mining district in the world ([6, 7], among others). This industry has produced almost 300,000 t of the metal during more than 2,000 years of uninterrupted activity since documented activity began in Roman times to the final closure of the mines and metallurgy in 2003. The district is the subject of the largest number of studies with reference to soil pollution, some of which focus on the (geo)chemistry of this pollution [8–20]; other studies are centred on the transfer from local soils to plants [21–36]; others are devoted to the transfer from soils to vertebrates [37, 38] or to humans [39, 40]; others refer to gaseous emissions from soils [41, 42], and in others, methodologies are proposed for soil decontamination [23, 43–47].

The *Asturias* region, in Northern Spain, can also be considered as an important Hg mining district at a world level, including evidence of 18 mineralised areas spread throughout the area of the Cantabrian Mountains [48, 49]. Regarding the volume of mineral extracted and treated, the most important sites are those of the El Terronal-La Peña group [50], located close to Mieres, and the Soterraña mine, located in the proximity of Pola de Lena. Some of these mines were active during Roman times, and Loredo et al. [51] indicated that the main production from the El Terronal-La Peña group (in the order of 500 flasks/month) corresponded to the late 1960s and early 1970s. Furthermore, smelting activities developed in some of the most important mining sites markedly enhanced the mobilisation of Hg and associated elements and led to their deposition in soils. Fernández-Martínez et al. [52, 53], Loredo et al. [54], Esbrí et al. [17] and Ordóñez et al. [55] described Hg contents in local soils, while López Alonso et al. [56, 57] and Miranda et al. [58] studied the transfer to cattle and Sierra et al. [47] described the possibility of soil washing for the extraction of Hg from the local soils.

Usagre (Badajoz province, SW Spain) corresponds to a medium- to small-sized cinnabar mine located in Cambrian marble from the Ossa-Morena Zone in the Iberian Massif. The mine was active from an unknown date to the early 1970s, when most Hg mines worldwide closed, and the total production is also unknown. García-Sánchez et al. [59] described Hg concentrations in soils from this area.

Valle del Azogue and Bayarque (Almería province, SE Spain) corresponds to a Hg-Sb district, with cinnabar and stibnite (Sb_2S_3) as the main ores [60, 61]. These are minor mercury mines that were exploited during the nineteenth century (1873–1888) by means of underground works and small open pits located close to two smelting sites [62]. Viladevall et al. [63], Navarro et al. [43, 61, 64] and Navarro [65] studied the soils and the mine passives in terms of Hg contents.

Flix (Tarragona, NE Spain) is the oldest chlor-alkali plant operating in Spain. The primitive technology favours significant emissions of gaseous Hg, as evidenced by the total gaseous mercury concentrations, which are well above the values measured in other Spanish plants [66]. In this case, Hg soil pollution arises from atmospheric deposition of gaseous Hg emitted by the plant along with downstream dissemination of plant residues that were disposed of on the banks of the Ebro River [67–70].

Furthermore, in several publications, the Hg contents in soils for general areas are described: FOREGS [71] presented data for the whole of Europe, including Spain; IGME [72] reported data for the whole of Spain; Rodríguez-Martín et al. [73] analysed Hg and other heavy metals from agricultural soils from the Ebro Basin; and Gil et al. [74] and Ramos-Miras et al. [75] studied Hg contents in non-contaminated calcareous-type soils from Almería and Valencia provinces (SE and S Spain, respectively).

3 Distribution of Total Mercury Concentrations in Soils

Mercury is emitted in different forms from known sources and its geographic distribution is controlled by numerous different parameters, both intrinsic and extrinsic (Fig. 1). Intrinsic parameters depend on the form of Hg being disseminated:

- Gaseous mercury includes the undifferentiated total gaseous mercury (TGM) and the three classical species, namely, gaseous elemental mercury (GEM), reactive gaseous mercury (RGM) and particulate mercury (PM). These are emitted to the atmosphere from all types of sources and they return to the soils through wet and/or dry deposition. In these forms, mercury can be disseminated over considerable distances, with the limitation of atmospheric dilution.
- Dissolved mercury is lixiviated from polluted soils or released directly into the environment by industries. The dispersion of dissolved mercury is channelled by water courses, and, in terms of soil processes, its presence leads more to pollution lixiviation than to pollution concentration.

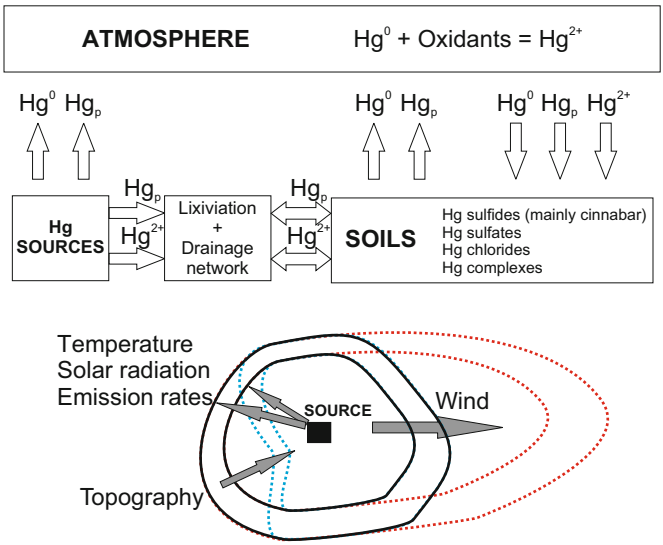

Fig. 1 Diagram of the mercury flows in soil and atmosphere

– Solid mercury species, including the most common one, cinnabar, is mainly emitted from mining sources. Other possible species include sulphides, sulphates, chlorides and others. The dispersion of mercury in this form is limited except for the finest particles, which can be dragged by wind in the form of atmospheric PM over variable distances.

Extrinsic parameters include the following:

– *Volumetric importance of the source area*: The volume (and its temporal extent of activity) influences the geographic extent of the polluted area and also the quantity of pollutants, which is reflected in the concentrations of mercury in the soils.
– *Climatology/meteorology*: Climatic and meteorological factors, and in particular wind, affect the directional extent of pollution, particularly for wind-driven species. Temperature and solar radiation promote gaseous mercury emissions from polluted soils [41, 42] and favour redeposition of mercury away from the source area.
– *Physiography*: The topographic array of an area influences the dissemination of all possible forms of mercury.

3.1 General Data

The Geochemical Atlas of Europe [71] shows the distribution of a significant number of elements, including Hg, in European soils. The Spanish territory is

covered by 87 samples and the concentrations measured range between 0.005 and 1.038 mg kg^{-1}. The median of the European data was 0.061 mg kg^{-1} in a range between 0.005 and 1.354 mg kg^{-1}.

The Geochemical Atlas of Spain [72] contains Hg concentrations for sediments and for two soil horizons, 0–25 cm and 25–50 cm, with higher values found in the topsoil than in the deeper soil samples (maximum concentrations = 73.5 and 11.1 mg kg^{-1}, respectively). The central 50% of the measured values range between 0.005 and 0.05 mg kg^{-1}, with a median at 0.02 mg kg^{-1} for both soil horizons; this figure can be stated as a general background level for Spanish soils. The main anomalous areas correspond to the most important Hg mining areas: Almadén, with an extensive area with values above 0.23–0.24 mg kg^{-1}; Asturias (including all of the Cantabrian Zone); the Sierra del Espadán area (Maripí mine, Chóvar, Castellón province); the Usagre area; and the Alpujarras area (Granada-Almería provinces). Minor Hg anomalies are also mentioned, and these are related to mining activity for other sulphide deposits such as Zn deposits in Cantabria, Lugo and Biscay; Pb-Zn deposits in Sierra Morena (Badajoz, Seville, Cordoba and Jaén provinces) and in the Betic Cordillera (Sierra de Lújar, Granada province); or polymetallic sulphide deposits in the Iberian Pyrite Belt (Huelva and Seville provinces), among others. Also of minor importance in comparison to the levels associated with the largest Hg mining deposits are other possible anthropogenic anomalies described for northern Asturias (possibly related to Zn smelting), the area affected by the Aznalcollar mine tailing spill accident [76] and in the outskirts of cities such as Madrid, Valencia, Seville and Huelva, which are related to local industrial activities.

Rodríguez-Martín et al. [73] and Gil et al. [74] analysed Hg and other heavy metals from non-contaminated agricultural soils from the River Ebro basin and Hg contents in calcareous-type soils from Almería and Valencia provinces (SE and S Spain) (Table 1). Results are comparable with those of general non-contaminated areas.

3.2 Almadén

Almadén is by far the largest Spanish Hg source in terms of production and also the most affected area from an environmental point of view. The distribution of measured Hg values (Table 1) indicates the extensive pollution that affects a number of areas in the district; particularly worrying is the situation inside the decommissioned Almadenejos metallurgical precinct (ADMP), which was studied by Martínez-Coronado et al. [20] and Millán et al. [19]. In this area concentrations reached 40,000 mg kg^{-1}, which corresponds to a content of 0.4% Hg in these soils. Gray et al. [40] studied the toxicity to humans of these materials and found them to be highly accessible via the ingestion pathway. Reclamation measures have not been carried out in this area, which is used by the inhabitants of Almadenejos for cattle breeding (also pigs, sheep, horses, poultry) with permission of the precinct

Table 1 Total Hg contents in soils in Spanish sites

	N	Hg (mg kg^{-1})	Reference
Spain			
Spanish soils	NA	0.005–73.5	IGME [72]
Almadén			
4 sites	67	6–8,889	Higueras et al. [10]
10 sites	NA	5–1,710	Millán et al. [24]
30 sites	34	0.13–2,695	Molina et al. [26]
Transect	22	3.4–7,315	Bueno et al. [16]
ADMP	16	25–15,900	Martínez-Coronado et al. [20]
ADMP	7	5–40,000	Millán et al. [19]
ADMP, surroundings	35	4–174	Martínez-Coronado et al. [20]
Huerta del Rey	26	80–3,510	Llanos [77]
Huerta del Rey, surroundings	32	8–1,530	Llanos [77]
Las Cuevas	55	6–4,153	Llanos et al. [18]
Las Cuevas, surroundings	36	1–185	Llanos et al. [18]
Almadén	NA	2.3–97	Lindberg et al. [21]
Nueva Concepción	60	6.96–245	Castillo [78]
Nueva Concepción, surroundings	20	6.42–721	Castillo [78]
Local background levels		20–22	Molina et al. [26]
Asturias			
La Peña-El Terronal	89	2–1,585	Ordóñez et al. [55]
La Soterraña	56	2–502	Ordóñez et al. [55]
Brañamalosa	28	1–895	Ordóñez et al. [55]
Maramuñiz	24	2–577	Ordóñez et al. [55]
Olicio	6	76–344	Ordóñez et al. [55]
Caunedo	7	6–14	Ordóñez et al. [55]
La Campa del Trave	34	8–759	Ordóñez et al. [55]
Usagre			
	6	5–778	García-Sánchez et al. [59]
	26	0.2–311	Villaseca [79]
Azogue Valley			
Azogue Valley wastes	16	<1–4,000	Navarro et al. [43]
Azogue Valley soils	NA	<1–2,300	Navarro et al. [43]
Bayarque wastes	3	66–4,600	Navarro et al. [43]
Bayarque soils	1	33	Navarro et al. [43]
Flix			
Soils on alluvial sediments (Ebro)	22	0.098–495	Esbrí et al. [80]
Soils	55	0.044–13	Esbrí et al. [80]
Spanish non-contaminated soils			
Almería	53	0.009–1.6	Gil et al. [74]
Ebro River basin	13	0.001–0.7	Rodríguez-Martín et al. [73]
Reference levels			
Intervention values (industrial)	NA	30	Agencia de Residus de Catalunya [81]
Intervention values (residential)	NA	3	Agencia de Residus de Catalunya [81]

(continued)

Table 1 (continued)

	N	Hg (mg kg^{-1})	Reference
Intervention values (others)	NA	2	Agencia de Residus de Catalunya [81]
Soil guidance value for residential (UK)	NA	170	Environment Agency [82]
Hg content in world soils	NA	0.01–0.5	Alloway [83]
Non-contaminated soils	NA	0.01–0.03	Senesi et al. [84]

NA Not available, *BDL* Below detection limits, *ADMP* Almadenejos decommissioned metallurgical precinct

owner, i.e. the mining company. Other areas of concern are the decommissioned Huerta del Rey metallurgical precinct, which is located very close to the Almadén urban area. In this area, Llanos [77] measured concentrations of 80–3,510 mg kg^{-1}, and in the Las Cuevas mine area, concentrations of 6–4,153 mg kg^{-1} were found [18].

3.3 Asturias

As described above, a significant number of Hg mining sites are present in Asturias province and this area is also relatively rich in As. Although all of the mines were closed at least 40 years ago, considerable quantities of Hg and As are still released into the environment in this mining district. The main Hg data corresponding to the different mining sites of this area are shown in Table 1. Average Hg concentrations in the abandoned Hg mine sites of Asturias are between 80 (Caunedo site) and 300 (La Campa del Trave site) times higher than the mean Hg content in world soils [83] and up to 37 times higher than the local background levels estimated by Ordóñez et al. [55]. Additionally, average As concentrations are 2 (Caunedo) to 80 (La Soterraña) times higher than the average As content in world soils [85] and up to 21 times higher than the local background levels reported by Ordóñez et al. [55]. These metal contents should be the cause of environmental concern. The statistical analysis of multielemental geochemical data reveals a clear positive correlation between the total Hg and As concentrations in soils, and a marked anomaly for both elements is observed in the area affected by the abandoned mine works [55]. This finding is consistent with a common origin for the accumulation of these elements in soils and it can be related to the weathering of low-grade ore stored in the spoil heaps. The effect of mining activity seems to be the main factor involved in metal dispersion, but it is localised in the vicinity of the mines. In all of the sites studied, the estimated level of risk exceeds the commonly established regulatory values and this is driven by the high concentrations of As and Hg. Fortunately, most of these mines are located in sparsely populated areas, so the chronic exposure of potential receptors is low [86].

3.4 Usagre

Usagre is a single mining site with minor metallurgical activity. Total Hg contents at this site were studied by García-Sánchez et al. [59]. The results, as expected for a single and not especially productive mine, are comparable to those obtained for minor mining sites from the AMMD, such as 'La Nueva Concepción' [78] (Table 1).

3.5 Valle del Azogue

The Valle del Azogue area corresponds, like Usagre, to minor cinnabar mines that have been abandoned since the late twentieth century without any reclamation measures. This activity left a legacy of mining and metallurgic installations, including dumps, dams and calcine piles [43, 61, 63–65]. The Hg concentration data for local soils and passives are summarised in Table 1. The values found are of the same order of magnitude as those from the Las Cuevas mine and Usagre and are clearly related to the presence of unreclaimed mine passives.

3.6 Flix

Flix (Tarragona province, NE Spain) corresponds to a different type of Hg-polluted site. The local source of this element is a chlor-alkali plant with very old technology that produces significant gaseous Hg emissions, which through dry and wet deposition have been transferred to the soils. A total of 350,000 t of hazardous industrial solid waste from this plant was also deposited on the banks of the River Ebro. The solid waste contained high Hg concentrations (170 mg kg^{-1}) in the surface sediments and up to 440 mg kg^{-1} at a depth of 100 cm [70]. Esbrí et al. [80] described the geochemical characteristics of soils from this area. The main data from this study are provided in Table 1. Higher concentrations were found in the alluvial sediments, where values comparable to those recorded in minor mines from the AMMD were reached. Soils affected exclusively by atmospheric Hg deposition gave much lower values, but these were still four orders of magnitude above the reference values for uncontaminated areas.

4 Mercury Mobility and Availability

The mobility, availability and toxicity of Hg depend upon the specific chemical forms and the interactions with the different soil constituents. Cinnabar and other Hg sulphides, Hg oxides and sulphates, elemental Hg and organomercury compounds are the most common Hg species found in mining areas. However, some clay materials, oxyhydroxides and organic matter have been described as scavengers of inorganic and organomercury compounds [87, 88]. Mercury in soils can be mobilised due to different factors [89, 90]. Consequently, detailed information about the interactions between Hg and the bulk soil is required in order to estimate the environmental impact.

A considerable number of studies have focused on the assessment of Hg mobility in soils from the Almadén mining district and these involve the application of selective sequential extractions (Table 2). Fernández-Martínez and Rucandio [8] applied a two-stage sequential extraction procedure (SEP) and found that Hg was predominantly present in the sulphide fraction, which ranged from 85 to 90% of the total Hg content. In contrast, in a similar study, Sánchez et al. [13] applied a six-step SEP and found that Hg was predominantly associated with crystalline Fe and Mn oxyhydroxides (15–37% of the total Hg) and only 8–20% of the total Hg content could be assigned to the nonmobile form, namely, cinnabar. Readily available Hg forms were not significant (<0.5% of the total Hg) and only low amounts of Hg associated with organic matter could be found (1.3–2.4% of the total Hg). A similar Hg distribution was identified by Sierra et al. [29] in a study carried out on soils from an agricultural and pastureland area in Almadén. A six-step SEP was applied to calcine wastes by Bernaus et al. [15]. The results showed significant Hg percentages in the readily available Hg fractions, and this finding is related to the presence of more soluble Hg compounds, which have a higher risk of Hg mobilisation. The same SEP was applied by Millán et al. [19] to highly polluted soil samples from ADMP. In this case, Hg was present mainly in the residual fraction (31–70% of the total Hg). High Hg percentages were found in the oxidisable fraction (8–20%) and the fraction that was soluble in 6 M HCl (22–59%), indicating significant association of the Hg to soil organic matter as well as to Fe and Mn crystalline oxyhydroxides. These authors attributed the high Hg contents in the least soluble fractions to the presence of unconverted cinnabar and other Hg species that are usually formed during the processing of the ore due to the incomplete roasting process. More recently, the application of a Hg-specific four-step SEP to soil profiles from Almadén [91, 93] revealed that Hg was mainly present as Hg sulphide (55–86%) and as elemental Hg (9–33%). In addition, elemental Hg increased with soil depth. Mobile Hg fractions were only relevant in deeper soil profiles, and humic and fulvic complexes had a small influence on the Hg distribution since they only represented a Hg percentage of <6%.

Regarding organic Hg speciation, Gray et al. [12] reported extremely high methylmercury concentrations (0.2–3,100 μg kg^{-1}) in mine waste calcines from Almadén. The authors suggested that the highly reactive Hg(II) concentrations in

Table 2 Mercury mobility data in historic mining areas in Spain

Location	Methodology	Target phases/identified Hg species	References
Almadén	Selective sequential extraction	F1: Non-sulphide Hg	Fernández-Martínez and Rucandio [8]
		F2: Bound to sulphide Hg	
		F1: Water soluble	Sánchez et al. [13], Sierra et al. [29],
		F2: Exchangeable	Bernaus et al. [15], Millán et al. [19]
		F3: Carbonates	
		F4: Easily reducible	
		F5: Oxidisable	
		F6: Residue	
		F1: Labile Hg species	Fernández-Martínez and Rucandio [91]
		F2: Humic and fulvic complexes	
		F3: Elemental Hg and bound to crystalline oxides	
		F4: Hg sulphide and refractory species	
	Organomercury speciation	MeHg	Gray et al. [12]
		Organic Hg	Fernández-Martínez and Rucandio [91]
	Thermodesorption analysis	Humic complexes, cinnabar	Higueras et al. [10]
	XAS speciation	Cinnabar, HgO, $Hg_3(SO_4)O_2$	Bernaus et al. [15]
		Cinnabar, metacinnabar, $HgCl_2$, Hg_2Cl_2, $Hg_3(SO_4)O_2$	Esbrí et al. [17]
Asturias	Selective sequential extraction	F1: Mobile Hg	Fernández-Martínez et al. [52, 53]
		F2: Semi-mobile Hg	
		F3: Nonmobile Hg	
		F1: Labile Hg species	Fernández-Martínez et al. [92]
		F2: Humic and fulvic complexes	
		F3: Elemental Hg and bound to crystalline oxides	
		F4: Hg sulphide and refractory species	
	Organomercury	Organic Hg	Fernández-Martínez and Rucandio [91]
	XAS speciation	Cinnabar, metacinnabar, $HgCl_2$, HgO, $HgSO_4$	Esbrí et al. [17]

(continued)

Table 2 (continued)

Location	Methodology	Target phases/identified Hg species	References
Usagre	Selective extraction	Exchangeable Hg	García-Sánchez et al. [59]
	Thermal desorption	Hg(0)	García-Sánchez et al. [59]
Valle del Azogue	Thermodesorption analysis	Cinnabar, matrix-bound Hg	Navarro et al. [43, 61]
	Water leaching	Mobilisable Hg species by runoff	Navarro et al. [43, 61]

calcine piles could be bioavailable for the microbial transformation of inorganic Hg to methylmercury. Therefore, ADMP was identified as a 'hot spot' for Hg methylation since it presented the highest reactive Hg(II) concentrations. Organic Hg concentrations ranging from 79 to 287 μg kg^{-1} were reported in a recent study carried out on soil profiles from two different sites in Almadén [91]. Positive correlations were found between organic Hg and total organic carbon and also between organic Hg and elemental Hg contents. These results suggest that the elemental Hg present in soils can be converted to reactive Hg(II), mostly by oxidation, and further methylated by microbial activity.

Thermal fractionation analyses were performed on soils from the ADMP and its surroundings [10]. Analysis of the Hg thermodesorption curves showed the presence of cinnabar and Hg-humic complexes.

μ-EXAFS speciation analysis [15] showed that cinnabar was the main species present in most of the studied particles of calcine samples (5–89% of the total Hg) together with more soluble species such as schuetteite ($Hg_3(SO_4)O_2$) and HgO in high proportions (5–55% of the total Hg). Evidence for the possible presence of $HgCl_2$ was also observed and this would be consistent with the higher Hg mobility observed in these samples by SEP. A more recent study performed by XANES revealed the presence of five Hg phases (cinnabar, metacinnabar, $HgCl_2$, Hg_2Cl_2 and schuetteite) [17] and that metacinnabar was linked with metallurgical activities and calomel and schuetteite with weathering processes.

Several studies on Hg mobility and speciation have been carried out in the Asturias mining district (Table 2). Fernández-Martínez et al. [52, 53] studied calcine piles and soils at the El Terronal mine and they found Hg enrichment in the finest grain-size fractions downslope from the mine. The element was present mainly in semi-mobile (about 50% of the total Hg) and nonmobile (about 50% of the total Hg) fractions, which correspond to cinnabar (nonmobile) and elemental Hg and Hg(II) complexes (semi-mobile), respectively. Although the mobile fraction represented only 1.1% of the total Hg, this fraction is an evident risk to the environment since it presented a relatively high Hg concentration (120 mg kg^{-1}). In soil samples, Hg was predominantly extracted in the semi-mobile fraction (52–56% of the total Hg) with contents of nonmobile Hg of around 40%. Samples collected downslope from the roasting site contained a higher percentage of mobile Hg (6.5% of the total Hg) as a consequence of the accumulation of leachates from the waste near to the roasting site. Regarding the Hg distribution in grain-size fractions, the semi-mobile fraction was more concentrated in the finest subsamples, while the nonmobile fraction was predominant in the coarsest fractions. A similar but more detailed study was recently carried out in the same area [92] and the results showed high Hg concentrations associated with Fe crystalline oxides, elemental Hg and cinnabar. In addition, extremely high Hg concentrations were extracted from the most soluble fractions (10–22% of the total Hg), especially in the finest grain-size subsamples. Furthermore, although organic Hg only represented 0.5–0.9% of the total Hg, high organic Hg concentrations were found in calcine pile samples (22–236 mg kg^{-1}). The authors attributed the high Hg mobility in calcine piles to the presence of reactive Hg(II) species, formed during ore processing. In

contrast, soil samples exhibited low Hg concentrations in terms of soluble and organic Hg fractions. Hg was mainly associated with Fe crystalline oxides and cinnabar. Significant Hg concentrations associated with humic and fulvic acids were also found.

Esbrí et al. [17] studied mercury levels in the La Peña-Terronal mine (Asturias province) and found that Hg was present as $HgCl_2$, HgO, $HgSO_4$, cinnabar and metacinnabar, with a predominance of sulphide species. The presence of highly soluble Hg species such as $HgCl_2$ indicates a higher Hg mobility in soils from Asturias than in those from Almadén. The ratios between cinnabar and metacinnabar were higher than those found in Almadén as a result of the less efficient metallurgical processes used in Asturias in comparison with those carried out in Almadén or Idria.

Very few studies have been performed on soils from the mining area of Usagre (Table 2). García-Sánchez et al. [59] found very low exchangeable Hg contents, which ranged from 0.008 to 0.038 mg kg^{-1} and represent less than 0.2% of the total Hg for all studied samples. Elemental Hg contents were also very low (0.4–8 mg kg^{-1}) compared to those found in other historic mining districts.

Regarding the Valle del Azogue mining area, thermodesorption curves obtained by Navarro et al. [43, 61] (Table 2) revealed that cinnabar was the predominant form of Hg in soil samples and mine wastes. In contrast, matrix-bound metallic Hg formed during the roasting process and readsorbed onto iron oxide surfaces was found in soil and waste samples and it was clearly predominant in calcine piles. The results of column leaching experiments suggested the possible mobilisation of $Hg^{(0)}$ under the environmental conditions in the Valle del Azogue mine [43, 61]. Speciation calculations on the water leachates were carried out using specialist software. The results showed that $Hg^{(0)}$ and $Hg(OH)_2$ were theoretically the dominant inorganic species in calcine samples, while $HgCl_2$, $HgCl_3^-$ and HgClOH were predominant in mine waste samples.

5 Mercury Transfer from Soils to Plants

Another important question concerning the possible toxic effects that Hg can have on the environment and human health is the transfer of the pollutant from soils to plants growing on Hg-polluted sites. Several different approaches are possible to study this process: (i) comparative analyses of Hg contents in soils (including extractable fractions) and in wild plants (Fig. 2), which allow the bioaccumulation index to be calculated and expressed as the soil/plant ratio of the metal. Huckabee et al. [22], Rodríguez et al. [23], Millán et al. [24, 25], Molina et al. [26], Higueras et al. [33] and, to a lesser extent, Martínez-Coronado et al. [20] reported data of this type in the AMMD, while García-Sánchez et al. [59] reported data for the Usagre area; (ii) experimental study of soil to plant transfer. This type of study can also be carried out by different approaches, which include laboratory-based studies of plant uptake from natural soils or from spiked soils; lysimeter-based experiments, as

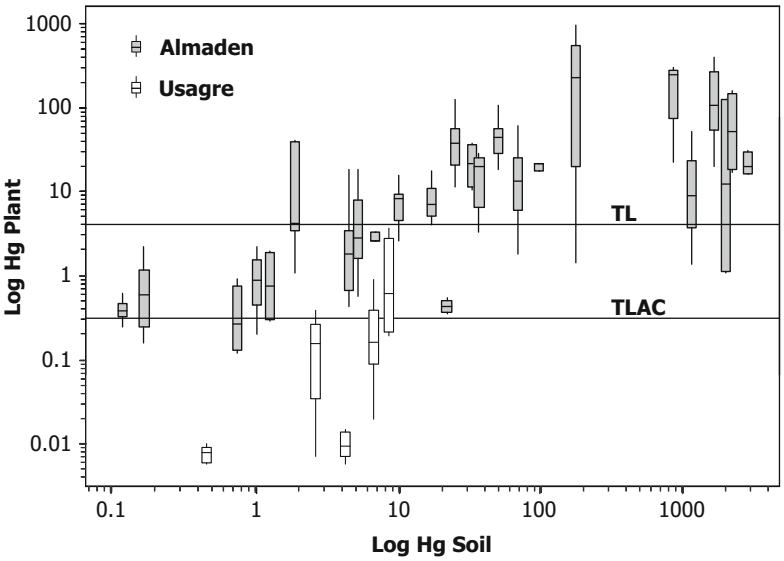

Fig. 2 Boxplot of total mercury contents in soil and wild plants from Almadén and Usagre [26, 59]. All mercury data in mg kg^{-1}. TL: Toxicity level; TLAC: Toxicity level for agronomic crops

described by Sierra et al. [27]; and other methods devoted to biochemical interactions between Hg and plant molecules or enzymes [36, 94]. Considering a different point of view, some of these publications refer to wild plants, most of which are not edible, while others are devoted to crop plants that are used directly for human consumption. The main conclusions from these studies are that Hg is a metal that in most plant species is taken up from the soils and it is accumulated to a lesser extent in aerial parts than in roots, although not (or scarcely) in edible fruit or grain.

6 Mercury Transfer to Animal Biota

The effect of exposure to heavy metals, and particularly mercury, on vertebrates from soil pollution is a crucial issue for risk assessment. Gray et al. [40] assessed the toxicity of soils developed over cinnabar retorting calcines in Almadenejos (ADMP) and analysed the leaching capacity of Hg from these materials by simulated human bodily fluids. The results show a high leaching capacity for simulated gastric fluid ($\leq$6,200 μg of Hg leached per g) as well as for simulated lung fluids ($\leq$9,200 μg of Hg leached/g), serum-based fluid ($\leq$1,600 μg of Hg leached per g) and water at pH 5 ($\leq$880 μg of Hg leached per g). This leaching capacity of Hg appears to be controlled by calcine mineralogy: calcines containing soluble Hg compounds contain higher leachate Hg concentrations.

Díez et al. [39] studied Hg contents in human hair for inhabitants of Almadén and the rest of the Castilla-La Mancha region. Although hair contents cannot be directly linked with soil pollution, it is interesting to note that in addition to the factors known to affect this parameter, such as fish consumption, age and gender, residence in Almadén also appears to be a significant factor, with higher average concentrations in Almadén (2.86 mg kg^{-1}) than in the region as a whole (2.26 mg kg^{-1}). The reason for this difference is probably the addition of local gaseous Hg inhalation exposure plus the intake of food containing Hg levels that are higher than normal, such as vegetables grown in local orchards on Hg-polluted soils or local fish and crayfish with high Hg contents [11].

In other studies, it was found that Hg levels in kidney and liver were higher in red deer (*Cervus elaphus L.*) and wild boar (*Sus scrofa L.*) [38] and in hair from pigs [37] in AMMD, with values of 8–10 μg g^{-1}. It is believed that gaseous Hg inhalation and ingestion of wild biota from contaminated soils are the main uptake routes.

7 Mercury Transfer from Soil to Atmosphere

In the absence of an active industrial source, such as a chlor-alkali plant or mining/metallurgical activity, polluted soils represent the major contributors to such emissions, as shown by Higueras et al. [95]. Two aspects can be considered regarding soil emissions: (i) experimental aspects, as studied by Llanos et al. [18], Llanos et al. [41] and Carmona et al. [42] for ADMP soils, and (ii) monitoring aspects, as studied by Llanos et al. [18], Llanos et al. [41], Martínez-Coronado et al. [20] and Herrera [96] in the ADMP and Huerta del Rey and Esbrí et al. [80] in the Flix area. The results obtained in these surveys are presented in Table 3.

Llanos et al. [18] and Llanos et al. [41] found that water-soluble Hg contents, temperature and solar radiation were the most important factors that affect Hg emission fluxes (MEF). The results allowed the average annual Hg emissions from the ADMP to be estimated as 16.4 kg $year^{-1}$, with significant differences between seasons. Carmona et al. [42] developed a soil emission physicochemical model based on mass transfer and equilibrium. They found that the soil to atmosphere mass transfer coefficient was proportional to the inverse of temperature and was independent of the radiation. It was also found that the Hg concentration in the gas phase was mainly dependent on the soluble Hg content in the soil.

With these data, and although data on Hg contents in the soil for most of these sites have been published, it is not possible to find a relationship between the contents in soils and the contents in air. This is due to the numerous factors involved in the soil to atmosphere transfer process, which is influenced, as mentioned above, by soil Hg speciation, meteorological conditions and time. García-Sánchez et al. [97], Higueras et al. [98] and Guerrero [99] found evidence that Hg contained in soils that remained undisturbed for long periods of time led to changes in

Table 3 Statistical summary for total Hg measurements carried out on areas with Hg-polluted soils. All mercury values in ng m^{-3}

Site	N	Average	SD	Max	GM	References
Flix						
Flix	51,483	112	445	27,439	19	Esbrí et al. [80]
Almaden						
ADMP	16	137	230	972		Martínez-Coronado et al. [20]
ADMP S	35	21	21	80		Martínez-Coronado et al. [20]
HR	180	44	72	491		Llanos [77]
NC	61	103	659	5,200		Castillo [78]

ADMP Almadenejos decommissioned metallurgical precinct, *ADMP S* surroundings of Almadenejos decommissioned metallurgical precinct, *HR* Huerta del Rey, *NC* Nueva Concepción, *SD* standard deviation, *GM* geometric mean

mercury speciation and this may reduce the capacity for the release of mercury into the atmosphere in gaseous form.

8 Remediation Possibilities for Mercury-Polluted Soils

Mercury-polluted soils represent significant environmental and health risks. The possibility of reducing these risks by applying different techniques has been tested, using soils from polluted areas in Spain as a reference.

Rodriguez et al. [23] used in situ phytoextraction in the proximity of ADMP. The results indicate that the three crops tested (lupine, lentil and barley) were effective for the extraction of Hg from the soil, although the uptake values were very low (less than 3% of the total Hg in the soil). Navarro et al. [43, 44] used solar energy for the remediation of Hg-polluted soils from the Valle del Azogue and Bayarque mines (Almería). A Hg removal efficiency of up to 76% was achieved in soil and mine waste samples. Navarro et al. [44] used solar energy to assess the vitrification of samples from the same area. Temperatures between 1,050 and 1,350°C were employed and very good results were achieved for the immobilisation of heavy metals. Subirés-Muñoz et al. [46] applied a standard sequential extraction procedure (SEP) together with lixiviation tests and the flushing technique in soils from ADMP. It was found that iodine, EDTA and thiosulphate were the most effective chelating agents, but they also noted the undesired effect of an increase in the mobility of Hg. As a consequence, they proposed an additional technique such as acid-enhanced electrokinetic remediation. García-Rubio et al. [45] assessed the use of the electrokinetic remediation technique (EKR) and achieved a removal efficiency similar to that obtained by Subirés-Muñoz et al. [46]. Sierra et al. [47] applied soil washing on soils from La Soterraña mine (Asturias). It was concluded that the required milling of the samples and its associated economic cost are the main drawbacks to consider in terms of making this technique feasible.

9 Conclusions

The main conclusions that can be drawn from this review are the following:

- The mercury contents in Spanish soils show significant variability, both on the regional and the local scales. Regional anomalies are mainly related to areas that are known to contain cinnabar and other sulphide deposits, such as the Asturias region and the Southern Central Iberian zone. Local anomalies appear to be related to minor cinnabar or other sulphide ore deposits, but Hg-related industrial activities such as zinc smelting may also contribute to anomalies. The background level can be set as 0.02 mg kg^{-1}, while extreme values of 40,000 mg kg^{-1} can be reached in mining areas.
- The mobility and availability of mercury has been established in different mining sites and high to extremely high total Hg concentrations were found. The results indicate that, as a consequence of the intense mining activity and ore processing carried out in these sites, Hg can be present in relatively mobilisable forms, especially in calcine piles.
- Translocation of Hg into plant tissue has proven to be effective for all studied taxa: Plants growing in polluted areas reach total Hg concentrations that in some areas are well above the accepted toxicity levels. On the other hand, studies focused on edible products did not identify concentrations above the maximum recommended levels for food consumption.
- The effect on vertebrates has not been studied in depth and the data analysed in this review only indicate a certain transfer to human hair, which could be related to indirect exposure, e.g. consumption of vegetables and animal-derived food grown on highly contaminated sites. A great deal of work is still required to assess the possible soil to vertebrate fauna transfer.
- Emission of gaseous Hg to the atmosphere has proven to be an important mechanism of air toxification in highly polluted areas. However, atmospheric dispersion, in particular during periods of high wind, reduces the risks related with this process. In the same way, time reduces the capacity of Hg contained in polluted soils to be emitted and this risk is also reduced if the soil remains undisturbed for a sufficient period of time.
- Technologies for the decontamination of Hg-polluted soils have been tested in several Spanish sites – always at the laboratory or pilot plant scale. The results have never been conclusive and the possibility of economically viable processes for the decontamination of specific polluted sites has yet to be demonstrated.
- As a general conclusion, there is a real need to establish appropriate criteria for the classification of soils polluted with mercury as ‘contaminated’ on a legal basis. Total contents do not appear to be appropriate, but this aspect should be based on parameters related to the mobility and availability of the element, as assessed by soil to biota and atmosphere transfer rates.

References

1. Kurland LT, Faro SN, Siedler H (1960) Minamata disease. The outbreak of a neurologic disorder in Minamata, Japan, and its relationship to the ingestion of seafood contaminated by mercuric compounds. World Neurol 1:370–395
2. Rustam H, Hamdi T (1974) Methyl mercury poisoning in Iraq. A neurological study. Brain 97 (3):499–510
3. Pavlish JH, Sondreal EA, Mann MD, Olson ES, Galbreath KC, Laudal DL, Benson SA (2003) Status review of mercury control options for coal-fired power plants (Review). Fuel Process Technol 82:89–165
4. Díaz-Somoano M, Unterberger S, Hein KRG (2007) Mercury emission control in coal-fired plants: the role of wet scrubbers. Fuel Process Technol 88(3):259–263
5. Widmer NC, Cole JA, Seeker WR, Gaspar JA (1998) Practical limitation of mercury speciation in simulated municipal waste incinerator flue gas. Combust Sci Technol 134(1–6): 315–326
6. Saupé F (1990) Geology of the Almaden mercury deposit, province of Ciudad Real, Spain. Econ Geol 85(3):482–510
7. Hernández A, Jébrak M, Higueras P, Oyarzun R, Morata D, Munhá J (1999) The Almaden mercury mining district, Spain. Miner Deposita 34(5–6):539–548
8. Fernández-Martínez R, Rucandio MI (2003) Study of extraction conditions for the quantitative determination of Hg bound to sulfide in soils from Almaden (Spain). Anal Bioanal Chem 375 (8):1089–1096
9. Fernández-Martínez R, Rucandio MI (2005) Study of the suitability of HNO3 and HCl as extracting agents of mercury species in soils from cinnabar mines. Anal Bioanal Chem 381 (8):1499–1506
10. Higueras P, Oyarzun R, Biester H, Lillo J, Lorenzo S (2003) A first insight into mercury distribution and speciation in soils from the Almadén mining district, Spain. J Geochem Explor 80(1):95–104
11. Higueras P, Oyarzun R, Lillo J, Sánchez-Hernández JC, Molina JA, Esbrí JM, Lorenzo S (2006) The Almadén district (Spain): Anatomy of one of the world's largest Hg-contaminated sites. Sci Total Environ 356(1–3):112–124
12. Gray JE, Hines ME, Higueras PL, Adatto I, Lasorsa BK (2004) Mercury speciation and microbial transformations in mine wastes, stream sediments, and surface waters at the Almadén Mining District, Spain. Environ Sci Technol 38(16):4285–4292
13. Sánchez DM, Quejido AJ, Fernández M, Hernández C, Schmid T, Millán R, González M, Aldea M, Martin R, Morante R (2005) Mercury and trace element fractionation in Almadén soils by application of different sequential extraction procedures. Anal Bioanal Chem 381 (8):1507–1513
14. Bernaus A, Gaona X, Valiente M (2005) Characterisation of Almadén mercury mine environment by XAS techniques. J Environ Monit 7(8):771–777
15. Bernaus A, Gaona X, Esbrí JM, Higueras P, Falkenberg G, Valiente M (2006) Microprobe techniques for speciation analysis and geochemical characterization of mine environments: the mercury district of Almadén in Spain. Environ Sci Technol 40(13):4090–4095
16. Bueno PC, Bellido E, Rubí JAM, Ballesta RJ (2009) Concentration and spatial variability of mercury and other heavy metals in surface soil samples of periurban waste mine tailing along a transect in the Almadén mining district (Spain). Environ Geol 56(5):815–824
17. Esbrí JM, Bernaus A, Ávila M, Kocman D, García-Noguero EM, Guerrero B, Gaona X, Alvarez R, Perez-Gonzalez G, Valiente M, Higueras P, Horvat M, Loredo J (2010) XANES speciation of mercury in three mining districts - Almadén, Asturias (Spain), Idria (Slovenia). J Synchrotron Radiat 17(2):179–186
18. Llanos W, Higueras P, Oyarzun R, Esbrí JM, López-Berdonces MA, García-Noguero EM, Martínez-Coronado A (2010) The MERSADE (European Union) project: Testing procedures

and environmental impact for the safe storage of liquid mercury in the Almadén district, Spain. Sci Total Environ 408(20):4901–4905
19. Millán R, Schmid T, Sierra MJ, Carrasco-Gil S, Villadóniga M, Rico C, Ledesma DMS, Puente FJD (2011) Spatial variation of biological and pedological properties in an area affected by a metallurgical mercury plant: Almadenejos (Spain). Appl Geochem 26 (2):174–181
20. Martínez-Coronado A, Oyarzun R, Esbrí JM, Llanos W, Higueras P (2011) Sampling high to extremely high Hg concentrations at the Cerco de Almadenejos, Almadén mining district (Spain): The old metallurgical precinct (1794 to 1861 AD) and surrounding areas. J Geochem Explor 109(1–3):70–77
21. Lindberg SE, Jackson DR, Huckabee JW (1979) Atmospheric emission and plant uptake of mercury from agricultural soils near the Almaden mercury mine. J Environ Qual 8(4):572–578
22. Huckabee JW, Sanz Diaz F, Janzen SA, Solomon J (1983) Distribution of mercury in vegetation at Almaden, Spain. Environ Pollut A 30(3):211–224
23. Rodriguez L, Lopez-Bellido FJ, Carnicer A, Alcalde-Morano V (2003) Phytoremediation of mercury-polluted soils using crop plants. Fresen Environ Bull 12(9):967–971
24. Millán R, Gamarra R, Schmid T, Sierra MJ, Quejido AJ, Sánchez DM, Cardona AI, Fernandez M, Vera R (2006) Mercury content in vegetation and soils of the Almadén mining area (Spain). Sci Total Environ 368(1):79–87
25. Millán R, Lominchar MA, López-Tejedor I, Rodríguez-Alonso J, Schmid T, Sierra MJ (2012) Behavior of mercury in the Valdeazogues riverbank soil and transfer to Nerium oleander L. J Geochem Explor 123:136–142
26. Molina JA, Oyarzun R, Esbrí JM, Higueras P (2006) Mercury accumulation in soils and plants in the Almadén mining district, Spain: One of the most contaminated sites on Earth. Environ Geochem Health 28(5):487–498
27. Sierra MJ, Millán R, Esteban E, Cardona AI, Schmid T (2008) Evaluation of mercury uptake and distribution in *Vicia sativa L.* applying two different study scales: Greenhouse conditions and lysimeter experiments. J Geochem Explor 96(2–3):203–209
28. Sierra MJ, Millán R, Esteban E (2008) Potential use of Solanum melongena in agricultural areas with high mercury background concentrations. Food Chem Toxicol 46(6):2143–2149
29. Sierra MJ, Millán R, Esteban E (2009) Mercury uptake and distribution in Lavandula stoechas plants grown in soil from Almadén mining district (Spain). Food Chem Toxicol 47(11):2761–2767
30. Sierra MJ, Millán R, Cardona AI, Schmid T (2011) Potential cultivation of *Hordeum vulgare L.* in soils with high mercury background concentrations. Int J Phytoremediation 13(8): 765–778
31. Sierra MJ, Rodríguez-Alonso J, Millán R (2012) Impact of the lavender rhizosphere on the mercury uptake in field conditions. Chemosphere 89(11):1457–1466
32. Ruiz-Díez B, Quiñones MA, Fajardo S, López-Berdonces MA, Higueras P, Fernández-Pascual M (2012) Mercury-resistant rhizobial bacteria isolated from nodules of leguminous plants growing in high Hg-contaminated soils. Appl Microbiol Biotechnol 96(2):543–554
33. Higueras P, Amorós JA, Esbrí JM, García-Navarro FJ, Pérez de los Reyes C, Moreno G (2012) Time and space variations in mercury and other trace element contents in olive tree leaves from the Almadén Hg-mining district. J Geochem Explor 123:143–151
34. Moreno-Jiménez E, Gimeno H, Gamarra R, Esteban E (2013) Evidence of a new Hg-tolerant ecotype of Rumex induratus from Almadén (Ciudad Real, Spain). Plant Biosyst 148(1):58–63
35. Quiñones MA, Ruiz-Díez B, Fajardo S, López-Berdonces MA, Higueras PL, Fernández-Pascual M (2013) Lupinus albus plants acquire mercury tolerance when inoculated with an Hg-resistant Bradyrhizobium strain. Plant Physiol Biochem 73:168–175
36. Dago A, González I, Ariño C, Martínez-Coronado A, Higueras P, Díaz-Cruz JM, Esteban M (2014) Evaluation of the mercury stress produced in plants by the analysis of phytochelatins and its Hg complexes induced in Asparagus acutifolius and Retama sphaerocarpa from the Almadén mining district. Environ Sci Technol 48(11):6256–6263

37. Moreno T, Higueras P, Jones T, McDonald I, Gibbons W (2005) Size fractionation in mercury-bearing airborne particles (HgPM10) at Almadén, Spain: implications for inhalation hazards around old mines. Atmos Environ 39:6409–6419
38. Berzas Nevado JJ, Rodríguez Martin-Doimeadios RC, Mateo R, Rodríguez Fariñas N, Rodríguez-Estival J, Patiño Ropero MJ (2012) Mercury exposure and mechanism of response in large game using the Almadén mercury mining area (Spain) as a case study. Environ Res 112:58–66
39. Díez S, Esbrí JM, Tobias A, Higueras P, Martínez-Coronado A (2011) Determinants of exposure to mercury in hair from inhabitants of the largest mercury mine in the world. Chemosphere 84:571–577
40. Gray JE, Plumlee GS, Morman SA, Higueras PL, Crock JG, Lowers HA, Witten ML (2010) In vitro studies evaluating leaching of mercury from mine waste calcine using simulated human body fluids. Environ Sci Technol 44(12):4782–4788
41. Llanos W, Kocman D, Higueras P, Horvat M (2011) Mercury emission and dispersion models from soils contaminated by cinnabar mining and metallurgy. J Environ Monit 13(12):3460–3468
42. Carmona M, Llanos W, Higueras P, Kocman D (2013) Mercury emissions in equilibrium: A novel approach for the quantification of mercury emissions from contaminated soils. Anal Methods 5(11):2793–2801
43. Navarro A, Cardellach E, Corbella M (2009) Mercury mobility in mine waste from Hg-mining areas in Almería, Andalusia (Se Spain). J Geochem Explor 101(3):236–246
44. Navarro A, Cardellach E, Cañadas I, Rodríguez J (2013) Solar thermal vitrification of mining contaminated soils. Int J Miner Process 119:65–74
45. García-Rubio A, Rodríguez-Maroto JM, Gómez-Lahoz C, García-Herruzo F, Vereda-Alonso C (2011) Electrokinetic remediation: The use of mercury speciation for feasibility studies applied to a contaminated soil from Almadén. Electrochim Acta 56(25):9303–9310
46. Subirés-Muñoz JD, García-Rubio A, Vereda-Alonso C, Gómez-Lahoz C, Rodríguez-Maroto JM, García-Herruzo F, Paz-García JM (2011) Feasibility study of the use of different extractant agents in the remediation of a mercury contaminated soil from Almaden. Sep Purif Technol 79(2):151–156
47. Sierra C, Menéndez-Aguado JM, Afif E, Carrero M, Gallego JR (2011) Feasibility study on the use of soil washing to remediate the As-Hg contamination at an ancient mining and metallurgy area. J Hazard Mater 196:93–100
48. Luque C (1985) Mercury mineralization in Cantabria mountains (Las mineralizaciones de mercurio de la Cordillera Cantábrica). PhD Dissertation, University of Oviedo, In Spanish
49. Luque C, Gutiérrez-Claverol M (2006) Mercury mining in Asturias; historic features (La minería del mercurio en Asturias; Rasgos históricos). Eujoa Artes Gráficas, Oviedo, In Spanish
50. Luque C, Martínez-Garcia E, Garcia-Iglesias J, Gutierrez-Claverol M (1991) Mineralization of Hg-As-Sb in the western edge of Central Asturias Carboniferous basin and its possible relation to tectonic: La Peña-El Terronal mine. (Mineralizaciones de Hg–As–Sb en el borde occidental de la cuenca Carbonífera central de Asturias y su posible relación con la tectónica: el yacimiento de El Terronal-La Peña). Bol Soc Esp Mineral 14:161–170, In Spanish
51. Loredo J, Ordóñez A, Gallego JR, Baldo C, García-Iglesias J (1999) Geochemical characterisation of mercury mining spoil heaps in the area of Mieres (Asturias, northern Spain). J Geochem Explor 67(1–3):377–390
52. Fernández-Martínez R, Loredo J, Ordóñez A, Rucandio MI (2005) Distribution and mobility of mercury in soils from an old mining area in Mieres, Asturias (Spain). Sci Total Environ 346:200–212
53. Fernández-Martínez R, Loredo J, Ordóñez A, Rucandio MI (2006) Physicochemical characterization and mercury speciation of particle-size soil fractions from an abandoned mining area in Mieres, Asturias (Spain). Environ Pollut 142(2):217–226

54. Loredo J, Ordóñez A, Álvarez R (2006) Environmental impact of toxic metals and metalloids from the Muñón Cimero mercury-mining area (Asturias, Spain). J Hazard Mater 136 (3):455–467
55. Ordóñez A, Álvarez R, Loredo J (2013) Asturian mercury mining district (Spain) and the environment: A review. Environ Sci Pollut Res 20(11):7490–7508
56. López Alonso M, Benedito JL, Miranda M, Castillo C, Hernández J, Shore RF (2003) Mercury concentrations in cattle from NW Spain. Sci Total Environ 302(1–3):93–100
57. López Alonso M, Benedito JL, Miranda M, Fernández JA, Castillo C, Hernández J, Shore RF (2003) Large-scale spatial variation in mercury concentrations in cattle in NW Spain. Environ Pollut 125(2):173–181
58. Miranda M, López-Alonso M, Castillo C, Hernández J, Prieto F, Benedito JL (2003) Some toxic elements in liver, kidney and meat from calves slaughtered in Asturias (Northern Spain). Eur Food Res Technol 216(4):284–289
59. García-Sánchez A, Murciego A, Álvarez-Ayuso E, Santa Regina I, Rodríguez-González MA (2009) Mercury in soils and plants in an abandoned cinnabar mining area (SW Spain). J Hazard Mater 168:1319–1324
60. Martínez J, Navarro A, Lunar R (1997) First reference of pyrite framboids in a Hg–Sb mineralization: the Valle del Azogue mineral deposit (SE Spain). N Jb Miner Mh Jg 4:175–184
61. Navarro A, Biester H, Mendoza JL, Cardellach E (2006) Mercury speciation and mobilization in contaminated soils of the Valle del Azogue Hg mine (SE, Spain). Environ Geol 49(8):1089–1101
62. Becker GF (1888) Geology of the quicksilver deposits of the Pacific Slope with Atlas. Monogr US Geol Surv 23442:27–32
63. Viladevall M, Font X, Navarro A (1999) Geochemical mercury survey in the Azogue Valley (Betic area, SE Spain). J Geochem Explor 66(1–2):27–35
64. Navarro A, Martínez-Frías J, Font X, Viladevall M (2000) Modelling of modern mercury vapor transport in an ancient hydrothermal system: environmental and geochemical implications. Appl Geochem 15:281–294
65. Navarro A (2008) Review of characteristics of mercury speciation and mobility from areas of mercury mining in semi-arid environments. Rev Environ Sci Biotechnol 7:287–306
66. Esbrí JM, Baselga L, Higueras P (2009) Evaluation of Mercury dispersion from Chlor-alkali industries in Spain. In: Theophanides M, Theophanides T (eds) Environmental Engineering and Management. ATINER, Atenas, pp 121–128
67. Carrasco L, Díez S, Soto DX, Catalan J, Bayona JM (2008) Assessment of mercury and methylmercury pollution with zebra mussel (Dreissena polymorpha) in the Ebro River (NE Spain) impacted by industrial hazardous dumps. Sci Total Environ 407:178–184
68. Navarro A, Quirós L, Casado M, Faria M, Carrasco L, Benejam L, Benito J, Díez S, Raldúa D, Barata C, Bayona JM, Piña B (2009) Physiological responses to mercury in feral carp populations inhabiting the low Ebro River (NE Spain), a historically contaminated site. Aquat Toxicol 93:150–157
69. Faria M, Huertas D, Soto DX, Grimalt JO, Catalan J, Riva MC, Barata C (2010) Contaminant accumulation and multi-biomarker responses in field collected zebra mussels (Dreissena polymorpha) and crayfish (Procambarus clarkii), to evaluate toxicological effects of industrial hazardous dumps in the Ebro river (NE Spain). Chemosphere 78:232–240
70. Grimalt JO, Sánchez-Cabeza JA, Palanques A, Catalán J (2003) Estudi de la dinàmica dels compostos organoclorats persistents i altres contaminants en els sistemes aquàtics continentals. Catalan Water Agency, Government of Catalonia, ACA/CIRIT, p 256; In Catalonian
71. FOREGS (2005) Geochemical Atlas of Europe. Part 1: background information, methodology and maps. In: Salminen R (ed) Geological survey of Finland, Espoo, p 526
72. IGME (2012) Geochemical atlas of Spain (Atlas Geoquímico de España), Instituto Geológico y Minero de España, Madrid, In Spanish

73. Rodríguez-Martín JA, Lopéz Arias M, Grau Corbí JM (2006) Heavy metals contents in agricultural topsoils in the Ebro basin: application of the multivariate geoestatistical methods to study spatial variations. Environ Pollut 144:1001–1012
74. Gil C, Ramos-Miras J, Roca-Pérez L, Boluda R (2010) Determination and assessment of mercury content in calcareous soils. Chemosphere 78(4):409–415
75. Ramos-Miras JJ, Gil C, Roca-Perez L, Boluda R (2012) Content and evolution of mercury in greenhouse soils of Almeria, Spain. Acta Hortic 927:821–826
76. Grimalt JO, Ferrer M, MacPherson E (1999) The mine tailing accident in Aznalcollar. Sci Total Environ 242:3–11
77. Llanos W (2011) Modelization of gaseous mercury emissions to the atmosphere in Almadén mining district (Ciudad Real province) (Modelización de las emisiones de mercurio gaseoso a la atmosfera en el distrito minero de almadén (provincia de Ciudad Real)). PhD Dissertation, University Complutense of Madrid, In Spanish
78. Castillo WO (2012) Mercury in soils of Nueva Concepción mine, Almadén mining district (Spain) (Mercurio en suelos del sector de la mina la Nueva Concepción, Distrito Minero de Almadén (España)). Dissertation, University Complutense of Madrid, In Spanish
79. Villaseca R (2012) Study of heavy metal pollution in Usagre mercury mine (Badajoz) (Estudio de la contaminación por metales pesados en el yacimiento de mercurio de Usagre (Badajoz)). Dissertation, University of Castilla-La Mancha, In Spanish
80. Esbrí JM, López-Berdonces MA, Fernández-Calderón S, Higueras P, Díez S (2014) Mercury atmospheric pollution around a Chlor-Alkali plant: an integrated analysis. Environ Sci Pollut Res. doi:10.1007/s11356-014-3305-x
81. Agencia de Residus de Catalunya (2014) NGR values for metals and metalloids and human health protection in Catalonia (Valores de los NGR para metales y metaloides y protección de la salud humana aplicables a Cataluña.), Available at GENCAT. http://www20.gencat.cat/portal/site/arc/menuitem.60fb2478680e61fd624a1d25b0c0e1a0/?vgnextoid=fd370431b17d6210VgnVCM1000008d0c1e0aRCRD&vgnextchannel=fd370431b17d6210VgnVCM1000008d0c1e0aRCRD&vgnextfmt=default. Accessed 21 Mar 2014, In Spanish
82. Environment Agency (2009) Soil guidance values for UK, Available at environment agency. http://www.environment-agency.gov.uk/research/planning/33714.aspx. Accessed 21 Mar 2014
83. Alloway BJ (1995) Heavy metals in soils, 2nd edn. Chapman and Hall, London
84. Senesi GS, Baldassarre G, Senesi N, Radina B (1999) Trace element inputs into soils by anthropogenic activities and implications for human health. Chemosphere 39(2):343–377
85. Bowen HJM (1979) Environmental chemistry of the elements. Academic, New York
86. Ordóñez A, Álvarez R, Charlesworth S, De Miguel E, Loredo J (2011) Risk assessment of soils contaminated by mercury mining, Northern Spain. J Environ Monit 13:128–136
87. Biester H, Muller G, Scholer HF (2002) Binding and mobility of mercury in soils contaminated by emissions from chlor-alkali plants. Sci Total Environ 284:191–203
88. Davies G, Ghabbour EA, Cherkasskiy A, Fataftah A (2001) Tight metal binding by solid phase peat and soil humic acids. In: Clapp CE, Hayes MHB, Senesi N, Bloom PR, Jardine PM (eds) Humic substances and chemical contaminants. Soil Science Society of America, Anaheim, pp 371–395
89. Bengtsson G, Picado F (2008) Mercury sorption to sediments: dependence on grain size, dissolved organic carbon, and suspended bacteria. Chemosphere 73:526–531
90. Sahuquillo A, Rauret G, Bianchi M, Rehnert A, Muntau H (2003) Mercury determination in solid phases from application of the modified BCR-sequential extraction procedure: a valuable tool for assessing its mobility in sediments. Anal Bioanal Chem 375:578–583
91. Fernández-Martínez R, Rucandio I (2014) Total mercury, organic mercury and mercury fractionation in soil profiles from the Almadén mercury mine area. Environ Sci Process Impacts 16:333–340

92. Fernández-Martínez R, Loredo J, Ordóñez A, Rucandio I (2014) Mercury availability by operationally-defined fractionation in granulometric distributions of soils and mine wastes from an abandoned Cinnabar Mine. Environ Sci Process Impacts 16(5):1069–1075
93. Fernández-Martínez R, Rucandio I (2013) Assessment of a sequential extraction method to evaluate mercury mobility and geochemistry in solid environmental samples. Ecotoxicol Environ Saf 97:196–203
94. Carrasco-Gil S, Álvarez-Fernández A, Sobrino-Plata J, Millán R, Carpena-Ruiz RO, Leduc DL, Andrews JC, Abadia J, Hernández LE (2011) Complexation of hg with phytochelatins is important for plant Hg tolerance. Plant Cell Environ 34(5):778–791
95. Higueras P, Oyarzun R, Kotnik J, Esbrí JM, Martínez-Coronado A, Horvat M, López-Berdonces MA, Llanos W, Vaselli O, Nisi B, Mashyanov N, Ryzov V, Spiric Z, Panichev N, McCrindle R, Feng XB, Fu XW, Lillo J, Loredo J, García ME, Alfonso P, Villegas K, Palacios S, Oyarzún J, Maturana H, Contreras F, Adams M, Ribeiro-Guevara S, Niecenski LF, Giammanco S, Huremović J (2014) A compilation of field surveys on gaseous elemental mercury (GEM) from contrasting environmental settings in Europe, South America, South Africa, and China: separating fads from facts. Environ Geochem Health 36:713–734
96. Herrera EA (2013) Mercury in air and lichens (Evernia Prunastri) in La Nueva Concepción mine, Almadén mining district (Spain). (Mercurio en aire y líquenes (Evernia prunastri) en el sector de la mina La Nueva Concepción, distrito minero de Almadén (España)). Dissertation, University Complutense of Madrid. In Spanish
97. García-Sánchez A, Contreras F, Adams M, Santos F (2006) Atmospheric mercury emissions from polluted gold mining areas (Venezuela). Environ Geochem Health 28:529–540
98. Higueras P, Llanos W, García ME, Millán R, Serrano C (2012) Mercury vapor emissions from the Ingenios in Potosí (Bolivia). J Geochem Explor 116–117:1–7
99. Guerrero S (2012) Chemistry as a tool for historical research: identifying paths of historical mercury pollution in the Hispanic New World. Bull Hist Chem 37:61–70

The Role of Earthworms in Mercury Pollution Soil Assessment

Rosa Carmen Rodríguez Martín-Doimeadiós, Francisco Javier Guzmán Bernardo, Nuria Rodríguez Fariñas, and María Jiménez Moreno

Abstract Mercury (Hg) is a global pollutant with different highly toxic chemical forms that can be bioaccumulated and biomagnified. Up to now most studies on Hg pollution have focused on aquatic ecosystems, and this is why little information about Hg in terrestrial ecosystems is currently available. However, the impact of Hg pollution on the terrestrial environment and food chain is of great interest for its human health implications. In this context, earthworms, which constitute a major component in soil ecosystems and act as a food source for a wide variety of organisms, are an excellent option to study Hg biochemistry in terrestrial ecosystems. The use of earthworms as bioindicators of Hg soil pollution involves a wide number of variables to be considered since the metal–biota interaction is very complicated in this case. Therefore, the aim of this chapter is to review the role of earthworms as bioindicators of Hg pollution in soils.

Keywords Bioaccumulation, Biomarkers, Earthworms, Mercury, Methylation, Soils

Contents

R.C. Rodríguez Martín-Doimeadiós (✉), F.J. Guzmán Bernardo, N. Rodríguez Fariñas, and M. Jiménez Moreno
Department of Analytical Chemistry and Food Technology, Faculty of Environmental Sciences and Biochemistry, University of Castilla-La Mancha, E-45071 Toledo, Spain
e-mail: RosaCarmen.Rodriguez@uclm.es

E. Jiménez et al. (eds.), *Environment, Energy and Climate Change I: Environmental Chemistry of Pollutants and Wastes*, Hdb Env Chem (2015) 32: 159–174,
DOI 10.1007/698_2014_271,
Published online: 29 July 2014

1 Introduction

Anthropogenic activities have dramatically increased the soil pollution during the last decades with a wide range of pollution sources (i.e. agricultural, urban, industrial, etc.). The main effects are soil fertility decrease and contamination of crops and groundwater. Therefore, soil pollution constitutes an important threat to all living organisms, and it is nowadays a matter of major concern in environmental studies.

Soils are exposed to contamination by many different types of pollutants, and heavy metals are one of the most important. Heavy metals are naturally present but anthropogenic input can highly exceed the natural sources. Moreover, they do not decompose or disappear as most of the organic contaminants do and can be mobilised by run-off or lixiviated to deeper layers which affect the groundwaters. These are the reasons why their adverse effects persist for many years.

Among heavy metal pollutants in soils, mercury (Hg) is especially disturbing for different reasons [1]. This element has some unique properties, such as its low melting point, the capacity to form amalgams and its occurrence in different chemical and physical forms, which make it useful for many human purposes. As a consequence, an important mobilisation of Hg natural resources has occurred with emissions to different environmental compartments. With respect to the atmosphere, Hg is mainly emitted as elemental Hg, which is a relatively stable form with a residence time of approximately 1 year [2]. Therefore the presence of Hg and its environmental impact can be found far away from the source, and this is why it is considered to be a global pollutant [3]. Moreover, Hg can exist in different oxidation states (0, +1 and +2) and chemical forms, mainly elemental Hg (Hg^0), inorganic Hg (Hg^{2+}) and alkyl compounds, with different properties. Most forms of Hg are toxic and not known to have a role in life processes, but it is monomethylmercury (MeHg) that causes a particular concern [4]. MeHg is an important neurotoxin, and it can be bioaccumulated in the biota and biomagnified in the aquatic food webs leading to the dangerous levels in food (mainly fish) for human consumption [5–7]. Additionally, MeHg can be generated under natural environmental conditions from other chemical forms [8]. Recognising the magnitude of this problem, a specific international treaty (i.e. *Minamata Convention on Mercury*) has recently been signed to "protect the human health and the environment from anthropogenic emissions and release of mercury and mercury compounds" [9], with the main objective of reducing the use and emissions of Hg at a global scale.

Therefore, there is an increasing interest in the monitoring and assessment of Hg soil pollution to estimate and/or remediate the associated risks. The traditional approach to soil pollution assessment is based on the determination of total or easily extractable Hg and the comparison to the reference values proposed by different organisations. However, soil analysis by itself does not accurately reflect the deleterious effects of contaminants on the biota because it cannot give information about the extent of pollutant penetration into the biotic compartments of the

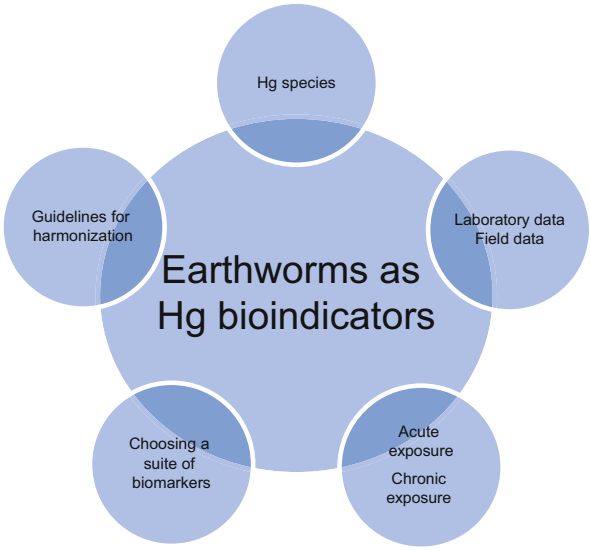

Fig. 1 Key aspects of earthworms as bioindicators of Hg pollution in soils

ecosystems or the interactive effects (synergism and antagonisms) of pollutants on the biota. To overcome these limitations, the use of bioindicator organisms has been proposed to supplement the data obtained from abiotic samples. In terrestrial ecosystems, earthworms can be identified as suitable bioindicators [10, 11]. Earthworms are essential components of the soil fauna since they contribute to the decomposition of organic matter, cycling of nutrients and pedogenesis. They are in full contact with the soil and ingest large quantities of it so pollutants can enter the earthworms through the skin, ingestion or both. Generally, earthworms increase the mobility and availability of metals, and many studies have demonstrated their efficiency on heavy metal accumulation from soils [12]. Moreover, earthworms constitute a major part (up to 80%) of the total biomass in terrestrial ecosystems, and they serve as food source for several higher organisms, such as birds, reptiles or mammals. They play a key role in the biomagnification processes of soil pollutants. With regard to Hg, the metal–biota interaction is more complicated than for other pollutants since bioaccumulation and interconversion of species can occur.

The use of earthworms as bioindicators of Hg soil pollution involves a number of variables to be considered such as the nature of the pollutant (Hg species), their levels, how long the exposure to a certain concentration exists (acute or chronic), the validation of the laboratory data in field studies, the information that biomarkers can provide and how our results compare with the results of other researchers (protocols and harmonisation). In this way, Fruend et al. provided a suite of recommendations for using earthworms as model organisms in the laboratory [13].

The aim of this chapter is to review the role of earthworms as bioindicators of Hg pollution in soils taking into account all the key aspects, summarised in Fig. 1.

2 Levels of Hg in Soils and Toxicity

The concentration of Hg in soil affects the levels and toxicity of Hg in earthworms. Since Hg is ubiquitous, the background levels have to be established. For instance, the median concentration of Hg in European soils is 0.037 mg/kg within a range of 0.005–1.354 mg/kg according to the *Geochemical Atlas of Europe* [14]. These figures have been used as consensus background levels of Hg in several works in comparison to local levels [15, 16].

Regulatory agencies have estimated guideline soil levels of Hg, aimed at protecting either human health or the environment. However, the levels issued are different depending on a number of factors, and this is why a value of consensus does not exist. For example, in the United Kingdom, there is a maximum Hg concentration to protect human health of 8 mg/kg [17], while that of Canada is 6.6 mg/kg [18]. Another complication for comparison of data is that some authors prefer to express these levels in terms of soil organic matter because of the well-established strong interaction between Hg^{2+} and the organic matter [19].

From the (eco)toxicological point of view, the total concentration of Hg in soil is not the key point, but the bioavailable concentration. Mercury is highly immobile in soil and accumulates due to its strong affinity to organic matter and soil minerals. This makes it a low bioavailable metal [20] with a big difference between total and bioavailable Hg [21]. In the particular case of earthworms, their levels may be a relevant measure of Hg bioavailability in soil [10]. In fact, levels of Hg in soil and in earthworms exposed to it have been reported in unpolluted and polluted locations, and the results always show that there is a big gap between the total concentration and the bioavailable concentration.

The ecotoxicological levels of pollutants can be derived from values of available toxicity data, and they can be expressed as critical limits. The critical limit is the soil concentration above which unacceptable effects are expected, but the way it is estimated is different among researchers. The critical limit for Hg^{2+} estimated by De Vries et al. was based on the results of long-term experiments with Hg^{2+} added to forest soils [22]. However, Tipping et al. derived critical limits from published laboratory toxicity data for Hg^{2+} [20]. As a result, De Vries et al. adopted a soil critical limit of 0.5 mg/kg soil organic matter, whereas Tipping et al. estimated a value of 3.3 mg/kg soil organic matter.

3 Bioaccumulation and Uptake of Hg Species by Earthworms

Bioindicators are organisms used to identify the factors controlling pollutant toxicity and bioavailability and can be used to evaluate hazards where pollution is present. An appropriate bioindicator organism should be reasonably well understood in terms of biological qualities and responses and be broadly applicable to

different external conditions. In this way, earthworms are ideal candidates as bioindicators because they are simple, well-studied creatures that are known to accumulate contaminants from the soils. In fact, earthworms have been used in a multitude of experiments either as a response variable, in experiments investigating the reaction of earthworms to their environment, or as a treatment variable, in experiments investigating the impact of earthworms on their environment.

The earthworm activity produces a reduction in soil pH and/or an increase in dissolved organic carbon resulting in changes in mobility and availability of metals [12]. Moreover, these bioindicators accumulate heavy metals from soils, and the extent this happens is very important for ecological risk assessment because it is related to the bioavailability of heavy metals in soils. Thus, the risk of primary poisoning of earthworms due to bioaccumulation and of secondary poisoning of vertebrate predators due to biomagnification increases with the availability of the metal [23]. There are many researches concerning heavy metal accumulation in earthworms, but few study total Hg and/or MeHg concentrations in earthworms [24].

Bioaccumulation can be quantified by means of bioaccumulation factors (BAFs). In the case of Hg species, BAFs are calculated as the total Hg or MeHg concentration in the tissues divided by the corresponding concentrations in the soils. In literature it is also common to find the terms bioconcentration and bioconcentration factor (BCF), which specifically refer to tissues instead of organisms. Bioaccumulation and bioconcentration can be assumed to be equivalent to earthworms. Although the use of BAFs is highly accepted among researchers, it also has limitations. In this way, Zagury et al. found that BAFs for total Hg were related to the ratio of bioavailable Hg to total Hg and not to the absolute concentration of bioavailable Hg [25].

Different experimental designs have been used to assess the metal uptake and bioaccumulation by earthworms leading to controversial results and sometimes noncomparable data. Nahmani et al. have reviewed on this topic and also have made some recommendations for further works [26]. Briefly, the authors claimed that internationally agreed protocols on time of exposure, time of depuration and determined soil properties (which should include pH, organic matter content, soil texture and cationic exchange capacity) should be standardised. Kinetic studies were also recommended as they may provide more useful toxicological information than the sole estimation of the BAFs. Studies with different earthworm species should be carried out so that application of data obtained for one species (and particularly *Eisenia fetida*/*Eisenia andrei*) to other species is possible. Moreover, experiments either in the field or terrestrial model ecosystems should be carried out so that experimental constraints do not influence earthworm's response. The recommendations of this work have been used as guidelines for researchers dealing with bioaccumulation of total Hg and, eventually, Hg species.

Some of the issues highlighted in this review have been addressed in recent studies, summarised in Table 1. Thus, the influence of the soil composition on the

Table 1 Studies reporting concentration intervals of total Hg, MeHg (mg/kg) in soils and earthworms (dry weight) and bioaccumulation factors (BAFs)

	Soil		Earthworms		BAF		
Reference	Total Hg	MeHg	Total Hg	MeHg	Total Hg	MeHg	Comments
Rieder et al. [27]	0.07–0.55	<0.001–0.003	0.20–2.12	0.014–0.242	1.1–14.5	15.1–191.5	Different earthworm species, unpolluted soil
Zhang et al. [28]	2.04–15.23	0.00201–0.01038	0.8–5.46	0.013–0.877	0.040–0.539	10.16–31.38	Different earthworm species, polluted soil
Hinton and Veiga [29]	0.4–11.0	–	0.037–1.63[a]	–	0.10–21.3	–	*E. fetida*, different soil composition
Ernst et al. [23]	0.046–0.553		0.01–4.79		1.1–15.2		Different earthworm species, unpolluted soil
Burton et al. [24]	0.085–11.542	0.00112–0.00735			0.6–3.3	175–249	Kinetic estimation of BAFs

[a]Fresh weight

bioaccumulation of total Hg in *E. fetida* was studied by Hinton and Veiga [29]. In this work, earthworms exposed to gold mining soils (0.445–11.021 mg/kg total Hg) showed BAFs from 0.10 to 21.3. Interestingly, the highest bioaccumulation took place in earthworms exposed to low-Hg-organic-rich soils instead of earthworms exposed to higher Hg concentrations in organic-poor tailings.

Other works have focused on the bioaccumulation in different earthworm species (i.e. epigeic, anecic and endogeic). Thus, Ernst et al. studied bioaccumulation of Hg in different groups of earthworms from unpolluted soil forest and found a high variability of BAFs among earthworm species, ranging from 1 (*Lumbricus rubellus*, epigeic) to 15 (*Aporrectodea rosea*, endogeic) [23]. Rieder et al. found the same pattern for soils containing similar concentrations of total Hg (0.07–0.55 mg/kg), with mean BAFs for total Hg of 2.9 ± 1.8 for epigeic earthworms (*Dendrodilus rubidus* and *L. rubellus*), of 6.0 ± 4.2 for anecic earthworms (*Aporrectodea longa* and *Lumbricus terrestris*) and of 10.9 ± 3.4 for endogeic earthworms (*Aporrectodea caliginosa*, *Aporrectodea rosea* and *Octolasion cyaneum*) [27]. Rieder et al. also measured MeHg in earthworms and calculated MeHg BAFs. The results indicated that MeHg was also highly species-specific, with values between 15.1 (*L. rubellus*, epigeic) and 191.5 (*O. cyaneum*, endogeic). In a heavily polluted region by chlor-alkali and metal smelting industries (up to 15.2 mg/kg Hg in soils), Zhang et al. also observed different BAFs both for total Hg and MeHg in different earthworm species (*Allolobophora* sp., endogeic; *Drawida* sp., anecic) [28].

As recommended by different authors, a kinetic study of the metal uptake is required to accurately predict its toxicity [26, 30]. Burton et al. estimated total Hg and MeHg BAFs from the rate of uptake and bioaccumulation of total Hg and MeHg in *E. fetida* from soils which had been contaminated with Hg for approximately 30 years, with total Hg concentrations from 0.085 up to 11.542 mg/kg and MeHg concentrations from 1.12 up to 7.35 μg/kg (both d.w.) [24]. The authors found total Hg BAFs from 0.6 up to 3.3, and MeHg BAFs from 175 up to 249, which is in the range of other studies in which the BAFs have not been calculated using kinetics.

The BAFs for total Hg in earthworms are typically from <1 up to 10, and, according to the scarce literature available, the BAFs for MeHg can be up to three orders of magnitude higher than for total Hg [27, 28]. For instance, Rieder et al. found that the MeHg BAF were between 6 (*A. longa*, anecic) and 25 (*A. caliginosa*, endogeic) times higher than the total Hg BAF [27]. Likewise, MeHg BAFs between 20 and 150 times higher than total Hg BAFs were reported by Zhang et al. in different earthworm species [28]. One of the reasons why a more efficient accumulation of MeHg is found in organisms compared to inorganic Hg could be the lipophilic nature of this organic species.

4 Earthworms as Bioindicators of Hg Toxicity

Earthworms are considered to be the model organisms for standard toxicity tests of terrestrial ecosystems by the American Society for Testing and Materials [31], the Organisation for Economic Cooperation and Development [32] for the testing of chemicals and the International Standards Organization [33–35]. *E. fetida* is the reference earthworm species used for these tests. In the particular case of Hg, a LC_{50} (concentration causing 50% mortality) of 170 mg Hg/kg soil [36] and an EC_{50} (concentration causing 50% effect) based on cocoon production of 9.16 mg Hg/kg soil [37] are some examples in literature following these guidelines.

Traditionally, the studies on earthworm toxicity bioassays have been carried out using survival, growth change, reproduction and avoidance as end points. Since these toxicity end points do not provide information on what is happening at a cellular or subcellular level, in the recent years, the study of biomarkers has experienced a sharp growth [11, 38–40]. Biomarkers can be defined as measurable biological changes, from molecular to behavioural levels, in response to one or more contaminants [11]. Although this definition includes the traditional end points mentioned above, which would be the behavioural, current research is focused on the study of the responses to the xenobiotic agent at cellular and subcellular level. This has been particularly intense in aquatic (eco)toxicology, but earthworm biomarkers are still far from being standardised even though these animals are the standard test organisms in soil toxicity tests [41].

Biomarkers can be classified in two groups, biomarkers of exposure and biomarkers of effect [11]. Biomarkers belonging to the first group are early reversible cellular changes that indicate pollutant exposure. They are usually enzymatic systems involved in xenobiotic detoxification (i.e. metallothioneins [MTs]), and they do not indicate that the individual health is seriously at risk. Biomarkers of effect show acute toxicity and are directly related to the risk of adverse health effects. The use of a multi-marker approach can provide information about both the causes and the effects of a hazard.

The response of earthworms at cellular and/or subcellular levels to different chemicals, with a wide variety of properties, may be different, and so they may be the biomarkers to be monitored. Thus, there is a full set of biomarkers; some of them are considered general (i.e. lysosomal membrane instability) and others are more closely related to a specific pollutant type such as heavy metals (i.e. MTs) or pesticides (i.e. acetylcholinesterase activity, AChE).

The aim of this section is not to make a full compilation of studies on earthworm biomarkers, but it is solely focused on biomarker currently used to evaluate Hg exposure and effects. The literature related to Hg, summarised in Table 2, is scarce compared to literature related to other heavy metals, such as Cd, Pb or Zn.

MTs induction is one of the most frequently applied biomarker of earthworm exposure to heavy metals. In addition to their function in homeostasis of essential metals like Cu and Zn, MTs are involved in detoxification of non-essential metals. Svendsen et al. confirmed the induction of MT-2 in *L. rubellus* exposed to field soils

Table 2 Biomarkers to evaluate Hg exposure and effects in earthworms

Reference	Earthworm species	Metal(s)	Biomarkers	Experimental conditions
Fugère et al. [42]	*L. rubellus*	Cd/Zn/Pb/Hg/MeHg	Phagocytic activity of coelomocytes	In vitro exposure of coelomic fluid to heavy metals
Svendsen et al. [43]	*Lumbricus rubelllus*	As/Cd/Cu/Hg/Pb/Zn	Metallothioneins Lysosomal membrane stability	Contaminated field soils under different laboratory temperatures and in the field at different seasons
Gudbrandsen et al. [36]	*E. fetida*	Hg	Oxidative stress biomarkers (GSH)	Soils spiked in the laboratory with Hg (up to 70 mg/kg)
Calisi et al. [44]	*L. terrestris*	Cd/Cu/Hg	Metallothioneins Haemoglobin oxidation	Laboratory exposure using a standard acute toxicity test on filter paper
Colacevich et al. [45]	*L. terrestris*	Hg	Metallothioneins Oxidative stress (antioxidant enzymes activities and GSH) Integrated biomarker	Short (2-day) and long-term (44-day) exposure to Hg-contaminated field soils
Calisi et al. [46]	*L. terrestris*	Cd/Cu/As/Zn/Hg	Lysosomal membrane stability Granulocyte morphometric alteration Haemoglobin oxidation Acetylcholinesterases Integrated biomarker	Native earthworms sampled in heavy metal-contaminated sites
Berzas Nevado et al. [47]	*L. terrestris*	Hg	Oxidative stress biomarkers (GSH)	Hg-contaminated field soils

contaminated with metals (As, Cd, Cu, Hg, Pb and Zn) [43]. However, this study evaluated the overall effect of all the metals, and it was not possible to distinguish the impact of Hg. The individual effect of Hg in MTs induction in *L. terrestris* was studied by Calisi et al. [44]. The organisms were exposed to increasing concentrations of Hg (10^{-8}–10^{-2} M) by means of the standard toxicity test in the filter paper [48]. MTs showed a typical dose–response increase, and the lowest metal concentration that increased MTs significantly was 10^{-5} M. In this experiment, Cd and Cu were also individually tested, and it should be pointed out that the effect of the three metals was quite similar. The same earthworm species (*L. terrestris*) were exposed for 2 and 44 days to four Hg-contaminated field soils (from 73 to 1,287 mg/kg) from a mining area [45]. In this study Hg was not spiked in the laboratory but it was naturally present, and therefore it could be more representative of natural processes. The level of Hg in soil did not cause earthworm mortality but had a significant impact on earthworm biomarkers. The duration of exposure had a significant effect on MTs induction, being higher at longer exposure times.

The earthworm coelomic fluid plays an important role in the animal physiology since it is involved in the transport of pollutants and in the internal defence mechanisms. Therefore, the health of the organisms is affected by any impairment of their functionality [42]. The coelomocyte lysosomal membrane stability is the most commonly used biomarker to evaluate coelomocyte alteration. The coelomocyte lysosomal membrane stability has been used as a general indicator of exposure to chemicals and associated to biological effects. Many elements, including Hg, are known to exert stress on lysosomal membrane stability in field soils [43]. More recently, the morphometric alterations in earthworm granulocytes has been proposed as a new biomarker related to coelomocytes [46, 49, 50]. This biomarker has shown high sensitivity to exposure to some pollutants (copper sulphate and methiocarb) in laboratory experiments. With respect to Hg, this biomarker has been included in a study with native earthworms (*L. terrestris*) sampled in heavy metal (Cu, Cd, As, Hg and Zn)-contaminated sites with a significant enlargement of the granulocyte dimension compared to those obtained from control sites [46].

The inhibition of AChE has been traditionally used as biomarker of pesticide exposure and toxicity [40, 51]. With respect to heavy metals, there are contradictory results. Thus, Calisi et al. found no effect of copper sulphate exposure on AChE activity in laboratory experiments with *E. fetida* [49] or *L. terrestris* [50], whereas Lionetto et al. reported AChE inhibition by metallic ions (Hg^{2+}, Cd^{2+}, Cu^{2+} and Pb^{2+}) in fish and invertebrates [11]. The sensitivity of this biomarker in *L. terrestris* to heavy metal exposure (Cd, Cu, As, Zn and Hg) under the field conditions was demonstrated by Calisi et al. [46]. In the case of Hg, the inhibition of different cholinesterases by $HgCl_2$ through different mechanisms has been demonstrated in incubation experiments [52]. One of the tested AChE was inhibited in micromolar Hg concentration, but the others were sensitive only in the millimolar range. Because of these controversial results, further studies are necessary before using AChE inhibition as biomarker of Hg exposure in earthworms.

Novel potential biomarkers have been proposed in earthworms, such as indicators of oxidative stress or changes in haematology. Several pollutants are able to induce oxidative stress in cells, which protect themselves against the oxidative damage using antioxidant enzymes and small molecular-weight antioxidants such as glutathione (GSH). The potential of GSH as a biomarker of exposure to Hg has been demonstrated in *E. fetida* [36] and in *L. terrestris* [45, 47]. On the other hand, blood haemoglobin concentration increase has been recently proposed as a biomarker in *L. terrestris* in both laboratory [44] and field experiments [46]. Further studies are necessary to demonstrate its suitability as exposure/effect biomarkers in earthworms.

In the environment under natural conditions, the organisms are exposed simultaneously to different pollutants, and therefore a suite of biomarkers is required to get environmental diagnosis. A current trend in biomarker studies is to develop integrated quantitative biomarker indexes to summarise biomarker responses and simplify their interpretation [53]. Some initial attempts have focused on assessing sublethal effects in Hg-exposed earthworms, but further studies are required [45, 46].

5 Methylation of Hg in Earthworms

The active or passive role of earthworms in MeHg production and accumulation in terrestrial ecosystems is unclear. As previously stated, the bioaccumulation is higher for MeHg than for total Hg [27]. Generally, the main hypothesis to explain this difference was that MeHg is produced in the substrate and then it is accumulated more efficiently than inorganic Hg because of its high lipid solubility. However, more recently, different authors opened the question about the possibility of a more active role of earthworms in the methylation process [23, 24, 28, 54]. Thus, the highest BAFs for MeHg in earthworms could be also explained because inorganic Hg is methylated inside the organisms by their digestive tract microbiota.

The internal Hg methylation capability has been explored with different experimental approaches. Rieder et al. studied sterile soils incubated (1) with earthworms to examine the methylation in the earthworms (*L. terrestris*), (2) without earthworms to test abiotic methylation in the soil and (3) without earthworms but with a suspension obtained by rinsing their body surface to test Hg methylation in the soil by microorganisms from the earthworm [55]. Each experimental condition was evaluated with inorganic Hg spike (6 mg/kg), with MeHg spike (0.75 mg/kg) and without Hg. The concentration of MeHg in earthworms grown in inorganic Hg was significantly higher than in earthworms incubated without Hg and in soils in all the experimental conditions. This means that inorganic Hg is methylated inside the earthworms and not by bacteria introduced by earthworms (cast/rinsing solution) into the soil. The Hg methylation capability of intestinal sulphate-reducing bacteria in earthworms (*E. fetida*) has also been studied by Kaschak et al. [56]. In this study, the earthworms were incubated in sterile and non-sterile soils with (4 mg/kg) and

without Hg spike. MeHg concentration in earthworms was significantly higher in spiked than in non-spiked soils and in non-sterile than in sterile soils spiked with Hg. The significant amounts of MeHg found (51 μg/kg) in earthworms grown in the sterile soils indicate that methylation activity of intestinal microbiota in earthworm is more important than soil microbiota methylation. The analysis by laser ablation inductively coupled plasma mass spectrometry (LA-ICP-MS) of thin section of earthworms exposed to Hg allowed measuring a gradient from highest concentration in the intestinal compartments to lower concentration in the epidermis [56]. Furthermore, gut epithelia and gut content obtained from earthworms demonstrated the capability for Hg methylation in biotic cultures [56]. This finding also confirms that intestinal methylation is more important than soil microbiota methylation. The hypothesis of intestinal Hg methylation is supported by the anaerobic internal conditions which may favour the growth of sulphate (SRB)- and iron (FeRB)-reducing bacteria, known as active methylators [57–59]. Parks et al. identified the genes required for methylation of Hg in some SRB (*Desulfovibrio* (*Dv*.) *desulfuricans* ND132 and *Geobacter sulfurreducens* PCA) [59]. A two-gene cluster, *hgcA* and *hgcB*, was present in confirmed methylators, but it was absent in non-methylating strains. This finding was a major contribution to understand the Hg methylation mechanisms [59]. These SRBs have also been detected in the intestine of other animals, and they may play an important role in the inorganic Hg methylation in terrestrial invertebrates [60, 61]. Limper et al. identified SRB (*Desulfovibrio intestinalis*) in the intestinal tract of termites (*Mastotermes darwiniensis*) and demonstrated its ability to methylate Hg [61]. Rieder et al. detected SRB in earthworms but not in the soil samples [55]. Kaschak et al. has reported MeHg formation by pure and enriched culture of SRBs obtained from animals (insects, annelids and mammals), including human beings' intestines [56]. This indicates the methylation capability of bacteria found in the intestines of terrestrial animals, not only earthworms, but additional studies should be carried out for the confirmation.

The intestinal biomethylation of Hg by earthworms, as well as other organisms, is particularly intriguing. Up to now, the generation of MeHg in terrestrial ecosystems and its transfer to terrestrial food chains have been neglected so the related information is scarce. Although some studies have indicated how important this process is [62–64], there is still a long way to go to fully understand it as well as its implications on the biomagnification of MeHg within terrestrial food chains.

References

1. Bank MS (2012) Mercury in the environment: pattern and process, 1st edn. University of California Press, California
2. Seigneur C, Vijayaraghavan K, Lohman K, Karamchandani P, Scott C (2004) Global source attribution for mercury deposition in the united states. Environ Sci Technol 38(2):555–569

3. Swartzendruber P, Jaffe D (2012) Sources and transport: a global issue. In: Bank MS (ed) Mercury in the environment: pattern and process. University of California Press, California, pp 3–18
4. Clarkson TW, Magos L (2006) The toxicology of mercury and its chemical compounds. Crit Rev Toxicol 36(8):609–662
5. USEPA (2001) Water quality criterion for the protection of human health: methylmercury. United States Environmental Protection Agency, Washington
6. EU (2006) Setting maximum levels for certain contaminants in foodstuffs. Commission Regulation no. 1881/2006. Offi J Eur Union
7. WHO (2011) Evaluation of certain food additives and contaminants. Seventy-second report of the Joint FAO/WHO Expert Committee on Food Additives. World Health Organization
8. Hintelmann H (2010) Organomercurials. Their formation and pathways in the environment. Met Ions Life Sci 7:365–401
9. UNEP (2013) Minamata convention on mercury. United Nations Environment Programme. http://www.mercuryconvention.org/Portals/11/documents/publications/MinamataConventiontextEn.pdf
10. Lanno R, Wells J, Conder J, Bradham K, Basta N (2004) The bioavailability of chemicals in soil for earthworms. Ecotoxicol Environ Saf 57(1):39–47
11. Lionetto MG, Calisi A, Schettino T (2012) Earthworms biomarkers as tools for soil pollution assessment. Soil Health Land Use Manage 305–332
12. Sizmur T, Hodson ME (2009) Do earthworms impact metal mobility and availability in soil? - a review. Environ Pollut 157(7):1981–1989
13. Fruend H-C, Butt K, Capowiez Y, Eisenhauer N, Emmerling C, Ernst G, Potthoff M, Schaedler M, Schrader S (2010) Using earthworms as model organisms in the laboratory: recommendations for experimental implementations. Pedobiol 53(2):119–125. doi:10.1016/j.pedobi.2009.07.002
14. Salminen R, Batista MJ, Bidovec M, Demetriades A, De Vivo B, De Vos W, Duris M, Gilucis A, Gregorauskiene V, Halamic J, Heitzmann P, Lima A, Jordan G, Klaver G, Klein P, Lis J, Locutura J, Marsina K, Mazreku A, O'Connor PJ, Olsson SÅ, Ottesen R-T, Petersell V, Plant JA, Reeder S, Salpeteur I, Sandström H, Siewers U, Steenfelt A, (2005) Geochemical atlas of europe, part 1, background information, methodology and maps, vol 1. FOREGS
15. Teršič T, Gosar M, Biester H (2011) Distribution and speciation of mercury in soil in the area of an ancient mercury ore roasting site, Frbejžene trate (Idrija area, Slovenia). J Geochem Explor 110(2):136–145. http://dx.doi.org/10.1016/j.gexplo.2011.05.002
16. Teršič T, Gosar M (2012) Comparison of elemental contents in earthworm cast and soil from a mercury-contaminated site (Idrija area, Slovenia). Sci Total Environ 430(0):28–33. http://dx.doi.org/10.1016/j.scitotenv.2012.04.062
17. EAW (2002) Soil guideline values for inorganic mercury contamination. Environment agency of England and Wales. R&D Publication, Swindon
18. CEAA (1995) Toxicity testing of national contaminated sites remediation program priority substances for the development of soil quality guidelines for contaminated sites. Evaluation and interpretation branch, guidelines division. Canadian Environmental Assessment Agency - Environment Canada, Ottawa
19. Meili M (1991) The coupling of mercury and organic-matter in the biogeochemical cycle - towards a mechanistic model for the boreal forest zone. Water Air Soil Pollut 56:333–347. doi:10.1007/bf00342281
20. Tipping E, Lofts S, Hooper H, Frey B, Spurgeon D, Syendsen C (2010) Critical Limits for Hg (II) in soils, derived from chronic toxicity data. Environ Pollut 158(7):2465–2471. doi:10.1016/j.envpol.2010.03.027
21. Ravichandran M (2004) Interactions between mercury and dissolved organic matter—a review. Chemosphere 55(3):319–331. http://dx.doi.org/10.1016/j.chemosphere.2003.11.011

22. de Vries W, Lofts S, Tipping E, Meili M, Groenenberg JE, Schütze G (2007) Impact of soil properties on critical concentrations of cadmium, lead, copper, zinc, and mercury in soil and soil solution in view of ecotoxicological effects. Rev Environ Contam Toxicol 191:42. doi:10.1007/978-0-387-69163-3_3
23. Ernst G, Zimmermann S, Christie P, Frey B (2008) Mercury, cadmium and lead concentrations in different ecophysiological groups of earthworms in forest soils. Environ Pollut 156 (3):1304–1313. doi:10.1016/j.envpol.2008.03.002
24. Burton DT, Turley SD, Fisher DJ, Green DJ, Shedd TR (2006) Bioaccumulation of total mercury and monomethylmercury in the earthworm *Eisenia fetida*. Water Air Soil Pollut 170 (1–4):37–54. doi:10.1007/s11270-006-3113-0
25. Zagury GJ, Neculita C-M, Bastien C, Deschênes L (2006) Mercury fractionation, bioavailability, and ecotoxicity in highly contaminated soils from chlor-alkali plants. Environ Toxicol Chem 25(4):1138–1147. doi:10.1897/05-302r.1
26. Nahmani J, Hodson ME, Black S (2007) A review of studies performed to assess metal uptake by earthworms. Environ Pollut 145(2):402–424. doi:10.1016/j.envpol.2006.04.009
27. Rieder SR, Brunner I, Horvat M, Jacobs A, Frey B (2011) Accumulation of mercury and methylmercury by mushrooms and earthworms from forest soils. Environ Pollut 159 (10):2861–2869
28. Zhang ZS, Zheng DM, Wang QC, Lv XG (2009) Bioaccumulation of total and methyl mercury in three earthworm species (Drawida sp., Allolobophora sp., and Limnodrilus sp.). Bull Environ Contam Toxicol 83(6):937–942. doi:10.1007/s00128-009-9872-8
29. Hinton JJ, Veiga MM (2009) Using earthworms to assess Hg distribution and bioavailability in gold mining soils. Soil Sedim Contam 18(4):512–524. doi:10.1080/15320380902978847
30. van Straalen NM, Donker MH, Vijver MG, van Gestel CAM (2005) Bioavailability of contaminants estimated from uptake rates into soil invertebrates. Environ Pollut 136 (3):409–417. http://dx.doi.org/10.1016/j.envpol.2005.01.019
31. ASTM (1999) Standard guide for conducting a laboratory soil toxicity test with the lumbricid earthworm Eisenia foetida. Annual book of ASTM standards. American Society for Testing and Materials, Philadelphia, PA
32. OECD (2004) Test No. 222: earthworm reproduction test (*Eisenia fetida*/*Eisenia andrei*). OECD Guidelines for testing of chemicals. OECD Publishing, Paris
33. ISO (1993) Soil quality-effects of pollutants on earthworms (*Eisenia fetida*). Part 1: determination of acute toxicity using artificial soil substrate, vol 11268–1. International Organization for Standardization, Geneve
34. ISO (1998) Soil quality- effects of pollutants on earthworms (*Eisenia fetida*). Part 2: determination of effects on reproduction, vol 11268–2. International Organization for Standardization, Geneve
35. ISO (2006) Soil quality-sampling of soil invertebrates (I): hand-sorting and formalin extraction of earthworms. International Organization for Standardization, Geneva
36. Gudbrandsen M, Sverdrup LE, Aamodt S, Stenersen J (2007) Short-term pre-exposure increases earthworm tolerance to mercury. Eur J Soil Biol 43(Suppl 1):S261–S267
37. Lock K, Janssen C (2001) Ecotoxicity of mercury to *Eisenia fetida*, Enchytraeus albidus and Folsomia candida. Biol Fertil Soils 34(4):219–221. doi:10.1007/s003740100392
38. Kammenga JE, Dallinger R, Donker MH, Köhler HR, Simonsen V, Triebskorn R, Weeks JM (2000) Biomarkers in terrestrial invertebrates for ecotoxicological soil risk assessment. Rev Environ Contam Toxicol 164:93–147
39. Scott-Fordsmand JJ, Weeks JM (2000) Biomarkers in earthworms. Rev Environ Contam Toxicol 165:117–159
40. Sanchez-Hernandez JC (2006) Earthworm biomarkers in ecological risk assessment. Rev Environ Contam Toxicol 188:85–126
41. Rodríguez-Castellanos L, Sanchez-Hernandez JC (2007) Earthworm biomarkers of pesticide contamination: current status and perspectives. J Pestic Sci 32(4):360–371

42. Fugère N, Brousseau P, Krzystyniak K, Coderre D, Fournier M (1996) Heavy metal-specific inhibition of phagocytosis and different in vitro sensitivity of heterogeneous coelomocytes from *Lumbricus terrestris* (Oligochaeta). Toxicology 109(2–3):157–166
43. Svendsen C, Hankard PK, Lister LJ, Fishwick SK, Jonker MJ, Spurgeon DJ (2007) Effect of temperature and season on reproduction, neutral red retention and metallothionein responses of earthworms exposed to metals in field soils. Environ Pollut 147(1):83–93
44. Calisi A, Lionetto MG, Sanchez-Hernandez JC, Schettino T (2011) Effect of heavy metal exposure on blood haemoglobin concentration and methemoglobin percentage in *Lumbricus terrestris*. Ecotoxicology 20(4):847–854
45. Colacevich A, Sierra MJ, Borghini F, Milian R, Sanchez-Hernandez JC (2011) Oxidative stress in earthworms short- and long-term exposed to highly Hg-contaminated soils. J Hazard Mater 194:135–143. doi:10.1016/j.jhazmat.2011.07.091
46. Calisi A, Zaccarelli N, Lionetto MG, Schettino T (2013) Integrated biomarker analysis in the earthworm *Lumbricus terrestris*: application to the monitoring of soil heavy metal pollution. Chemosphere 90(11):2637–2644. http://dx.doi.org/10.1016/j.chemosphere.2012.11.040
47. Berzas Nevado JJ, Rodríguez Martin-Doimeadios RC, Guzman Bernardo FJ, Rodriguez Alvarez C (2014) Determination of total glutathione in earthworms by ultra-high performance liquid chromatography with fluorescence detection. Analyt Method. doi:10.1039/c4ay00085d
48. OECD (1984) Test No. 207: earthworm, acute toxicity tests. OECD guidelines for the testing of chemicals. OECD Publishing, Paris
49. Calisi A, Lionetto MG, Schettino T (2009) Pollutant-induced alterations of granulocyte morphology in the earthworm Eisenia foetida. Ecotoxicol Environ Saf 72(5):1369–1377
50. Calisi A, Lionetto MG, Schettino T (2011) Biomarker response in the earthworm *Lumbricus terrestris* exposed to chemical pollutants. Sci Total Environ 409(20):4456–4464
51. Lionetto MG, Caricato R, Calisi A, Giordano ME, Schettino T (2013) Acetylcholinesterase as a biomarker in environmental and occupational medicine: new insights and future perspectives. Biomed Res Int 2013:1–8. doi:10.1155/2013/321213
52. Frasco MF, Colletier JP, Weik M, Carvalho F, Guilhermino L, Stojan J, Fournier D (2007) Mechanisms of cholinesterase inhibition by inorganic mercury. FEBS J 274(7):1849–1861
53. Beliaeff B, Burgeot T (2002) Integrated biomarker response: a useful tool for ecological risk assessment. Environ Toxicol Chem 21(6):1316–1322
54. Hinton JJ, Veiga JM (2008) The influence of organic acids on mercury bioavailability: insight from an earthworm assessment protocol. Environ Bioindicat 3:47–67
55. Rieder SR, Brunner I, Daniel O, Liu B, Frey B (2013) Methylation of mercury in earthworms and the effect of mercury on the associated bacterial communities. PLoS One 8(4). 10.1371/journal.pone.0061215
56. Kaschak E, Knopf B, Petersen JH, Bings NH, König H (2014) Biotic methylation of mercury by intestinal and sulfate-reducing bacteria and their potential role in mercury accumulation in the tissue of the soil-living Eisenia foetida. Soil Biol Biochem 69(0):202–211. http://dx.doi.org/10.1016/j.soilbio.2013.11.004
57. Drake HL, Horn MA (2007) As the worm turns: the earthworm gut as a transient habitat for soil microbial biomes. Annu Rev Microbiol 61:169–189
58. Gilmour CC, Elias DA, Kucken AM, Brown SD, Palumbo AV, Schadt CW, Wall JD (2011) Sulfate-reducing bacterium Desulfovibrio desulfuricans ND132 as a model for understanding bacterial mercury methylation. Appl Environ Microbiol 77(12):3938–3951
59. Parks JM, Johs A, Podar M, Bridou R, Hurt RA Jr, Smith SD, Tomanicek SJ, Qian Y, Brown SD, Brandt CC, Palumbo AV, Smith JC, Wall JD, Elias DA, Liang L (2013) The genetic basis for bacterial mercury methylation. Science 339(6125):1332–1335
60. Dröge S, Limper U, Emtiazi F, Schönig I, Pavlus N, Drzyzga O, Fischer U, König H (2005) In vitro and in vivo sulfate reduction in the gut contents of the termite Mastotermes darwiniensis and the rose-chafer Pachnoda marginata. J Gen Appl Microbiol 51(2):57–64
61. Limper U, Knopf B, König H (2008) Production of methyl mercury in the gut of the Australian termite Mastotermes darwiniensis. J Appl Entomol 132(2):168–176

62. Gnamus A, Byrne AR, Horvat M (2000) Mercury in the soil-plant-deer-predator food chain of a temperate forest in Slovenia. Environ Sci Tech 34(16):3337–3345. doi:10.1021/es991419w
63. Cristol DA, Brasso RL, Condon AM, Fovargue RE, Friedman SL, Hallinger KK, Monroe AP, White AE (2008) The movement of aquatic mercury through terrestrial food webs. Science 320(5874):335. doi:10.1126/science.1154082
64. Berzas Nevado JJ, Rodríguez Martin-Doimeadios RC, Mateo R, Rodríguez Fariñas N, Rodriguez-Estival J, Patiño Ropero MJ (2012) Mercury exposure and mechanism of response in large game using the Almaden mercury mining area (Spain) as a case study. Environ Res 112:58–66. doi:10.1016/j.envres.2011.09.019

Pb–Zn–Cd–As Pollution in Soils Affected by Mining Activities in Central and Southern Spain: A Scattered Legacy Posing Potential Environmental and Health Concerns

Javier Lillo, Roberto Oyarzun, José María Esbrí, Mari Luz García-Lorenzo, and Pablo Higueras

Abstract In this chapter, published geochemical data for soils from several Pb–Zn mine sites and districts from Spain are reviewed. Although most of the mines have closed down, a legacy of highly polluted soils still remains throughout the sites constituting a potential hazard for the environment and human health. The fate of the studied metals and metalloids in these soils is mainly controlled by factors such as mining methods, concentration and metallurgical operations, mineralogy of the ore, gangue and host rock, fracturing of the host rocks, physiography, climate, and soil types (pedogenic evolution). It can be concluded that the most polluted soils (identified on the basis of an enrichment factor) are those of the Sierra Minera (La Unión District – SE Spain), at more than 488 (Pb), 163 (Zn), 99 (Cd), and 98 (As) times the background values from non-contaminated soils. Pb is usually related to As, which in turn is bound to Fe oxides and oxyhydroxides. Metal bearing jarosite and other soluble phases also play a relevant role in the studied soil–water

J. Lillo (✉)
Departamento de Biología, Geología, Física y Química Inorgánica, ESCET, Universidad Rey Juan Carlos, 28029 Móstoles, Madrid, Spain

IMDEA Water Inst., Parque Científico Tecnológico de la Universidad de Alcalá, 28805 Alcalá de Henares, Madrid, Spain
e-mail: javier.lillo@urjc.es

R. Oyarzun
Departamento de Cristalografía y Mineralogía, Facultad de Ciencias Geológicas, Universidad Complutense, 28040 Madrid, Spain

J.M. Esbrí and P. Higueras
Instituto de Geología Aplicada-Área de Explotación de Minas, Universidad de Castilla-La Mancha, 13400 Almadén (Ciudad Real), Spain

M.L. García-Lorenzo
Departamento de Petrología y Geoquímica, Facultad de Ciencias Geológicas, Universidad Complutense, 28040 Madrid, Spain

E. Jiménez et al. (eds.), *Environment, Energy and Climate Change I: Environmental Chemistry of Pollutants and Wastes*, Hdb Env Chem (2015) 32: 175–206,
DOI 10.1007/698_2014_278,
Published online: 9 August 2014

systems, because these minerals are dissolved during intense rainy events, thus resulting in high rates of metal leaching and mobilization by runoff.

Keywords Arsenic, Environmental geochemistry, Iberian Peninsula, Metals, Mine sites, Soils

Contents

Abbreviations

A	Agricultural
AFS	Atomic fluorescence spectroscopy
AMD	Acid mine drainage
BDL	Below detection limit
EDXRF	Energy dispersive X-ray fluorescence
ETAAS	Electrothermal atomization atomic absorption spectrometry
FAAS	Flame atomic absorption spectrometry
ICP-AES	Inductively coupled plasma atomic emission spectroscopy
ICP-MS	Inductively coupled plasma mass spectrometry
INAA	Instrumental neutron activation analysis
IPB	Iberian Pyrite Belt
MCL	Maximum contaminant levels
Q1	First quartile
Q3	Third quartile
REF_{metal}	Relative enrichment factor
RPL	Residential or parkland

1 A Brief Revision of the Most Relevant Pb–Zn Ore Deposits from the Southern and Central Iberian Peninsula

Given that this chapter is focused on metal pollution and Pb–Zn mineral deposits from the Iberian Peninsula, it is worth mentioning here that metal (and metalloid) dispersion can have both a natural and industrial origin. In this regard, once a mineral deposit is in the surface or near surface environment, fracturing will result in increased permeability and, therefore, in enhanced movement of oxygen-rich meteoric solutions throughout the ore bodies. This implies higher rates of oxidation and metal leaching. This case can be understood in terms of natural (geological) metal pollution. The second case is far more obvious and relates to the mining, processing, and smelting of Pb–Zn sulfides. Thus, to fully understand the combination of natural and industrial, a concise geological revision of the studied mine sites and districts follows.

There are numerous Pb–Zn ore deposits in southern and central Spain (Fig. 1), and these formed in different geological scenarios throughout the Iberian Peninsula from Paleozoic to Cenozoic time. With the exception of a few ore deposits in the Iberian Pyrite Belt (e.g., Las Cruces in Spain, Neves Corvo in Portugal), all mining operations in the described districts have ceased. However, a legacy of tailings deposits, waste rock dumps, and highly polluted soils still remains there constituting a potential hazard for the environment and public health.

1.1 Variscan Age Ore Deposits and Districts

These ore deposits are Pb–Zn hydrothermal vein deposits of Variscan to late Variscan age emplaced along faults crosscutting metasedimentary sequences of Neoproterozoic to Silurian age:

- Alcudia Valley and the San Quintín mining group, southern–central Spain (Fig. 1, Table 1), with about 453 ore deposits (most of them are of very small size). Total Pb production from the Alcudia Valley has been estimated at 1.4 Mt, of which 1.25 Mt was produced between 1840 and 1988. Estimated Ag production was 350 t. Lack of data prevents a reliable estimation of Zn production. For more info, see the comprehensive paper of Palero et al. [1]. Environmental impact: minor and very localized [2]. However, tailings deposits and acid mine drainage (AMD) may pose an environmental hazard for surrounding agricultural lands such as at the San Quintín mining group [3].
- Py–(Cu)–Zn–Pb–(Sn) stockwork and stratiform massive sulfides of volcanogenic origin and Upper Famennian–Lower Visean age occur in southern Portugal and Spain defining the so-called Iberian Pyrite Belt (IPB) (Fig. 1, Table 1), with more than 80 known deposits containing 1,700 Mt of sulfides

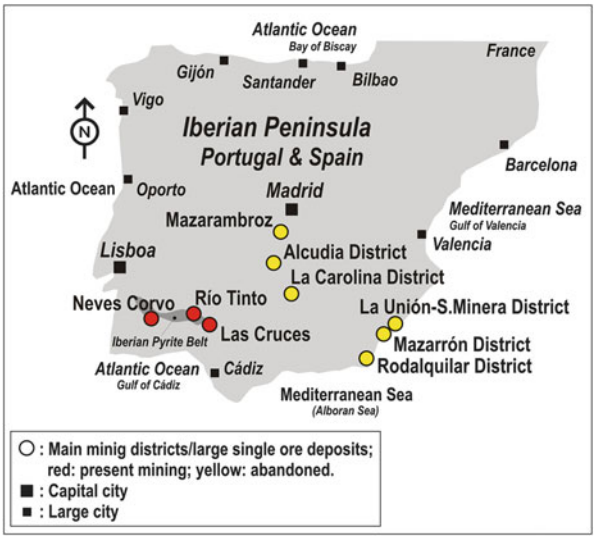

Fig. 1 Location of the Pb–Zn mining districts considered in this chapter

(250 Mt have been extracted; [25]), amounting 14.6 Mt Cu, 13 Mt Pb, 34.9 Mt Zn, 46,100 t Ag, and 880 t Au. For more info on the belt, see the comprehensive paper of Leistel et al. [9]. A few mines are currently operating along the belt, e.g., Las Cruces (Spain) and Neves Corvo (Portugal). Environmental impact: huge, including complete degradation of the River Tinto which owes its deep red color (and name) to massive AMD. The high pollution by heavy metals affecting the soils of the IPB deserved a noteworthy number of studies (e.g., [10–12]). The good news is that the red color is a tourist attraction and the river serves as a world-class natural laboratory for the study of specialized algae and bacteria (e.g., [18]).

- The Linares–La Carolina Ba–Pb–Zn–Cu–(Ag) vein deposits in central Spain (Fig. 1, Table 1) were mainly mined in the period 1875–1920 and constituted one of the most outstanding mining districts of Europe, with an average lead production of 65,000 t $year^{-1}$ and up to 500 g/t silver obtained as a by-product. The workings were concentrated on vein-type hydrothermal mineralization hosted by granitoids and metasediments. The El Cobre vein, a cordilleran vein-type deposit, is representative of the veins in the district and is also one of the largest. The vein strikes northeast–southwest for about 5 km, has an average thickness of 2–3 m, and is hosted by monzogranitic rocks (the so-called Monzogranito de Linares) and minor Carboniferous metasediments. For more info on this district, see the paper of [5]. The soils of the district [6] are extremely rich in Pb (up to 410 times the world average for soils, [26]) whereas for Zn the enrichment is much lower (up to 7 times the world average for soils [26]).

Table 1 Summary of basic information (ore and gangue, soils, and climate) from the districts considered in this chapter. Main references have been included

District	Metal association/ore type/main ore/gangue mineralogy	Soil uses/types/parent material	Climate	References
Alcudia, San Quíntin	Pb–Zn–(Cu)–(Ag) Vein-type deposits Sulfides, sulfosalts Quartz, ankerite, siderite, barite, calcite	*Dehesa* pastures (clear forest of evergreen oaks), Mediterranean forest Soil parent material[a]: metasediments	Mediterranean (dry season from June to September, average annual temperature is 14–15°C, average annual precipitation is 430–550 mm)	[1–4]
Linares–La Carolina	Ba–Pb–Zn–Cu–(Ag) Vein-type deposits Sulfides, sulfosalts Quartz, ankerite, barite, calcite,	*Dehesa* pastures, agriculture (olive groves, minor cereal crops) Soil parent material[a]: granites, metasediments, sedimentary rocks (sandstones, lutites, and marls)	Mediterranean (dry season from June to September, average annual temperature is 17°C, average annual precipitation is ~470 mm)	[5–8]
Iberian Pyrite Belt (IPB)	Py–(Cu)–Zn–Pb–(Sn) Stockwork and stratiform massive deposits. Gossans Sulfides Silicates (quartz, chlorite, sericite), carbonates, barite	Degraded scrub, forest scrub, agriculture (orange plantations, horticulture), reclaimed for forest land Leptosols, Regosols, Cambisols, Fluvisols, Entisols Soil parent material[a]: shales, volcanic and volcanic-sedimentary rocks	Semiarid Mediterranean (xeric–aridic moisture regime, dry season from April to September, average annual temperature is 15–20 °C, average annual precipitation is 400–700 mm)	[9–11]: IPB2 data set [12]: IPB1 data set [13]
Mazarambroz	Pb–Zn–(Ag) Vein-type deposits Sulfides, minor sulfosalts Quartz, siderite, barite	*Dehesa* pastures (clear forest of evergreen oaks), agriculture (extensive cereal crops) Cambisols, Anthrosols Soil parent material[a]: granites, migmatites, metasediments	Mediterranean (dry season from June to September, average annual temperature is ~16°C, average annual precipitation is ~370 mm)	[14–16]
Mazarrón	Pb–(Ag)–Zn–(As) Vein and stockwork type Sulfides Quartz, calcite, siderite, dolomite, and gypsum	Degraded scrub Anthrosols Soil parent material: volcanic rocks (dacites and rhyodacites)	Semiarid Mediterranean (dry season from June to August, average annual temperature is 16.5–18.8 °C, average annual precipitation is 185–310 mm)	[17] [18–22]

(continued)

Table 1 (continued)

District	Metal association/ore type/main ore/gangue mineralogy	Soil uses/types/parent material	Climate	References
La Unión (Sierra Minera, Cartagena)	Pb–(Ag)–Zn–(Sn)–(As) Stratabound ore deposits, disseminations in sedimentary facies, stockworks. Gossans Sulfides, sulfosalts Quartz, carbonates, clays, chlorite, sulfates	Degraded scrub, agriculture? Anthrosols Soil parent material[a]: sedimentary rocks (sands and conglomerates), subvolcanic (rhyolite, dacite, and andesite) and volcanic (alkaline basalt)	Semiarid Mediterranean (dry season from June to August, average annual temperature is 17°C, average annual precipitation is ~300 mm)	
Rodalquilar	High-sulfidation-type Au–(As)–alunite vein deposits Peripheral low-sulfidation Pb–Zn–Cu–(Au) veins Sulfides, sulfosalts Quartz, clays, alunite, chlorite	Degraded scrub, agriculture Inceptisols, Anthrosols Soil parent material[a]: ignimbrites, felsic domes	Semiarid Mediterranean (dry season from May to August, average annual temperature is 18°C, average annual precipitation is 200 mm)	[23, 24]

[a]In addition to mine wastes and modern sediments

1.2 Alpine Age Ore Deposits and Districts

- The Mazarrón district mineral deposits (SE Spain) (Fig. 1, Table 1) formed in Miocene time in relation to the emplacement of dacitic–rhyodacitic domes. The Pb–(Ag)–Zn–(As) ore deposits are of vein and stockwork type. There are three main mining sites (from east to west): San Cristóbal–Perules (adjacent to the town of Mazarrón), Pedreras Viejas, and Coto Fortuna. The area is located in the southern realm of a Miocene–Pliocene marine basin surrounded by mountains in its western, eastern, and southern flanks. The mines were exploited for lead, silver, and zinc during the nineteenth to twentieth centuries (until the early 1960s). The latter corresponds to the peak period of mineral extraction when 3 Mt of ore at 10% Pb and 150 g t^{-1} Ag was extracted between 1920 and 1941. This was followed by a decline in the period 1951–1962, when only 1 Mt of ore at 3% Pb, 5% Zn, and 115 g t^{-1} Ag was extracted. Despite strong AMD (seasonal ponds) and extremely high contents of Pb and Zn (and As) in the tailings and soils, ionic metal migration is limited by the presence of carbonate rocks (Alpujárrides Complex) and soils. The anthropic soils of the district are extremely rich in Pb (up to 200 times the world average for soils, [26]), whereas for Zn the enrichment is lower (up to 80 times the world average for soils, [26]). However, some extremely metal-rich tailings deposits reach the Las Moreras seasonal stream. For more info on this district, see Oyarzun et al. [17].
- The La Unión–Sierra Minera Pb–(Ag)–Zn–(Sn)–(As) district in Cartagena (SE Spain) (Fig. 1, Table 1) hosts ore deposits of different types, having in common a late Miocene age. These include stratabound ore deposits (the so-called mantos) (e.g., Emilia, Brunita), disseminations in the Miocene marine facies (e.g., Sultana), stockworks in felsic domes (e.g., Cabezo Rajao), and gossans. The mining district covers an area of about 10×5 km^2 that contains one of the largest densities of Pb–Zn ore deposits in Spain. Modern mining at the Sierra de Cartagena can be divided into two periods. The first one comprised traditional, underground operations that were active until the early 1950s. From 1957 onwards the Sociedad Minero-Metalúrgica Peñarroya España (a French mining group) began large open pit mining operations, which led first to the generation of large volumes of tailings and mineral dumps and eventually to huge abandoned pits. The Roberto froth flotation plant disposed directly onto the Portman bay about 60 Mt of tailings during the period 1957–1990, eventually making the shoreline advance between 500 and 600 m seaward [19]. For more info on the district, see López_García et al. [18]. A myriad of tailings and waste rock deposits (nineteenth and twentieth centuries) are scattered throughout the district, although metal dispersion is restricted by the presence of carbonate rocks (Alpujárrides Complex) and soils. However, the area affected by mining activities is not small and covers about 1,000 km^2 [20]. Besides, agricultural soils surrounding old mining works (e.g., Cabezo Rajao) may have up to 2,000 mg kg^{-1} Pb and 1,200 mg kg^{-1} Zn [21].

- The Rodalquilar district in Almería (SE Spain) (Fig. 1, Table 1) is well known for its high-sulfidation-type Au–(As)–alunite vein deposits within a large volcanic caldera of Miocene age, with an ore mineralogy consisting of native gold (Au^0), pyrite, enargite (Cu_3AsS_4), tennantite ($Cu_{12}As_4S_{13}$), tetrahedrite ($Cu_{12}Sb_4S_{13}$), cinnabar (HgS), bismuthinite (Bi_2S_3), cassiterite (SnO_2), galena, and sphalerite. However, the district also hosts peripheral low-sulfidation Pb–Zn–Cu–(Au) veins. The geological setting of Rodalquilar district includes Upper Miocene felsic domes, ignimbrites, ash fall deposits, massive volcanic rocks, and a limestone complex of Messinian age. The sulfide mineralogy of the peripheral low-sulfidation deposits consists of native gold, sphalerite, galena, chalcopyrite, and pyrite. Mining initiated around 1825 for Pb, Zn, and Cu, and it was not until 1864 that the miners realized that the ore contained some gold as well. Mining operations belonging to this period are those of Consulta, María Josefa, San Diego, and Triunfo. The larger mining operation relates to the El Cinto high-sulfidation deposits and took place between 1943 and 1966, when about 1.6 Mt of ore grading 3.5 g t^{-1} Au was extracted. Most if not all of the tailings (between 900,000 and 1,250,000 m^3) around the town of Rodalquilar can be related to this mining period. For more info on the district, see the papers of Arribas et al. [23] and Oyarzun et al. [24]. Main environmental concerns relate to the high contents of As in anthropic and agricultural soils.
- The Mazarambroz Pb–Zn mineralization in the Toledo Mountains (central Spain) (Fig. 1, Table 1) is filling E–W fractures following the main direction of the so-called Mylonitic Band of Toledo. The veins are hosted by migmatites, metasediments, and granitic rocks related to the Mora Plutón [14]. Ag-rich galena and sphalerite are the main ore minerals, being accompanied by arsenopyrite (FeAsS), pyrite and marcasite (FeS_2), chalcopyrite ($CuFeS_2$), and gersdorffite (NiAsS), with quartz (SiO_2), siderite ($FeCO_3$), and barite ($BaSO_4$) as the dominant gangue minerals [15]. Mines in this area were exploited until the late 1970s [15]. The soils in this area show Pb, Zn, and As concentrations much higher than the regional averages for soils [16].

2 Understanding of the Geochemical Behavior of Pb and Zn in Natural Environments

2.1 Environmental Mineralogy and Geochemistry of Pb and Zn: A Brief Introduction

Lead and zinc are base metals that form one of the classic associations in ore deposits. Galena (PbS) and sphalerite (ZnS) are their common sulfide minerals, and they can be found together with chalcopyrite ($CuFeS_2$), pyrite (FeS_2), and arsenopyrite (FeAsS) (among others) in a variety of geological and ore-forming settings, such as skarns in limestones and dolostones (dolomites), hydrothermal veins, and

replacements in plutonic or volcanic rocks of felsic composition, volcanogenic massive sulfide deposits, and Mississippi Valley-type Pb–Zn ore deposits. Other common lead and zinc minerals are anglesite ($PbSO_4$), cerussite ($PbCO_3$), and smithsonite ($ZnCO_3$), together with the less common willemite (Zn_2SiO_4) and zincite (ZnO). The presence of silver in galena (either as mineral inclusions or solid solution) is relatively common.

The environmental legislation of most countries has progressively retired lead from common uses such as plumbing, additives for petrol, and paints, while it remains nevertheless being widely used in lead–acid batteries for cars. On the other hand, the major environmental and health concerns regarding Zn are not strictly related to the element but to its most common mineral: sphalerite, which usually hosts Cd. Cadmium and zinc belong to the same group of the periodic table (IIB) and share chemical properties such as the tetrahedral covalent bond and other crystal structures. They have similar ionic radii: Zn^{2+} (0.74 Å) and Cd^{2+} (0.97 Å), which accounts for the observation that cadmium occurs in sphalerite as an isomorphous impurity [27].

Lead and zinc ([28, 29]) can be regarded as chalcophile (i.e., those elements that combine easily with sulfur) although Zn also has lithophile affinities (i.e., those elements that concentrate in the silicate phase and combine readily with oxygen in the Earth's crust). The solubility of their ionic species (Pb^{2+}, Zn^{2+}) is controlled by the ionic potential, being extremely high in the case of Zn or extremely low in the case of Pb, which will form insoluble sulfates or carbonates ($PbSO_4$, $PbCO_3$). This is crucial to understand their geochemical behavior in the environment because while Pb will remain close to the source, Zn can move and disperse easily. This will happen even in extremely dry scenarios such as the Atacama Desert, where Zn forms vast geochemical halos surrounding the source (e.g., [30]).

Pb in freshwater systems will be complexed by carbonate species ($Pb(CO_3)_2^{2-}$) at pH 6–8, whereas stable species below and above this range will be $PbSO_4$ (or Pb^{2+} in low-sulfate waters) and $Pb(OH)_2$, respectively [26]; besides, Zn^{2+} is the most stable species of zinc below pH 8, whereas $ZnCO_3$ is stable at higher pH. Complexing of Zn with SO_4^{2-} becomes important only in sulfate-rich acidic waters [26], a geochemical scenario where important oxidation of pyrite (FeS_2) has occurred (1) leading to formation of AMD:

$$4FeS_2 + 10H_2O + 15O_2 \rightarrow 4FeO(OH) + 16H^+ + 8SO_4^{2-}. \quad (1)$$

This is also important to understand oxidation and hydrolysis of galena and sphalerite in the supergene environment of the higher sections of sulfide ore deposits (2, 3), because if pyrite is volumetrically unimportant, reaction (4) will be insignificant and no important formation of Fe^{3+} will occur [31]:

$$4FeS_2 + 14O_2 + 4H_2O \rightarrow 4FeSO_4 + 4H_2SO_4, \quad (2)$$

$$4FeSO_4 + 2H_2SO_4 + O_2 \rightarrow 2Fe_2(SO_4)_3 + 2H_2O, \quad (3)$$

$$Fe_2(SO_4)_3 \rightarrow 2Fe^{3+} + 3SO_4{}^{2-}. \quad (4)$$

The chemical evolution of the system from (2) to (4) is the main prerequisite to induce oxidation and hydrolysis of galena (5) and sphalerite (6) [31]:

$$PbS + 8Fe^{3+} + 4H_2O \rightarrow Pb^{2+} + 8Fe^{2+} + SO_4{}^{2-} + 8H^+, \quad (5)$$

$$ZnS + 8Fe^{3+} + 4H_2O \rightarrow Zn^{2+} + 8Fe^{2+} + SO_4{}^{2-} + 8H^+. \quad (6)$$

Given that sphalerite often contains Cd, the oxidation and leaching of this metal can be expressed in the following way (7):

$$Zn_{1-x}Cd_xS + 8Fe^{3+} + 4H_2O \rightarrow (1-x)Zn^{2+} + xCd^{2+} + 8Fe^{2+} + SO_4{}^{2-} + 8H^+. \quad (7)$$

Arsenopyrite is present in many Pb–Zn deposits (e.g., the Mazarrón district), and therefore it is worth showing here how the oxidation of this mineral occurs [32] (8–11):

$$FeAsS \rightarrow Fe^{2+} + \tfrac{1}{2}As_2S_2 + 2e^-, \quad (8)$$

$$As_2S_2 + 14H_2O \rightarrow 2H_3AsO_3 + 2\,SO_4{}^{-2} + 22H^+ + 18\,e^-, \quad (9)$$

$$H_3AsO_3 + H_2O \rightarrow H_3AsO_4 + 2H^+ + 2\,e^-, \quad (10)$$

$$Fe^{2+} \rightarrow Fe^{3+} + 1\,e^-. \quad (11)$$

If fO_2 conditions are high, then oxidation of As^{3+} to As^{5+} may proceed in the following way [33] (12):

$$H_3AsO_3 + \tfrac{1}{2}O_2 \rightarrow H_2AsO_4{}^- + H^+. \quad (12)$$

The concentrations of these ionic or complex ion species in water are a particularly sensitive case regarding public health; in this regard, maximum contaminant levels (MCLs) for drinking water (USA) for these elements are Pb (0.015 mg L^{-1}), Zn (5 mg L^{-1}), Cd (0.005 mg L^{-1}), and As (0.01 mg L^{-1}) [34]. MCLs have to be understood as the highest level of a contaminant that is allowed in drinking water using the best available treatment technology and taking cost into consideration [34]. However, do these MCL figures reveal the complete picture regarding metal toxicity? Not really, because toxicity does not depend on concentration but on the bioavailability of the metal species [35]. In fact, strongly complexed metals, especially those complexed by natural chelating agents such as the humic acids, appear to be completely unavailable and nontoxic [35]; thus, metal speciation studies are of paramount importance to fully understand the potential health hazards derived from the existence of high concentrations of metals in waters (surface or underground). The same applies to sediments and soils.

Regarding sediment quality guidelines for freshwater ecosystems, the following threshold effect concentrations (meaning that below these levels, no adverse effects for the biota should happen) are suggested for lead, zinc, and cadmium: Pb (35 mg kg^{-1}), Zn (121 mg kg^{-1}), Cd (0.99 mg kg^{-1}), and As (9.79 mg kg^{-1}) [36]. Nevertheless, natural systems are to be regarded for what they are, nonlinear highly complex systems in which the outcome cannot be fully predicted based only on the study of just a few variables. For example, the ultimate fate of free cadmium (Cd^{2+}) may be strongly influenced by the presence of pyrite, which is particularly important in anoxic media. In this regard, two reactions (13, 14) are to be taken into account [35]:

$$FeS_{(s)} \leftrightarrow {Fe^{2+}}_{(aq)} + {S^{2-}}_{(aq)}, \tag{13}$$

$${Cd^{2+}}_{(aq)} + {S^{2-}}_{(aq)} \leftrightarrow CdS_{(s)}. \tag{14}$$

In this regard, if the free (and therefore available) Cd^{2+} metal ion is combined with free sulfur (S^{2-}), then CdS will precipitate and become unavailable. Given that cadmium has more affinities for sulfur than iron, then the overall reaction will proceed towards the products (right-hand side) (15):

$${Cd^{2+}}_{(aq)} + FeS_{(s)} \rightarrow {Fe^{2+}}_{(aq)} + CdS_{(s)}. \tag{15}$$

A similar concern regarding these elements is observed in the Canadian Soil Quality Guidelines [37], which indicate maxima levels of (A, agricultural; RPL, residential or parkland): 70 mg kg^{-1} (A) and 140 mg kg^{-1} (RPL) for Pb, 200 mg kg^{-1} (A and RPL) for Zn, 1.4 mg kg^{-1} (A) and 10 mg kg^{-1} (RPL) for Cd, and 12 mg kg^{-1} (A and RPL) for As.

2.2 Speciation of Pb and Zn in Contaminated Soils

Speciation of metals in soils depends on the type of soil matrix, pH, Eh, colloidal activity, and climate. For example, in soils with abundant organic matter, Pb^{2+} may be complexed to salicylate- and catechol-type functional groups of humic substances [38], whereas Zn is not expected to significantly bind to organic matter [39]. Conversely, Zn^{2+} in these acidic soils can be found as franklinite ([(Zn, Mn^{2+}, Fe^{2+})(Fe^{3+},Mn^{3+})$_2O_4$]) or bound by adsorption to Fe and Mn oxyhydroxides as inner-sphere sorption complexes [39]. To understand lead speciation in carbonate-rich soils, the formation of carbonic acid has to be considered since it is a key reactant for the ultimate fate of this metal (16):

$$CO_{2(g)} + H_2O \leftrightarrow H_2CO_{3(aq)}. \tag{16}$$

Pb^{2+} in alkaline soils such as pedocals (which form in semiarid and arid regions) will first form Pb oxides (17), followed by the formation of cerussite ($PbCO_3$) (18)

at nearly neutral to slightly alkaline pH and even hydrocerussite (19) if pH is high enough:

$$Pb^{2+}{}_{(aq)} + \tfrac{1}{2}O_{2(g)} \rightarrow PbO_{(s)}, \tag{17}$$

$$PbO_{(s)} + H_2CO_{3(aq)} \rightarrow PbCO_{3(s)} + H_2O, \tag{18}$$

$$3PbO_{(s)} + 2H_2CO_{3(aq)} \rightarrow Pb_3(CO_3)_2(OH)_{2(s)}. \tag{19}$$

In the same environment, Zn^{2+} may form smithsonite ($ZnCO_3$) or hydrozincite ($Zn_5(CO_3)_2(OH)_6$).

Arsenic is usually bound to Fe oxide/hydroxide phases in soils [33] and river sediments (e.g., [40]). Colloidal goethite has a net positive charge in acid media [41], which binds by adsorption of the negatively charged arsenic complex ions of general composition $H_xAsO_y^{-z}$ (where $x = 1$, 2, or 3; $y = 3$ or 4; and $z = 0$, -1, or -2). These complex ions may remain strongly bound to goethite up to higher pH of 8.0–8.5 [42–44]. Desorption of arsenic from goethite may occur by competition between negative charges for the positive colloid, a reduction of the iron oxide mineral phase [45], or high pH values (>8.5). If plants are present, then the chemical interactions that take place in the soil–rhizosphere–plant system have to be considered. According to [46], both plant-induced reductions and drastic pH decreases in the rhizosphere may dissolve Fe oxides/hydroxides. This would result in the release of As and the potential uptake by the plant of As^{3+} (enhanced bioavailability and toxicity to plants) [46]. Alternatively, in carbonate-rich rocks and soils, the acid solutions will become neutral to alkaline, and two arsenic minerals will precipitate: first weilite ($Ca(AsO_3OH)$) and then pharmacolite ($CaHAsO_4 \cdot 2H_2O$) [33]. Besides, the same authors found remarkable redox seasonal changes for arsenic in river sediments; winter is characterized by a dominance of As^{3+} species within an environment ruled by the activity of bacteria, which leads to the formation of amorphous Fe^{3+}-As^{3+} precipitates together with nanocrystalline tooeleite ($Fe_6(AsO_3)_4SO_4(OH)_4 \cdot 4H_2O$). On the other hand, biotic oxidation of As^{3+} and Fe^{2+} leads to the precipitation of mixed Fe^{3+}-As^{5+} hydrous oxides during spring and summer [33].

3 Mining and Pb–Zn Dispersion in Soils: Some Facts and Fads

3.1 How Bad Is the Case?

Mining has indeed a bad press. Poor public relations skills of mining company officials, the action of environmental groups, and a traditional mistrust from the ordinary citizens have contributed to create an increasingly poisoned social scenario. There is no question on whether mining strongly polluted the environment

(atmosphere, soils, underground and surface waters, biota, etc.) with heavy metals and/or metalloids prior to the enforcement of environmental regulation laws (from the 1980s onwards) in most countries. However, different to popular beliefs, mining is by no means at present the evil force that many environmental lobbies claim to be. In this regard, if the Earth's land area modified by human action mostly during the last 500 years ($53.5 \pm 5.1\%$) [47] is taken into account, mining and quarrying have contributed with a mere 0.3% (there is a 67% probability that the actual value lies between 0.2% and 0.6%); for comparison, agriculture and forestry contribute with a huge $46.6 \pm 5.0\%$ [48]. This is particularly significant if it is considered that modern agriculture is the kingdom of chemicals, which are nevertheless a key prerequisite to maintain and even increase global production to sustain an ever-growing human population.

Having said all this, it must be clear on this matter that it is not suggested here that mining (and particularly the smelting of lead minerals) does not pose an important health risk. In fact, lead can affect the nervous system, kidney function, immune system, reproductive and developmental systems, and the cardiovascular system, also affecting the oxygen carrying capacity of the blood; in this regard, this metal is persistent in the environment and accumulates in soils and sediments through deposition from air sources, direct discharge of waste streams to water bodies, mining, and erosion [49]. For example, a comprehensive geochemical and epidemiologic study carried out in 1974 at Coeur d'Alene (Idaho, USA) revealed the following [50]:

- Lead levels in air, soil, and dust were highest at the smelter and decreased with distance, with peak concentrations in soils and vegetation of 9,000 and 3,478 mg kg^{-1}, respectively.
- 99% of 1- to 9-year-old children living within 1.6 km from the smelter had blood lead levels $\geq$40 μg dl^{-1}, indicating increased absorption (22% had levels $\geq$80 μg dl^{-1}).
- Lead levels $\geq$40 μg dl^{-1} decreased with distance, for example, at 72 km from the smelter, it was 1%.
- 17% of children with lead levels of $\geq$80 μg dl^{-1} were anemic.

Another example is related to the Antofagasta (Chile) incident involving lead poisoning in children. Lead was gathered in bulk (Pb mineral concentrates from Bolivia) within the urban zone of the city, which resulted in severe contamination of the surrounding schools and houses. This contamination was in turn significantly associated with high blood lead levels in children [51].

On the other hand, mining and smelting of zinc has been by far the most important contributor of this metal to the environment [26]. For a long time, Zn was not considered to be harmful for the environment, and it was thought to pose minimal health risks compared to other heavy metals; however, at present zinc is known to cause toxic effects in the aquatic biota [26]. Besides, the almost ubiquitous presence of Cd in sphalerite (ZnS) is another factor to be taken into account. Zinc is an essential element, necessary for the function of more than 300 enzymes; however, oral exposure to high levels of zinc in humans can result in several

systemic effects [52]. In this regard, the major concerns about Zn are not usually related to the element but to sphalerite, which usually hosts Cd. This toxic element causes the so-called itai-itai disease, that is, osteomalacia with various degrees of osteoporosis accompanied by severe renal tubular diseases [53]. Low-molecular-weight proteinuria has been reported among people living in contaminated areas in Japan and exposed to cadmium via food and drinking water [53]. Regarding arsenic, acute and chronic poisoning involves the respiratory, gastrointestinal, cardiovascular, nervous, and hematopoietic systems; besides arsenic is carcinogenic and may cause lung, bladder, liver, renal, and skin cancers [54]. The toxicity of this metalloid depends on its binding form. For example, the organic arsenic compounds are less toxic than inorganic species. In fact, As^{3+} is 10 times more toxic than As^{5+} and 70 times more toxic than the organic species.

Although mining and processing of Pb and Zn in the Iberian Peninsula is currently restricted to a few mines in the IPB, a myriad of abandoned mines, tailings, and waste rock dumps are scattered in the old mining districts, and some of them are in close proximity to towns. For example, Pb–Zn tailings are part of the urban landscape of Mazarrón [17].

3.2 When Should We (Really) Worry About?

This is an important question that should be addressed from a combined industrial and environmental perspective including the following factors: mining methods (underground – open pit); concentration and metallurgical operations; mineralogy of the ore, gangue, and host rock; fracturing of the host rocks; physiography (hilly vs. flat terrain); climate; and, last but not least, soil types (pedogenic evolution):

- *Mining methods*: It does not escape to anyone that the impact of open pit mining is far larger than the underground procedures. It is a matter of simple mathematics: a usual rate of waste to mineralized rock in open pit operations is 3:1 (or more), meaning that for each ton of rock that will undergo milling and mineral concentration, three will go into waste; moreover, this three tons will not be entirely "barren" because they may host subeconomic mineralization (usually rich in pyrite). In this case, the sulfides present in huge waste rock piles will be exposed to oxygen and water, which implies generation of AMD and metal leaching. Besides, once the mining operations have ceased, a huge rock surface within the pit will be also left to undergo chemical reactions, which may have disastrous consequences for the chemistry of groundwaters. On the contrary, underground mining is more selective (it has to be; otherwise it would turn out to be uneconomic), and therefore waste rock piling will be minimal. However, these galleries and stopes placed above the water table may also undergo oxidation and leaching.
- *Mineral concentration*: As any other industrial activity, mining has undergone a complete transformation since the second half of the nineteenth century.

Different to the froth flotation (introduced in the early twentieth century), mineral concentration in the nineteenth century (and well into the twentieth century) was performed by gravity using jigs (e.g., as at Mazarrón and La Unión), an inefficient procedure that contributed to generate tailings deposits extremely rich in Pb and Zn; for example, 4830–21,600 mg kg^{-1} Pb and 2410–13,100 mg kg^{-1} Zn [17].

- *Mineralogy of the ore, gangue, and host rock*: As previously discussed (1–7), key for the oxidation and leaching of Pb and Zn from galena and sphalerite is the presence of pyrite in the system. Thus, the relative abundance of pyrite among the sulfide species in one particular ore deposit will rule the rate of oxidation during weathering. Other important factors to be taken into account are the fO_2 (no oxygen–no oxidation), water (these are also hydrolytic chemical processes), and biological activity. The latter is driven by the presence of chemolithotrophic bacteria such as (among others) *Thiobacillus ferrooxidans* or *Leptospirillum* spp. [55]. In this regard, the rate of pyrite oxidation directly relates to the rate at which aqueous Fe^{3+} can be produced from Fe^{2+} by microbial catalysis [56]. In turn, abiotic and biotic oxidation of pyrite generates two powerful chemical leaching agents: sulfuric acid and ferric sulfate (2, 3). However, if the gangue minerals or the host rock includes species such as calcite ($CaCO_3$), the acid will react with the carbonate, H^+ will be consumed, and leaching will be reduced or stopped altogether (20):

$$CaCO_3 + H^+ \leftrightarrow Ca^{2+} + HCO_3^-. \tag{20}$$

The same applies to the feldspars (21) and their hydrolytic by-products (22) that can be found in volcanic or plutonic rocks [57]:

$$3KAlSi_3O_8 + 2H^+ \rightarrow KAl_3Si_3O_{10}(OH)_2 + 6SiO_2 + 2K^+, \tag{21}$$

$$2KAl_3Si_3O_{10}(OH)_2 + 2H^+ + 3H_2O \rightarrow 3Al_2Si_2O_5(OH)_4 + 2K^+. \tag{22}$$

- *Fracturing*: The intensity of fracturing also plays a major role in the oxidation leaching of sulfides. A high density of major fractures facilitates erosion and, therefore, the unroofing of mineral deposits. Once the mineral deposit is in the surface or near surface environment, fracturing will result in increased permeability and, therefore, in enhanced movement of oxygen-rich meteoric waters throughout the ore bodies. This implies higher rates of oxidation and metal leaching [57].
- *Climate and physiography*: They do play a major role in metal dispersion. Given that leaching of metals is an essentially chemical process, temperature will play a crucial role: warmer conditions will enhance the process, whereas cold conditions will slow it down. Total rain precipitation is also important [17]. For example, rainfall and dry events cause increases and decreases, respectively, in acid and metal concentrations. The process does not end until pyrite is fully weathered, which can take hundreds to thousands of years [58]. As noted by

[58], long dry spells result in gradual increases in metal concentrations, whereas sudden large increases are observed during initiation of rains. However, as precipitations reach their peak, the solutions become diluted. On top of this, the flash floods generated during stormy episodes must be added as they have the capacity to remove contaminated soils and tailings deposits. If this occurs, massive transport of contaminated materials will go to the rivers and, from there, to the lowlands. This is a process that will be enhanced by the high-altitude environment. In this regard, the rule of thumb is: the higher a mining operation is located, the greater the risk of mass movement of contaminated materials. This is well exemplified by cases in Chile (Pascua – Lama, El Indio Belt) and New Guinea (OK Tedi, Grasberg, Porgera) (e.g., [2, 40, 57], of this chapter).

- *Soil types (pedogenic evolution)*: The retention and accumulation of metals in the soil depends on various soil characteristics such as solid phase components (organic matter, sulfates, carbonates and clay minerals, oxides, etc.), texture, structure, pH, and ion exchange capacity (e.g., [13, 17]). These soil characteristics are intimately related to the climate and physiography in terms of soil evolution. Organic matter plays a key role as they may form very stable organic-mineral complexes and they have a very high ion exchange capacity. Alternatively, soluble humic substances as fulvic acids may form quelates that facilitate the metal leaching from the soil. Soil mineralogy is crucial because of the importance of adsorption processes and ion exchange capacity in clays and oxides, hydroxides, and oxyhydroxides and metal coprecipitation in sulfates and carbonates. The presence of soluble salts may affect the pH and the ion (cation) exchange of metals. Texture and structure control the water–rock interaction and solid phase reactivity through specific surface and hydraulic conductivity. The pH in terms of active and potential acidity plays a dual role, firstly because it controls the ion exchange capacity (especially in organic matter) and secondly because metal solubility depends on pH.

These reasons explain why risk assessment of metal leaching from ore deposits, tailings, and waste rock dumps is so complex. In fact, it involves complex nonlinear systems in which the measurements of the pollutant phase(s) (and other variables: see above) alone cannot provide a complete picture of the state of the system, because they are limited in space and time. However, at least a partial answer may be provided to the initial question on when we should be worried regarding metal leaching. In this process nothing is as decisive as: (1) the proportion of pyrite in the sulfide mineral assemblage and (2) the reactivity of the gangue and host rock minerals. This puts the IPB deposits in the worst possible case scenario (extremely rich in pyrite).

4 Pb, Zn, Cd, and As in Soils from the Studied Iberian Mining Sites and Districts

To study the Pb, Zn, Cd, and As distribution in soils from the revised mining sites and districts (Fig. 1, Table 1), published data from soils subjected to different uses (agricultural, natural, and anthropic) have been considered (Table 2). The more polluted soils were identified on the basis of a relative enrichment factor (REF_{metal}), defined by the ratio ([metal concentration in polluted soil – metal background concentration in soil]/[metal background concentration in soil]). By using the REF value, it is assumed that soils may have high background metal concentrations in natural, nonpolluted conditions as they are in areas that host ore deposits. Indeed, ore deposits induce the generation of geochemical dispersion halos, which can be regarded as a "natural contamination process" different to these of industrial origin generated by mining, processing, and smelting of sulfide ores. The relationships between metals and As (arsenic is a metalloid) were studied by correlation matrices, and cluster and factor analyses were also used to investigate whether different geological and industrial scenarios resulted in the formation of differentiated clusters of mineral deposits. Below detection limit (BDL) data were set to a value of half the BDL concentration for each element [59]. Besides, given that a sizeable proportion of data with identical value can seriously influence any multivariate analysis [60], the sets with BDL data >10% of the population were excluded. Log transformation was applied to data to get more symmetrical (Gaussian) distributions. In this regard, many trace element distributions show important skewness, which may disappear if the logarithm of the values (log x) is considered. If this is the case, it can be said that log x has a normal distribution, or simpler, that the distribution is lognormal [61].

Although there are significant differences in size among the data sets, the following facts can be highlighted in terms of mean concentrations and enrichment factors.

4.1 Mean Concentrations

- The highest Pb and Zn mean concentrations are found in soils located in the Sierra Minera (La Unión District) with values of 6,241 and 9,111 mg kg^{-1}, respectively (Fig. 2, Table 2). However, the data population shows a large dispersion with some outliers of very high concentrations that displace the mean outside the first quartile (Q1) and third quartile (Q3) range (Fig. 2, Table 2). The lowest Pb and Zn mean concentrations are found in soils located in Rodalquilar (226.3 and 118.9 mg kg^{-1}, respectively) (Fig. 2, Table 2).
- The highest As mean concentration (1,309 mg kg^{-1}) is also found in soils from the Sierra Minera (Fig. 2, Table 2), whereas the lowest As mean concentration (26.1 mg kg^{-1}) is found in Linares (Fig. 2, Table 2).

Table 2 Descriptive basic statistics of trace element concentrations. Mean, median, minimum, maximum, first quartile (Q1), and third quartile (Q3) values are expressed in mg kg^{-1}

Variable	Analysis method	Mean	St. Dev.	Min.	Q1	Median	Q3	Max.
Linares ($n = 126$) (*Source:* [64])								
Ag	ICP-AES	2.1	4.3	0.3	0.3	0.5	1.8	29.2
As	ICP-AES	26.1	29.2	2.5	11	17	26	175.5
Cd	ICP-AES	0.8	2.9	0.2	0.2	0.2	0.6	31.8
Cu	ICP-AES	145.4	242.5	14	32.8	53.5	128.4	1,654
Pb	ICP-AES	4077	7,016	27	267	1,279	4,867	37,356
Sb	ICP-AES	18.6	90	2.5	2.5	2.5	10	992
Zn	ICP-AES	123.9	206	26	46	71.5	133.5	1,988
Mn	ICP-AES	1,210.7	802.1	194	530.8	1,086	1,608	3,981
Rodalquilar ($n = 31$) (*Source:* [18])								
As	ICP-MS	422	473.1	27.4	70.4	169	784	1,510
Bi	ICP-MS	8.5	13.9	0	1	2.8	10.2	73.5
Cd	ICP-MS	0.3	0.2	0.1	0.1	0.2	0.2	0.8
Cu	ICP-MS	73.6	49.5	11.2	39.8	57.5	102	178
Hg	Pyrolysis	0.4	0.6	0	0.1	0.2	0.5	2.6
Pb	ICP-MS	226.3	158.7	28.2	115	193	270	798
Sb	ICP-MS	19.4	18.8	0.6	4.6	10.7	32.2	62.6
Se	ICP-MS	15.7	14.5	1.5	3.9	8.9	27.5	49.8
Sn	ICP-MS	25.7	28.5	2	5	11	37	108
Zn	ICP-MS	118.9	103.3	1.3	42.4	77.2	160	401
Mazarrón ($n = 15$) (*Source:* [13])								
Ag	ICP-MS	9.7	11.2	0.4	2.5	6.4	12.4	36
As	ICP-MS	252.3	206.6	58	98	189	299	744
Ba	ICP-MS	1,212	1,425	149	485	774	1,390	6,050
Bi	ICP-MS	0.3	0.6	0.01	0.1	0.2	0.4	2.4
Cd	ICP-MS	11.4	9.9	0.7	5	7.6	18	32.8
Cu	ICP-MS	88.7	59.4	27	41	80	123	259
Pb	ICP-MS	2,955	2,570	235	908	2,600	4,820	9,110
Sb	ICP-MS	54.4	42.2	10.3	27.3	40.5	80.1	174
Se	ICP-MS	1.2	0.4	0.5	1.1	1.2	1.4	2
Sn	ICP-MS	14.3	10.6	4	9	11	14	48
Zn	ICP-MS	1,651	1,584	331	563	791	3,030	5,250
Sierra Minera ($n = 54$) (*Source:* [59])								
As	AFS	1,309	1,123	67	453	1,020	1,597	4,429
Cd	ETAAS	37.6	22.6	2.2	22.2	33.7	44.5	123.2
Cu	ETAAS	352.1	293.4	21.5	140.5	258.4	576.2	1,335
Hg	AFS	0.3	0.5	0	0	0.1	0.4	2
Pb	ETAAS	6,241	9,390	25	2,287	3,328	4,222	47,619
Zn	FAAS	9,111	6,911	516	3,223	7,844	11,336	30,405
Alcudia ($n = 142$) (*Source:* [2])								
As	EDXRF	37.4	83.16	0.5	17	22	26	792
Cd	EDXRF	10.53	51.83	0.5	0.5	0.5	2	530
Cr	EDXRF	33.84	33.39	0.5	14	26	44.25	253
Cu	EDXRF	56.6	150	1	11	15.5	31	1,283
Hg	EDXRF	71.4	342.7	0.5	0.5	0.5	0.5	2,665

(continued)

Table 2 (continued)

Variable	Analysis method	Mean	St. Dev.	Min.	Q1	Median	Q3	Max.
Mo	EDXRF	3.067	3.702	0.5	0.5	1	5	19
Ni	EDXRF	12.3	21.63	0.5	0.5	4.5	16	137
Pb	EDXRF	1,575	5,581	69	112	169	544	52,207
Sb	EDXRF	2.98	12.37	0.5	0.5	0.5	0.5	110
Se	EDXRF	33.7	27.56	18	25	27	31	282
Zn	EDXRF	517	1,232	30	61	112	259	8,336
Mazarambroz ($n = 50$) (*Source:* [21])								
As	EDXRF	161.8	417.5	11	30	61	140.5	2,955
Cd	EDXRF	5.69	10.02	0.5	0.5	0.5	7.25	47
Cr	EDXRF	52.11	45.45	0.5	21.75	46	75	244
Cu	EDXRF	40.78	36.22	8	17.75	32.5	50.5	232
Hg	EDXRF	0.5	0	0.5	0.5	0.5	0.5	0.5
Mo	EDXRF	9.84	3.285	3	8	10	12	19
Ni	EDXRF	22.3	23.49	0.5	6	18	29	112
Pb	EDXRF	307.9	472.8	86	97	109.5	267.3	2,867
Sb	EDXRF	0.73	1.626	0.5	0.5	0.5	0.5	12
Se	EDXRF	22.64	6.444	0.5	21	24	26	32
Zn	EDXRF	603	1,251	67	110	160	389	762
IPB1 ($n = 32$) (*Source:* [8])								
As	INAA	562.4	441.9	51	185.5	443.5	896	1,560
Cd	ICP-AES	1.744	3.99	0.15	0.15	0.65	1	22
Cr	INAA	77.84	51.34	2.5	48.25	73	94.25	226
Cu	ICP-AES	684	678	24	238	413	992	2,874
Hg	INAA	6.78	14.5	0.5	0.5	0.5	4.75	62
Ni	ICP-AES	34.69	29.93	0.5	12	30.5	51.75	138
Pb	ICP-AES	1,705	1,839	59	239	1,165	2,637	6,500
Zn	ICP-AES	599	1,192	22	175	354	500	6,890
IPB2 ($n = 15$) (*Source:* [7])								
As	INAA	226.8	315.8	18.8	30.2	78.7	361	994
Cd	ICP-AES	0.917	0.529	0.15	0.5	0.8	1.2	2.3
Cr	INAA	129.3	56.8	35	98	111	173	236
Cu	ICP-AES	259.7	296.8	27	90	159	253	1,160
Ni	ICP-AES	45.93	20.23	14	26	51	60	75
Pb	ICP-AES	810	1,341	41	93	197	1,270	4,890
Zn	ICP-AES	303.1	233.9	95	147	206	356	897

ICP-AES, inductively coupled plasma atomic emission spectroscopy; ICP-MS, inductively coupled plasma mass spectrometry; AFS, atomic fluorescence spectroscopy; FAAS, flame atomic absorption spectrometry; ETAAS, electrothermal atomization atomic absorption spectrometry; EDXRF, energy dispersive X-ray fluorescence; INAA, instrumental neutron activation analysis

- The highest Cd mean concentration (37.6 mg kg^{-1}) is also from the Sierra Minera (Fig. 2, Table 2), whereas the lowest is found in Rodalquilar (0.2 mg kg^{-1}) (Fig. 2, Table 2).

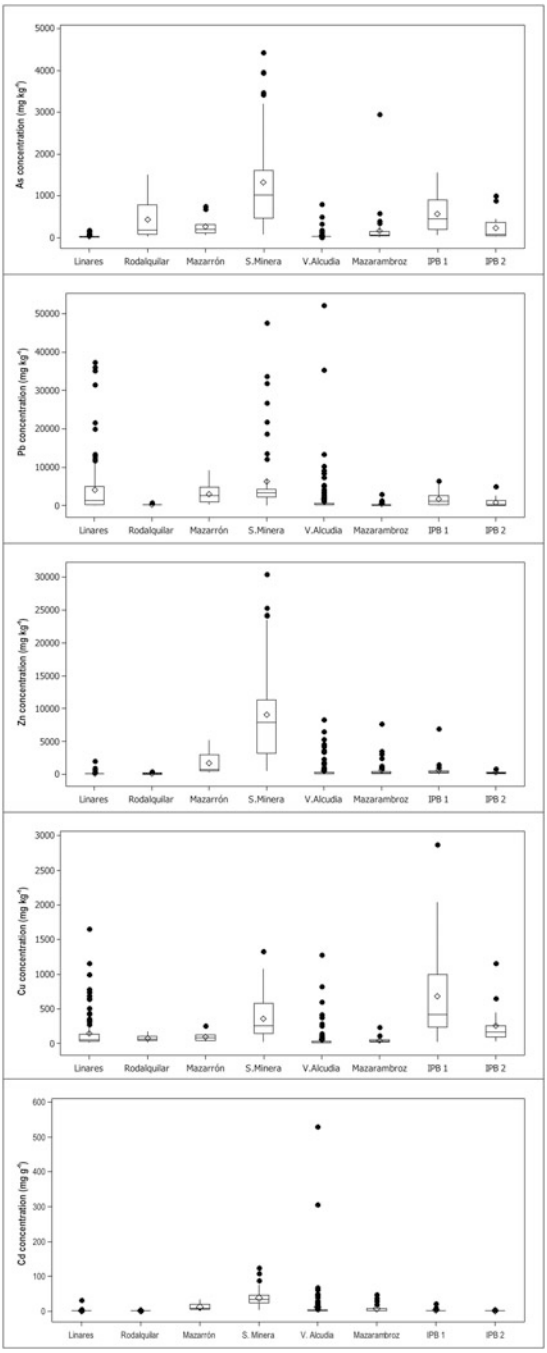

Fig. 2 Box-and-whisker plot for As, Pb, Zn, Cu, and Cd concentrations. The central box covers the middle half of the data, extending from the lower (Q1) to the upper quartile (Q3). The lines extending above and below the box (*whiskers*) show the range from which the not included data are considered as outsiders. The median of the data is indicated by the *horizontal line* within the box, whereas the *diamond sign* shows the location of the arithmetic mean

4.2 Enrichment Factors (REFmetal)

- The most Pb–Zn polluted soils correspond to those of the Sierra Minera (Fig. 3, Table 3) with Pb and Zn at more than 488 and 163 times the background, respectively. Conversely, the least Pb–Zn polluted soils are those of Linares, with Pb at 2.5 times the background value and Zn close to the background.
- The most As polluted soils are those of the Sierra Minera (Fig. 3, Table 3) at ~98 times the background value. On the other hand, the less polluted soils correspond to those located in Linares (Fig. 3, Table 3) at less than 0.5 times the background value.
- The most Cd polluted soils are found in the Sierra Minera (Fig. 3, Table 3) at more than 99 times the background value, whereas the less polluted soils are those from IPB, close to the background values.

4.3 Correlations and Clustering of Data

- The highest correlations in soils from the Alcudia Valley are found for the Pb–Zn and Pb–Cu pairs (0.86), whereas insignificant correlations are found for As–Zn and As–Cr (0.02 and 0.07, respectively) (Table 4). Thus, the lack of relation among As and metals is remarkable (Fig. 4).
- Contrary to the results for the Alcudia Valley, the strongest correlation in the (IPB) is found for the As–Pb pair (0.80 in the data set IPB1 and 0.91 in data set IPB2) (Table 4). In this regard, As gests clustered with Pb and Cu in the two populations, whereas Zn appears to show more affinity for Cd and Cr with Ni (Fig. 4).
- The strongest correlation in Linares is found for the pair As–Pb (0.81) (Table 4), which is also indicated by the cluster analysis (Fig. 4). Besides, the lowest correlation is shown by the Pb–Zn and Cu–Zn pairs (0.65) (Table 4), a fact also shown by the cluster analysis (Fig. 4).
- The data from Mazarrón show a pattern similar on that observed for the IPB data sets, with As clustering with Pb and Cu (and also Ag in the Mazarrón case) (Fig. 4). Zn clusters with Cd, whereas Cr does it with Ni. The As–Pb is well correlated (0.81) (Table 4) although the highest correlation corresponds to the Ag–Pb pair (0.94) (Table 4). The pairs Ba–Cu and Ba–Sn display the lowest correlations (−0.06 and 0, respectively) (Table 4).
- The strongest correlation in the data from Sierra Minera is shown by the As–Cu pair (0.70) (Table 4), and the lowest corresponds to the As–Hg pair (−0.01) (Table 4). The cluster analysis allows the observation of some patterns reflecting the moderate correlation indexes among As, Cu, Pb, Zn, and Cd pairs and the low affinity of Hg with the other metals and As (Fig. 4).
- The strongest correlation in Rodalquilar is found for the pair As–Sn (0.95) (Table 4), with As being weakly related to the Pb–Zn–Cu group (Fig. 4).

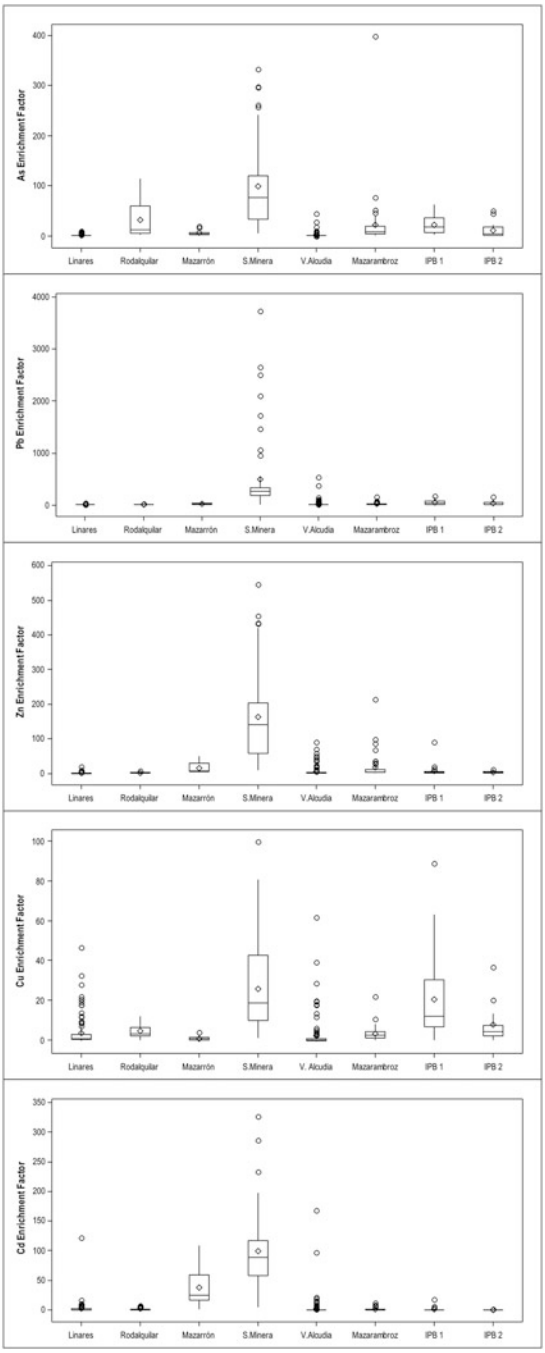

Fig. 3 Box-and-whisker plot for As, Pb, Zn, Cu, and Cd relative enrichment factors (REF_{metal} = [metal concentration in polluted soil – metal background concentration in soil]/[metal background concentration in soil]). Explanation as in Fig. 2

Table 3 Descriptive basic statistics of relative enrichment factors (REFmetal) of As, Pb, Zn, Cu, and Cd. Mean, median, minimum, maximum, first quartile (Q1), and third quartile (Q3) values are expressed in per unit of the background value

District	Backgrd	Source	N	Mean	St. Dev.	Min.	Q1	Median	Q3	Max.
As										
Linares	18.09	[7, 8]	126	0.4	1.6	−0.9	−0.4	−0.1	0.4	8.8
Rodalquilar	13.15	[24]	31	31.1	36	1.1	4.4	11.9	58.6	113.8
Mazarrón	39.33	[17]	15	5.4	5.3	0.5	1.5	3.8	6.6	17.9
S. Minera	13.25	[22]	54	97.8	84.8	4.1	33.2	76	119.6	333.2
V. Alcudia	17.5	[2]	142	1.1	4.8	−1	0	0.3	0.5	44.3
Mazarambroz	7.4	[62]	50	20.9	56.4	0.5	3.1	7.2	18	398.3
IPB1	25	[63]	32	21.5	17.7	1	6.4	16.7	34.8	61.4
IPB2	20	[11]	15	10.3	15.8	−0.1	0.5	2.9	17.1	48.7
Pb										
Linares	1,212	[7, 8]	126	2.4	5.8	−1	−0.8	0.1	3	29.8
Rodalquilar	33	[24]	31	5.9	4.8	−0.1	2.5	4.8	7.2	23.2
Mazarrón	159.67	[17]	15	17.5	16.1	0.5	4.7	15.3	29.2	56.1
S. Minera	12.75	[22]	54	488	736	1	178	260	330	3,734
V. Alcudia	96.9	[2]	142	15.3	57.6	−0.3	0.2	0.7	4.6	537.8
Mazarambroz	19.3	[62]	50	15	24.5	3.5	4	4.7	12.9	147.6
IPB1	38	[63]	32	43.9	48.4	0.6	5.3	29.7	68.4	170.1
IPB2	31	[11]	15	25.1	43.3	0.3	2	5.4	40	156.7
Zn										
Linares	100.79	[7, 8]	126	0.2	2	−0.7	−0.5	−0.3	0.3	18.7
Rodalquilar	54	[24]	31	1.2	1.9	−1	−0.2	0.4	2	6.4
Mazarrón	103.67	[17]	15	14.9	15.3	2.2	4.4	6.6	28.2	49.6
S. Minera	55.5	[22]	54	163.2	124.5	8.3	57.1	140.3	203.2	546.8
V. Alcudia	92	[2]	142	4.6	13.4	−0.7	−0.3	0.2	1.8	89.6
Mazarambroz	35.7	[62]	50	15.9	35	0.9	2.1	3.5	9.9	212.6
IPB1	76	[63]	32	6.9	15.7	-0.7	1.3	3.7	5.6	89.7
IPB2	72	[11]	15	3.2	3.2	0.3	1	1.9	3.9	11.5
Cu										
Linares	34.82	[7, 8]	126	3.2	7	−0.6	−0.1	0.5	2.7	46.5
Rodalquilar	14.1	[24]	31	4.2	3.5	−0.2	1.8	3.1	6.2	11.6
Mazarrón	55.33	[17]	15	0.6	1.1	−0.5	−0.3	0.4	1.2	3.7
S. Minera	13.25	[22]	54	25.6	22.1	0.6	9.6	18.5	42.5	99.8
V. Alcudia	20.5	[2]	142	1.8	7.3	−1	−0.5	−0.2	0.5	61.6
Mazarambroz	10.3	[62]	50	3	3.5	−0.2	0.7	2.2	3.9	21.5
IPB1	32	[63]	32	20.4	21.2	−0.3	6.4	11.9	30	88.8
IPB2	31	[11]	15	7.4	9.6	−0.1	1.9	4.1	7.2	36.4
Cd										
Linares	0.26	[7, 8]	126	2	11	−0.2	−0.2	−0.2	1.4	121.3
Rodalquilar	0.1	[24]	31	1.5	2.1	0	0	1	1	7
Mazarrón	0.3	[17]	15	37.1	33.1	1.3	15.7	24.3	59	108.3
S. Minera	0.38	[22]	54	99.2	60.3	4.8	58.3	88.9	117.5	327.4
V. Alcudia	3.14	[2]	142	2.4	16.5	−0.8	−0.8	−0.8	−0.4	168.1
Mazarambroz	3.9	[62]	50	0.5	2.6	−0.9	−0.9	−0.9	0.9	11.1
IPB1	1.2	[12]	32	0.5	3.3	−0.9	−0.9	−0.5	0.1	17.2
IPB2	1.2	[12]	15	−0.2	0.4	−0.9	−0.6	−0.3	0	0.9

Sources of the background concentrations used in this chapter are indicated in the Backgrd column. *Backgrd* background, *St. Dev.* standard deviation, *Min.* minimum, *Max.* maximum

Table 4 Correlation index matrices for element concentrations (log10) from all data sets. For the correlation analysis, metal sets with more than 10% of all values of BDL data have been excluded from the original data sets (Linares Ag, Cd, Sb; Rodalquilar Cd; Mazarrón Bi; Alcudia Cd, Hg, Mo, Ni, Sb; Mazarambroz Cd, Cr, Hg, Ni, Sb; IPB1 Hg)

Linares									
	As	Cu	Pb						
Cu	0.76								
Pb	0.81	0.78							
Zn	0.68	0.65	0.65						
Rodalquilar									
	As	Bi	Cu	Hg	Pb	Sb	Se	Sn	
Bi	0.82								
Cu	0.62	0.7							
Hg	0.26	0.33	0.2						
Pb	0.42	0.46	0.72	0.21					
Sb	0.87	0.71	0.58	0.27	0.28				
Se	0.91	0.71	0.46	0.4	0.22	0.87			
Sn	0.95	0.85	0.57	0.29	0.34	0.86	0.91		
Zn	0.54	0.33	0.58	−0.16	0.65	0.29	0.26	0.35	
Mazarrón									
	Ag	As	Ba	Cd	Cu	Pb	Sb	Se	Sn
As	0.89								
Ba	0.17	0.29							
Cd	0.18	0.23	0.30						
Cu	0.66	0.77	−0.06	0.55					
Pb	0.94	0.81	0.14	0.37	0.74				
Sb	0.51	0.58	0.83	0.41	0.21	0.50			
Se	0.13	0.23	0.45	0.19	0.09	0.12	0.46		
Sn	0.42	0.42	0.00	0.60	0.53	0.55	0.42	0.52	
Zn	0.34	0.30	0.37	0.73	0.48	0.58	0.54	0.37	0.63
Sierra Minera									
	As	Cd	Cu	Fe	Hg	Pb			
Cd	0.25								
Cu	0.70	0.31							
Fe	0.57	0.50	0.55						
Hg	−0.01	0.18	0.23	0.14					
Pb	0.61	0.42	0.58	0.68	0.21				
Zn	0.32	0.46	0.56	0.42	0.31	0.43			
Alcudia Valley									
	As	Cr	Cu	Pb	Se				
Cr	0.07								
Cu	0.15	0.22							
Pb	0.14	0.21	0.86						
Se	0.23	0.25	0.79	0.84					
Zn	0.02	0.17	0.86	0.86	0.68				

(continued)

Table 4 (continued)

Mazarambroz						
	As	Cu	Mo	Pb	Se	
Cu	0.64					
Mo	0.01	0.18				
Pb	0.56	0.49	0.27			
Se	−0.65	−0.3	0.09	−0.27		
Zn	0.58	0.62	0.33	0.89	−0.24	
IPB1						
	As	Cd	Cr	Cu	Ni	Pb
Cd	0.16					
Cr	0.06	0.09				
Cu	0.42	0.47	0.19			
Ni	0.25	0.27	0.71	0.49		
Pb	0.80	0.29	0.16	0.71	0.43	
Zn	0.25	0.68	−0.02	0.65	0.45	0.51
IPB2						
	As	Cd	Cr	Cu	Ni	Pb
Cd	0.53	1.00				
Cr	0.16	−0.30	1.00			
Cu	0.90	0.55	0.13	1.00		
Ni	0.64	0.44	0.49	0.67	1.00	
Pb	0.91	0.57	0.00	0.87	0.46	1.00
Zn	0.80	0.61	−0.20	0.69	0.33	0.91

- The strongest correlation from the Mazarambroz soils occurs in the Pb–Zn pair (0.89) (Table 4), whereas the most weak corresponds to the As–Mo pair (0.02) (Table 4). The cluster analysis of the Mazarambroz data is consistent with the correlation matrix, showing the Pb–Zn and As–Cu affinities (Fig. 4).

5 Conclusions

From the above results, some conclusions may be attained. The clustering of As and metals allows identification of several pollution modes, which in turn may correspond to significant differences in metal partitioning and solid phase bounding:

- The As–Pb–(Cu) + Zn–Cd mode that can be regarded as representative of the IPB, Linares, and Mazarrón. This suggests that the metals of each pair are similarly partitioned into the soil and bound to the same mineral phases, for example, As and Pb to iron oxyhydroxides ([12, 17]); alternatively, [11] and [13] have suggested that As, Pb, and Zn are mainly bound to Fe and Mn oxides with some Pb and Zn associated with the exchangeable fraction consisting of phyllosilicates and carbonates.

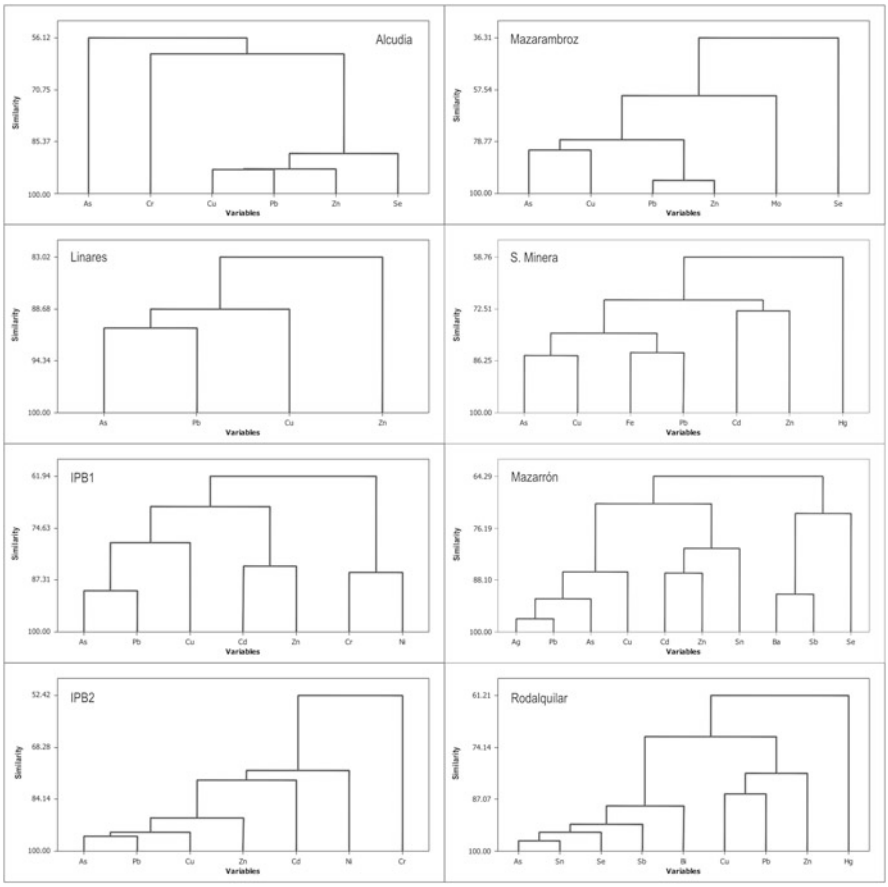

Fig. 4 Dendrogram (clusters by group average) for all data sets. Data are log-transformed, and metal sets with more than 10% of all values of BDL data have been excluded for the cluster analysis (Linares Ag, Cd, Sb; Rodalquilar Cd; Mazarrón Bi; Alcudia Cd, Hg, Mo, Ni, Sb; Mazarambroz Cd, Cr, Hg, Ni, Sb; IPB1 Hg)

- The As–Cu mode that may be regarded as representative of: (a) the Sierra Minera with As–Cu + Pb–Zn + Cd–Zn pattern and (b) Mazarambroz with a Pb–Zn + As–Cu pattern. The As–Cu pair appears to be related to jarosite in the Sierra Minera [22]. At Mazarambroz Pb seems to be bound to supergenic carbonates and sulfates, whereas As would be bound to iron oxyhydroxides [16].
- The As–Sn + Cu–Pb–(Zn) mode is observed at Rodalquilar where Pb is bound to Mn oxide phases and As is bound to goethite [24].
- The Cu–Pb–Zn mode with As showing a weak affinity for those metals as observed at the Alcudia Valley. In the San Quintín mines, most of Pb is bound to reducible forms (Fe and Mn oxides), whereas Zn occurs mainly as a exchangeable, water- and acid-soluble form (e.g., carbonates; [4]).

A second conclusion is that these modes do not necessarily relate to the intensity of pollution in terms of absolute concentrations of metals or REF_{metal}. For example, the most As–Pb–Cd polluted district (Sierra Minera) does not show the same pattern as the IPB, Rodalquilar, or Mazarrón (Fig. 2, 3) (Tables 2, 3).

A third conclusion relates to the fact that the As–metal affinities seem to be controlled by other factors than exclusively mineral paragenesis and/or pyrite abundance. For example, Linares (a district where the ore deposits are characterized by low contents of pyrite and an important presence of carbonates that preclude a significant AMD production, [64]) displays nevertheless a similar (As–Pb–(Cu)) pattern to that of the IPB, the most representative district of AMD in the Iberian peninsula (e.g., [65]) and of the worst cases worldwide. On the other hand, the distinct pattern of metal clustering in some districts could be related to the mineral paragenesis as seen in Rodalquilar where the alteration type and minerals associated to the high-sulfidation ore-forming processes ultimately played a key role in the As and metal fate in soils (Table 1, [24]).

A fourth conclusion is that some of the most As–Pb–Zn–Cd polluted districts in terms of REF_{metal} (Sierra Minera, Rodalquilar, IPB, and Mazarrón) have a semiarid Mediterranean climate, characterized by a high evapotranspiration during the dry and hot summer. That process induces the ascent of metal-rich water in the soil by capillarity and the subsequent metal enrichment in the top soil, mostly in the form of soluble phases as sulfates and carbonates [66], which in turn will be dissolved during heavy rain stormy episodes. Thus, these rain events can produce high rates of metal leaching and mobilization by runoff (e.g., [17, 22]).

Acknowledgments The study presented in this chapter was partly funded by the Spanish Ministry of Economy and Competitiveness (Project CTM2012-33918).

References

1. Palero FJ, Both RA, Arribas A, Boyce AJ, Mangas J, Martin-Izard A (2003) Geology and metallogenic evolution of the polymetallic deposits of the Alcudia Valley Mineral Field, eastern Sierra Morena, Spain. Econ Geol 98:577–605
2. Higueras P, Oyarzun R, Iraizoz JM, Lorenzo S, Esbrí JM, Martínez Coronado A (2014) Low-cost geochemical surveys for environmental studies in developing countries: testing a field portable XRF instrument under quasi-realistic conditions. J Geochem Explor 113:3–12
3. Oyarzun R, Fernández Barrenechea J, Esbrí JM, Higueras P, Lillo J, Martínez Coronado A, López García JA, López Andrés S (2010) Geoquímica Ambiental en San Quintín. Grupo Minero San Quintín (Ciudad Real): Sitio docente de entrenamiento activo para evaluaciones ambientales (Environmental Geochemistry in San Quintín. San Quintín Mining Group,Ciudad Real: learning site for training in environmental assessments). http://www.aulados.net/GEMM/Documentos/San_Quintin_Innova/index.html. Accessed 12 Jun 2014
4. Rodríguez L, Ruiz E, Alonso-Azcárate J, Rincón J (2009) Heavy metal distribution and chemical speciation in tailings and soils around a Pb-Zn mine in Spain. J Environ Manage 90:1106–1116
5. Lillo J (2002) Hydrothermal alteration in the Linares-La Carolina Ba-Pb-Zn-Cu-(Ag) vein district, Spain: mineralogical data from El Cobre vein. T I Min Metall B 111:114–118

6. Martínez J, Llamas JF, De Miguel E, Rey J, Hidalgo MC (2008) Soil contamination from urban and industrial activity: example of the mining district of Linares (southern Spain). Environ Geol 54:669–677
7. Martínez J, Llamas J, De Miguel E, Rey J, Hidalgo MC (2007) Determination of geochemical back ground in a metal mining site: example of the mining district of Linares (south Spain). J Geochem Explor 94:19–29
8. Martínez López J, Llamas Borrajo J, De Miguel GE, Rey Arrans J, Hidalgo Estévez MC, Sáez Castillo AJ (2008) Multivariate analysis of contamination in the mining district of Linares (Jaén, Spain). Appl Geochem 23:2324–2336
9. Leistel JM, Marcoux E, Thiéblemont D, Quesada C, Sánchez A, Almodovar GR, Pascual E, Sáez R (1998) The volcanic-hosted massive sulphide deposits of the Iberian Pyrite Belt. Miner Deposita 33:2–30
10. Chopin EIB, Alloway BJ (2007) Trace element partitioning and soil particle characterisation around mining and smelting areas at Tharsis, Riotinto and Huelva, SW Spain. Sci Total Environ 373:488–500
11. López M, González I, Romero A (2008) Trace elements contamination of agricultural soils affected by sulphide exploitation (Iberian Pyrite Belt, SW Spain). Environ Geol 54:805–818
12. Fernández-Caliani JC, Barba-Brioso C, González I, Galán E (2009) Heavy metal pollution in soils around the abandoned mine sites of the Iberian Pyrite Belt (Southwest Spain). Water Air Soil Poll 200:211–226
13. González I, Galán E, Romero A (2011) Assessing soil quality in areas affected by sulfide mining. Application to soils in the Iberian Pyrite Belt (SW Spain). Minerals 1:73–108
14. Villaseca C, López-García JA, Barbero L (2005) Estudio de la composición isotópica (Pb-S-O) de las mineralizaciones Pb–Zn de Mazarambroz (Banda Milonítica de Toledo) (Study of the isotopic composition (Pb-S-O) of the Mazarambroz (Toledo Mylonitic Band) mineralization). Geogaceta 38:271–274
15. López-García JA, Villaseca C, Barbero L (2003) Estudio preliminar de las mineralizaciones de Pb-Zn de Mazarambroz, Banda Milonítica de Toledo (Preliminary study of the Pb-Zn mineralization in Mazarambroz (Toledo Mylonitic Band)). Boletín de la Sociedad Española de Mineralogía 26-A:171–172
16. González-Corrochano B, Esbrí JM, Alonso-Azcárate J, Martínez-Coronado A, Jurado V, Higueras P (2014) Environmental geochemistry of a highly polluted area: the La Union Pb-Zn mine (Castilla-La Mancha region, Spain). Dig J Geochem Explor. doi:10.1016/j.gexplo.2014.02.014
17. Oyarzun R, Lillo J, López-García JA, Esbrí JM, Cubas P, Llanos W, Higueras P (2011) The Mazarrón Pb-(Ag)-Zn mining district (SE Spain) as a source of heavy metal contamination in a semiarid realm: Geochemical data from mine wastes, soils, and stream sediments. J Geochem Explor 109:113–124
18. López-García JA, Oyarzun R, López-Andrés S, Manteca Martínez JI (2011) Scientific, educational, and environmental considerations regarding mine sites and geoheritage: a perspective from SE Spain. Geoheritage 3:267–275
19. Oyarzun R, Manteca-Martínez JI, López-García JA, Carmona C (2013) An account of the events that led to full bay infilling with sulfide tailings at Portman (Spain), and the search for "black swans" in a potential land reclamation scenario. Sci Total Environ 454–455:245–249
20. Robles-Arenas VM, Rodríguez R, García C, Manteca JI, Candela L (2006) Sulphide-mining impacts in the physical environment: Sierra de Cartagena-La Unión (SE Spain) case study. Environ Geol 51:47–64
21. Navarro MC, Pérez-Sirvent C, Martínez-Sánchez MJ, Vidal J, Tovar PJ, Bech J (2008) Abandoned mine sites as a source of contamination by heavy metals: a case study in a semiarid zone. J Geochem Explor 96:183–193
22. García-Lorenzo ML, Pérez-Sirvent C, Martínez-Sánchez MJ, Molina-Ruiz J (2012) Trace elements contamination in an abandoned mining site in a semiarid zone. J Geochem Explor 13:23–35

23. Arribas A Jr, Cunningham CG, Rytuba JJ, Rye RO, Kelly WC, Podwysocki MH, McKee EH, Tosdal RM (1995) Geology, geochronology, fluid inclusions, and isotope geochemistry of the Rodalquilar gold alunite deposit, Spain. Econ Geol 90:795–822
24. Oyarzun R, Cubas P, Higueras P, Lillo J, Llanos W (2009) Environmental assessment of the arsenic-rich, Rodalquilar gold-(copper-lead-zinc) mining district, SE Spain: data from soils and vegetation. Environ Geol 58:761–777
25. Urbano Vicente R (1998) Guía para la investigación de los recursos minerales en España (Guideline on the investigation of mineral resources in Spain). IGME, Madrid
26. Callender E (2004) Heavy metals in the environment-historical trends. In: Lollar BS (ed) Treatise on Geochemistry 9. Environmental Geochemistry. Elsevier, Amsterdam, pp 67–105
27. Lin Y, Tiegeng L (1999) Sphalerite chemistry, Niujiaotang Cd-rich zinc deposit, Guizhou, Southwest China. Chin J Geochem 18:62–68
28. Goldschmidt V (1937) The principles of distribution of chemical elements in minerals and rocks. J Chem Soc, March, pp 655–673. doi:10.1039/JR9370000655
29. Gill R (1996) Chemical fundamentals of geology. Chapman and Hall, London
30. Oyarzun R (1976) Alteración hidrotermal y distribución de Cu, Mo, Pb y Zn en el prospecto Kilómetro Catorce, El Salvador, III Región (Hydrothermal alteration and distribution of Cu, Mo, Pb and Zn in the prospect Kilómetro Catorce, El Salvador, III Region). In: Proceedings of the 1st Congreso Geológico Chileno, 2–7 August 1976. Santiago, Chile, 2, E125–E143
31. Blanchard R (1968) Interpretation of Leached Outcrops. Nevada Bureau of Mines Bulletin 66
32. Lázaro I, Cruz R, González I, Monroy M (1997) Electrochemical oxidation of arsenopyrite in acidic media. Int J Miner Process 50:3–75
33. Morin G, Calas G (2006) Arsenic in soils, mine tailings, and former industrial sites. Elements 2:97–101
34. USEPA (2013). Drinking water contaminants. Water, United States Environmental Protection Agency. http://water.epa.gov/drink/contaminants/index.cfm. Accessed 10 Feb 2014.
35. Benjamin MM, Honeyman BD (2006) Trace Metals. In: Jacobson MC, Charlson RJ, Rodhe H, Orians GH (eds) Earth system science, International Geophysics Series 72. Elsevier, Amsterdam, pp 377–418
36. MacDonald DD, Ingersoll CG, Berger TA (2000) Development and evaluation of consensus-based sediment quality guidelines for freshwater ecosystems. Arch Environ Contam Toxicol 39:20–31
37. CCME (1999) Canadian soil quality guidelines for the protection of environmental and human health. Canadian Environmental Guidelines, Canadian Council of Ministers of the Environment, http://ceqg-rcqe.ccme.ca/. Accessed 12 Jun 2014
38. Manceau A, Boisset MC, Sarret G, Hazemann JL, Mench M, Cambier P, Prost R (1996) Direct determination of lead speciation in contaminated soils by EXAFS spectroscopy. Envir Sci Technol 30:1540–1552
39. Roberts DR, Scheinost AC, Sparks DL (2002) Zinc speciation in a smelter-contaminated soil profile using bulk and microspectroscopic techniques. Envir Sci Technol 36:1742–1750
40. Oyarzun R, Lillo J, Higueras P, Oyarzún J, Maturana H (2004) Strong arsenic enrichment in sediments from the Elqui watershed, Northern Chile: industrial (gold mining at El Indio-Tambo district) vs. geologic processes. J Geochem Explor 84:53–64
41. Seaman JC, Bertsch PM, Strom RN (1997) Characterization of colloids mobilized from southeastern coastal plains sediments. Envi Sci Technol 31:2782–2790
42. Davis JA, Kent DB (1990) Surface complexation modeling in aqueous geochemistry. In: Hochella MF, White AF (eds) Mineral-Water Interface Geochemistry. Reviews in Mineralogy, 23, Mineralogical Society of America, Washington DC, pp 177–260
43. Smith KS (1999) Metal sorption on mineral surfaces: an overview with examples relating to mineral deposits. In: Plumlee GS, Logsdon MJ (eds) The environmental geochemistry of mineral deposits. Reviews in Economic Geology 6A, Society of Economic Geologists, Chelsea, Michigan, pp 161–182

44. Smedley PL, Kinniburgh DG (2002) A review of the source, behaviour and distribution of arsenic in natural waters. Appl Geochem 17:517–568
45. Meng X, Korfiatis GP, Bang S, Bang KW (2002) Combined effects of anions on arsenic removal by iron hydroxides. Toxicol Lett 133:103–111
46. Fitz WJ, Wenzel WW (2002) Arsenic transformations in the soil-rhizosphere-plant system: fundamentals and potential application to phytoremediation. J Biotechnol 99:259–278
47. Ellis EC, Kaplan JO, Fuller DQ, Vavrus S, Goldewijk KK, Vervurg PH (2013) Used planet: a global history. Proc Natl Acad Sci USA 110:7978–7985
48. Hooke RLEB, Martín-Duque JF, Pedraza J (2012) Land transformation by humans: a review. GSA Today 22:4–10
49. USEPA (2012). Health. Six common pollutants, lead in air; United States Environmental Protection Agency, http://www.epa.gov/oar/lead/health.html. Accessed 10 Feb 2014
50. Landrigan PJ, Baker EL Jr, Feldman RG, Cox DH, Eden KV, Orenstein WA, Mather JA, Yankel AJ, Lindern IHV (1976) Increased lead absorption with anemia and slowed nerve conduction in children near a lead smelter. J Pediatr 89:904–910
51. Sepúlveda V, Vega J, Delgado I (2000) Exposición severa a plomo ambiental en una población infantil de Antofagasta, Chile (Childhood environmental lead exposure in Antofagasta, Chile). Rev Med Chile 128:221–232
52. USEPA (2005) Toxicological review of zinc and compounds. United States Environmental Protection Agency, CAS No. 7440-66-6, http://www.epa.gov/iris/toxreviews/0426tr.pdf. Accessed 10 Feb 2014
53. WHO (2011) Cadmium in drinking-water. Background document for development of WHO Guidelines for Drinking-water Quality, World Health Organization, WHO/SDE/WSH/03.04/80/Rev/1, http://www.who.int/water_sanitation_health/dwq/chemicals/cadmium.pdf. Accessed 10 Feb 2014
54. Bissen M, Frimmel FH (2003) Arsenic – a review. Part I: occurrence, toxicity, speciation, mobility. Acta Hydroch Hydrob 31:9–18
55. Edwards KJ, Schrenk MO, Hamers R, Bandfield JF (1998) Microbial oxidation of pyrite: experiments using microorganisms from an extreme acidic environment. Am Mineral 83:1444–1453
56. Nordstrom DK, Alpers CN (1999). Geochemistry of acid mine waters. In: Plumlee GS, Logsdon MJ (eds) Reviews in economic geology, 6A, The environmental geochemistry of mineral deposits. Part A. Processes, methods and health issues. Society of Economic Geologists, Littleton, pp 133–160
57. Oyarzun R, Lillo J, Oyarzun J, Maturana H, Higueras P (2007) Mineral deposits and Cu-Zn-As dispersion-contamination in stream sediments from the semiarid Coquimbo Region, Chile. Environ Geol 53:283–294
58. Nordstrom DK (2009) Acid rock drainage and climate change. J Geochem Explor 100:97–104
59. Singh A, Nocerino J (2002) Robust estimation of mean and variance using environmental data sets with below detection limit observations. Chemometr Intell Lab 60:69–86
60. Templ M, Filzmoser P, Reimann C (2008) Cluster analysis applied to regional geochemical data: problems and possibilities. App Geochem 23:2198–2213
61. Limpert E, Stahel WA, Abbot M (2001) Log-normal distributions across the sciences: keys and clues. Bioscience 51:341–352
62. Jiménez-Ballesta R, Bueno PC, Rubí JAM, Gimenez RG (2010) Pedo-geochemical baseline content levels and soil quality reference values of trace elements in soils from the Mediterranean (Castilla-La Mancha, Spain). Central Eur J Geosci 2:441–452
63. Galán E, Fernández-Caliani JC, González I, Aparicio P, Romero A (2008) Influence of geological setting on geochemical baselines of trace elements in soils. Application to soils of Southwest Spain. J Geochem Explor 98:89–106
64. Hidalgo Estévez MC, Benavente Herrera J, Rey Arrans J (1999) First results on the presence of metallic contaminants in waters after the abandonment of a sulphide mining district (Linares,

Spain). In: Proceedings of the mine, water & environment for the 21st century, International Mine Water Association, Sevilla
65. Sánchez España J, López Pamo E, Santofimia E, Aduvire O, Reyes J, Barettino D (2005) Acid mine drainage in the Iberian Pyrite Belt (Odiel river watershed, Huelva, SW Spain): geochemistry, mineralogy and environmental implications. App Geochem 20:1320–1356
66. Oyarzun R, Higueras P, Lillo J (2011) Minería Ambiental: Una Introducción a los Impactos y su Remediación (Environmental mining: an introduction to impacts and remediation techniques). http://www.aulados.net/Libros_Aula2puntonet_GEMM/Libros.html. Accessed 12 Jun 2014

In Situ Chemical Oxidation Based on Hydrogen Peroxide: Optimization of Its Application to an Hydrocarbon Polluted Site

S. del Reino, M. Rodríguez-Rastrero, O. Escolano, L. Welte, J. Bueno, J.L. Fernández, T. Schmid, and R. Millán

Abstract In situ chemical oxidation (ISCO) is an effective technology for the cleanup of contaminated sites by organic compounds, such as hydrocarbons. Such remediation involves the introduction of a chemical oxidant into the subsurface in order to transform organic pollutants, present in groundwater or soil, into less harmful chemical species. Commonly applied oxidants are permanganate, hydrogen peroxide, ozone, and persulphate.

To implement the ISCO effectively, an enhancement of the contact oxidant-contaminant is required. This can be difficult in many soils and aquifers where natural features can result in significant heterogeneities in the flow of water, or in which the presence of natural reducing substances can generate non-productive reactions that consume oxidants, thus compromising their adequate distribution and efficiency. In this regard, a detailed previous knowledge of some morphological and physicochemical properties of soils and aquifers to be treated will contribute to optimize the ISCO treatments.

A present case study is currently being developed on a site with particular features that significantly influence the applicability of ISCO in any reagents. This features include: the irregular distribution of pollutants, high spatial and temporal variability of water table, generally low permeability as well as a remarkable heterogeneity of the main physicochemical soil properties (salinity, aeration, grain size or organic matter), both in the vertical and the horizontal distribution.

This chapter provides a short review of the main challenges associated to an in situ chemical oxidation treatment, specifically referred to as a site that represents a significant source of inefficiency in its application, focusing on the main issues that need to be accounted for the design of such treatment.

S. del Reino (✉), L. Welte, J. Bueno, and J.L. Fernández
AITEMIN, Río Cabriel s/n, 45007 Toledo, Spain
e-mail: susana.del.reino@aitemin.es

M. Rodríguez-Rastrero, O. Escolano, T. Schmid, and R. Millán
CIEMAT, Avda, Complutense 40, 28040 Madrid, Spain

E. Jiménez et al. (eds.), *Environment, Energy and Climate Change I: Environmental Chemistry of Pollutants and Wastes*, Hdb Env Chem (2015) 32: 207–228,
DOI 10.1007/698_2014_272, © Springer-Verlag Berlin Heidelberg 2014,
Published online: 2 October 2014

Keywords Catalysed hydrogen peroxide, Conceptual site model, ISCO, Soil organic pollution

Contents

1 In Situ Chemical Oxidation Technology

The in situ chemical oxidation (ISCO) technique involves the introduction of a chemical oxidant into the subsurface for transforming groundwater or soil contaminants into less harmful chemical species. This is commonly described as in situ because it is carried out in the exact location of the contaminant, without having to excavate soil or pump out groundwater for an aboveground cleanup.

To treat soil and groundwater, the oxidants are injected into the ground by pumping them into wells in the source area (Fig. 1). Once the oxidant is pumped down the wells, it spreads into the surrounding soil and groundwater where it mixes and reacts with contaminants.

Typically, the ISCO technique is performed using oxidant formulations based on hydrogen peroxide [1–5], permanganate [6], persulphate [7–12] and ozone [13–17]. Solid peroxides such as sodium percarbonate and calcium peroxide are also being applied [18, 19].

Oxidant-specific characteristics must be considered to determine which oxidant is most appropriate. Table 1 provides a qualitative list of reactive species, stability and oxidation potential for oxidants used for in situ chemical oxidation.

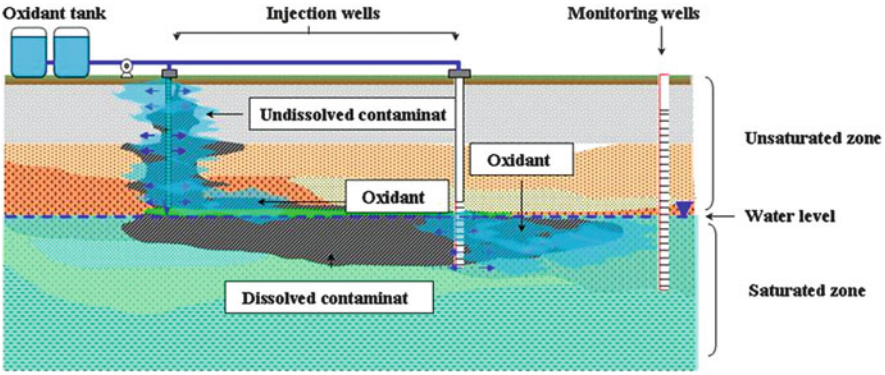

Fig. 1 Treatment scheme of soil and groundwater by ISCO

Table 1 Reactive species, stability and oxidation potential for oxidants used for in situ chemical oxidation (adapted from [20])

Oxidant	Reactive species	Form	Catalyser	Persistence	Oxidant potential
Permanganate	MnO_4^-	Powder liquid	None	>3 months	1.7 V
Hydrogen peroxide	•OH $•O_2^-$ $•HO_2$ HO_2^-	Liquid	None, Fe (II) and Fe (III)	Minutes to hours	1.8 V
Ozone	O_3 •OH	Gas	None	Minutes to hours	2.1 V
Persulphate	$•SO_4^{2-}$	Powder liquid	None, Fe (II), Fe (III), heat, H_2O_2	Hours to weeks	2.1 V
Percarbonate	•OH	Powder	Fe (II)	Weeks	2.8 V

Several previous case study reviews have focused on the ISCO, or contained a significant number of ISCO case studies, especially in the United States [20–30] that provided general information on how the remediation process works. The information include: the parameters to consider, metrics to assess performance or databases. In this context, Krembs et al. [31] created a database with 242 ISCO projects from 42 US states and 7 nations and a list of selected publicly accessible ISCO case study resources.

In contrast, in Europe the development of a full-scale ISCO is more limited [30]. References are restricted to APAT [32] and CityChlor [19]. In the Spanish case, AITEMIN has developed a protocol for the application of the ISCO technology using catalysed hydrogen peroxide (patent pending), supported on its results coming from treatability tests, pilot tests and full-scale applications in Spain.

Catalysed hydrogen peroxide (CHP) has been among the most widely applied oxidants through the standard Fenton's reaction, where the decomposition of a solution of dilute hydrogen peroxide is catalysed by excess iron (II) yielding the hydroxyl radical (•OH) and ferric (Fe(III)) and hydroxyl ions (OH^-) (1). Fe(III) reacts with H_2O_2 or the superoxide radical (O_2^-), yielding Fe(II) (2) at pH of 2.5–3.5:

$$H_2O_2 + Fe^{2+} \rightarrow Fe^{3+} + OH^- + OH\bullet \quad (1)$$

$$H_2O_2 + Fe^{3+} \rightarrow Fe^{2+} + H^+ + HO_2\bullet \quad (2)$$

The possibility of applying Fenton's process to contaminated soil has been demonstrated by several authors: Tyre et al. [33], Watts and Dilly [34], Kakarla and Watts [35], Watts et al. [36], Xu et al. [37] and Ndjou'ou and Cassidy [38].

The radical of interest in Fenton has always been the hydroxyl radical, a relatively non-specific oxidant that reacts with most organic compounds; but many other catalysts and radicals that are not present in the original "Fenton's" process play major roles in contaminant degradation reactions when hydrogen peroxide is applied in situ [39, 40]. These radicals are formed as the result of a reaction between hydrogen peroxide and certain catalysts which prevent the OH• formation. This non-productive reaction may be a source of treatment inefficiency, so it is necessary to note that reaction rates of hydrogen peroxide are dependent not only on the concentration of the contaminants of concern, but on many other subsurface parameters including temperature, pH, reaction by-products and other naturally occurring reductants [41–43].

Another source of inefficiency is related to an ineffective distribution of the oxidant on the subsurface owing to the fact that the chemical oxidant needs direct contact with the contaminant in order to be effective. A correct distribution requires enough knowledge about contaminant distribution, subsurface lithology and hydrogeology, as well as location and characteristics of surface structures and underground utilities that could act as preferential pathways [26].

To ensure the success of the ISCO technique, all these parameters must be evaluated during site characterization, prior to the design of ISCO implementation.

The objective of this chapter is to provide an overview of challenges associated to site condition that could represent a source of inefficiency applying the ISCO treatment. Likewise, this chapter presents the key elements of the conceptual site model (CSM), needed to ensure ISCO treatment success on the basis of the current case study that is being performed by AITEMIN within the framework of the BIOXISOIL project funded by the EU's LIFE Programme.

2 ISCO Based on Hydrogen Peroxide

2.1 Chemical Oxidation Mechanisms

The chemistry of the hydrogen peroxide reaction is remarkably complex because it includes free radical chain reactions, radical scavenging for the transformation and degradation of organic contaminants.

The process is often based on the catalysed decomposition of hydrogen peroxide by salt-iron, iron chelates or iron minerals to generate the strong oxidant hydroxyl radical (OH•), as well as other reactive oxygen species like the superoxide radical (O_2^-•) and the perhydroxyl radical (HO_2•), at pH of 2.5–3.5, responsible for the transformation and degradation of organic contaminants. In this process, it is possible to distinguish between direct and indirect oxidation. Direct oxidation refers to a direct electron-transfer reaction between a reactant and hydrogen peroxide, and indirect oxidation refers to free radical reactions and mechanisms resulting in a reaction between hydrogen peroxide and inorganic compounds.

Section 1 presents the basic hydroxyl radical chain initiating Fenton's reaction (1).

The hydroxyl radical reacts with organic compounds by electrophilic substitution to aromatic compounds and addition to alkenes, hydrogen abstraction from saturated compounds or direct electron transfer [44, 45]; the reaction product includes an organic radical, which may react with water or other species and degrade (3 and 4):

$$OH\bullet + RH \rightarrow R\bullet + OH^- \quad (3)$$

$$R\bullet + H_2O_2 \rightarrow ROH + OH\bullet \quad (4)$$

Therefore, hydroxyl radicals are extremely reactive and short-lived as they react as soon as they are formed in the very same location. However, other radical species formed in the CHP system, such as the superoxide radical anion or the perhydroxyl radical, are relatively long-lived in water and soil organic matter [39], allowing a higher transport into the subsoil (5 to 12) [40]:

$$OH\bullet + H_2O_2 \rightarrow H_2O + HO_2\bullet \quad (5)$$

$$H_2O + HO_2\bullet \rightarrow H_2O_2 + O_2 + OH\bullet \quad (6)$$

$$Fe^{2+} + OH\bullet \rightarrow Fe^{3+} + OH^- \quad (7)$$

$$HO_2\bullet \rightarrow O_2^-\bullet + H^+ \quad (8)$$

$$Fe^{3+} + HO_2\bullet \rightarrow Fe^{2+} + O_2 + H^+ \quad (9)$$

$$Fe^{3+} + HO^{2-} \rightarrow Fe^{2+} + HO_2\bullet \quad (10)$$

$$Fe^{3+} + H_2O_2 \rightarrow Fe\,(HO_2)^{2+} + H^+ \quad (11)$$

$$Fe(HO_2)^{2+} \rightarrow Fe^{2+} + HO_2\bullet \quad (12)$$

In summary, according to (1) to (12), the main species involved are hydroxyl radicals and other radicals such as the superoxide anion ($O_2^{-}\bullet$), the perhydroxyl radical ($HO_2\bullet$) or intermediate species like the hydroperoxide anion (HO_2^{-}) formed when the hydroxyl radical generated in Fenton's initiation reaction (1) reacts with hydrogen peroxide.

The perhydroxyl radical is a weak oxidant in Fenton's systems, the superoxide anion is a weak reductant and nucleophile, and the hydroperoxide anion is a strong nucleophile. These intermediates increment their reactivity in slurry systems that have solutes and sufficient hydrogen peroxide [4, 46].

Reactions (1) to (9) will generally continue to occur until hydrogen peroxide is depleted. In these systems, iron is continually regenerated between Fe(II) and Fe (III) forms unless it becomes unavailable due to precipitation or complexation reactions (13) [29]:

$$Fe^{3+} + nOH^{-} \rightarrow \text{Amorphous iron oxides (precipitate)} \quad (13)$$

2.2 *Challenges and Limitations of ISCO Based on Catalysed Hydrogen Peroxide (CHP)*

The success of the ISCO treatment depends on getting enough oxidant in contact with the contaminant. In this sense, several parameters associated to the site condition could represent a source of inefficiency in Fenton's systems. These parameters include site chemical characteristics like the presence of scavengers and pH, which can affect the natural oxidant demand, or the oxidant stability as well as physical site characteristics like low permeability, low hydraulic conductivity and heterogeneities that control oxidant distribution and transport capacity in the subsurface and consequently the efficiency of the treatment [43].

Moreover, other factors associated with reagent injection like surfacing of reagents and fouling of wells also represent an additional source of inefficiency in CHP systems.

2.2.1 Site Chemical Characteristics

The effective radius of oxidation treatment may be less than the hydraulic radius of influence if the reagents are depleted when they move through the subsurface [26]. Faster rates of oxidation reactions are linked to the presence of natural scavengers, which react with the oxidant before the contaminant, or to changes in pH, which may affect the solubility of the catalyst.

Scavengers

The presence of scavengers, nontarget species at a treatment site including natural organic (e.g. humic acids) and inorganic matter (oxidizable metals and minerals), affects hydrogen peroxide stability [44–47]. When this oxidant comes into contact with inorganic compounds, such as iron oxyhydroxide and manganese oxyhydroxide catalysts, or with organic compounds commonly found in surface soils, it can quickly decompose, limiting the utility of ISCO for the remediation of contaminated sites. According to Baciocchi et al. [48], these non-productive reactions may well lead to a loss of hydrogen peroxide above 50%.

The most important scavengers are:

- Natural organic matter (NOM) ([3, 33, 49–53]; Tarr and Lindsay 1998). Besides, NOM can serve as an adsorbent for the target compounds (making it less available in solution) and as an electron acceptor or donor. Nevertheless, Huling et al. [54] indicate that NOM may have no significant effect on the oxidation effectiveness and efficiency.
- Anions like carbonate, bicarbonate, chloride and sulphate with the capability to scavenge hydroxyl radicals and to form inorganic radicals with much lower reactivity and propensity to degrade organic contaminants than the hydroxyl radicals. In addition, these anions have the capability to form complexes with soluble iron limiting the mineral catalytic sites [55–59].
- Other metals, including chromium and selenium, can be oxidized to more soluble forms, thereby increasing their migration potential [26].

Several stabilizers of hydrogen peroxide can be used to slow down the reaction of catalysed hydrogen peroxide [35, 60]. Several chelating agents have been used to reduce the decomposition of hydrogen peroxide by suppressing the catalytic activity of naturally occurring transition metals [1, 35, 44, 61, 62]. In recent years "green" hydrogen peroxide stabilizers have been studied [63, 64] like *S*,*S*-′-ethylenediaminedisuccinate (EDDS), citric acid or cyclodextrin [65–68].

pH

This parameter can determine the success of ISCO using catalysed hydrogen peroxide as it controls the solubility of iron and therefore its reactivity towards hydrogen peroxide.

Soluble iron, iron chelates and iron oxide minerals naturally present in the subsurface serve as catalysts. Soluble iron and iron minerals are most effective at acidic pH, while iron chelates are also effective at neutral pH regimes and they may travel farther in the subsurface compared to soluble iron [4].

2.2.2 Site Physical Characteristics

Hydrogeological conditions, especially permeability, hydraulic conductivity and substrate heterogeneities, control oxidant distribution and transport capacity in the subsurface and consequently the efficiency of the treatment. In this sense, it is possible to obtain a greater oxidant transport in homogeneous soils with higher effective porosity than in soil with low or variable effective porosity or with horizontal and vertical heterogeneities [69].

Additionally, the presence of subsurface structures, artefacts, previous boreholes or pits can provide preferential pathways for the migration of contaminants, injected oxidation reagents and by-products from the reactions.

2.2.3 Additional Sources of Inefficiency

Surfacing

The common delivery system to introduce and distribute hydrogen peroxide into the aquifer is the direct injection by a vertical well from an external source. Injection of hydrogen peroxide and catalyst solutions into the subsoil results in the mixing and displacement of the aquifer water present that can cause changes in water table, a phenomenon termed “mounding”. Furthermore, when the injection flow rate exceeds the acceptance rate of the aquifer, this results in fluid being found on the surface in an event termed “surfacing” [70]. According to Technical Report TR-NAVFAC-EXWC-EV-1303 (2013) [71] of NAVFAC surfacing can also occur as follows:

- Shallow depth of groundwater
- High excess pressure, caused by:
  - Low hydraulic conductivity and permeability
  - High injection flow rates
  - Application of reagents that generate a substantial volume of gas
- Preferential pathways that connect the area of mounding to the surface

Fouling

Fouling can occur as a result of introducing reagents into the aquifer. There are several types of fouling: biofouling, fouling due to the formation of inorganic precipitates and gas fouling.

In the case of CHP, gas fouling tends to be particularly problematic. Gases like carbon dioxide, oxygen, methane and hydrogen sulphide can partially block aquifer pore spaces, which can reduce the permeability of the aquifer and adversely impact the distribution of reagents [71].

Rebound

Rebound, defined as an increase in the contaminant concentrations observed in groundwater, following an initial reduction is a common occurrence observed at ISCO sites [31]. This phenomenon occurs when the oxidant degrades the dissolved-phase contaminant mass but not entirely the sorbed phase mass or free-phase mass.

The typical rebound causes are the mass transfer from adsorbed and DNAPL phases into the groundwater [20] due to the desorption effect from the oxidants that tends to mobilize adsorbed hydrocarbons rather than chemically break them down [26]. Increases in contaminant concentrations due to an influx of contaminated groundwater from untreated upgradient locations at the site are not considered as a rebound.

Although rebound requires further remediation efforts [72], it can be used to find unknown areas with high sorbed and free-phase mass [31].

Partially Oxidized Products

The ideal CHP reaction will be to transform the contaminants of concern (COCs) to carbon dioxide and water. However, in most cases the production of partially oxidized by-products is observed especially when the organic contaminant is composed of a large or complex chemical structure that could require multiple oxidation steps.

Typical by-products are organic compounds with low-molecular-weight carboxylic acids, such as formic acid, oxalic acid, acetic acid and others [29], which in almost all cases are more biodegradable when compared to the parent compound [26].

According to Regenesis [73], the presence of by-products could be used to test if the oxidation has occurred or not, i.e. by-products can be used as an indicator to follow the success of a remediation.

3 Site Characterization: Conceptual Site Model

3.1 Introduction

Successful design and implementation of ISCO technology is dependent on the correct understanding of site conditions, changes to site conditions and the ability to address unexpected conditions and challenges that arise to ensure adequate distribution and contact of the reagent with the contaminant of concern [71]. Natural or human-induced subsurface heterogeneities, preferential flow paths or the presence of scavengers that consume oxidant could compromise the remediation effectiveness. According to ITRC [23], the most critical success factors are associated with

the ability to control the ISCO reaction with the contaminant of concern and with an effective delivery of the reagents to the zone to be treated.

An effective site characterization that allows the development of a valid conceptual site model (CSM) is essential for the design of the ISCO technology to determine treatment goals and operating conditions. According to Siegrist et al. [29], particular emphasis needs to be on subsurface hydrogeology and geochemical conditions including:

- Reactivity of hydrogen peroxide with the subsurface media (can control oxidant depletion rate)
- Oxidation-reduction potential (can provide insight into oxidant persistence)
- pH and alkalinity (can influence oxidant chemistry and the scavenging of free radicals)
- Presence of redox and pH-sensitive metals (can result in posttreatment toxicity)

3.2 Conceptual Site Model

The CSM compiles all known site data. It is an iterative tool that should be developed and refined as information is obtained during the review of the site history and continues throughout the site and/or remedial investigation. For more details on CSM characteristics, refer to New Jersey Department of Environmental Protection [74]. Always, a CSM should incorporate the location and mass of contaminant of concern; an understanding of the pedology, geology and hydrogeology, aquifer geochemistry, major migration pathways for the contaminants of concern and groundwater flow direction/gradient; and the identification of surface and subsurface structures, underground utilities and potential receptors in the area.

There are several types of checklists available to develop the conceptual site model, with the type of information that is recommended to be collected during the remedial process [69, 75].

3.3 Treatability and Field Pilot Test

Areas of uncertainty identified in the CSM have to be determined by treatability and pilot scale tests. Treatability and pilot tests could give the following information: the ability and rate of the proposed oxidant dose to destroy the target contaminants, estimation of oxidant and activator dosage, determination of the volume of oxidant that the scavengers potentially consume and by-product formation of the oxidation-reduction reactions and potential metals mobilization. In general, treatability test guidelines often include simple batch studies in aqueous systems or soil slurry systems containing the majority of the contaminant(s) and other parameters that will largely influence oxidant demand.

In the case of pilot tests, the information provided also includes the determination of optimum injection flow rates, radius of influence (ROI), geochemical impacts to the aquifer and the potential for rebound [76].

4 ISCO Project Design Based on Site-Specific Conditions

Oxidant injection plan must include oxidant dosing and persistence and oxidant delivery strategy, well spacing ensuring that the wells are placed appropriately to achieve adequate treatment within the affected zone, injection flow rate and total fluid volume, number of injections and the monitoring programme to evaluate the effectiveness of the injection strategy.

4.1 Oxidant Dosage

It is recommended to base the oxidant dosage calculation on the type and nature of contaminant, aquifer properties and chemical and physical properties of the reagent.

A number of chemical and physical factors contribute to the total oxidant demand (TOD) of a subsurface environment. These include dissolved-phase contaminant, sorbed phase contaminants, free-phase contaminants, dissolved-phase reduced minerals, solid phase (or sorbed phase) reduced minerals, dissolved and sorbed phase natural organic matter (NOM), chemical decomposition and quenching. The total oxidant mass delivered must satisfy the stoichiometric requirements of the target organics plus non-productive oxidant depletion in the subsurface.

The dissolved-phase mass can be calculated from the concentration of contaminants found in wells. Data collection of groundwater samples represents an integrated measure of the type, phase and magnitude of contaminants in the subsurface.

The sorbed phase can be calculated from the concentration of contaminants of soil samples obtained from constructed wells.

Natural oxidant demand due to nontarget species that consume the oxidant is commonly calculated with a bench scale test in uncontaminated samples or samples from which the volatile organic compounds have been removed [26]. Several authors [77–81] suggest that the natural oxidant demand measurement is determined rapidly using acidified dichromate chemical oxygen demand (COD) method.

4.2 Oxidant Delivery and Monitoring Design

The choice of oxidant delivery and monitoring strategy should be based on site-specific conditions, especially on pedology, geology, contaminant mass distribution

and site architecture since all of them determine the capacity of the subsurface to accept fluid volume.

4.2.1 Well Characteristics and Layout

Normally, wells are constructed of polyvinylchloride (PVC) pipe with the screen interval placed in the vertical section intended for treatment. Injection wells are constructed with slot well screens and coarse sand packs located at the same depth, or slightly deeper than the bottom of the most contaminated horizon.

The most important considerations when designing and installing oxidant injection wells are the quality of the bentonite seal above the sand pack and the proper construction of a surface seal surrounding the well box. Packers can also be used to isolate the injection depth.

Wells have been placed to achieve adequate treatment within the target treatment zone. In general, injection wells are built on a grid maintaining the same distance between each of them based on the expected radius of influence (ROI) calculated in the field test.

In the case of catalysed hydrogen peroxide, it is important to take into account the injection of catalyst solution with iron in acid solution either coinjected or injected separately and sequentially. It is recommended to carry out the latter option because the reaction not only occurs in the injection point but also when the oxidant finds the catalyst, thus permitting increase of the radius of influence [26].

The sequence of the injections depends on the water flow direction. The most common strategies are work upgradient to reduce the potential to push contamination further downgradient and push the contaminant towards the centre [29].

4.3 Injection Health and Safety

Catalysed hydrogen peroxide generates large amounts of oxygen gas which creates excessive backpressures in the subsurface as well as excessive heat (exothermic reaction).

Pressure should be maintained and monitored to limit fracturing unless required to obtain flow due to reagent physical characteristics or tight soil conditions, and temperature should be limited to minimize vapour generation (temperature should be limited below 66°C to minimize vapour generation) [70].

4.4 Design Monitoring

The monitoring plan to demonstrate contact/distribution of oxidant/activator and contaminant of concern must include the monitoring injection and the performance

Table 2 Typical process monitoring during remediation

Measurement	Method	Purpose
Groundwater levels	Hydrolevel	Changes in levels during injection to assess hydraulic connection between injection monitoring wells
		Evaluate change to flow direction and gradient
Pressures	Transducers	Pressure increases may indicate that the injection flow rate exceeds the acceptance rate of the aquifer
Flow rates	Flowmeter	Decrease in flow rate may indicate plugging of injection well or formation
Oxidant	Colorimetric kits	Presence in monitoring wells to determine ROI
Visual observations	Visual	Bubbles are present if oxygen and carbon dioxide are produced
		Surfacing of reagents or groundwater is noted if the injection flow rate exceeds the acceptance rate of the aquifer
Groundwater temperature	Thermocouples	Temperature above 40°C could indicate possible vapour generation
Groundwater quality (DO, ORP, pH, conductivity)	Groundwater quality meter	Change of these parameters to indicate arrival of reagents (oxidants can increase ORP and DO and decrease pH)
Soil gas and well vapours	Photoionization detector (PID)	Presence of VOCs due to gas generation

Table 3 Process and performance monitoring ISCO parameters

Parameter	Purpose of the data/information
Target contaminant	Assess the treatment performance success via reduction in concentrations in groundwater, aquifer material and NAPL
By-products	Indicator to follow the success of a remediation, particularly if rebound is noted (dissolution, desorption or an influx of new mass could hide the contaminant mass removal)

monitoring. Injection monitoring includes those parameters that provide information on the state of the remedial action during implementation, and performance monitoring provides information on the efficacy of the remedy to achieve remedial goals for ISCO [76].

Typical process monitoring during remediation and their purpose are presented in Table 2 (based on [20, 76]).

Typical process and performance monitoring parameters and their purpose are presented in Table 3 (based on [20]).

5 Site Characterization of the Case Study

5.1 Background

This case study describes the conceptual design of a full-scale CHP remediation of hydrocarbon polluted soils, corresponding to a coastal area of Cadiz (Andalucía, Spain), subjected to eventual and localized hydrocarbon spills from ancient fuel storage tanks and transport facilities, during previous decades. The specific working area has a surface of approximately 1.5 ha.

The ISCO remedial goal consists of a significant reduction of hydrocarbon concentration, determined by the percent of reduction of hydrocarbons in soil and water in relation to the baseline.

The working area is a complex site with a substrate consisting of irregularly distributed anthropic deposits over marsh sediments, usually clayey; both anthropogenic and natural marsh deposits show a remarkable heterogeneity in their morphological and physicochemical properties. The work area presents a water table with high spatial and temporal variability, in a context of a Mediterranean climate with mild and wet winters and warm and dry summers.

In such conditions, an adequate characterization of the work area is an initial primary objective, which first requires the development of a large number of prospections in order to assess the type of materials present, its thickness and its spatial distribution. This activity, carried out with pedological criteria, has enabled to define horizons or levels where initial physicochemical and morphological characterizations have been carried out. In parallel, groundwater sampling has been carried out by establishing a network of monitoring wells, which allowed the initial hydrochemical characterization of the site and the establishment of groundwater levels, which were subsequently monitored.

5.2 Site Characterization Method

The initial direct push technologies were used to assess the condition of contamination at the site. A total of 25 soil pits were realized with pedological criteria including soil sampling and a detailed soil profile description. Hydraulic parameters such as flow pattern or hydraulic conductivity were determined implementing a topographical survey of the site and by pumping tests in soil pits and pre-existing boreholes.

A deeper characterization of substrates and groundwater, in order to design an efficient targeted hydrogen peroxide injection programme, consisted of well drilling in the source area and the continuous monitoring of the underground water-level evolution by the installation of automatic Diver-type registration systems.

Monitoring wells were pumped, to evacuate a minimum of three volumes of water, prior to collecting a groundwater sample. Water samples were collected 24 h

following well purging with bailers made of Teflon®. Sampling occurred in a progression from the least to the most contaminated well. Likewise, measurements of temperature, pH, oxidation-reduction potential (ORP), conductivity and O_2 were taken at the same time of the sampling.

Besides, non-invasive technologies such as ground-penetrating radar were used in order to test its potential use for measuring and interpreting physical properties to determine subsurface conditions, including an eventual presence of artefacts as preferential paths for CHP flow.

Soil and water sampling has allowed a morphological and physical characterization of the site, which serves as a basis for essential properties concerning permeability, thickness and degree of contamination at different levels. Furthermore, the analysis of the samples obtained has made it possible to establish the set of chemical parameters that will determine the ISCO treatment provided, as indicated in point 3.3.

Morphological soil parameters include determining the different levels or horizons, depth, colour, smell, presence of roots and other biological features, structure and consistence. Physicochemical soil parameters include fragments (% >2 mm fraction), fine earth fraction (% sand, silt and clay), pH, electrical conductivity (μS cm^{-1}), carbonates (%), organic matter (%) and total petroleum hydrocarbons (TPH, mg kg^{-1}).

Water analyses include chemical oxygen demand (COD), anions (Cl^-, SO_4^{2-}, HCO_3^-, PO_4^{2-}, F^-, Br^-) and cations (Na^+, K^+, Ca^{2+}, Mg^{2+})

Total aliphatic and aromatic hydrocarbons are also determined in both soil and water selected samples with EC_{10}-EC_{12}, EC_{13}-EC_{16}, EC_{17}-EC_{21}, EC_{22}-EC_{35} and $>EC_{35}$ fractions.

Figure 2 shows the site layout and the monitoring network including data of the TPH concentration observed per sample point, both in soil (mg kg^{-1}) and in groundwater (μg L^{-1}). Soil data show the highest value of hydrocarbons found within the soil profile (commonly from four to five sampling levels per profile).

Data show a remarkable heterogeneity in the values of hydrocarbons in soil and water. Thus, areas virtually free of hydrocarbons are compared to other areas with high levels of contamination at very close vicinity. Additionally, significant differences were observed between different depths in the same pit.

Pollutant distribution patterns have been roughly defined according to the presence of old tanks and pipes. This consequently required a specific treatment in different plots within the study area.

5.3 Conceptual Site Model

The study area, from a lithological point of view, corresponds to anthropogenic fill deposits located on marshes. According to IGME [82, 83], these deposits consist of sands, silts and clays of the Holocene age.

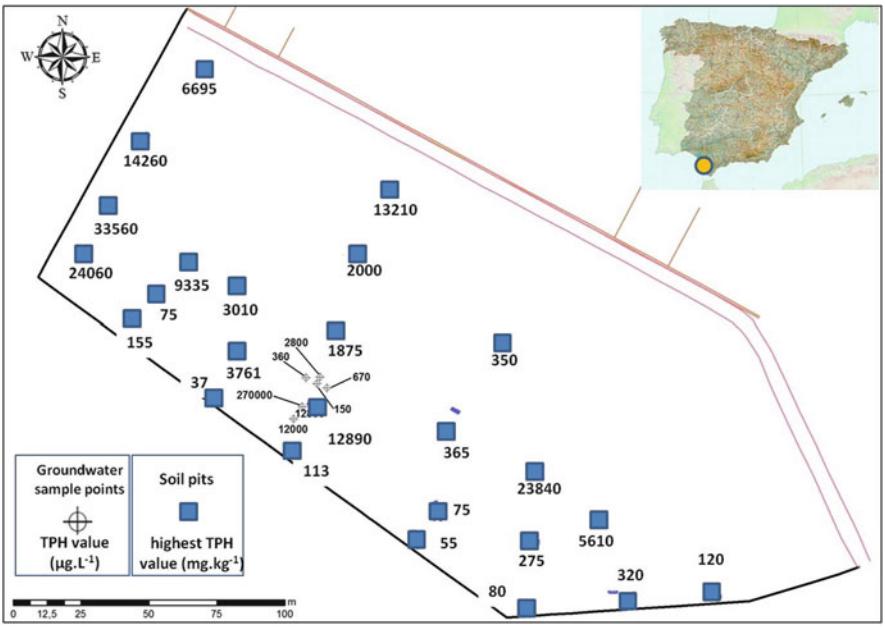

Fig. 2 Working area with soil and groundwater sampling points indicating the maximum TPH concentration data

From a geomorphological point of view, it is a transition zone between "high *slikke*" marsh formations (sand and clay, flooded during high tides, and with very sparse vegetation) and "schorre" formations (silts and clay, flooded only at extreme tides, with abundant vegetation). It is to note the abundance of shell fragments in marsh deposits.

The information obtained from the description of the 25 soil pits, as well as records of groundwater level and the detailed topographic study, has allowed establishing, for the whole work area, a conceptual soil and water model.

The characteristics of the substrate materials constituting the study area are summarized in Fig. 3 that shows a profile description based on one of the 25 test pits performed.

The so-called shell level is defined as the level of interest regarding the application of ISCO due to TPH mass. The density of pits and wells drilled has allowed spatially define the presence of that level, and the description and characterization of these points has established its depth in the entire study area.

Hydrogeologically, basic pH and the high carbonate, sulphate and chloride concentrations founded will affect iron solubility and peroxide lifetime.

Hydraulically, the shell level is located within an average depth between 0.20 and 1.20 m limited in the upper part by an anthropogenic fill more permeable and in the lower part by a sludge or "mud" level, rich in clay, compacted and virtually

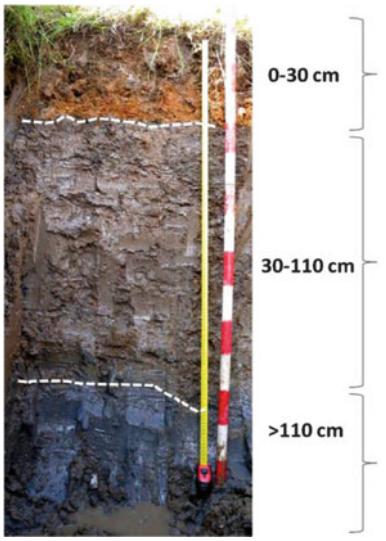

0-30: Anthropogenic fill level. Coarse grain size (sandy with fragments), basic pH; abundant $CaCO_3$; moderate organic matter content; variable salinity generally low; well rooted; well oxygenated (reddish colours).

30-110: "Shells" level. Fine-grained (clayey-sandy) trend to laminar structure. Abundant presence of traces of ostreids, pectinids and others, occasionally cobble and sand levels. Basic pH, abundant $CaCO_3$; moderate organic matter content. Variable salinity, generally high and increasing with depth. Very few roots. Variable oxygenation, generally decreasing with depth.

>110: "Mud" level. Very fine grain size (clay), occasionally with more sandy levels smelling to hydrogen sulfide; massive and compact structure. Basic pH, abundant $CaCO_3$, moderate content of organic matter. Very high salinity. Anoxic.

Fig. 3 Conceptual site soil model from characteristical soil profile

impermeable; according to pumping test, soil transmissivity has been estimated in 0.14 m^2/day. The water table across the site varies in an average depth of 0.72–1.35 m throughout the year. The groundwater flow is predominately to the north, without a clearly defined tidal influence.

5.4 Description of Target Treatment Volume

Chromatographic analysis of organic compounds in soil and groundwater samples indicates that sorbed and dissolved contaminants consisted of TPH in C_{16}-C_{21} and $>C_{21}$-C_{35} aliphatic ranges. The highest concentration is found in the so-called shell level within a depth between 0.20 and 1.20 m. Furthermore, high levels of NAPL were detected in the vadose zone.

The total volume of contaminated soil in the specific area of the ISCO treatment is about 5 tn.

Treatability-scale slurry-system testing of hydrogen peroxide treatment of the site contaminants indicated that TPH was oxidized, but the total soil and groundwater oxidant demand was not accurately determined during the treatability tests due to an insufficient duration of test. In return, several hydrogen peroxide

stabilizers (cyclodextrin, gallic acid, EDTA, gluconic acid and citric acid) were tested. The highest peroxide hydrogen lifetime was obtained using citric acid.

A field pilot test was performed on a much smaller portion of the plume, using approximately six groundwater wells to demonstrate the effectiveness of ISCO treatment and to calculate the radius of influence. The pilot test consisted of one injection of pressurized hydrogen peroxide and catalyst solution (chelated iron) into a double groundwater injection well (total injection quantity of 1,500 L). The radius of influence was determined to be approximately 4 m by field measurement of water quality changes (i.e. redox, specific conductance), presence of hydrogen peroxide by Merckoquant® Peroxide test strips and laboratory analysis of TPH concentration reduction in the surrounding wells. Significant rebound of TPH was monitored for 3 months following the pilot test in one of injection well. No evidence of surfacing was detected.

5.5 ISCO Consideration Full-Scale Design

Hydrogeochemical characteristics (basic pH and high carbonate, sulphate and chloride concentration) involve the use of iron chelates to keep the iron in solution and to increase peroxide lifetime.

Hydraulic characteristics (low permeability of shell level, possible preferential pathways – anthropogenic fill with more permeability – and shallow depth of groundwater) determine well construction, well layout, delivery strategy and injections sequence:

- Injection wells were constructed of polyvinylchloride (PVC) pipe with the screen interval placed in the vertical section intended for treatment. Injection wells are constructed with slot well screens and coarse sand pack located at the same depth or slightly deeper than the bottom of shell level (the most contaminated level). To isolate the injection depth, packers were also used.
- Regarding well layout, because the calculated radius of influence (ROI) in field test was 4 m, injection wells will be done on a grid maintaining a distance about 6.5 m between them; radius of influence might be extended by inducing a hydraulic gradient via the pumping of groundwater from a downgradient well.
- Regarding injection strategy, pressurized hydrogen peroxide and catalyst solution with iron and hydrogen peroxide stabilizer will be injected separately to increase the radius of influence. Taking into account hydrogeological characteristic of the site and the gas generation due to reagent injection, the injection flow will be less than 1 L/min to avoid high pressure that might generate surfacing.
- The sequence of the injections will depend on the water flow direction in the injection period: it could be work upgradient to reduce the potential to push contamination further downgradient or by pushing the TPH towards the centre.

5.6 Monitoring

Process monitoring during and post remediation will be presented in Tables 2 and 3.

References

1. Watts RJ, Stanton PC (1999) Mineralization of sorbed and napl-phase hexadecane by catalyzed hydrogen peroxide. Water Res 33:1405–1414
2. Watts RJ, Stanton PC, Howsawkeng J, Teel AL (2002) Mineralization of a sorbed polycyclic aromatic hydrocarbon in two soils using catalyzed hydrogen peroxide. Water Res 36 (17):4283–4292
3. Baciocchi R, Boni MR, D'Aprile L (2003) Hydrogen peroxide lifetime as an indicator of the efficiency of 3-chlorophenol Fenton's and Fenton-like oxidation in soils. J Hazard Mater B96:305–329
4. Watts RJ, Teel AL (2005) Chemistry of modified Fenton's reagent (catalyzed H_2O_2 propagations—CHP) for *in situ* soil and groundwater remediation. J Environ Eng 131(4):612–622
5. Kong SH, Watts RJ, Choi JH (1998) Treatment of petroleum-contaminated soils using iron mineral catalyzed hydrogen peroxide. Chemosphere 37(8):1473–1482
6. De Souza e Silva PT, da Silva V, de Barros-Neto B, Simonnot M-O (2009) Potassium permanganate oxidation of phenanthrene and pyrene in contaminated soils. J Hazard Mater 168(2–3):1269–1273
7. Kislenko VN, Berlin AA, Litovchenko NV (1996) Kinetics of the oxidation of organic substances by persulfate in the presence of variable-valence metal ions. Kinet Catal 37:767–774
8. Block PA, Brown RA, Robinson D (2004) Novel activation technologies for sodium persulfate in situ chemical oxidation. In: Proceedings of the 4th international conference on the remediation of chlorinated and recalcitrant compounds
9. Boulos N, Carvel D, Mucssig J (2008) Ex-situ and in-situ remediation with activated persulfate. US Patent application 2008/0272063
10. Liang C, Huang CF, Chen YJ (2008) Potential for activated persulfate degradation of BTEX contamination. Water Res 42(15):4091–4100
11. Liang C, Lee I (2008) In situ iron activated persulfate oxidative fluid sparging treatment of TCE contamination. A proof of concept study. J Contam Hydrol 100(3–4):91–100
12. Romero A, Santos A, Vicente F, González C (2010) Diuron abatement using activated persulphate: effect of pH, Fe(II) and oxidant dosage. Chem Eng J 162(1):257–265
13. Nam K, Kukor JJ (2000) Combined ozonation and biodegradation for remediation of mixtures of polycyclic aromatic hydrocarbons in soil. Biodegradation 11:1–9
14. O'Mahony MM, Dobson ADW, Barnes JD, Singleton I (2006) The use of ozone in the remediation of polycyclic aromatic hydrocarbon contaminated soil. Chemosphere 63 (2):307–314
15. Yu DY, Kang N, Bae W, Banks MK (2007) Characteristics in oxidative degradation by ozone for saturated hydrocarbons in soil contaminated with diesel fuel. Chemosphere 66(5):799–807
16. Rivas J, Gimeno O, de la Calle RG, Beltrán FJ (2009) Ozone treatment of PAH contaminated soils: operating variables effect. J Hazard Mater 169(1–3):509–515
17. Pierpoint AC, Hapeman CJ, Torrents A (2003) Ozone treatment of soil contaminated with aniline and trifluralin. Chemosphere 50:1025–1034
18. Bennedsen LR (2011) Activated peroxygens for remediation of contaminated soil and groundwater. Ph.D. Thesis
19. CityChlor (2013) Code of good practice: in situ chemical oxidation. http://www.citychlor.eu/sites/default/files/code_of_good_practice_isco.pdf. Accessed 04 Dec 2013
20. Huling SG, Pivetz BE (2006) *In situ* chemical oxidation. Engineering Issue. Prepared for the U.S. EPA. EPA/600/R-06/072. August

21. EPA (1998) In situ remediation technology: in situ chemical oxidation. Office of Solid Waste and Emergency Response, 542-R-98-008, September
22. ESTCP (1999) Technology status review: in situ oxidation. November
23. ITRC (The Interstate Technology & Regulatory Council) (2001) Technical and regulatory guidance for *in situ* chemical oxidation of contaminated soil and groundwater
24. GeoSyntec Consultants Inc (2004) Assessing the feasibility of DNAPL source zone remediation: review of case studies. Contract Report CR-04-002-ENV for NAVFAC, May
25. EPA (2004) DNAPL remediation: selected projects approaching regulatory closure. Office of Solid Waste and Emergency Response, 542-R-04-016, December
26. ITRC (The Interstate Technology & Regulatory Council) (2005) Technical and regulatory guidance for in situ chemical oxidation of contaminated soil and groundwater, 2nd ed. Washington DC
27. McGuire TM, McDade JM, Newell CJ (2006) Performance of DNAPL source depletion technologies at 59 chlorinated solvent-impacted sites. Ground Water Monit R 26(1):73–84
28. Johnson et al for ESTCP (2007) Critical evaluation of state-of-the-art in situ thermal treatment technologies for DNAPL source zone treatment (ER-03 14) project fact sheet. http://www.estcp.*org*/*Technology*/*ER-03 1 4-FS.cfm*. Accessed 29 Aug
29. Siegrist RL, Crimi M, Simpkin TJ (2011) In situ chemical oxidation for groundwater remediation series: SERDP ESTCP environmental remediation technology, vol 3, first edition, p 678
30. Baciocchi R (2013) Principles, developments, and design criteria of *in situ* chemical oxidation. Water Air Soil Pollut 224(12):1–11
31. Krembs FJ, Siegrist RL, Crimi ML, Furrer RF, Petri BG (2010) ISCO for groundwater remediation: analysis of field applications and performance. Ground Water Monit R 30 (4):42–53
32. APAT (2005) Protocol for ISCO application (In Italian). http://www.isprambiente.gov.it/files/temi/tec-protocolli-luglio-2005-protocollo-isco.pdf. Accessed 04 Dec 2013
33. Tyre BW, Watts RJ, Miller GC (1991) Treatment of four biorefractory contaminants in soils using catalyzed hydrogen peroxide. J Environ Qual 20:832–838
34. Watts RJ, Dilly SE (1996) Evaluation of iron catalysts for the Fenton-like remediation of diesel-contaminated soils. J Hazard Mater 51:209–224
35. Kakarla PKC, Watts RJ (1997) Depth of Fenton-like oxidation in remediation of surface soil. J Environ Eng 123:11–17
36. Watts RJ, Haller DR, Jones AP, Teel AL (2000) A foundation for the risk-based treatment of gasoline-contaminated soils using modified Fenton's reactions. J Hazard Mater 76:73–89
37. Xu P, Achari G, Mahmoud M, Joshi RC (2006) Application of Fenton's reagent to remediate diesel contaminated soils. Pract Period Hazard Toxic Radioact Waste Manage 10:19–27
38. Ndjou'ou AC, Cassidy D (2006) Surfactant production accompanying the modified Fenton oxidation of hydrocarbons in soil. Chemosphere 65:1610–1615
39. Afanas'ev IB (1989) Superoxide ion: chemistry and biological implications. CRC Press, Boca Raton, FL, p 296
40. De Laat J, Gallard H (1999) Catalytic decomposition of hydrogen peroxide by Fe(III) in homogeneous aqueous solution: mechanism and kinetic modeling. Environ Sci Technol 33:2726–2732
41. Lou JC, Lee SS (1995) Chemical oxidation of BTX using Fenton's reagent. Hazard Mater 12 (2):185–193
42. Lin SH, Lo CC (1997) Fenton process for treatment of desizing wastewater. Water Res 31:2050–2056
43. Tsitonaki A (2008) Treatment trains for the remediation of aquifers polluted with MTBE and other xenobiotic compounds. PhD Thesis
44. Watts RJ, SERDP (2006) Improved understanding of fenton-like reactions for the in situ remediation of contaminated groundwater including treatment of sorbed contaminants and destruction of DNAPLs
45. Bossmann SH, Oliveros E, Göb S, Siegwart S, Dahlen EP, Payawan LM, Matthias S, Wörner M, Braun AM (1998) New evidence against hydroxyl radicals as reactive

intermediates in the thermal and photochemically enhanced Fenton reactions. J Phys Chem A 102:5542–5550
46. Smith BA, Teel AL, Watts RJ (2004) Identification of the reactive oxygen species responsible for carbon tetrachloride degradation in modified Fenton's systems. Environ Sci Technol 38 (20):5465–5469
47. Pignatello JJ, Oliveros E, MacKay A (2006) Advanced oxidation processes for organic contaminated destruction based on the Fenton reaction and related chemistry. Criti Rev Environ Sci Technol 36:1–84
48. Baciocchi R, Ciotti C, Cleriti G, Innocenti I, Nardella A (2010) Design of *in situ* Fenton oxidation based on the integration of experimental and numerical modeling. J Adv Oxid Technol 13(2):153–161
49. Tarr M, Lindsay ME (1998) Role of dissolved organic matter in Fenton degradation of hydrophobic pollutant. Abstract presented at the 19th annual meeting of SETAC, Charlotte, NC, USA
50. Gates DD, Siegrist RL (1995) *In situ* chemical oxidation of trichloroethylene using hydrogen peroxide. J Environ Eng 121:39–644
51. Bissey LL, Smith JL, Watts RJ (2006) Soil organic matter–hydrogen peroxide dynamics in the treatment of contaminated soils and groundwater using catalyzed H_2O_2 propagations (modified Fenton's reagent). Water Res 40:2477–2484
52. Bogan BW, Trbovic V (2003) Effect of sequestration on PAH degradability with Fenton's reagent: roles of total organic carbon, humin, and soil porosity. J Hazard Mater 100:285–300
53. Vicente F, Rosas JM, Santos A, Romero A (2011) Improvement soil remediation by using stabilizers and chelating agents in a Fenton-like process. Chem Eng J 172:689–697
54. Huling SG, Arnold RG, Sierka RA, Miller MR (2001) Influence of peat on Fenton oxidation. Water Res 35(7):1687–1694
55. Kiwi J, Lopez A, Nadtochenko V (2000) Mechanism and kinetics of the OH-radical intervention during Fenton oxidation in the presence of a significant amount of radical scavenger (Cl^-). Environ Sci Technol 34:2162–2168
56. Siedlecka EM, Wieckowska A, Stepnowski P (2007) Influence of inorganic ions on MTBE degradation by Fenton's reagent. J Hazard Mater 147:497–502
57. De Laat J, Le GT, Legube B (2004) A comparative study of the effects of chloride, sulfate, and nitrate ions on the rates of decomposition of H_2O_2 and organic compounds by Fe(II)/H_2O_2 and Fe(III)/H_2O_2. Chemosphere 55:715–723
58. Lipczynska-Kochany E, Sprah G, Harms S (1995) Influence of some groundwater and surface waters on the degradation of 4-chlorophenol by the Fenton reaction. Chemosphere 30:9–20
59. Tang WZ, Huang CP (1996) 2,4-dichlorophenol oxidation kinetics by Fenton's reagent. Environ Technol 17:1371–1378
60. Watts RJ, Finn DD, Cutler LM, Schmidt JT, Teel AL (2007) Enhanced stability of hydrogen peroxide in the presence of subsurface solids. J Contam Hydrol 91:312–326
61. Sun Y, Pignatello JJ (1992) Chemical treatment of pesticide wastes: evaluation of Fe(III) chelates for catalyzed hydrogen peroxide oxidation of 2,4-D at circumneutral pH. J Agric Food Chem 40:322–327
62. Tandy S, Ammann A, Schulin R, Nowack B (2006) Biodegradation and speciation of residual SS-ethylenediaminedisuccinic acid (EDDS) in soil solution after soil washing. Environ Pollut 142:191–199
63. Ramo J (2003) Hydrogen peroxide-metals-chelating agents: interactions and analytical techniques. Oulu University Press, Oulu
64. Jones PW, Williams DR (2002) Chemical speciation simulation used to assess the efficiency of environment-friendly EDTA alternative for use in pulp and paper industry. Inorg Chim Acta 339:41–50
65. Tarr MA, Wei B, Zheng W, Xu G (2002) Cyclodextrin-modified fenton oxidation for in situ remediation. In: Proceedings, third international conference on remediation of chlorinated and recalcitrant compounds, Monterey, CA, USA, May 20–23, Paper 2C-17

66. Lindsey ME, Xu G, Lu J, Tarr MA (2003) Enhanced Fenton degradation of hydrophobic organics by simultaneous iron and pollutant complexation with cyclodextrins. Sci Total Environ 307:215–229
67. Jazdanian AD, Fieber LL, Tisoncik D, Huang KC, Mao F, Dahmani A, (2004) Chemical oxidation of chloroethanes and chloroethenes in a rock/groundwater system proceedings. In: Fourth international conference on remediation of chlorinated and recalcitrant compounds, Monterey, CA, USA, May 24–27, Paper 2F-01
68. Kang N, Hua I (2005) Enhanced chemical oxidation of aromatic hydrocarbons in soil systems. Chemosphere 61:909–922
69. The Colorado Department of Labor and Employment Division of Oil and Public Safety (2007) Petroleum hydrocarbon remediation by *in situ* chemical oxidation at Colorado Sites
70. In Situ Remediation Reagents Injection Working Group (2009) Subsurface injection of in situ remedial reagents (ISRRs) within the Los Angeles Regional Water Quality Control Board Jurisdiction
71. Rosansky S et al (2013a) Best practices for injection and distribution of amendments. Technical report TR-NAVFAC-EXWC-EV-1303
72. Ciotti C (2008) Advanced oxidation processes as innovative technologies for the remediation of contaminated sites. Ph.D. Thesis. University of Rome Tor Vergata
73. Regenesis (2007) Principles of chemical oxidation technology for the remediation of groundwater and soil, RegenOx™ design and application manual – Version 2.0. San Clemente, CA, USA
74. New Jersey Department of Environmental Protection (2011) Technical guidance for preparation and submission of a conceptual site model
75. British Columbia (2005) Technical guidance on contaminated sites. Checklist for reviewing a detailed site investigation
76. Rosansky S (2013) Design and quality assurance/quality control considerations for *in situ* chemical oxidation. Technical Memorandum TM-NAVFAC EXWC-EV-1302
77. Barcelona MJ, Holm T (1991) Oxidation–reduction capacities of aquifer solids. Environ Sci Technol 25(9):1565–1572
78. Powell RM, Callaway RW, Michalowski JT, Vandegrift SA, White MV (1988) Comparison of methods to determine oxygen demand for bioremediation of a fuel contamination of a fuel contaminated aquifer. Int J Environ Anal Chem 34:253–263
79. Lee W, Batchelor B (2003) Reductive capacity of natural reductants. Environ Sci Tech 37:535–541
80. Korom SF, McFarland MJ, Sims RC (1996) Reduced sediments: a factor in the design of subsurface oxidant delivery systems. GWMR, Winter 1996, pp 100–105
81. Pedersen JK, Bjerg PL, Cheristensen TH (1991) Correlation of nitrate profiles with groundwater and sediment characteristics in a shallow sandy aquifer. J Hydrol 124:263–277
82. IGME (1987) Mapa Geológico de España. Escala 1:50.000. San Fernando. Segunda Serie. Primera Edición. Madrid.
83. IGME (1990) Mapa Geológico de España. Escala 1:50.000. Chiclana de la Frontera. Segunda Serie. Primera Edición. Madrid

Sustainable Polyurethanes: Chemical Recycling to Get It

D. Simón, A.M. Borreguero, A. de Lucas, C. Gutiérrez, and J.F. Rodríguez

Abstract Nowadays polyurethanes are one of the most important classes of polymers in the chemical market due to the huge diversity of their applications. Polyurethane is placed the sixth of the most used plastics in the world ranking. As a consequence of their commercial success, a great quantity of wastes are generated, not only post-consumer products but also scrap from slabstock manufacturing. In the past, landfilling was the solution to the problem, but, nowadays, the new environmental laws do essential to develop environmental sustainable recycling processes. On the one hand, there are physical methods that do not modify the internal structure of the polyurethane and only convert mechanically the wastes in flakes, granules or powder to be used as fillers for new PUs or to be rebounded. However, these physical processes can be only applied with thermoplastic polyurethane, while the majority of polyurethane specialties are thermostable polymers. Therefore, chemical processes are mainly used to recycle polyurethane wastes. These chemical recycling processes allow to obtain basic hydrocarboned units known as monomers that are able to be used as synthesis materials in chemical and petrochemical industry. This way, it is possible to achieve high value-added products that can be used in the synthesis of new polyurethane products. Thus, the main aim of this chapter is to describe the presently known technologies for the chemical recycling of polyurethane wastes.

Keywords Glycolysis, Polyol, Polyurethane, Recycling, Wastes

D. Simón, A.M. Borreguero, A. de Lucas, C. Gutiérrez, and J.F. Rodríguez (✉)
Institute of Chemical and Environmental Technology (ITQUIMA), University of Castilla, La Mancha, Spain
e-mail: Diego.Simon@uclm.es; Anamaria.Borreguero@uclm.es; Antonio.LucasM@uclm.es; Cristina.Gutierrez@uclm.es; juan.rromero@uclm.es

E. Jiménez et al. (eds.), *Environment, Energy and Climate Change I: Environmental Chemistry of Pollutants and Wastes*, Hdb Env Chem (2015) 32: 229–260,
DOI 10.1007/698_2014_275,
Published online: 8 September 2014

Contents

1 Introduction

Polyurethane is the sixth most used polymer all over the world with a production of approximately 12 million tons per year [1]. Opposite to other commonly used plastics, they are no polymerisation but condensation polymers, synthesised from polyols and isocyanates.

The diversity of polyols and isocyanates allows the synthesis of numerous different compounds covering a huge range of application. The polyurethanes (PU) can be classified mainly in foams and in the denominated CASEs (Coatings, Adhesives, Sealants and Elastomers). Furthermore, foams can be divided in flexible, such as the ones used in mattresses and automotive seats, and rigid, commonly applied in buildings isolation and commercial refrigeration. Regarding the CASEs uses, they can be found as part of sporty shoes, athletics tracks, electronic products and ships structures.

As a direct consequence of their commercial success, an increasing quantity of wastes is disposed by landfilling. Such wastes comprise not only post-consumer products but also scrap from slabstock manufacturing, which can reach the 10% of the total foam production. Recycling is an alternative approach to landfilling. On the one hand, there are physical processes, which do not modify polymer internal structure. These processes consist basically on the wastes' mechanical transformation into flakes, granules or powder to be used in new materials production. The main advantages of these methods are their simplicity and their low cost with successful results for the thermoplastic polyurethane recovery. Physical processes consume at present about 120,000 tons per year, which represent the 1% of the total amount of produced polyurethane [1]. However, they cannot be applied for the PU foams recycling due to their cross-linked structure. Only rebonding has been developed for carpet underlay. Considering that the PU volume percentage corresponding to the foams part is about 80%, the development of chemical

recycling processes for their recovery has attracted considerable interest in the last decades. The goal of this chapter is to describe the presently known technologies for the chemical recycling processes of polyurethane wastes.

2 Chemistry of Polyurethanes

The basis of the polyurethane chemistry is the condensation reaction between diols or polyols and diisocyanates or polyisocyanates. However, depending on the polyurethane type, the reactive process of the polyurethane production can involve more reactions, as, for example, the gas formation in the case of the polyurethane foams. These main reactions are the chain extension, the gas formation, the cross-linking and the isocyanate polymerisation reactions.

2.1 Primary or Chain Extension Reaction

The primary reaction, also known as chain extension reaction, is the reaction between a compound containing active hydrogen groups and an isocyanate giving as a result a substituted carbamic acid ester or urethane. The mechanism of this reaction is a nucleophilic addition of the polyalcohol oxygen to the carbon of the isocyanate group, by six-centred ring as reaction intermediate [2].

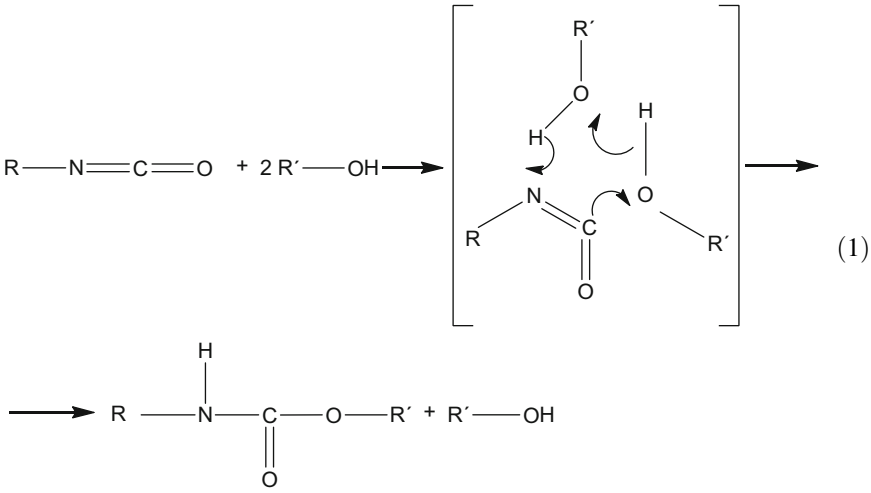

(1)

This reaction is exothermic but happens slowly at room temperature in the absence of any catalyst. Therefore, catalysts are usually added in order to accelerate the reaction. Some of the most used ones are nitrogen compounds (*N*, *N*-dimethylcyclohexylamine, triethylamine, *N*-ethylmorpholine, diaminobicyclooctane (DABCO),

N-methyl-*N*′-dimethylaminoethylpiperazine, *N*,*N*,*N*′,*N*′-tetramethyl-1,3-butanediamine, ethoxylated hydroxyamines), organometallic compounds (stannous octoate, dibutyltindiacetate, dibutyltindilaurate) or Lewis acid [3]. Dialkyltin compounds and stannous carboxylates are about ten times more powerful catalyst than the ones based in tertiary amines.

2.2 Gas Formation Reaction

Water reacts with isocyanate giving as a result a substituted carbamic acid that is decompounded in an amine and carbon dioxide. This reaction provides the principal source of gas for blowing the foam, as well as the main heat power for the expansion and cure of the polyurethane. This reaction also provides both covalent and hydrogen-bonding sites on the polymer chains [3].

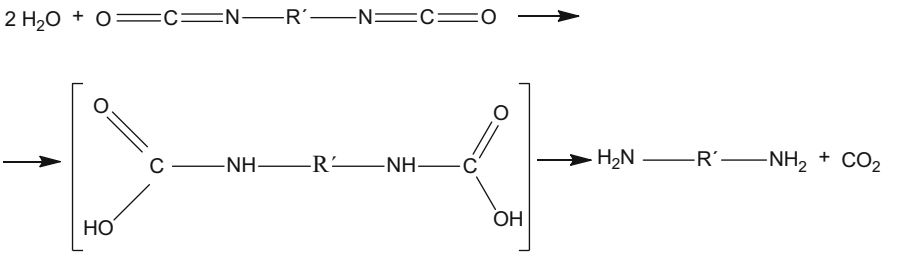

(2)

This reaction can be catalysed by tertiary amines. The catalyst selection of this reaction will determine the final polyurethane properties, since the rate of the gas formation regarding the rates of the chain extension and cross-linking reactions will determine the material structure [4, 5].

On the other hand, the blowing process can be also performed by the addition of blowing agents such as hydrochlorofluorocarbons (HCFCs), hydrofluorocarbons (HFCs) and hydrocarbons (HCs) such as cyclopentane, *n*-pentane, isopentane and *n*-butane. Furthermore, methyl chloroform and acetone are also used as blowing agents mainly in the production on non-insulation foams [6].

2.3 Cross-Linking Reactions

Additionally, to the chain extension reaction, the isocyanate participates in other reactions due to its high reactivity in the presence of labile protons. These reactions are known as cross-linking reactions.

For instance, the amines formed in the gas formation reaction may react with free isocyanate giving as a result a substituted urea Eq. (3). It is important to take into

account that the reaction of isocyanates with primary amines at room temperature in the absence of catalyst is much faster than the reaction with primary alcohols.

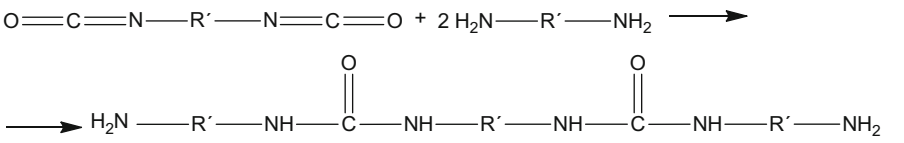

(3)

Furthermore, isocyanate may react with the active hydrogen atoms in urethanes to form more complex structures, known as allophanates Eq. (4).

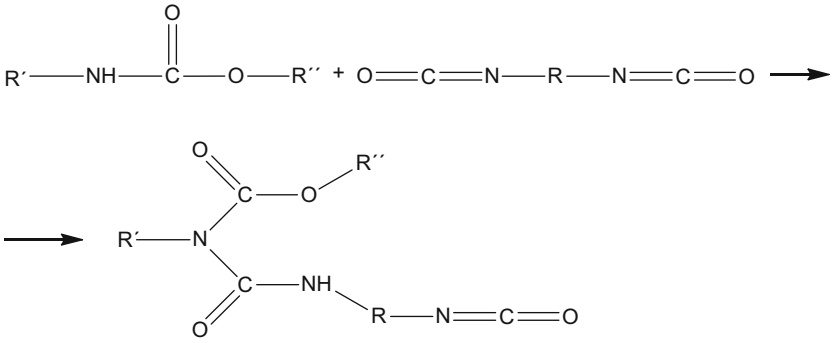

(4)

Finally, the labile protons of the substituted urea or the ones of the allophanates may react with more free isocyanate to yield a biuret structure Eq. (5). However, urethanes are less reactive to isocyanates than ureas, being necessary temperatures in the range of 120–140°C to achieve a significant allophanate cross-linking in the absence of catalyst. Besides, tertiary amines usually used as catalyst do not enhance in a significant way the allophanate linkages.

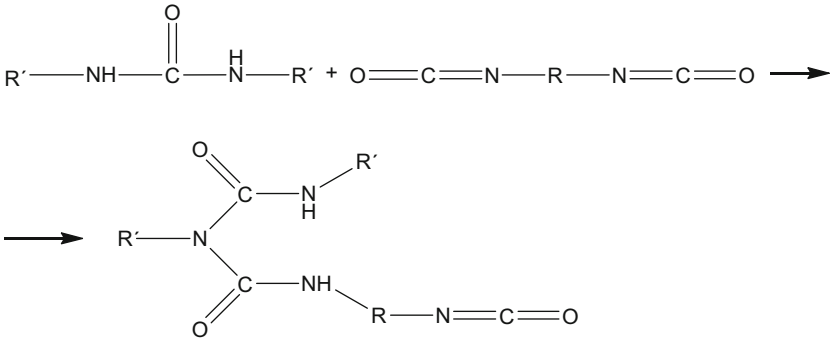

(5)

2.4 Isocyanate Polymerisation Reactions

The isocyanate polymerisation reactions can provide three main kinds of products: uretdiones, isocyanurates and carbodiimides.

Uretdiones are formed due to the dimerisation of the isocyanate group (Eq. 6). This dimerisation process is reversible.

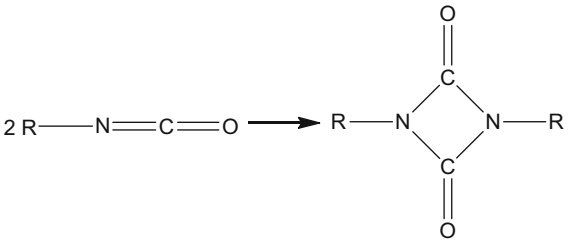

(6)

The trimerisation of the isocyanate group gives as a result 1,3,5-triazinones (isocyanurates) (Eq. 7). The formation of isocyanurate is not an easy reversible reaction because the branch formed is very stable [3].

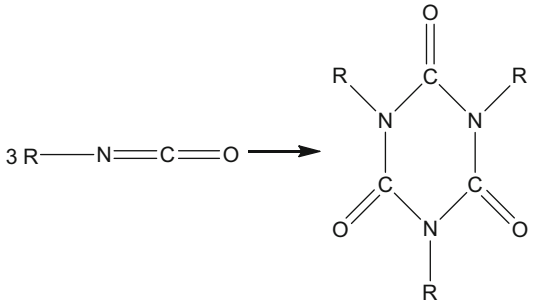

(7)

Finally, carbodiimides are synthesised by a reaction of two isocyanate groups with the evolution of CO_2 (Eq. 8).

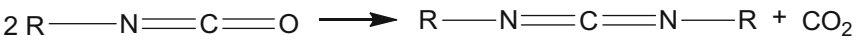

(8)

Furthermore, isocyanate may further react with the carbodiimides giving uretonimine as a product (Eq. 9).

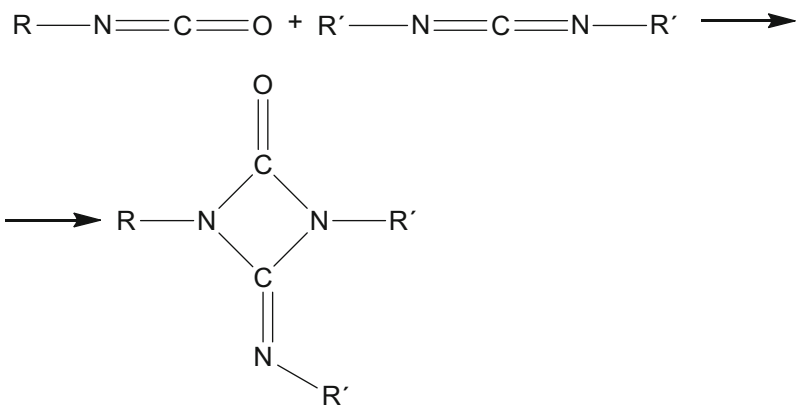

(9)

Therefore, the polyurethane structure presents a huge range of density and flexibility depending on the extension of the commented reactions.

3 Types of Polyurethanes

As commented before, depending on the polyol and the isocyanate types involved in the reaction, it is possible to obtain a huge variety of products, linear and reticulated.

Besides, in the current polyurethane synthesis processes, different additives (chain extenders, cross-linking agents, catalysts and foaming agents) are used in order to modify the final product characteristics.

From an application point of view, polyurethanes can be classified in foams (rigid or flexible) and in the denominated CASEs (Coatings, Adhesives, Sealants and Elastomers).

3.1 Polyurethane Foams

3.1.1 Flexible Foams

Flexible foams represent about the 45% of the total polyurethane production that means about 5.4 million tons per year [7]. They can be separated into three different groups: conventional foams that represent about the 80% of the total production; viscoelastic foams, with the 15% of the production; and high resilience (HR) foams, which represent the 5%.

The conventional ones are produced as slabstocks. High resilience foams are used for cushions, especially in the automotive industry. Viscoelastic foams are

usually employed for mattresses and pillows, since they adjust themselves to accommodate the various pressure points, such as the shoulder and hips, which are body areas that press hardest into the bed during sleep.

The 90% of the flexible foams are synthesised from long-chain polyether polyols based on ethylene and propylene oxide. Conventional foams are produced using only a flexible polyether polyol (uncommon) or a mixture of a flexible polyether polyol with a polymeric one and toluene diisocyanate (TDI) as isocyanate. The polymeric polyol consists of an acrylonitrile-styrene copolymer (SAN) dispersion in a flexible polyether polyol containing little ethylene oxide. Molecular weights of the polyols involved in the synthesis of conventional foams are in the range from 2,800 to 4,000 g/mol, and the most common functionality is three, since the majority of these polyols are synthesised using glycerine as initiator. On the other hand, high resilience (HR) foams are produced by long-chain polyether polyols with higher molecular weight (4,000–6,000 g/mol) and a higher proportion of ethylene oxide [1]. In the synthesis of HR foams, polymeric methylene diphenyl isocyanate (PMDI) is the isocyanate used, instead of TDI. Finally, viscoelastic foams are produced by a mix of two kinds of polyols: a high molecular weight polyether polyol and a short chain one. The isocyanate employed in the synthesis of viscoelastic foams is the same than for the HR ones, that is, PMDI. However, in some cases, TDI is also used.

3.1.2 Rigid Foams

Rigid foams are mainly used in buildings isolation and commercial refrigeration. The main differences between the flexible and the rigid foams are the molecular weight of the polyol used and its functionality. Rigid foams are synthesised using short-chain polyols, with molecular weights in the range 290–670 g/mol, although some polyols can achieve a molecular weight of 1,050 g/mol in some one-component rigid foams. On the other hand, the used initiator determines the functionality of the polyol and as a consequence its reactivity. Rigid polyols are usually synthesised with initiators with reactivity higher than three, promoting higher reticulation grades in the synthesised polyurethanes. The most common initiators contain active hydroxyl groups, such as sorbitol, triethanolamine and sucrose or active amine groups, such as toluenediamine and ethylenediamine. It is also important to point out that rigid polyols do not usually contain ethylene oxide in their structure [8]. Sometimes, a mixture of polyols is used, even a polyester and a polyether polyol. Furthermore, some rigid foams are synthesised using polyols based on natural oils [9]. Regarding the isocyanate, the mainly used in the synthesis of rigid polyurethane foams is the polymeric MDI.

3.2 CASES (Coatings, Adhesives, Sealant and Elastomers)

Coatings, adhesives and sealants are used in construction, in transport and in shipbuilding industry. Therefore, their applications are based in their hardness, humidity resistance and durability. On the other hand, elastomers are used in sporty shoes, athletics tracks and electronic products.

In the synthesis of CASEs, not only long-chain or medium-chain polyols are used but also different chain extenders of functionality 2, such as 1,4-butanediol (BDO). Recent studies have demonstrated the use of 1,3-propanediol (PDO) as an alternative replacement for BDO giving a polyurethane with very interesting properties [10]. Some of the improvements are flexibility and toughness, compression set and rebound and transparency as a result of less crystallinity. The PDO elastomers have higher heat resistance and approximately 40% less deformation [10]. Furthermore, PDO-based elastomers present lower hysteresis, indicating that material absorbs less energy and is more resilient when stretched. Therefore, it is an optimal product to be used in applications where material is exposed to dynamic forces.

Other chain extenders used are diethylene glycol, *N*,*N*′-bis-(2-hydroxypropyl) aniline (DHPA) and 1,4-di-(2-hydroxyethyl) hydroquinone (HQEE) [10]. Instead of hydroxylated chain extenders as BDO and PDO, diamine ones are also employed. Some of them are hydrazine, 1,4-cyclohexanediamine, diethyl-toluene diamine (DETDA), 4,4′-methylene-bis-(2-chloroaniline) (MOCA) and 3,5-dimethylthio-toluene diamine (DMTDA) [10]. Cross-linkers of functionality 3 are also used, such as diethanolamine, triethanolamine, trimethylolpropane (TMP) and glycerine [10].

3.2.1 Elastomers

There are four major types of polyurethane elastomers: cast elastomers, thermoplastic polyurethane elastomers (TPU), millable polyurethane gums and microcellular elastomers.

The *cast elastomers* can be classified by the way in which they are processed: prepolymer process (a prepolymer is a special isocyanate where it has been partially reacted with a polyol), quasi-prepolymer process and one-shot process. The isocyanate content as % NCO determines if the isocyanate is a prepolymer or not; an NCO content of less than 12% is enough to be considered prepolymer, and between 12 and 25% is considered quasi-prepolymer [10]. Elastomers with better properties are achieved using prepolymers.

Thermoplastic polyurethanes (*TPUs*) are elastomers fully thermoplastic, that is, elastic and melt processable. Nowadays, TPUs represent a 5% of the total production of polyurethanes; however, their growth is one of the fastest. They can be processed on extrusion as well as injection, blowing and compression moulding equipment. They are extremely flexible materials adaptable to dozens of uses such

as architectural glass lamination, auto-body side moulding, automotive lumbar supports, drive belts, film and sheet, flexible tubing, food processing equipment, medical tubing and wire and cable coatings.

The thermoplastic polyurethanes are compounded by hard and soft segments. The hard segments consists of pure 4,4′-diphenylmethane diisocyanate (MDI) and 1,4-butanediol (BDO) as chain extender [10]. The soft segments are the macrodiols of molecular weight generally between 1,000 and 2,000 g/mol. The most common macrodiol is polytetramethylene glycol (PTMEG or PTHF, 650–2,800 g/mol). PTMEG, produced by cationic polymerisation of tetrahydrofuran, is a waxy solid at room temperature. It is insoluble in water and in aliphatic hydrocarbons but soluble in alcohols, esters and ketones, aromatic solvents and chlorinated hydrocarbons. Other common polyether polyols used are polypropylene glycol diol (400–4,000 g/mol), polypropylene glycol-capped diol (400–4,000 g/mol) and poly (trimethylene ether)glycol (650–2,400 g/mol) [10]. Polyesters polyols are also employed such as polybutanediol adipate and polycaprolactone polyol [10]. Less commonly, polybutadiene polyols are also used. Almost all TPUs are based on pure MDI, have high molecular weight (>100,000 g/mol) and contain no chemical cross-linking. In the TPUs, formulations only used are difunctional components with a ratio NCO:OH of approximately one [10]. The synthesis of these polymers is crucial to remove the water by vacuum stripping to a maximum of 100 ppm. Polyether-based TPUs present an excellent low temperature flexibility and hydrolysis resistance. However, polyester-based TPUs are superior in abrasion resistance and mechanical properties, due to the interchain hydrogen bonding between the ester groups, chemical resistance and injectability.

Millable gum polyurethanes or *millable polyurethane rubbers* were one of the first polyurethane elastomers technology developed. They are made from both polyester and polyether polyols. Millable gums are under-indexed urethanes, that is, in their formulation, there is a stoichiometric deficiency of isocyanate groups compared to hydroxyl groups (NCO:OH ratio is less than 1.0). As a consequence of the low index, it is necessary to vulcanise the millable urethanes with peroxides or sulphurs. The cure sites can be introduced by different ways: using the methylene hydrogens of MDI for a peroxide cure or introducing unsaturation (carbon–carbon double bonds) in the chain extender. Then, vulcanisation can be accomplished with heat and pressure utilising sulphur or peroxide cure systems.

One of the main applications of the millable gums is the footwear industry. Table 1 summarises some synthesis systems [11]:

Microcellular elastomers are the last type of polyurethane to be commented. They can be considered as very high density flexible foams or more typically polyurethane elastomers with micro-fine bubbles and reduced density [10]. Microcellular elastomers are polymers based on polymeric MDI and polyether polyol. They are manufactured by the addition of surfactants and specific catalysts, generally an amine-based one. Silicone surfactants are used to control the cell size and to improve the foam stability. Chain extenders such as ethylene glycol and butane diol are also employed. It is essential to control the quantity of added water in order to produce a limited foaming. Some of their main applications are the

Table 1 Millable polyurethane rubber for footwear

Polyol	Isocyanate	Cure	Use
Polyether	TDI	Sulphur	High abrasion
Polyether	Aliphatic	Peroxide	Clear outsoles
Polyether	MDI	Peroxide	Clear outsoles
Polyester	MDI	Peroxide	Low cost transparent soles

steering wheels, the air bag door covers and the shoe soles. Polyether polyols provide good flexibility at low temperatures, which is a crucial property for the footwear industry.

3.2.2 Coatings

Polyurethane coatings are usually classified as water-based coatings, solvent-based ones and totally solids coatings.

In the synthesis of the polyurethane, coatings used are polyester, polyether and acrylic polyols. The most common polyether polyols used are polypropylene glycol diol (400–4,000 g/mol), polypropylene glycol-capped diol (400–4,000 g/mol), polytetramethylene glycol (PTMEG or PTHF, 650–2,800 g/mol) and polycarbonate polyol. On the other hand, the main polyester polyols involved are polybutanediol adipate, polycaprolactone polyol and polyethylene terephthalate [10].

With respect to the isocyanate used for coating synthesis, they can be classified in aliphatic and aromatic isocyanates. Some of the most important aliphatic isocyanates are hexamethylene diisocyanate (HDI), isophorone diisocyanate (IPDI) and methylene dicyclohexylisocyanate (H12MDI). By the aromatic side, the most used ones are toluene diisocyanate (TDI) and methylene diphenyl isocyanate (MDI). However, aliphatic isocyanates are approximately five times more used than the aromatic ones for the coating synthesis since the aliphatic isocyanates provide very good colour stability. Among them, HDI is the most used, followed by the IPDI. H12MDI is only used to produce very high-quality products and water-borne systems [10].

Apart from polyol and isocyanate, in the synthesis of coatings, other products are involved, such as solvents and coalescing agents. These are added to reduce the Tg of the polymer or to reduce the repulsive forces between the polymer particles. Besides, plasticisers are also used to reduce the Tg, at the time that increase the free polymer molecule volume. They interact just in a physical way (without chemical reaction) with the polymer molecule forming a homogeneous system.

Well-known coating plasticisers are phthalate esters. Pigments addition allows to colour the coating, and with some fillers, an improvement in the toughness and texture can be produced. Diatomaceous earth, lime, talc, barites and clay are some of the most common fillers, being all of them inert and cheap materials. Additionally, other coatings additives are thickeners, stabilisers, texturisers, UV stabilisers, biocides, etc.

Thanks to this amount of additives, coatings present a high versatility, and as a consequence, they can be applied in many different sectors and applications such as the aerospace market, the automotive industry, packaging, pipes, wires, wood furnitures, marine roofs, architectural, etc.

3.2.3 Sealants

A sealant is a material designed only to fill up a space. The spaces can be joints, gaps or cavities that occur between two substrates. Frost and Sullivan define a sealant as a liquid, paste or foam material, that, when applied to a joint or orifice, forms a tight seal against liquids or gases. Some of the main properties of the sealants are corrosion resistance, insolubility and environmental resistance, and they are involved in many sectors such as automotive, construction and aerospace. It is important to comment that, many times, sealants and adhesives are considered together due to some formulations can perform a role as either an adhesive or a sealant. However, sealants are generally lower in strength than adhesives, but present a better flexibility. An adhesive is defined as a material that joins two surfaces together by bonding them and is usually applied as a thin layer between two surfaces.

Polyurethane sealants are classified as high-performance ones because they present a greater than 12% movement capability and a service life between 10 and 50 years, while the low-performance sealants based on polyvinyl acetate, epoxy or oil and resin-based sealants only present a 0–5% movement capability and a service life of less than 10 years [12]. The only drawback of the polyurethane sealants is their moderate resistance to hydrolysis and UV radiation.

The chemistry of the polyurethane sealants is similar to that of elastomers. For their synthesis are used either polyester or polyether polyols. Among the most used polyester polyols, the polycaprolactone polyol and the polybutanediol adipate stand out. On the other hand, the main polyether polyols for the synthesis of polyurethane sealants are polypropylene glycol diol and polypropylene glycol-capped diol, although polybutadiene polyols are also used [12].

With respect to the isocyanates involved in the synthesis of sealants, TDI and MDI are the most used ones. If a nonyellowing sealant is required, then aliphatic isocyanates are the ones to be employed.

Besides, the sealants characteristics are improved by adding solvents (improve processability), plasticisers (increase hydrophobicity and reduce viscosity), fillers as calcium carbonate (improve mechanical properties and reduce cost), etc.

3.2.4 Adhesives

An adhesive is defined as a non-metallic material which is able to join together substances by means of surface adhesion and inner strength [13].

The effectiveness of adhesives is based on surface adhesion (adhesion) and the power of attraction of the adhesive molecules exerted between themselves (cohesion). The adhesion can take place by mechanical or chemical mechanisms.

The urethane adhesives present some interesting properties, for instance, they can interact with the substrate through polar interactions (hydrogen bonds), they can form covalent bonds with substrates that present active hydrogen atoms and they effectively wet the surface of most substrates. Furthermore, their relatively low size and molecular weight allows them to permeate porous substrates. Thus, they can be applied in many sectors; some of the most important ones are footwear industry, construction, woodworking, transportation, packaging and assembly operations.

The most used polyols in the synthesis of polyurethane adhesives are the crystalline polyester polyols such as butane or hexanediol adipates [12]. These polyols provide an excellent plasticiser resistance. When higher tensile resistance is needed, polyester polyols such as polycaprolactone polyol are used and also polyether polyols such as polytetramethylene glycol (PTMEG). On the other hand, polybutadiene polyols are used to synthesise hydrophobic adhesives. Propylene and ethylene oxide polyols are also used extensively because of their low cost and hydrolytic stability.

In general, soft adhesives are synthesised by means of higher molecular weight polyols (1,000–6,000), lower functionality (2–3), lower hydroxyl value (28–160 mg KOH/g), lower NCO/OH ratio and low levels of chain extenders [12].

On the other hand, hard adhesives are achieved using lower molecular weight polyols (150–1,500) with a functionality higher than 3 (generally 3–8), higher hydroxyl value (250–1,000 mg KOH/g), higher NCO/OH ratio and higher quantities of chain extenders [12].

MDI and TDI are the most common isocyanates employed in the synthesis of polyurethane adhesives. Aliphatic isocyanates are only used when a nonyellowing adhesive is needed.

As previously commented for the other urethane specialties, in the synthesis of polyurethane adhesives, some additives allow to modify the final product properties. For instance, solvents are used to adjust viscosity and improve the processability, and plasticisers achieve an improvement in the elongation and lower hardness of the adhesives. The most common used plasticiser is a phthalate kind one [12]. Tertiary amines and transition metals compounds are used as catalysts and diamines or diols as chain extenders. These chain extenders react with the isocyanate producing hard segments, while soft segments are formed by the polyol. Cross-linkers are also commonly used. These compounds have low molecular weight and contain active hydrogen with a minimum functionality of 3. Furthermore, fillers are added in structural adhesive formulations to improve properties and to reduce the cost.

With the aim of providing a global view of the polyurethane specialties, Table 2 summarises the main products involved in the synthesis of the polyurethane products.

Table 2 Global overview of the main products involved in the synthesis of PU specialties

	Polyol				Isocyanate			
Polyurethane type	Polyether	Polyester	Polybutadiene	Acrylic	Pure MDI	Polymeric MDI	TDI	Aliphatic
Flexible foam								
Conventional	PEOB ($f=2$–3) PPOB ($f=2$–3) PP ($f=2$–3)	–	–	–	–	–	√	–
High resilience	PEOB ($f=2$–3) PPOB ($f=2$–3)	–	–	–	–	√	–	–
Viscoelastic	PEOB($f=2$–3) PPOB ($f=2$–3)	–	–	–	–	√	–	–
Rigid foam								
	PPOB ($f>3$)	√	–	–	–	√	–	–
CASE								
Elastomer	PTMEG ($f=2$) PPGD ($f=2$) PPGCD ($f=2$) PTRIMEG ($f=2$)	PBDA PCLP	√	–	√	–	–	–
Coating	PTMEG ($f=2$) PPGD ($f=2$) PPGCP ($f=2$) PCP	PBDA PCLP PET	–	√	√	–	√	HDI IPDI H12MDI
Sealant	PPGD ($f=2$) PPGCD ($f=2$)	PBDA PCLP	√	–	√	√	√	HDI IPDI H12MDI
Adhesive	PTMEG ($f=2$) PEOB PPOB	PBDA PCLP	√	–	√	√	√	HDI IPDI H12MDI

PEOB polyethylene oxide based, *PPOB* polypropylene oxide based, *PP* polymeric polyol, *PTMEG* polytetramethylene glycol, *PPGD* polypropylene glycol diol, *PPGCD* polypropylene glycol-capped diol, *PTRIMEG* poly(trimethylene ether)glycol, *PBDA* polybutanediol adipate, *PCLP* polycaprolactone polyol, *PCP* polycarbonate polyol, *PET* polyethylene terephthalate

As can be observed in Table 2, polyethylene oxide- and polypropylene oxide-based polyols with a functionality of 2–3 are the ones used in the synthesis of flexible PU foams. However, in the synthesis of rigid foams, polyethylene oxide-based polyols are no longer used, and as a consequence, polypropylene oxide-based polyols are the ones employed. It is really important to remark that the functionality of polyols involved in the synthesis of rigid foams is higher than three. What is more, rigid polyols have a higher hydroxyl number and a lower molecular weight that the polyols involved in the synthesis of flexible foams.

On the other hand, the main polyol used in the synthesis of CASEs is polytetramethylene glycol (PTMEG or PTHF), produced by cationic polymerisation of tetrahydrofuran. As shown in Table 2, PTMEG has a functionality of 2. It is important to take into account that difunctional components are mainly used in the synthesis of CASEs.

Table 2 shows that toluene diisocyanate (TDI) is the isocyanate employed in the synthesis of conventional flexible foams. However, in the synthesis of HR and viscoelastic flexible foams, polymeric methylene diphenyl isocyanate (PMDI) is the one used, instead of TDI. PMDI is also the isocyanate employed in the synthesis of rigid PU foams as shown in Table 2. Regarding the CASEs, the most common isocyanate is the pure methylene diphenyl isocyanate (MDI); however, in some cases TDI, PMDI and aliphatic isocyanates as hexamethylene diisocyanate (HDI), isophorone diisocyanate (IPDI) and methylene dicyclohexylisocyanate (H12MDI) are also used.

4 Chemical Recycling of Polyurethanes

As commented above, polyurethane is the sixth polymer most used with a production of approximately 12 million tons per year. As a direct consequence of their commercial success, a lot of wastes are generated, and their treatment is an environmental challenge. In the past, landfilling was the solution to the problem. However, there is little information about the behaviour of PU in landfills due to the large life period of the polyurethanes (>10 years) [14]. This fact, joined to the new environmental laws, is essential to develop environmental sustainable recycling processes. According to the standard ASTM D5033 [15], recycling processes can be classified in this way:

Primary recycling is "the processing of scrap plastic product into a product with characteristic similar to those of the original product".

Secondary recycling is "the processing of scrap plastic product into a product that has characteristics different from those of the original product".

Tertiary recycling is "the production of basic chemicals or fuels from segregated plastic scrap or plastic material that is part of a municipal waste stream of other source".

Quaternary recycling is "the useful retrieval of the energy content of scrap plastic by its use as a fuel to produce products such as steam, electricity and so forth".

Physical recycling processes include the primary and the secondary recycling. These kinds of processes do not modify polymer internal structure. In physical processes, polymer wastes are mechanically turned into flakes, granules or powder to be used in new material production. The main polyurethane physical recycling processes are:

Rebonding: Moulded polyurethane products made from pieces of chopped flexible polyurethane foam. It is applied to produce carpet underlay and sports mats [16].

Regrind or powdering: Polyurethane wastes are powdered and mixed with one of the virgin reagents (generally with the polyol up to 30%) to create a new polyurethane product [17].

Compression moulding: Polyurethane wastes are powdered and then subjected under high pressures and heat in a mould. It allows to obtain up to 100% recycled content [18].

These physical processes are successfully used with thermoplastic polymers, but, unfortunately, they are useless for the majority of the polyurethane specialties due to their thermostable nature. On the other hand, the chemical recycling processes allow to obtain basic hydrocarboned units known as monomers (tertiary recycling) that are able to be used as synthesis materials in chemical and petrochemical industry. This way, it is possible to achieve high value-added products [19].

Therefore, a deeper description of the main polyurethane chemical recycling processes is going to be done.

4.1 Hydrolysis

Hydrolysis was the first process developed to recycle polyurethane wastes in a chemical way, in particular flexible polyurethane foams. Ford Motor Company studied this process in the sixties. It consists on the reaction of the urethane wastes with water steam in a wide range of pressures and high temperatures. In the first stage of development, the hydrolysis process was carried out at 300°C and 15 atm, but the next tries were focused on more extreme conditions such as temperatures around 450°C and pressures about 50 atm [1]. The reaction between the polyurethane and the water allows to recover the polyol (Eq. 10):

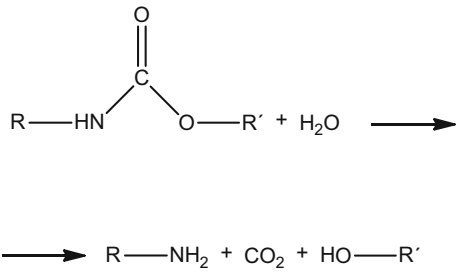

(10)

Hydrolysis studies by other authors, focused on the recovery and recycling of the polyol, demonstrated that steam temperatures around 288°C produced a polyol excellent for the synthesis of new PU foam for seat cushions when mixed with a 5% of virgin material. Higher temperatures provide a decrease in the polyol recovery yield, but polyols recovered at lower steam temperatures produce more unstable new PU foams [20]. Hydrolysis processes in supercritical water have been also described in the literature [21].

Gerlock et al. [22] described the hydrolysis process of polyether-based polyurethane foams at temperatures between 190 and 230°C yielded high-quality polyol, isomeric toluenediamines and carbon dioxide as primary products. Matuszak et al. [23] determined that polyurethanes are more susceptible to alkaline hydrolysis than to acidic one. Anon [24] also reported the recovery of expanded polyurethanes by steam hydrolysis. Campbell [20] reported polyurethane foam waste hydrolysis with dry superheated steam at atmospheric pressure and from 232 to 316°C. Foams with a replacement up to 20% were synthesised. Grigat [25] by means of an extruder developed a continuous method of hydrolytically reconverting shredded polyurethane foams.

Recently, Shi et al. [26] carried out several studies and stated that the increase of temperature and the presence of catalyst accelerate the hydrolysis reaction.

An improvement of the hydrolysis process is the hydroglycolysis, in which water and glycols are combined under softer operating conditions. Gerlock et al. [27] suggested that hydroglycolysis could be used to recover polyols from mixed and/or contaminated water-blown polyurethane wastes. Recently, Alavi Nikje et al. [28, 29] developed a hydroglycolysis process under microwave irradiation at atmospheric pressure and 160°C using mixtures of glycerine, sorbitol, water and sodium hydroxide as hydroglycolysis agent. Two phases were observed, the upper phase contained recycled polyol susceptible of being mixed with raw flexible polyol to synthesise new flexible polyurethane foams and the lower phase was a brown liquid containing aromatic amines that can be applied in rigid polyurethane foam formulations. It was also observed that, in order to produce high-quality recovered polyols, it is necessary to carry out a purification process. With this propose, Braslaw et al. [30] described the liquid–liquid extraction of the polyol obtained from base-catalysed hydroglycolysis of waste polyurethane foams. After this treatment, the recovered polyol could replace up to the 50% of the virgin polyol in PU foams synthesis.

It is really important to emphasise that hydrolysis has been only developed for the recycling of flexible polyurethane foam wastes. Flexible polyurethane foams hydrolysis processes have been scaled up to pilot plant, but they have not achieved the commercial scale [31] due to the high energy input required into the reactor [1].

4.2 Glycolysis

Glycolysis is the most widely used chemical recycling process for PU. It consists of a transesterification reaction, in which the ester group joined to the carbolinic carbon of the urethane is interchanged by the hydroxyl group of the glycol.

The main reaction that takes place is the following one:

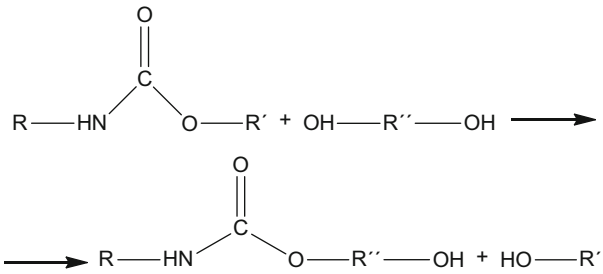

(11)

Nearly all types of catalyst have been used: alkaline hydroxides such as sodium hydroxide and potassium hydroxide [27], alkaline acetate such as potassium acetate [32], Lewis acids [33], amines such as diethanolamine [34], organometallic compounds such as titanium butoxide [35, 36], metallic octoates [37, 38] and stannous compounds such as stannous octoate [39, 40].

Polyurethane structure is not only formed by urethane units, but it is also compounded by other functional groups such as urea. These urea groups appear due to the amines formed in the gas formation reaction of the polyurethane synthesis (Eq. 2). In a following step, the amines may react with free isocyanate giving as a result a substituted urea (Eq. 3). Urea groups are also susceptible of the glycolysis process giving as a result a low-weight carbamate and an aromatic amine [41]:

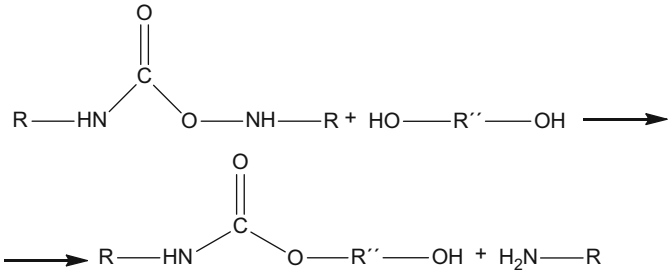

(12)

Furthermore, the urethane group may react with water giving as a result a hydrolysis reaction that would be a competitive reaction for the glycolysis one. The reaction is the following one:

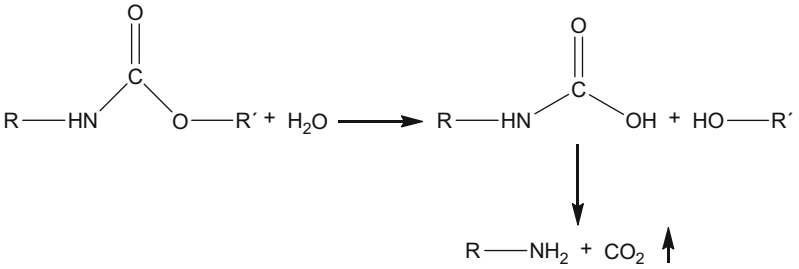

(13)

As can be observed, this reaction leads to the formation of a polyol and an unstable carbamic acid that at the reaction temperatures decarboxiles and leads to the formation of a secondary amine, while carbon dioxide is evolved [42].

What is more, the urethane group may react with amines (see Eqs. 12 and 13) to form a urea [41]. However, glycolysis is the main reaction since glycol is much abundant than amines in the reaction system.

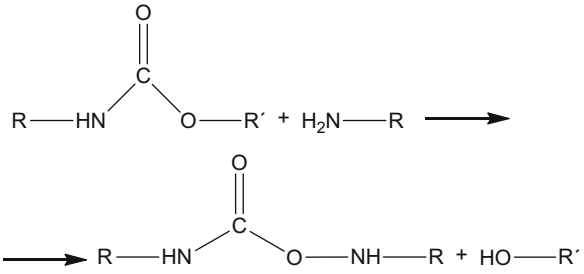

(14)

Finally, at the reaction temperatures, urethane may be degraded in a thermal way giving as a result carbon dioxide, amines and unsaturated compounds.

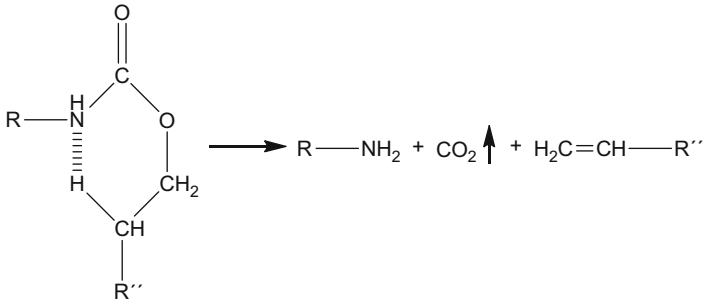

(15)

It is also really important to comment that with a large glycol excess, the reaction product splits in to two phases, where the upper layer is mainly formed by the recovered polyol and the bottom layer by the excess of glycolysis agent and reaction by-products. This process allows to recover the polyol with the highest quality in comparison to single-phase processes.

As has been commented before, glycolysis is the most important process to recover polyurethane wastes, and as a consequence, it is noteworthy to summarise the glycolysis advances depending on the polyurethane type treated. The types of polyurethane have been explained in Sect. 3 of this book chapter.

4.2.1 Elastomers

Borda et al. [34] described the glycolysis of elastomers based on polyether polyol and MDI. They employed ethylene glycol (EG), 1,2-propylene glycol (PG), triethylene glycol (TEG) and poly(ethylene glycol) (PEG) as glycols and diethanolamine (DEA) as catalyst. The reaction temperature described was 170–180°C, with a glycolysis agent:PU waste ratio of 2:1 and an DEA:ethylene glycol ratio between 1:1 and 1:9. A two-phase mixture was obtained where the upper liquid phase was the starting polyol. In another manuscript of these series, Borda et al. [43] stated that the obtained glycolysates could be used as components in the synthesis of urethane adhesives.

Wang et al. [44] described the glycolysis of thermoplastic polyurethane elastomers (TPU) based on 4,4′-diphenylmethane diisocyanate (MDI) and polyether polyol (PEG).

Diethylene glycol (DEG) and ethylene glycol (EG) were used as low-weight glycols, whereas ethanolamine (EA) and lithium acetate were employed as catalysts. The degradation reactions were carried out at 160–190°C. They found that, by using a 9/9/2 ratio of DEG/EG/EA, the decomposition products were completely separated into two layers, where the upper one was the polyether polyol.

4.2.2 Coatings

Datta et al. [45] proposed the glycolysis of polyurethane coating wastes with mass ratios of scrap polyurethane coating to glycol ranging from 2:1 to 10:1, potassium acetate (KAc) and sodium hydroxide (NaOH) as catalysts and reaction temperatures from 190 to 240°C. It would allow to obtain recycled semi-products, the so-called urethane oligomers that have the properties and structures suitable for using to manufacture new polyurethane products.

4.2.3 Rigid Foams

Simioni et al. [46] described the glycolysis of rigid polyurethane foams using dipropylene glycol as low-weight glycol and potassium acetate as catalyst. A single-phase product was obtained that could be used in the synthesis of new rigid urethane foams.

Xue et al. [47] obtained by means of glycolysis of rigid polyurethane foam wastes, using diethylene glycol (DEG) as glycol and monoethanolamine (EA) as catalyst, a glycolysate that could be applied as hardeners for epoxy adhesives

Morooka et al. [48] carried out the glycolysis of rigid PU foam wastes that came from refrigerators using diethylene glycol (DEG) as solvent and BaO or diethanolamine (DEA) as catalysts. They stated that up to a 10% wt of the glycolysate obtained can be added to raw virgin polyol to produce a new rigid polyurethane foam with similar thermal conductivities and compressive strengths as those of a standard foam. Murai et al. [49] employed dipropylene glycol and tetraethylene glycol as glycols and KOH and dibutyltindilaurate as catalysts and a reaction temperature from 170 to 200°C.

Nikje et al. [50] carried out glycolysis reactions of rigid polyurethane foams by means of microwave irradiation at atmospheric pressure. In microwave heating, the energy can be applied directly to the sample rather than conductively, via the vessel. They used diethylene glycol (DEG) as low-weight glycol, and as catalysts, they tried various ones such as sodium hydroxide (NaOH), potassium hydroxide (KOH), sodium acetate (NaAc) and zinc acetate (ZnAc2). The reactions were carried out with a glycolysis agent/PU foam ratio of 2:1 and at different microwave powers of 180, 300, 450, 600 and 900 W. They found that in the absence of catalyst, the transesterification reaction is difficult to carry out, even under high MW powers. The optimal catalysts were sodium hydroxide (NaOH) and potassium hydroxide (KOH), whereas the worse one was the zinc acetate (ZnAc2) considering that the glycolysis reaction time was very high when using this catalyst. The single-phase products were obtained and used to be mixed with virgin polyol up to 40% by weight to synthesise new rigid foams.

4.2.4 Flexible Foams

Modesti et al. [51] carried out glycolysis reactions of flexible PU foams based on polyether polyol (mostly triol) and toluene diisocyanate (TDI). Ethylene glycol (EG) was used as low-weight glycol, and the temperature reaction was 190°C. When a foam:EG ratio of 1:1 was used, a product containing two liquid phases and a solid one, with ratios, respectively, of 44:54:2 w:w:w was achieved. The upper phase was mostly the original polyether polyol, and the bottom one consisted of mostly aromatic products with traces of polyether solve in EG, whereas the solid phase was formed mostly by ureas, but also by carbamates. On the other hand, when a foam:EG ratio of 4:1 was used the quantity of this solid phase was increased. However, when hexamethylenetetramine (HMTA) was used, a two liquid-phase system was achieved without solid phase obtaining this way a glycolysate that presented a low free-amine content (lower than 100 ppm).

Wu et al. [32] also reported glycolysis reactions of flexible PU foams under atmospheric pressure and isothermal condition (220°C) using diethylene glycol (DEG) and potassium acetate (KAc) as solvent and catalyst, respectively. They stated that the optimal concentrations of DEG and KAc are about 150 and 1%wt of the PU flexible foam and that glycolysis reaction was concluded when reaction time was 90 min. The glycolysate obtained presented a high hydroxyl value, and, therefore, the authors proposed a distillation process in order to reduce it and obtain a final product susceptible of being used in the synthesis of new PU products.

Borda et al. [34] investigated the glycolysis of flexible PU foams in the temperature range from 170 to 180°C. The low-weight glycols used were EG, 1,2-propylene glycol, triethylene glycol and poly(ethylene glycol), whereas diethanolamine was used as catalyst. A split-phase product was achieved where the recovered polyol was the main component of the two-phase liquid mixture and could be used as an industrial adhesive [43].

Nikje et al. [52] carried out microwave-assisted split-phase glycolysis reactions of flexible PU foam wastes. They used glycerine, instead of a low-weight glycol as reported by other authors, and sodium and potassium hydroxides as catalysts. Reactions were carried out at various temperatures of 160, 180, 200 and 220°C. They observed that the higher the reaction temperature, the lower the reaction time. Nevertheless, it is important to take into account that at a temperature greater than 220°C, unwanted secondary reaction rates become competitive with respect to the glycolysis transesterification reaction, producing a glycolysate with high amine content [35, 53]. Nikje et al. reported that with the use of microwave irradiation, a glycolysis reaction 20–30 times faster than with conventional heating methods can be achieved. In another article of these series, Nikje et al. [54] evaluated DEG-pentaerythritol (PER) as a new solvent-reactant mixture by a traditional split-phase glycolysis process with sodium hydroxide as catalyst. The four hydroxyl functional groups contained in the pentaerythritol would accelerate the degradation of urethane structure. However, Nikje et al. stated that the higher the ratio DEG/PER, the higher the upper phase quantity and, as a consequence, the

recovered polyol content. Furthermore, the upper phase was reused in the synthesis of flexible foams, and the lower phase was used in rigid foams production. In another work, Nikje et al. [55] carried out glycolysis reactions by means of microwave irradiation using pentaerythritol in combination with glycerine and sodium hydroxide, as a PU bond degradation reagent environmentally sustainable, with the aim of obtaining an amine-free recovered polyol. They observed that the higher the pentaerythritol content in the composition of degradation solvent, the greater the reaction times.

Datta et al. [56] reported the glycolysis reaction of elastic PU foams using 1,6-hexanediol (HDO) as low-weight glycol and potassium acetate (KAc) as catalyst. Datta and his colleagues carried out the glycolysis reactions in the temperature range 230–245°C with a PU foam:HDO mass ratios of 1:1, 2:1, 4:1, 6:1, 8:1 and 10:1 and an amount of catalyst of 0.5% by weight with respect to the PU foam mass. They observed that at PU foam:HDO ratios of 1:1, 2:1 and 4:1, a single-phase liquid product was obtained. On the other hand, the reaction ran as "split-phase" glycolysis when PU foam:HDO ratios of 6:1, 8:1 and 10:1 were used. They also reported that the higher the PU foam:HDO ratio, the lower the hydroxyl number value and the higher the molecular weight of the obtained glycolysates. Besides, they found that the reaction time was a function of the PU foam:HDO mass ratio. This way, the reaction time was in the range 9–70 min. Furthermore, the glycolysates obtained with the highest PU foam:HDO mass ratios were successfully used as the only polyol components in polyurethane elastomers synthesis. In another work, Datta [57] studied the effect of using different low molecular weight glycols in the structure of the glycolysates obtained. They used ethylene glycol (EG), propane 1,3 diol (PG), butane 1,4 diol (BDO), pentane 1,5 diol (GP) and hexanediol HDO with a PU foam:HDO mass ratios of 10:1 that had been demonstrated as the optimal one in the previously commented manuscript [57]. FTIR spectra results demonstrated the presence of similar chemical substances in glycolysates irrespective of the glycolysis agent used. Moreover, the higher the molecular weight of the glycol used is, the higher the molecular weight of the glycolysate obtained is and the lower the polydispersity and the hydroxyl number are.

A complete development of the flexible foams glycolysis has been performed by the group of Professor De Lucas at the University of Castilla-La Mancha. This work has achieved the whole recovery of the flexible foams components. Firstly, this group carried out a study to determine the optimal glycol to be used in the split-phase chemolysis reaction of flexible PU foams [58]. In this work, diethanolamine (DEA) was used as catalyst and monoethylene glycol (MEG), diethylene glycol (DEG), 1,2-propylene glycol (MPG) and dipropylene glycol (DPG) as low-weight glycols. It was found that propylenic glycols increased the solubility between phases, worsening the phase separation. On the other hand, MEG provided a slow degradation rate, while DEG showed a good degradation capacity of the urethane chain requiring lower time to achieve their complete degradation and obtaining a polyol with properties similar to those of the raw one.

Once selected DEG as glycol, Molero et al. [38] carried out a study to determining the optimal catalyst to be used in the glycolysis process, trying with different octoate salts. Stannous octoate yielded the greatest quality for the recovered polyol as well as the highest decomposition rate. The next step was to determine the optimal conditions to carry out the glycolysis reaction using DEG and the stannous octoate [40]. It was reported that the glycolysis reactions must be carried out with a catalyst concentration in the glycolysis agent of 1.3% by weight since for higher concentrations, the improvement in the reaction rate was unnoticeable, approaching zero-order behaviour with respect to the catalyst content. The optimal mass ratio of glycolysis agent to PU foam was determined to be between 1.125:1 and 1.5:1, observing that a larger ratio did not produce a significant improvement of the process [59], while it would imply larger volume equipment requirements and larger amounts of bottom phase to be recycled by distillation. On the other hand, ratios lower than 1:125:1 provided low polyol content in the upper phase due to the presence of non-dissolved portions of the PU scraps in the reaction media, causing stirring problems. As a result, a proper phase separation could not be achieved, and not only the reaction proceeded slowly but also the polyol concentration was lower than using other ratios. The optimal temperature was found to be around 190°C because lower temperatures provided a slow recovery process and a low polyol percentage in the upper phase, while higher temperatures caused a diethylene glycol-excessive evaporation and an increase of the secondary reactions extension, reducing the purity of the recovered polyol.

Furthermore, Molero et al. [60] proposed a purification process of the recovered polyols. It consisted of a liquid extraction with a slightly acid pH solvent. It was found that a temperature of 60°C or higher and a minimum solvent/upper phase ratio of 1:1 provided a purified polyol with properties susceptible of being foamed [61]. Amounts up to 25% by weight of recovered polyol could be applied instead of the raw one without any relevant change in the required physical properties of commercial PU foam [61].

Finally, to get a complete utilisation of the foam wastes, Simón et al. [62] developed a process for the valorisation of the glycolysis bottom phase. It consisted of recycling the excess of glycol employed in the split-phase glycolysis of PU wastes by means of distillation under reduced pressure. It was found that 50 m bar was the most appropriate pressure. On the other hand, the residue of the distillation column, containing the isocyanate part of the glycolysis by-products that had been considered as a dangerous waste up to now, was characterised showing properties similar to the toluenediamine (TDA) commonly used as initiator in the synthesis of new polyols. Thus, this vacuum residue was used as initiator for polyol synthesis. As a final point, rigid PU foams with suitable technical properties were successfully foamed in a TDA-polyol-based formulation using this synthesised polyol.

A deep revision of the literature relative to polyurethane glycolysis has been carried out. Finally, with the goal of providing a general overview of the polyurethane glycolysis, Table 3 summarises the main parameters involved in the chemolysis process.

Table 3 Global overview of the polyurethane glycolysis

Polyurethane type	Catalyst	Glycol	Glycol: PU by weight	Temperature (°C)	Bibliography
Elastomer	EA	Monoethylene glycol	2:01	160–190	[34, 43, 44]
	DEA	Monopropylene glycol			
	LiAc	Triethylene glycol			
		Poly(ethylene glycol)			
		Diethylene glycol			
Coating	KAc	Monoethylene glycol	1:2–1:10	190–240	[45]
	NaOH				
Rigid Foam	EA	Diethylene glycol	2:01	170–200	[46–50]
	DEA	Dipropylene glycol			
	BaO	Tetraethylene glycol			
	KOH				
	NaOH				
	Dibutyltindilaurate				
	NaAc				
	$ZnAc_2$				
Flexible Foam	KAc	Monoethylene glycol	1:10–1.5:1	160–245	[32, 34, 35, 38, 40, 43, 51–62]
	DEA	Diethylene glycol			
	TiBut	Monopropylene glycol			
	LiOct	Dipropylene glycol			
	SnOct	Triethylene glycol			
		Poly(ethylene glycol)			
		Glycerine			
		Butane 1,4 diol			
		Pentane 1,5 diol			
		1,6-hexanediol			

As can be observed in Table 3, the catalysts involved in the glycolysis process of polyurethanes are amines such as ethanolamine and diethanolamine; alkaline acetates such as lithium, potassium, and sodium acetates; hydroxides such as sodium hydroxide and potassium hydroxide; organometallic compounds such as titanium

butoxide; metallic octoates such as lithium octoate; and stannous compounds such as stannous octoate.

Regarding the glycol employed, monoethylene glycol (MEG), monopropylene glycol (MPG), diethylene glycol (DEG) and dipropylene glycol (DPG) are some of the most widely used, mainly DEG.

Table 3 also shows the most common glycolysis agent:PU ratios employed in the transesterification reaction. It can be observed that ratio glycolysis agent:PU is generally higher than one with the aim of getting a proper split-phase glycolysis and as a result a high-quality glycolysate, susceptible of being used in the synthesis of a new PU product.

With respect to the optimal temperature to carry out the glycolysis reaction, Table 3 shows a range between 160 and 240°C because lower temperatures provide a slow recovery process and a low polyol percentage, while higher temperatures may cause glycol-excessive evaporation and an increase of the secondary reactions extension. As shown in Table 3, glycolysis temperature is depending on the kind of PU treated.

4.3 Aminolysis

Aminolysis consists of a transesterification reaction, in which the ester group joined to the carbolinic carbon of the urethane is interchanged by the amine group (Eq. 16).

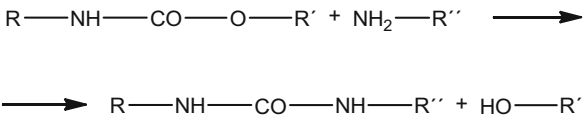

(16)

In the aminolysis process, polyurethanes are cleaved with mono- and dialkanolamines, and the recycling reaction is carried out with monoethanolamine, diethanolamine and dimethylethanolamine at 80–190°C. The reaction generally proceeds under inert atmosphere and accelerated by catalysts [63] such as sodium hydroxide, aluminium hydroxide and sodium methoxide.

Kanaya et al. [58] reported the split-phase aminolysis of methylene diphenyl isocyanate (MDI)-based polyurethane flexible foams using alkanolamines in the absence of catalyst at 150°C. After the decomposition reaction, two layers were obtained in the same way that commented for the split-phase glycolysis. The upper phase was mainly formed by the recovered polyether polyol, and the lower one was composed by methylene diphenyl amine (MDA) and alkanolamine derivatives such as 2-hydroxyethyl carbamic acid ester.

It is worthy to point out that MDA is a monomer used for poly(*p*-diphenyl-methylterephthalamide) synthesis [64]. This polymer is an aromatic polyamide

generally used to improve several properties of some polymers, such as Nylon 6 and Kevlar. Furthermore, MDA can be used as a hardener for epoxy resin [65].

Kanaya et al. [66] also reported that the decomposition process of polyurethane foam by alkanolamines was probably not aminolysis but alcoholysis. The reaction scheme proposed is shown in Eq. 17.

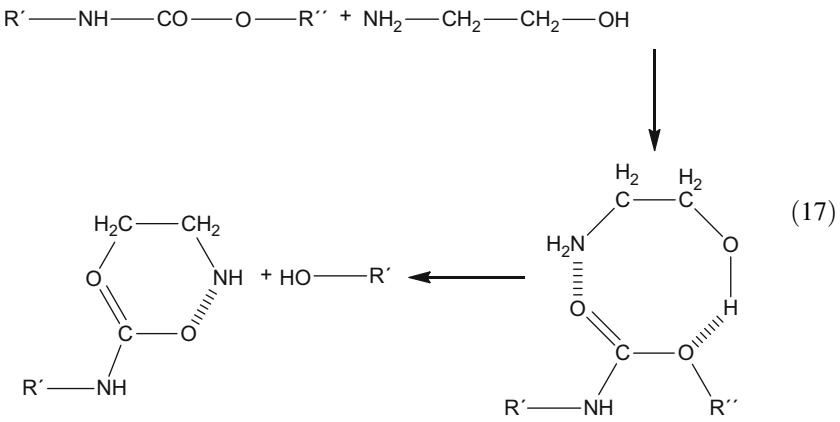

(17)

On the other hand, aminolysis of rigid foams have been also investigated by several authors. Chuayjuljit et al. [67] carried out aminolysis reactions with rigid polyurethane foam scraps using diethylenetriamine (DETA) as degrading agent and sodium hydroxide (NaOH) as catalyst. Previously, Xue et al. [65] had reported the improvement in the reaction rate and in the reduction of the product viscosity when diethylenetriamine (DETA) was used instead of using other common aminolysis reagents such as triethylene tetramine (TETA) and tetraethylene pentamine (TETP). Xue et al. carried out the aminolysis reaction without the presence of any catalyst. However, Van der Wal [68] found that potassium hydroxide could catalyse the depolymerisation of PU foam when alkanolamine was used as a degrading agent.

Taking all things into consideration, Chuayjuljit et al. [67] decided to study the possibility of carrying out aminolysis reactions of rigid PU foam scraps using DETA as aminolysis agent and an alkaline hydroxide, as sodium hydroxide (NaOH), as catalyst. Aminolysis reactions were carried out at 180°C with a rigid PU foam:DETA ratio of 2:1. It was reported an improvement in the recovery process when the NaOH amount was increased since NaOH not only acts as a catalyst for aminolysis but also reacts with urethane linkage and urea linkage of PU foam to form related amines and polyols according to reactions (18) and (19).

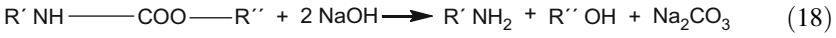

(18)

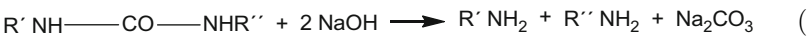

(19)

These reactions were proposed by Van Der Wal for the PU depolymerisation using KOH as a catalyst [68]. Chuayjuljit et al. reported [67] that the main aminolysis products were methylene diphenyl amine (MDA), low molecular weight urethane oligomers and other chemicals. It was also stated that the greater the amount of NaOH used, the lower the quantity of MDA obtained due to the aminolysis of PU foam by MDA catalysed with NaOH.

4.4 Phosphorolysis

Phosphorolysis is a reaction analogous to hydrolysis in which esters of phosphonic or phosphoric acids perform in a similar way to that of water with the formation of a phosphate. Phosphorolysis let to obtain glycolysates that can be used in the synthesis of polyurethanes with flame retardant properties due to the phosphate functionality of the recovered product.

An extensive work has been performed by Troev et al. in the study of the phosphorolysis of different polyurethane plastics.

Initially, Troev et al. developed a phosphorolysis process for flexible polyurethane foams based on toluene diisocyanate (TDI) and polyester polyol [69]. As degradation reagents, phosphonic acid diesters such as dimethyl phosphonate and diethyl phosphonate were used. The degradation reactions were carried out at 160°C, with a phosphonic acid dialkyl ester/flexible PU foam ratio of 3:1 and in the absence of a catalyst. After removing the unreacted dimethyl phosphonate, two liquid layers were obtained. It was found that the upper layer was mainly formed by the recovered polyol with the phosphate group functionality and the bottom one consisted mostly of aromatic products. Then, the study was extend to flexible polyurethane foams based on toluene diisocyanate (TDI) but now with polyether polyols, using dimethyl phosphonate and the same reaction conditions [70]. Again, two layers were obtained: the upper one containing phosphorus oligomers and a bottom one mainly formed by phosphorus-containing aromatic compounds.

Further, the phosphorolysis of elastomers was also studied, in particular with microcellular elastomers. Initially, Troev et al. [71] carried out phosphorolysis reactions of microcellular elastomers based on diphenylmethane diisocyanate (MDI) and polyester polyol. In this case, reactions were performed using dimethyl phosphonate at 142°C, in the absence of catalyst and with a ratio dimethyl phosphonate/microcellular elastomer of 2:1. In a further work, Troev et al. [72] changed the phosphorous compound, using triethyl phosphate and tris (2-chloroethyl) phosphate as degradation agents and increase the reaction temperature up to 180°C and a degradation agent/microcellular elastomer ratio up to 3:1, obtaining similar results. Using this last degradation agent:microcellular elastomer ratio, diethyl phosphonate and tris(1-methyl-2-chloroethyl) phosphate as

degradation agents and at 170°C, Troev et al. obtained phosphorus- or phosphorus- and chlorine-containing oligomers due to the use of a degradation agent containing chloro as tris(1-methyl-2-chloroethyl) phosphate [73].

It is really important to remark that the global aim of all the phosphorolysis glycolysates is the possibility of being used directly or after chemical treatment for the synthesis of polyurethanes with flame retardant properties or as additives to improve the fire resistance of several polymers.

5 Future Challenges

From the deep revision about the different polyurethane chemical recycling processes carried out in this chapter, it can be highlighted the glycolysis as the most important technology all over the world to recover PU wastes.

The main advantage of the glycolysis is its versatility since it has been studied for a lot of polyurethane specialties, including flexible and rigid foams and also the denominated CASES. On the contrary, the hydrolysis has just been applied for flexible PU foams, due to its high energy requirements; the aminolysis processes have been only described for flexible and rigid foams and phosphorolysis technologies for microcellular elastomer and flexible foams.

Despite the bigger development of the glycolysis, there is still a big amount of PU specialties in which it has not been assayed. On the other hand, considering that the flexible foams mean about the 45% of the total polyurethane production, the more immediate challenge is the extension of the glycolysis to all this PU type. Up to now, all the publications developed only describe the glycolysis of conventional flexible PU foams (80% of the total production of the flexible foams) synthesised only with a flexible polyether polyol, but there is no report about works performed with conventional foams synthesised with blends of flexible polyether polyols with polymeric ones.

Another interesting future challenge would be to study the glycolysis of flexible viscoelastic foams since they mean the 15% of the total flexible PU foam production, and there is also no description in bibliography about the glycolysis of these kinds of foams.

Finally, the biggest challenge would be the extension of the glycolysis to the treatment of foam blends since this would avoid the necessity of a selective collection or a previous separation step.

References

1. Behrendt G, Naber BW (2009) The recycling of polyurethanes (review). J Univ Chem Technol Metallurg 44(1):3–23

2. Herlinger H (1970) Struktur und Reaktivit der Isocyante (Structure and reactivity of isocyanate). Stuttgart
3. Woods G (1982) Flexible polyurethane foams: chemistry and technology. Applied Science Publishers, Barking, Essex
4. Wu J, Wang Y, Wan Y, Lei H, Yu F, Liu Y, Chen P, Yang L, Ruan R (2009) Processing and properties of rigid polyurethane foams based on bio-oils from microwave-assisted pyrolysis of corn stover. Int J Agric Biol Eng 2(1):40–50
5. Ullmann's Encyclopedia (2005) Polyurethanes. Wiley, Weinheim. doi:10.1002/14356007.a21_665.pub2
6. Singh SN (2001) Blowing agents for polyurethane foams, vol 12, Number 10. Rapra Review Reports. Report 142
7. Zevenhoven R (2004) Treatment and disposal of polyurethane wastes: options for recovery and recycling. Energy Engineering and Environmental Protection Publications Espoo 2004. Report TKK-ENY-19
8. Oertel G (1985) Polyurethane handbook. Hanser Publishers, Munich
9. Tan S, Abraham T, Ference D, Macosko CW (2011) Rigid polyurethane foams from a soybean oil-based polyol. Polymer 52:2840–2846
10. O'Connor JM (2012) Polyurethane coatings and elastomers. American Chemistry Council. Center for the Polyurethanes Industry. September 24–26, 2012. Atlanta, Georgia
11. De SK, White JR (eds) (2001) Rubber technologist's handbook. Rapra Technology, Shawbury
12. O'Connor JM (2012) Polyurethane sealants, adhesives and binders. American Chemistry Council. Center for the Polyurethanes Industry. September 24–26, 2012. Atlanta, Georgia
13. DIN 16920 (1981) standard published by Deutsches Institut Fur Normung E.V. (German National Standard)
14. Bastian C (1994) A European strategy for recycling. Paper 50 presented at UTECH 94 Conf. The Hague
15. ASTM D5033-00 Standard Guide for Development of ASTM Standards Relating to Recycling and Use of Recycled Plastics (Withdrawn 2007)
16. ISOPA (2001) Recycling and recovering polyurethanes: rebonded flexible foam. Brussels
17. ISOPA (2001) Recycling and recovering polyurethanes: regrinding/powdering. Brussels
18. ISOPA (2001) Recycling and recovering polyurethanes: compression moulding. Brussels
19. Hicks DA, Krommenhoek M, Soderberg DJ, Hooper JFG (1994) Polyurethanes recycling and waste management. Paper 51 presented at UTECH 94 Conf. The Hague
20. Campbell GA, Meluch WC (1976) Polyurethane foam recycling – superheated steam hydrolysis. Environ Sci Tech 10(2):182–185
21. Dai Z, Hatano B, Kadokawa J, Tagaya H (2002) Effect of diaminotoluene on the decomposition of polyurethane foam waste in superheated water. Polym Degrad Stabil 76(2):179–184
22. Gerlock JL, Braslaw J, Mahoney LR, Ferris FC (1980) Reaction of polyurethane foam with dry steam: kinetics and mechanism of reactions. J Polym Sci Pol Chem 18(2):541–557
23. Matuszak ML, Frisch KC, Reegen SL (1973) Hydrolysis of linear polyurethanes and model monocarbamates. J Polym Sci Pol Chem 11(7):1683–1690
24. Anon (1976) Recovery of expanded polyurethanes by steam hydrolysis. Mater Plast Elastomeri 3:202–205
25. Grigat E (1978) Hydrolysis of plastics wastes. Kunstst Ger Plast 68(5):12–13
26. Shi Y, Zhan X, Zhang Q, Chen F (2009) Interfacial hydrolysis of isocyanate in monomer miniemulsion. Chem React Eng Technol 25:88
27. Gerlock J, Braslaw J, Zimbo M (1984) Polyurethane waste recycling 1. Glycolysis and hydroglycolysis of water-blown foams. Ind Eng Chem Proc Des Dev 23(3):545–552
28. Nikje MMA, Nikrah M, Mohammadi FHA (2008) Microwave-assisted polyurethane bond cleavage via hydroglycolysis process at atmospheric pressure. J Cell Plast 44(5):367–380
29. Nikje MMA, Mohammadi FHA (2009) Sorbitol/glycerin/water ternary system as a novel glycolysis agent for flexible polyurethane foam in the chemical recycling using microwave radiation. Polim Polym 54(7–8):541–545

30. Braslaw J, Gerlock JL (1984) Polyurethane waste recycling 2. Polyol recovery and purification. Ind Eng Chem Proc Des Dev 23(3):552–557
31. Weigand E, Raβhofer W (1999) Present state of polyurethane recycling in Europe. In: Advances in Plastic Recycling, vol 1: recycling of polyurethanes. Technomic Publishing CO, Lancaster
32. Wu CH, Chang CY, Cheng CH, Huang HC (2003) Glycolysis of waste flexible polyurethane foam. Polym Degrad Stabil 80(1):103–111
33. Bauer G (1996) Recycling of polyurethanes. In: Weigand E (ed) Recycling and recovery of plastics. Hanser Publishers, München, pp 518–537
34. Borda J, Päsztor G, Zsuga M (2000) Glycolysis of polyurethane foams and elastomers. Polym Degrad Stabil 68(3):419–422
35. Simioni F, Modesti M, Rienzi SA (1987) Polyol recovery from elastomer polyurethane waste. Cell Polym 6(6):27–41
36. Simioni F, Modesti M (1991) Controlled degradation of polyurethane for recycling. Mater Sci Eng 2:127–144
37. Molero C, de Lucas A, Rodríguez JF (2006) Recovery of polyols from flexible polyurethane foam by "split-phase" glycolysis with new catalysts. Polym Degrad Stabil 91:894–901
38. Molero C, de Lucas A, Rodríguez JF (2009) Activities of octoate salts as novel catalysts for the transesterification of flexible polyurethane foams with diethylene glycol. Polym Degrad Stabil 94(4):533–539
39. Molero C, de Lucas A, Romero F, Rodríguez JF (2009) Glycolysis of flexible polyurethane wastes using stannous octoate as the catalyst. J Mater Cycles Waste Manage 11(2):130–132
40. Simón D, García MT, de Lucas A, Borreguero AM, Rodríguez JF (2013) Glycolysis of flexible polyurethane wastes using stannous octoate as the catalyst: study on the influence of reaction parameters. Polym Degrad Stabil 98(1):144–149
41. Modesti M (1996) Recycling of polyurethane polymers. Advances in urethane science and technology, vol 13. Technomic Publishing CO., Lancaster
42. Ullmann's Encyclopedia of Industrial Chemistry (2003). 6th edition. Wiley-VCH, Weinheim
43. Borda J, Rácz A, Zsuga M (2002) Recycled polyurethane elastomers: a universal adhesive. J Adhes Sci and Technol 16(9):1225–1234
44. Wang X, Chen H, Chen C, Li H (2011) Chemical degradation of thermoplastic polyurethane for recycling polyether polyol. Fiber Polym 12(7):857–863
45. Datta J, Haponiuk JT (2008) Advanced coating of interior of tanks for rising environmental safety - novel applications of polyurethanes. Pol Marit Res Special Issue 2008:8–13
46. Simioni F, Bisello S, Tavan M (1983) Polyol recovery from rigid polyurethane waste. Cell Polym 2(4):281–293
47. Xue S, He F, Omoto M, Hidai T, Imai Y (1993) General purpose adhesives prepared from chemically decomposed waste rigid polyurethane foams. Kobunshi Ronbunshu 50(11):847–853
48. Morooka H, Nakakawaji T, Okamoto S, Araki K, Yamada E (2005) Chemical recycling of rigid polyurethane foam for refrigerators. Polym Prepr 54(1):1951
49. Murai M, Sanou M, Fujimoto T, Baba F (2003) Glycolysis of rigid polyurethane foam under various reaction conditions. J Cell Plast 39(1):15–27
50. Nikje MMA, Nikrah M (2007) Chemical recycling and liquefaction of rigid polyurethane foam wastes through microwave assisted glycolysis process. J Macromol Sci Pure 44(6):613–617
51. Modesti M, Simioni F, Munari R, Baldoin N (1995) Recycling of flexible polyurethane foams with a low aromatic amine content. React Funct Polym 26:157–165
52. Nikje MMA, Nikrah M, Haghshenas M (2007) Microwave assisted "split-phase" glycolysis of polyurethane flexible foam wastes. Polym Bull 59:91–104
53. Scheirs J (ed) (1998) Polymer recycling. Wiley, UK, pp 339–377
54. Nikje MMA, Garmarudi AB (2010) Regeneration of polyol by pentaerythritol-assisted glycolysis of flexible polyurethane foam wastes. Iran Polym J 19(4):287–295

55. Nikje MMA, Mohammadi FHA (2010) Polyurethane foam wastes recycling under microwave irradiation. Polym-Plast Technol 49:818–821
56. Datta J, Rohn M (2007) Thermal properties of polyurethanes synthesized using waste polyurethane foam glycolysates. J Therm Anal Calorim 88(2):437–440
57. Datta J (2012) Effect of glycols used as glycolysis agents on chemical structure and thermal stability of the produced glycolysates. J Therm Anal Calorim 109:517–520
58. Molero C, de Lucas A, Rodríguez JF (2006) Recovery of polyols from flexible polyurethane foam by "split-phase" glycolysis: glycol influence. Polym Degrad Stabil 91(2):221–228
59. Molero C, de Lucas A, Rodríguez JF (2008) Recovery of polyols from flexible polyurethane foam by "split-phase" glycolysis: study on the influence of reaction parameters. Polym Degrad Stabil 93(2):353–361
60. Molero C, de Lucas A, Rodríguez JF (2006) Purification by liquid extraction of recovered polyols. Solv Extr Ion Exch 24(5):719–730
61. Molero C, de Lucas A, Romero F, Rodríguez JF (2008) Influence of the use of recycled polyols obtained by glycolysis on the preparation and physical properties of flexible polyurethane. J Appl Polym Sci 109(1):617–626
62. Simón D, Borreguero AM, de Lucas A, Molero C, Rodríguez JF (2013) Novel polyol initiator from polyurethane recycling residue. J Mater Cycles Waste Manage. doi:10.1007/s10163-013-0205-y
63. Sheratte MB (1978) Process for converting the decomposition products of polyurethane and novel compositions thereby obtained. US Pat 4,110,266
64. Higashi F, Taguchi Y, Kokubo N, Ohta H (1981) Effect of initiation condition on the direct polycondensation reaction using triphenyl phosphite and pyridine. J Polym Sci Pol Chem 19 (11):2745–2750
65. Xue S, Omoto M, Hidai T, Imai Y (1995) Preparation of epoxy hardeners from waste rigid polyurethane foam and their applications. J Appl Polym Sci 56(2):127–134
66. Kanaya K, Takahashi S (1994) Decomposition of polyurethane foams by alkanolamines. J Appl Polym Sci 51(4):675–682
67. Chuayjuljit S, Norakankorn C, Pimpan V (2002) Chemical recycling of rigid polyurethane foam scrap via base catalyzed aminolysis. JOM 12(1):19–22
68. Van Der Wal HR (1994) New chemical recycling process for polyurethane. J Reinf Plast Compos 51:87–96
69. Troev K, Tsekova A, Tsevi R (2000) Chemical degradation of polyurethanes: degradation of flexible polyester polyurethane foam by phosphonic acid dialkyl esters. J Appl Polym Sci 78 (14):2565–2573
70. Troev K, Tsekova A, Tsevi R (2000) Chemical degradation of polyurethanes II. Degradation of flexible polyether foam by dimethyl phosphonate. Polym Degrad Stabil 67:397–405
71. Troev K, Atanasov VI, Tsevi R, Grancharov G, Tsekova A (2000) Chemical degradation of polyurethanes. Degradation of microporous polyurethane elastomer by dimethyl phosphonate. Polym Degrad Stabil 67:159–165
72. Troev K, Atanasov VI, Tsevi R (2000) Chemical degradation of polyurethanes II. Degradation of microporous polyurethane elastomer by phosphoric acid esters. J Appl Polym Sci 76:886–893
73. Troev K, Grancharov G, Tsevi R (2000) Chemical degradation of polyurethanes III. Degradation of microporous polyurethane elastomer by diethyl phosphonate and tris(1-methyl-2-chloroethyl) phosphate. Polym Degrad Stabil 70:43–48

Polystyrene Wastes: Threat or Opportunity?

Cristina Gutiérrez, Juan C. de Haro, M. Teresa García, Ignacio Gracia, Antonio de Lucas, and Juan F. Rodríguez

Abstract The recycling of polystyrene (PS) wastes could be considered even economically feasible if, apart from the intrinsic environmental benefits, the wastes are transformed into high-added value products with enhanced properties. In this work, the development of an integral recycling process for polystyrene wastes by means of a new and cost-effective alternative to traditional plastic recycling techniques has been proposed. The methodology consists of the selective dissolution of the plastic wastes with suitable natural solvents (terpene oils) to get a volume reduction without degradation of the polymer chains. The employment of a natural solvent for the treatment of polystyrene wastes transforms the process in an environmentally friendly technology. High pressure CO_2 is proposed to perform the solvent removal in order to avoid the formation of undesirable by-products and to improve the quality of the recycled plastic, since it acts as a physical foaming agent. The use of CO_2 is very attractive because it makes the polymer–solvent separation easier, improves the mass transfer into the highly swelled polymer bulk and allows the tuning of the final properties of the recovered PS. A controlled foaming of the polystyrene–solvent mixtures can be easily carried out at moderate temperatures and pressures by exploiting the advantages that provide the recycling with a natural solvent, obtaining completely free of solvent PS foams. Adjusting the

C. Gutiérrez, J.C. de Haro, M.T. García, I. Gracia, and A. de Lucas
Department of Chemical Engineering, Faculty of Chemical Science and Technology, University of Castilla-La Mancha, Avda. Camilo José Cela 12, 13071 Ciudad Real, Spain
e-mail: jcarlos.haro@uclm.es

J.F. Rodríguez (✉)
Faculty of Chemical Science and Technology, Institute of Chemical and Environmental Technology (ITQUIMA). University of Castilla-La Mancha, Avda. Camilo José Cela 12, 13071 Ciudad Real, Spain
e-mail: juan.rromero@uclm.es

E. Jiménez et al. (eds.), *Environment, Energy and Climate Change I: Environmental Chemistry of Pollutants and Wastes*, Hdb Env Chem (2015) 32: 261–286,
DOI 10.1007/698_2014_279, © Springer International Publishing Switzerland 2014,
Published online: 23 August 2014

working conditions, the structure of the foams produced can be tailored enhancing the initial properties of the PS wastes.

Keywords Polystyrene, Recycling, Supercritical CO_2, Terpene oils

Contents

1 Plastics

History has been usually categorised according to the materials that the man used for making his tools and his basic facilities. The Stone Age, the Iron Age and the Bronze Age are best recognised. During the last century, a new class of material has been established; it has not only challenged the older material for their uses but has also made possible the creation of new products. Without plastics, it is difficult to conceive our everyday life [1]. The term plastic is derived from the Greek word *plastikos*, meaning fit for moulding. An adequate definition of plastic is difficult to achieve, but on a regular basis, plastic materials are synthetic or semi-synthetic organic solid widely used in the manufacture of industrial products. Attending to their molecular structure, they are mainly polymer of high molecular weight. The word polymer literally means many units (*mer*), in which a chemical unit (monomer) is repeated itself a very large number of times to create the polymer [2, 3].

Nowadays, the majority of commodity plastics are derived from gas or from crude oil which, after their processing and refining, monomers are generated. Then, they are used in the manufacture of polymers. There are as many processing routes as the kinds of polymers, and several routes could be used to obtain one polymer (Fig. 1).

The huge variety of plastics shown in Fig. 1 makes essential its classification in order to group by properties and applications. The most commonly used classification is based on thermoplastics (80–90%) and thermosets (10–20%) since they constitute the majority of the market accounting for around 75% of the total polymer consumption. Thermoplastics are capable of changing shape on application of force and retaining this shape on removal of force (stress produces a nonreversible strain). They are softened when heated above the glass transition temperature (T_g) and can be reshaped and will toughen in this form upon cooling.

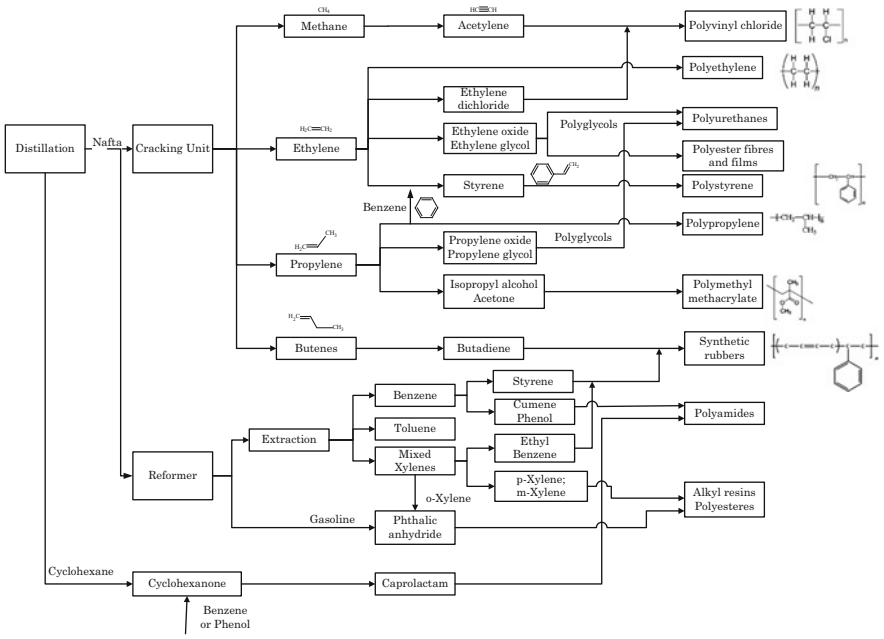

Fig. 1 Conventional production routes for polymer raw materials to commodity products

Multiple cycles of heating and cooling can be repeated without severe damage, allowing reprocessing and recycling since they are generally linear or branched polymers which present few chemical interactions between chains. On the other hand, thermosets do not soften on heating, but elevated temperatures produce chemical reactions that could harden the material into an infusible solid. Generally, they are more brittle and insoluble in organic solvents than thermoplastics because thermosets present a three-dimensional structure obtained by chemical cross-linking produced after or during the processing. By this reason, thermosets cannot tolerate repeated heating cycles as thermoplastics can [4].

According to their demand, the most representative thermoplastics are polypropylene (PP), low-density polyethylene (LDPE), high-density polyethylene (HDPE), polyvinyl chloride (PVC), polyethylene terephthalate (PET) and polystyrene (PS). The thermosets are largely represented by amino resins, polyurethanes, phenolics, polyesters, alkyd resins and epoxy resins (Fig. 2).

Figure 2 represents the most representative thermoplastics in Europe during the year 2012. Polypropylene, polyethylene, polyvinyl chloride and polystyrene are considered as the most demanded commodity plastics in Europe.

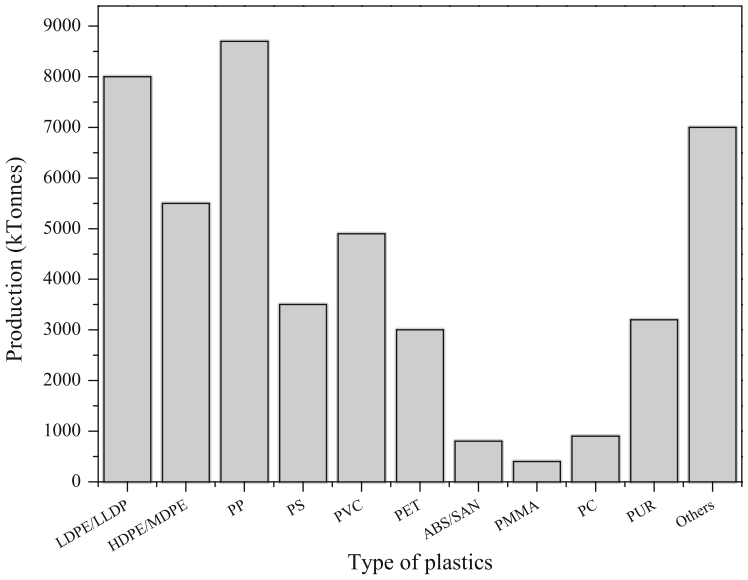

Fig. 2 The most representative thermoplastics attending to their demand in Europe 2012 (Figure taken from http://www.plasticseurope.es) [6]

1.1 Plastic Production and Demand

In the second half of the twentieth century, plastics became one of the most universally used materials all over the world due to their excellent characteristics. Today, plastics are used in an increasing number of applications being essential to our modern economy [5]. Among the most important properties are versatility, low price, lightweight, durability and strength. Due to their excellent characteristics, the plastic industry has benefited from 50 years of growth with a year-on-year expansion of 8.7% from 1950 to 2012. The production and consumption of plastic materials have been growing steadily. For instance, the production of plastics increased to 288 million tonnes from 2011 to 2012, meaning an increment of 2.8%. Nevertheless, in Europe and according to the general economic crisis, plastic production decreased by 3% from 2011 to 2012 (Fig. 3) [6].

The first plastic producer country around the world is China, followed by Europe, the United States, Canada and Mexico (NAFTA). European countries produced 50 Mt in 2012 and the main producers were Germany, Italy and France. The United Kingdom and Spain got the fourth and fifth positions, respectively.

In Europe, packaging purposes are the most important application sector for the plastic industry and constitute 39.4% of the total plastic demand. In the second position, building and construction sector reaches 20.3% followed by the automotive sector, electrical and electronic applications. Other application sectors such as

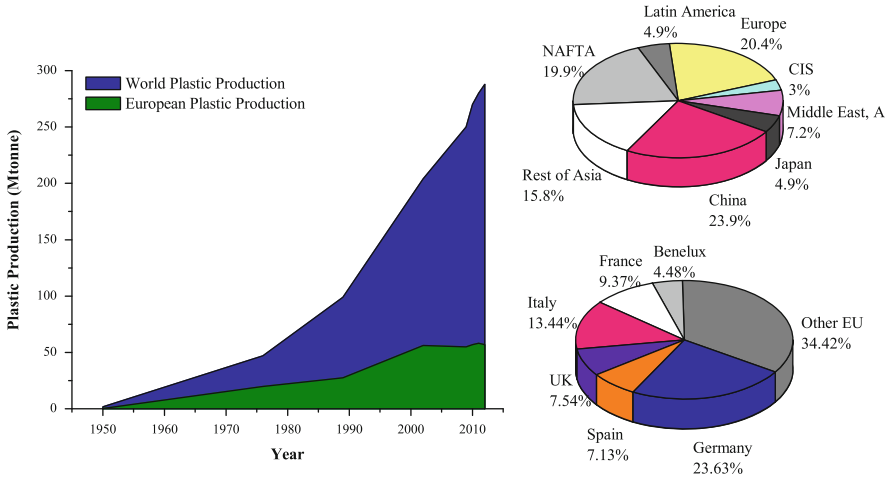

Fig. 3 Plastic production from 1950 to 2012. The production includes thermoplastics, polyurethanes, thermosets, elastomers, adhesives, coating, sealants and fibres. But PET, PA and polyacryl fibres are not included [6] (Figures inspired by http://www.plasticseurope.es)

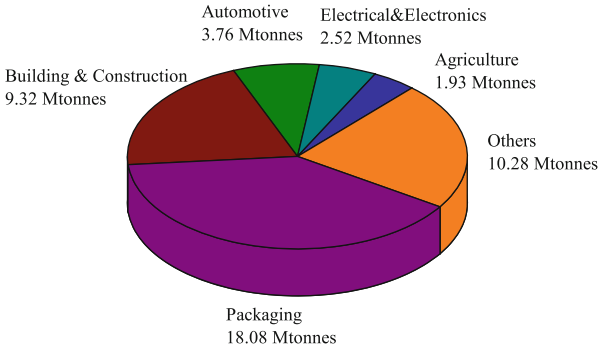

Fig. 4 Main sectors of application of the plastic industry in Europe 2012 (Figure taken from http://www.plasticseurope.es)

appliances, household and consumer products, furniture and medical products comprise a total of 22.4% of the European plastic demand (Fig. 4).

1.2 Plastic Wastes

According to the data showed in the previous section, it is obvious that plastics are used in our daily lives in a great number of purposes, but at the end of their useful life, polymers enter in waste streams as either post-consumer waste or industrial scrap.

Household, distribution and industry sectors are the main suppliers of the wastes. But also, the automotive sector, the electrical and electronic, as well as building and

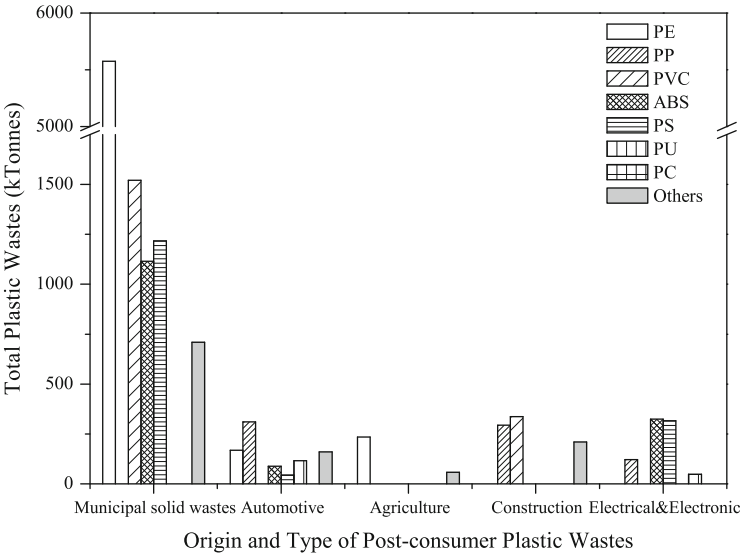

Fig. 5 Classification of the amount of plastics produced as a function of the origin and the type of polymer in Europe

construction provide important amounts of plastic wastes. The composition of the plastic waste streams depending on the sources and the types of polymer is shown in Fig. 5.

Plastic waste has been involved in the municipal solid waste considerably, concentrated in packaging, films, covers, bags, containers and so on that are widely used in our daily lives. As shown in Fig. 5, municipal solid wastes involved the largest volume of plastic wastes. Particularly, packaging materials make up the largest contribution to polymer wastes in the stream, and they are mainly constituted by LDPE/LLDPE, PP, HDPE, EPS/PS, PVC and PET. The main reason is that polyolefins used for packaging materials are often discarded after a single use, which results in a large amount of polymer waste [7].

In the automotive sectors, plastics have increasingly been used to replace metals for many components because of their greater processability, lighter weight and corrosion resistance. The percentage by weight of polymers in the average European car has risen in the last years, in contrast with packaging applications. Polymers found in automotive wastes are PP, ABS, HDPE, PP, PU and PVC.

The plastic wastes coming from the construction are mainly PVC and thermosetting resins together with acrylics or PP. The nature of the plastics generated in the large industry is mainly PE from the sheet used exclusively for all secondary packaging.

LDPE is the predominant plastic from the agricultural plastic wastes. And eventually, electrical and electronic wastes are a significant contributor of ABS poly(acrylonitrile-co-butadiene-co-styrene), polycarbonate and modified PP.

From the comparison of Figs. 2 and 5, significant differences between the plastic demand and plastic waste generation can be observed. The most demanded plastic in Europe in 2012 was polypropylene, while the polyethylene was the most common plastic present in waste streams. Although the vast majority of the industrial wastes are recycled with the processing, the rests are usually sent for reprocessing. On the other hand, the majority of post-consumer plastic waste reaches the environment, and hence the emphasis in polymer waste management is on this type of waste stream.

1.3 Plastic Waste Management

European waste policy has evolved the municipal solid wastes through "environmental actions plans and a framework of Legislation" for the last 30 years (European Commission 2010). The target of the environmental policy is the reduction of waste negative impacts. In 2005, a long-term strategy on waste management began a new period of EU waste policy. The new plan originated from the EU's Sixth Environment Action Programme has been shown in the Waste Framework Directive (WFD-2008/98/EC). The Directive (WFD-2008/98/EC) is focused on the encouragement of a recycling society with the targets for "EU Member States to recycle 50% of their municipal waste and 70% of construction waste by 2020" [8]. Waste management legislation in Europe differs in each country; however, basic principles and restrictions are in accordance with the European Landfill Directive and other important EU legislations in the field of waste reduction.

Regardless, since the last years, a positive trend in the recovery and recycling of plastics in Europe is growing. In 2012, post-consumer plastic waste reached 25.2 Mt, of which 62% of plastics were recovered and only 38% ended up in landfills. It is important to highlight that almost 70% of plastic packaging wastes were recovered, 34.5% went through energy recovery (incineration or additive as refuse derived fuel), 34.2% were mechanically recycled, and only 0.7% went to feedstock recycling [6].

It should be outlined that the recycling of plastic wastes is attractive not only environmentally but also from an economic point of view due to their high potential value [9]. The European Commission marked a shift away from thinking about waste as an unwanted trouble to perceive it as a valued resource (European Commission 2010). Nevertheless, the recycling will be only economically advantageous if the design of the process consider the amount of energy necessary to produce the virgin polymer plus the energy to dispose equal to the energy to recover the waste plastic plus the energy during the reprocessing. The high cost would be balanced by the reduction cost of landfilling and of course by the social benefit [10] since the recycling of plastics greatly contributes to the preservation of the natural resources.

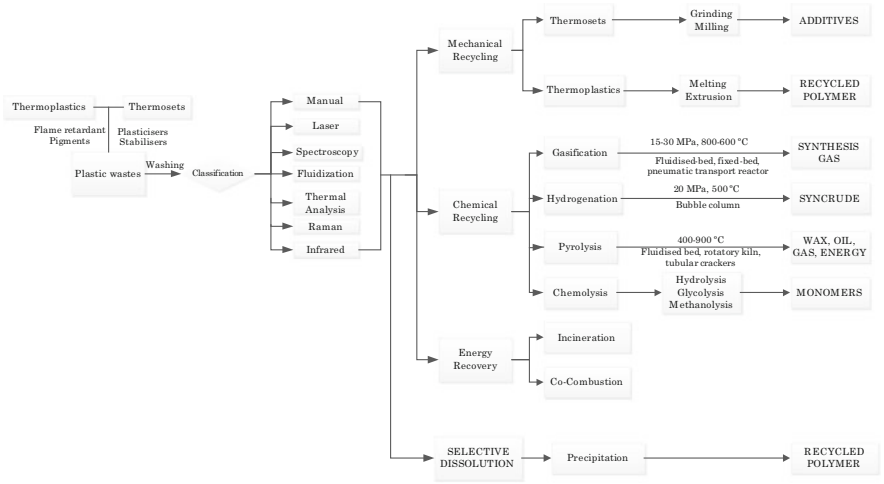

Fig. 6 Routes for the management of the plastic wastes: from the sorting to the recycling

According to the European policy, recycling methods are being established as priority techniques for the recovery of polymers from plastic wastes. But the recycling of materials requires the separation of the different polymers in order to recover plastics of acceptable quality. Plastic recycling streams are made of dirty mixed polymers including dyes, fillers, flame retardant and other additives [9]. The use of polymers in different market sectors complicates the identification and separation of waste streams because their use in one sector does not guarantee that they will appear as waste in the same sector [4]. By these reasons, the separation of different polymers by type is crucial. Moreover, the differences among the melting temperature and some chemical incompatibilities hinder the mixture of plastics previously to its classification, especially if the target recycled product should present high value [11].

Adequate and cost-effective techniques are demanded for the identification of plastics (Fig. 6) since the recycling processes are priority [12]. Separation is further complicated by the current design of products in which polymers are blended with other materials and polymers are currently sorted and separated manually or mechanically, which means its high cost and inefficiency [13]. Considerable work has been undertaken to develop automated technologies that can separate mixed waste streams according to polymer type or to remove foreign matter (contaminants) from them [14]. Nevertheless, plastic exhibits similar properties which make the automatic classification a challenge.

Figure 6 shows some of the developed techniques for the identification and sorting of different types of plastics. The substantial development occurred in the last decade has achieved the classification of plastics even if they contain only small amounts of other types of polymers [15]. Choi et al. [16] proposed gravity separation based on air or centrifugal force. Although, the most studied techniques are

related with spectroscopy, laser [17], Raman [18], infrared [19] or fluorescence [9], FT-Raman has been proved to be the most rapid and selective technique to recognise the most usual polymers. But generally, the combination of different analytical techniques is required to sort perfectly the polymers from the plastic waste streams. This fact makes the recycling technologies very expensive, and their efficiency is always limited by the feed composition. By these reasons, the choice of the most appropriate sorting technology will depend on the complexity of the polymer mixture, its physical form, the quality or the additives and/or the contaminants [4].

The proposal of a general methodology for the classification of plastic wastes is still nowadays a challenge. There is no clear relationship between quantities of plastics produced and plastic residues generated, because of the gap between production and disposal, which depends mainly on the lifespan of each product. Post-consumer plastic waste may spring from a host of products or applications, each with differing life cycles, and therefore, they should be treated individually. While containers and packaging waste generally have a lifespan under a year, durable and nondurable plastics can reach a lifespan estimated at 5 years for transportation applications; 10 years for furnitures, housewares, electric and electronics; and 50 years or more for building and construction materials [19]. Generally and according to the mentioned data, packaging dominates the waste generated from plastics, covering 62.2% of the total. Other applications like building and construction, electrical and electronic products and agriculture count for 5 till 6% each. It should be more appropriate to divide in new categories the waste streams in which plastics may be found as it was shown in Fig. 5.

Years of research, study and testing have resulted in a number of treatment, recycling and recovery methods that could be feasible and economically advantageous. Important efforts are made to manage the plastic products efficiently at the end of their service life; new routes are improving constantly and fewer of them are ending up in landfills.

1.4 Plastic Waste Recycling

In Fig. 6, plastic waste management can be performed mainly by three different ways: mechanical recycling, chemical recycling and energy recovery [20]. A fourth approach was defined by Scott [21] as the biological recycling, but only the biodegradable plastic wastes are capable of being recycled following this methodology. By this reason, this alternative is not generally considered as a regular recycling way [10]. Each method provides a unique set of advantages that make it particularly beneficial for specific applications [22]. Next, a brief summary of the different alternatives is shown.

1.4.1 Mechanical Recycling

Mechanical recycling is the recovery of materials from wastes while maintaining the polymers' molecular structure using mechanical techniques: grinding, washing, separating, drying, re-granulating and compounding.

Separation of different polymers is particularly important for mechanical recycling because processing mixed materials would produce recycled products of low quality, which could only be used in a limited number of applications. Hence, mechanical recycling is really best suited to clean plastic wastes such as packaging materials. Mechanical recycling of mixed waste necessarily starts with the manual sorting process because it can only be performed on single-polymer plastics, and the mixed or contaminated wastes cannot be recycled following this method. This fact implies high costs and low-quality products when the separation is not as efficient as is required.

Depending on the type of polymer, the mechanical recycling follows different processes. Thermosets are grinded and particulated for its reuse as filler in new materials since they cannot be remelted. They are generally used as additives to improve the properties of other polymers providing better values of modulus, elongation at break or impact strength. On the other hand, thermoplastics are remelted, extruded and pelletised to be sold as a raw material for further processing. Although thermoplastics are soften above their glass transition temperature, degradation and heterogeneity of wastes should be considered. Polymerisation reactions are irreversible, but the heat provided during the mechanical recycling could cause photo-oxidation. Consequently, length or branching of polymers could occur, and the polymer would present worse properties in comparison with the virgin plastic as a result of the ageing. Despite this, mechanical recycling has been the oldest and most extended practice by common plastic manufacturers [23].

1.4.2 Chemical Recycling

Chemical recycling is based on the conversion of polymers into monomers (monomer recycling) or useful petrochemicals (feedstock recycling). Generally, polyolefin plastics with a massive production have been subjected to be recycled chemically to produce a mixture of hydrocarbons that could be useful as fuel [22, 24]. Several processes are included in the chemical recycling and the most relevant are explained below (Fig. 6).

Gasification is the partial oxidation of hydrocarbons in the presence of low oxygen levels. The process is typically carried out at temperatures from 800 up to 1,600°C, pressures of 15–30 MPa and in the presence of a gasifying agent (air, oxygen, steam, fuel gas). The main products of gasification are synthesis gases [25].

Once plastic wastes are depolymerised, they can be hydrogenated to produce bitumen and a synthetic crude oil, known as syncrude, which presents a very high-added value. The syncrude is refined for its use in the petrochemical industry.

Pyrolysis consists of thermal decomposition of the plastic wastes at temperature from 350 to 700°C in the absence of oxygen or other gasifying gases. The polymers decompose to their monomers, oligomers and other organic substances that can be collected separately and used as a feedstock or for energy generation [26].

Finally, chemolysis is a treatment which uses solvolytic processes (hydrolysis, glycolysis or alcoholysis) to recycle and convert plastics into their basic monomers for repolymerisation into new plastics. This method allows up to 90% of the plastic (by weight) to be reused, but it works best with homogeneous plastic types.

1.4.3 Energy Recovery

When the recycling of plastic wastes is not feasible, they could be used in energy recovery due to its high calorific values. The high calorific value of plastics underscores the need for an alternative energy recovery technology that is affordable, efficient, safe and user-friendly. The two ways to obtain energy from plastic wastes are the incineration and the co-combustion. Incineration without energy recovery would be also possible but is not acceptable from the sustainability point of view because it only reduces the amount of wastes, but waste valuable non-renewable resources, and it cannot be defined as a recycling option. Furthermore, the incineration of polymer provokes important social opposition [4].

Despite the fact that plastic recycling is increasing and many different alternatives are proposed, important efforts are still required to recycle efficiently the plastic wastes. Mechanical recycling is only economically feasible if the plastic wastes are classified in a single-polymer stream, and energy recovery must also separate PVC from the rest of the polymers due to the formation of dioxins. The fact that most of the recycling options require a severe previous classification of polymers by type is a challenge that nowadays constrains the recycling. Consequently, the increase of the costs of these processes entails that the recycling is established as a priority option, but not the top priority.

2 Polystyrene Production and Wastes

The research work of our group in this field during the last years has been focused on the recycling of polystyrene wastes because in the last years, it has been considered a plague on the environment taking more space in landfills than paper. The first commercial production of polystyrene began in the early 1930s by the Farben Company in Germany. Polystyrene is the polymerisation product of styrene monomer, which is a colourless liquid with a strong odour derived from petroleum and natural gas by-products (Fig. 1) [27]. Vinyl monomers may be polymerised via free-radical polymerisation, a type of chain growth; nevertheless, due to the reactivity of the monomer, it is often necessary to add an inhibitor to stabilise the monomers and prevent premature radical formation.

Generally, polystyrene is a clear, hard, glassy material with a bulk density between 0.94 and 1.05 g/cm^3. Its purpose is mainly in packaging, food and beverage containers and building and insulation applications. It is widely used since it is very cheap, light and versatile; also, it presents low dielectric constant and low thermal conductivity.

Unfortunately, due to its resistance to biodegradation, PS plastic wastes have become one of the major problems to the environment. PS is made from petroleum, a non-renewable resource, through a very complicated process. From oil to monomer, monomer to polymer and polymer to final product (Fig. 1), not only are massive amounts of energy and resource consumed but also serious environmental contamination during the productive processes [28, 29]. The Environmental Protection Agency (EPA) established PS as the fifth largest source of hazardous wastes. Furthermore, according to Kyoto protocol, PS foams were banned to the ozone-depleting CFC gases used as blowing agents. Nowadays, several governments are considering the extension of the ban on PS foam containers because of its impact on marine pollution. Scientists are concerned that plastic debris in the ocean can transport toxic substances which may end up in the food chain causing potential harm to the ecosystem and human health (UNEP 2011).

Regarding the aforementioned restrictions, the traditional disposal of plastic wastes in landfills is not an option due to the high costs, legislative pressures and public concern on resource conservation. Particularly, New York City officials are considering a ban on foam containers of polystyrene, which will take effect in July 2015. However, PS should be considered a raw material with high potential value and its recycling a priority, not only for the environmental but also from an economic point of view. Nevertheless, its excellent properties entail some environmental inconveniences. It is extremely lightweight, and due to the high volume/weight ratio, it does not look economically viable to store or transport nor is an attractive material for collection, taking up huge volume in landfills. But if PS is landfilled, there is an important loss of the potentially valuable materials. Its versatility means a wide variety of applications which often makes the PS wastes a mixture of different grades and types of polymer. This fact could result in variable and low-quality recycled products, which limit the further uses of the recovered material.

On the other hand, PS wastes (especially expanded polystyrene, EPS) are frequently contaminated by food, and they are generally not recycled because clean wastes are required in order to recover high-quality plastics. It should be emphasised that recycled plastics should not present a lower grade than the "virgin" polymer because it could prevent its use in some applications, such as that for food packaging. Eventually, it should be underlined that PS generally is a one-time use material and its cost per unit is around cents. The world's oversupply of this virgin polymer, due to the excess of production capacity, has driven its price down. So it is a challenge the recycling of PS wastes to achieve a high market value product from an easy and cheap process since the costs for collecting, sorting, cleaning and reprocessing often become excessive [30]. The main idea to overcome the economic boundaries is the recovery of materials with enhanced properties and at the

same time with new uses [10]. Mechanical recycling has been selected as the most adequate way to recover styrenic plastic wastes from packaging applications. But during the remelting and compression of PS, their chemical structure, long-term stability or mechanical properties could be altered [31]. Although the recycling of the cited polymer has been highly promoted, nowadays, the rate of PS recycling is very low in comparison to the recycling rate of all other plastic wastes.

2.1 Polystyrene Recycling

According to the different aspects about the recovery of PS wastes, all the scientific efforts should be focused on the recycling since it allows saving energy and raw materials. This fact is crucial due to the existing situation that Europe relies upon imports of scarce resources (European Commission, 2010).

New processing schemes should be explored in order to reduce the cost of the traditional and expensive recycling processes. Dissolution and shrinking has been proposed as one of the cheapest and most efficient methods for the recycling of PS [32–34]. The selection of the most suitable solvent is the crucial step for the selective recycling of polymers by dissolution [35]. The main advantages of the dissolution of polymeric wastes are shown below:

- The dissolution of PS in a suitable solvent will cause considerable volume reduction (it could be achieved with a volume reduction of more than 100 times).
- Any insoluble contaminants will be dissolved and they could be removed by filtration, obtaining a cleaner polymer that could be reprocessed.
- The selective dissolution allows the separation of plastics from other types of waste and non-soluble polymers depending on their chemical nature. For instance, a solvent can be used to dissolve selectively one polymer at a temperature, while others remain insoluble.
- The polymer does not suffer further degradation, unless heat is used for the dissolution of the plastic wastes.

In view of these numerous advantages, the design of a process for the recycling of PS wastes by dissolution can be performed. The dissolution of PS wastes has been studied but focused on the thermal recycling (pyrolysis) [36]. With this aim, Zhang et al. [37] proposed the use of biodiesel as a solvent to obtain a solution with a high specific heat; Kodera et al. [38] developed a bench scale process to combine PS and the solvents derived from the pyrolysis of their own wastes; Karaduman et al. [39] studied the thermal degradation of PS in aliphatic, cyclic and aromatic solvents. And recently, Kim et al. [40] employed automobile lubricating oil wastes as solvent to swell PS wastes observing improved heat transfer. The heat of combustion of PS is approximately 41 MJ/kg, comparable to the traditional value for oil. In a properly designed combustion device, complete combustion could be achieved resulting in water, carbon dioxide and trace levels of ash [41].

The use of these solvents has been focused on the dissolution of PS wastes in low-cost solvents but with high specific heat in order to be pyrolysed. Nevertheless, after the pyrolytic treatment, only the energy is recovered but not the polymer. However, it can be checked that the concept of dissolution could be useful to propose new methodologies for the recycling of PS wastes.

2.1.1 Recycling of Polystyrene Wastes by Dissolution in Terpene Oils

According to the literature, aromatic solvents are efficient for the solubilisation of PS, but they are not environmentally friendly and would make the further application of the recycled polymer difficult. The development of a recycling technology must consider the global benefit, sense and coherence of the process; by this reason, the screening of the solvents should be carried out according to the principles of the green chemistry [42]. The replacement of aromatic solvents and/or lubricating oils by natural ones, such as terpene oils, could transform the dissolution in an environmentally friendly technology. Several researches have checked the viability of terpenes to solubilise PS [33, 34, 43–46].

Terpenes are natural compounds originated mainly from plants and containing molecule part similar to the isoprene subunit; by this reason, they are also denoted as isoprenoids. They are included in numerous plants and flowers that smell pleasantly, taste spicy or exhibit pharmacological activities. By these reasons, they have been used throughout history for a broad variety of purposes including perfume, medicine and flavouring [46]. There are more than 30,000 terpenes defined in the literature, which present the general structure shown below (Fig. 7).

In nature, terpenes are found mainly as hydrocarbons, alcohols, aldehydes or ketones [47]. In accordance with the wide variety of structures presented by terpenes, the most suitable solvents to carry out the dissolution of PS should present similar structures to the traditional aromatic solvents. By this reason, monoterpenes were selected the most suitable.

Monoterpenes containing between 10 and 16 carbon atoms are derivatives from 2,6-dimethyloctane. Some of the most well-known monoterpenes are α-/β-myrcene, geraniol, *o*-/*m*-/*p*-cymene, linalool, α-/β-phellandrene, terpinolene, α-/γ-terpinene, limonene, cymene, etc. They are present in basil, bay, hops, roses, lemons, oranges, lavender, mandarins, eucalyptus or orchids, among others. Therefore, it implies that they can be obtained from renewable sources.

The feasibility of the recycling process could be achieved if the terpene solvent solubilise selectively the PS, but the rest of the polymers in the waste stream remain

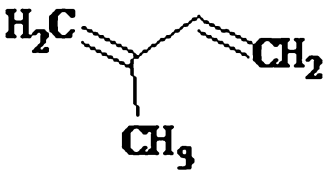

Fig. 7 2-Methyl-1,3-butadiene or isoprene

insoluble. An initial approach could be carried out theoretically according to Hildebrand theory. Hildebrand theory proposed that polymers will be soluble in those solvents whose solubility parameters (δ) are similar. The calculation of δ could be carried out by approximated or group contribution methods [35] although most of the solubility parameters of typical solvents are summarised in the literature [48].

They are the numerical expression of the popular quotation "like dissolves like". A first screening could be performed according to the chemical structure of polymers and solvents. In the case of PS, solvents which exhibit similar solubility parameters will present low tendency to form hydrogen bonds and relatively low polarity. But also, solubility behaviour of polymers could be predicted by graphical methods. Crowley et al. developed a three-component graph using the Hildebrand parameter, a hydrogen-bonding number and the dipole moment. The markers represent the intersection of the cited values. The ability of solvents to dissolve a polymer is indicated by the proximity between the polymer and the studied solvent. The solubility of PS in terpene oils was studied and results are shown in Fig. 8.

In the depicted diagram, the solubility parameters of PS is placed in the centre of the sphere of radius δ_h. If the solvent parameters remain inside the sphere, terpene is considered as a good solvent, whereas if the solvent parameters remain outside, it may be assumed that the studied terpene will not dissolve the polymer [49]. In Fig. 9, the most suitable solvents to perform the recycling of PS by dissolution are *p*-cymene, limonene, γ-terpinene, α-phellandrene and α-pinene.

The solubility of PS in the studied terpenes was determined experimentally to check the feasibility of the theoretical methods for the prediction of the polymer dissolution. Table 1 shows the values of solubility of PS in a set of terpene oils at 25°C.

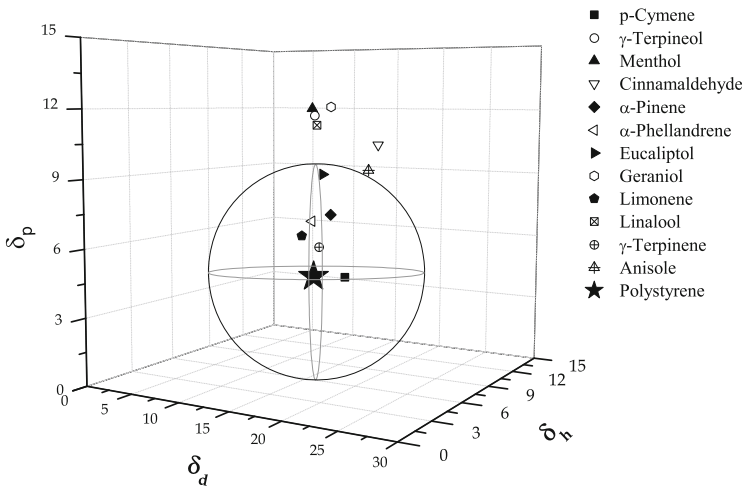

Fig. 8 Prediction of PS solubility in terpene oils according to Hildebrand parameters

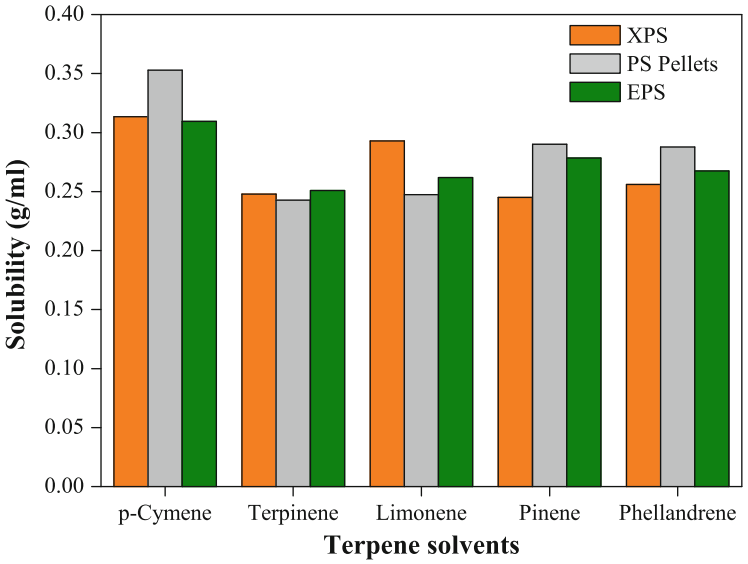

Fig. 9 Influence of the processed on the solubility of PS and PS wastes in terpene oils at 25°C

According to Table 1, the most suitable solvent to carry out the dissolution process agrees with the predicted theoretically (Fig. 9). γ-terpinene and p-cymene are the most suitable solvents to carry out the dissolution process, because they present the greatest solubility values. Moreover to dissolve the PS easily, a good solvent to carry out its recycling should show high volatility, which allows its removal from the polymer. Also, it is also appreciated that the selected terpenes present low cost, low toxicity and easy availability, which are also the appreciated properties [50]. Nevertheless, the strong interactions between PS and some of the cited solvents (those who exhibited high solubility values) could prevent its complete removal from the polymer-rich solution [51, 52]. According to the described reasons, the most suitable terpene oils for the recycling of PS wastes are p-cymene, γ-terpinene, limonene, α-pinene and α-phellandrene.

PS is processed in different ways to adapt the market needs. Generally, PS wastes can be found as expanded (EPS) or extruded (XPS) polystyrene, which provide a wide applicability field. The processing of polymers could affect to their dissolution in terpene oils since besides the molecular weight of the polymer, the dissolution process can also be affected by the chain chemistry, composition and stereochemistry [53]. The dissolution of a polymer into a solvent is not immediate, and it involves two transport processes, namely, solvent diffusion and chain disentanglement. A comparison between the solubility of pure PS (in pellets) and real wastes is shown in Fig. 9.

Figure 9 shows similar values of PS solubility independently of the processing of polymer wastes. The molecular weight of the pure polymer and the wastes was higher than 100,000 g/mol (typically used in the plastic industry [54]), and above

Table 1 Experimental solubility of PS in terpene oils at 25°C

Solvent		Solubility (g/mL)	Solvent		Solubility (g/mL)
p-Cymene	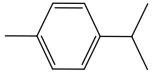	0.3529	α-Terpineol	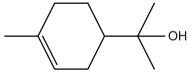	0.0063
Anisole	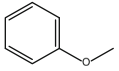	0.2578	α-Pinene	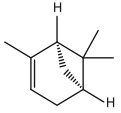	0.2901
Cinnamaldehyde	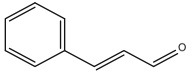	0.1957	α-Phellandrene	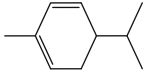	0.2879
Linalool	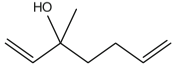	0.0059	Geraniol	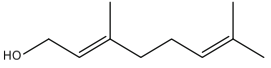	0.0029
γ-Terpinene	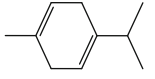	0.2427	D-Limonene	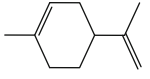	0.2473
Eucalyptol	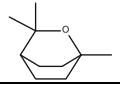	0.2977			

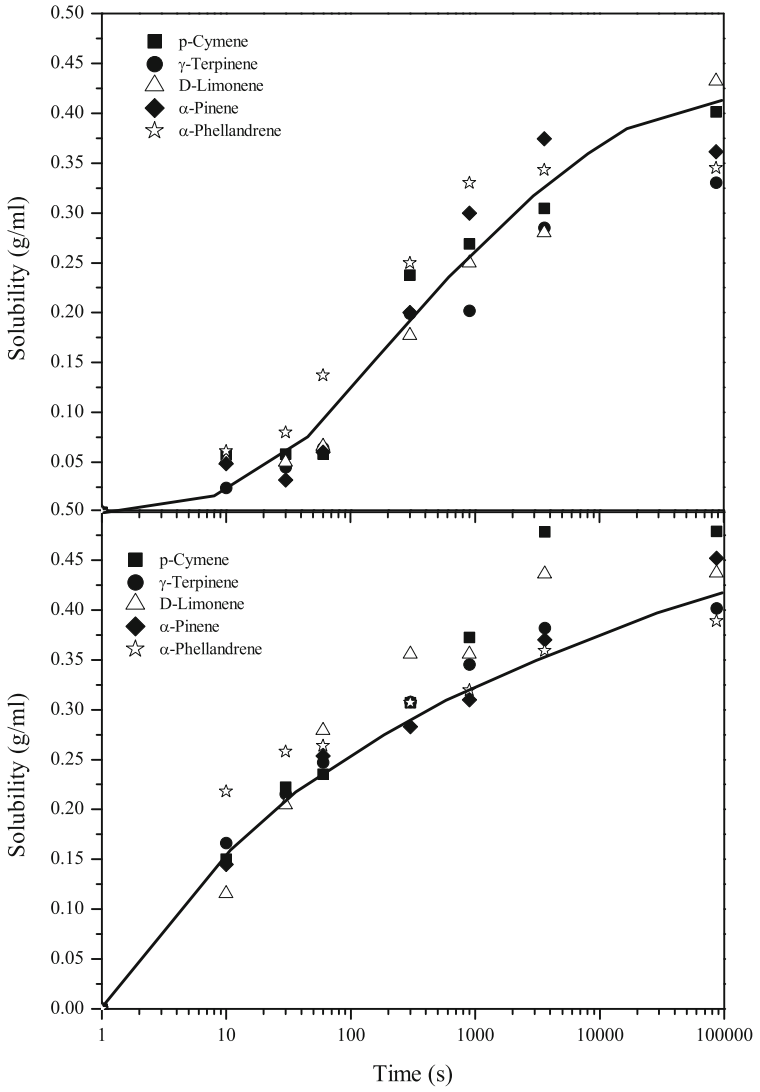

Fig. 10 Time influence in PS pellet solubility (*upper*) and XPS waste solubility (*below*)

this value, the solubility was not influenced by the type of processing. Although the values of solubility were similar in the case of the wastes and the pure PS, it is remarkable that the dissolution of the PS scraps was faster than PS pellets. Figure 10 shows the evolution of the concentration of PS and XPS solutions as a function of time.

The tendency shows that during the initial 100 s PS in pellets is practically insoluble in the solvent, but since that time, the dissolution process starts following

an exponential behaviour. The higher porosity and surface area of the wastes (generally foamed) make the absorption and diffusion of the solvents into the polymer easier, and consequently the dissolution process is faster. Polymer solubility reaches similar values after 24 h, and by this reason, it is confirmed that results obtained for pure PS are applicable to PS wastes.

2.1.2 Solvent Removal

On the basis of the achievements described in the previous sections, it can be stated that the treatment of PS with terpene oils is an attractive option for the recovery of PS wastes [35, 44, 46]. However, traditional solvent removal process by atmospheric or vacuum distillation presents several disadvantages: formation of undesirable by-products by thermal degradation of polymer chains, important energy consumption and a worse plastic quality [50]. The recycling process will only be economically beneficial if the recycled materials present high-quality being prepared from post-consumer waste plastic. During the dissolution process, any chain degradation or ageing that occurred was checked, so the solvent removal must respect the PS integrity. Furthermore, vacuum distillation produces an incipient degradation of the polymer although it can be performed at mild temperature (~80–90°C). A slight increase of polydispersity that could be attributed to the chain degradation was observed. This fact will entail the ageing of the PS and, consequently, a decrease on its quality. Also, the high energy consumption required for the solvent removal should be considered into the economic evaluation of the process [50].

Liquid–liquid extraction could be considered as an option to recover terpene oils while the polymer is precipitated. Nevertheless, the use of another solvent (named antisolvent) in which the polymer is insoluble while terpenes are soluble is highly expensive, and further purification would be needed. However, the use of CO_2 to remove terpenes from the solution has been considered a very attractive alternative to replace the use of traditional organic solvent used for liquid–liquid extraction. Due to the small size of CO_2, diffusion is much faster than in the case of conventional liquid antisolvent and the separation process can be quickly facilitated.

A fluid is considered as supercritical when it is at temperature greater than its critical temperature and pressure greater than its critical pressure [55]. The supercritical fluids (scF) combine properties of gases and liquids in a chemically interesting manner. Supercritical fluids have physicochemical properties in between a liquid and a gas. They can have a liquid-like density and very low surface tension while interacting with solid surfaces and a solvent power similar to liquids easily dissolving many chemicals. They can have gas-like low viscosity and high diffusivity [55]. Another interesting attribute of supercritical fluids is the capacity of adjusting their properties by small changes in their temperature or pressure [56]. These special characteristics give supercritical fluids great possibilities to carry out separations, chemical reactions and material processing in environmentally friendly conditions. The cited advantages acclaimed CO_2 as the optimum

candidate to precipitate PS and recover terpene. Furthermore of being a green solvent, it presents several advantages since it presents low reactivity and is non-flammable, non-toxic, environmentally acceptable and relatively inexpensive. Due to its low operating temperature required to get its critical pressure, it is able to preserve the thermolabile compounds (as the terpenoids) [57, 58]. In addition, CO_2 is able of swelling the polymer, making accessible the internal part of the polymer bulk to the CO_2; by this way, the removal of organic solvent is easier and it enables the polymeric chains to remain intact [59]; and finally, when the pressure is reduced, the total removal of the solvent with the carbon dioxide [60]. According to the explanations mentioned, CO_2 can be used as antisolvent to remove terpene oils from the PS solution in order to obtain a solvent-free solid material with enhanced properties. Low operating temperature and pressure are suitable to perform the separation process, minimising the degradation of polymer chains and reducing the operating costs.

2.1.3 Global Process

The process could be summed up according to the next diagram.

With regard to Fig. 11, the general process for the recycling of polystyrene wastes can be divided in two main steps: the dissolution of polystyrene wastes in terpene oils and the separation of the polymer from the solution by CO_2 at high pressure. The dissolution of wastes in terpenes allows the effective decrease of the PS volume, since the density of the oils is higher than those of PS wastes and the volume could be reduced between 5 and 15 times depending on the concentration. Next, CO_2 solubilises terpene, while the polymer remains changeless except that CO_2 is absorbed among the polymeric chains and is able to tune the polymer structure.

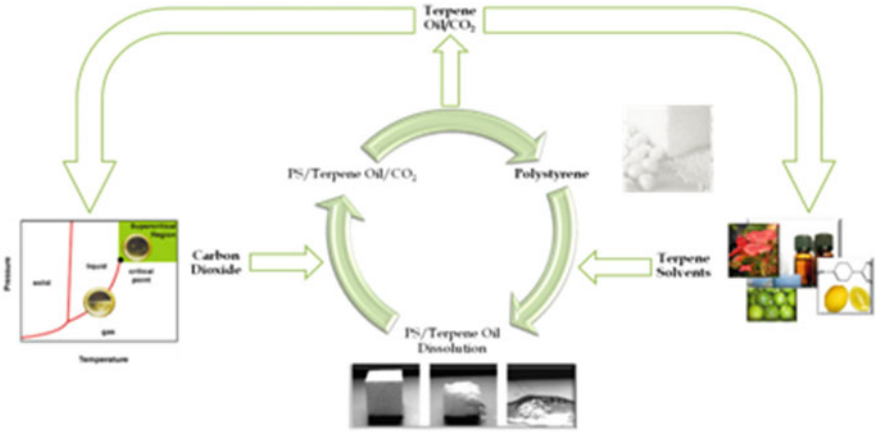

Fig. 11 Global process for the recycling of PS wastes by dissolution in terpene solvents and recovery by CO_2 at high pressure

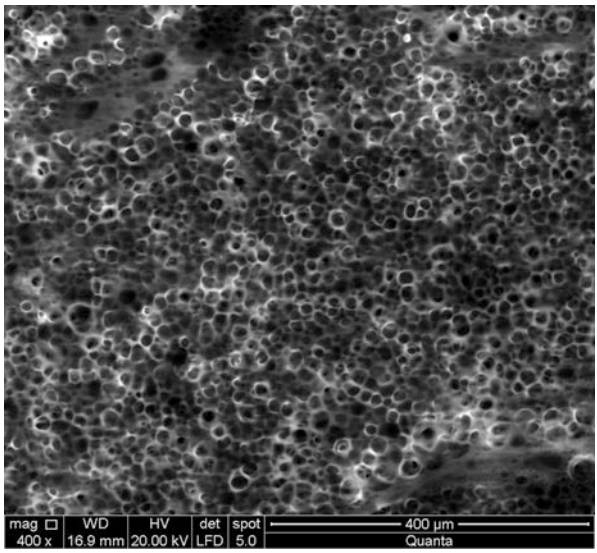

Fig. 12 SEM images with 400× magnification of the recycled PS microcellular foam obtained at 90 bar and 30°C

Finally, polystyrene is recovered as microcellular foam, a very high-added value product.

The recovered polymer presented high-added value since the process was designed to obtain microcellular foams of PS, which show average cell sizes of less than 10 μm and cell densities greater than 10^9 cells/cm^3. They are the target products since they typically exhibit high impact strength, toughness and thermal stability, as well as low dielectric constant and thermal conductivity, becoming a high-quality product [61]. The process to prepare microcellular foams using CO_2 as foaming agent is usually divided into three steps: (1) sorption of CO_2 until saturation in the plastic; (2) nucleation of foam bubbles, it is need induce a phase separation by a thermodynamic instability (either a temperature increase or a pressure decrease); and (3) growth of foam cells. Following the described process, polystyrene can be recovered under mild working conditions, and its structure can be tailored by altering mainly the pressure and the temperature of the process in order to get microcellular foams (Fig. 12) [60].

The global process shown in this chapter has succeeded the use of PS wastes as raw material for the microcellular foam production. The use of plastic wastes as source of high-added value products offers a great opportunity by many reasons: the reduction of raw material consumption, the increase of free volume in landfills, and obviously, the environmental and social benefits. Furthermore, the new proposed process (Fig. 11) allows the integration of CO_2 (substance considered as ozone depleting) and natural oils, which means that the global methodology is environmentally friendly. Any waste stream from the process is obtained because terpenes and CO_2 can easily be recovered and reused in several cycles, minimising the environmental impact. The traditional high costs involved in the recycling of PS wastes are compensated mainly because of the high-quality recycled polymer, but also due to the mild operating conditions required to carry out the process and the

Fig. 13 Pilot plant for the recycling of polystyrene wastes by dissolution at ambient conditions and solvent recovery by $scCO_2$

selective dissolution technique which eliminates the need to previously sort the polymer from mixed plastic waste streams.

Due to the promising results obtained for the recycling of PS by terpene oils and CO_2 as antisolvent, the scaleup of the process was performed. The pilot plant was installed in the facilities of the Institute for Chemical and Environmental Technologies (University of Castilla-La Mancha) and is shown in Fig. 13.

The pilot plant allows the study of the recycling of PS wastes (it is mainly focused on XPS wastes) by dissolution in natural solvents and the recovery of the polymer and terpenes using CO_2 at high pressure. It was designed for the treatment of 75 m^3 of wastes/month; working for 8 h/day, it means 100 kg XPS/day. If dissolution would be performed in the source of residue production, transportation will be more efficient than in the conventional recycling system. The dissolution process in the source of the residues decreases the transport costs dramatically and makes the process economically beneficial. Furthermore, the target products are microcellular foams, and due to their excellent properties, the recycled polymer will reach higher sales prices. Finally, the process can be described as a cycle because terpene oils and CO_2 can be recovered easily by depressurisation. Thus, only new waste raw material is needed to perform the recycling process. According to the discussion shown along this chapter, the exposed process allows the environmental friendly management and recycling of PS wastes independently of its processed or origin.

3 Conclusions

The efficient recycling of plastics is nowadays a challenge, but important efforts are necessary to achieve economical and environmental advantageous processes. Our research group is focused on the recycling of polystyrene wastes due to the huge volume produced and its unsettling effect on the environment. But the threat could

not be taken for granted since it can become an opportunity applying new green and environmentally friendly recycling techniques. The selective dissolution of the polymer in natural terpene oils followed by the recovery of the solvents using CO_2 is outlined as a promising alternative for the efficient recycling of the PS wastes.

References

1. Brydson JA (1999) The historical development of plastics materials. In: Brydson JA (ed) Plastics materials, 7th edn. Butterworth-Heinemann, Oxford, pp 1–18, http://dx.doi.org/10.1016/B978-075064132-6/50042-5
2. Council PP (n.d.) Polystyrene Packaging Council. http://www.polystyrenepackaging.co.za/. Accessed March, 10 2014
3. Ghosh P (2001) Polymer science and technology: plastics, rubbers, blends and composites. Tata McGraw-Hill, New Delhi
4. Azapagic A, Emsley A, Hamerton I (2003) Polymers: the environment and sustainable development. Wiley, Guildford
5. Van Krevelen DW, Te Nijenhuis K (2009) Typology of polymers. In: Krevelen DWV, Nijenhuis KT (eds) Properties of polymers, 4th edn. Elsevier, Amsterdam, pp 7–47, http://dx.doi.org/10.1016/B978-0-08-054819-7.00002-9
6. PlasticsEurope. http://www.plasticseurope.org/. Accessed March 7 2014
7. Borsoi C, Scienza LC, Zattera AJ (2013) Characterization of composites based on recycled expanded polystyrene reinforced with curaua fibers. J Appl Polym Sci 128(1):653–659. doi:10.1002/app.38236
8. Zelenović Vasiljević T, Srdjević Z, Bajčetić R, Vojinović Miloradov M (2012) GIS and the analytic hierarchy process for regional landfill site selection in transitional countries: A case study from Serbia. Environ Manage 49(2):445–458. doi:10.1007/s00267-011-9792-3
9. Brunner S, Fomin P, Zhelondz D, Kargel C (2012) Investigation of algorithms for the reliable classification of fluorescently labeled plastics. In: 2012 I.E. international instrumentation and measurement technology conference, I2MTC 2012, Graz, pp 1659–1664. doi:10.1109/i2mtc.2012.6229451
10. Ávila AF, Duarte MV (2003) A mechanical analysis on recycled PET/HDPE composites. Polym Degrad Stab 80(2):373–382. doi:10.1016/s0141-3910(03)00025-9
11. Carvalho T, Durão F, Ferreira C (2010) Separation of packaging plastics by froth flotation in a continuous pilot plant. Waste Manage (Oxford) 30(11):2209–2215. doi:10.1016/j.wasman.2010.05.023
12. Inada K, Matsuda R, Fujiwara C, Nomura M, Tamon T, Nishihara I, Takao T, Fujita T (2001) Identification of plastics by infrared absorption using InGaAsP laser diode. Resour Conservat Recycl 33(2):131–146. doi:10.1016/s0921-3449(01)00080-5
13. Martínez SS, Paniza JML, Ramírez MC, Ortega JG, García JG (2012) A sensor fusion-based classification system for thermoplastic recycling. In: 18th international conference on automation and computing, ICAC 2012, Loughborough, Leicestershire, pp 290–295
14. Anzano J, Lasheras RJ, Bonilla B, Casas J (2008) Classification of polymers by determining of C1:C2:CN:H:N:O ratios by laser-induced plasma spectroscopy (LIPS). Polym Test 27(6):705–710. doi:10.1016/j.polymertesting.2008.05.012
15. Luijsterburg B, Goossens H (2013) Assessment of plastic packaging waste: material origin, methods, properties. Resour Conservat Recycl. doi:10.1016/j.resconrec.2013.10.010
16. Choi WZ, Yoo JM, Park EK (2006) Separation of individual plastics from mixtures by gravity separation processes. In: TMS fall extraction and processing division, Sohn International Symposium, San Diego, pp 459–468

17. Unnikrishnan VK, Choudhari KS, Kulkarni SD, Nayak R, Kartha VB, Santhosh C (2013) Analytical predictive capabilities of Laser Induced Breakdown Spectroscopy (LIBS) with Principal Component Analysis (PCA) for plastic classification. RSC Adv 3(48): 25872–25880. doi:10.1039/c3ra44946g
18. Anzano J, Casanova ME, Bermúdez MS, Lasheras RJ (2006) Rapid characterization of plastics using laser-induced plasma spectroscopy (LIPS). Polym Test 25(5):623–627. doi:10.1016/j.polymertesting.2006.04.005
19. Alter H (2005) The recovery of plastics from waste with reference to froth flotation. Resour Conservat Recycl 43(2):119–132. doi:10.1016/j.resconrec.2004.05.003
20. Hamad K, Kaseem M, Deri F (2013) Recycling of waste from polymer materials: an overview of the recent works. Polym Degrad Stab 98(12):2801–2812. doi:10.1016/j.polymdegradstab.2013.09.025
21. Scott G (2000) "Green" polymers. Polym Degrad Stab 68(1):1–7. doi:10.1016/s0141-3910(99)00182-2
22. Al-Salem SM, Lettieri P, Baeyens J (2010) The valorization of plastic solid waste (PSW) by primary to quaternary routes: From re-use to energy and chemicals. Prog Energy Combust Sci 36(1):103–129. doi:10.1016/j.pecs.2009.09.001
23. Al Shrah M, Janajreh I (2013) Mechanical recycling of cross-link polyethylene: assessment of static and viscoplastic properties. In: 1st international renewable and sustainable energy conference, IRSEC 2013, Ouarzazate, pp 456–460. doi:10.1109/irsec.2013.6529674
24. De La Puente G, Sedran U (1998) Recycling polystyrene into fuels by means of FCC: performance of various acidic catalysts. Appl Catal Environ 19(3–4):305–311. doi:10.1016/s0926-3373(98)00084-8
25. Wilk V, Hofbauer H (2013) Conversion of mixed plastic wastes in a dual fluidized bed steam gasifier. Fuel 107:787–799. doi:10.1016/j.fuel.2013.01.068
26. Kaminsky W, Predel M, Sadiki A (2004) Feedstock recycling of polymers by pyrolysis in a fluidised bed. Polym Degrad Stab 85 (3 Spec. iss.):1045–1050. doi:10.1016/j.polymdegradstab.2003.05.002
27. Teach WC, Kiessling GC (1960) Polystyrene. Reinhold Publishing Corporation, New York
28. Andrady AL (2003) Plastics and the environment. Wiley, New Jersey
29. Brandrup J (1996) Recycling and recovery of plastics. Hanser Publishers, Munich
30. Ambrose CA, Hooper R, Potter AK, Singh MM (2002) Diversion from landfill: quality products from valuable plastics. Resour Conservat Recycl 36(4):309–318. doi:10.1016/s0921-3449(02)00030-7
31. Vilaplana F, Ribes-Greus A, Karlsson S (2006) Degradation of recycled high-impact polystyrene. Simulation by reprocessing and thermo-oxidation. Polym Degrad Stab 91(9): 2163–2170. doi:10.1016/j.polymdegradstab.2006.01.007
32. Noguchi T, Lnagaki Y, Miyashita M, Watanabe H (1998) A new recycling system for expanded polystyrene using a natural solvent. Part 2. Development of a prototype production system. Packag Tech Sci 11(1):29–37
33. Noguchi T, Miyashita M, Lnagaki Y, Watanabe H (1998) A new recycling system for expanded polystyrene using a natural solvent. Part 1. A new recycling technique. Packag Tech Sci 11(1):19–27
34. Shikata S, Watanabe T, Hattori K, Aoyama M, Miyakoshi T (2011) Dissolution of polystyrene into cyclic monoterpenes present in tree essential oils. J Mater Cycles Waste Manag 13(2): 127–130. doi:10.1007/s10163-011-0005-1
35. Gutiérrez C, García MT, Gracia I, De Lucas A, Rodríguez JF (2011) A practical approximation to design a process for polymers recycling by dissolution. Afinidad 68(553):181–188
36. Arandes JM, Ereña J, Azkoiti MJ, Olazar M, Bilbao J (2003) Thermal recycling of polystyrene and polystyrene-butadiene dissolved in a light cycle oil. J Anal Appl Pyrolysis 70(2):747–760. doi:10.1016/s0165-2370(03)00056-1
37. Zhang Y, Mallapragada SK, Narasimhan B (2010) Dissolution of waste plastics in biodiesel. Polym Eng Sci 50(5):863–870. doi:10.1002/pen.21598
38. Kodera Y, Ishihara Y, Kuroki T, Ozaki S (2005) Selected papers presented at the 3rd International Symposium on Feedstock Recycling of Plastics. In: Müller-Hagedorn M,

Bockhorn H (eds) Solvo-cycle process: AIST's new recycling process for used plastic foam using plastics-derived solvent, Karlshrue, pp 217–222
39. Karaduman A, Imşek EH, Çiçek B, Bilgesü AY (2002) Thermal degradation of polystyrene wastes in various solvents. J Anal Appl Pyrolysis 62(2):273–280. doi:10.1016/s0165-2370(01)00125-5
40. Kim SS, Kim J, Jeon JK, Park YK, Park CJ (2013) Non-isothermal pyrolysis of the mixtures of waste automobile lubricating oil and polystyrene in a stirred batch reactor. Renew Energy 54:241–247. doi:10.1016/j.renene.2012.08.001
41. Sovová H, Stateva RP, Galushko AA (2007) High-pressure equilibrium of menthol + CO_2. J Supercrit Fluids 41(1):1–9
42. Kerton F, Marriott R (2013) Alternative solvents for green chemistry, 2nd edn, RSC green chemistry. RSC publishing, Cambridge
43. Hattori K, Shikata S, Maekawa R, Aoyama M (2010) Dissolution of polystyrene into p-cymene and related substances in tree leaf oils. J Wood Sci 56(2):169–171. doi:10.1007/s10086-009-1073-x
44. Gutiérrez C, García MT, Gracia I, De Lucas A, Rodríguez JF (2013) The selective dissolution technique as initial step for polystyrene recycling. Waste Biomass Valorization 4(1):29–36
45. Hattori K, Naito S, Yamauchi K, Nakatani H, Yoshida T, Saito S, Aoyama M, Miyakoshi T (2008) Solubilization of polystyrene into monoterpenes. Adv Polym Tech 27(1):35–39. doi:10.1002/adv.20115
46. García MT, Duque G, Gracia I, De Lucas A, Rodríguez JF (2009) Recycling extruded polystyrene by dissolution with suitable solvents. J Mater Cycles Waste Manag 11(1):2–5. doi:10.1007/s10163-008-0210-8
47. Breitmaier E (2006) Terpenes: flavors, fragrances, pharmaca, pheromones. Wiley, Weinheim
48. Hansen CM (2000) Hansen solubility parameters: a user's handbook. CRC, New York
49. Güner A (2004) The algorithmic calculations of solubility parameter for the determination of interactions in dextran/certain polar solvent systems. Eur Polym J 40(7):1587–1594. doi:10.1016/j.eurpolymj.2003.10.030
50. García MT, Gracia I, Duque G, Ad L, Rodríguez JF (2009) Study of the solubility and stability of polystyrene wastes in a dissolution recycling process. Waste Manag (Oxford) 29(6):1814–1818. doi:10.1016/j.wasman.2009.01.001
51. Subra P, Jestin P (2000) Screening design of experiment (DOE) applied to supercritical antisolvent process. Ind Eng Chem Res 39(11):4178–4184
52. Lin IH, Liang PF, Tan CS (2010) Preparation of polystyrene/poly(methyl methacrylate) blends by compressed fluid antisolvent technique. J Supercrit Fluids 51(3):384–398. doi:10.1016/j.supflu.2009.10.008
53. Miller-Chou BA, Koenig JL (2003) A review of polymer dissolution. Prog Polym Sci (Oxford) 28(8):1223–1270. doi:10.1016/s0079-6700(03)00045-5
54. Okubo M, Ahmad H (1995) Synthesis of temperature-sensitive submicron-size composite polymer particles. Colloid Polym Sci 273(9):817–821
55. Cooper AI (2000) Polymer synthesis and processing using supercritical carbon dioxide. J Mater Chem 10(2):207–234. doi:10.1039/a906486i
56. Bogel-Łukasik E, Szudarska A, Bogel-Łukasik R, Nunes da Ponte M (2009) Vapour-liquid equilibrium for β-myrcene and carbon dioxide and/or hydrogen and the volume expansion of β-myrcene or limonene in CO_2 at 323.15 K. Fluid Phase Equilib 282(1):25–30
57. Reverchon E, Sesti Osseo L, Gorgoglione D (1994) Supercritical CO2 extraction of basil oil: characterization of products and process modeling. J Supercrit Fluids 7(3):185–190
58. Varona S, Martin A, Cocero MJ, Gamse T (2008) Supercritical carbon dioxide fractionation of Lavandin essential oil: experiments and modeling. J Supercrit Fluids 45(2):181–188. doi:10.1016/j.supflu.2007.07.010
59. Gutiérrez C, Rodríguez JF, Gracia I, de Lucas A, García MT (2013) High-pressure phase equilibria of Polystyrene dissolutions in Limonene in presence of CO_2. J Supercrit Fluid 84:211–220. doi:http://dx.doi.org/10.1016/j.supflu.2013.08.017

60. Gutiérrez C, Rodríguez JF, Gracia I, de Lucas A, García MT (2014) Preparation and characterization of polystyrene foams from limonene solutions. J Supercrit Fluid 88:92–104. doi:http://dx.doi.org/10.1016/j.supflu.2014.02.002
61. Bao JB, Liu T, Zhao L, Hu GH, Miao X, Li X (2012) Oriented foaming of polystyrene with supercritical carbon dioxide for toughening. Polymer (United Kingdom). doi:10.1016/j.polymer.2012.10.011

Microbial Fuel Cell: The Definitive Technological Approach for Valorizing Organic Wastes

F.J. Fernández, J. Lobato, J. Villaseñor, M.A. Rodrigo, and P. Cañizares

Abstract Microbial fuel cells (MFC) are promising bioelectrochemical devices which are currently being developed to harvest energy from wastes. Its state of the art is within a stage of maturity that makes research on this topic ambitious and feasible at the same time, and hence, development of MFC can be considered as research at the edge of knowledge embracing multidisciplinary and the hottest topics of research in chemical engineering: energy, environment, and biotechnology. This chapter describes the fundamentals of the MFC technology and some of its applications, also focusing on the most relevant challenges, which include solving two key problems: cost of comburent and target of applications. Regarding to the first one, a comprehensive review of the main references published during the recent years in algae and natural MFC is presented. Regarding the second, attention is focused on wastewater treatment but other applications are also described. A complete review of the most relevant references on the technology using SCOPUS and WoS is included in the chapter.

Keywords Bioelectrochemical system, Energy, Microbial fuel cells, Organic wastes

Contents

F.J. Fernández, J. Lobato, J. Villaseñor, M.A. Rodrigo (✉), and P. Cañizares
Department of Chemical Engineering, University of Castilla La Mancha, Campus Universitario s/n 13071, Ciudad Real, Spain
e-mail: manuel.rodrigo@uclm.es

E. Jiménez et al. (eds.), *Environment, Energy and Climate Change I: Environmental Chemistry of Pollutants and Wastes*, Hdb Env Chem (2015) 32: 287–316,
DOI 10.1007/698_2014_273, © Springer-Verlag Berlin Heidelberg 2014,
Published online: 29 July 2014

1 Need for New Energy Technological Approaches

In recent years there has been a great deal of discussion regarding the huge environmental damage and accelerated global climate change caused by, among other factors, the enormous demand for power. In this context, any effort made to decrease the CO_2 or increase the energy efficiency should be greatly welcomed, and there is a consensus in the fact that new energy sources should be renewable and carbon neutral. Numerous researchers have focused on new alternatives to fossil fuels, that is, green power devices. This explains the noteworthy success of the research on photovoltaic panels, air windmills, and fuel cell during the recent years.

Fuel cells offer an environmentally friendly alternative to fossil fuels. In a first view (Fig. 1), these devices consist of an electrochemical cell in which simultaneously a fuel (typically, but not exclusively, hydrogen) is oxidized on an anode surface and a comburent (typically air) is reduced at a cathode surface. Electrons flow through an external circuit allowing the use of the energy contained in the fuel directly as electric energy. Currently, fuel cells are considered to be very interesting devices to make use of the chemical energy of a fuel. Ideally, they can reach efficiencies much higher than those which can be obtained with other more conventional energy-transformation devices.

There are several types of fuel cells, being the type of electrolyte that separates the electrodes, the key point to differentiate among them. This electrolyte also defines the operation conditions (in particular temperature) because a high ionic conductivity is required to minimize ohmic loses of energy.

Solid oxide and polymer electrolyte membrane fuel cells (typically known by their acronyms as SOFC and PEMFC, respectively) are the most applied technologies nowadays. In order to be effective, the reaction conditions in traditional fuel cells are usually harsh, in particular in SOFC technology. Softer operation conditions technologies, like those of PEMFC, require the use of platinum as catalyst. This noble metal is expensive, the resources are limited, and it is easily poisoned by CO, which can be formed if the used fuel is not pure hydrogen. Nevertheless, the versatility and wide range of power generated by PEMFC makes them the most common and advanced nowadays. Among PEM fuel cells, those that work at temperature higher than 100°C are the most promising, since the important operation problems derived from liquid water management and the catalyst poisoning, which are inherent to conventional PEM fuel cells, are precluded.

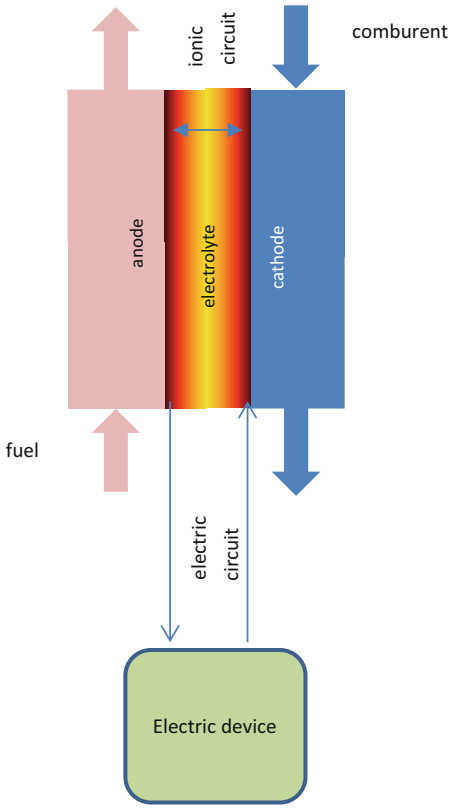

Fig. 1 Typical scheme of a fuel cell

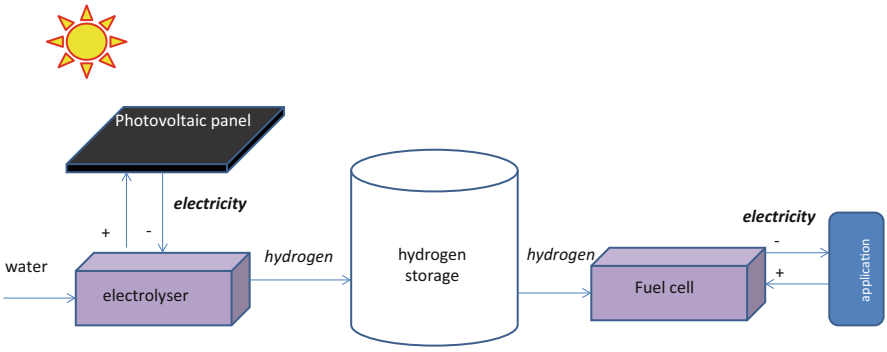

Fig. 2 Coupling green and electrochemical technology to regulate energy supply

From the academic point of view, a very interesting combination was expected to be obtained when this electrochemical fuel cell technology was coupled with electrolysis and with solar (or wind) energy to produce and use hydrogen as an energy vector (Fig. 2). In fact, it was a very important challenge for many research

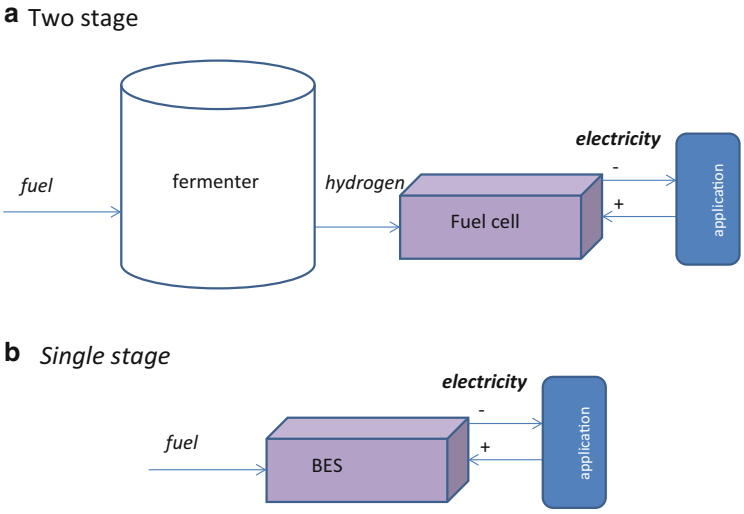

Fig. 3 Production of electricity using biological technology

groups during the last decade. However, unfortunately, this technological approach has found some disadvantages in the storage of energy as hydrogen and in the fuel cell operation. Thus, although there are many commercial applications in the market, robust hydrogen energy storage is far away from the desired feasibility nowadays.

At this point, energy production from biomass (bioenergy) can be considered as one important alternative. Thus, processes involving microorganisms are promising, because they have the potential to produce green energy on a large scale, without disrupting strongly the environment or human activities. The biological fuel cell development is an interesting and promising innovation to already existing fuel cell types. There are two types of biological-based fuel cell (Fig. 3):

1. Processes using a primary fuel (usually an organic waste such as corn husks, whey, urban wastewater, etc.) to generate species such as hydrogen or ethanol, which later are used as a secondary fuel within a conventional fuel cell.
2. Cells which generate electricity directly from an organic fuel such us glucose, using either enzymes or complete microorganisms. Electron mediators are often required to transfer electrons from the microorganisms to an electrode [1] or from enzymes to the electrode [2, 3], but in some cases, the electrons are directly transferred [4, 5].

The first case is a combination of two well-known processes, and it should not be considered properly as a bioelectrochemical system. The other type of device is commonly referred to as microbial fuel cells (MFC), and they can be properly

considered as bioelectrochemical systems (BES) for electric power generation, because they are based on the exploration of biocatalytic reactions with active microbial cells.

In contrast to the harsh operation conditions of conventional fuel cells, the MFCs have mild reaction conditions (ambient temperature, normal pressure, and neutral pH) and, overall, platinum is not required (although it might be used in order to increase efficiencies). Instead of platinum, the catalyst is either a microorganism or an enzyme. The biological fuel cell can then convert the chemical energy of organic matter directly into electric energy. Hence, an MFC consists of a bioreactor that is able to convert chemical energy, from chemical bonds in organic compounds, directly into electrical energy through catalytic reactions of microorganisms under anaerobic conditions. These microorganisms use mediators or direct transfer of electrons to oxidize the organic molecules and transform them into carbon dioxide and protons. The electrons produced in the oxidation of the organic matter are used to reduce oxygen or other acceptor of electrons in the cathodic chamber flowing electricity through an external electric circuit where a device harvests the energy liberated by the reactions [6]. Protons and/or other cations in solution migrate to the cathode through an ionic circuit (cation exchange membrane, salt bridge, etc.), and this allows the MFC maintaining electroneutrality of the anodic and cathodic compartments of the cell.

MFCs are now considered as promising bioelectrochemical systems (BES) for electric power generation. They have been studied for decades with an increasing interest, and nowadays they have become a hot multidisciplinary research topic in the edge between biotechnology and electrochemical engineering [7]. In the literature, it is often proposed that the greatest potential for practical application of MFCs is in the treatment of urban and industrial wastewaters. As it is known, the costs associated to the treatment of wastewaters are very high, and the development of a technology that allows to simultaneously treat a waste and to produce directly energy would have a very high significance. Unfortunately, the efficiencies obtained presently are far away from those required for commercial applications, and a lot of fundamental work has to be done during the next years in order to develop a ready-to-use technology in this field. In particular, the low current densities obtained in MFC leads to extremely huge electrode areas, causing serious concerns related to design and to amortization of the potential facilities of wastewater treatment. Thus, this is a prospectively important subject, not for present applications but for future ones. However, there are other applications in which MFC can be applied successfully such as those requiring less extensive production of energy. One of them is the replacement of photovoltaic cell, trying to extract energy directly from sun in order to be used in small devices (such as robots) and giving them autonomy.

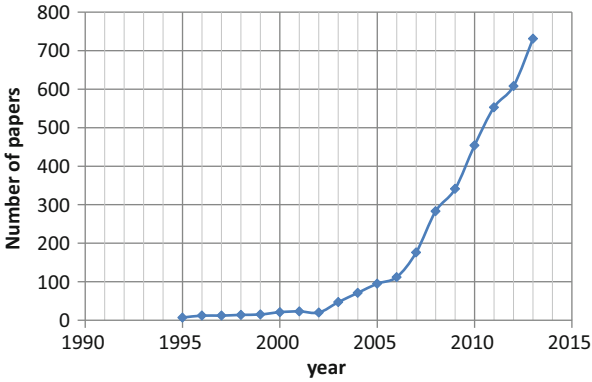

Fig. 4 Number of manuscript focus on microbial fuel cells (*source*: WoS, March 2014)

2 Microbial Fuel Cells: An Interesting Way to Use Organic Contents of Wastes in Harvesting Energy

The MFC may be understood as a device that converts directly the chemical energy of a fuel (organic substrate) into electrical energy with the aid of biocatalytic reactions carried out by microorganisms [8]. The MFC concept has been known for a long time [9]. However, this technology is still at an early lab-scale research stage, although its applications are growing fast, and nowadays, MFCs are expected to provide new opportunities for the sustainable production of energy, in the form of electricity produced directly from biodegradable compounds. The number of articles published on this topic in recent years is very high as can be observed in Fig. 4, which clearly indicates that MFC can be considered hot topic nowadays.

The huge number of papers makes important the existence of reviews that summarize the most important information. At this point, it is considered relevant to cite here only some of them, such as recent comprehensive reviews [10–13] and some studies on carbon and nitrogen removal [14, 15] and on the application of MFCs to treat industrial wastewater [16].

Wastewater containing a high percentage of biodegradable organic compounds can be used as fuel in MFCs, achieving simultaneous wastewater treatment and energy production. To illustrate this fact, Fig. 5 shows a graph in which the effect of the organic load on power production is plotted for an MFC fed with urban wastewater. A clear relationship can be observed between the influent chemical oxygen demand (COD) and the power produced.

As a typical biological process, in addition to the organic load, performance of MFC systems depends strongly on many factors such as temperature, pH, etc. At this point it is important to take in mind that time constants (to assess transitory responses) of electrochemical and biological processes are not comparable, and in MFC there are always two types of transient responses [18]:

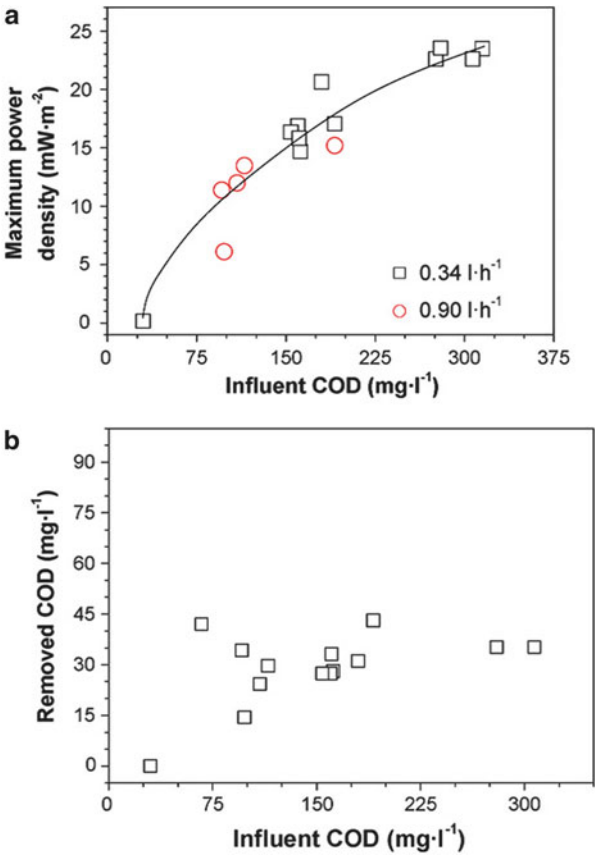

Fig. 5 Influence of the COD on the maximum power density (**a**) and on the COD removal rate (**b**) during the treatment with an MFC of an urban wastewater [17]

1. A short-term response which is produced by the direct response of the metabolisms of the microorganisms contained in the anodic chamber of the MFC
2. A long-term response, associated to changes in the microorganisms' cultures caused by the competitive adaptation to new conditions

Excess sludge production in an MFC is very low compared to conventional aerobic processes [19], which will help to minimize the overall operating cost of a treatment plant by decreasing the cost of sludge management. Numerous microorganisms have the ability to transfer the electrons derived from the metabolism of organic compounds to the anode, and these include *Aeromonas hydrophila*, *Desulfovibrio desulfuricans*, *Escherichia coli*, *Geobacter metallireducens*, *and Shewanella oneidensis* [20]. It has been pointed out that the choice of inoculum source is a key parameter in MFC design [21]. In most studies, the source of electroactive microorganisms has been domestic wastewater [6, 17, 22–26]. Alternative sources have been reported, and these include heat-treated soils [27], garden compost [28], manure [29], and waste from agricultural and food industries [21]. Anaerobic sewage sludge is also a good source for inoculating the anodic

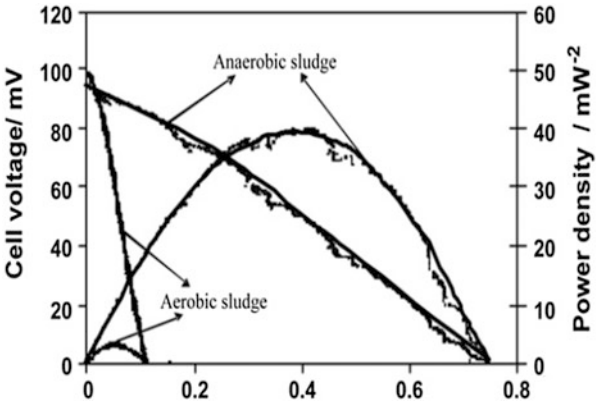

Fig. 6 Polarization curves obtained in the MFC seeded with aerobic (20 days after start-up) and anaerobic (30 days after start-up) sludges [32]

chamber of an MFC [30]. Typically, this sludge consists of fermentative bacteria, methanogens, and sulfate reducers [31]. In this context, the presence of highly varied bacterial communities, including electrochemically active strains of bacteria, has been reported for the mixed anaerobic sludge [20]. Pretreatments of the inoculum have been carried out to suppress the activity of methanogens and increase the performance of the MFCs [30]. Figure 6 compares operation of all MFC seeded with aerobic and anaerobic sludges. As it can be observed, both sludges produce electrogenic cultures when properly acclimated to the MFC operation conditions.

Hence, the production of an electrogenic culture of microorganisms cannot be considered a difficult task, and these biological cultures can be obtained from the raw sludge of aerobic or anaerobic processes [6] under a proper acclimation process.

Regarding the comburent of MFC, air is the most applied reagent, although in the literature, the role of other electron acceptors different from oxygen such as nitrates or sulfates has been demonstrated [33]. This is important because one of the main drawbacks of MFC is the slow rate of the oxygen reduction. Thus, although MFCs are promising for wastewater treatment processes, there are still many technical and economic obstacles to overcome before practical applications will be feasible [34]. Currently, platinum is often used to catalyze oxygen reduction, which requires a significant investment cost. For this reason, some researchers have recently started working on the concept of biocathodes. There are three different concepts:

1. Aerobic biocathodes that use oxygen as the oxidant and microorganisms to assist the oxidation of transition metal compounds, such as Mn(II) or Fe(II), for electron delivery to oxygen [35].
2. Anaerobic biocathodes that use compounds such as nitrate, sulfate, iron, manganese, selenate, arsenate, urinate fumarate, and carbon dioxide as terminal electron acceptors [36].

3. Algal biocathodes in which the cost of aeration is reduced by changing the mechanical aeration device to an algal oxygen supply, which can also reduce CO_2 emissions from a factory [37]. Hence, a photosynthetic culture of algae at the cathode, with light radiation, utilizes CO_2 as the carbon source for photosynthesis and produces oxygen, which acts as an electron acceptor for electricity generation. Algae can also act as a biological electron acceptor while simultaneously reducing carbon dioxide to biomass [38, 39]. For example, it is possible to couple photosynthetic bioreactors using microalgae in the cathode with anaerobic oxidation of organic substrates in the anode produced by photosynthesis [40] or contained in a wastewater flow [41]. Other configurations with the same purpose are the plant-MFC [42–44] which integrates the roots of a living plant into the anode compartment and the sediment MFC or benthic MFC [45].

3 Comparison of Microbial/Enzymatic, Biofilm/Suspended Culture and Pure/Mixed Culture Fuel Cells

The use of whole cells in MFC is advantageous since multiple enzymes, and therefore multiple fuels, can be used. Because of that, the use of whole cells increases the potential applications of the MFC. Moreover, the use of the whole microorganism eliminates the need for enzyme isolation.

The microbial cultures used in MFC can either be suspended in the anode chamber or immobilized, forming a biofilm. The use of suspended cultures limits the operational feeding mode of the MFC to a batch mode whereas the use of biofilm allows the MFC to operate under batch and continuous mode. When an MFC is continuously fed, the biofilm-forming species will be selected based on the hydrodynamic conditions. Moreover, these organisms will be preferred because of their ability to directly transfer the electron to the electrode. When the MFC is operated under batch conditions, redox mediators can be accumulated in the anodic chamber [46] which allows to its further use with the advantages related.

In the literature, a comparison of the batch and continuous operational modes showed that the power output and efficiency were lower when working with suspended cultures [47]. This could be explained because of the better efficiency of the electron transfer to the electrode in the biofilm systems. Anyway, when working with biofilms, it must be noted that mass transfer limitations may occur which, in the case of thick biofilms, would reduce the performance of the MFC.

Regarding to the purity of the culture, MFC can be operated based on either pure or mixed cultures. In the literature the performance of pure cultures has been deeply described in order to elucidate mechanisms and electrochemical reaction kinetics. The main organisms used in these studies are *S. oneidensis* MR-1 and *Geobacter sulfurreducens* PCA [48].

On one hand, the main advantages of pure culture systems versus the mixed ones are the higher coulombic efficiency and, from the scientific point of view, the

possibility of clear identification of the reaction and electron transfer mechanisms. On the other hand, mixed microbial electrogenic cultures are more versatile.

Microbial communities that were enriched in MFCs have been characterized [49]. In the mixed cultures, the electrochemically active microorganisms or species used to be *Geobacter*, *Desulfuromonas*, *Alcaligenes* [49], *Enterococcus* [49], *Pseudomonas aeruginosa*, *Proteobacteria* [50], *Clostridium*, and also nitrogen-fixing bacteria such as *Azoarcus* and *Azospirillum* [51].

In the mixed microbial electrogenic cultures also appear a great number of non-electrogenic organisms performing alternative metabolisms which would lead to a low coulombic efficiency. Moreover, sometimes a large percentage of the microorganisms remain uncharacterized. In the literature it has been reported that in an MFC fed with starch and inoculated with wastewater, the microbial community that developed consisted of 36% unidentified, 25% β- and 20% α-Proteobacteria, and 19% *Cytophaga*, *Flexibacter*, and *Bacteroides* groups [52].

The main role of the non-electrogenic microorganisms is the transformation of the slowly biodegradable organic substrates into more easy ones [53]. Later on, these compounds could be oxidized by the electrogenic culture with the associated electricity production.

4 Interaction Between Electrogenic Organisms and the Electrode

One of the key aspects of MFC development is the electron transfer to the electrode. The electron transfer can be defined as the process in which electrons derived from the oxidation of organic compounds are transferred to a terminal electron acceptor. Usually, the electron donors and acceptors are dissolved. However, some microorganisms are able to release the electrons to solid electrodes [54]. Usually, the biofilms with microorganisms capable of electron transfer to and from solid electron acceptors are known electricigens, electrochemically active microbes, exoelectrogenic bacteria, and anode-respiring or anodophilic species [55].

The ability of bacteria to transfer electrons to soluble and/or insoluble terminal electron acceptor allows to use MFC as energy-producing systems that collect the electrons originated from the microbial metabolism [56]. Then, these electrons can be derived to an external electrical circuit generating an electrical current.

The electron transfer can be achieved either by direct contact with the electrode via membrane-associated cytochromes or through the use of natural, secreted by the microorganisms itself, or artificial, added externally, mediators. Therefore, the electron transfer mechanisms can be divided into two groups: direct and indirect interactions through extracellular mediators.

In the case of the direct electron transfer, two subgroups can be identified: cytochromes and pili. Similar situation appears when studying the mediated electron transfer in which internal and external mediators can be distinguished.

S. oneidensis MR-1 uses both mechanisms: the indirect one, via biosynthesized mediators, and the direct one by means of pili [57, 58].

When mediators are used as electron shuttles, they are required to have a fast kinetics, to easily interact with the microorganisms, to be chemically stable, not to be adsorbed on the bacteria or anode, and have a potential that matches that of the reductive metabolite [59]. Different types of mediators, such as thionine, quinone, phenazines, Fe(III) ethylenediaminetetraacetic acid (EDTA), methylene blue, and neutral red (NR), have been used in MFCs. In order to enhance the efficiency of the mediator, it can be immobilized on the anode surface. In the literature a significant increase, threefold, of the current exerted when operating with the mediator immobilized instead of solubilized in the liquid bulk has been described [60].

The mediators can also be synthesized by the microorganisms, e.g., Clostridium butyricum [61] and *P. aeruginosa* [46], which release their own mediators. Below the main aspects of the direct and indirect, mediated, electron transfer will be described.

4.1 Mediated Electron Transfer (MET)

Mediators are redox molecules that are stable in both oxidized and reduced form and that are neither degraded by the microbial culture nor toxic to the microorganisms in the culture [60]. The mediator serves as shuttled for the electron transfer between the microorganisms and the electrode surface, facilitating electron transport. The use of mediators may increase the reaction rates by one to several orders of magnitude, increasing therefore the electricity production [62]. Externally added flavin-based compounds as well as quinone-based compounds have been reported as redox mediators [63]. Unfortunately, although externally supplied mediators can considerably enhance the electron transfer efficiency, the use of external mediators is neither recommended nor feasible in the real implementation of MFCs. Hopefully, in recent years, it has been described in the literature that several metabolic intermediates released by microorganisms during substrates oxidation can play an important role as electron mediator, enhancing in situ the electricity generation in MFCs [19, 49] and also the degradation of the fuel [24, 64]. This is very interesting in the case of an MFC fed with wastewater, because the fuel is the pollutants contained in the wastewater.

In Fig. 7 it is presented a scheme of the working principles of mediators in MFC.

4.2 Direct Electron Transfer (DET)

Direct electron transfer to anode electrode is possible due to the existence of internal electron transport mechanisms in the microorganisms. The direct electron transfer takes place by means of a physical contact between the microorganisms and

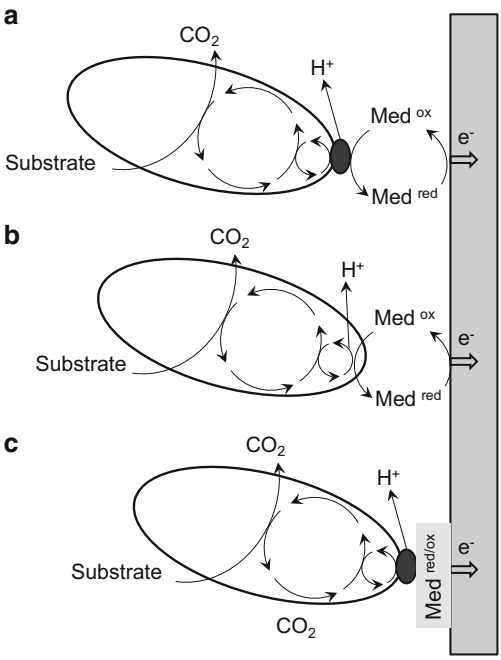

Fig. 7 Schematic overview of the working principles of soluble mediated electron transfer. (**a**) Soluble mediator reduction at the external bacteria surface through membrane-bound complexes, (**b**) soluble mediators transported into the bacteria for reduction, (**c**) soluble mediators incorporated on the surface of the electrode

the electrode. In the case of DET, any chemical is involved in the electron transfer, and the only requisite is the existence in the microorganisms of an electron transfer system that allows it to directly transport electrons outside and the existence of a system which finally releases the electron to electrode. In the literature the role of c-type cytochromes and multi-heme proteins has been proposed to act in these mechanisms when working with different microorganisms.

In the literature it has also been demonstrated that some microbial strains, mainly *Geobacter* and the *Shewanella*, can develop electronically conducting molecular pili to establish physical electrical connections with an electrode not directly in contact with the cell [56]. These pili, usually named nanowires, allow the microorganism to distance electron transport to the final solid electrode. Therefore, the nanowires allow these microorganisms to transfer the electrons to an electrode without the physical contact requirement. The nanowires are connected to the membrane cytochromes, which supply the electrons that are conducted through the nanowire.

A schematic description of the electron transfer mechanism of the DET is shown on Fig. 8.

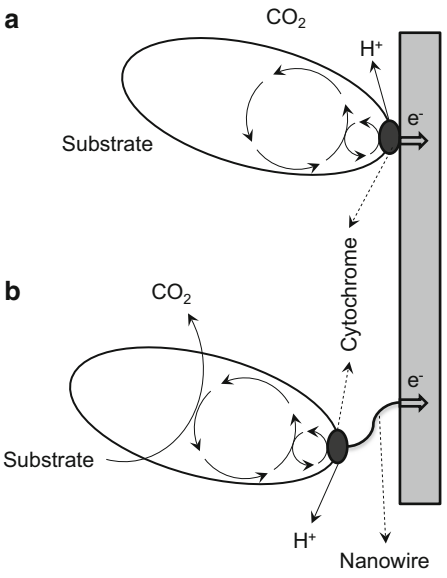

Fig. 8 Direct electron transfer by means of membrane-bound cytochromes (**a**) and electronically conducting nanowires (**b**)

5 Photosynthetic Microbial Fuel Cells

As it has been stated previously, MFCs are bioelectrochemical systems for electric power generation based on the exploitation of biocatalytic reactions with active microorganisms. When sunlight is converted into electricity within the metabolic reaction scheme of an MFC, this system is described as a photosynthetic MFC [39]. These solar-powered MFCs are an emerging technology for direct renewable energy production from solar energy through organic matter produced by organisms like algae [65], cyanobacteria [66], and higher plants [44].

There are different approaches of photo-synthetic MFCs (photo-MFCs) where the sunlight is used. This concept is not new, and in the 1960s, biohydrogen was obtained from photosynthetic bacteria with an electrocatalytic anode. In this photochemical reactor, hydrogen was produced from photosynthetic microbial metabolisms and the couple H_2/H^+ served as a natural electron mediator between the microbial metabolism and the anode. Other MFCs of the last century consisted of the use of cyanobacterial species and artificial redox compounds such as 2-hydroxy-1,4-naphtoquinone as an artificial mediator to shuttle electrons from the microorganism to the anode. Nevertheless, this configuration was not appealed, from technical point of view, because of the cost of the mediators and its toxicity.

One of the photo-MFCs which is receiving great attention during the last years is those which use algae in the system. Figure 9 shows the way in which in the recent years the number of publications focused on photosynthetic MFCs has increased. Thus, the algae can be used as organic substrates for their oxidation in the anodic chamber of an MFC [63]. In this case, an external photobioreactor must be disposed for optimal grow of algae. Low coulombic efficiencies have been reported less than

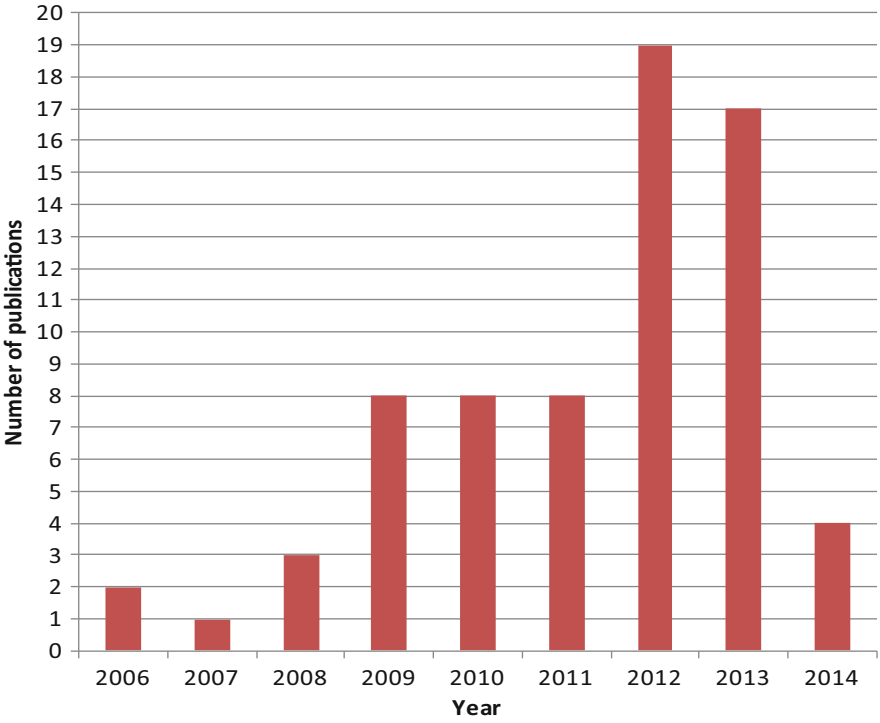

Fig. 9 Evolution of publication during last years on photo-MFC (source from Scopus and Science Direct, used keywords for searching: algae; microbial fuel cell; photosynthetic MFC, in abstract, keywords, and title)

3% because of the lower degradation rate of the complex organic matter (algae cells) by the bacterial community in the anode [40]. In order to overcome this limitation, later, Rosembau et al. proposed a system where the photobioreactor generates easy-to-degrade metabolic products, such as carboxylic acids, in order to increase the power and hence the coulombic efficiency; a scheme of the system can be observed in Fig. 10a [67]. On the other hand, algae can be used in the cathode side of the MFC, where photosynthetic microorganisms generate in situ [38] or ex situ [68] the required oxygen for the cathode electrode. A scheme of this system can be observed in Fig. 10b.

The use of algae in the cathode led to many advantages for a wastewater system based on a photo-MFC. Thus, aeration costs can be decreased considerably because the oxygen is provided from photosynthesis reactions. MFCs can effectively degrade various organic substrates (an interesting review focused on these substrates can be found in a work by Pant et al. [69]), but nutrient degradation is generally limited under anaerobic condition with a few specially designed nutrient removal processes [15]. Microalgae can assimilate significant amounts of nutrients because of high N and P demand for synthesis of proteins (45–60% of algae dry

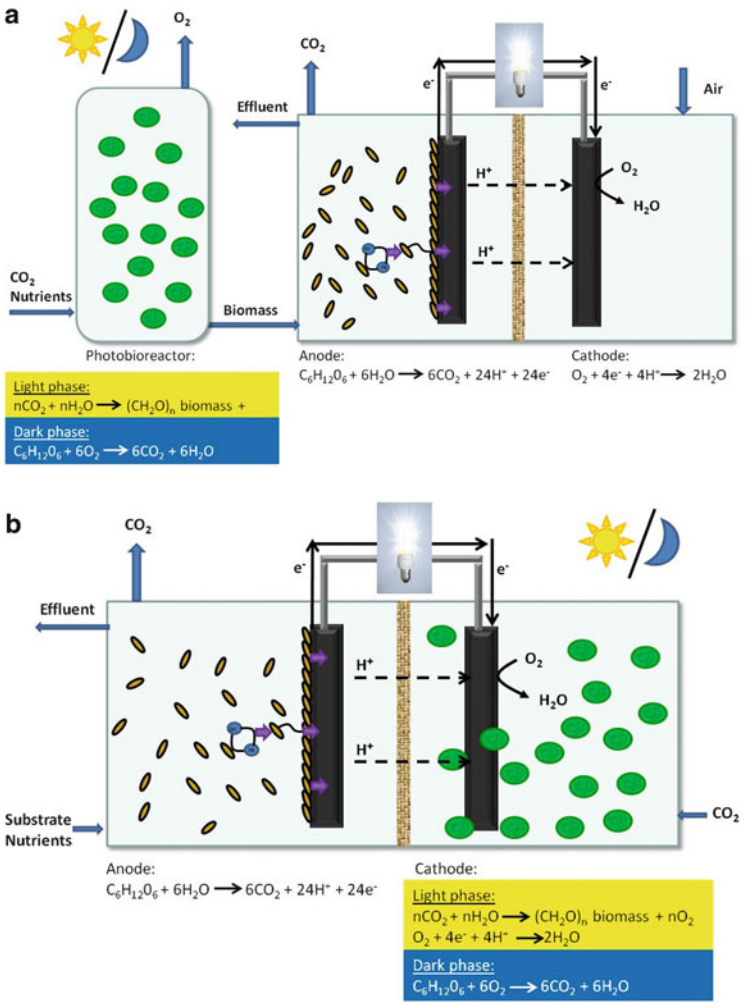

Fig. 10 (**a**) Scheme of a photo-MFC using the algae in the anode side. (**b**) Scheme of a photo-MFC using the algae in the cathode side for oxygen production

weight), nucleic acids, phospholipids, and other cellular constituents [70]. The produced algae biomass can be used for producing biofuels, including biodiesel [71], or can be used as a carbon energy source in the same MFC anodes [72]. Algae could be used as a biological electron acceptor while simultaneously reducing carbon dioxide to biomass [38]. Moreover, as the algae needs an inorganic carbon source for their metabolism, the cathode side with the algae can be used as a CO_2 sink system [73].

On the other hand, one of the main drawbacks of the photo-MFCs is that the sunlight is not always available. This means that the production of oxygen is not

constant, and during the dark period (not sunlight), algae consumes oxygen instead of producing it and let to a decrease of the performance of the MFC. Thus, in an integrated bioelectrochemical system where MFCs are coupled to a photobioreactor with algae to produce oxygen, it was observed that its performance was affected by the illumination cycles (16 h light, 8 h dark) and dissolved oxygen (DO) [74]. In this system, a peak power density of 2.2 ± 0.2 W/m^3 under illumination period was reached. Because no aeration was provided in the light period, the cathode reaction relied on the DO produced by the algae. The dissolved oxygen profiles varied in the same way that the MFC performance and under illumination period the DO concentration reached 20 mg/L more than twice the saturated dissolved oxygen in water at the same temperature. But when the system was working under the dark period, the dissolved oxygen was gradually gone down to below 1 mg/L resulting in a power density of 0.1 W/m^3. Other authors [75] were able to produce power during the dark period using a photo-MFC with a reversible bioelectrode. During the dark period the depletion of oxygen occurred, but the current density was 5 mA/m^2 and recovered immediately once the illumination was established (26 mA/m^2). Because the reduction reactions took place under lack of oxygen, other final electron acceptors should be presented like nitrate [76] or ferric ions [77]. More recently, González del Campo et al. [78] have observed the same tendency in their system (a photo-MFC with a membrane to separate anode compartment from the cathode one and with algae for the oxygen production in the cathode chamber). They observed also that the evolution of DO and the voltage output during the operation of the photo-MFC, 12 h light to 12 h dark, achieved the same profiles but in the dark period power generation still was produced (11 mV with an external resistance of 120 Ω), more than 60% of the cell voltage obtained during the illuminated period operating in continuous mode.

Although it is clear that the illumination period affects strongly to the performance of the photo-MFC as it was expected by the other hand, the behavior of the photo-MFC is also affected by the operation mode [41]. Thus, a photo-MFC was running in batch and continuous mode, with cycles of 12 h light and 12 h of dark with an external resistance of 120 Ω. Figure 11 shows the evolution of cell voltage and dissolved oxygen during 24 h of the photo-MFC with algae for the production of oxygen in the cathode chamber running in batch and continuous mode. It can be observed that four periods or behaviors are observed when the photo-MFC was operated under batch mode. It was found that periods 1 and 2 of the daylight time and the night period were cathodically controlled while periods 3 and 4 of the daylight time were controlled by the oxidation processes of the anode. In the case of the photo-MFC running under continuous feeding mode, only the periods 1 and 2 of the daylight time were observed which means that the oxygen production controlled the performance of the photo-MFC under continuous mode.

It is well known that the pH gradient through the membrane in MFCs is a significant problem because cell voltage and power output decrease. This gradient is formed because at the anode, the pH is low due to the oxidation of organic substrate by the microorganisms, whereas at the cathode side, alkaline production by oxygen reduction is produced and there is nonspecific proton exchange through

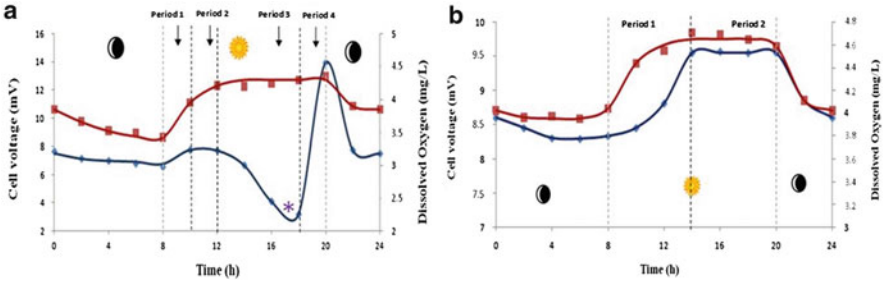

Fig. 11 Cell voltage and dissolved oxygen profiles of a photo-MFC with algae in the cathodic chamber for oxygen production. (**a**) Batch mode and (**b**) in continuous mode (◆ cell voltage; ■ dissolved oxygen). Sun (daylight period: 8:00 to 20:00), Moon (night period: 20:00 to 8:00). *Feeding time in batch mode. Reproduced with permission from [41]

the membrane [79]. Strik et al. [75] solved this problem with a solar energy-powered MFC with reversible bioelectrodes responsible for both biocatalyzed anodic and cathodic electron transfer. The identified organisms within biofilm of the reversible bioelectrodes were algae, (cyano)bacteria, and protozoa [75]. On the other hand, the use of algae in the catholyte does not mean a great problem for the pH, because as a result of the combined effect of the oxygen reduction and CO_2 buffering, the MFC cathode reaction could elevate the pH of the cathode chamber above 11 [80], but when the pH is low in the anode, because of the oxidation of organic compounds, the pH in the cathode chamber is around 7–9 which is optimal for the algal growth [81].

Algae are autotrophic photosynthetic organisms which use inorganic carbon (such as CO_2) source for growth. Different sources of carbon dioxide (e.g., waste gas from the purification of gas reformate streams) may be added to the algal bioreactor for algal growth which makes this system appealing for large-scale application [82]. Nevertheless, flowrate of CO_2 has to be carefully managed: González del Campo et al. [78] studied the influence of the time for bubbling CO_2 in their system (the amount of CO_2 added) and found that for their photo-MFC (0.8 L each compartment) 30 min each day was enough time to get the required amount of inorganic carbon for the alga growth, the algae concentration being stable around 350 ppm.

Although there has been much development on photo-MFC during the past few years, more work still requires to be focused on this attractive system. Assessment of valuable by-product coupled with simultaneous pollutant removal and electricity generation from photo-MFCs may be promising. If not platinum catalyst is used in the cathode, low-power densities are reached, and this is one of the main challenges for the next future. Electrons transfer mechanisms are still being explored looking for synergic interactions between biofilms of the cathode electrode and algae to improve the power output of this technology. Thus, it has been observed that in situ phototrophic biofilms formed on an electrode, immersed in a river stream, were able to catalyze the oxygen reduction [83], demonstrating that that biofilm can be better

than a suspension of planktonic cells as suggested by Huang et al. [79]. Recently Walter et al. [84] confirmed that the presence of an oxygenic biofilm can enhance the current produced by the photo-MFC only during the illumination period, but this effect was stable over time which suggests that the enhancement of the power output could be due to the oxygen supersaturation effect. Nevertheless, more effort is currently performed in order to confirm this hypothesis.

6 MFC Based on Natural Systems

The MFC fundamentals have been applied in some natural ecosystems or low-cost environmental remediation technologies with the already known objective: to harvest the energy contained in the environmental natural organic matter or contained in environmental pollutants. There are currently three main technologies: the sediment microbial fuel cells (SMFC) also called as benthic MFC, the plant-type microbial fuel cells (PMFC), and the MFC coupled to constructed wetlands (CWMFC).

The SMFC is the most usually studied and applied type. The research focused in SMFC began in 2001 [85], and since then the amount of research studies and applications has increased, especially since 2008. An SMFC (Fig. 12) is just an MFC where the anode is located in the bottom of a freshwater or marine-water sediment, which contains organic matter under anaerobic conditions or under absence of oxygen or alternative electron acceptors. The cathode is usually located next to the overlying of the surface water in order to get direct access to atmospheric oxygen, which is the usual final electron acceptor. In such environments there is a natural redox potential difference between the two electrodes and no membranes are located between them. The organic matter in the sediment is the fuel or electron donor for the MFC, and it can be of natural origin (e.g., humic acids, decomposing biomass) but also can be organic pollution (e.g., oil hydrocarbons). Marine sediments near the continental border usually contain organic matter (2–5% dry weight). Under such conditions, and according to the MFC fundamentals, electric power can be obtained and the organic matter is simultaneously removed, thus representing a sustainable method for polluted sediments remediation.

The SMFC studies were primarily done in marine sediments [45, 85, 86], although fresh water sediments were later used. Some of them were polluted sediments [87–92], but also the technology has been applied for polluted soil remediation [79, 93, 94].

The SMFC produce approximate electric power values in the range from 10 to 100 mW m^{-2} (electrode surface expressed as electrode footprint area) and, in some successful cases, obtained maximum power values between 100 and 300 mW m^{-2} [88, 95–98], and there is much variability in the results depending on the environmental conditions and the SMFC design. The most important variables currently under study are (1) the type of organic substrate used as electron donor and (2) the electrodes configuration (electrode materials, size, and distance between anode and

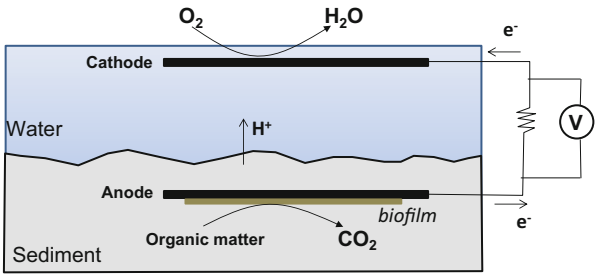

Fig. 12 A sediment microbial fuel cell (SMFC)

cathode). The results monitored are usually the electric power obtained, the pollutant removal efficiency, and the microbiological population responsible for the organic matter consumption and the electron transfer with the electrodes. The anode is covered by a microbial biofilm. The most related organisms for anodes residing from marine sediments are *Desulfuromonas acetoxidans*, and for freshwater sediments, the most related species are *Geobacter* [43].

The organic matter exhaustion in sediments is one of the problems which affect the SMFC performance. Several research works have studied the effect of organic matter addition. Different materials have been tested: chitin [12, 99], cellulose [89, 100], acetate [94, 98, 101], glucose [102], or plant biomass [96]. As a general result, the organic matter addition improved the power generation, although it was necessary to use readily biodegradable materials. Song and Jiang [88] reported that the sediment pretreatment was useful to increase the organic matter biodegradability and obtain higher-power efficiencies. Some pollutants such as phenol [93] or petroleum hydrocarbons [91] have been removed. The SMFC have been also used to avoid greenhouse effect methane emissions from aquatic sediments [103].

The SMFC anode is usually built from graphite, with many examples available in the literature [45, 103–105], and several times stainless steel [89, 106] or granular carbon [107] is also used. Babu and Mohan [105] studied the positive effect of including small graphite flakes in the sediment. Arends et al. [107] observed the most adequate size of carbon granules used as anode material, while Hong et al. [108] observed that SMFC using porous electrodes showed a superior performance when compared with the use of nonporous electrodes. The cathode is usually next to the atmospheric air-water interface and O_2 is the universal electron acceptor. The cathode is usually also graphite and several times stainless steel [68, 89, 106, 109]. The biofilm presence upon the cathode (biocathode) usually improved the cell performance [68, 110]. Zhang and Angelidaki [98] used SMFC to remove nitrates from wastewater, thus using nitrate as alternative electron acceptor in the cathode.

The SMFC are currently used to feed small remote electrical devices such as modems, temperature sensors, or dissolved oxygen sensors [111–115], and the first attempts for scale-up have been also reported [116].

The second natural-type MFC described here are the plants microbial fuel cell (PMFC). The anode of a PMFC is located into the soil and in contact with the plants rhizosphere, while the cathode is in direct contact with atmospheric oxygen (Fig. 13).

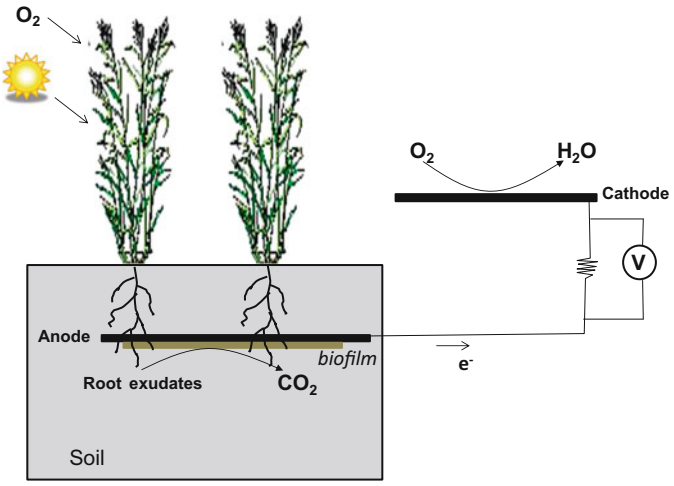

Fig. 13 The plants microbial fuel cell (PMFC)

The main difference between SMFC and PMFC is that the plant-MFC receives the organic matter (electron donor in the anode) from the rhizodeposits, that is, the organic matter exudates produced by the plant roots which were synthesized by the plant photosynthesis. The first PMFC was presented by Strik et al. [44], and these authors later developed several studies in which the effect of some variables was tested, such as the effect of the plants [117], using ferrocyanide as electron mediator in the cathode [118] or the microbial community developed in the root zone [119]. The role of plants as source of organic matter is very important. Recently, these authors proposed the application of PMFC as roof in buildings [120, 121]. The PMFC is very similar to the SMFC, and some works proposed studies which could be considered as a combination between these two systems [42, 68]. Some PMFC studies [122, 123] have reported low-power density values (around 10 mW m^{-2}) and higher values such as 88 mW m^{-2} [121], 222 mW m^{-2} [117] or 100 mW m^{-2} [118].

The third and more recently appeared natural-type MFC described here is the coupling between MFC and constructed wetlands for water pollution control (the CW-MFC). The constructed wetlands (CW) are well-known natural low-cost systems for wastewater treatment. There are several types of CW, and some of them, depending on the water flow direction and the wastewater pollution, present similar environmental conditions to the SMFC (i.e., a bottom section under anaerobic conditions and a top section next to the atmospheric oxygen), and it allowed to couple an MFC system in order to obtain energy from the water pollutants. Figure 14 shows, as example, a horizontal subsurface flow constructed wetland treating wastewater and coupled to an MFC system. There are also many similarities with SMFC, and indeed some studies reported can also be considered as a combination of SMFC and CW-MFC [124–126].

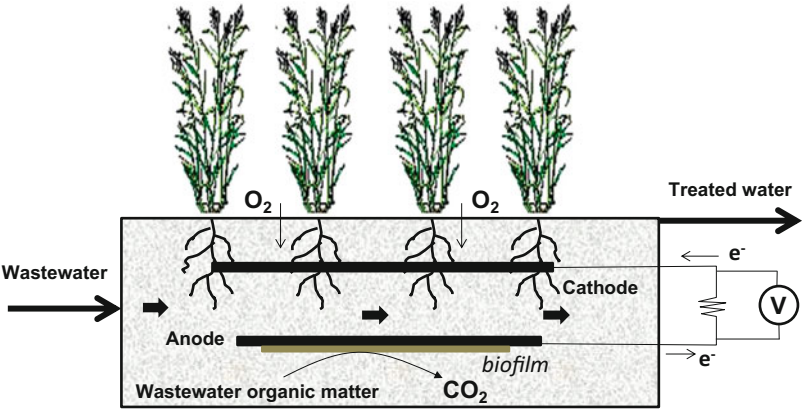

Fig. 14 A constructed wetland-microbial fuel cell (CW-MFC)

There are two important differences between this system (CW-MFC) and the other two systems previously described (SMFC and PMFC). First, the CW-MFC technology works usually under continuous flow mode; it receives a wastewater flow and discharges a treated water flow. Secondly, the role of the plants is opposite to the PMFC. They act as aeration systems instead of organic matter generation systems, and thus they must be located in the cathode zone. It is well known by wetland researchers that the macrophyte species usually used in CW for wastewater treatment can supply oxygen to the rhizosphere. Thus, the CW-MFC technology considers that the oxygen supply potential would be stronger than the organic matter generation potential in the form of root exudates.

The first CW-MFC was very recently reported by Yadav [127], and later several systems have been tested: vertical flow subsurface systems [128–130], a horizontal subsurface flow system [131], or surface flow systems with floating macrophytes [124, 125]. The few known systems based on constructed wetlands reported maximum power density values of 35 mW m^{-2} [127, 130], 16 mW m^{-2} [130], 43 mW m^{-2} [131], and values between 17 and 80 mW m^{-2} [124].

7 Challenges for Microbial Fuel Cells

In the recent years, many efforts have been done to increase knowledge on the fundamentals of the bioelectrochemical process as well as to apply it to wastewater treatment. This particular interest is based in the fact that microorganisms can degrade a great variety of organic molecules. Thus, opposite to conventional fuel cells, the type of fuel does not need to be a single molecule like hydrogen or methanol (low-temperature FC) or methane (high-temperature FC), but it can be even the complex mixture organics contained in a wastewater. However, presently

there are two important drawbacks for this use of MFC technology in wastewater treatment:

1. Oxygen should flow into the cathodic chamber, and the cost of aeration can be even higher than the energy obtained in the MFC.
2. Electric power densities obtained are not very high, and today they are far away from those required to make an economical feasible process, because of the extremely large areas of electrodes that would be required for an industrial-scale process.

To face the first drawback, and partially the second, one of the currently more interesting research topics is the algae and the natural MFC. Thus, this variety of MFC combines the utilization of photochemically active systems and biological moieties to harvest the energy from sunlight and convert this into electrical energy [41, 78]. This concept has been obtained from an extensively used process in a natural treatment of wastewaters: the lagooning treatment technology [132]. The lagooning technique is a well-known and widely used natural treatment process that consists of the accumulation of wastewater in ponds or basins, known as biological or stabilization ponds, where a series of biological, biochemical, and physical processes take place. During this treatment, process synergistic effects of heterotrophic microorganisms and algae occur. Thus, algae produce oxygen using sunlight energy and assimilate nutrients and bicarbonates, while heterotrophic microorganisms deplete organic matter using oxygen, providing as reaction products bicarbonates and nutrients. Lagooning is very efficient technology to purify wastewater from small or medium communities and from communities having variable population, because they are a robust technology to manage with highly changing flowrates. Some lagoon plants could also be built to purify wastewater produced by food seasonal industries. An algae MFC consists of a photosynthetic system providing oxygen at the cathode coupled to a microbial anodic system. By working in this way, a mixed culture of green algae generates, in situ, the oxygen required for the electrochemical reactions taking place in the cathodic chamber. The main advantage of this integration is that the photosynthetic system substituted the traditional aeration systems, which is a more sustainable option in both environmental and economic terms. No artificial mediators are needed, and it is also noticeable that not precious metals are required as catalyst in the cathode electrode. A similar behavior is also observed in other more complex bioelectrogenic processes such as wetlands [131]

To face the second drawback is more difficult nowadays. Currently, fundamentals of MFC are not well understood, and although efficiency of MFC has been largely increased in the last decade, there is a still a long way to scale-up the process [7]. In our opinion the current challenge of MFC should not be the application in large systems like urban wastewater treatment plants but the search for application at lower scale in which operation conditions are better controlled, energy requirements are smaller, and energy production and demand could be easily coupled. One of these applications may be the energy production for small applications replacing solar photovoltaic panels.

8 Concluding Remarks

Although not mature yet, MFC technology has improved significantly during the recent years, and presently it is within a stage of maturity that makes research on this topic ambitious and feasible at the same time. Thus, development of MFC can be considered as research at the edge of knowledge embracing multidisciplinary and the hottest topics of research in chemical engineering: energy, environment, and biotechnology. For sure its application will go further beyond the current expectations, but the search for application at a low scale in which energy requirements would not be very high seems to be applications that will be seen more sooner than later.

Acknowledgements Financial support from Ministerio de Economia y Competitividad of the Spanish Government through projects CTM2013-45612-R and CTQ2013-49748-EXP are gratefully acknowledged.

References

1. Park DH, Zeikus JG (2000) Electricity generation in microbial fuel cells using neutral red as an electronophore. Appl Environ Microbiol 66(4):1292–1297. doi:10.1128/aem.66.4.1292-1297.2000
2. Palmore GTR, Bertschy H, Bergens SH, Whitesides GM (1998) A methanol/dioxygen biofuel cell that uses NAD(+)-dependent dehydrogenases as catalysts: application of an electro-enzymatic method to regenerate nicotinamide adenine dinucleotide at low overpotentials. J Electroanal Chem 443(1):155–161. doi:10.1016/s0022-0728(97)00393-8
3. Topcagic S, Minteer SD (2006) Development of a membraneless ethanol/oxygen biofuel cell. Electrochim Acta 51(11):2168–2172. doi:10.1016/j.electacta.2005.03.090
4. Bond DR, Lovley DR (2003) Electricity production by *Geobacter sulfurreducens* attached to electrodes. Appl Environ Microbiol 69(3):1548–1555. doi:10.1128/aem.69.3.1548-1555.2003
5. Jang JK, Pham TH, Chang IS, Kang KH, Moon H, Cho KS, Kim BH (2004) Construction and operation of a novel mediator- and membrane-less microbial fuel cell. Process Biochem 39 (8):1007–1012. doi:10.1016/s0032-9592(03)00203-6
6. Rodrigo MA, Canizares P, Garcia H, Linares JJ, Lobato J (2009) Study of the acclimation stage and of the effect of the biodegradability on the performance of a microbial fuel cell. Bioresour Technol 100(20):4704–4710. doi:10.1016/j.biortech.2009.04.073
7. Bebelis S, Bouzek K, Cornell A, Ferreira MGS, Kelsall GH, Lapicque F, Ponce de León C, Rodrigo MA, Walsh FC (2013) Highlights during the development of electrochemical engineering. Chem Eng Res Des 91(10):1998–2020
8. Kim HJ, Park HS, Hyun MS, Chang IS, Kim M, Kim BH (2002) A mediator-less microbial fuel cell using a metal reducing bacterium, Shewanella putrefaciense. Enzyme Microb Technol 30(2):145–152. doi:10.1016/s0141-0229(01)00478-1
9. Bannetto H (1991) Electricity generation by microorganisms. Biotechnol Edu 1:168
10. Logan BE (2012) Essential data and techniques for conducting microbial fuel cell and other types of bioelectrochemical system experiments. ChemSusChem 5(6):988–994. doi:10.1002/cssc.201100604

11. Logan BE, Rabaey K (2012) Conversion of wastes into bioelectricity and chemicals by using microbial electrochemical technologies. Science 337(6095):686–690. doi:10.1126/science.1217412
12. Logan BE, Hamelers B, Rozendal RA, Schrorder U, Keller J, Freguia S, Aelterman P, Verstraete W, Rabaey K (2006) Microbial fuel cells: methodology and technology. Environ Sci Technol 40(17):5181–5192. doi:10.1021/es0605016
13. Mook WT, Aroua MKT, Chakrabarti MH, Noor IM, Irfan MF, Low CTJ (2013) A review on the effect of bio-electrodes on denitrification and organic matter removal processes in bio-electrochemical systems. J Ind Eng Chem 19(1):1–13. doi:10.1016/j.jiec.2012.07.004
14. Virdis B, Rabaey K, Yuan Z, Keller J (2008) Microbial fuel cells for simultaneous carbon and nitrogen removal. Water Res 42(12):3013–3024. doi:10.1016/j.watres.2008.03.017
15. Virdis B, Rabaey K, Rozendal RA, Yuan Z, Keller J (2010) Simultaneous nitrification, denitrification and carbon removal in microbial fuel cells. Water Res 44(9):2970–2980. doi:10.1016/j.watres.2010.02.022
16. Velasquez-Orta SB, Head IM, Curtis TP, Scott K (2011) Factors affecting current production in microbial fuel cells using different industrial wastewaters. Bioresour Technol 102 (8):5105–5112. doi:10.1016/j.biortech.2011.01.059
17. Rodrigo MA, Canizares P, Lobato J, Paz R, Saez C, Linares JJ (2007) Production of electricity from the treatment of urban waste water using a microbial fuel cell. J Power Sources 169(1):198–204. doi:10.1016/j.jpowsour.2007.01.054
18. Gonzalez del Campo A, Lobato J, Canizares P, Rodrigo MA, Fernandez Morales FJ (2013) Short-term effects of temperature and COD in a microbial fuel cell. Appl Energy 101:213–217. doi:10.1016/j.apenergy.2012.02.064
19. Rabaey K, Lissens G, Siciliano SD, Verstraete W (2003) A microbial fuel cell capable of converting glucose to electricity at high rate and efficiency. Biotechnol Lett 25(18):1531–1535. doi:10.1023/a:1025484009367
20. Du Z, Li H, Gu T (2007) A state of the art review on microbial fuel cells: a promising technology for wastewater treatment and bioenergy. Biotechnol Adv 25(5):464–482. doi:10.1016/j.biotechadv.2007.05.004
21. Cercado-Quezada B, Delia M-L, Bergel A (2010) Testing various food-industry wastes for electricity production in microbial fuel cell. Bioresour Technol 101(8):2748–2754. doi:10.1016/j.biortech.2009.11.076
22. Oh S, Min B, Logan BE (2004) Cathode performance as a factor in electricity generation in microbial fuel cells. Environ Sci Technol 38(18):4900–4904. doi:10.1021/es049422p
23. Logan BE (2005) Simultaneous wastewater treatment and biological electricity generation. Water Sci Technol 52(1–2):31–37
24. Moon H, Chang IS, Jang JK, Kim BH (2005) Residence time distribution in microbial fuel cell and its influence on COD removal with electricity generation. Biochem Eng J 27(1):59–65. doi:10.1016/j.bej.2005.02.010
25. Morris JM, Jin S (2009) Influence of NO3 and SO4 on power generation from microbial fuel cells. Chem Eng J 153(1–3):127–130. doi:10.1016/j.cej.2009.06.023
26. Larrosa A, Lozano LJ, Katuri KP, Head I, Scott K, Godinez C (2009) On the repeatability and reproducibility of experimental two-chambered microbial fuel cells. Fuel 88(10):1852–1857. doi:10.1016/j.fuel.2009.04.026
27. Niessen J, Harnisch F, Rosenbaum M, Schroder U, Scholz F (2006) Heat treated soil as convenient and versatile source of bacterial communities for microbial electricity generation. Electrochem Commun 8(5):869–873. doi:10.1016/j.elecom.2006.03.025
28. Parot S, Delia M-L, Bergel A (2008) Acetate to enhance electrochemical activity of biofilms from garden compost. Electrochim Acta 53(6):2737–2742. doi:10.1016/j.electacta.2007.10.059
29. Scott K, Murano C (2007) Microbial fuel cells utilising carbohydrates. J Chem Technol Biotechnol 82(1):92–100. doi:10.1002/jctb.1641

30. More TT, Ghangrekar MM (2010) Improving performance of microbial fuel cell with ultrasonication pre-treatment of mixed anaerobic inoculum sludge. Bioresour Technol 101 (2):562–567. doi:10.1016/j.biortech.2009.08.045
31. Kim JR, Min B, Logan BE (2005) Evaluation of procedures to acclimate a microbial fuel cell for electricity production. Appl Microbiol Biotechnol 68(1):23–30. doi:10.1007/s00253-004-1845-6
32. Lobato J, Canizares P, Jesus Fernandez F, Rodrigo MA (2012) An evaluation of aerobic and anaerobic sludges as start-up material for microbial fuel cell systems. N Biotechnol 29 (3):415–420. doi:10.1016/j.nbt.2011.09.004
33. Rodrigo MA, Canizares P, Lobato J (2010) Effect of the electron-acceptors on the performance of a MFC. Bioresour Technol 101(18):7014–7018. doi:10.1016/j.biortech.2010.04.013
34. Franks AE, Nevin KP (2010) Microbial fuel cells: a current review. Energies 3(5):899–919. doi:10.3390/en3050899
35. Clauwaert P, Van der Ha D, Boon N, Verbeken K, Verhaege M, Rabaey K, Verstraete W (2007) Open air biocathode enables effective electricity generation with microbial fuel cells. Environ Sci Technol 41(21):7564–7569. doi:10.1021/es0709831
36. Hu Z (2008) Electricity generation by a baffle-chamber membraneless microbial fuel cell. J Power Sources 179(1):27–33. doi:10.1016/j.jpowsour.2007.12.094
37. Freguia S, Rabaey K, Yuan Z, Keller J (2007) Electron and carbon balances in microbial fuel cells reveal temporary bacterial storage behavior during electricity generation. Environ Sci Technol 41(8):2915–2921. doi:10.1021/es062611i
38. Powell EE, Mapiour ML, Evitts RW, Hill GA (2009) Growth kinetics of Chlorella vulgaris and its use as a cathodic half cell. Bioresour Technol 100(1):269–274. doi:10.1016/j.biortech.2008.05.032
39. Rosenbaum M, He Z, Angenent LT (2010) Light energy to bioelectricity: photosynthetic microbial fuel cells. Curr Opin Biotechnol 21(3):259–264. doi:10.1016/j.copbio.2010.03.010
40. Strik DPBTB, Terlouw H, Hamelers HVM, Buisman CJN (2008) Renewable sustainable biocatalyzed electricity production in a photosynthetic algal microbial fuel cell (PAMFC). Appl Microbiol Biotechnol 81(4):659–668. doi:10.1007/s00253-008-1679-8
41. Lobato J, Gonzalez del Campo A, Fernandez FJ, Canizares P, Rodrigo MA (2013) Lagooning microbial fuel cells: a first approach by coupling electricity-producing microorganisms and algae. Appl Energy 110:220–226. doi:10.1016/j.apenergy.2013.04.010
42. de Schamphelaire L, van den Bossche L, Dang HS, Hofte M, Boon N, Rabaey K, Verstraete W (2008) Microbial fuel cells generating electricity from rhizodeposits of rice plants. Environ Sci Technol 42(8):3053–3058. doi:10.1021/es071938w
43. De Schamphelaire L, Rabaey K, Boeckx P, Boon N, Verstraete W (2008) Outlook for benefits of sediment microbial fuel cells with two bio-electrodes. J Microbial Biotechnol 1(6):446–462. doi:10.1111/j.1751-7915.2008.00042.x
44. Strik DPBTB, Hamelers HVM, Snel JFH, Buisman CJN (2008) Green electricity production with living plants and bacteria in a fuel cell. Int J Energy Res 32(9):870–876. doi:10.1002/er.1397
45. Reimers CE, Girguis P, Stecher HA III, Tender LM, Ryckelynck N, Whaling P (2006) Microbial fuel cell energy from an ocean cold seep. Geobiology 4(2):123–136. doi:10.1111/j.1472-4669.2006.00071.x
46. Rabaey K, Boon N, Höfte M, Verstraete W (2005) Microbial phenazine production enhances electron transfer in biofuel cells. Environ Sci Tech 39(9):3401–3408
47. Allen RM, Bennetto HP (1993) Microbial fuel-cells - electricity production from carbohydrates. Appl Biochem Biotechnol 39–40(1):27–40
48. Jung S (2012) Impedance analysis of *Geobacter sulfurreducens* PCA, *Shewanella oneidensis* MR-1, and their coculture in bioeletrochemical systems. Int J Electrochem Sci 7(11):11091–11100

49. Rabaey K, Boon N, Siciliano SD, Verhaege M, Verstraete W (2004) Biofuel cells select for microbial consortia that self-mediate electron transfer. Appl Environ Microbiol 70(9):5373–5382
50. Yates MD, Kiely PD, Call DF, Rismani-Yazdi H, Bibby K, Peccia J, Regan JM, Logan BE (2012) Convergent development of anodic bacterial communities in microbial fuel cells. ISME J 6(11):2002–2013
51. Yong XY, Feng J, Chen YL, Shi DY, Xu YS, Zhou J, Wang SY, Xu L, Yong YC, Sun YM, Shi CL, OuYang PK, Zheng T (2014) Enhancement of bioelectricity generation by cofactor manipulation in microbial fuel cell. Biosens Bioelectron 56:19–25
52. Kim BH, Park HS, Kim HJ, Kim GT, Chang IS, Lee J, Phung NT (2004) Enrichment of microbial community generating electricity using a fuel-cell-type electrochemical cell. Appl Microbiol Biotechnol 63(6):672–681
53. Infantes D, González Del Campo A, Villaseñor J, Fernández FJ (2011) Influence of pH, temperature and volatile fatty acids on hydrogen production by acidogenic fermentation. Int J Hydrogen Energy 36(24):15595–15601
54. Nealson KH, Finkel SE (2011) Electron flow and biofilms. MRS Bull 36(5):380–384
55. Marsili E, Sun J, Bond DR (2010) Voltammetry and growth physiology of *Geobacter sulfurreducens* biofilms as a function of growth stage and imposed electrode potential. Electroanalysis 22(7–8):865–874
56. Logan BE, Hamelers B, Rozendal R, Schröder U, Keller J, Freguia S, Aelterman P, Verstraete W, Rabaey K (2006) Microbial fuel cells: methodology and technology. Environ Sci Tech 40(17):5181–5192
57. Von Canstein H, Ogawa J, Shimizu S, Lloyd JR (2008) Secretion of flavins by Shewanella species and their role in extracellular electron transfer. Appl Environ Microbiol 74(3):615–623
58. Marsili E, Baron DB, Shikhare ID, Coursolle D, Gralnick JA, Bond DR (2008) Shewanella secretes flavins that mediate extracellular electron transfer. Proc Natl Acad Sci U S A 105 (10):3968–3973
59. Shukla AK, Suresh P, Berchmans S, Rajendran A (2004) Biological fuel cells and their applications. Curr Sci 87(4):455–468
60. Park DH, Zeikus JG (2003) Improved fuel cell and electrode designs for producing electricity from microbial degradation. Biotechnol Bioeng 81(3):348–355
61. Park HS, Kim BH, Kim HS, Kim HJ, Kim GT, Kim M, Chang IS, Park YK, Chang HI (2001) A novel electrochemically active and Fe(III)-reducing bacterium phylogenetically related to Clostridium butyricum isolated from a microbial fuel cell. Anaerobe 7(6):297–306
62. Dos Santos AB, Traverse J, Cervantes FJ, Van Lier JB (2005) Enhancing the electron transfer capacity and subsequent color removal in bioreactors by applying thermophilic anaerobic treatment and redox mediators. Biotechnol Bioeng 89(1):42–52
63. Velasquez-Orta SB, Head IM, Curtis TP, Scott K, Lloyd JR, Von Canstein H (2010) The effect of flavin electron shuttles in microbial fuel cells current production. Appl Microbiol Biotechnol 85(5):1373–1381
64. Chang BV, Yuan SY, Ren YL (2012) Anaerobic degradation of tetrabromobisphenol-A in river sediment. Ecol Eng 49:73–76
65. Rosenbaum M, Schroder U, Scholz F (2005) Utilizing the green alga Chlamydomonas reinhardtii for microbial electricity generation: a living solar cell. Appl Microbiol Biotechnol 68(6):753–756. doi:10.1007/s00253-005-1915-4
66. Tanaka K, Tamamushi R, Ogawa T (1985) bioelectrochemical fuel-cells operated by the cyanobacterium, anabaena-variabilis. J Chem Technol Biotechnol 35(3):191–197
67. Rosenbaum M, Agler MT, Fornero JJ, Venkataraman A, Angenent LT (2010) Integrating BES in the wastewater and sludge treatment line. In: Rabaey K, Angenent LT, Schröder U, Keller J (eds) Bioelectrochemical system: from extracellular electron transfer to biotechnological application. International Water Association, London, UK

68. De Schamphelaire L, Cabezas A, Marzorati M, Friedrich MW, Boon N, Verstraete W (2010) Microbial community analysis of anodes from sediment microbial fuel cells powered by rhizodeposits of living rice plants. Appl Environ Microbiol 76(6):2002–2008. doi:10.1128/aem.02432-09
69. Pant D, Van Bogaert G, Diels L, Vanbroekhoven K (2010) A review of the substrates used in microbial fuel cells (MFCs) for sustainable energy production. Bioresour Technol 101 (6):1533–1543. doi:10.1016/j.biortech.2009.10.017
70. Munoz R, Guieysse B (2006) Algal-bacterial processes for the treatment of hazardous contaminants: a review. Water Res 40(15):2799–2815. doi:10.1016/j.watres.2006.06.011
71. Rittmann BE (2008) Opportunities for renewable bioenergy using microorganisms. Biotechnol Bioeng 100(2):203–212. doi:10.1002/bit.21875
72. De Schamphelaire L, Verstraete W (2009) Revival of the biological sunlight-to-biogas energy conversion system. Biotechnol Bioeng 103(2):296–304. doi:10.1002/bit.22257
73. Wang X, Feng Y, Liu J, Lee H, Li C, Li N, Ren N (2010) Sequestration of CO2 discharged from anode by algal cathode in microbial carbon capture cells (MCCs). Biosens Bioelectron 25(12):2639–2643. doi:10.1016/j.bios.2010.04.036
74. Xiao L, Young EB, Berges JA, He Z (2012) Integrated photo-bioelectrochemical system for contaminants removal and bioenergy production. Environ Sci Technol 46(20):11459–11466. doi:10.1021/es303144n
75. Strik DPBTB, Hamelers HVM, Buisman CJN (2010) Solar energy powered microbial fuel cell with a reversible bioelectrode. Environ Sci Technol 44(1):532–537. doi:10.1021/es902435v
76. Clauwaert P, Rabaey K, Aelterman P, De Schamphelaire L, Ham TH, Boeckx P, Boon N, Verstraete W (2007) Biological denitrification in microbial fuel cells. Environ Sci Technol 41 (9):3354–3360. doi:10.1021/es062580r
77. Ter Heijne A, Hamelers HVM, Buisman CJN (2007) Microbial fuel cell operation with continuous biological ferrous iron oxidation of the catholyte. Environ Sci Technol 41 (11):4130–4134. doi:10.1021/es0702824
78. Gonzalez del Campo A, Canizares P, Rodrigo MA, Fernandez FJ, Lobato J (2013) Microbial fuel cell with an algae-assisted cathode: a preliminary assessment. J Power Sources 242:638–645. doi:10.1016/j.jpowsour.2013.05.110
79. Huang L, Cheng S, Chen G (2011) Bioelectrochemical systems for efficient recalcitrant wastes treatment. J Chem Technol Biotechnol 86(4):481–491. doi:10.1002/jctb.2551
80. Rozendal RA, Hamelers HVM, Buisman CJN (2006) Effects of membrane cation transport on pH and microbial fuel cell performance. Environ Sci Technol 40(17):5206–5211. doi:10.1021/es060387r
81. Park JBK, Craggs RJ, Shilton AN (2011) Wastewater treatment high rate algal ponds for biofuel production. Bioresour Technol 102(1):35–42. doi:10.1016/j.biortech.2010.06.158
82. Fornero JJ, Rosenbaum M, Cotta MA, Angenent LT (2010) Carbon dioxide addition to microbial fuel cell cathodes maintains sustainable catholyte pH and improves anolyte pH, alkalinity, and conductivity. Environ Sci Technol 44(7):2728–2734. doi:10.1021/es9031985
83. Lyautey E, Cournet A, Morin S, Bouletreau S, Etcheverry L, Charcosset J-Y, Delmas F, Bergel A, Garabetian F (2011) Electroactivity of phototrophic river biofilms and constitutive cultivable bacteria. Appl Environ Microbiol 77(15):5394–5401. doi:10.1128/aem.00500-11
84. Walter XA, Greenman J, Ieropoulos IA (2013) Oxygenic phototrophic biofilms for improved cathode performance in microbial fuel cells. Algal Res 2(3):183–187. doi:10.1016/j.algal.2013.02.002
85. Reimers CE, Tender LM, Fertig S, Wang W (2001) Harvesting energy from the marine sediment-water interface. Environ Sci Technol 35(1):192–195. doi:10.1021/es001223s
86. Tender LM, Reimers CE, Stecher HA, Holmes DE, Bond DR, Lowy DA, Pilobello K, Fertig SJ, Lovley DR (2002) Harnessing microbially generated power on the seafloor. Nat Biotechnol 20(8):821–825. doi:10.1038/nbt716

87. Song T-S, Yan Z-S, Zhao Z-W, Jiang H-L (2010) Removal of organic matter in freshwater sediment by microbial fuel cells at various external resistances. J Chem Technol Biotechnol 85(11):1489–1493. doi:10.1002/jctb.2454
88. Song T-S, Jiang H-L (2011) Effects of sediment pretreatment on the performance of sediment microbial fuel cells. Bioresour Technol 102(22):10465–10470. doi:10.1016/j.biortech.2011.08.129
89. Song T-S, Yan Z-S, Zhao Z-W, Jiang H-L (2011) Construction and operation of freshwater sediment microbial fuel cell for electricity generation. Bioprocess Biosyst Eng 34(5):621–627. doi:10.1007/s00449-010-0511-x
90. Yuan Y, Zhou S, Zhuang L (2010) A new approach to in situ sediment remediation based on air-cathode microbial fuel cells. J Soils Sediments 10(7):1427–1433. doi:10.1007/s11368-010-0276-5
91. Morris JM, Jin S (2012) Enhanced biodegradation of hydrocarbon-contaminated sediments using microbial fuel cells. J Hazard Mater 213:474–477. doi:10.1016/j.jhazmat.2012.02.029
92. Yan Z, Song N, Cai H, Tay J-H, Jiang H (2012) Enhanced degradation of phenanthrene and pyrene in freshwater sediments by combined employment of sediment microbial fuel cell and amorphous ferric hydroxide. J Hazard Mater 199:217–225. doi:10.1016/j.jhazmat.2011.10.087
93. Huang D-Y, Zhou S-G, Chen Q, Zhao B, Yuan Y, Zhuang L (2011) Enhanced anaerobic degradation of organic pollutants in a soil microbial fuel cell. Chem Eng J 172(2–3):647–653. doi:10.1016/j.cej.2011.06.024
94. Dominguez-Garay A, Berna A, Ortiz-Bernad I, Esteve-Nunez A (2013) Silica colloid formation enhances performance of sediment microbial fuel cells in a low conductivity soil. Environ Sci Technol 47(4):2117–2122. doi:10.1021/es303436x
95. Nielsen ME, Reimers CE, White HK, Sharma S, Girguis PR (2008) Sustainable energy from deep ocean cold seeps. Energy Environ Sci 1(5):584–593. doi:10.1039/b811899j
96. Song T-S, Wang D-B, Han S, X-y W, Zhou CC (2014) Influence of biomass addition on electricity harvesting from solid phase microbial fuel cells. Int J Hydrogen Energy 39 (2):1056–1062. doi:10.1016/j.ijhydene.2013.10.125
97. Zhang Y, Angelidaki I (2012) Bioelectrode-based approach for enhancing nitrate and nitrite removal and electricity generation from eutrophic lakes. Water Res 46(19):6445–6453. doi:10.1016/j.watres.2012.09.022
98. Zhang Y, Angelidaki I (2012) Self-stacked submersible microbial fuel cell (SSMFC) for improved remote power generation from lake sediments. Biosens Bioelectron 35(1):265–270. doi:10.1016/j.bios.2012.02.059
99. Jung SP, Yoon M-H, Lee S-M, Oh S-E, Kang H, Yang J-K (2014) Power generation and anode bacterial community compositions of sediment fuel cells differing in anode materials and carbon sources. Int J Electrochem Sci 9(1):315–326
100. Sajana TK, Ghangrekar MM, Mitra A (2014) Effect of presence of cellulose in the freshwater sediment on the performance of sediment microbial fuel cell. Bioresour Technol 155:84–90
101. Zhao J, Li X-F, Ren Y-P, Wang X-H, Jian C (2012) Electricity generation from Taihu Lake cyanobacteria by sediment microbial fuel cells. J Chem Technol Biotechnol 87(11):1567–1573. doi:10.1002/jctb.3794
102. Kim M, Ekpeghere KI, Kim SH, Chang JS, Koh SC (2012) Analysis of microbial communities in aquatic sediment microbial fuel cells injected with glucose. Kor J Microbiol 48 (4):254–261
103. Ueno Y, Kitajima Y (2012) Suppression of methane Gas emission from sediment using a bioelectrochemical system. Environ Eng Manage J 11(10):1833–1837
104. Ajayi FF, Weigele PR (2012) A terracotta bio-battery. Bioresour Technol 116:86–91. doi:10.1016/j.biortech.2012.04.019
105. Babu ML, Mohan SV (2012) Influence of graphite flake addition to sediment on electrogenesis in a sediment-type fuel cell. Bioresour Technol 110:206–213. doi:10.1016/j.biortech.2012.01.064

106. Dumas C, Mollica A, Feron D, Basseguy R, Etcheverry L, Bergel A (2007) Marine microbial fuel cell: use of stainless steel electrodes as anode and cathode materials. Electrochim Acta 53(2):468–473. doi:10.1016/j.electacta.2007.06.069
107. Arends JBA, Blondeel E, Tennison SR, Boon N, Verstraete W (2012) Suitability of granular carbon as an anode material for sediment microbial fuel cells. J Soils Sediments 12(7):1197–1206. doi:10.1007/s11368-012-0537-6
108. Hong SW, Chang IS, Choi YS, Kim BH, Chung TH (2009) Responses from freshwater sediment during electricity generation using microbial fuel cells. Bioprocess Biosyst Eng 32 (3):389–395. doi:10.1007/s00449-008-0258-9
109. Dumas C, Mollica A, Feron D, Basseguy R, Etcheverry L, Bergel A (2008) Checking graphite and stainless anodes with an experimental model of marine microbial fuel cell. Bioresour Technol 99(18):8887–8894. doi:10.1016/j.biortech.2008.04.054
110. Wang A, Cheng H, Ren N, Cui D, Lin N, Wu W (2012) Sediment microbial fuel cell with floating biocathode for organic removal and energy recovery. Front Environ Sci Eng 6 (4):569–574. doi:10.1007/s11783-011-0335-1
111. Donovan C, Dewan A, Peng H, Heo D, Beyenal H (2011) Power management system for a 2.5 W remote sensor powered by a sediment microbial fuel cell. J Power Sources 196 (3):1171–1177. doi:10.1016/j.jpowsour.2010.08.099
112. Donovan C, Dewan A, Heo D, Lewandowski Z, Beyenal H (2013) Sediment microbial fuel cell powering a submersible ultrasonic receiver: new approach to remote monitoring. J Power Sources 233:79–85. doi:10.1016/j.jpowsour.2012.12.112
113. Gong Y, Radachowsky SE, Wolf M, Nielsen ME, Girguis PR, Reimers CE (2011) Benthic microbial fuel cell as direct power source for an acoustic modem and seawater oxygen/temperature sensor system. Environ Sci Technol 45(11):5047–5053. doi:10.1021/es104383q
114. Zhang F, Tian L, He Z (2011) Powering a wireless temperature sensor using sediment microbial fuel cells with vertical arrangement of electrodes. J Power Sources 196 (22):9568–9573. doi:10.1016/j.jpowsour.2011.07.037
115. Thomas YRJ, Picot M, Carer A, Berder O, Sentieys O, Barriere F (2013) A single sediment-microbial fuel cell powering a wireless telecommunication system. J Power Sources 241:703–708. doi:10.1016/j.jpowsour.2013.05.016
116. Hsu L, Chadwick B, Kagan J, Thacher R, Wotawa-Bergen A, Richter K (2013) Scale up considerations for sediment microbial fuel cells. RSC Adv 3(36):15947–15954. doi:10.1039/c3ra43180k
117. Helder M, Strik DPBTB, Hamelers HVM, Kuhn AJ, Blok C, Buisman CJN (2010) Concurrent bio-electricity and biomass production in three plant-microbial fuel cells using Spartina anglica, Arundinella anomala and Arundo donax. Bioresour Technol 101(10):3541–3547. doi:10.1016/j.biortech.2009.12.124
118. Timmers RA, Strik DPBTB, Hamelers HVM, Buisman CJN (2010) Long-term performance of a plant microbial fuel cell with Spartina anglica. Appl Microbiol Biotechnol 86(3):973–981. doi:10.1007/s00253-010-2440-7
119. Timmers RA, Rothballer M, Strik DPBTB, Engel M, Schulz S, Schloter M, Hartmann A, Hamelers B, Buisman C (2012) Microbial community structure elucidates performance of Glyceria maxima plant microbial fuel cell. Appl Microbiol Biotechnol 94(2):537–548. doi:10.1007/s00253-012-3894-6
120. Helder M, Chen W-S, van der Harst EJM, Strik DPBTB, Hamelers HVM, Buisman CJN, Potting J (2013) Electricity production with living plants on a green roof: environmental performance of the plant-microbial fuel cell. Biofuels Bioprod Biorefin Biofpr 7(1):52–64. doi:10.1002/bbb.1373
121. Helder M, Strik DPBTB, Timmers RA, Raes SMT, Hamelers HVM, Buisman CJN (2013) Resilience of roof-top plant-microbial fuel cells during Dutch winter. Biomass Bioenergy 51:1–7. doi:10.1016/j.biombioe.2012.10.011

122. Timmers RA, Strik DPBTB, Hamelers HVM, Buisman CJN (2013) Electricity generation by a novel design tubular plant microbial fuel cell. Biomass Bioenergy 51:60–67. doi:10.1016/j.biombioe.2013.01.002
123. Liu S, Song H, Li X, Yang F (2013) Power generation enhancement by utilizing plant photosynthate in microbial fuel cell coupled constructed wetland system. Int J Photoenergy. doi:10.1155/2013/172010
124. Mohan SV, Mohanakrishna G, Chiranjeevi P (2011) Sustainable power generation from floating macrophytes based ecological microenvironment through embedded fuel cells along with simultaneous wastewater treatment. Bioresour Technol 102(14):7036–7042. doi:10.1016/j.biortech.2011.04.033
125. Chiranjeevi P, Chandra R, Mohan SV (2013) Ecologically engineered submerged and emergent macrophyte based system: an integrated eco-electrogenic design for harnessing power with simultaneous wastewater treatment. Ecol Eng 51:181–190. doi:10.1016/j.ecoleng.2012.12.014
126. Chen Z, Y-c H, J-h L, Zhao F, Y-g Z (2012) A novel sediment microbial fuel cell with a biocathode in the rice rhizosphere. Bioresour Technol 108:55–59. doi:10.1016/j.biortech.2011.10.040
127. Yadav AK (2010) Design and development of novel constructed wetland cum microbial fuel cell for electricity production and wastewater treatment. In: Paper presented at the 12th international conference on wetlands systems for water pollution control. International Water Association, Venice, Italy
128. Zhao Y, Collum S, Phelan M, Goodbody T, Doherty L, Hu Y (2013) Preliminary investigation of constructed wetland incorporating microbial fuel cell: batch and continuous flow trials. Chem Eng J 229:364–370. doi:10.1016/j.cej.2013.06.023
129. Fang Z, Song H-L, Cang N, Li X-N (2013) Performance of microbial fuel cell coupled constructed wetland system for decolorization of azo dye and bioelectricity generation. Bioresour Technol 144:165–171. doi:10.1016/j.biortech.2013.06.073
130. Yadav AK, Dash P, Mohanty A, Abbassi R, Mishra BK (2012) Performance assessment of innovative constructed wetland-microbial fuel cell for electricity production and dye removal. Ecol Eng 47:126–131. doi:10.1016/j.ecoleng.2012.06.029
131. Villasenor J, Capilla P, Rodrigo MA, Canizares P, Fernandez FJ (2013) Operation of a horizontal subsurface flow constructed wetland - microbial fuel cell treating wastewater under different organic loading rates. Water Res 47(17):6731–6738. doi:10.1016/j.watres.2013.09.005
132. Kruzic AP, Kreissl JF (2009) Natural treatment and onsite systems. Water Environ Res 81 (10):1346–1360. doi:10.2175/106143009x12445568399659

Removal of Organic Pollutants from Industrial Wastewater by Treatment with Oxidoreductase Enzymes

Edelmira Valero, María-Isabel González-Sánchez, and María-Teresa Pérez-Prior

Abstract Removal of persistent organic pollutants in wastewaters of industrial origin is an increasingly relevant issue in industrialized countries that needs addressing. Remarkable research efforts have been made for the development and implementation of new efficient and eco-friendly treatments capable of reducing, or even eliminating, toxic compounds in effluents prior to their disposal. Enzymatic methods appear to be a promising technology for this task, with a minor impact on ecosystems as compared to physicochemical methods. The applicability of such technology has been explicitly demonstrated in a huge number of publications and patents registered to date.

The present chapter focuses on the application of oxidoreductase enzymes in industrial wastewaters treatment. Numerous redox enzymes, including peroxidases, tyrosinases, and laccases from different sources, and even hemoglobin from animal blood have exhibited their potential for the remediation of a broad spectrum of recalcitrant organic compounds. However the implementation of this technology on an industrial scale still needs further research. Here the most important aspects about the current situation of the subject and future perspectives for the use of redox enzymes in industrial wastewaters treatment are highlighted.

Keywords Aromatic pollutants, Immobilization, Industrial wastewater, Oxidation, Oxidoreductase enzymes

E. Valero (✉) and M.-I. González-Sánchez
Department of Physical Chemistry, School of Industrial Engineering, University of Castilla-La Mancha, Campus Universitario, 02071 Albacete, Spain
e-mail: Edelmira.Valero@uclm.es; MIsabel.Gonzalez@uclm.es

M.-T. Pérez-Prior
Department of Materials Science and Chemical Engineering, University Carlos III of Madrid, Campus Universitario, Leganés, 28911 Madrid, Spain
e-mail: maperezp@ing.uc3m.es

E. Jiménez et al. (eds.), *Environment, Energy and Climate Change I: Environmental Chemistry of Pollutants and Wastes*, Hdb Env Chem (2015) 32: 317–340,
DOI 10.1007/698_2014_266,
Published online: 22 July 2014

Contents

Abbreviations

BOD	Biochemical oxygen demand
BPA	Bisphenol A
CLEAs	Cross-linked enzyme aggregates
COD	Chemical oxygen demand
CoI	Compound I of peroxidase
CoII	Compound II of peroxidase
CPO	Chloroperoxidase
EDCs	Endocrine disrupting compounds
Hb	Hemoglobin
HRP	Horseradish peroxidase
LiP	Lignin peroxidase
metHb	metHemoglobin
MnP	Manganese peroxidase
PAHs	Polycyclic aromatic hydrocarbons
PCBs	Polychlorinated biphenyls
PCDDs	Polychlorinated dibenzodioxins
PCDFs	Polychlorinated dibenzofurans
PEG	Polyethylene glycol
POPs	Persistent organic pollutants
QSAR	Quantitative structure–activity relationship
SBP	Soya bean peroxidase
US EPA	United States Environmental Protection Agency
WRF	White-rot fungi
WWT	Wastewater treatment
WWTPs	Wastewater treatment plants

1 Introduction

Water is an essential raw material for all organisms on our planet. Freshwater supply has historically been a determining factor for society development, and its scarcity or lack has led to poverty, disease, or even the complete disappearance of population centers. Nowadays in the "omic" era, governments, companies, and environmental scientists face one of the most crucial challenges for life: improving access and availability of natural freshwater resources for the whole population and ensuring sustainability for future generations.

Since the Industrial Revolution in the 19th century, the number and variety of industries have immensely grown with a clear aim to improve the human quality of life and, in fact, it has profoundly transformed society year in year out. However, the same activities that have allowed industrialized countries to gain prosperity have also damaged the environment. The American Chemical Society currently has more than 81 million organic and inorganic substances registered [1], which gives us an idea of the huge number of chemicals handled worldwide industrially on a daily basis. Many of these chemicals are discharged in industrial effluents with little or no treatment, which can result in a huge negative impact on the environment. Thus, there is considerable pressure on industry to clean effluents prior to their disposal. For all these reasons, the development and implementation of low-cost, efficient, and environmentally acceptable technologies to remove a wide variety of pollutants present in different kinds of industrial streams is essential to attain true sustainable development.

There are many kinds of industry that generate wastewater effluents that contain a number of hazardous organic compounds. These most notably include oil refineries, coking plants, mining, agricultural activity, different manufacturing plants, such as food, textile, dyes, timber, pulp and paper, plastics, solvents, detergents, other chemicals and pharmaceutical industries, and thousands of laboratories worldwide. The chemical composition of industrial effluent discharges varies according to the particular kind of industry that has generated them. Many of these compounds are toxic, persistent organic pollutants (POPs) in the environment, which are generally resistant to natural environmental degradation, and also to conventional wastewater treatment (WWT) techniques. They are also semi-volatile organic compounds that can travel long distances from the emission source, do not dissolve readily in water, but in fats and lipids, and so tend to bioaccumulate. Therefore their impact on humans and ecosystems is significant, even in the microamounts in which they are found in waters. The European Community Regulation No. 850/2004 [2] declares that: "The POP content in waste is to be destroyed or irreversibly transformed into substances that do not exhibit similar characteristics, unless other operations are environmentally preferable."

Different technologies have been developed and tested to evaluate their relative potential for treating industrial streams containing POPs. They can be classified into non-oxidative and oxidative techniques. Among non-oxidative approaches, physicochemical adsorption with different materials, wetlands, microalgae, and other

unit operations of the chemical industry have proven effective [3]. Oxidative approaches are also well suited for the treatment of industrial wastewaters. They are based on the conversion of organic matter into carbon dioxide and water (total oxidation) or into harmless intermediate products (partial oxidation), which are more suitable for biological treatment in conventional wastewater treatment plants (WWTPs). Among these technologies, catalytic wet air oxidation, electrochemical methods, chemical oxidation with ozone or hydrogen peroxide, photocatalysis, and biocatalytic oxidation with enzymes [4] are noteworthy.

The applicability of redox enzymes to remove different organic pollutants from industrial wastewaters was first reported by Klibanov et al in 1980 [5]. Since then, it has become increasingly clear that oxidoreductase enzymes are a promising tool for industrial WWT in an environment-friendly way. Proof of that is the large number of patents and articles reported yearly in numerous high-impact scientific journals about the optimization and cost reduction of the biocatalytic process. Most focus on the search for new ways to increase the oxidation potential of the enzymes used in order to act on a broader spectrum of organic pollutants, new technologies that increase the stability of the biocatalyst allowing reutilization, and new methodologies for large-scale enzymes production [6]. There is also presently a wide variety of ongoing scientific investigation about the possible application of other groups of enzymes in WWT, like hydrolases [7], although their substrates and action mechanism are different. However, despite the use of enzymes as biocatalysts on an industrial scale becoming increasingly widespread, their application in the environmental field is still not a reality. In this chapter, the use of different oxidoreductase enzymes to remove aromatic pollutants from industrial wastewaters is discussed.

2 Pollutants in Industrial Wastewaters

Thousands of organic pollutants, including phenols, aromatic amines, polycyclic aromatic hydrocarbons (PAHs), polychlorinated aromatic compounds, pesticides, biocides, pharmaceuticals, dyes, solvents, and so on, are present in industrial wastewaters and derive from different manufacturing operations. Their effects on environment and human health have occupied environmental scientists' attention since the early 1970s. This is currently one of the most active research lines at the multidisciplinary level as numerous studies start each year. In this section, a brief description of those that can be effectively removed by enzymatic biocatalysis is provided.

2.1 Phenols

Phenol and its numerous derivatives are widespread pollutants whose sources are both biogenic and anthropogenic. Phenol is an inexpensive massively produced

reagent used as starting material for synthetic polymers and fibers. Although some phenolics play important physiological roles in living systems, many others are extremely hazardous pollutants in waters because they show poor biodegradability, high toxicity, or are even carcinogens. Therefore, presence of phenols in ecosystems poses a serious health concern for life. As a result of this, the United States Environmental Protection Agency (US EPA) has included some, particularly chlorophenols, in its list of priority pollutants [8].

2.2 Aromatic Amines

Major sources of amines in the environment include several chemical industry sectors such as oil refining, synthetic polymers, dyes, adhesives and rubbers, pharmaceuticals, pesticides, and explosives [9]. These compounds are highly toxic and play a role in cancer development in humans, so some have been classified as priority pollutants by the US EPA [8] and their levels in wastewaters are strictly regulated.

2.3 Polycyclic Aromatic Hydrocarbons

PAHs are fused aromatic rings that are poorly soluble in aqueous media. So they are normally found as traces (ng to μg/L) in wastewater, but are powerful pollutants, even at these low levels. Some have been identified as being carcinogenic, mutagenic, and teratogenic. Main anthropogenic sources giving rise to their presence in waters are combustion processes (by incomplete combustion or pyrolysis), including food preparation, discharges of certain petroleum products, storm runoffs with PAHs from car exhaust particles and road runoffs, and even urban landfills. Industrial plants (cement works, metal smelting, aluminium production) also contribute to PAHs emissions. Forest fires represent natural sources. Given their low biodegradability, PAHs concentrate in sewage sludge. The US EPA has designated 16 PAHs as priority pollutants [8].

2.4 Polychlorinated Aromatic Compounds

Polychlorinated aromatic compounds are among the most problematic and persistent water pollutants given their chemical inertness, lipid solubility, and toxicity. In particular, polychlorinated derivatives of dibenzo-*p*-dioxins (PCDDs), dibenzofurans (PCDFs), and biphenyls (PCBs) are the most dangerous because they have a very powerful toxic effect on human health (neurotoxic, carcinogens, endocrine disruptors). Their biodegradability is inversely proportional to the degree of

chlorination. PCDDs and PCDFs are not commercial chemical products, but are trace level unintentional by-products of most forms of combustion and several industrial chemical processes. PCBs were produced commercially in large quantities until production was stopped in 1977 [10]. Some of these compounds are listed as priority pollutants by the US EPA [8].

2.5 Endocrine Disrupting Compounds

In the last few years, there has been growing concern about a group of anthropogenic water pollutants that are able to mimic hormones, the so-called endocrine disrupting compounds (EDCs), which have major negative adverse health effects on aquatic organisms, even at very low concentrations (pg/L–ng/L). The US EPA defines EDCs as "exogenous agents that interfere with the production, release, transport, metabolism, binding, action, or elimination of the natural hormones in the body responsible for the maintenance of homeostasis and the regulation of developmental processes" [11]. Thousands of chemicals can be considered potential EDCs, including steroids (e.g., 17α-ethinylestradiol), surfactants (e.g., nonylphenol), preservatives (e.g., butylated hydroxyanisole), parabens, disinfectants (e.g., triclosan), musk fragrances, plasticizers (e.g., phthalates and bisphenol A (BPA)), pesticides, PAHs and PCBs. These pollutants have been detected in effluents from WWT facilities, so they can reach surface waters. Last year, the US EPA reported in the Federal Register [12] a priority list of 109 chemicals occurring in drinking water in its Endocrine Disruptor Screening Program. However, the wide variety of EDCs makes the establishment of regulations complex [13]. Current research works tend, therefore, to refocus on a regulation based on an endocrinal effect threshold rather than on a concentration threshold of a specific chemical. An excellent review about the enzymatic removal of BPA and other EDCs has been recently reported by Husain and Qayyum [14].

2.6 Dyes

Synthetic dyes are a set of recalcitrant organic compounds with different chemical structures and countless applications in different industries, ranging from textiles, food, pharmaceutical, cosmetics, and printing. The discharge of wastewaters containing high concentration of aromatic dyes is a well-known problem associated with dyestuff activities. Their highly variable, complex chemical structures make them difficult to remove by conventional WWT systems [15].

Azo dyes and anthraquinone derivatives constitute the largest, most versatile class of synthetic dyes used. The chemical structure of azo compounds consists in the functional group R-N=N-R′, where R and R' are usually aromatic derivatives, to establish a system of delocalized double-bonds, thus yielding intense coloration.

The biological treatment of azo dyes is efficient under low oxygen to anaerobic conditions, but has the deterrent effect of generating toxic and carcinogenic amines that are resistant to further detoxification under low oxygen conditions. Presence of dyes, or their degraded products, in wastewaters has a high impact on human health and aquatic life. This has led to new, stricter regulations on maximum accepted concentrations in colored wastewater discharges, and compels manufacturers to adopt "cleaner technology" approaches [16]. Different redox enzymes have been shown to be most efficient for the decolorization of textile dyes and their effluents.

3 Treatment of Wastewaters with Oxidoreductase Enzymes

Oxidoreductases are enzymes that catalyze electron transfer reactions from a donor molecule (the reductant, the organic matter in WWT) to the receptor (the oxidant, usually O_2 or added H_2O_2 in WWT). They are classified as EC 1 in the EC number classification of enzymes. A huge number of international reports and patents endorse the use of enzymes as potent "clean" biocatalysts for recalcitrant pollutants removal in industrial effluents that offer numerous advantages over other technologies. In this section some key redox enzymes in WWT, peroxidases, tyrosinases, and laccases are reviewed, and future prospects where technological developments can lead to the real application of these biocatalysts are outlined.

3.1 Peroxidases

Peroxidases (EC 1.11.1.x) are ubiquitous oxidative enzymes that contain a heme group (ferriprotoporphyrin IX) as a prosthetic group. These enzymes have been classified into two large superfamilies: the first includes the peroxidases found in bacteria, fungi, and plants, while the second contains those found in animals. In turn, the first superfamily includes three groups: Class I, which comprises intracellular peroxidases, including cytochrome *c* peroxidase, ascorbate peroxidase, and gene-duplicated bacterial and fungal catalase-peroxidases; Class II, which comprises secretory fungal enzymes, such as manganese peroxidase (MnP) and lignin peroxidase (LiP); Class III, which consists in secretory plant peroxidases, the best known representative of which is horseradish peroxidase (HRP) [17].

The classic action mechanism that appears to be universally accepted currently for most peroxidases is shown in Fig. 1 but, obviously, there might be some differences depending on the peroxidase type. The enzymatic catalytic cycle is initiated by the rapid $2e^-$ oxidation of the native ferric enzyme (resting state) by H_2O_2 (or other hydroperoxides) to give an intermediate, Compound I (CoI). CoI is not a classical enzyme-substrate complex, rather a reactive intermediate with a

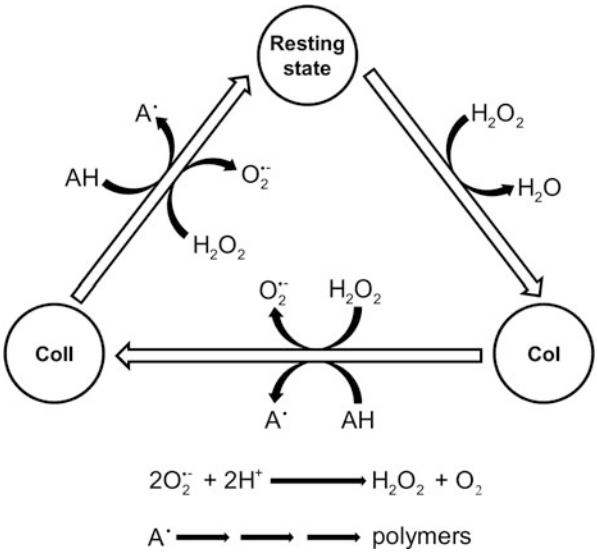

Fig. 1 Schematic depiction of the catalytic cycle of peroxidases. The pollutant substrate, AH, is transformed into its corresponding free radical, A$^{\bullet}$, which afterwards evolves to the formation of insoluble polymers

higher formal oxidation state (V). Thus, it is able to oxidize a broad spectrum of reducing substrates in two sequential one-electron steps, first through Compound II (CoII) and then CoII back to the native enzyme. The reaction products are the corresponding free radicals, which are unstable chemical species leading to the formation of insoluble high-molecular-weight polymers that can be easily removed from solution by conventional technologies like sedimentation or filtration [18].

Theoretically, peroxidases are the most oxidizing enzymes found in nature, according to the redox potential of H_2O_2 [6]. They have been shown able to oxidize different pollutants deriving from industrial activity, such as phenols, halogenated phenols, amines, PAHs, EDCs, pesticides, dioxins, PCBs, industrial dyes, and other xenobiotics. It is well known that compounds such as PCBs, naphthalene, or azobenzene which themselves are not substrates for peroxidases, can be effectively oxidized in the presence of phenols and anilines by co-oxidation [19]. This fact makes these enzymes powerful and very suitable biotools to remove pollutants from industrial wastewaters. Furthermore given this broad versatility, peroxidases are widely applied in other fields, including biopulping and biobleaching in the paper industry, soil detoxification, enzyme-linked immunoassays [20], biosensors [21, 22], analytical applications [23], and others.

In the absence of a reducing substrate, H_2O_2 performs a dual role in the catalytic cycle of most peroxidases, as oxidant in CoI formation and as typical one-electron reducing agent for both CoI and CoII, which leads to the evolution of oxygen gas [24]. This activity has been called "catalase-like" as it is reminiscent of the action of catalases, and the extent to which it is observed vastly varies between different peroxidases. If exogenous substrates electron-donors are present, like organic pollutants in wastewaters, competition for CoI and CoII takes place between H_2O_2 and the electron donor compound (Fig. 1). Consequently, and besides the

kinetic progress curve corresponding to the disappearance of organic matter, there is a parallel progress curve that corresponds to oxygen evolution in the reaction medium. This means that the peroxidase-H_2O_2 system not only catalyzes the removal of organic pollutants in wastewater, but is also strongly related to the amount of dissolved oxygen present in the medium, a very important wastewater quality parameter. Although this fact implies a clear advantage of peroxidase-based technologies for pollutants removal, it has its drawbacks: H_2O_2 is a relatively expensive reagent for the treatment of large volumes of water. It has also been shown to behave like a suicide substrate for the protein [25], which considerably limits the lifetime and reuse of the catalyst.

Apart from the cost of the enzyme and the oxidizing agent, suicide inactivation of peroxidases by H_2O_2 is the weakest point for using such catalysts in bioremediation processes. This has been successfully addressed on the laboratory scale by different approaches, including the gradual addition of H_2O_2 to minimize biocatalyst inactivation, in situ H_2O_2 generation, research into numerous supports and approaches to immobilize the protein, which offers the additional benefit of reusability and improved stability of the biocatalyst, thus minimizing costs, as well as the use of modern protein engineering techniques to obtain new, more stable catalysts in large amounts [26]. In this scenario, the main challenges that should be solved to make peroxidases become a reality in future industrial WWTPs are the following: (1) enhancing operational stability, particularly towards H_2O_2, by designing and developing new techniques and materials to immobilize the protein so that only the strictly necessary amount of oxidant agent to carry out the biocatalytic process comes into contact with the enzyme; (2) extending the range of substrates that can be oxidized by designing new peroxidases with a higher redox potential and greater catalytic activity; (3) producing low-cost enzymes in the huge amounts demanded by industry by improving heterologous expression technologies; (4) designing suitable bioreactors to optimize processes and to make them economically viable [6].

In the following paragraphs, the latest innovations in the bioremediation of industrial pollutants by peroxidases are summarized. The most used peroxidases for this purpose are of plant origin, including HRP and soya bean peroxidase (SBP); extracellular ligninolytic fungal peroxidases, including LiP and MnP; other fungal peroxidases like chloroperoxidase (CPO); and lastly, a protein with peroxidase-like activity, hemoglobin (Hb).

3.1.1 Plant Peroxidases

HRP

HRP (EC 1.11.1.7) is one of the most studied peroxidases worldwide, so many of the most significant discoveries and achievements in peroxidase research have first been made by experiments with this enzyme. In fact, it was the first enzyme whose use was proposed to remove toxic phenols and aromatic amines from industrial

aqueous effluents [5]. HRP is particularly suitable for this application because it retains its activity over a wide range of pH and temperature [27]. It is able to catalyze the oxidation of a wide variety of organic compounds, particularly phenols and aromatic amines, in the presence of H_2O_2, but other chemical non-substrates of this enzyme can also be removed by co-oxidation [19]. HRP, like other peroxidases, is irreversibly inactivated by excess H_2O_2 and by the free radical products of the biocatalytic process [25]. Nevertheless, the catalytic lifetime of the enzyme can be substantially extended in the presence of hydrophilic polymers, such as high-molecular-weight polyethylene glycol (PEG) or chitosan, leading to a significantly reduced amount of enzyme required to achieve the desired level of treatment [28].

Among the POPs susceptible to being removed by HRP, it is worth noting synthetic dyes. HRP can effectively catalyze the degradation of a wide spectrum of azo aromatic dyes by either precipitation or opening the aromatic ring structure under mild environmental conditions [16]. It has also been shown to efficiently remove some EDCs. Auriol et al [29] checked the performance of HRP to remove four steroid hormones in synthetic water and from a municipal WWTP. They found an optimum molar H_2O_2/estrogens ratio of about 0.5 that completely removed these compounds in the presence of a sufficient amount of HRP. Other authors [30] have calculated the kinetic parameters for both single and multiple-EDCs HRP-mediated removal and constructed a quantitative structure-activity relationship (QSAR) to easily predict the K_M values from molecular volumes and hydration energies.

To improve HRP performance, the protein has been immobilized in a wide variety of supports. On this particular topic, numerous articles can be found in the scientific literature. It is not possible to exhaustively review them here, therefore only the latest most significant articles will be mentioned. HRP immobilization on Eupergit C for the elimination of phenol has been tested [31]. Application of immobilized HRP in porous calcium alginate is another example of an inexpensive support [32]. The protein capsules thus obtained were reusable by up to four cycles with no changes in their retention activity noted. Microgels have also been employed for HRP-immobilization. A series of temperature-sensitive *N*,*N*-diethylacrylamide-co-acrylic acid microgels were synthesized [33] for this purpose, obtaining exceptional advantages such as high reactive activity, high thermostability and storage and reuse convenience. HRP encapsulation into poly(D,L-lactide-co-glycolide) electrospun fibrous membranes has been recently reported [34], which attained a yield as high as 83% for pentachlorophenol removal at pH 3, although no activity was observed at higher pHs. These fibers have several advantages, like their biodegradability, biocompatibility, and outstanding mechanical properties against other materials. HRP has also been immobilized on magnetic beads to be operated in a magnetically stabilized fluidized bed reactor [35]. The main advantage of this approach is the possibility of reusing beads by collecting them with an external magnetic field.

Nowadays, nanotechnology is being increasingly used to immobilize enzymes. Nano-structured compounds have a high surface area that, in most cases, can help in the immobilization and bioremediation process. HRP loading on graphene oxide has been found to be an ideal immobilization support for this enzyme [36]. The

immobilized protein showed improved thermostability and a wide active pH range for phenolics removal, which is most appealing for practical applications. Furthermore, chitosan-halloysite hybrid-nanotubes [37] and phospholipid-templated titania particles [38] are other inexpensive materials more recently used for this purpose.

In summary, HRP is an efficient biocatalyst to eliminate pollutants in wastewater. However it is still necessary to overcome some drawbacks, like minimizing H_2O_2-induced suicide inactivation and denaturation at high temperatures for its real application on the industrial scale. Production of chemically modified or mutated peroxidases with improvements, in-situ H_2O_2 production, or the use of peroxidases from other sources are possible lines of action to enhance the effectiveness of peroxidase-based industrial processes.

SBP

It is a heterogeneous glycoprotein belonging to plant peroxidases class III [17] that can be easily extracted from soya bean hulls, a by-product of the food industry. Therefore it can become readily available in large quantities at a minimal cost, leading to the revaluation of waste. Thus, it represents an attractive less expensive alternative to HRP for bioremediation and other possible commercial uses. The enzyme is catalytically similar to LiP, and is able to oxidize veratryl alcohol and other phenolic and non-phenolic aromatics directly in the presence of H_2O_2 [39].

SBP exhibits significantly higher thermo- and conformational stability than HRP due to a stronger heme-apoprotein affinity [40] which, when taking into account its high oxidation potential even in organic solvents, makes it a very suitable catalyst for a larger number of commercial and environmental applications. In fact there are several patents on the use of SBP for the biocatalytic oxidation of phenols and dyes and, based on an economic analysis of the extraction process, it has been suggested that investment in an SBP extraction facility is profitable [41]. Recently, the performance of SBP, HRP, and artichoke peroxidase has been tested in a continuous tank reactor associated with an ultrafiltration membrane module for 4-chlorophenol oxidation [42], which resulted in SBP attaining higher conversion yields for all the experimental conditions used.

3.1.2 Extracellular Ligninolytic Fungal Peroxidases

There are some fungi, particularly white-rot fungi (WRF), which have the ability to degrade and mineralize recalcitrant plant polymer lignin by an extraordinary nonspecific extracellular enzymatic machinery. They are gaining worldwide importance in recent years for a number of biotechnological applications, including removal of POPs in industrial wastewater, mainly due to their high quality/price relationship, related to their high redox potential. The enzymes involved are mainly

LiP, MnP, and laccase, this latter a phenol oxidase. In this section, a brief summary of the use of LiP and MnP is provided.

LiP (EC 1.11.1.14) is an interesting enzyme in WWT because it catalyzes difficult transformations, so in some cases it is more appropriate than other classical peroxidases. By way of example, LiP is able to slowly oxidize 2,7-dichlorodibenzo-*p*-dioxin [43]. Recently, a comparison made between LiP and HRP for the catalytic removal of nonylphenol in an aqueous medium has been reported [44], showing that the performance of LiP towards this EDC was far better. The main drawback of this protein is that it is readily inactivated at a low pH [45]. Regarding MnP (EC 1.11.1.13), despite having been efficiently used to catalyze the removal of phenolic and non-phenolic aromatic compounds, and even dyes [16], this enzyme's requirement of high concentrations of Mn(III) makes its feasibility for WWT application doubtful [27].

3.1.3 Other Fungal Peroxidases: Chloroperoxidase

CPO (EC 1.11.1.10) is a heme-containing glycoprotein secreted by various fungi that does not match any of the three peroxidase classes [17]. Although its primary biological function is chlorination, it also shows peroxidase, catalase, and cytochrome P450 activities in the absence of chloride ions, which is why it is the most versatile of all known heme enzymes. CPO differs from classical peroxidases in some key aspects, the most important of which is that the oxidation process of organic substrates is modified in the presence of chloride [46] since chlorination reactions may take place. This situation means that it can diminish the efficiency of the removal process, although CPO is relatively resistant to H_2O_2 inactivation. CPO-mediated removal of phenols [47] and aromatic amines [48] was reported some years ago. More recently, this enzyme has been suggested as being a highly efficient catalyzer for the degradation of azo dyes in the presence of H_2O_2 [49].

3.1.4 Other Proteins with Peroxidase-Like Activity: Hemoglobin

Hb is the most important respiratory hemoprotein whose main function is to bind oxygen reversibly and, hence, function as oxygen-transport protein. More than just simple oxygen-binding protein, Hb in the met form (metHb, Hb-Fe(III)) shows catalytic properties in the presence of H_2O_2, such as peroxidase-like [50, 51] and catalase-like [52] activities, be it several orders of magnitude lower than monofunctional peroxidases and catalases, respectively. At this point, the redox chemistry of this hemoprotein plays an important role in not only living systems, but also in processes of environmental interest, like industrial WWT, where the metHb/H_2O_2 system can be used as biocatalyst to remove POPs.

From the early studies conducted by Woodward et al [53], in which the use of the system metHb/H_2O_2 for monitoring phenol concentration in coal conversion wastewaters was shown, the number of reported articles describing diverse applications

of this protein has exponentially grown. There are several reasons which justify the use of metHb for these purposes as alternative to other peroxidases, and the most important reason is that it can be easily extracted from animal blood, a waste of the slaughter industry. Therefore, using this protein for the biocatalytic oxidation of recalcitrant organic matter from industrial wastewaters offers the additional advantage of minimizing wastes, thus rendering the process more eco-friendly. The versatility of Hb as a biocatalyst in bioremediation processes and other applications is reflected in the huge range of chemicals that can be oxidized.

Among the chemicals that can be substrates of the peroxidase-like activity of metHb, there are numerous phenolic compounds that are normally present in wastewaters from various industries [54]. Recently, a kinetic study into the metHb-catalyzed oxidation of 13 phenolic compounds with different functional groups in their structure has been reported [55]. The kinetic data obtained in this study indicated that the protein shows non-Michaelian behavior during its catalytic action on phenolic compounds, and a good QSAR correlation was found between the catalytic constant values and Hill coefficients with the E_{HOMO} and the pK_a of each phenol derivative. The equations thus obtained may serve as a basis to further not only explore the potential use of metHb-mediated reactions in the treatment of phenols in wastewaters, but to also predict which phenol can be removed most efficiently with satisfactory reliability.

The study of the biocatalytic oxidation of aromatic amines by metHb is just as important. The nearly complete removal of benzidine and *o*-dianisidine, two carcinogenic aromatic amines often found in surface water, with immobilized blood hemolysate in the presence of H_2O_2 was reported [56]. More recently, the protein has been encapsulated in a silica-based matrix by a modified "fish-in-net" approach [57]. These authors obtained aniline removal of up to 65% with metHb under these conditions. Furthermore, metHb immobilized in this way displays more stable peroxidase-like activity than the free protein, and its storage and pH stability substantially increase. These results suggest that metHb thus immobilized can be a promising biocatalyst for WWT.

Another family of compounds susceptible of being oxidized by metHb in the presence of H_2O_2 is formed by PAHs. It has been shown that Hb is able to catalyze the oxidation of chemicals like styrene, stilbene, 7,8-dihydroxy-7,8-dihydrobenzo [*a*]pyrene, thianthrene 5-oxide, and other PAHs [50, 57]. It has also been shown that PEG-modified metHb has a significantly higher catalytic efficiency to destroy PAHs than the unmodified protein [58]. Later studies [59] have demonstrated that anthracene, a carcinogenic pollutant from petroleum refineries, can be successfully oxidized by bovine metHb to show improved biocatalytic oxidation when the protein was immobilized on mesoporous silica supports. The applicability of an Hb-based bioelectrocatalytic system for the treatment of wastewaters contaminated by chlorinated organic compounds has also been reported [60], which significantly increases the usability of this protein for WWT.

As previously indicated, metHb also displays catalase-like activity in the presence of H_2O_2 [52]. This means that the metHb/H_2O_2 system significantly contributes to BOD and COD removal in wastewaters. A good linear correlation between

the biocatalytic activity of metHb towards a variety of phenolic compounds and oxygen evolution has recently been found [55]. From these results, the amount of oxygen released in the reaction medium can be predicted and this value is directly related to COD and BOD.

Finally, the application of Hb as biocatalyst in industrial WWT can prove to be a good alternative to using other more expensive enzymes. Nevertheless, more studies are required to improve the stability of the protein and the process yield in order to implement it on the industrial scale.

3.2 Tyrosinases

Tyrosinases (EC 1.14.18.1) are copper-containing enzymes belonging to the family of polyphenol oxidases, which are widely distributed in microorganisms, plants, and animals. Tyrosinase catalyzes two different O_2-dependent reactions that consecutively take place: the *o*-hydroxylation of monophenols to form *o*-diphenols (cresolase activity) and the oxidation of *o*-diphenols to *o*-quinones (catecholase activity) (Fig. 2). The stoichiometry of the reaction is 1 O_2/1 monophenol, but ½ O_2/1 *o*-diphenol. A lag period is observed in the time course of the oxidation of monophenols, whose duration depends substantially on the experimental conditions, the nature of the substrate, and the presence of other diphenols in the reaction medium [61]. The *o*-quinones product of catalytic activity are unstable in aqueous solution, so they tend to react either with themselves or other nucleophilic agents present in the reaction medium [62, 63] to form oligomers and insoluble polymers, which can be easily removed from aqueous media by conventional technologies.

These enzymes are extensively used in many industrial fields such as pharma, fruit, healthcare industries, or WWT [14, 64]. Tyrosinase from mushroom is commercially available, so it has been the most widely studied and used as a model in many reports. Regarding WWT applications, early studies [65, 66] showed the effectiveness of tyrosinases in remediation processes for the removal of phenols and aromatic amines of industrial origin. The potential use of tyrosinases for dye removal has also been tested [67]. To avoid the protein inactivation, some additives like PEG, Tween 20, SDS, or Triton X-100 have been employed to improve the quality of the process. Wastes from olive oil processing have been proposed as an inexpensive source of tyrosinase activity for WWT [68].

More recent studies have proposed the combination of tyrosinase-induced oxidation and heat-induced deposition of chitosan-conjugated thermo-responsive polymers as an effective method to remove phenols in water [69]. The results revealed that pollutants were completely removed (>98%). The immobilization of mushroom tyrosinase in the form of cross-linked enzyme aggregates (CLEAs) is also a highly efficient method to eliminate phenolic compounds from wastewater [70] as it achieved the complete conversion of substrates like phenol, *p*-cresol, *p*-chlorophenol, and BPA.

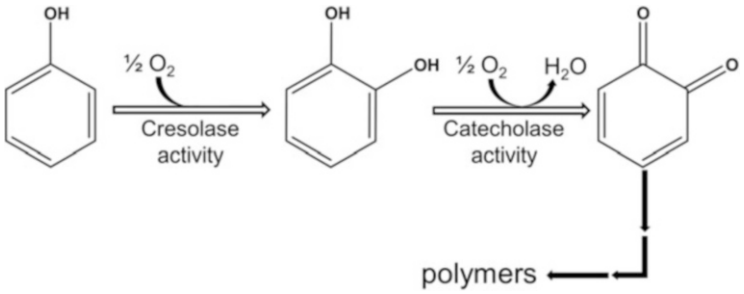

Fig. 2 Catalytic activities of tyrosinase. Monophenolic compounds are first oxidized to their corresponding *o*-diphenolic compounds by the cresolase activity, and then to *o*-quinones by the catecholase activity. The products of the biocatalytic process evolve towards the formation of insoluble polymers

In summary, the use of tyrosinases as biocatalysts in industrial processes of environmental interest like WWT has many advantages against peroxidases, and is one of the most relevant which does not require the addition of H_2O_2, which offers considerable economic savings. Nevertheless, they are not free of certain limitations for large-scale applications because, as a result of catalytic activity, the amount of dissolved oxygen significantly decreases in water, the protein undergoes irreversible inactivation during the course of the reaction and they show a smaller substrate spectrum than laccases.

3.3 Laccases

Laccases (EC 1.10.3.2) are multicopper blue oxidases produced by higher plants, bacteria, insects, and selected fungi [71]. In the last few decades, these enzymes have considerably attracted the interest of many environmental researchers because they are able to very effectively catalyze the one-electron oxidation of a surprisingly huge number of aromatic and non-aromatic compounds. These compounds include phenols, aminophenols, methoxyphenols, polyamines, lignins, aryl diamines, as well as some inorganic ions, and a variety of non-phenolic compounds [72]. An interesting comparative study with 11 laccases from different sources towards a substrate screen of 91 natural and non-natural industry-relevant compounds has been recently reported [73]. The only co-substrate that these proteins need for biocatalysis is molecular oxygen, which offers two important advantages over peroxidases: significant cost savings and less protein inactivation since the addition of H_2O_2 is not necessary. The products of the biocatalytic process are water and the corresponding radical to the reducing substrate, which then evolves to the formation of insoluble polymers that can be easily removed by conventional technologies. For this reason, laccases are seen as one of the most promising classes of enzymes for future "green" biotechnological applications.

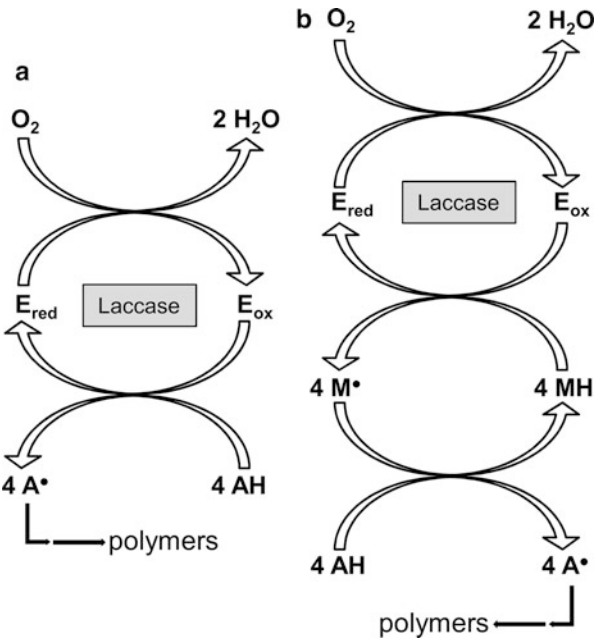

Fig. 3 Redox cycle of laccase-catalyzed oxidation of organic pollutants, AH, (**a**) in the absence and (**b**) in the presence of a mediator (MH). The products of the biocatalytic process evolve towards the formation of insoluble polymers

Laccases are glycoproteins with four copper atoms termed T1 (where substrate oxidation takes place) and the T2/T3 trinuclear cluster (where oxygen binds). They are thought to act as batteries by storing electrons from individual substrate oxidation reactions in order to reduce oxygen to water (a four-electron process). Hence the stoichiometry of the process is 1 O_2/4 reducing substrate molecules (Fig. 3a). This is an added advantage of laccases versus tyrosinases, since the consumption of dissolved oxygen in water is lower. The redox potentials reported for laccases are lower than those of non-phenolic compounds, so in principle, these enzymes cannot oxidize such substances. However, it has been shown that in the presence of small molecules that are capable of acting as electron transfer mediators between the active site of the enzyme and the non-phenolic substrate (Fig. 3b), laccases are able to catalyze the oxidation of these compounds [74, 75], thereby vastly extending the range of substrates. Different organic and inorganic compounds have been reported as effective mediators, including phenols, quinones, thiols, *N*-hydroxy compounds, 2,2′-azino-di-(3-ethyl-benzthiazoline-6-sulfonic acid, ferrocyanide, copper ions, etc. Mediators, however, are mostly toxic, unstable, or expensive. As they are truly substrates of the enzyme, they are also transformed into their corresponding free radicals, which can evolve through polymerization to lead to dark precipitates that confer undesirable coloration to wastewater, or can even inactivate the enzyme. An ideal low-cost eco-friendly mediator that enhances the oxidation efficiency of pollutants at low levels (<μm) for WWT is still to be discovered.

The biochemical and catalytic properties of fungal laccases have been comprehensively reviewed [76]. In general, they typically exhibit pH optima within the acidic pH range, which may be a drawback for the treatment of more alkaline industrial wastewaters. In line with this, bacterial laccases are advantageous. Combi-CLEAs of laccase and tyrosinase have recently been tested [77] to form a stable biocatalyst with an expanded oxidative pH-spectrum, though further research is still needed to fully evaluate the potential of this bienzymatic system for real WWT. Optima temperatures for laccases range from 25°C to even 80°C in some cases [76], which means that, in general, they are highly thermostable enzymes. Considerable efforts have been made to develop effective immobilization techniques that increase the operational stability of laccases in order to reduce the cost of the process. This topic has been recently reviewed [78], with particular emphasis placed on the use of CLEAs and enzyme polymer-engineered structures for WWT.

The large number of biotechnological applications of laccases [79], particularly their uses in the environmental field, demands the industrial-scale production of stable and active enzymes. Among the different laccase-producing organisms, WRF are becoming more important because they possess a very powerful extracellular enzymatic system that is involved in lignin degradation, including LiP, MnP, and laccases isoforms. Besides the organism, laccases production is strongly dependent on fungi culture conditions and the nature of the lignocellulosic material used. Other critical factors for the effective production of fungal laccases are carbon and nitrogen sources, their relative concentrations, and the presence of an inducer compound to optimize the process [80]. The most effective, commonly used inducers are 2,5-xylidine and copper sulfate, but other compounds like guaicol, veratryl alcohol, ethanol, some lignin monomers, amino acids, or vitamins, can also be used [81]. The most traditionally used technology for ligninolytic enzymes production has been submerged fermentation, mainly because it is easier to scale up and to control the process parameters [82]. In recent years, solid-state fermentation is arousing much interest for laccases production because it is a simpler technique, with less energy requirements and wastewater output which offers higher yields in a shorter time [83, 84]. Nevertheless, the bioreactors design for profitable laccases production on the industrial scale still needs further research to be implemented.

Laccases are also widespread in bacteria, which might open up vast opportunities for their use in biotechnology if the currently available tools for genetic manipulation are considered. Nevertheless, if compared with fungal laccases, very little is known about the potential of bacterial laccases for bioremediation applications, most likely because of their lower redox potential. A recent comparative study of four laccase-producing strains of *Streptomyces* bacteria with the WRF *Trametes versicolor* has shown fungal laccase to be the best candidate to remove micropollutants from wastewater [85]. An interesting approach that is currently being investigated, and has yielded promising results to obtain laccase variants with a higher redox potential and increased specific activity towards phenolic and non-phenolic substrates, as well as increased stability under harsh

conditions (e.g., extreme pH and temperature values), is the use of modern directed molecular evolution technologies [86].

Among the different strategies proposed to remove harmful POPs from wastewater, many research efforts indicate the extraordinary potential of laccases owing to their numerous advantages in environmental terms. Recently it has been shown that it is possible to transform some EDCs that are frequently observed in wastewaters into other chemicals with no estrogenic activity by the application of laccases both in the free form or immobilized on different supports [87]. Synthetic dyes are another example of hazardous pollutants that are efficiently removed by laccases [4]. An excellent review about this topic can be read in [80].

Despite laccases seeming to be the most attractive enzymes for bioremediation of POPs in industrial wastewaters, their use is still limited to the laboratory scale. Thus the different processes involved need to be optimized and tested for enzyme production in large-scale reactors. The use of lignocellulose waste material and/or wastewater as culture media for the growth of microorganisms producing laccases can be a good alternative to the use of purified enzymes. In this case, the presence of other extracellular enzymes and whole cells is an advantage for increasing the effectiveness of in situ bioremediation process, and for reducing costs [80].

4 Perspectives and Future Challenges

In the last few decades, the use of enzymes as biocatalysts in large-scale processes like WWT has aroused great interest in the scientific community since it forms part of the technology that encompasses the so-called Green Chemistry. In fact under current legal restrictions, industry needs to implement environmentally sustainable processes that require low-cost biocatalysts, and that are able to effectively work under non-polluting conditions.

Enzymes offer numerous advantages over other catalysts because of their natural origin, biodegradability, and ability to work under mild pressure and temperature conditions, so it is a natural process that is accepted by society more readily than other physicochemical treatments. Furthermore, the reaction products are usually insoluble polymers that can be easily removed by conventional treatments.

The use of enzymes for the removal of recalcitrant organic matter from industrial origin has been demonstrated on a small scale. As has just been explained, there is a vast variety of well-characterized enzymes that would allow the choice of the most appropriate biocatalyst (or mix) for each particular case. Peroxidases show the highest redox potential, but require the addition of hydrogen peroxide, a relatively expensive reagent that also behaves as a suicide substrate for the biocatalyst. Tyrosinases can be used as a cheaper alternative to peroxidases as they need only molecular oxygen as a cosubstrate. However they have a smaller substrate spectrum and are also inactivated during the course of the reaction. Laccases seem to be the most promising enzymes for industrial wastewater applications thanks to their wider substrate range and lower oxygen consumption in water.

The challenge is to scale up the process to industrial proportions in an efficient, economical, and environmentally benign way. High costs, low stability, and reusability become major obstacles for the application of enzymes in industrial WWT. It is essential to increase the robustness of the biocatalyst to withstand the continuous arrival of a water flow with physicochemical parameters that are far removed from the allowed values. In this context, well-developed immobilization techniques have been proposed to overcome this problem. Therefore a key point for future research is the design of new materials and immobilization methodologies to improve the performance/price ratio for the biocatalyst. To that end, the availability of large amounts of enzymes with a high redox potential at low cost is essential. Thus, molecular biology will play a decisive role on the road to the true competitiveness of enzymes in the environmental sector. Moreover, having optimized the biocatalyst parameters, a suitable chemical reactor, based on a careful analysis of the oxidative process kinetics, will guarantee the success of the treatment.

References

1. ACS (2014) CAS Registry. https://www.cas.org/content/chemical-substances. Accessed 11 Feb 2014
2. European Community (2004) Regulation No 850/2004 of the European Parliament and of the Council of 29 April 2004 on Persistent Organic Pollutants and Amending Directive 79/117/EEC. http://eur-lex.europa.eu/LexUriServ/LexUriServ.do?uri¼OJ:L:004:158:0007:0049:EN:PDF
3. Busca G, Berardinelli S, Resini C et al (2008) Technologies for the removal of phenol from fluid streams: a short review of recent developments. J Hazard Mater 160:265–288
4. Husain Q (2006) Potential applications of the oxidoreductive enzymes in the decolorization and detoxification of textile and other synthetic dyes from polluted water: a review. Crit Rev Biotechnol 26:201–221
5. Klibanov AM, Alberti BN, Morris ED et al (1980) Enzymatic removal of toxic phenols and anilines from waste waters. J Appl Biochem 2:414–421
6. Torres E, Ayala M (2010) Biocatalysis based on heme peroxidases. Springer-Verlag, Berlin/Heidelberg
7. Cammarota MC, Freire DMG (2006) A review on hydrolytic enzymes in the treatment of wastewater with high oil and grease content. Bioresource Technol 97:2195–2210
8. EPA (2013) Water: CWA Methods, Priority Pollutants. http://water.epa.gov/scitech/methods/cwa/pollutants.cfm Accessed 26 Feb 2014
9. Pinheiro HM, Touraud E, Thomas O (2004) Aromatic amines from azo dye reduction: status review with emphasis on direct UV spectrophotometer detection in textile industries wastewater. Dyes Pigments 61:121–139
10. EPA (2011) Persistent Bioaccumulative and Toxic (PBT) Chemical Program. Dioxins and Furans. http://www.epa.gov/pbt/pubs/dioxins.htm Accessed 26 March 2014
11. EPA (2013) Ecosystems & Environment: Wastewater treatment. http://www.epa.gov/research/endocrinedisruption/wastewater.htm Accessed 4 March 2014
12. Federal Register, The Daily Journal of the US Government (2013) Endocrine disruptor screening program; final second list of chemicals and substances for tier 1 screening. document 78 FR 35922
13. Vuorinen A, Odermatt A, Schuster D (2013) In silico methods in the discovery of endocrine disrupting chemicals. J Steroid Biochem Mol Biol 137:18–26

14. Husain Q, Qayyum S (2013) Biological and enzymatic treatment of bisphenol A and other endocrine disrupting compounds: a review. Crit Rev Biotech 33:260–292
15. Dos Santos AB, Cervantes FJ, van Lier JB (2007) Review paper on current technologies for decolourisation of textile wastewaters: Perspectives for anaerobic biotechnology. Bioresource Technol 98:2369–2385
16. Husain (2010) Peroxidase mediated decolorization and remediation of wastewater containing industrial dyes: a review. Rev Environ Sci Biotechnol 9:117–140
17. Dunford HB, Jones PA (2010) Peroxidases and catalases: biochemistry, biophysics, biotechnology and physiology. Wiley, New Jersey
18. Nicell JA, Bewtra JK, Biswas N et al (1993) Reactor development for peroxidase catalyzed polymerization and precipitation of phenols from wastewater. Water Res 27:1629–1639
19. Klibanov AM (1982) Enzymatic removal of hazardous pollutants from industrial aqueous effluents. Enzyme Eng 6:319–323
20. Regalado C, García-Almendárez BE, Duarte-Vázquez MA (2004) Biotechnological applications of peroxidases. Phytochem Rev 3:243–256
21. González-Sánchez MI, Laurenti M, Rubio-Retama J et al (2011) Fluorescence decrease of conjugated polymers by the catalytic activity of horseradish peroxidase and its application in phenolic compounds detection. Biomacromolecules 12:1332–1338
22. González-Sánchez MI, Rubio-Retama J, López-Cabarcos E et al (2011) Development of an acetaminophen amperometric biosensor based on peroxidase entrapped in polyacrylamide microgels. Biosen Bioelectron 26:1883–1889
23. Valero E, García-Carmona F (1998) A continuous spectrophotometric method based on enzymatic cycling for determining L-glutamate. Anal Biochem 259:265–271
24. Hiner A, Hernández-Ruiz J, Williams GA et al (2001) Catalase-like oxygen production by horseradish peroxidase must predominantly be an enzyme-catalyzed reaction. Arch Biochem Biophys 392:295–302
25. Arnao MB, Acosta M, del Río JA et al (1990) A kinetic study on the suicide inactivation of peroxidase and hydrogen peroxide. Biochim Biophys Acta 1041:43–47
26. Valderrama B, Ayala M, Vazquez-Duhalt R (2002) Suicide inactivation of peroxidases and the challenge of engineering more robust enzymes. Chem Biol 9:555–565
27. Karam J, Nicell JA (1997) Potential applications of enzymes in waste treatment. J Chem Techn Biotech 69:141–153
28. Wagner M, Nicell JA (2001) Peroxidase-catalyzed removal of phenols from a petroleum refinery wastewater. Water Sci Technol 43:253–260
29. Auriol M, Filali-Meknassi Y, Tyagi RD et al (2007) Oxidation of natural and synthetic hormones by the horseradish peroxidase enzyme in wastewater. Chemosphere 68:1830–1837
30. Zheng W, Colosi LM (2011) Peroxidase-mediated removal of endocrine disrupting compound mixtures from water. Chemosphere 85:553–557
31. Pramparo L, Stüber F, Font J et al (2010) Immobilisation of horseradish peroxidase on Eupergit C for the enzymatic elimination of phenol. J Hazard Mater 177:990–1000
32. Alemzadeh I, Nejati S (2009) Phenols removal by immobilized horseradish peroxidase. J Hazard Mater 166:1082–1086
33. Zhang YP, Liu TH, Wang Q et al (2012) Synthesis of novel poly(*N*,*N*-diethylacrylamide-co-acrylic acid) (P(DEA-co-AA)) microgels as carrier of horseradish peroxidase immobilization for pollution treatment. Macromol Res 20:484–489
34. Niu JF, Xu JJ, Da YR et al (2013) Immobilization of horseradish peroxidase by electrospun fibrous membranes for adsorption and degradation of pentachlorophenol in water. J Hazard Mater 246–247:119–125
35. Bayramoglu G, Arica MY (2008) Enzymatic removal of phenol and *p*-chlorophenol in enzyme reactor: Horseradish peroxidase immobilized on magnetic beads. J Hazard Mater 156:148–155
36. Zhang F, Zheng B, Zhang J et al (2010) Horseradish peroxidase immobilized on graphene oxide: physical properties and applications in phenolic compound removal. J Phys Chem C 114:8469–8473

37. Zhai R, Zhang B, Wan YZ et al (2013) Chitosan-halloysite hybrid nanotubes: Horseradish peroxidase immobilization and applications in phenol removal. Chem Eng J 214:304–309
38. Jiang Y, Tang W, Gao J et al (2014) Immobilization of horseradish peroxidase in phospholipid-templated titania and its applications in phenolic compounds and dye removal. Enzyme Microb Technol 55:1–6
39. McEldoon JP, Pokora AR, Dordick JS (1995) Lignin peroxidase-type activity of soybean peroxidase. Enzyme Microb Technol 17:359–365
40. Kamal JKA, Behere DV (2002) Thermal and conformational stability of seed coat soybean peroxidase. Biochemistry 41:9034–9042
41. Hailu G, Weersink A, Cahlík F (2010) Examining the prospects for commercialization of soybean peroxidase. AgBioForum 13:263–273
42. Gómez M, Murcia MD, Ortega S et al (2012) Removal of 4-chlorophenol in a continuous membrane bioreactor using different commercial peroxidases. Desalin Water Treat 37:97–107
43. Valli K, Wariishi H, Gold MH (1992) Degradation of 2,7-diclorodibenzo-*p*-dioxin by the lignin-degrading basidiomycete *Phanerochaete chrysosporium*. J Bacteriol 174:2131–2137
44. Dong SP, Mao L, Luo SQ et al (2014) Comparison of lignin peroxidase and horseradish peroxidase for catalyzing the removal of nonylphenol from water. Environ Sci Pollut Res Int 21:2358–2366
45. Aitken MD, Irvine RL (1989) Stability testing of ligninase and Mn-peroxidase from *Phanerochaete-chrysosporium*. Biotechnol Bioeng 34:1251–1260
46. Aitken MD, Massey IJ, Chen TP et al (1994) Characterization of reaction-products from the enzyme-catalyzed oxidation of phenolic pollutants. Water Res 28:1879–1889
47. Carmichael R, Fedoruk PM, Pickar MA (1985) Oxidation of phenols by chloroperoxidase. Biotechnol Lett 7:289–294
48. Dr D, Corbett MD (1991) Peroxygenation mechanism for chloroperoxidase-catalyzed N-oxidation of arylamines. Chem Res Toxicol 4:556–560
49. Zhang J, Feng MY, Jiang YC et al (2012) Eficient decolorization/degradation of aqueous azo dyes using buffered H_2O_2 oxidation catalyzed by a dosage below ppm level of chloroperoxidase. Chem Eng J 191:236–242
50. Ortiz-Leon M, Velasco L, Vazquez-Duhalt R (1995) Biocatalytic oxidation of polycyclic aromatic hydrocarbons by hemoglobin and hydrogen peroxide. Biochem Biophys Res Commun 215:968–973
51. González-Sánchez MI, Manjabacas MC, García-Carmona F et al (2009) Mechanism of acetaminophen oxidation by the peroxidase-like activity of methemoglobin. Chem Res Toxicol 22:1841–1850
52. González-Sánchez MI, García-Carmona F, Macià H et al (2011) Catalase-like activity of human methemoglobin: a kinetic and mechanistic study. Arch Biochem Biophys 516:10–20
53. Woodward J, Allen BF, Scott MA (1984) Measurement of phenol concentrations using hemoglobin. Biotechnol Bioeng Symp 14:435–438
54. Chapsal JM, Bourbigot MM, Thomas D (1986) Oxidation of aromatic compounds by hemoglobin. Water Res 20:709–713
55. Pérez-Prior MT, Gómez-Bombarelli R, González-Sánchez MI et al (2012) Biocatalytic oxidation of phenolic compounds by bovine methemoglobin in the presence of H_2O_2. Quantitative structure-activity relationships. J Hazard Mater 241–242:207–215
56. Liu J, Guan J, Lu M et al (2012) Hemoglobin immobilized with modified "fish-in-net" approach for the catalytic removal of aniline. J Hazard Mater 217–218:156–163
57. Ortiz de Montellano PR, Catalano CE (1985) Epoxidation of styrene by hemoglobin and myoglobin. Transfer of oxidizing equivalents to the protein surface. J Biol Chem 260:9265–9271
58. Torres E, Vazquez-Duhalt R (2000) Chemical modification of hemoglobin improves biocatalytic oxidation of PAHs. Biochem Biophys Res Commun 273:820–823

59. Laveille P, Falcimaigne A, Chamouleau F et al (2010) Hemoglobin immobilized on mesoporous silica as effective material for the removal of polycyclic aromatic hydrocarbons pollutants from water. New J Chem 34:2153–2165
60. Liu Q, Yu J, Xu Y et al (2013) Bioelectrocatalytic dechlorination of trichloroacetic acid at gel-immobilized hemoglobin on multiwalled carbon nanotubes modified graphite electrode: kinetic modeling and reaction pathways. Electrochim Acta 92:153–160
61. Valero E, Varón R, García-Carmona F (2002) Tyrosinase-mediated oxidation of acetaminophen to 4-acetamido-*o*-benzoquinone. Biol Chem 383:1931–1939
62. Valero E, Escribano J, García-Carmona F (1988) Reactions of 4-methyl-*o*-benzoquinone, generated chemically or enzymatically, in the presence of L-proline. Phytochemistry 27:2055–2061
63. Valero E, Carrión P, Varón R et al (2003) Quantification of acetaminophen by oxidation with tyrosinase in the presence of Besthorn's hydrazone. Anal Biochem 318:187–195
64. Mukherjee S, Basak B, Bhunia B et al (2013) Potential use of polyphenol oxidases (PPO) in the bioremediation of phenolic contaminants containing industrial wastewater. Rev Environ Sci Biotechnol 12:61–73
65. Atlow SC, Bonadonna-Aparo L, Klibanov AM (1984) Dephenolization of industrial wastewaters catalyzed by polyphenol oxidase. Biotechnol Bioeng 26:599–603
66. Wada S, Ichikawa H, Tatsumi K (1995) Removal of phenols and aromatic amines from wastewater by a combination treatment with tyrosinase and a coagulant. Biotechnol Bioeng 45:304–309
67. Amjad K, Qayyum H (2007) Potential of plant polyphenol oxidases in the decolorization and removal of textile and non-textile dyes. J Environ Sci 19:396–402
68. Toscano G, Colarieti ML, Greco G Jr (2003) Oxidative polymerisation of phenols by a phenol oxidase from green olives. Enzyme Microb Technol 33:47–54
69. Saitoh T, Asano K, Hiraide M (2011) Removal of phenols in water using chitosan-conjugated thermo-responsive polymers. J Hazard Mater 185:1369–1373
70. Xu DY, Yang Z (2013) Cross-linked tyrosinase aggregates for elimination of phenolic compounds from wastewater. Chemosphere 92:391–398
71. Sirim D, Wagenr F, Wang L et al (2011) The laccase engineering database: a classification and analysis system for laccases and related multicopper oxidases. Database (Oxford). doi:10.1093/database/bar006
72. Thurston CF (1994) The structure and function of fungal laccases. Microbiology 140:19–26
73. Reiss R, Ihssen J, Richter M et al (2013) Laccase versus Laccase-like multi-copper oxidase: a comparative study of similar enzymes with diverse substrate spectra. PLoS One 8:e65633
74. Bourbonnais R, Paice MG (1990) Oxidation of non-phenolic substrates: an expanded role of laccase in lignin biodegradation. FEBS Lett 267:99–102
75. Husain M, Husain Q (2008) Applications of redox mediators in the treatment of organic pollutants by using oxidoreductive enzymes: a review. Crit Rev Environ Sci Technol 38:1–42
76. Baldrian P (2006) Fungal laccases-occurrence and properties. FEMS Microbiol Lett 30:215–242
77. Ba S, Haroune L, Cruz-Morató C et al (2014) Synthesis and characterization of combined cross-linked laccase and tyrosinase aggregates transforming acetaminophen as a model phenolic compound in wastewaters. Sci Total Environ 487:748–755
78. Ba S, Arsenault A, Hassani T et al (2013) Laccase immobilization and insolubilization: from fundamentals to applications for the elimination of emerging contaminants in wastewater treatment. Crit Rev Biotechnol 33:404–418
79. Durán N, Rosa MA, D'Annibale A et al (2002) Applications of laccases and tyrosinases (phenoloxidases) immobilized on different supports: a review. Enzyme Microb Technol 31:907–931
80. Majeau JA, Brar SK, Tyagi RD (2010) Laccases for removal of recalcitrant and emerging pollutants. Bioresource Technol 101:2331–2350

81. Ikehata K, Buchanan ID, Smith DW (2004) Recent developments in the production of extracellular fungal peroxidases and laccases for waste treatment. Environ Eng Sci 3:1–19
82. Songulashvili G, Elisashvili V, Wasser SP et al (2007) Basidiomycetes laccase and manganese peroxidase activity in submerged fermentation of food industry wastes. Enzyme Microb Technol 41:57–61
83. Elisashvili V, Penninckx M, Kachlishvili E et al (2008) *Lentinus edodes* and *Pleurotus* species lignocellulolytic enzymes activity in submerged and solid-state fermentation of lignocellulosic wastes of different composition. Bioresource Technol 99:457–462
84. Qiu W, Zhang W, Chen H (2014) Flavonoid-rich plants used as sole substrate to induce the solid-state fermentation of laccase. Appl Biochem Biotechnol 172:3583–3592
85. Margot J, Bennati-Granier C, Maillard J et al (2013) Bacterial versus fungal laccase: potential for micropollutant degradation. AMB Express 3:63
86. Camarero S, Cañas AI, Martínez A et al (2010) Laccases having high redox potential obtained through directed evolution. Patent WO2010058057 A1
87. Debaste F, Songulashvili G, Penninckx MJ (2014) The potential of *Cerrena unicolor* laccase immobilized on mesoporous silica beads for removal of organic micropollutants in wastewaters. Desalin Water Treat 52:2344–2347

Livestock Waste: Fears and Opportunities

Jesús M[a] Martín-Marroquín and Dolores Hidalgo

Abstract One of the common tendencies of livestock activities in developed countries is to intensify the animal production and to increase the size of the production units. High animal density is always accompanied by production of a surplus of manure, representing a considerable pollution threat for the environment in these areas. Intensive animal production needs therefore suitable manure management, aiming to optimise their recycling. Treatment technologies can play an important role in the management of livestock manure by providing a more flexible approach to land application and acreage limitations, and by solving specific problems such as odours, pathogens, water pollution, ammonia emissions, greenhouse gas emissions, and phosphorus and heavy metal contamination of soils. Treatment can be enhanced with the use of biological, chemical, and physical methodologies, especially in combination as part of holistic systems. This chapter discusses sustainable treatment practices, emerging technologies, and holistic systems to solve related problems and to provide direction on animal waste treatment systems of the future.

Keywords Animal waste, Livestock, Manure, Nutrient recycling, Waste valorisation

J.M[a]. Martín-Marroquín (✉) and D. Hidalgo
CARTIF Technology Centre, Parque Tecnológico de Boecillo, 205, Boecillo, 47151 Valladolid, Spain

ITAP Institute, University of Valladolid, P° del Cauce, 59, 47011 Valladolid, Spain
e-mail: jesmar@cartif.es; dolhid@cartif.es

E. Jiménez et al. (eds.), *Environment, Energy and Climate Change I: Environmental Chemistry of Pollutants and Wastes*, Hdb Env Chem (2015) 32: 341–374,
DOI 10.1007/698_2014_268,
Published online: 29 July 2014

Contents

1 Introduction

Intensified livestock farming has meant an increase in livestock waste. Currently, the potential impact of manure on the environment represents one of the world agriculture's major challenges. Once dominated by many small operations as part of traditional crop-livestock farms, livestock production has become highly concentrated in large operations. This development has separated animal production from crop production. Thus, the amount of manure produced often exceeds local demand for use as fertiliser [1].

Until recently, farmers have tried to minimise the environmental problems caused by slurry management through recycling on farm. It has been recognised that livestock slurry represents a valuable resource that, if used appropriately with minimal loss, can replace significant amounts of mineral fertilisers. However, an increasing number of large, intensive livestock production units with insufficient area for the sustainable recycling of slurry nutrients have emerged in recent years. This specialisation in livestock production tends to weaken the link between livestock and plant production and increases the farm's impact on the environment.

Intensification of livestock production led to the development of large indoor animal houses. Another important consequence of this intensification is the concentration of animals in limited areas in order to reduce the production costs. As an example, European pig production is mainly developed in eight zones: Denmark, Belgium, Netherlands, northern Germany, Brittany (France), Catalonia and Aragon (Spain) and Po valley (Italy). In the USA, the case of North Carolina is another example of concentrated area [2]. Within these areas, local use of manure as organic fertiliser leads to an over-application of nutrient (nitrogen and phosphorus, mainly) on agricultural soils resulting in water and soil pollutions. As an example, average nitrate (NO_3^-) concentration of surface water in Brittany (France) increased from 5 mg $NO_3^- L^{-1}$ before the intensification of livestock production in this region (1970) to 35 mg $NO_3^- L^{-1}$ nowadays.

Table 1 Projected trend in production of various livestock products, 2011–2020

Region/Product	Projected annual growth 2011–2020[a] (%)	Total production 2011 (Mt)	2020 (Mt)
Developed world			
Cattle	0.6	29	31
Pork	0.4	45	47
Poultry	1.2	42	47
Meat	0.7	125	132
Milk	0.4	362	375
Developing world			
Cattle	2.6	18	22
Pork	2.7	48	60
Poultry	3.0	32	41
Meat	2.7	110	137
Milk	3.2	171	220

Source: FAOSTAT [3]
[a]Adapted from Delgado et al. [4]

Since 1960, the world population has doubled while animal numbers have increased by 50% for ruminants, 200% for pork, and 280% for poultry. In terms of meat, pork accounts for the largest proportion at 45 million tons per year compared to 42 and 29 million tons for cattle and poultry, respectively [3].

Furthermore, the concurrent growth in demand for livestock products suggests that by 2020, annual production will have to grow by another 13 million tons of milk and 7 million tons of meat, only in the developed world (Table 1). Such a large increase will require more than the simple adaptation of current livestock waste managing and treatment practices as they exist in developed countries.

By 2050, the world population is expected to reach over 9 billion people, and, combined with increasing incomes in developing nations leading to higher per capita consumption of animal products, global dairy and meat consumption are expected to increase by 74% and 58%, respectively [5]. The increased demand for animal products in developing nations has already led to an increase in livestock populations in these nations. To meet growing demand, between 2000 and 2011, China increased its pig population by 32 million (a 7% increase), whereas Brazil increased its cattle population by 42.9 million head (a 25% increase) over the same time period [3].

Manure is an inevitable by-product of livestock production. When properly managed, manure can be used as a nutrient source for crops and to improve soil properties through accretion of soil organic matter. On the other hand, improperly managed manure can pose a threat to soil, water and air quality, and human and animal health.

The properties of manure depend on several factors: animal species; ration digestibility, protein, and fibre content; and animal age, environment, and productivity. The waste system also handles added bedding, soil, water, hair, etc. Waste with 20–25% solids content (80–75% moisture content) can usually be handled as a

solid, e.g. it can be stacked and can be picked up with a fork loader. Liquids need to be drained and the waste dried or bedding added to get solid waste. In the 10–20% solids content range, handling characteristics vary depending on the type of solids present. In this range, the percent solids content does not necessarily define handling characteristics. Waste with 4–10% solids content can usually be handled as a liquid, but may need special pumps. Waste with 0–4% solids content is handled as a liquid with irrigation or flushing consistency. Liquids which have had the larger solids settled or filtered out or wastes with dilution water added may have 4% or less solids.

Table 2 lists average manure properties. These values are approximate since the actual characteristics of a given manure can easily vary 20% or more above or below the average. Also the volume of waste that a waste handling system has to handle can be much larger than the gathered in Table 2 due to the addition of water, bedding, etc. For example, liquid waste systems for swine farrowing and gestation units may have to handle twice as much waste volume as indicated; swine nurseries 3 to 4 times as much, because of large amounts of wash and wasted water.

Key issues of concern for ecological and human health related to manure production include the contamination of water resources (ground and surface) with nutrients, industrial and agricultural chemicals, and microorganisms such as viruses, bacteria, and parasites. Contamination of soil is another pervasive problem caused by the unsustainable, year-round deposition of excess nutrients, chemicals, and pathogens on land in the vicinity of industrial feeding operations. Poor air quality results from the localised release of significant quantities of toxic gases and odorous substances, as well as particulates and bioaerosols containing a variety of microorganisms and human pathogens. Adverse ecological outcomes include excessive nutrient loading and eutrophication of surface waters resulting in oxygen-depleted dead zones in both inland and marine surface waters, recurring algal blooms, fish kills, and a decline in species populations and biodiversity [7].

Livestock are responsible for 64% of anthropogenic ammonia (NH_3) emissions, 37% of anthropogenic methane (CH_4) and 65% of anthropogenic nitrous oxide (N_2O) [8]. About 30% of the green house gases (GHG) produced by livestock production are attributed to manure management. Concerning methane emissions in France, for example, animal manure management is responsible for the 32% of agriculture-forestry emissions, and about 44% of N_2O emissions from this sector come from animal manure management [9].

A wide range of equipment and systems are potentially available to treat manures [10] in order to avoid their negative impacts, but few were adopted on a large scale because of: heavy investment and operating costs without an equivalent return; their complexity and impracticality for the livestock operator; poor adaption for the livestock farm; and further environmental problems arising from the process, such as odours [11].

Table 2 Manure production and characteristics by animal species. Source: adapted from [6]

Animal	Size[a]	Manure production		Water	Density	TS[b]	VS[c]	BOD_5[d]	Nutrient content		
									N	P_2O_5	K_2O
	kg	kg d^{-1}	L d^{-1}	%	kg L^{-1}	kg d^{-1}	kg d^{-1}	kg d^{-1}	kg d^{-1}	kg d^{-1}	kg d^{-1}
Dairy cattle											
	68	6	5.7	88	1.0	0.6	0.6	0.09	0.023	0.005	0.018
	113	10	9.1	88	1.1	1.0	0.9	0.15	0.036	0.009	0.032
Heifer	340	29	28.3	88	1.0	3.1	2.6	0.45	0.104	0.032	0.100
Lactating cow	454	48	48.2	88	1.0	4.5	3.9	0.73	0.263	0.136	0.141
	635	67	68.0	88	1.0	6.4	5.4	1.02	0.372	0.191	0.218
Dry cow	454	37	36.8	88	1.0	4.3	3.7	0.54	0.163	0.050	0.127
	635	52	51.6	88	1.0	6.0	5.1	0.77	0.227	0.091	0.181
Veal	113	4	4.0	96	1.0	0.1	0.1	0.10	0.018	0.014	0.027
Beef cattle											
Calf	204	12	5.7	92	2.1	1.5	1.3	0.26	0.064	0.045	0.050
High forage	340	28	28.3	92	1.0	2.6	2.4	0.48	0.186	0.064	0.113
High forage	499	42	39.7	92	1.1	3.9	3.4	0.68	0.277	0.095	0.163
High energy	340	24	24.7	92	1.0	1.9	1.8	0.45	0.172	0.064	0.100
High energy	499	36	35.7	92	1.0	2.8	2.6	0.68	0.245	0.095	0.145
Cow	454	29	28.3	88	1.0	3.5	2.7	0.64	0.141	0.082	0.118
Swine											
Nursery	11	1.2	1.1	89	1.1	0.1	0.1	0.04	0.009	0.005	0.005
Grow-Finish	68	4.3	4.3	89	1.0	0.5	0.4	0.14	0.036	0.023	0.018
Gestating	125	3.4	3.4	91	1.0	0.3	0.3	0.10	0.023	0.018	0.018
Lactating	170	10.2	10.2	90	1.0	1.0	0.9	0.34	0.082	0.059	0.064
Boar	159	3.3	3.4	91	1.0	0.3	0.3	0.10	0.023	0.018	0.018
Sheep	45	1.8	1.7	75	1.1	0.5	0.4	0.05	0.018	0.009	0.018
Poultry											
Layer	2	0.12	0.1	75	1.0	0.0	0.0	0.01	0.002	0.001	0.001

(continued)

Table 2 (continued)

Animal	Size[a] kg	Manure production kg d^{-1}	Manure production L d^{-1}	Water %	Density kg L^{-1}	TS[b] kg d^{-1}	VS[c] kg d^{-1}	BOD_5[d] kg d^{-1}	Nutrient content N kg d^{-1}	Nutrient content P_2O_5 kg d^{-1}	Nutrient content K_2O kg d^{-1}
Broiler	1	0.08	0.1	74	1.0	0.0	0.0	0.00	0.001	0.001	0.0005
Turkey	9	0.41	0.4	75	1.0	0.1	0.1	0.30	0.006	0.005	0.002
Duck	3	0.15	0.1	73	1.1	0,0	0.0	0.01	0.002	0.002	0.001
Horse	454	23	22.7	78	1.0	5.0	4.2	0.64	0.127	0.050	0.104

[a]Weights represent the average size of the animal during the stage of production
[b]Total solids
[c]Volatile solids
[d]Biochemical oxygen demand

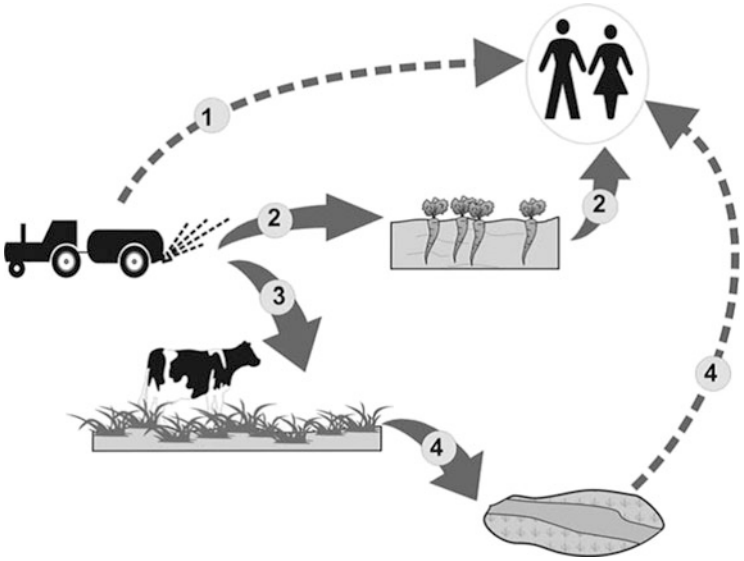

Fig. 1 Potential health impacts from the handling and land application of livestock manure: (1) direct transfer of zoonotic agents to farm staff and people nearby; (2) contamination of soil and food crops; (3) spread of disease via pasture; (4) contamination of surface water

2 Environmental Impact of Livestock Waste

Like many industries, livestock production results in a number of environmental impacts that affect populations both near and far (Fig. 1).

Industrial farm operations impact all major environmental media, including water, soil, and air. Of most concern are the pollution of ground and surface water resources with nutrients, industrial and agricultural chemicals, and microorganisms; the use of freshwater resources; the contamination and degradation of soils; and the release of toxic gases and odorous substances, as well as particulates and bioaerosols containing microorganisms and pathogens (Table 3). Interest in GHG emissions from livestock agriculture has been growing in the past two decades, with increasing awareness of the consequences of anthropogenic climate change and a desire to find strategies to mitigate GHG emissions. Other air pollutants from livestock agriculture have come under particular scrutiny in regions that suffer from poor air quality, which has led to governmental emissions regulations for livestock operations as well as serious efforts by researchers to characterise emission sources. Issues of water quality were the first area of focus, leading to regulation of livestock farms, but concerns have expanded into the impacts of manures on human health.

Table 3 Categories of environmental concerns from livestock operations

Item	Source(s) from livestock production	Area of concern
Carbon dioxide (CO_2)	Fossil fuel combustion, respiration	Climate change
Methane (CH_4)	Enteric fermentation, anaerobically stored manure	Climate change
Nitrous oxide (N_2O)	Manure-amended soil	Climate change
Ammonia (NH_3)	Manure	Air quality, eutrophication, odour
Volatile organic compounds	Fermented feeds, fresh manure	Tropospheric ozone formation
Particulate matter	Dry-lot housing for livestock, formation from ammonia	Air quality
Nitrate (NO_3^-)	Manure-amended soil	Eutrophication
Phosphorous runoff	Manure-amended soil	Eutrophication
Salts	Manure-amended soil	Soil quality
Bacteria	Manure-amended soil	Soil and water quality
Antimicrobials	Manure-amended soil	Soil and water quality

Source: Adapted from [12]

2.1 Soil Pollution

Animal wastes were historically disposed of on agricultural land oftentimes year-round and frequently without a suitable nutrient management plan. The latter practice results in over-fertilisation of the soils, toxic runoff, and leaching of contaminants, which then pose additional risks to adjacent environments.

Repeated soil over-applications of manure, above crop requirements, lead to the accumulation of not only macro nutrients such as nitrogen (N), phosphorus (P) and potassium (K), but also heavy metals, particularly copper (Cu) and zinc (Zn), impacting animal health through grazing and crop feeding [13–15].

Another important defined group of chemicals found in animal waste are endocrine disrupting compounds or EDCs. They can occur as natural constituents of animal excreta or represent drugs added to the feed of certain food animals. They are of both organic and inorganic nature and share the ability to interfere with hormonal signalling in animals and humans, thereby possessing the potential for causing adverse health effects in the exposed organism or its progeny [16]. EDCs can mimic the function of estrogenic or androgenic hormones, or they can interfere with hormone receptors to alter the outcome of internal signalling events. A major concern of EDCs is that some may display activity at very low concentrations in the parts-per-trillion or nanogram-per-litre range. Examples of EDCs in animal wastes include steroids and possibly arsenic in the form of arsenate [17].

The main consequence of nutrient or EDCs overloaded soils is related to the interaction between soils and its water and air fractions.

Table 4 Examples for animal sources of zoonotic pathogens which can be transmitted via manure

Pathogen	Excreted by
Salmonella spp	Cattle, poultry, pigs
Pathogenic *Escherichia coli*	Cattle
Yersinia enterocolitica	Pigs
Rotavirus	Cattle, pigs
Avian influenza virus	Poultry
Campylobacter spp.	Cattle, poultry, pigs
Cryptosporidium parvum	Cattle
Giardia lamblia	Cattle

Source: Adapted from [24]

2.2 Water Quality Impacts

The water quality parameters of greatest concern have traditionally been sediment, nitrogen, phosphorus and microorganisms. Each of these parameters present in livestock waste has the potential to pollute both, surface and groundwater. The processes by which pollution may occur are very complex. Both the presence and form of the pollutants are dependent on manure management practices (method of application, rate of application, etc.) [18].

Water pollution by animal production is often caused by the leaching and runoff of minerals from the soil or by direct disposal of wastes into watercourses. Animal manure nutrients in excess of crop uptake accumulate and even saturate soils. At saturation, nutrients are lost to either surface or groundwaters. Nitrogen and phosphorus are the two nutrients of special agricultural importance with the greatest potential to create water pollution [19]. Both N and P surplus can pollute surface waters through runoff while limited amounts are immobilised by the soil organic matter. Free ammonia (NH_3), rather than the ammonium salt (NH_4^+), has a greater impact on water systems because of its toxicity to many fish species. For instance, Salmon, an ammonia sensitive fish, is affected by 5 mg L^{-1} of ammonia [11].

While documenting the water quality concerns in livestock areas, different authors [20] specifically illustrated the problem and concluded that there is a general uncoupling of nutrient cycles, and problems related to nutrient loss are either short-term direct losses or long-term, related to accumulated nutrient surpluses.

There have been several well-reported cases of drinking water becoming contaminated by effluents from livestock agriculture resulting with the serious illness of local people [21–23]. Such events demonstrate that manures can easily enter surface waters adding a large bacterial load to the system (Table 4).

Various methods can be proposed for better management of manure land spreading practice to protect rivers and streams but in some high risk areas this may not be considered enough and the farmer may find himself with greatly restricted options. If water quality is likely to be affected by this practice, the reaction of local people and in consequence, politicians, can be expected to be very determined and restrictive measures on manure use may well follow [25].

2.2.1 Surface Water

Potential pollutants in manure are transported off the surface of treated areas by one of the three modes: (1) in solution/suspension, (2) sorbed to soil particles, or (3) in particulate form. Pollutants transported by the first mode include some organic nitrogen species (e.g. uric acid), soluble phosphorus and carbon, nitrates and ammonium. NH_4^+ and P may sorb to soil particles and be transported by erosion, while transport in particulate form is possible for forms of organic C, P, and N. Microorganisms appear capable of transport by both the first and second modes [18].

Runoff and erosion are the principal processes governing surface losses of potential pollutants present in the soil-waste system. Surface water quality impacts of land-applied manure depend on the numerous variables which influence runoff and erosion: soil, rainfall intensity and duration, roughness characteristics of the surface, topography, and many others. In the context of pollution, management practices such as loading rate and application timing can also play a significant role.

2.2.2 Groundwater Impacts

Groundwater quality may be impacted due to movement of water containing pollutants present in livestock waste. The overall process of groundwater pollution encompasses the sub-processes of saturated and unsaturated water flow, sorption/desorption, diffusion, and others. Subsurface transport is thus dependent on the hydraulic characteristics of the soil-waste system as well as the amounts and forms of potential pollutants present, which are in turn dependent on transformations and management practices. The pollutants which have received the most research attention include microorganisms, soluble nitrogen forms (particularly NO_3^-), salts, and soluble phosphorus forms.

2.3 Air Emissions

Besides being a producer of animal manure, livestock farming is an important emitter of airborne pollutants. These pollutants include in particular ammonia, odour and non-CO_2 greenhouse gases (CH_4 and N_2O). The risks of ammonia emissions relate to acidification of soils and waters and high levels of nitrates found in drinking waters. The emission of greenhouse gases is related to global warming which means that global temperatures might rise as a result of increasing atmospheric concentrations of certain gases. In recent years, odour emissions from animal housing and land application of manure are being increasingly considered a nuisance in densely populated countries as the scale of livestock operations [9].

Airborne contaminant emissions from manure can include toxic gases and particulates. In particular, large livestock facilities emit significant levels of several compounds, including endotoxins, particulate matter, ammonia, hydrogen sulphide, nitrous oxide, methane, and volatile organic compounds. Exposures to these compounds are associated with a wide range of airway diseases, including mucous membrane irritation, bronchitis, asthma, asthma-like syndrome, and chronic obstructive pulmonary disease, as demonstrated in studies of farm workers [26]. Organic aerosols, combined with inflammatory agents and endotoxins, have been associated with the development of respiratory illness among swine workers and the community surrounding the farms [27]. Some manure emissions such as ammonia can travel beyond the immediate farm location, thereby causing unwanted effects at the regional level.

The largest proportion of the gases arising from animal husbandry is produced from freshly deposited or stored faeces and urine, through microbial activity [11].

Methane emissions from livestock agriculture generally result either from enteric fermentation in the digestive tracts of ruminants or from manure of all livestock species stored under anaerobic conditions. In both instances, obligate anaerobic microorganisms known as methanogenic archaea are directly responsible for methane emissions. Total methane emissions per animal per day will depend largely on the forage-to-concentrate ratio of the diet, the level of feed intake, the degree of fat inclusion in the diet, the digestibility of the carbohydrates in the diet, and the presence of any feed additives that may alter the microbial populations of the rumen [28]. The Intergovernmental Panel on Climate Change (IPCC) calculated that 1 kg of methane has 63 times the warming effect of 1 kg of CO_2, over a period of 20 years following the gas release (calculated over 100 years, the warming effect of methane is 21–23 times the warming effect of CO_2).

N_2O emissions related to livestock agriculture are typically associated with emission from soil that has been fertilised with manure or solid manure storage systems [29].

CH_4 and N_2O are major greenhouse gases implicated in the global warming phenomenon. They are also involved in the photochemical reactions in the troposphere that determine concentrations of ozone.

Livestock are also estimated to be the single largest source of ammonia emissions. Ammonia results from the mixing of urine and faeces (together, manure), with the urea in urine hydrolysed by the enzyme urease found in livestock faeces. Volatilisation of NH_4^+ in the liquid phase to ammonia gas is dependent on pH, temperature, and wind speed; therefore, ammonia emissions from an animal feeding facility can be highly variable.

In Table 5 the production of nitrogen as urine and faeces substituent, e.g. the excretion, by growing-finishing pigs is divided into the part that ends up in the liquid manure that is removed from the farm after storage and the part that is emitted to the atmosphere as ammonia, either from the outside manure storage tanks or by means of the ventilation air of the pig house. Table 5 shows that a significant amount of all nitrogen that is excreted (one quarter) is emitted as ammonia with the exhaust air and three quarters end up in the liquid manure storage. Because 1/4 of all nitrogen is emitted to the atmosphere it can be concluded

Table 5 Excretion on nitrogen and emission to the atmosphere, expressed per growing-finishing pig place

	Nitrogen flux (kg N/year)	Relative contribution (%)
Excretion[a]	11.7	100
Emission from pig house by ventilation air	2.9[b]	25
Emission from liquid manure storage	0.5	4
Remaining in liquid manure	8.3[c]	71

Source: Adapted from [9]

[a]The N excretion is defined as the amount of N fed to the animals, viz 18.7 kg N per growing-finishing pig per year, minus the N retained in the animals, viz 7.0 kg N per growing-finishing pig per year

[b]Traditional housing system without emission reduction measures

[c]Calculated as excretion minus total emission

that abatement technologies for ammonia emission from these animal houses, e.g. by end-of-pipe treatment of exhaust air, are of major importance when we are trying to close nitrogen nutrient cycles in sustainable livestock farming [9].

Dust emissions can occur from livestock facilities through the locomotion of the animals on dry lots, the exhaust of animal-housing ventilation systems, or the movement of farm equipment on site or indirectly through the formation of secondary aerosol particles that form in part from ammonia emissions from the livestock manure [30].

Volatile organic compounds (VOC) result primarily from the fermented feeds fed to livestock, though some minor emissions result from the fresh manure of livestock as well. Photochemical ozone (O_3) production is driven in part by VOC, as VOC can lead to oxidation of NO to NO_2 (together known as NO_x), and in the presence of sunlight, O_3 production can result [31].

Odours are a perceived response to certain volatile organic compounds, but these odorants (the compounds) are not necessarily correlated with the presence or amounts of pathogens or faecal indicator microorganisms in the materials, particulate matter, or endotoxin [32]. All animal operations generate odorous volatile compounds from microbial metabolism of the various organic materials present in the systems, including feed, bedding, and excreta. Schiffman et al. [33] reported 331 different VOCs and fixed gases from swine facilities.

In confined interior spaces with intensive animal stocking densities, some odorous compound concentrations (NH_3 and H_2S) can accumulate rapidly and become a respiratory hazard for workers and animals. Beyond animal facility perimeters, odour complaints often lead to complaints about feeling ill (health symptoms) [33].

2.4 Food Safety and Public Health Fears

Livestock waste may contain various pathogenic microorganisms (bacteria, viruses, or parasites) that can present a sanitary risk during their subsequent spreading on

agricultural land. Whilst some pathogens are obligate parasites and are of limited concern, others can survive in the environment for long period.

Although the potential spread of zoonotic diseases to people will always cause the greatest concern, it is disease amongst livestock that represents by far the largest number of confirmed cases of illness [25]. In the case of a disease outbreak amongst farm animals, the manure and related effluents are often a principle vector for transfer and in the absence of good bio-security and good waste management there is a much increased rate of spread, with the real risk of transferring the disease to neighbouring farms.

Hygiene concerns resulted from a series of food scares resulting from the microbiological contamination of agricultural food products such as *Salmonella*, *Escherichia coli*, *Campylobacter* and also BSE (Bovine Spongiform Encephalopathy).

There is certainly published evidence of food crops contaminated by pathogens and, in some cases, this is linked to the use of animal manures as fertiliser [34–36]. The application of manures to any food crops that may be consumed raw can only increase the risk of contamination from a range of common pathogens such as *salmonella* or *campylobacter*. The number of cases of food crops contamination remains relatively small but the perceived risk from the retailers and the general public is leading to increasing restrictions of such manure use.

The health risk with respect to people in close proximity to manure (farm staff) is high but this can also be the result of the internal environment of the animal buildings (e.g. dust inhalation, high ammonia concentrations, etc.) as much as from a direct infection from the waste materials present [25]. Beyond the farm, the main impact on local people will be via the land spreading practice and the aerosols produced as a result. This activity causes odour nuisance, but this should not be confused with an exposure to an infective dose of a zoonotic disease.

Few incidences of water contamination by zoonoses were reported but each tends to be a very serious event with human fatalities [37, 38]. Zoonoses are most likely to contaminate food when manure contaminates water that is later used for irrigation or comes in contact with food. The irrigation route is of particular concern in the production of leafy vegetables eaten raw. Water used in washing such vegetables, as well as other foods, can also present a risk [39].

3 Livestock Waste Treatment Technologies

A common goal with regard to livestock waste management is the need for ‘closed-loop’ systems; making full use of the residual values of livestock waste in ways that do not impact negatively on the environment and that are both socially and economically acceptable. These goals principally include the retrieval of energy or its sequestration as organic or chemical carbon, the recycling of nutrients and, especially in drought-stressed regions, the reuse of water [40].

The objectives of manure treatment depend on the needs of a particular farm and applicable regulations. However, some general objectives of manure treatment are: stabilisation of the manure; odour reduction; nutrient management; proper storage and utilisation; pathogen reduction; and reduction of gaseous emissions such as ammonia, hydrogen sulphide, and greenhouse gases.

Treating manure can result in [41]:

1. Reduced Manure Mass. Treatment Results in Less Material to Transport and apply to cropland.
2. Reduced amounts of nutrients; thus, less land is required for manure application. Alternatively, a treatment technology can be used to produce "modified" manure in which nutrients are in the right agronomic proportions for use as a fertiliser. Producing modified manure minimises the risk of nutrient pollution of the environment.
3. Controlled pathogens and antibiotics. Reduced concentrations of pathogens and antibiotics in animal manure lessen biosecurity and health risks.
4. Production of value-added by-products. Treatment processes that produce energy (heat, electricity), fertiliser, and organic materials can be used on the farm or sold to provide an extra income source to the farm.

The basic principles underlying manure-treatment systems or technologies can be grouped into: biological, physical, and chemical processes. Manure-treatment technologies typically include a combination of these basic processes.

In general, the most common treatment methods are within the category of the biotechnological treatments. For costs reason, only composting or anaerobic treatment (biogas) can be applied as routinely used preventive measures on a farm level. Anaerobic treatment technology is particularly becoming more and more important, so that the hygienic aspect of this treatment should always be kept in mind. Physical and chemical manure treatment is more useful in cases of outbreaks of notifiable animal infectious diseases. Both will lead to reliable results. Depending on the infective agent to be treated, e.g. chemical disinfection of manure will be the favoured procedure in order to avoid spread of the diseases via the environment [24].

3.1 Microbiological Processes

The manure treatment technology most widely used is the anaerobic biodigestor. The biogas generated can be used to produce energy in form of heat or electricity [42, 43]. Swine producers can obtain additional benefits by using digested effluents and sludge as soil fertilisers, as well as the gaining carbon credit, which can be managed through certified broker companies and financial institutions. However, the biodigestors and other anaerobic systems present some limitations. Biodigestors are a partial solution to manure disposal problem, considering that they do not

remove nitrogen and phosphorus from the treated effluents; nor do they reduce crop area needed to absorb these nutrients.

Anaerobic digestion involves the breakdown of complex organic wastes and produces biogas, mainly methane and carbon dioxide, by a community of anaerobic microorganisms. This process occurs in three main stages – hydrolysis, fermentation, and methanogenesis. During hydrolysis the complex compounds are broken down into soluble components. Thus, they are readily available for fermentative bacteria (acidogenic and acetogenic) to convert into alcohols, acetic acid, other volatile fatty acids and off-gas containing H_2 and CO_2. These intermediate products are then metabolised into primarily CH_4 (60–70%), CO_2 (30–40%). The digestate can be sent to a solid–liquid separator with the liquid portion being utilised as a fertiliser, directly or previous transformation into secondary fertilisers by ammonia stripping or struvite crystallisation [44].

Co-digestion of animal manure with various biomass substrates in completed-mixed reactors increases the biogas yield and offers a number of advantages for the management of manure and organic wastes. Anaerobic co-digestion of manure and digestible organic wastes from food industry is very important for the corporate economy of the biogas plants and for the socio-economic reasons [45]. Biogas from co-digestion of animal manure and suitable organic wastes is also a very attractive solution from a socio-economic point of view, when biogas externalities, including environmental, human, and animal health benefits are quantified and integrated in the overall economic benefits [46]. It has been also demonstrated that the pre-treatment of manure (e.g., by sonication) enhances the subsequent anaerobic digestion, resulting in increased production of biogas [47].

The two-phase anaerobic digestion system permits the selection and enrichment of different bacteria in each digester; in the first phase, complex pollutants are degraded by acidogenic bacteria into volatile fatty acids, which are subsequently converted to methane and carbon dioxide by acetogenic and methanogenic bacteria in the second phase. This configuration also increases the stability of the process by controlling the acidification-phase in order to prevent overloading and the build-up of toxic material. Moreover, the first stage may act as a metabolic buffer, preventing pH shock to the methanogenic population; in addition, low pH, a high organic loading rate, and a short hydraulic retention time (HRT) are all factors which favour the establishment of the acidogenic phase, and preclude the establishment of methanogens [48].

Plug-flow digesters are unmixed systems operating semi-continuously by regularly receiving a new, untreated "plug" of manure while ejecting digested waste out the other digester end. The digesters have a normal HRT between 20 and 30 days [49]. This technology accounted for 51% of all installed digesters designs in the USA in 2007 [50].

Other advanced anaerobic bio-reactors (such as fixed film digesters) are capable of recovering energy from wastes with much shorter residence times on the order of 1–6 days [51]. The fixed-film digestion uses a tank packed with an inert media for which the anaerobic microorganisms can attach and grow to form a biofilm.

Biomass retention gives the fixed-film digestion the advantages of higher conversion efficiency, shorter HRT, and smaller footprint.

Biohydrogen fermentation using manure as substrate is currently being investigated [52, 53] since hydrogen is a clean energy source that has the potential to replace the fossil fuel in the global energy supply.

Open-air, anaerobic lagoons are the most trouble-free, low maintenance systems available for livestock waste treatment. Unfortunately, its use results in emission of GHGs such as CO_2, CH_4, and other odorous intermediate products. Reduction of GHGs and air pollutants brought on the need to cover lagoons and harvest the biogas.

In many countries, farm effluents are treated biologically using passive two-pond systems where the first pond is anaerobic and the second pond, often termed aerobic, is usually a facultative one, with an aerobic top layer over an anaerobic base. This treatment removes much of the biological oxygen demand and the suspended solids of the waste. The two-pond systems, however, are not primarily designed to remove nutrients, such as nitrogen, phosphorus, and potassium. Nutrients remaining in farm pond effluents are significant pollutants and when discharged to streams stimulate weed and algal growth, and result in the eutrophication of the waterways [54].

Advanced pond systems (APS) have only recently been applied to the treatment of farm effluents, particularly within New Zealand [55]. The first treatment step is anaerobic digestion, be it in a simple anaerobic pond, or a more advanced digester, where organic solids are microbially converted into methane and organic nutrients converted into "plant-available" inorganic forms. The effluent from this stage is then discharged into "high rate ponds" that are shallow, and shaped to form a meandering channel raceway where the water is continuously mixed by a paddlewheel. Rates of microbial disinfection are elevated in the high rate pond due to greater exposure to solar radiation. The wastewater is then treated in one or more maturation ponds. An APS treating dairy milking parlour effluent in Waikato Region, New Zealand's most intensive dairying region, produced effluent with 50–60% less biochemical oxygen demand (BOD5), chemical oxygen demand (COD), solids, total Kjeldahl N (TKN) and ammoniacal-N than equivalently sized two-pond systems. Total P was reduced by 70% [56].

Composting of manure is another alternative that has been promoted to manage livestock wastes [57]. Composting allows water evaporation and transforms liquid manure into a solid. This technology does not reduce the crop area needed for manure application, but it reduces manure volume while increasing nutrients concentration. Thus, composting makes the handling of manure easier by reducing manure transportation costs. Manure composting can also potentially increase farm income through the sale of an organic compound with high agronomic value.

Certain chemical characteristics of the animal manures are not adequate for composting and could limit the efficiency of the process: excess of moisture, low porosity, high N concentration for the organic-C, which gives a low C/N ratio, and in some cases high pH values. Thus, adequate composting management of the manure is required in order to obtain a quality compost. Therefore, different

aeration strategies, substrate conditioning-feedstock formulation, bulking agents, and process control options have been used in manure composting in order to reduce composting time and costs and enhance the quality of the end-products [58].

Composting of manure can be done with different techniques in windrows and reactors, under open air conditions and under a roof. It is hard to formulate standards here, because every technique applied has different properties concerning the process parameters necessary for effective hygienisation.

In aerobic processes-based technologies, oxygen is provided to the manure so that microorganisms can:

- Remove organic matter, often referred to as BOD or COD.
- Remove nitrogen and phosphorus through biological uptake.
- Manage nitrogen by converting ammonia in the manure to nitrogen gas (through a process called nitrification and denitrification).

Manure biological aerobic treatment was firstly developed in order to remove nitrogen surplus. However, additional steps were added to the biological processes in order to manage also the phosphorus excess. The most widespread treatment process is composed of, firstly, a filtering system allowing a separation of the manure into liquid and solid phases. Following this mechanical separation, the solid phase can be composted and the liquid phase is biologically treated. Biological treatment is usually performed in a single reactor, intermittently fed and aerated providing necessary conditions for nitrification and denitrification [2].

Four large-scale aerobic treatment plants with a nitrification-denitrification process for veal calf slurry have been in operation since 1976 at four locations in the Netherlands [9]. The continuously running systems comprise of three concentric compartments: the outer is aerated continuously, whereas the inner ring is not aerated but mixed continuously by two mechanical mixers. The central part is a clarifier. In the outer ring nitrification takes place under aerobic conditions and organic material is converted mainly to carbon dioxide, heat, and water. Also some lime is added for phosphate removal. In the inner ring denitrification takes place under anoxic conditions. Typical removal efficiencies of the systems are 95% for COD, 99% for BOD5, 99% for TKN, 99% for NH_4-N, and 95% for P.

In North Caroline, a second-generation treatment system that can achieve high standards at reduced costs was implemented in 2007. It was developed to replace the anaerobic swine lagoon technology commonly used in the USA to treat swine waste. The new system used solids separation, nitrification-denitrification, and phosphorus removal-disinfection. Removal efficiencies were: 98% suspended solids, 97% ammonia, 95% phosphorus, 99% copper and zinc, 99.9% odours, and 99.99% pathogens at 1/3 the cost of the previous version [59].

The running cost of this treatment is mainly due to the energy required for oxygen transfer to achieve nitrification and filtration of raw manure. Thus, anammox (anaerobic ammonium oxidation) process could be seen as an alternative allowing reducing the cost of treatment by reducing significantly the O_2 required [60].

Sequencing batch reactors (SBRs) are among the most effective activated sludge treatment plants for the treatment of the separated liquid fraction. SBRs use temporised cycles in a single reactor to perform the same reactions that continuous flow treatment trains do in different reactors, allowing integration of anaerobic-anoxic-oxic conditions. SBRs add flexibility due to the capability to modify the time duration of the different operational phases instead of having a fixed reaction volume as in continuous flow configurations. This flexibility can allow to regulate N removal efficiency according to the specific nutrient needs of a farm or to increase removal efficiency to meet the discharge limits [61].

On the opposite side there are authors who think that aerobic treatment of manure (nitrification-denitrification) cannot be considered as sustainable, as this process uses a lot of energy, emits nitrous oxide, and finally 'destroys' nitrogen forms (ammonia, nitrates and nitrites) by converting them to N_2, dinitrogen gas, that cannot be utilised anymore for fertilisation of crops. [9].

Low-technology solutions, as soil filter systems or constructed wetlands, try to take advantage of the natural environment (sun, wind, land, seeds, etc.) when treating animal waste [11, 40]. Treatment costs are much lower than those resulting for technological solutions but also treatment efficiencies use to be less.

Table 6 summarised the main characteristics of the biological treatment technologies.

3.2 Physical Processes

3.2.1 Liquid–Solid Separation

The cost of transporting manure can be reduced, and its fertiliser value increased, by separating the manure into (1) a liquid fraction intended for on-farm use, and (2) a dry-matter- and nutrient-rich fraction that can be exported to other areas requiring fertilisers or to centralised treatment systems. Separation may also contribute to a reduction in odour emission and assist in producing energy-rich biomass that can be used for incineration or biogas production [63]. In combination with chemicals, liquid–solid separation can be used also to remove nutrients from manure.

Furthermore, liquid–solid separation through settling (sedimentation) or by using mechanical methods (e.g. use of screens, centrifuges, or belt presses) is a necessary first-step to prevent manure particles from overloading subsequent chemical or biological processes in multi-step advanced treatments systems [64, 65].

Sedimentation in a thickener is an attractive option for separation, due to the low cost and simple technology. Most thickeners consist of a container that is cylindrical at the top and conical at the bottom. To encourage settling and increase the transfer of solids settled on the upper part of the conical section, thickeners can be vibrated or included a rake [64].

Table 6 Manure-treatment technologies: biological processes

Technology	Application	Pros	Cons	Comments
Anaerobic digestion	Biological treatment of animal manure and other biomass in the absence of oxygen (wet or liquid manure – dairy, swine, but dry manure – beef, poultry – if hydrated first)	(a) Reduced odour (b) Reduces the effects of greenhouse gases (methane, CO_2, and small amounts of N_2, CO, H_2,O_2, and H_2S) (c) Biogas used for energy production (d) Pathogens significantly reduced (e) End products: liquid and solids can be used as fertiliser (f) Potential income from carbon credits	(a) No nutrient reduction (b) No reduction of manure volume (c) Large construction footprint required for practice (d) High cost (e) Solid/liquid separation needed to reduce maintenance costs and cost of pumping (<25% solids) (f) Effluent product may need more treatment	(a) Nutrients are retained through the digestion process (b) A portion of the N and P is converted to more plant available forms (c) Through the digestion process the manure tends to become more liquid in nature (d) Anaerobic digestion is a relatively slow process (e) Reduced air emissions issues (f) Many successful applications when operation and maintenance are done by dedicated staff, or by a third party
Aerobic digestion	Biological treatment of animal manure and other biomass in the presence of oxygen (most commonly liquid)	(a) Reduced methane and NO_x (b) Pathogens significantly reduced (c) Reduced odour (d) Phosphorus and potassium can be recovered and used as fertiliser (e) Effluent product – cleaner than w/ anaerobic process	(a) High operating cost because of electricity demand for aerator (b) Significant loss of nitrogen to the atmosphere	(a) Available technology makes it possible to nearly eliminate air emissions issues (b) Does a better job removing suspended solids resulting in generally cleaner water output than with anaerobic digestion
Aerobic digestion "composting"	Processing of animal manure or other organic by-products	(a) Reduced manure volume/weight (b) Stable product (c) Phosphorus and potassium retained (d) Pathogens significantly reduced (e) Can be used as a soil amendment	(a) Significant amounts of NH_3, CO_2, methane, and NO_x can be lost to the atmosphere (properly aerated compost will have minimal NO_x emissions)	(a) Markets would need to be developed for efficient sale of composted materials (b) Markets may become saturated in areas of high animal production density

(continued)

Table 6 (continued)

Technology	Application	Pros	Cons	Comments
	into biologically stable organic matter (solid animal manure)	(f) Depending on the nutrient content may qualify as an organic fertiliser (g) Efficient means of dead animal disposal (h) Soil quality benefits	(b) Processing may take 3–6 months or more for a finished product (c) Salts within the manure are concentrated (d) Markets can become quickly saturated	(c) Many on-farm attempts are hindered by the workload involved with turning the pile of compost several times during the composting process, and by lack of marketing expertise (d) Use of rotary drum composters can reduce the composting period
Anaerobic + aerobic digestion	Anaerobic digestion followed by aerobic digestion	(a) Reduced methane/NO_x (b) Pathogens significantly reduced (c) Reduced odour	(a) High combined expense to maintain both systems (b) Large construction foot print (c) Significant loss of nitrogen to the atmosphere	Combined process is more efficient at removing solids and pathogens from slurry manures resulting in cleaner water exiting the system

Source: Adapted from [62]

Increasing the gravitational force can reduce the settling time needed to achieve a given separation efficiency. In practice, this is accomplished in decanter centrifuges (vertical or horizontal), where a centrifugal force is generated to cause the separation.

Screens and filter belts filter out solids from liquids by gravity. Most of the filter separators are screens consist of a rotating perforated cylinder with a loading area at the top and a scraper to remove the solids. The liquid flows through the screen and is drained off.

Pressurised filtration is another phases-separation option. The typical equipment used for filtration with applied pressure is a screw press or a press auger.

In general, the separation efficiency of mechanical separators for the removal of dry matter and phosphorus is ranked as follows: centrifugation> sedimentation > non-pressurised filtration > pressurised filtration. Also the separation of total nitrogen and NH_4^+ follows the same pattern, but the separation efficiency is lower than in the previous case [63].

Treatment with a flocculant before separation improves separation efficiency significantly [57]. The best mechanical separation techniques for flocculated slurry are screens or filter belts [66]. In these cases it should be borne in mind that the separation of animal slurry may create new problems; for example, a change in the ratio of plant nutrients to heavy metals in the biomass. Recent studies showed that solid–liquid separation with flocculation as a pre-treatment transferred zinc (Zn), copper (Cu), and cadmium (Cd) to the solid fraction [67, 68]. The additives used when optimising the separation of slurry (e.g. polymers and aluminum) may also pose an environmental problem [69].

After the initial liquid–solid separation, membrane filtration of the liquid fraction could be used to separate and concentrate dissolved K, P, and N nutrients, producing a nutrient-rich liquid phase and, in principle, pure water for reuse or safe discharge to the environment [63]. Problems associated with surplus nutrients in areas with high livestock density could be partly solved by the use of membrane technology to concentrate manure nutrients in small volumes that could be exported as fertilisers to other agricultural regions. Microfiltration and ultrafiltration membranes basically act as very efficient solid–liquid separators that can isolate nutrients associated with particles such as phosphorus. Ammonia and potassium retention requires nanofiltration or reverse osmosis [70].

3.2.2 Thermal Treatments

The thermal treatments are the physical conversion of biomass using high temperatures to break the bonds of organic matter and reform these intermediates into synthesis gas, hydrocarbon fuels, and/or a charcoal residual. While the biological-based conversion processes require an extended amount of reaction time, thermal conversion processes can quickly yield multiple complex end-products [71].

Thermal conversion processes include combustion, pyrolysis, gasification, and liquefaction (Fig. 2). These processes can be designed to solve odour problems,

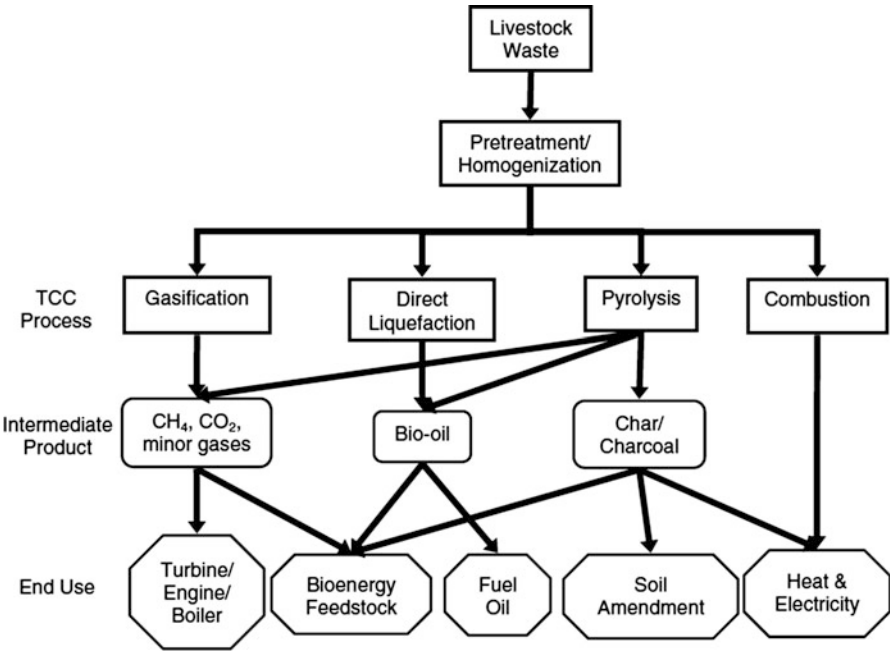

Fig. 2 Livestock waste thermal treatments. Adapted from [43]

reduce volume, recover inherent nutrients, decrease pollution potential, as well as recover energy from the manure. But since all of the thermal treatments are heat intensive, heat recovery is an essential component to make these processes energy feasible [43].

Combustion converts manure's energy into heat; however, this method does not provide a way to store the energy until it is needed. Additionally, the ash product from combustion has yet to find a suitable recycle use [72].

Pyrolysis uses heat and a non-oxygen atmosphere to convert the organic portion of manure into a mixture of char and volatile gases containing both non-condensable vapours and condensable tars (oxygenated hydrocarbons), which form a combustible pyrolytic oil or bio-oil [73].

Slow pyrolysis converts animal wastes into char, providing farmers with potential economic benefits due to energy production and carbon credits generated from carbon sequestration. Char can be used as a feedstock ("green coal") for existing coal combustion and gasification plants. Char can also be applied to soil as a soil amendment to improve fertility [74].

Liquefaction hydrolyses the lignocellulosic components in biomass and converts the biomass into lighter organic oils (bio-oils). Liquefaction process proceeds in a pressurised environment (5–20 MPa) and typically occurs at lower temperatures than the pyrolysis (250–350°C). In batch studies under a CO atmosphere and reactor temperatures ranging 285–350°C, volatile solid conversion to oil was

76.2%. The swine bio-oil product was energy dense with an average heating value of 36.4 MJ kg^{-1} [75].

The principle of manure gasification is to produce syngas through the thermochemical conversion of biomass, usually involving partial oxidation of the feedstock in a reducing atmosphere in the presence of air, oxygen, and/or steam. Experiments with dairy manure showed that the lower heating value of the syngas obtained varied from 2.0 to 4.7 MJ m^{-3}, indicating gasification could be used as a waste management option to produce bioenergy, and potentially reduce problems associated with the disposal of animal waste [76].

Incineration is not a broadly implemented technology. In August 2006 the construction of a central incineration plant (440,000 tons capacity) for poultry manure was started in Moerdijk, the Netherlands (BMC Moerdijk BV). The plant aims to produce electricity and fly ash. The incinerator is a fluidised bed boiler. The steam of the boiler is used to drive a steam turbine with a generator of 36.5 MWe. The generated 'green' electricity is sold to the national electricity grid. The flue gasses are purified before they are released to the atmosphere. The fly ashes are used by the fertiliser industry as a base material for the production of fertilisers.

As a post treatment to solid–liquid separation, water and volatiles can be removed from the slurry or the liquid fraction by evaporation. The liquid is heated to boiling point, which for slurry will be a little over 100°C at atmospheric pressure. At this temperature, both water and volatile organic compounds, such as free fatty acids and ammonia, will evaporate. This vapour phase has to be condensed in order to retrieve the energy used to evaporate the water and volatiles. The energy consumed in the process is high, as the heat needed for evaporation represents roughly 670 kWh per metric ton of water evaporated [63].

Table 7 summarised the main characteristics of the physical treatment technologies.

3.3 Chemical Processes

Principal chemical processes for manure include chemical coagulation, chemical precipitation, chemical disinfection, chemical oxidation, chemical neutralisation, chemical stabilisation, and ion exchange. Chemicals, in conjunction with physical processes, can be used to remove and recover nitrogen, phosphorus, and heavy metals.

Flocculation, coagulation, and precipitation are chemical pre-treatments that improve the mechanical solid–liquid separation of many suspensions.

In a recent research [77], swine manure was treated by coagulation/flocculation followed by an oxidation step. This physicochemical treatment removed suspended solids (32%), total organic carbon (78%), and nutrients (82% N and 50% P). Also a complete total coliforms reduction was achieved.

Chemical disinfection of manure may be done with several substances: lime-wash, caustic soda, peracetic acid, calcium cyanamide, and others. Generally, this

Table 7 Manure-treatment technologies: physical processes

Technology	Application	Pros	Cons	Comments
Solid/liquid separation	Processes used to partition the waste streams of animal manures and other materials (wet and liquid manure systems)	(a) Processes partition solids, liquids, and nutrients in the waste stream (b) Separated solids are lighter and more economical to transport (c) Separated solids may be used for animal bedding or as a fuel source (d) Multiple waste streams can provide additional flexibility in farm operations (e) Makes separated solid/liquids easier to handle (f) Separation of solids from liquids can reduces odours	(a) Mechanical separation process can be quite expensive (b) Multiple waste streams need to be addressed – separate transference, storage, and treatment considerations	(a) Various separation methods are available including both mechanical and non-mechanical processes (b) Separation efficiencies vary by process and manure type (c) Separation of solids and/or nutrients can be enhanced by chemical means (polymers)
Incineration	Thermal conversion of animal manure and other biomass in an oxygen rich environment (well suited for dry or dried manures)	(a) Reduced manure volume (b) Heat energy production (c) Phosphorus and potassium retained in ash has fertiliser value (d) Pathogens destroyed	(a) Potential air emission issues – air scrubbing may be necessary (b) Nitrogen lost through air emissions (NO_x) (c) Sand and other inorganics may affect performance (d) High initial cost	For wet or liquid manures solid/liquid separation methods may be required
Gasification	Thermal conversion of animal manure and other biomass in an oxygen starved environment (well suited for dry or dried manures)	(a) Reduced manure volume (b) Syngas used for energy production (c) Phosphorus and potassium retained in char has fertiliser value (d) Reduces the effects of greenhouse gases (methane, CO_2 H_2O, and small amounts of other gases)	(a) Nitrogen lost through air emissions (N_2) (b) Sand and other inorganics may affect performance (c) Syngas may need further processing before being used for power production (d) High initial cost	(a) For wet or liquid manures solid/liquid separation methods may be required (b) Gasification technology is old, but applications using manure are limited (c) Minimal air emissions issues

		(e) Smaller construction footprint than anaerobic digestion (f) Pathogens destroyed		
Pyrolysis	Thermal conversion of animal manure and other biomass under anaerobic conditions (well suited for dry or dried manures)	(a) Reduced manure volume (b) Syngas used for energy production alternatives (c) Bio-oil has various uses including energy production (d) Phosphorus and potassium retained in char has fertiliser value (e) Reduces the effects of greenhouse gases (methane, CO_2 H_2O, and small amounts of other gases) (f) Smaller construction footprint than anaerobic digestion (g) Pathogens destroyed	(a) Some nitrogen lost through air emissions (N_2) (b) Bio-oil may not be stable (c) Production rates between feed sources can vary greatly (d) Uses for bio-oil may be limited without additional processing (e) High initial cost	(a) For wet or liquid manures solid/liquid separation methods may be required (b) Pyrolysis technology is old, but applications using manure are limited (c) Products include: bio-oil, and bio-char (d) Minimal air emissions issues

Source: Adapted from [62]

Table 8 Manure-treatment technologies: chemical processes

Technology	Application	Pros	Cons	Comments
Chemical enhancement	Application of metal salts and/or polymers to manure to improve solid/liquid separation	(a) Enhanced separation of suspended and dissolved solids from the liquid waste stream (b) Improved partitioning of nutrients, especially phosphorus	(a) Chemical reaction can vary day-to-day (b) Testing needed to determine proper chemical and application rate (c) Chemicals expensive	(a) Chemical enhancement in conjunction with solid/liquid separation can remove 90% or more of total phosphorus from the liquid waste stream (b) Large number of chemicals and polymers are available
Manure amendments	Application of amendments during manure production or storage to address a resource concern	(a) Generally easy to use (b) Can select amendment for specific need (c) Effectively reduces ammonia emissions (d) Can be used as a phosphorus binder (e) Can be used to enhance solid/liquid separation	(a) Difficult to determine product effectiveness (b) Generally only a "stop-gap" solution (c) Amendments can be expensive	(a) For poultry, research shows that certain amendments increased productivity and lowered ammonia emission (b) Manure amendments have been shown to phosphorus in run-off and to lower leaching potential

Source: Adapted from [62]

type of treatment is used in the case of an epidemic and not routinely after every service period. Chemical disinfection of liquid manure will only be successful if the slurry has been carefully mixed prior to the addition of the chemicals and subsequently stirred.

Table 8 summarised the main characteristics of the chemical treatment technologies.

3.4 Exhaust Air Treatment Technologies

In regions with high animal density and limited availability of arable land not only manure treatment but also air treatment of mechanically ventilated housings is necessary for closing nutrient cycles (e.g. a quarter of all nitrogen excreted by pigs

Table 9 Factors influencing decision on on-farm or centralised approach

Collective/centralised management and treatment
Economical profile of the area: industrial and farming
High farming density and intensity
Low general impact of manure transportation
Existence of strong farmers leadership and/or a qualified contractor
Existence of other organic waste to help plant economy (co-digestion)
Potential uses of waste heat in the area (district heating, in-plant uses)
Existence of professional technology suppliers and consultants
Centralised treatment as a service to the collective management
Social variables: ease in involving farmers in a common project
On-farm management and treatment
Economical profile of the area: tourism, services, and residential
High impact of manure transportation
Involvement of farmer
Potential uses of waste heat in the farm (in the case of biogas plants)
Existence of professional technology suppliers and consultants
Treatment facilities fully integrated in the farm
Technological simplicity, ease of maintenance and operation

Source: Adapted from [80]

is emitted as ammonia). Furthermore, treatment of exhaust air is a means of reducing other environmental impacts of livestock production caused by the emission of ammonia, odour, and particulate matter (dust). Therefore both manure treatment and treatment of exhaust air are essential for sustainable livestock operations in areas with a high livestock density [9].

Currently, a new generation of scrubbers is being developed for livestock operations that, besides ammonia, also addresses odour and particulate matter emission abatement. These so-called multi-pollutant scrubbers usually consist of two or more scrubbing stages, each stage aims for the removal of one type of compounds. The first prototypes of multi-pollutant scrubbers for pig farms, combining the concepts of acid scrubbing, bio-scrubbing, water curtains, and biofiltration have been tested in the USA [78], Germany [79], and the Netherlands [9] and are in operation now at a limited number of farms.

3.5 On-Farm Versus Centralised Treatment

When considering treating livestock waste on-farm or in a centralised plant managing aspects are usually more critical than technological aspects. Economical factors, which affect the decision about management and facilities scale are influenced by the density and the intensity of farming in a given area. Areas with

high intensity take benefit from a centralised treatment system, since it allows optimising logistics [80]. Table 9 gathers the elements to be considered when deciding if follows an on-farm or centralised approach.

4 Current Challenges and Future Perspectives

Livestock wastes have traditionally been thought of as a problem, both for those who generate it and society in general. But now that there is a scarcity of many products, livestock wastes have become an interesting source of energy and certain raw materials.

Proper planning and installation of a livestock waste management system open up opportunities for a variety of uses of these wastes. No system is right or wrong for every situation, but the way these wastes are handled affects their value as plant nutrients or for other purposes. In all cases the farms should be required to apply an efficient nutrients management.

Nowadays it is clear that the world population is growing, the energy prices are continuously increasing and the phosphorus is depleting; also larger livestock concentrations are expected in the near future. This is why priority should be given to livestock waste processing technologies which produce energy and facilitate nutrients recovery (e.g. anaerobic digestion or pyrolysis).

Development of appropriate livestock wastes processing schemes requires also an appropriate regulatory framework, so that international trading of end and by-products from livestock wastes processing would be regulated and facilitated. Policies should stimulate a transition to a bio-based economy, with energetic valorisation and maximum recycling and valorisation of nutrients and water from these wastes. Financial support mechanisms could be made available to develop technologies and market mechanisms for recycling of nutrients, even though the polluter pays principle should always be taken into account.

Some of the topics that should be made subject of additional research as an important pre-requisite for continued sustainable dissemination of livestock wastes processing activities are the following:

- Setting up an EU-wide network of livestock manure processing plants to serve research needs.
- Optimal change of commonly used techniques.
- Long-term research on the effects of heavy metals and other recalcitrant compounds on soil, due to applications of treated manure.
- Improve gaseous emissions treatment technologies and sampling methodologies.
- Investigations on real livestock manure qualities and amounts available for processing.

– Improvement of nutrients balances in livestock farming systems includes also the optimisation of feed composition. The whole chain from feed to manure application should be considered.
– New ideas and opportunities should be investigated, with respect to optimising of already existing manure processing technologies and concerning new technologies. Examples are, among others, algae production from liquid manure products, bio-electrochemical systems to recover/produce new products and energy, or the management of different waste types (livestock, biomass, industrial, municipal) at integrated plants to take advantage of potential synergies.

Acknowledgments The authors gratefully acknowledge support of this work by the LIFE+ Program under the responsibility of the Directorate General for the Environment of the European Commission through the agreement LIFE 12 ENV/ES/000727-REVAWASTE project.

References

1. Vanotti M, Szogi A, Pilar Bernal M, Martinez J (2009) Livestock waste treatment systems of the future: a challenge to environmental quality, food safety, and sustainability. OECD Workshop. Bioresource Technol 100(22):5371–5373
2. Bernet N, Béline F (2009) Challenges and innovations on biological treatment of livestock effluents. Bioresource Technol 100(22):5431–5436
3. FAOSTAT (2013) http://faostat3.fao.org. Accessed 6 Feb 2014
4. Delgado C, Rosegrant M, Steinfeld H, Ehui S, Courbois C (1999) Livestock to 2020. International Food Policy Research Institute, Washington
5. Garg M, Makkar H (2012) Balanced feeding for improving livestock productivity: increase in milk production and nutrient use efficiency and decrease in methane emission. Anim Prod Health 173, Rome
6. American Society of Agricultural Engineers (2001) Committee S&E-412 report AW-D-1, revised 6-14-73
7. Halden U, Schwab J (2008) Environmental impact of industrial farm animal production. A Report of the Pew Commission on Industrial Farm Animal Production
8. Steinfeld H, Gerber P, Wassenaar T, Castel V, Rosales M, de Haan C (2006) Livestock's long shadow. FAO, Rome
9. Melse R, Timmerman M (2009) Sustainable intensive livestock production demands manure and exhaust air treatment technologies. Bioresource Technol 100(22):5506–5511
10. Burton C, Turner C (eds) (2003) Manure management-treatment strategies for sustainable agriculture, 2nd edn. Silsoe Research Institute, Bedford
11. Martinez J, Dabert P, Barrington S, Burton C (2009) Livestock waste treatment systems for environmental quality, food safety, and sustainability. Bioresource Technol 100(22):5527–5536
12. Place S, Mitloehner F (2014) The Nexus of environmental quality and livestock welfare. Annu Rev Anim Biosci 2:1.1–1.15
13. Giola P, Basso B, Pruneddu G, Giunta F, Jones J (2012) Impact of manure and slurry applications on soil nitrate in a maize-triticale rotation: field study and long term simulation analysis. Eur J Agron 38:43–53
14. Maillard É, Angers D (2014) Animal manure application and soil organic carbon stocks: a meta-analysis. Glob Change Biol 20(2):666–679

15. Bernard E, Larkin R, Tavantzis S, Erich M, Alyokhin A, Sewell G, Gross S (2012) Compost, rapeseed rotation, and biocontrol agents significantly impact soil microbial communities in organic and conventional potato production systems. Appl Soil Ecol 52:29–41
16. European Union (2014) Endocrine disruptors website: how the European Union uses the precautionary principle to tackle endocrine disruptors. http://ec.europa.eu /environment/endocrine/definitions/endodis_en.htm. Accessed 7 Feb 2014
17. Combalbert S, Bellet V, Dabert P, Bernet N, Balaguer P, Hernandez-Raquet G (2012) Fate of steroid hormones and endocrine activities in swine manure disposal and treatment facilities. Wat Res 46(3):895–906
18. Edwards D, Daniel T (1992) Environmental impacts of on-farm poultry waste disposal – a review. Bioresource Technol 41(1):9–33
19. EEC/91/676, O.J. NL 375, 31.12.1991.p1. Protection of waters against pollution caused by nitrates from agricultural sources
20. Hooda P, Edwards A, Anderson H, Miller A (2000) A review of water quality concerns in livestock farming areas. Sci Total Environ 250:143–167
21. Ali S (2004) A socio-ecological autopsy of the *E. coli* O157:H7 outbreak in Walkerton, Ontario, Canada. Soc Sci Med 58(12):2601–2612
22. Thorne P (2007) Environmental health impacts of concentrated animal feeding operations: anticipating hazards searching for solutions. Environ Health Perspect 115:296–307
23. Gilchrist M, Greko C, Wallinga D (2007) The potential role of concentrated animal feeding operations in infectious disease epidemics and antibiotic resistance. Environ Health Perspect 115:313–316
24. Martens W, Böhm R (2009) Overview of the ability of different treatment methods for liquid and solid manure to inactivate pathogens. Bioresource Technol 100(22):5374–5378
25. Burton C (2009) Reconciling the new demands for food protection with environmental needs in the management of livestock wastes. Bioresource Technol 100(22):5399–5405
26. May S, Romberger D, Poole J (2012) Respiratory health effects of large animal farming environments. J Toxicol Environ Health B 15(8):524–541
27. Leytem A, Dungan R, Bjorneberg D, Koehn A (2011) Emissions of ammonia, methane, carbon dioxide, and nitrous oxide from dairy cattle housing and manure management systems. J Environ Qual 40(5):1383–1394
28. Dammgen U, Amon B, Hutchings N, Haenel H, Rosemann C (2012) Data sets to assess methane emissions from untreated cattle and pig slurry and solid manure storage systems in the German and Austrian emission inventories. Archiv Naturschutz Landschaftsforschung 62(1–2):1–20
29. Junior C, Cerri C, Dorich C, Maia S, Bernoux M, Cerri C (2013) Towards a representative assessment of methane and nitrous oxide emissions and mitigation options from manure management of beef cattle feedlots in Brazil. Mitig Adapt Strat Gl:1–14
30. Cambra-López M, Aarnink A, Zhao Y, Calvet S, Torres A (2010) Airborne particulate matter from livestock production systems: a review of an air pollution problem. Environ Pollut 158:1–17
31. Ling Z, Guo H (2014) Contribution of VOC sources to photochemical ozone formation and its control policy implication in Hong Kong. Environl Sci Policy 38:180–191
32. Millner P (2009) Bioaerosols associated with animal production operations. Bioresource Technol 100(22):5379–5385
33. Schiffman S, Walker J, Dalton P, Lorig T, Raymer J, Shusterman D, Williams C (2000) Potential health effects odor from animal operations, wastewater treatment, and recycling of byproducts. J Agromed 7:7–81
34. Ackers M, Mahon B, Leahy E (1998) An outbreak of E. coli O157: H7 infections associated with leaf lettuce consumption. J Infect Dis 177(6):1588–1593
35. Bezanson G, Ells T, Prange R (2014) Effect of composting on microbial contamination and quality of fresh fruits and vegetables-a mini-review. In: I International symposium on organic matter management and compost use in horticulture. ISHS Acta Horticulturae 1018:631–638

36. Dufour A (ed) (2012) Animal waste, water quality and human health. IWA Publishing, London
37. Guan T, Holley R (2003) Pathogen survival in swine manure environments and transmission of human enteric illness – a review. J Environ Qual 32:383–392
38. Cooley M, Carychao D, Crawford-Miksza L, Jay M, Myers C, Rose C, Keys C, Farrar J, Mandrell R (2007) Incidence and tracking of Escherichia coli O157:H7 in a major produce production region in California. PLoS One 2:e1159
39. Cliver D (2009) Disinfection of animal manures, food safety and policy. Bioresource Technol 100(22):5392–5394
40. Harrington R, McInnes R (2009) Integrated Constructed Wetlands (ICW) for livestock waste-water management. Bioresource Technol 100(22):5498–5505
41. Ogejo, J (2009) Selecting a treatment technology for manure management. Virginia Coopeative Extension 442–306. http://pubs.ext.vt.edu/442/442-306/442-306.html. Accesed 11 Feb 2014
42. Sommer S (2013) Animal manure- from waste to raw materials and goods. In: Sommer S (ed) Animal manure recycling: treatment and management. Wiley, New York, pp 1–4.
43. Cantrell K, Ducey T, Ro K, Hunt P (2008) Livestock waste-to-bioenergy generation opportunities. Bioresource Technol 99:7941–7953
44. Hidalgo D, Corona F, Álamo J, Aguado A (2014) Resource recovery from anaerobic digestate: struvite crystallisation versus ammonia stripping. In: Abstracts of the international congress on water, waste and energy management, Oporto, 16–18 July 2014
45. Nieto P, Hidalgo D, Irusta R, Kraut D (2012) Biochemical methane potential (BMP) of agro-food wastes from the Cider Region (Spain). Water Sci Technol 66(9):1842–1849
46. Holm-Nielsen J, Al Seadi T, Oleskowicz-Popiel P (2009) The future of anaerobic digestion and biogas utilization. Bioresource Technol 100(22):5478–5484
47. Hidalgo D, Sastre E, Gómez M, Nieto P (2012) Evaluation of pre-treatment processes for increasing biodegradability of agro-food wastes. Environmen Technol 33(13):1497–1503
48. Hidalgo D, Martín-Marroquín J, Sastre E (2013) Single-phase and two-phase anaerobic co-digestion of residues from the treatment process of waste vegetable oil and pig manure. BioEnergy Res 1–11
49. Massé L, Massé D, Pellerin Y (2007) The use of membranes for the treatment of manure: a critical literature review. Biosyst Eng 98:371–380
50. USEPA (2007) AgSTAR Guide to operational systems. U.S. Environmental Protection Agency, Washington, D.C
51. Hidalgo D, Álamo J, Irusta R (2008) Pig manure digestion assays under anaerobic conditions in fluidized bed reactors. Arch Environ Prot 34:3–11
52. Wu X, Zhu J, Miller C (2013) Kinetics study of fermentative hydrogen production from liquid swine manure supplemented with glucose under controlled pH. J Environ Sci Health B 48 (6):477–485
53. Wu X, Lin H, Zhu J (2013) Optimization of continuous hydrogen production from co-fermenting molasses with liquid swine manure in an anaerobic sequencing batch reactor. Bioresource Technol 136:351–359
54. Luo Y, Stichnothe H, Schuchardt F, Li G, Huaitalla R, Xu W (2014) Life cycle assessment of manure management and nutrient recycling from a Chinese pig farm. Waste Manage Res 32 (1):4–12
55. Bolan N, Laurenson S, Luo J, Sukias J (2009) Integrated treatment of farm effluents in New Zealand's dairy operations. Bioresource Technol 100(22):5490–5497
56. Craggs R, Sukias J, Tanner C, Davies-Colley R (2004) Advanced pond system for dairy-farm effluent treatment. New Zealand J Agric Res 47:449–460
57. Kunz A, Miele M, Steinmetz R (2009) Advanced swine manure treatment and utilization in Brazil. Bioresource Technol 100(22):5485–5489
58. Liu J, Xu X, Li H, Xu Y (2011) Effect of microbiological inocula on chemical and physical properties and microbial community of cow manure compost. Biomass Bioenerg 35(8):3433–3439

59. Vanotti M, Szogi A, Millner P, Loughrin J (2009) Development of a second-generation environmentally superior technology for treatment of swine manure in the USA. Bioresource Technol 100(22):5406–5416
60. Magrí A, Béline F, Dabert P (2013) Feasibility and interest of the anammox process as treatment alternative for anaerobic digester supernatants in manure processing – an overview. J Environ Manage 131:170–184
61. Scaglione D, Tornotti G, Teli A, Lorenzoni L, Ficara E, Canziani R, Malpei F (2013) Nitification denitrification via nitrite in a pilot-scale SBR treating the liquid fraction of co-digested piggery/poultry manure and agro-wastes. Chem Eng J 228:935–943
62. Porter J, Davis J, Hickman D (2010) Selection guidance for manure management technologies. In: Abstracts of the international symposium on air quality and manure management in agriculture, Dallas, Texas, 13–16 September 2010
63. Hjorth M, Christensen K, Christensen M, Sommer S (2010) Solid–liquid separation of animal slurry in theory and practice. A review. Agron Sustain Dev 30(1):153–180
64. Christensen M, Christensen K, Sommer S (2013). Solid–liquid separation of animal slurry. In: Sommer S (ed) Animal manure recycling: treatment and management. Wiley, New York, pp 105–130
65. Riaño B, García-González M (2014) On-farm treatment of swine manure based on solid–liquid separation and biological nitrification- denitrification of the liquid fraction. J Environ Manage 132:87–93
66. Guerdat T, Losordo T, DeLong D, Jones R (2013) An evaluation of solid waste capture from recirculating aquaculture systems using a geotextile bag system with a flocculant-aid. Aquacult Eng 54:1–8
67. Møller H, Jensen H, Tobiasen L, Hansen M (2007) Heavy metal and phosphorus content of fractions from manure treatment and incineration. Environ Technol 28:1403–1418
68. Kwon S, Jang Y, Owens G, Kim M, Jung G, Hong S, Kim K (2013) Long-term assessment of the environmental fate of heavy metals in agricultural soil after cessation of organic waste treatments. Environ Geochem Health, 1–11
69. Nahm K (2005) Environmental effects of chemical additives used in poultry litter and swine manure. Crit Rev Environ Sci Technol 35:487–513
70. Massé D, Gilbert Y, Saady N, Liu C (2013) Low-temperature anaerobic digestion of swine manure in a plug-flow reactor. Environ Technol 34(18):2617–2624
71. Wu H, Hanna M, Jones D (2012) Thermogravimetric characterization of dairy manure as pyrolysis and combustion feedstocks. Waste Manage Res 30(10):1066–1071
72. Edström M, Schüßler I, Luostarinen S (2011) Combustion of manure: manure as fuel in a heating plant. In: Baltic forum for innovative technologies for sustainable manure management. Technical Report. http://balticmanure.eu/download/Reports/baltic_manure_combustion_final_2_2011_total.pdf. Accesed 11 Feb 2014
73. Ro K, Cantrell K, Hunt P (2010) High-temperature pyrolysis of blended animal manures for producing renewable energy and value-added biochar. Ind Eng Chem Res 49(20):10125–10131
74. Liu X, Li Z, Zhang Y (2013) Energy balance analysis on the slow pyrolysis process of cattle manure. Appl Mech Mater 392:531–534
75. Ocfemia K, Zhang Y, Funk T (2006) Hydrothermal processing of swine manure to oil using a continuous reactor system: Effects of operating parameters on oil yield and quality. Trans ASABE 49:1897–1904
76. Wu H, Hanna M, Jones D (2012) Fluidized-bed gasification of dairy manure by Box–Behnken design. Waste Manage Res 30(5):506–511
77. Chelme-Ayala P, El-Din M, Smith R, Code K, Leonard J (2011) Advanced treatment of liquid swine manure using physico-chemical treatment. J Hazard Mater 186(2):1632–1638
78. Kangas P, Mulbry W (2014) Nutrient removal from agricultural drainage water using algal turf scrubbers and solar power. Bioresource Technol 152:484–489

79. Arends F, Franke G, Grimm E, Gramatte W, Häuser S, Hahne J (2008) Exhaust air treatment systems for animal housing facilities: techniques-performance-costs. KTBL-Schrift 464, KTBL, Darmstadt, Deutschland
80. Flotats X, Bonmatí A, Fernández B, Magrí A (2009) Manure treatment technologies: on farm versus centralized strategies. NE Spain as case study. Bioresource Technol 100(22):5519–5526

Greenhouse Effect Mitigation Through Photocatalytic Technology

Jesusa Rincón, Rafael Camarillo, Fabiola Martínez, Carlos Jiménez, and Susana Tostón

Abstract Climate change is one of the most critical issues facing the world. One of the pillars of the fight against this phenomenon is the mitigation of greenhouse gas (GHG) emissions, CO_2 in particular. Although many achievements have already been made in CO_2 capture and storage technologies, promising methods to convert waste streams concentrated in this gas into valuable products are currently under way. This chapter intends to describe one of them, the photocatalytic reduction of CO_2 to fuel products, that is, the reaction to produce fuel between the CO_2 molecules and a reducing agent (usually water), in the presence of a semiconductor material that provides electrons (e^-) and holes (h^+) when it is illuminated by light of appropriate energy. Moreover, if solar energy were employed as light source, this type of energy difficult to store could be transformed into liquid or gaseous fuels, useful in conventional power production systems. In this chapter, firstly, a wide review about photocatalysis fundamentals, photocatalysts, synthesis of particles in supercritical fluids, characterization techniques, photocatalytic reactors, etc., is carried out. Subsequently, previous results from the authors' research on this subject are shown. More specifically, the characteristics of photocatalysts synthesized in a supercritical medium to convert CO_2 into fuels are presented and discussed.

Keywords Carbon dioxide, Photocatalysis, Supercritical synthesis, Titanium dioxide

J. Rincón (✉), R. Camarillo, F. Martínez, C. Jiménez, and S. Tostón
Faculty of Environmental Sciences and Biochemistry, University of Castilla-La Mancha, Campus Tecnológico de la Antigua Fábrica de Armas, Avda. Carlos III, s/n., 45071 Toledo, Spain
e-mail: Jesusa.Rincon@uclm.es

E. Jiménez et al. (eds.), *Environment, Energy and Climate Change I: Environmental Chemistry of Pollutants and Wastes*, Hdb Env Chem (2015) 32: 375–404,
DOI 10.1007/698_2014_274,
Published online: 29 July 2014

Contents

1 Introduction

Seven years ago the Fourth Assessment Report from IPCC (Intergovernmental Panel on Climate Change) presented a devastating landscape for both environment and economy of the Earth unless vigorous actions were adopted to slow down climate change. It also showed the need to reduce CO_2 emissions around 50–85% by 2050 to keep our climate safe. Additionally, it was pointed out that the costs of measures to reduce emissions would be lower than those derived from the fight against consequences from climate change [1].

In its recent Fifth Assessment Report, the IPCC has confirmed with a 95% of certainty that climate change is caused by human activity and that its effects are evident in most regions of the world [2]. Actually, CO_2 emissions from fossil fuel burning constitute the main cause of the problem. Further, in IPCC report several scenarios were defined, being the most optimistic one that showing an increase in the global temperature of about 2°C by the year 2100, with regard to the preindustrial stage. It should be noticed at this point that, even at this situation, serious and irreversible damages would be suffered by the world population and the environment.

Consequently, and due to the expected increase in CO_2 emissions related to energy production by about 50% up to 2035 [3], experts warn about the necessity of slowing down the rise so that the trend is reversed by 2020 [2] in order to minimize impacts on our climate.

Regarding the best strategy to solve the problem, a multidimensional solution is chosen. It combines a series of credible actions, many of which have already been implemented, although not yet at a global level and without the necessary determination: firstly, *to use the energy much more efficiently* in all sectors, from transport to housing, industry and power generation (Fig. 1), and, secondly, to *reduce deforestation* and develop technologies to obtain energy from *low-carbon alternative sources*, in particular renewable such as solar and wind energies, which do not use carbon neither emit CO_2.

In this sense, the pillars of the new framework of the European Union (EU) for climate and energy by 2030 are cutting greenhouse gas (GHG) emissions 40%

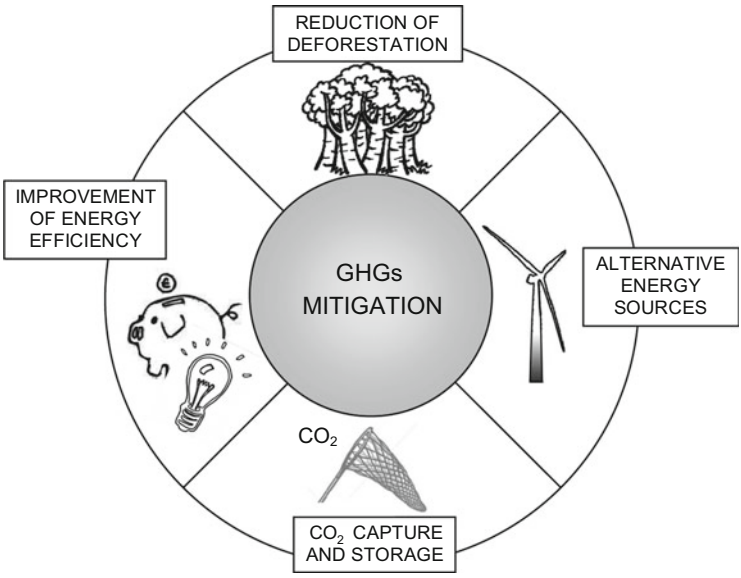

Fig. 1 Measures to reduce greenhouse gases (GHGs)

below 1990 levels and setting a binding target for all Member States of at least 27% of renewable energies above 1990 levels [4].

The first target is an intermediate stage of a more ambitious one: cutting GHG emissions 80–95% by 2050. EU wants to continue to lead the fight against climate change, and this has been reflected in a GHG reduction of 18% between 1990 and 2012, very encouraging to fulfil the objectives of EU 2020 Strategy (a reduction of GHG emissions of 20–30%, the use of 20% of renewable sources of energy, and an increase of 20% in energy efficiency) [5]. The second target is to increase the use of renewable energies in the power sector from 21% today to at least 45% by 2030.

Moreover, fossil-fuelled plants provided with *CO_2 capture and storage* technology would help meet the challenges of increasing energy demand with decreasing CO_2 emissions [6]. In other words, together with putting brakes on deforestation, improving energy efficiency and development of renewable energies, CO_2 capture and storage technologies are the fourth way to mitigate GHGs (Fig. 1).

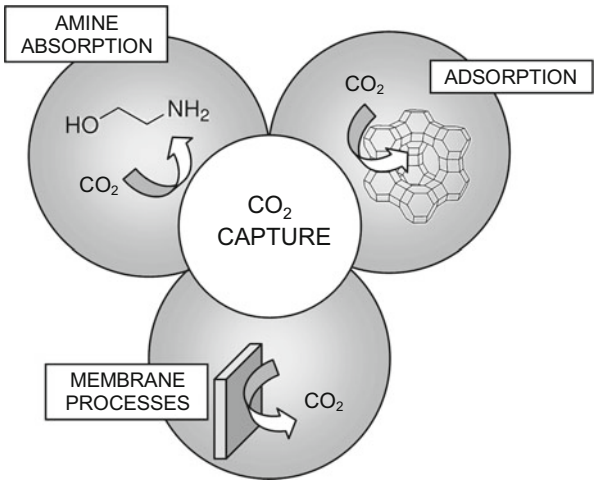

Fig. 2 Processes of CO_2 capture

2 Overview of the Technologies Used in CO_2 Conversion/ Mitigation

2.1 CO_2 Capture and Storage Technologies

The aim of these technologies is to prevent the input of anthropogenic CO_2 emissions in the atmosphere by means of capture, isolation (separation) and deviation (storage) towards secure places or by conversion into stable and/or high-added value products.

Current technology for direct capture and separation of CO_2 in the sources where emissions are generated exists, but it is expensive because CO_2 concentration is not high enough. So, refineries separate CO_2 to produce hydrogen, and since the 1970s, the petroleum industry injects pure compressed CO_2 in the subsoil to mobilize oil harder to extract. The challenge is therefore to increase CO_2 concentration to make storage economically viable.

A wide range of methods for CO_2 capture are available (absorption, adsorption and membrane processes), but gas *absorption* with nonaqueous solutions of amines is considered the most appropriate (Fig. 2). Bibliography lists numerous papers about absorption with monoethanolamine (MEA) and new amine-based absorbers. Most of them reach acceptable performances in capture [7, 8].

Apart from design improvements in contact systems, a technology that combines absorption (with amines) and the use of hollow-fibre inorganic *membranes* has been proposed to increase the efficiency of absorption process. In this technology, the membrane allows only the passage of CO_2 from gaseous phase to absorbing phase, leading to a substantial improvement over the conventional absorption [8, 9].

Other process employed for CO_2 capture is gas adsorption on different materials, both natural (kaolinite, dolomite, anthracite, etc.) and synthetic ones (active carbon,

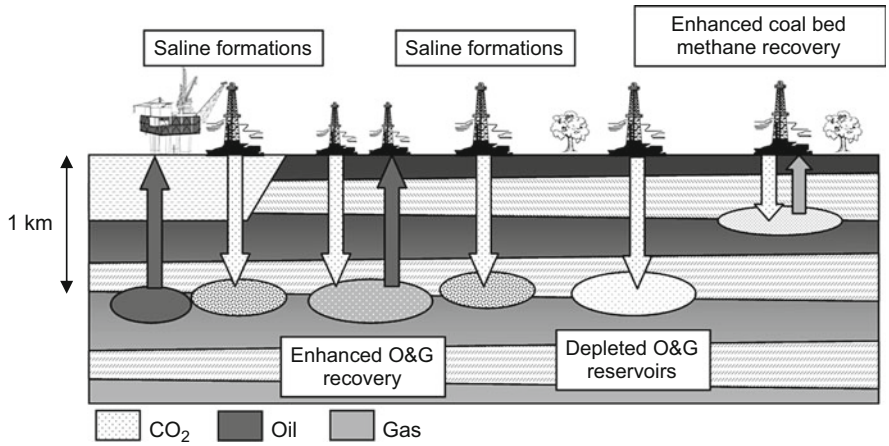

Fig. 3 CO_2 storage in underground reservoirs (based on [14])

resins, zeolites, etc.). However, the potential of this classical and well-known technology seems to be uncompetitive compared with absorption. In the same way, membrane processes, a still emerging technology for CO_2 separation, are not competitive either [8, 10].

It should be noted that the decrease of emissions can be achieved not only *after combustion* (separation of CO_2 from flue gas by means of absorption, adsorption and membrane processes) but also *before combustion* (conversion of conventional fuel into a low-carbon fuel) and *during combustion* (using oxygen instead of air, we can obtain a stream with higher concentration in CO_2, thus more easily to be captured) [11, 12].

After capture and separation of CO_2, its *storage* is required. This storage can take place in *underground reservoirs* (depleted oil and gas reservoirs, deep saline formations, coal mines of difficult exploitation, etc.), *terrestrial sinks* (forests, crops, wetlands) and *oceans* [11, 13].

In principle, CO_2 storage in *underground reservoirs* would be plausible because they have ability, structure, porosity and other properties necessary to store it during decades and centuries (Fig. 3). However, some question marks surrounding safety and environmental acceptability (CO_2 leakage towards land surface and sources of drinking water) hinder their development [15].

In *terrestrial reservoirs*, ecosystems are manipulated to store CO_2 beyond normal conditions. However, the possibility of enhanced natural systems to fix all emitted CO_2 appears doubtful, given the current generation rates.

Regarding storage capacity of *oceans*, it could be important and some experiments have already been performed to determine its probable use, both through direct injection and stimulating its natural absorption ability by means of fertilizers [11]. Research is primarily directed to determine operation efficiency and resulting ecological impact but also to ensure the environmental acceptability of procedures. It is commonly known that small changes in biogeochemical cycles can lead to

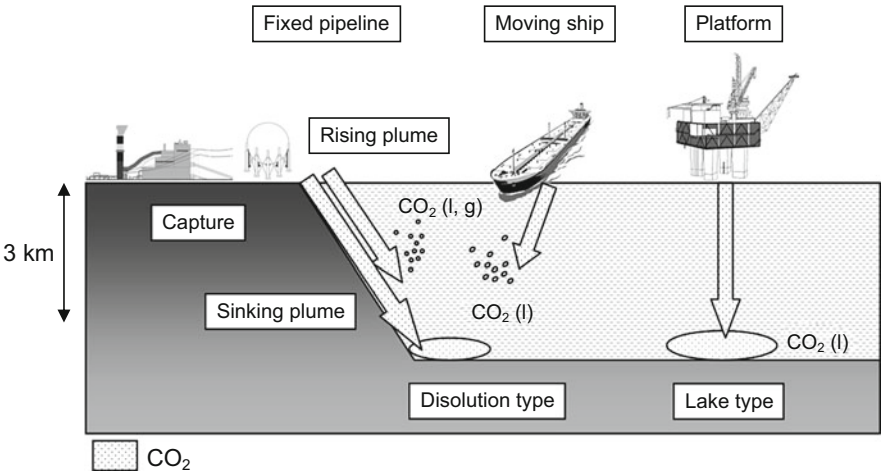

Fig. 4 CO_2 storage in ocean (based on [14])

huge impacts, most of them secondary and difficult to foresee, being the increasing acidity of sea water of particular concern. Figure 4 depicts different methods of CO_2 storage in ocean.

Ultimately, we can conclude that capture, transport and storage of CO_2 have some drawbacks. In addition to increasing the costs of energy production by 30% [6, 16], it also implies a cost of additional energy (with corresponding CO_2 emissions), conditioning of storage sites and unknowns about their ultimate safety.

2.2 *Chemical and Biological CO_2 Conversion*

An alternative to these previous procedures is (chemical or biological) conversion of CO_2 into stable and inert, tradable or non-tradable products [17]. It is an option with guarantees, since in nature there are many examples of CO_2 conversion: photosynthesis and CO_2 mineral reactions to form carbonates.

Briefly, we can say that the biological CO_2 recycling pathway involves growing algae to reduce CO_2 emissions. Further, at the same time pollution "trapped" by the algal biomass may be converted into biodiesel and/or ethanol. Obviously it is an attractive idea, but not without drawbacks. The main issue is that for an algae culture to be profitable, and also sustainable, both ecologically and economically, the possibility of using tap water and commercial fertilizer on crops should be discarded. In addition, it should be noted that algae can only assimilate between 20 and 50% of CO_2 supplied to them, while the rest is lost to the atmosphere [18].

Regarding chemical conversion, it should be underlined that although CO_2 molecule is very stable, leading to slow conversion processes, the potential for chemical processing is immense. Current technology allows turning it into

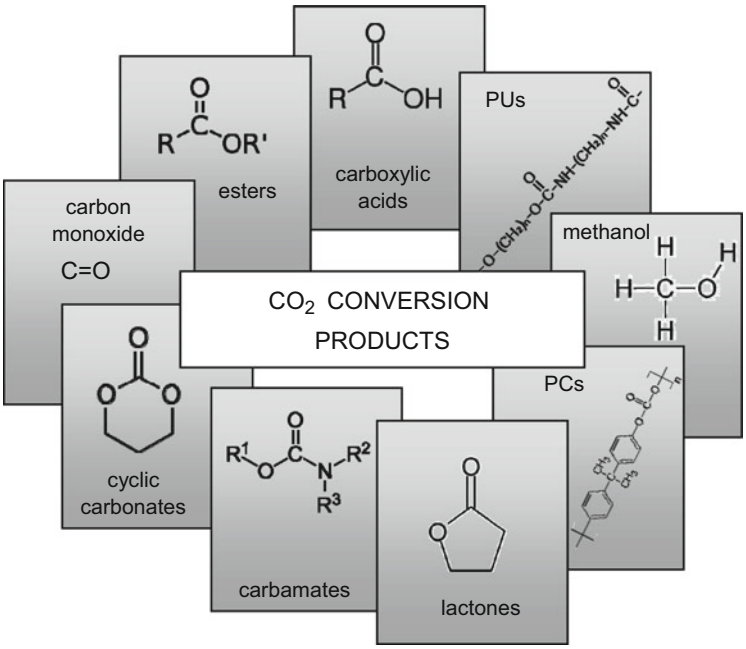

Fig. 5 Products from conventional CO_2 conversion

conventional chemical products, polymers, fuelling, etc. (Fig. 5), although with a low yield. However, given that, in terms of carbon dioxide equivalent, chemical industry can only absorb 1–3% anthropogenic CO_2 emissions [17], the synthesis of fuels emerges as the only conversion path to have a real significant impact on emission mitigation.

In this context of CO_2 reuse to produce a new fuel, some reactions deserve particular consideration: *coal gasification* ($C + CO_2 + 171\ kJ \rightarrow 2CO$), *catalytic reforming of* CH_4 to obtain syngas ($CH_4 + CO_2 + 247\ kJ \rightarrow 2CO + 2\ H_2$) and *enhanced photosynthesis* ($6CO_2 + 6H_2O + \text{energy} \rightarrow C_6H_{12}O_6 + 6O_2$) [19]. The main drawback is high energy requirements. Therefore, in order to mitigate emissions, the ideal would be to use *alternative energy sources*, such as renewable energy. In this case, the process would imply the transformation of energy difficult to store or transport (wind, sunlight) into liquid or gaseous fuels that can be used in conventional energy or heat production systems. For this, the photocatalytic conversion of the gas using solar energy is a process that despite being in its early stage of development has an enormous future potential [20].

Obviously, this technology, like capture and storage, is directed to major electric power plants and other industries where the amount of CO_2 generated is huge and concentrated, excluding transport, which comprises numerous small mobile sources.

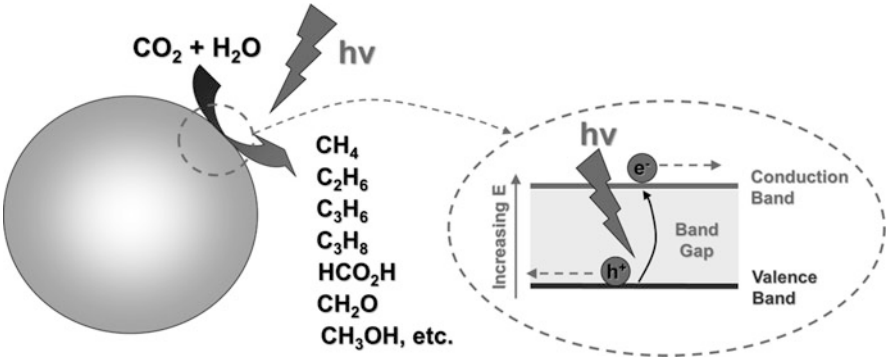

Fig. 6 Photocatalytic conversion of CO_2 process [21]

Table 1 Energy of band gap of different semiconductors [22]

Photocatalyst	Band gap energy (eV)	Photocatalyst	Band gap energy (eV)
Si	1.10	TiO_2 rutile	3.02
WSe_2	1.20	Fe_2O_3	3.10
α-Fe_2O_3	2.20	TiO_2 anatase	3.23
CdS	2.40	ZnO	3.20
V_2O_5	2.70	$SrTiO_3$	3.40
WO_3	2.80	SnO_2	3.50
SiC	3.00	ZnS	3.70

2.3 *A Chemical Process with Huge Future Potential: The Photocatalytic Reduction of CO_2*

Photocatalytic methods involve the use of semiconductors to cause reactions in the presence of light. Unlike metals, with continuous electronic states, when semiconductors are exposed to light, they show a band gap that extends from the upper part of the valence band (VB) to the lower part of the conduction band (CB) (Fig. 6). Kabra et al. [22] provide information about the energy of the band gap for different semiconductors generally employed in photocatalytic processes (Table 1).

When one photon interferes with a photocatalyst, electron–hole pairs (e^-–h^+) are generated through a photoexcitation process. If photon energy is equal to or more than band gap energy, the electron migrates into the conduction band, whereas the hole remains in the valence band. The following equations describe the generation of electron–hole pairs (photoexcitation) and the reverse process (recombination):

$$\text{Photocatalyst} + h\upsilon \rightarrow e^- + h^+ \quad (1)$$

$$e^- + h^+ \rightarrow \text{heat} \quad (2)$$

where $h\upsilon$ is photon energy, e^- represents one electron in CB and h^+ is a hole in VB.

The half-life of electron–hole pairs is short, a few nanoseconds [23], but enough to provoke redox reactions. Once electrons reach the surface, photoinduced transfer of electrons to close molecules takes place. If these molecules are adsorbed to the semiconductor, the process is more efficient [24]. Regarding holes, they can combine with electrons from donor species in surface. The charge-transfer rate depends on band gap energy and redox potential of adsorbed species. Sometimes electrons and holes can recombine before reaching semiconductor surface, which hinders the reactions of adsorbed molecules.

In general, photocatalytic processes take place at best conditions when as follows: (1) Redox potential of photo-generated hole in VB is positive enough to act as electron acceptor; (2) redox potential of photo-generated electron in CB is negative enough to act as electron donor.

More specifically, the mechanism of CO_2 photoreduction implies the formation of two important intermediate species: H· and $\cdot CO_2^-$, produced through electron transference from CB:

$$H^+ + e^- \rightarrow H\cdot \quad (3)$$

$$CO_2 + e^- \rightarrow \cdot CO_2^- \quad (4)$$

A set of reactions as follows lead to different products (among others):

$$CO_2 + 2H^+ + 2e^- \rightarrow CO + H_2O \quad \text{Carbon monoxide} \quad (5)$$

$$CO_2 + 2H^+ + 2e^- \rightarrow HCOOH \quad \text{Formic acid} \quad (6)$$

$$CO_2 + 4H^+ + 4e^- \rightarrow HCHO + H_2O \quad \text{Formaldehyde} \quad (7)$$

$$CO_2 + 6H^+ + 6e^- \rightarrow CH_3OH + H_2O \quad \text{Methanol} \quad (8)$$

$$CO_2 + 8H^+ + 8e^- \rightarrow CH_4 + 2H_2O \quad \text{Methane} \quad (9)$$

In spite of the above, other side reactions (consuming H^+ and e^-, producing H_2 and H_2O_2) take place together with CO_2 photoreduction [25]:

$$2H_2O + 4h^+ \rightarrow O_2 + 4H^+ \quad \text{Water splitting} \quad (10)$$

$$2H^+ + 2e^- \rightarrow H_2 \quad \text{Hydrogen formation} \quad (11)$$

$$O_2 + 2H^+ + 2e^- \rightarrow H_2O_2 \quad \text{Hydrogen peroxide formation} \quad (12)$$

Photocatalytic reduction of CO_2 develops under milder conditions (less energy consumption) than chemical reduction. The latter requires huge amounts of energy to reach pressure and/or temperature necessary to destabilize CO_2 molecule [26].

The first works about photocatalytic reduction of CO_2 in aqueous solution were published in 1978 and 1979 [27, 28]. Afterwards, many researchers [29–49] have studied the mechanism and efficiency of the process using different *catalysts* (titanium, zinc and cadmium oxides, cadmium sulphur, silicon carbide), *reducing agents* (water, amines, alcohols) and *light sources* (xenon, mercury, halogen lamps). These works have shown that a wide variety of products (methane, methanol, formol, formic acid, ethanol, ethane, etc.) can be obtained by means of specific semiconductors and reducing agents.

The latest relevant studies [50–64] have continued the analysis of a variety of parameters affecting both the selectivity and efficiency of the process. However, it should be noticed that the comparison of results of photocatalysts activity reported by different groups is a serious question, given the different reaction conditions in different labs.

Generally speaking, *pressure* effect has been analysed in several works [46, 51, 64] using water and organic solvents as reducing agents and TiO_2 as catalyst. Pressure has been found to increase CO_2 conversion and to affect selectivity, due to the different changes in adsorption rates for each reactive species with increasing pressure.

Regarding *temperature*, it should be noted that although photonic irradiation is the primary energy source in the formation of electron–hole pair at ambient temperature (because band gap energy is too large to be overcome with thermal excitation), at higher temperatures reaction rates can increase, so do collision frequency and diffusion rates. Global reaction rate increases because a higher temperature activates thermal stages (e.g. desorption) that follow photochemical reaction [42]. Despite these hypotheses, some references report a negative effect of high temperatures on half-life of excited states originated after photoexcitation, leading to deactivation. Nevertheless, Fox and Dulay [35] found that photocatalytic reactions (like most reactions) are not sensitive to small changes in temperature.

The effect of different *reducing agents* on mechanism and selectivity of reaction has been also analysed. Photoreduction of CO_2 with water is cheap and relatively simple. However, it raises concerns about the low solubility of CO_2 in water and the existence of side reactions consuming H^+ and e^- and leading to H_2 and H_2O_2 to the detriment of other reaction products from CO_2 (formic acid, formaldehyde, methanol, methane, CO, etc.). Therefore, yields in organic compounds are generally low when employing water [59].

To overcome these limitations, there are two alternatives: on the one hand, to replace liquid water with water vapour, which has just been described in different papers [65–67], that will be discussed later and, on the other hand, to replace water with other reducing agents (trimethylamine, triethanolamine, dimethylformamide and isopropyl alcohol), since it has been observed that solvent polarity significantly affects reaction mechanisms and the use of organic solvents enhances the efficiency and selectivity of the process towards the desired products [47].

Also to avoid the previous drawbacks, photoreduction has been accomplished with gases such as hydrogen sulphide [32], hydrogen [39, 68] and methane [56]. The photocatalytic reduction of supercritical CO_2 in the absence of reducing

agents and using TiO_2 and xenon arc lamps has even been suggested [49, 69]. Kaneko et al. [49] did not identify any reduced gaseous products after irradiation, but a washing of catalyst with water led to the presence of formic acid (through protonation of adsorbed anionic radicals $\cdot CO_2^-$). Moreover, if other washing solutions (methanol, ethanol, propyl alcohol, nitric acid, hydrochloric acid, phosphoric acid) were used, formic acid concentration increased inversely with solution pH, probably because the greater availability of H^+ favours the desorption of intermediates from catalyst surface.

In short, the reproduction in the laboratory of photosynthesis by means of photocatalytic procedures is not only possible, but short-chain hydrocarbons production with yields up to 1% (photosynthesis yields 3–5%) has been reported [70]. However, in order the process to be feasible at industrial scale, their main problems (low efficiency and slow kinetics) should be solved through the development of advanced catalysts and new design of reactors [71–75]. For this reason, both topics are addressed in the following sections.

2.3.1 Photocatalysts

Properties

Regarding the properties of potential catalysts, it could be highlighted that they should be semiconductor materials with a wide band gap, leading to high negative and positive redox potentials in CB and VB, respectively. The disadvantage of a wide band gap could be the necessity of a higher energy input, a minor problem from the photocatalytic point of view. The materials should also be stable against corrosion, nontoxic, low cost, and with physical-chemical properties that enable them to act as catalysts.

Although a variety of *semiconductors* have been employed, such as TiO_2, ZnO, ZrO_2, CdS, MoS_2, Fe_2O_3, WO_3, etc. and their combinations [51, 55, 56, 58, 71, 76], it has been noted that the material with the best photocatalytic behaviour and quantum yield is TiO_2, being the allotropic form anatase more active than rutile, due to its larger surface area and higher density of active sites for adsorption and catalysis [74]. The band gap energy is 3.02 eV for rutile and 3.23 eV for anatase [22] (Table 1).

The morphology of TiO_2 also has influence on the photocatalytic activity of catalysts. So, TiO_2 nanorods and nanotubes are currently being studied [77] due to the large surface area, reduced grain boundaries and facile charge transport paths of 1-D nanomaterials [71].

Doping of Catalyst

As indicated above, for photocalytic reduction to happen, the formation of electron–hole pairs after photon absorption by a semiconductor is essential.

Nevertheless, sometimes the recombination of electron–hole pairs may take place, leading to a decrease in efficiency of photoreduction. For this reason, some authors [34, 36, 52, 55, 57, 59, 60, 62, 63, 78, 79] have looked into the possibility of improving the efficiency and selectivity of photocatalyst through surface modification with metals (Cu, Pt, Pd, Rh, Au, Ag and Ru).

From previous works, one can conclude that *metal doping* avoids recombination and, consequently, lengthens the independent half-life of electrons and holes. The efficiency always increases, whatever the metal is introduced, and the selectivity towards specific products changes with the metal employed, increasing the production of formaldehyde, methanol and methane, which consume more electrons. As metal and semiconductor surfaces are in contact, electrons flow freely from catalyst to metal and distribute across the surface (Fig. 6). At the same time, holes are free to move towards semiconductor surface, where oxidation can take place.

This improvement has been also associated with the increase in the absorption of visible radiation by the catalysts with metal doping [58]. This is a very important fact, given that UV radiation only contributes less than 4% to the whole solar spectrum and 43% of the solar energy lies in the visible light region [71].

However, metal loading should be optimized and distributed evenly across catalyst surface. An excess would lead to a decrease in illuminated surface of catalyst, being the photons not absorbed as a consequence of reflection. The incorporation of metal to semiconductor has been performed by impregnation, electrostatic sol-spray deposition (ESSD) or ionic exchange.

It should not be forgotten that the incorporation of non-metal elements (B, N, I, C, S, P, F, Cl, etc.) also brings a redshift of the adsorption edge into visible light region [64, 80]. Special mention must be made of graphene- and C-based materials, due to their excellent transparency, superior electron conductivity and mobility, high specific surface area and high chemical stability [67, 81].

Immobilization

Another factor that may affect the process substantially is the way the catalyst is used: as powder or immobilized over a support. Investigations undertaken show that, generally speaking, powdered catalysts are more efficient due to their higher surface area and more favourable conditions for mass transference [33, 41, 50, 71, 75].

Nevertheless, the use of powdered catalysts at industrial scale is intrinsically difficult, given the necessity of including an additional separation of small particles of catalyst after photocatalysis. For this reason, the development of efficient, low-cost, *supported catalysts* is an alternative that deserves thoughtful consideration [50]. The bigger particle size of supported catalyst would make solid–fluid easier to separate after photocatalytic reaction.

In both cases, the activity of catalyst has been found to increase when particle size decreases [37, 43]. For supported catalysts, the reactivity and selectivity

towards specific products increase with the degree of dispersion of semiconductor over the support [48, 71].

Regarding supported catalysts, it is widely accepted [40] that a good support material should possess the following properties: (a) transparency to light radiation, (b) promoting the formation of strong bonds with catalyst particles with no negative impact on reactivity, (c) with a large surface area, (d) exhibiting a high adsorption capacity of species to treat, (e) allowing reactor designs that facilitate mass transference and (f) being chemically inert.

Fulfilling all previous requirements, the supports most often used have been siliceous materials as nonporous silica microspheres, silica gel, quartz, glass, etc. Special mention must be made of silicates and aluminosilicates with zeolitic structure due to their unique properties related to pore size, inner surface topology and ionic exchange capacity [38, 44, 45, 48, 53, 54].

From the point of view of coating, the ideal situation happens with the existence of two core conditions: (a) good adhesion between catalyst and support and (b) the absence of degradation in catalyst during fixation process [72].

The first one is essential, since catalyst-support union must withstand the stresses resulting from mechanic interactions (particle–particle, particle–fluid) in reactor and avoid the breakdown of catalyst particles and the release from support.

In relation to the second condition, the modification of catalytic activity is of prime importance. It can occur due to many factors: (a) changes in energy levels of VB and CB through catalyst-support bonds and/or the small particle size of coating, (b) changes in crystal structure of catalyst as a result of fixation treatment at relatively high temperatures, (c) the decrease of catalyst surface area due to particle agglomeration and catalyst-support bonds and (d) the fixation of catalyst particles inside the inner micropores of support, where the light cannot penetrate.

The fixation of catalyst over the support has taken place through two methods [40]. In the first one, the fixation of catalyst over the support is performed after the synthesis of catalyst. In the second one, there is an in situ generation of catalyst by means of sol–gel, GSP [57] or chemical vapour deposition, CVD [55].

2.3.2 Photocatalytic Reactors

The effect of using different *types of reactors* on photoreduction of CO_2 has been little studied, having performed most research in batch reactors. These reactors can be gathered in two categories: fluidized bed reactors and fixed bed reactors.

Fluidized bed reactors are the most common ones. These reactors work in batch mode with two phases (heterogeneous). The photocatalyst is suspended as solid particles in a fluidlike state by a magnetic stirrer, which provides high dispersion. Reaction starts with filling CO_2 into the reactor containing the reducing agent (usually liquid water) and catalyst particles. Then light source is switched on. Samples are taken at fix time intervals by syringe or online automatic sampling system and sent to gas chromatography (GC) systems. One of the main variables, apart from lamp type and reactor size, is lamp position. There are examples where

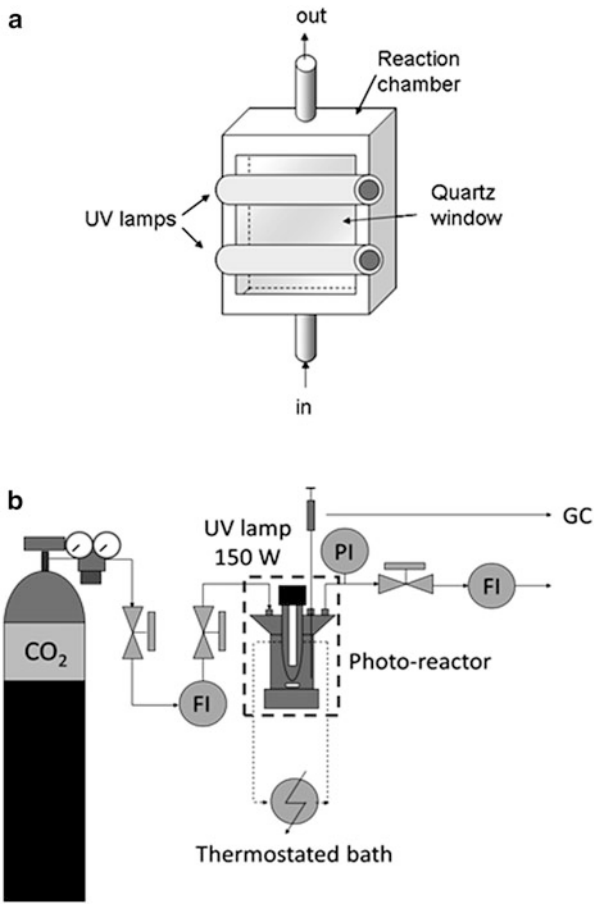

Fig. 7 Fluidized bed photocatalytic reactors: (**a**) lamp parallel to reactor, (**b**) lamp placed in an inner radiation cell

the lamp is located parallel to the reactor [82] (Fig. 7a) or placed in an inner radiation cell [83, 84] (Fig. 7b).

Regarding fixed bed reactors [21, 64] (Fig. 8a), CO_2 photoreduction usually takes place in gas phase. In this way, a CO_2 stream flows through a water bubbler to achieve a controlled humidity. The resulting mixture is introduced in a reaction chamber with a quartz window, which receives the light energy. The catalyst particles are dispersed on a glass fibre filter inside the reaction chamber. Once the reaction has finished, the gaseous sample is taken by syringe or online automatic sampling system towards a GC.

A specific type of fixed bed reactor are fibre reactors, where photocatalysts are coated optical fibres and the fluid is guided to form a plug flow state [85] (Fig. 8b). The fibre serves as a medium to deliver light effectively and uniformly to the surface of the photocatalyst [71].

Another special type of photocatalytic reactors are solar reactors [86]. The design takes into account two options: (a) immobilization of catalyst over a support

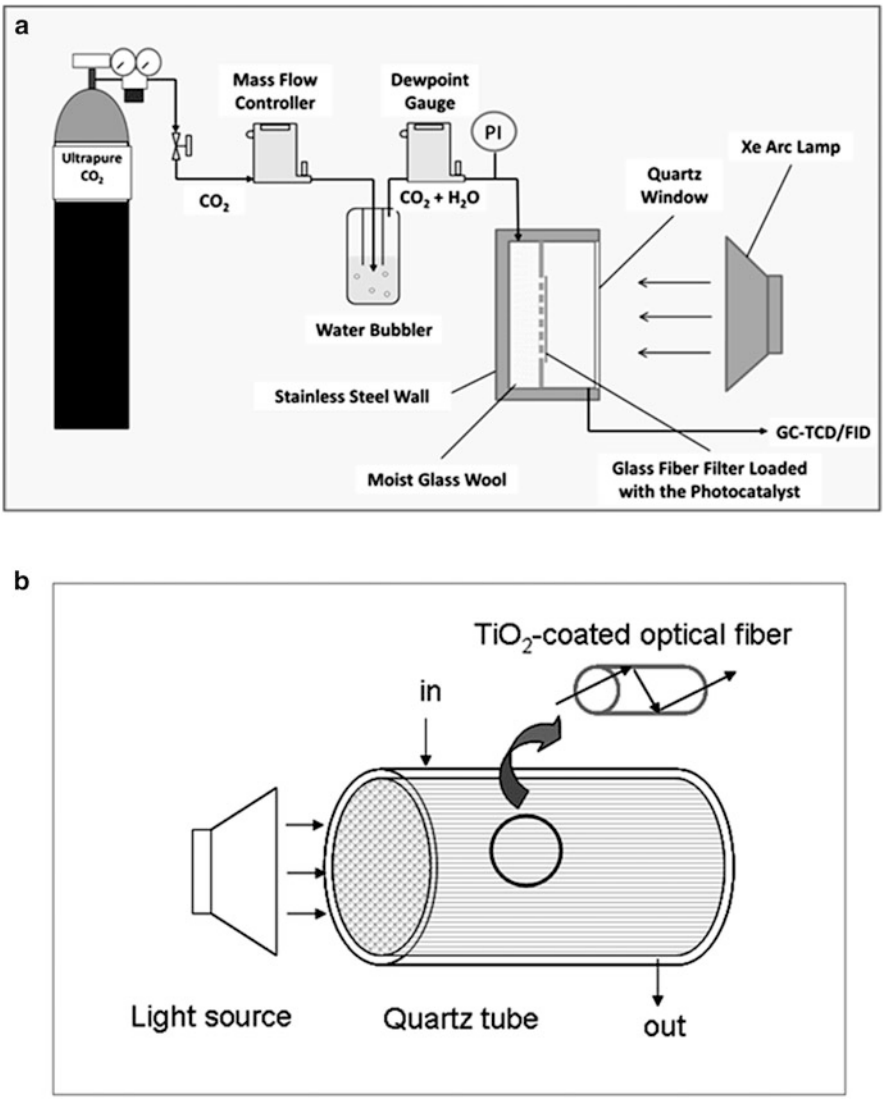

Fig. 8 Fixed bed photocatalytic reactors: (**a**) conventional [21], (**b**) fibre reactor

and (b) concentration of sunlight. As in nonsolar reactors, the advantage of supported systems is a simplification in the separation of catalyst after photocatalytic reaction. The drawback is lower efficiency than nonsupported systems. As regards the systems that do not concentrate light, they make use of both diffuse UV light and direct sunlight, and they capture the light more efficiently. On the other hand, their volume is higher than concentrated systems for an equivalent area of light energy collection.

3 Photocatalytic Conversion of CO_2 into Fuels by Means of Catalysts Synthesized at Supercritical Conditions

Given that the catalyst plays an important role during a photocatalytic reaction, one of the challenges in this area is the development of innovative methods for the synthesis of advanced catalysts. In this sense, the experience gained by authors in extraction with supercritical fluids (SCFs) encouraged the group to study the production of efficient TiO_2-based photocatalysts by means of SCFs technology for CO_2 conversion into fuels, a specific issue not studied so far. As a matter of fact, most works dealing with photocatalyst synthesis apply conventional methods to obtain this type of materials [80, 87, 88] or the few studies employing SCFs synthesis process destine photocatalysts for other purposes [89].

Thus, in this section we will discuss results obtained in the experimental investigation planned to study the supercritical synthesis of TiO_2 to convert CO_2 into fuel. Before that, a brief overview on SCFs and their use to produce photocatalysts is presented.

3.1 Overview on Supercritical Fluids and Their Use to Produce Photocatalysts

The peculiarity of supercritical fluids (SCFs) lies in their hybrid nature, since they combine density and solvent power of liquids with transport properties (viscosity and diffusivity) of gases, being these parameters tunable with changes in operating conditions [90, 91].

Thus, due to the unique physicochemical and thermodynamic properties of SCFs, this technology is interesting in the development of certain processes, such as advanced micro- or nano-structured/sized material generation, supporting and impregnation, compound extraction, solid decontamination or recycling, destruction of organic wastes or even sterilization and virus deactivation [92–97].

In the field of catalysis, numerous works have shown that the synthesis conditions of a catalyst have strong influence on its properties [98–100], so the reactivity of synthetic solids could exceed that of commercial catalysts provided that an appropriate synthesis method is employed. A clear example of this is found in wastewater reclamation [101]. Moreover, a recent work has revealed a higher catalytic activity for electrocatalysts synthesized in supercritical medium in comparison to commercial catalysts [102].

Regarding processes in supercritical media, results from recent research indicate that the synthesis of photocatalysts (as TiO_2) in supercritical CO_2 can be performed under milder temperature conditions [89] and in a faster way [103] than using classical synthesis techniques (sol–gel process, SGP, and chemical vapour deposition, CVD).

Another reason why SCFs are an attractive alternative in the synthesis of nanoparticles is the control of properties as size, morphology, structure and size distribution, very important for the final application of synthesized product [89, 104].

The most common solvents in supercritical technology are water and carbon dioxide. The use of supercritical water (SCW) is due to its excellent qualities as inorganic solvent in oxidation reactions, acting as both a reagent and a reaction medium. It has been proved that oxidation processes in SCW provide rapid destruction of a wide variety of organic species normally considered to be refractory or difficult to break down under conventional means such as incineration [96].

On the other hand, supercritical CO_2 ($scCO_2$) is particularly interesting, not only because it is a nontoxic, nonflammable compound, with high compressibility and abundance (low cost), but also with milder supercritical conditions ($T_c = 304.4$ K; $P_c = 73.8$ bar) than SCW [102]. In addition, the ease with which $scCO_2$ is removed from the final reaction mixture contrasts with the costly drying process to remove conventional solvents. Its relatively high solvent power, together with the simple change of density, makes an easy control of reactions and processes possible [93]. All these properties make $scCO_2$ the ideal candidate for preparation of nanoparticles [104]. It can also be used in other processes as an antisolvent or extracting agent for organic phases in water emulsions or even to improve the spraying process in different techniques [105].

Despite the abovementioned, the synthesis of metal oxides nanoparticles has been also addressed in SCW with satisfactory results [106, 107]. Interestingly, rapid reaction kinetics in SCW makes possible to prepare metal oxide nanoparticles in continuous processes, which is more attractive for industrial-scale production. Nevertheless, some drawbacks such as corrosion of the high-pressure apparatus, with the subsequent increase in capital costs, normally appear [106].

3.2 Particle Generation in Supercritical Fluids

According to the above section, the use of SCF technology implies significant savings in conventional organic solvents, being substituted by fluids as $scCO_2$, a nondestructive and clean solvent, very suitable for the production and processing of sensible materials and complex micro- and nanostructures [92, 102].

For this reason, the first stage of our study on the photocatalytic conversion of CO_2 into fuels (CH_4, C_2H_6, etc.) using UV–visible light was the design of a suitable catalyst to improve the efficiency of the reaction. With this purpose, a semiconductor with appropriate band gap energy was chosen. The candidate was TiO_2, with high stability against corrosion, good photocatalytic behaviour and high quantum yield [84, 108–110].

However, given that the efficiency of TiO_2 can be significantly improved through the incorporation of metals, the effect of metal doping on photoreduction of CO_2 was also studied. This surface modification opens the doors to the use of this

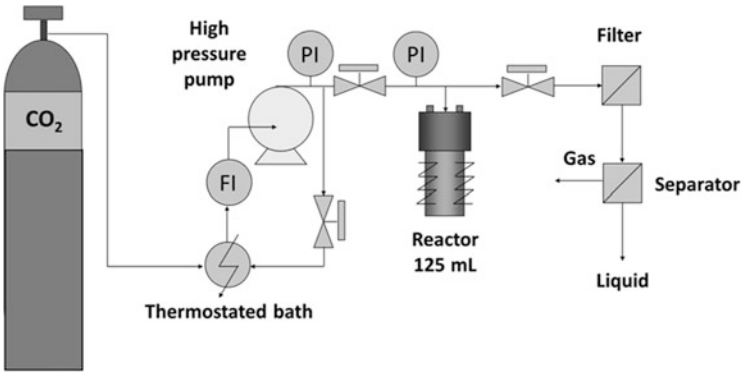

Fig. 9 Experimental setup of supercritical synthesis of photocatalysts. *FI* and *PI*, flow and pressure indicators, respectively [21]

catalyst in solar reactors, since metal-doped TiO_2 activates under visible light [111, 112]. In this case, copper in concentrations <5% wt. was selected as a doping agent [34, 36, 52, 55, 57, 59, 60].

The synthesis of TiO_2 and Cu–TiO_2 was carried out using supercritical CO_2 as reaction medium. Thereby, titanium dioxide has been synthesized from diverse combinations of two titanium precursors (titanium tetraisopropoxide, TTIP, and diisopropoxititanium bis(acetylacetonate), DIPBAT) and two hydrolytic agents (isopropyl alcohol and ethanol) in a thermohydrolysis process [113, 114].

An ad hoc experimental setup comprising 3 subsystems (fluid pumping, reaction chamber and separation module) was used (Fig. 9). This installation was designed to operate under pressure (200 bar) and temperature (300°C) required by process, whose duration was 2 h once these values were achieved [113]. The main components in the system were a high-pressure pump preceded by a thermostated bath and a stainless steel reactor (125 mL inner volume) followed by a particle filter. Once the reaction had finished and ambient conditions were recovered in reactor, the solid was extracted by means of washing with the same alcohol used in the reaction, dried at 105°C, and finally calcinated at 400°C during 6 h [21]. Although this thermohydrolytic process is based on previous studies [113, 114], this last calcination step was included to improve solid crystallinity and guarantee the primacy of anatase phase, very suitable in photocatalysis [74]. It is important to mention that calcination temperature was established taking into account that transition between anatase–rutile phases happens at temperature about 700°C [115, 116].

3.2.1 Synthesis Yield

A set of more than 60 synthesis experiments were performed, covering all possible combinations of precursor and alcohol in the absence and presence of copper in concentrations 0.5–3% by weight. A variable called “yield” can be calculated as the

ratio between the moles of product obtained and the moles of the precursor, following a 1:1 stoichiometry for both precursors. The yields for TTIP were higher (about 90%) than those observed for DIPBAT (about 60%). Regarding hydrolytic agents, no significant effect has been found, although the yields are slightly higher in TTIP–ethanol system [21].

Despite this statement, the selection of an ideal precursor-alcohol combination is also dependent on photocatalysis results, given that DIPBAT has been considered as the best candidate by different authors [113] due to its higher surface area in adsorption and catalysis, and isopropyl alcohol is related to higher photocatalytic activity in oxidation than ethanol [103].

3.2.2 Particle Characterization

UV–Visible Diffuse Reflectance

The solids thus synthesized were *characterized* through different usual techniques, namely, diffuse reflectance UV–Vis spectroscopy, X-ray diffraction, particle size and particle size distribution analysis and BET area measurement.

To start with the analysis of the catalyst, *UV–Vis absorbance* is considered of prime importance because it gives idea of the utilization of light source, both artificial lamps in this work and sunlight in the upcoming stages of project.

As it is depicted in Fig. 10a, a redshift takes place for all synthesized catalysts (in contrast to commercial TiO_2), particularly for materials from DIPBAT. These materials will have a better use of visible light (400–700 nm), where the Xenon arc lamp (with AM 1.5G Standard filter) employed in most photocatalysis experiments shows some emission peaks (Fig. 10d) [21].

Some authors [80] have related this redshift to the presence of carbonaceous wastes in materials from DIPBAT, since this molecule possesses very thermally and kinetically stable ligands, which hinder hydrolysis [113].

In Fig. 10b the influence of metal doping can be observed. In the case of catalysts from TTIP, an increase of absorbance in visible range with copper concentration (up to 3% wt.) is observed. Nevertheless, catalysts from DIPBAT exhibit this behaviour at low concentrations, since a shielding phenomenon seems to take place at concentrations higher than 2% wt. [58].

Figure 10c depicts that catalysts from ethanol show higher absorbances in visible range than those from isopropyl alcohol. This effect has not been previously studied in bibliography, since papers about traditional synthesis of TiO_2-based catalysts usually employ a single alcohol and/or each research is developed under different synthesis conditions [80, 117].

In summary, the curve with higher absorbance in visible range is DIPBAT–ethanol–Cu (2% wt.) (Fig. 10c).

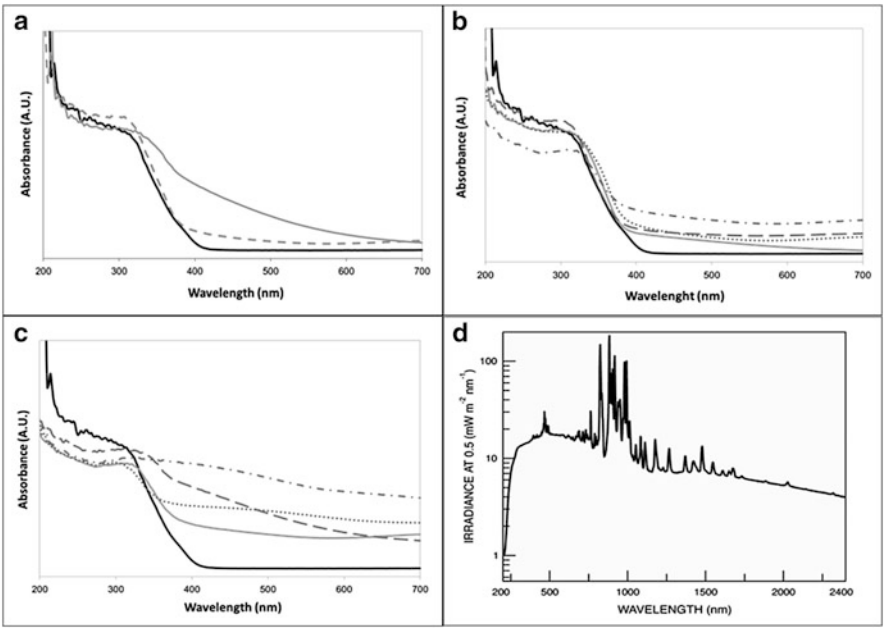

Fig. 10 Diffuse reflectance UV–Vis spectra of catalysts: (**a**) non-doped materials (*black*, commercial; *grey*, DIPBAT; *dashed line*, TTIP), (**b**) doped TTIP-based materials (*black*, commercial; *grey*, TTIP–isop.; *dot line*, TTIP–isop.–Cu 1%; *dashed line*, TTIP–isop.–Cu 2%; *dot-dashed line*, TTIP–isop.–Cu 3%), (**c**) maximum absorbances in visible range (*black*, commercial; *grey*, TTIP–isop.–Cu 3%; *dashed line*, DIPBAT–isop.–Cu 2%; *dot line*, TTIP–ethanol–Cu 3%; *dot-dashed line*, DIPBAT–ethanol–Cu 2%), (**d**) irradiance spectrum of a Xe arc lamp (Newport, model 6266, 450 W) [21]

X-Ray Diffraction

Another important analytic technique is *X-ray diffraction* (XRD). XRD patterns give information about both the allotropic forms of TiO_2 (anatase and rutile) present in the sample, according to the position of peaks, and the crystallinity of the catalyst related to the height and resolution of peaks. It has been proved that a photocatalytic process is favoured when anatase phase prevails (higher surface area, higher density of active sites) and peaks are high and well resolved (higher crystallinity) [74].

According to Fig. 11, all precursor-alcohol combinations exhibit XRD patterns similar to commercial TiO_2. The combination with the best resolution and peak height is TTIP–isopropyl alcohol (Fig. 11a), whereas the crystallinity is worse for TTIP–ethanol (Fig. 11b). Catalysts from DIPBAT (Fig. 11c, d) are less crystalline. In the case of photocatalysts with copper, those synthesized from TTIP appreciably resemble commercial catalyst (not shown).

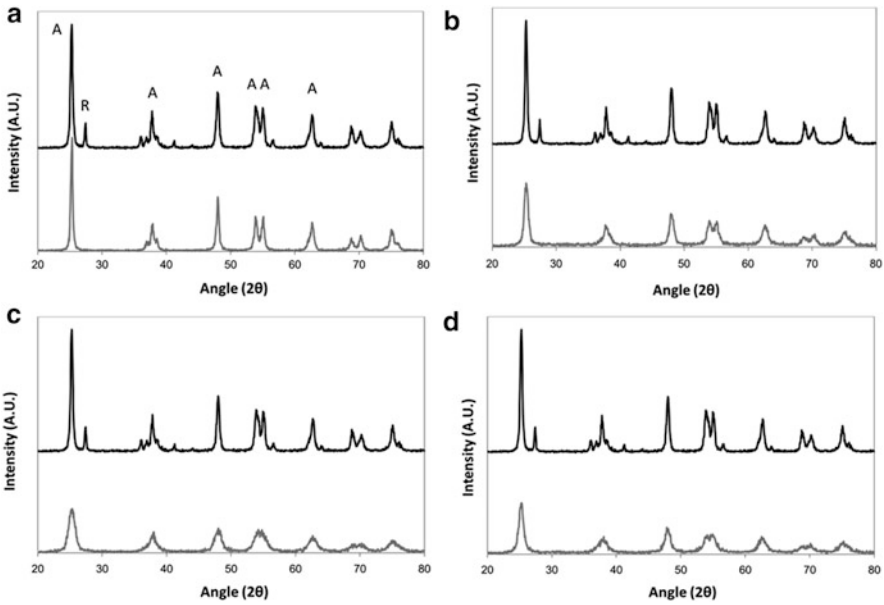

Fig. 11 XRD patterns of catalysts: (**a**) TTIP–isopropyl alcohol, (**b**) TTIP–ethanol, (**c**) DIPBAT–isopropyl alcohol, (**d**) DIPBAT–ethanol (*black lines*, commercial TiO_2; *grey lines*, synthesized materials; *A* anatase, *R* rutile) [21]

Mean Particle Size and Particle Size Distribution

The third parameter analysed is *mean particle size* of synthesized particles, which is slightly bigger than that for commercial catalyst (not shown). This variable has a strong relationship with *particle size distribution*, which is wider for synthesized catalysts. It must be emphasized that almost 50% in volume of synthesized particles possess a particle size greater than 1 μm, while 70% in volume of commercial particles have 0.6–5 μm diameter [21].

Taking into account the type of precursor, catalysts from DIPBAT show smaller mean particle size than those from TTIP [113]. Significant differences have not been observed between different hydrolytic agents.

Surface Area

Regarding surface area (*BET area*), it is a variable sensitive to certain parameters as synthesis temperature or crystallinity [103]. In this study, materials from DIPBAT show higher surface area, which could be related to their lower degree of crystallinity [113]. To understand this issue, it should be noted that particle porosity decreases with increasing crystallinity degree [118] and amorphous or poorly crystalline particles will show, consequently, higher surface areas.

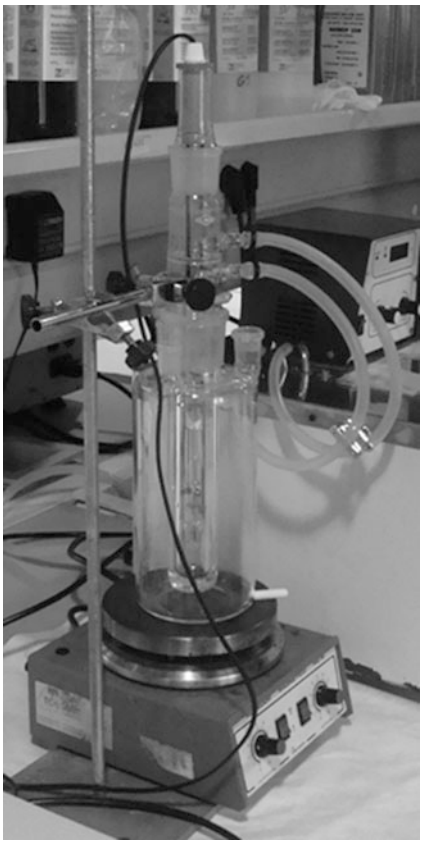

Fig. 12 Photocatalytic reactor equipped with inner UV radiation source

3.2.3 Photocatalytic Reduction of CO_2

Finally, to evaluate the photocatalytic activity of catalysts, two series of experiments in liquid and gaseous phases were performed.

When liquid water was used as a reducing agent, the solid was in aqueous suspension (concentration 1 g/L) and gaseous CO_2 was bubbled until total pressure 1.1 bar [119, 120]. A first ad hoc experimental setup consisted in a fluidized bed reactor (glass cylindrical flask, inner volume 1 L) and an UV radiation source (150-W medium pressure mercury UV lamp) was used [59, 83] (Fig. 7b). These experiments were performed in batch mode, and liquid and gaseous samples were taken at intervals through the reactor cover, which has different caps with *septum* (Fig. 12). These samples were analysed in a gas chromatograph (GC) with flame ionization detector (FID).

As earlier pointed out, due to the low solubility of CO_2 in water, the efficiency of the process was very limited and the products obtained were so diluted that they were very difficult to detect.

As a consequence, we decided to use a reaction medium where water was in gaseous state, with the corresponding increase in moles CO_2/mol H_2O ratio. Thus, a second ad hoc experimental installation was designed on the basis of bibliography (Fig. 8a) [64, 121, 122].

The new installation consists of a CO_2 mass flow controller, a water bubbler to saturate with humidity this gaseous stream, a dew-point gauge and the photocatalytic reactor. It is a fixed bed reactor, made of stainless steel, with cylindrical shape and inner volume 50 cm^3. It has a quartz window and a stainless steel grill to support glass fibre filter loaded with the photocatalyst (Fig. 8a) [21].

The reaction chamber is illuminated by a Xe arc lamp with an AM 1.5G Standard filter, with an emission spectrum similar to sunlight [64, 122].

This system works in batch mode. Once experimental time is over, reaction products are sent to a gas chromatography system (GC-TCD/FID). For this reason, it was necessary to design different methods to detect and quantify the different products: CO, CH_4, light hydrocarbons (C1–C7) and hydrogen.

As example, results of two experiments using 100 mg of undoped commercial and synthesized catalysts (supported on a glass fibre filter, dried at 180°C during 30 min and illuminated with UV light during 30 min to avoid any organic contamination) are presented. Ultrapure CO_2 (99.998% with a certified maximum of hydrocarbons less than 1 ppm) [120], and further moistened with deionized water until relative humidity 85%, was used. Initial pressure inside reactor was 1.07 bar [121] and illumination time was 3 h.

Methane (CH_4) was identified as the major product from the photocatalytic reaction in both cases, together with alkanes (ethane and propane) and some alkenes (propylene) at lower concentrations (Fig. 13a) [121, 122]. Intermediate compounds as CO and hydrogen were also analysed to elucidate reaction mechanism [64].

Finally, if we compare the results with undoped synthesized catalyst (TTIP–isopropyl alcohol) (Fig. 13b) and those for commercial TiO_2 (Fig. 13a), the variety of products obtained is similar. Moreover, in the case of synthesized catalyst, peaks are about 1.5 times larger in area in comparison to commercial catalyst [21]. It should be highlighted that these results are in agreement with those obtained by other authors when using catalysts synthesized through conventional methods [57].

4 Conclusions

To sum up, this chapter shows that although the reproduction in the laboratory of photosynthesis by means of photocatalytic procedures is possible, its implementation on an industrial scale will not be feasible until their main drawbacks (low efficiency and slow kinetics) are solved. It also shows that the solution to these problems may be accomplished through the development of advanced photocatalysts.

Moreover, the chapter intends to demonstrate that supercritical fluids (SCFs) may be used as a synthesis medium to improve the properties of catalysts employed

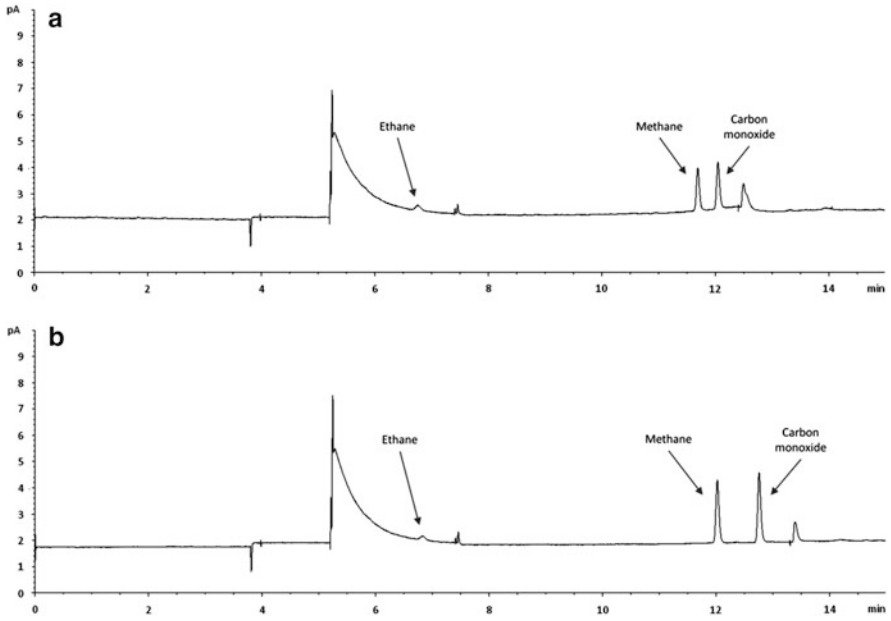

Fig. 13 GC Chromatograms of experiments of photocatalytic conversion of CO_2: (**a**) commercial TiO_2, (**b**) TTIP–isopropyl alcohol (only majority compounds are labelled) [21]

for the photocatalytic conversion of CO_2 into fuel products. Particularly, the behaviour at the photocatalytic conversion of commercial TiO_2 and TiO_2-based catalysts synthesized in supercritical carbon dioxide is assessed. Results attained indicate that SCF synthesized catalysts are unquestionably more efficient than the commercial catalyst.

References

1. Intergovernmental Panel on Climate Change (IPCC) (2007) Fourth assessment report mitigation of climate change. http://www.ipcc.ch/pdf/assessment-report/ar4/wg3/ar4_wg3_full_report.pdf. Accessed 12 Jun 2014
2. Intergovernmental Panel on Climate Change (IPCC) (2013) Fifth assessment report climate change: the physical science basis. https://www.ipcc.ch/report/ar5/wg1/. Accessed 12 Jun 2014
3. International Energy Agency (IEA) (2013) IEA world energy outlook
4. European Commission (28 Jan 2014) La CE establece los objetivos de clima y energía para 2030. Por una economía más competitiva, segura y baja en carbono en la UE. http://ec.europa.eu/spain/actualidad-y-prensa/noticias/energia/energia-cc_es.htm. Accessed 12 Jun 2014
5. European Commission (2014) Europa 2020. http://ec.europa.eu/europe2020/index_es.htm. Accessed 12 Jun 2014

6. European Technology Platform for Zero Emission Fossil Fuel Power Plants (2007) CO_2 capture and storing: a key solution for combating climate change. www.zero-emissionplatform.eu. Accessed 12 Jun 2014
7. Abu-Zahra MRM, Schneiders LHJ, Niederer JPM, Feron PHM, Versteeg GF (2007) CO_2 capture from power plants. Part I. A parametric study of the technical performance based on monoethanolamine. Internat J Greenhouse Gas Control 1:37–46
8. Patricia L, Van Gerven T, Van der Bruggen B (2012) Recent developments in membrane-based technologies for CO_2 capture. Prog Energ Combust 38:419–448
9. van Loo S, van Elk EP, Versteeg GF (2007) The removal of carbon dioxide with activated solutions of methyl-diethanol-amine. J Petrol Sci Eng 55:135–145
10. Chaffee AL, Knowles GP, Liang Z, Zhang J, Xiao P, Webley PA (2007) CO_2 capture by adsorption: materials and process development. Internat J Greenhouse Gas Control 1:11–18
11. US Department of Energy (USDOE) (2006) Carbon sequestration research and development. www.fe.doe.gov/programs/sequestration/cslf/sequestrationfactsheet_06_18.pdf. Accessed 12 Jun 2014
12. Kanniche M, Gros-Bonnivard R, Jaud P, Valle-Marcos J, Amann J-M, Bouallou C (2010) Pre-combustion, post-combustion and oxy-combustion in thermal power plant for CO_2 capture. Appl Therm Eng 30:53–62
13. Reiche DE, Houghton JC, Kane RL, DOE (2007) A review of carbon sequestration science and technology opportunities by the US Department of Energy. www.lib.kier.re.kr/balpyo/ghgt5/Papers/E1%202.pdf. Accessed 12 Jun 2014
14. Intergovernmental Panel on Climate Change (IPCC) (2005) Special report carbon dioxide capture and storage, technical summary. http://www.ipcc.ch/pdf/special-reports/srccs/srccs_technicalsummary.pdf. Accessed 12 Jun 2014
15. Monastersky R (2013) Seabed scars raise questions over carbon-storage plan. Nature 504:339–340
16. Office of Scientific and Technical Information (OSTI) (2007) Carbon sequestration research and development: advanced chemical approaches to sequestration. www.osti.gov/energycitations/servlets/purl/8107229s7bTP/native/810722.pdf. Accessed 12 Jun 2014
17. Royal Society of Chemistry (RSC) (2006) Converting CO_2 to chemicals, workshop of the RSC: environmental, sustainability and energy forum, London (UK). www.rsc.org/images/converting%20CO2%20to%20chemicals%20report_FINAL_tcm18-65202.pdf. Accessed 12 Jun 2014
18. Sudhakar K, Suresh S, Premalatha M (2011) An overview of CO_2 mitigation using algae cultivation technology. Int J Chem Res 3(3):110–117
19. Edwards JH (1995) Potential sources of CO_2 and the options for its large-scale utilisation now and in the future. Catal Today 23:59–66
20. Tahir M, Amin NS (2013) Recycling of carbon dioxide to renewable fuels by photocatalysis: prospects and challenges. Renew Sust Energ Rev 25:560–579
21. Tostón S, Camarillo R, Martínez F, Jiménez C, Rincón J (2014) Carbon dioxide recycling for fuel production by UV–vis photochemistry. Res J Chem Environ in press
22. Kabra K, Chaudhary R, Sawhney RL (2004) Treatment of hazardous organic and inorganic compounds through aqueous phase photocatalysis: a review. Ind Eng Chem Res 43:7683–7696
23. Bussi J, Ohanian M, Vazquez M, Dalchiele DA (2002) Photocatalytic removal of Hg from solid wastes of chlor-alkali plant. J Environ Eng 128:733–739
24. Linsebigler AL, Lu G, Yates JT Jr (1995) Photocatalysis on TiO_2 surfaces: principles, mechanism and selected results. Chem Rev 95:735–758
25. Centi G, Perthoner S (2009) Opportunities and prospects in the chemical recycling of carbon dioxide to fuels. Catal Today 148:191–205
26. Kohno Y, Hayashi H, Takenaka S, Tanaka K, Funabiki T, Yoshida S (1999) Photoenhanced reduction of carbon dioxide with hydrogen over Rh/TiO_2. J Photochem Photobiol A Chem 126:117–123

27. Halmann M (1978) Photoelectrochemical reduction of aqueous carbon dioxide on P-type gallium phosphide in liquid junction solar cells. Nature 275:115–116
28. Inoue T, Fujishima A, Konishi S, Honda K (1979) Photoelectrocatalytic reduction of carbon dioxide in aqueous suspensions of semiconductor powders. Nature 277:637–638
29. Hemminger JC, Carr R, Somorjai GA (1978) The photoassisted reaction of gaseous water and carbon dioxide adsorbed on the $SrTiO_3$ (111) crystal face to form methane. Chem Phys Lett 57:100–104
30. Chandrasekaran K, Thomas JK (1983) Photochemical reduction of carbonate to formaldehyde on TiO_2 powder. Chem Phys Lett 99:7–10
31. Halmann M, Katzir Y, Borgarello E, Kiwi J (1984) Photoassisted carbon dioxide reduction on aqueous suspensions of titanium dioxide. Sol Energy Mater 10:85–91
32. Aliwi SM, Aljubori KF (1989) Photoreduction of CO_2 by metal sulphide semiconductors in the presence of H_2S. Sol Energy Mater 18:223–229
33. Ollis DF, Turchi C (1990) Heterogeneous photocatalysis for water purification: contaminant mineralization kinetics and elementary reactor analysis. Environ Prog 9:229–234
34. Hirano K, Inoue K, Yatsu T (1992) Photocatalysed reduction of CO_2 in aqueous TiO_2 suspension mixed with copper powder. J Photochem Photobiol A Chem 64:255–258
35. Fox MA, Dulay MT (1993) Review: heterogeneous photocatalysis. Chem Rev 93:341–357
36. Ishitani O, Inoue C, Suzuki Y, Ibusuki T (1993) Photocatalytic reduction of carbon dioxide to methane and acetic acid by an aqueous suspension of metal-deposited TiO_2. J Photochem Photobiol A Chem 72:269–271
37. Yamashita H, Kamada N, He H, Tanaka K, Ehara S, Anpo M (1994) Reduction of CO_2 with H_2O on TiO_2(100) and TiO_2(110) single crystals under UV irradiation. Chem Lett 5:855–858
38. Anpo M, Yamashita H, Ichihashi Y, Fujii Y, Honda M (1997) Photocatalytic reduction of CO_2 with H_2O on titanium oxides anchored within micropores of zeolites: effects of the structure of the active sites and the addition of Pt. Phys Chem B 101:2632–2636
39. Kohno Y, Tanaka T, Funabiki T, Yoshida S (1997) Photoreduction of carbon dioxide with hydrogen over ZrO_2. Chem Commun 9:841–842
40. Pozzo RL, Baltans MA, Cassano AE (1997) Supported titanium dioxide and photocatalyst in water decontamination: state of the art. Catal Today 39:219–231
41. Ray AK, Beenackers AACM (1997) Novel swirl-flow reactor for kinetic studies of semiconductor photocatalysis. AIChE J 43:2571–2578
42. Saladin F, Alxneit I (1997) Temperature dependence of the photosynthetic reduction of CO_2 with H_2O at the solid/gas interface of TiO_2. Chem Soc Faraday Trans 93:4149–4163
43. Yoneyama H (1997) Photoreduction of carbon dioxide on quantized semiconductor nanoparticles in solution. Catal Today 39:169–175
44. Zhang SG, Fujii Y, Yamashita H, Koyano K, Talsumi T, Anpo M (1997) Photocatalytic reduction of CO_2 with H_2O on Ti-MCM-41 and Ti-MCM-48 mesoporous zeolites at 328 K. Chem Lett 7:659–660
45. Anpo M, Yamashita H, Ikeue K, Fujii Y, Zhang SG, Ichihashi Y, Park DR, Suzuki Y, Koyano K, Tatsuni T (1998) Photocatalytic reduction of CO_2 with H_2O on Ti-MCM-41 and Ti-MCM-48 mesoporous zeolite catalyst. Catal Today 44:327–332
46. Kaneko S, Shimizu Y, Ohta K, Mizuno T (1998) Photocatalytic reduction of high pressure carbon dioxide using TiO_2 powders with a positive hole scavenger. J Photochem Photobiol A Chem 115:223–226
47. Liu BJ, Torimoto T, Yoneyama H (1998) Photocatalytic reduction of CO_2 using surface-modified CdS photocatalysts in organic solvent. J Photochem Photobiol A Chem 113:93–97
48. Yamashita H, Fuji Y, Ichihashi Y, Zhang SG, Ikeue K, Park DR, Koyano K, Tatsumi T, Anpo M (1998) Selective formation of CH_3OH in the photocatalytic reduction of CO_2 with H_2O on titanium oxides highly dispersed within zeolites and mesoporous molecular sieves. Catal Today 45:221–227
49. Kaneko S, Kurimoto H, Shimizu Y, Ohta K, Mizuno T (1999) Photocatalytic reduction of CO_2 using TiO_2 powders in supercritical CO_2. Energy 24:21–30

50. Cassano AE, Alfano OM (2000) Reaction engineering of suspended solid heterogeneous photocalytic reactors. Catal Today 58:167–197
51. Hori H, Takano Y, Koike K, Sasaki Y (2003) Efficient rhenium-catalyzed photochemical carbon dioxide reduction under high pressure. Inorg Chem Commun 6:300–303
52. Matsuoka M, Anpo M (2003) Review: local structures, excited states and photocatalytic reactivities of highly dispersed catalysts constructed within zeolites. J Photochem Photobiol C Rev 3:225–252
53. Shioya Y, Ikeue K, Ogawa M, Anpo M (2003) Synthesis of transparent Ti-containing mesoporous silica thin film materials and their unique photocatalytic activity for the reduction of CO_2 with H_2O. Appl Catal A Gen 254:251–259
54. Chun H, Yuchao T, Hongxiao T (2004) Characterization and photocatalytic activity of transition-metal-supported surface bond-conjugated TiO_2/SiO_2. Catal Today 90:325–330
55. Shi D, Feng Y, Zhong S (2004) Photocatalytic conversion of CH_4 and CO_2 to oxygenated compounds over Cu/CdS-TiO_2/SiO_2 catalyst. Catal Today 98:505–509
56. Teramura K, Tanaka T, Ishikawa H, Cono Y, Funabiki T (2004) Photocatalytic reduction of CO_2 in the presence of H_2 or CH_4 as a reductant over MgO. J Phys Chem B 108:346–354
57. Tseng IH, Wu JCS, Chou HY (2004) Effects of sol–gel procedures on the photocatalysis of Cu/TiO_2 in CO_2 photoreduction. J Catal 221:432–440
58. Slamet, Nasution HW, Purnama E, Kosela S, Gunlazuardi J (2005) Photocatalytic reduction of CO_2 on copper-doped titania catalysts prepared by improved-impregnation method. Catal Commun 6:313–319
59. Sasirekha N, Basha SJS, Shanthi K (2006) Photocatalytic performance of Ru doped anatase on silica for reduction of carbon dioxide. Appl Catal B Environ 62:169–180
60. Kitano M, Matsuoka M, Ueshima M, Anpo M (2007) Recent developments in titanium oxide-based photocatalysts. Appl Catal A Gen 325:1–14
61. Tan SS, Zou L, Hu E (2008) Kinetic modelling for photosynthesis of hydrogen and methane through catalytic reduction of carbon dioxide with water vapour. Catal Today 131:125–129
62. Zhao Z, Fan J, Xie M, Wang Z (2009) Photo-catalytic reduction of carbon dioxide with in-situ synthesized CoPc/TiO_2 under visible light irradiation. J Clean Prod 17:1025–1029
63. Yui T, Kan A, Saitoh C, Koike K, Ibusuki T, Ishitani O (2011) Photochemical reduction of CO_2 using TiO_2: Effects of organic adsorbates on TiO_2 and deposition of Pd onto TiO_2. Appl Mater Interfaces 3:2594–2600
64. Zhang Q, Li Y, Ackerman EA, Gajdardziska-Josifovska M, Li H (2011) Visible light responsive iodine-doped TiO_2 for photocatalytic reduction of CO_2 to fuels. Appl Catal A 400:195–202
65. Anpo M, Yamashita H, Ichihashi Y, Ehara S (1995) Photocatalytic reduction of CO_2 with H_2O on various titanium oxide catalysts. J Electroanal Chem 396:21–26
66. Tan SS, Zou L, Hu E (2006) Photocatalytic reduction of carbon dioxide into gaseous hydrocarbon using TiO_2 pellets. Catal Today 115:269–273
67. Xia XH, Jia ZJ, Yu Y, Liang Y, Wang Z, Ma LL (2007) Preparation of multi-walled carbon nanotube supported TiO_2 and its photocatalytic activity in the reduction of CO_2 with H_2O. Carbon 45:717–721
68. Lo CC, Hung CH, Yuan CS, Wu JF (2007) Photoreduction of carbon dioxide with H_2 and H_2O over TiO_2 and ZrO_2 in a circulated photocatalytic reactor. Sol Energy Mater Sol Cell 91:1765–1774
69. Baiker A (1999) Supercritical fluids in heterogeneous catalysis. Chem Rev 99:453–474
70. ELCAT (2007) Electrocatalytic gas phase conversion of CO_2 in confined catalysts. www.elcat.org.gu.se. Accessed 12 Jun 2014
71. Li K, An X, Park KH, Khraisheh M, Tang J (2014) A critical review of CO_2 photoconversion: catalysts and reactors. Catal Today 224:3–12
72. Alexiadis A, Mazarino I (2005) Design guidelines for fixed-bed photocatalytic reactors. Chem Eng Proc 44:453–459

73. Song C (2006) Global challenges and strategies for control, conversion and utilization of CO_2 for sustainable development involving energy, catalysis, adsorption and chemical processing. Catal Today 115:2–32
74. Usubharatana P, McMartin D, Veawab A, Tontiwachwuthikul P (2006) Photocatalytic process for CO_2 emission reduction from industrial flue gas stream. Ind Eng Chem Res 45:2558–2568
75. Izumi Y (2013) Recent advances in the photocatalytic conversion of carbon dioxide to fuels with water and/or hydrogen using solar energy and beyond. Coord Chem Rev 257:171–186
76. Li G, Ciston S, Saponjic ZV, Chen L, Dimitrijevic NM, Rajh T, Gray HD (2008) Synthesizing mixed-phase TiO_2 nanocomposites using a hydrothermal method for photo-oxidation and photo-reduction applications. J Catal 253:105–110
77. Devan RS, Patil RA, Lin J-H, Ma Y-R (2012) One-dimensional metal-oxide nanostructures: recent developments in synthesis, characterization, and applications. Adv Funct Mater 22:3326–3370
78. Pelaez M, Nolan N, Pillai S, Seery M, Falaras P, Kontos A, Dunlop P, Hamilton J, Byrne J, O'Shea K, Entezari M, Dionysiou D (2012) A review on the visible light active titanium dioxide photocatalysts for environmental applications. Appl Catal B Environ 125:331–349
79. Dozzi MV, Selli E (2013) Doping TiO_2 with p-block elements: effects of photocatalytic activity. J Photochem Photobiol C 14:13–28
80. Dolat D, Quici N, Kusiak-Nejman E, Morawski AW, Li Puma G (2012) One-step, hydrothermal synthesis of nitrogen, carbon co-doped titanium dioxide (N, CTiO2) photocatalysts. Effect of alcohol degree and chain length as carbon dopant precursors on photocatalytic activity and catalyst deactivation. Appl Cat B Environ 115–116:81–89
81. Zhang Q, Gao T, Andino JM, Li Y (2012) Copper and iodine co-modified TiO_2 nanoparticles for improved activity of CO_2 photoreduction with water vapour. Appl Catal B Environ 123–124:257–264
82. Brandi RJ, Rintoul G, Alfano OM, Cassano AE (2002) Photocatalytic reactors. Reaction kinetics in a flat plate solar simulator. Catal Today 76:161–175
83. Camarillo R, Rincón J (2011) Photocatalytic discoloration of dyes: relation between effect of operating parameters and dye structure. Chem Eng Technol 34:1675–1684
84. Liu G, Hoivik N, Wang K, Jakobsen H (2012) Progress on free-standing and flow-through TiO_2 nanotube membranes. Sol Energy Mater Sol Cell 105:53–68
85. Wu JCS (2009) Photocatalytic reduction of greenhouse gas CO_2 to fuel. Catal Surv Asia 13:30–40
86. Alfano OM, Bahnemann D, Cassano AE, Dillert R, Goslich R (2000) Photocatalysis in water environments using artificial and solar light. Catal Today 58:199–230
87. Ahmed MA, El-Katori EE, Gharni ZH (2013) Photocatalytic degradation of methylene blue dye using Fe_2O_3/TiO_2 nanoparticles prepared by sol–gel method. J Alloys Compd 553:19–29
88. Dai K, Zhang X, Fan K, Peng T, Wei B (2013) Hydrothermal synthesis of single-walled carbon nanotube-TiO_2 hybrid and its photocatalytic activity. Appl Surf Sci 270:238–244
89. Wang M, Chen C, Zhao B, Zeng Q, He D (2013) Solvothermal synthesis of nanostructured TiO_2 photocatalyst in supercritical CO_2 fluids. Mater Lett 109:104–107
90. McHugh MA, Krukonis VJ (eds) (1994) Supercritical fluid extraction: principles and practice. Butterworth-Heinemann, Boston
91. Leitner W, Jessop PG (eds) (1999) Chemical synthesis using supercritical fluids. Wiley-VCH, Weinheim
92. Reverchon E, Cardea S (2012) Supercritical fluids in 3-D tissue engineering. J Supercrit Fluid 69:97–107
93. Haldorai Y, Shim J-J, Lim KT (2012) Synthesis of polymer-inorganic filler nanocomposites in supercritical CO_2. J Supercrit Fluid 71:45–63
94. Meyer F, Stamenic M, Zizovic I, Eggers R (2012) Fixed bed property changes during scCO2 extraction of natural materials – experiments and modeling. J Supercrit Fluid 72:140–149

95. Morin C, Loppinet-Serani A, Cansell F, Aymonier C (2012) Near- and supercritical solvolysis of carbon fibre reinforced polymers (CFRPs) for recycling carbon fibers as a valuable resource: state of the art. J Supercrit Fluid 66:232–240
96. Marrone PA (2013) Supercritical water oxidation – current status of full-scale commercial activity for waste destruction. J Supercrit Fluid 79:283–288
97. Perrut M (2012) Sterilization and virus inactivation by supercritical fluids (a review). J Supercrit Fluid 66:359–371
98. Pijarn N, Jeimsirilers S, Jinawath S (2013) Photocatalytic activity of mixed phase TiO_2 from microwave-assisted synthesis. Adv Mat Res 664:661–666
99. Seck EI, Doña-Rodríguez JM, Pulido Melián E, Fernández-Rodríguez C, González-Díaz OM, Portillo-Carrizo D, Pérez-Peña J (2013) Comparative study of nanocrystalline titanium dioxide obtained through sol–gel and sol–gel-hydrothermal synthesis. J Colloid Interf Sci 400:31–40
100. Chen J, Li G, Huang Y, Zhang H, Zhao H, An T (2012) Optimization synthesis of carbon nanotubes-anatase TiO_2 composite photocatalyst by response surface methodology for photocatalytic degradation of gaseous styrene. Appl Catal B Environ 123–124:69–77
101. Hamdy MS, Saputera WH, Groenen EJ, Mul G (2014) A novel TiO_2 composite for photocatalytic wastewater treatment. J Catal 310:75–83
102. Bozbag SE, Erkey C (2012) Supercritical fluids in fuel cell research and development. J Supercrit Fluids 62:1–31
103. Alonso E, Montequi I, Cocero MJ (2009) Effect of synthesis conditions on photocatalytic activity of TiO_2 powders synthesized in supercritical CO_2. J Supercrit Fluids 49:233–238
104. Sanli D, Bozbag SE, Erkey C (2012) Synthesis of nanostructured materials using supercritical CO_2: part I. Physical transformations. J Mater Sci 47:2995–3025
105. Tabernero A, Martín del Valle EM, Galán MA (2012) Supercritical fluids for pharmaceutical particle engineering: methods, basic fundamentals and modelling. Chem Eng Proc 60:9–25
106. Sui R, Charpentier P (2012) Synthesis of metal oxide nanostructures by direct sol–gel chemistry in supercritical fluids. Chem Rev 112:3057–3082
107. Leino E, Mäki-Arvela P, Eta V, Kumar N, Demoisson F, Samikannu A, Leino A-R, Shchukarev A, Murzin DY, Mikkola J-P (2013) The influence of various synthesis methods on the catalytic activity of cerium oxide in one-pot synthesis of diethyl carbonate starting from CO_2, ethanol and butylene oxide. Catal Today 210:47–54
108. López-Muñoz MJ, van Grieken R, Aguado J, Marugán J (2005) Role of the support on the activity of silica-supported TiO_2 photocatalysts: structure of the TiO_2/SBA-15 photocatalysts. Catal Today 101:307–314
109. Aguado J, van Grieken R, López-Muñoz MJ, Marugán J (2006) A comprehensive study of the synthesis, characterization and activity of TiO_2 and mixed TiO_2/SiO_2 photocatalysts. Appl Catal A Gen 312:202–212
110. Leary R, Westwood A (2011) Carbonaceous nanomaterials for the enhancement of TiO_2 photocatalysis. Carbon 49:741–772
111. Castro CA, Jurado A, Sissa D, Giraldo SA (2012) Performance of Ag-TiO_2 photocatalysts towards the photocatalytic disinfection of water under interior-lighting and solar-simulated light irradiations. Int J of Photoenergy 2012:261045 (10 pages)
112. Veréb G, Ambrus Z, Pap Z, Kmetykó Á, Dombi A, Danciu V, Cheesman A, Mogyorósi K (2012) Comparative study on UV and visible light sensitive bare and doped titanium dioxide photocatalysts for the decomposition of environmental pollutants in water. Appl Catal A Gen 417:26–36
113. Alonso E, Montequi I, Lucas S, Cocero MJ (2007) Synthesis of titanium dioxide particles in supercritical CO_2: effect of operational variables in the characteristics of the final product. J Supercrit Fluids 39:453–461
114. Chhor K, Bocquet JF, Pommier C (1992) Syntheses of submicron TiO_2 powder in vapour, liquid and supercritical phases, a comparative study. Mater Chem Phys 32:249–254

115. Aman N, Satapathy PK, Mishra T, Mahato M, Das NN (2012) Synthesis and photocatalytic activity of mesoporous cerium doped TiO_2 as visible light sensitive photocatalyst. Mater Res Bull 47(2):179–183
116. Pap Z, Karácsonyi É, Cegléd Z, Dombi A, Danciu V, Popescu IC, Baia L, Oszkó A, Mogyorósi K (2012) Dynamic changes on the surface during the calcination of rapid heat treated TiO_2 photocatalysts. Appl Catal B Environ 111–112:595–604
117. Nam CT, Yang W-D, Duc LM (2013) Study on photocatalysis of TiO_2 nanotubes prepared by methanol-thermal synthesis at low temperature. B Mater Sci 36(5):779–788
118. Reverchon E, Della Porta G (2003) Particle design using supercritical fluids. Chem Eng Technol 26:840–845
119. Wu JCS, Lin H-M (2005) Photo reduction of CO_2 to methanol via TiO_2 photocatalyst. Int J Photoener 7:115–119
120. Kočí K, Obalová L, Matějová L, Plachá D, Lacný Z, Jirkovský J, Šolcová O (2009) Effect of TiO_2 particle size on the photocatalytic reduction of CO_2. Appl Catal B Environ 89:494–502
121. Varghese OK, Paulose M, LaTempa TJ, Grimes CA (2009) High-rate solar photocatalytic conversion of CO_2 and water vapor to hydrocarbon fuels. Nano Lett 9:731–737
122. Li Y, Wang WN, Zhan Z, Woo MH, Wu CY, Biswas P (2010) Photocatalytic reduction of CO_2 with H_2O on mesoporous silica supported Cu/TiO_2 catalysts. Appl Catal B Environ 100:386–392

Microwaves in Green and Sustainable Chemistry

Antonio de la Hoz, Ángel Díaz-Ortiz, and Pilar Prieto

Abstract Since the creation of the group of microwaves and sustainable organic synthesis (MSOC) we have been interested in the development and applications of synthetic methodologies for green and sustainable synthesis. In this account major contributions in microwave-assisted organic synthesis (MAOS) related to green and sustainable chemistry are described.

Keywords Computational calculations, Green Chemistry, Microwaves, Solvent-free

Contents

A. de la Hoz (✉), Á. Díaz-Ortiz, and P. Prieto
Departamento de Química Inorgánica, Orgánica y Bioquímica, Facultad de Ciencias y Tecnologías Químicas, Universidad de Castilla-La Mancha, 13071 Ciudad Real, Spain
e-mail: Antonio.Hoz@uclm.es

E. Jiménez et al. (eds.), *Environment, Energy and Climate Change I: Environmental Chemistry of Pollutants and Wastes*, Hdb Env Chem (2015) 32: 405–428,
DOI 10.1007/698_2014_267,
Published online: 22 July 2014

Table 1 The 12 principles of green chemistry [1]

1. Prevent waste
2. Maximize atom economy
3. Design less hazardous chemical syntheses
4. Design safer chemicals and products
5. Use safer solvents and reaction conditions
6. Increase energy efficiency
7. Use renewable feedstocks
8. Avoid chemical derivatives
9. Use catalysts, not stoichiometric reagents
10. Design chemicals and products to degrade after use
11. Analyze in real time to prevent pollution
12. Minimize the potential for accidents

1 Green Chemistry

The American Chemical Society (ACS) code of conduct includes the following statements (https://www.acs.org/content/acs/en/careers/profdev/ethics/the-chemical-professionals-code-of-conduct.html. Accessed 19 Feb 2014), "Chemical professionals have a responsibility to serve the public interest and safety and to further advance the knowledge of science. They should actively be concerned with the health and safety of co-workers, consumers and the community. Public comments on scientific matters should be made with care and accuracy, without unsubstantiated, exaggerated, or premature statements." In this context, publication of the book of Anastas and Warner [1] in 1998 can be considered as the starting point of green chemistry.

Green chemistry is defined by the Environmental Protection Agency (EPA) (http://www2.epa.gov/green-chemistry. Accessed 19 Feb 2014) as "the design of chemical products and processes that reduce or eliminate the use or generation of hazardous substances." There is an increasing expectation on what chemists and chemical engineers should produce greener and more sustainable processes in the future. In the words of the Nobel prize Noyori, [2] "Green Chemistry is not a mere catch phrase; it is the key for the survival of mankind."

It is not surprising that green chemistry has increase in importance in the last years in research [3], industry [4], and education [5] and in this way it is considered that the green chemical market will increase up to 100 billion dollars by 2020 [6].

The design of environmentally benign processes and products has been guided by the 12 principles of green chemistry defined by Anastas and Warner [1] (Table 1). These principles are a categorization of the fundamental approaches taken to achieve the green chemistry goals and have been used as guidelines by synthetic chemists. As a consequence the 12 principles of green engineering have been postulated [7].

Other key points in the development of green chemistry were the development of green chemistry metrics [8, 9].

2 Microwaves and Green Chemistry

The research of the Microwaves and Sustainable Organic Chemistry (MSOC) group has been focused on the application of enabling and environmentally benign techniques in organic synthesis, microwave activation for organic reactions, and the synergy with solvent-free reactions and catalysis. Since 1993 we have been involved in the development and application of microwave irradiation in organic synthesis and lately in green chemistry and now in the use of other environmental methodologies as mechanochemistry, and flow chemistry.

Microwave heating is very attractive for chemical applications and has become a widely accepted non-conventional energy source for performing organic synthesis [10, 11]. Microwave-assisted organic synthesis (MAOS) is characterized by the spectacular accelerations produced in many reactions as a consequence of the heating rate, which cannot be reproduced by classical heating. Higher yields, milder reaction conditions, and shorter reaction times can be used and many processes can be improved. Indeed, even reactions that do not occur by conventional heating can be performed using microwaves.

The use of microwave irradiation has led to significant added value in chemistry and also to the introduction of new concepts, mainly because the absorption and transmission of the energy is completely different from the conventional mode of heating (Table 2). Conventional forms of heating are rather slow and inefficient methods for transferring energy into a reaction mixture. In contrast, microwave (MW) irradiation produces efficient internal heating by direct coupling of MW energy with the molecules that are present in the reaction mixture. The magnitude of the energy transfer depends on the dielectric properties of the molecules; as a guide, compounds with high dielectric constants tend to absorb MW energy whereas less polar substances and highly ordered crystalline materials are poor absorbers. In this way, absorption of the radiation and heating may be performed selectively.

Considering the application of microwave irradiation in green chemistry and the 12 principles, the use of microwaves could apply for principle 6, increase energy efficiency. It has been traditionally considered that microwave irradiation is more efficient than conventional heating [12]. However some recent reports consider that relative “greenness” of microwave-assisted transformations is a complex task that must take many different factors into account. First, the efficiency of the magnetron is low, 65% conversion of electric energy into electromagnetic radiation. Second, the transformation of the electromagnetic radiation into heat could be low in apolar systems. They conclude that it is highly questionable whether this non-classical form of heating should be labeled as being green, sustainable, or environmentally friendly, based on energy efficiency considerations [13, 14]. Ondrushka et al. also

Table 2 Characteristics of microwave and conventional heating

Microwave heating	Conventional heating
Energetic coupling	Conduction/convection
Coupling at the molecular level	Superficial heating
Rapid	Slow
Volumetric	Superficial
Selective	Nonselective
Dependent of the properties of the material	Less dependent

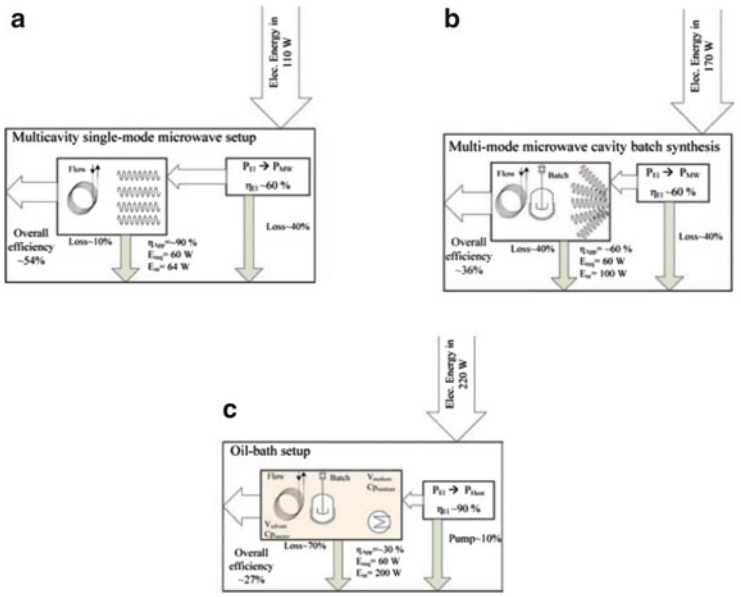

Fig. 1 Energy flow diagrams for three heating systems studied; that is, single-mode (**a**), multimode (**b**) microwaves, and oil-bath (**c**) heating (Reproduced from Hessel [16])

consider that Ball milling is more efficient (regarding the energy consumption) than microwave irradiation or the combination of both methods in a Suzuki–Miyaura reaction in solvent-free conditions [15]. On the contrary, Hessel et al. performed a complete cost analysis of a production plant and they consider that an integrated microwave heating and microflow processing led to a cost-efficient system using a micropacked-bed reactor in comparison with wall-coated microreactor (Fig. 1) [16].

Regardless of these considerations it seems to be clear that microwave irradiation is more efficient when using a substrate with a high loss tangent (tan δ) than a good microwave absorbent and that transforms easily microwave energy into heat.

Our approach in MAOS has been the use of solvent-free conditions because microwave irradiation is directly absorbed by the substrate and not by the solvent. In these conditions the effect of microwave irradiation is more clearly seen in terms

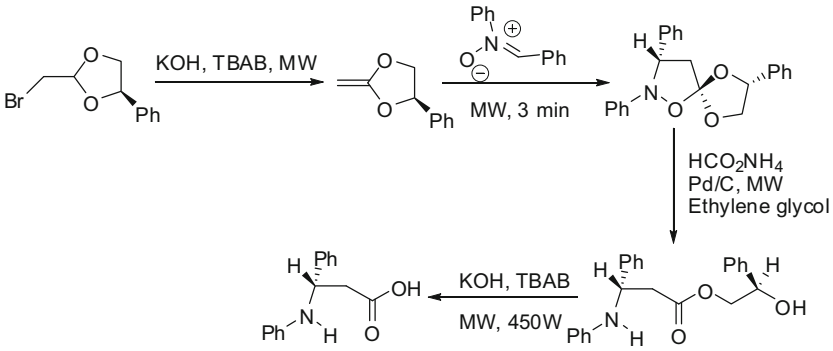

Scheme 1 Multi-step synthesis under microwave irradiation

of energy efficiency and especially in yield, selectivity, and simplification of the work-up procedure. Using this approach we point to principle 5, use safer solvents and reaction conditions.

Similarly we have focused also on heterogeneous catalysis. It is known that many solid supports absorb microwave irradiation efficiently while they are poor heat conductors. In terms of sustainability many mineral acids and mineral oxidant can be replaced by recyclable solid supports. In this regard, principle 9, use catalysts, not stoichiometric reagents can be applied also.

We have used this approach in most of the chemistry developed in our group. This includes cycloadditions palladium catalyzed reactions, synthesis of heterocyclic compounds, etc. In each subsection we will focus on some representative reactions, more that showing an exhaustive collection of different reactions.

3 Microwaves in Solvent-Free Conditions

3.1 Multi-Step Sequences

Following our approach the first multi-step sequence using microwave irradiation and solvent-free conditions was reported by our group (Scheme 1).

An enantiomerically pure bromoacetaldehyde acetal was transformed into an enantiomerically pure β-amino acid in four steps: (1) Elimination under phase transfer catalysis (PTC) conditions, (2) 1,3-dipolar cycloaddition with nitrones, (3) hydrogenolysis using ammonium formiate as a source of hydrogen, and (4) hydrolysis again under PTC conditions. Microwave irradiation was used in the four steps under solvent-free conditions in all but one step, the reductive cleavage where ethylene glycol was used as the solvent [17–19]. Problems such as codistillation and low stability of ketene acetals could be efficiently solved using solvent-free conditions and the short reaction time induced by microwaves.

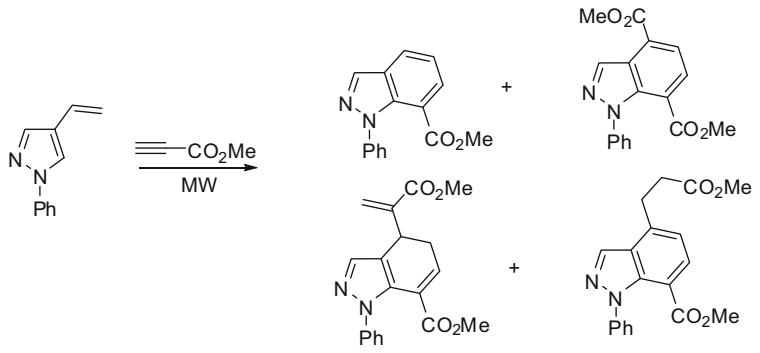

Scheme 2 Reaction of vinylpyrazoles with acetylenic esters

3.2 *Process Improvements*

Under solvent-free conditions, the radiation is directly absorbed by the substrates and the beneficial effects of microwaves are more evident. We have shown that processes that do not occur or occur in low yield under conventional heating occur in good yield under microwave irradiation in solvent-free conditions.

Cycloadditions of vinylpyrazoles and pyrazolylimines are good examples of process improvement in these conditions [20–23]. Synergy between microwave irradiation and solvent-free conditions induces vinylpyrazoles to undergo Diels–Alder cycloadditions with acetylenic dienophiles within a few minutes avoiding the drastic reaction conditions described by classical heating. Using this methodology, yields were improved remarkably, diminishing the polymerization process and increasing the purity of the products and intermediates, and products not described by classical heating were isolated (Scheme 2).

Pyrazolylimines are very reluctant to participate in cycloaddition reactions because of the aromaticity of pyrazoles and its nature of 2-azadienes. However, Diels–Alder cycloadditions of alkylidene derivatives of 5-aminopyrazole with nitroalkenes, as electron-poor dienophiles, under microwave irradiation in solvent-free conditions afforded the corresponding pyrazolo[3,4-*b*]pyridines in good to excellent yields (Scheme 3).

All the cycloadditions were performed in the absence of solvent at atmospheric pressure in a focused microwave reactor with full control of the incident power and the reaction temperature. It is remarkable that most of these cycloadditions do not occur under classical heating in comparable reaction conditions.

3.3 *Modification of Selectivity*

Selectivity is an essential objective in organic synthesis. A very attractive application of microwave irradiation is the possibility of modifying the selectivity just

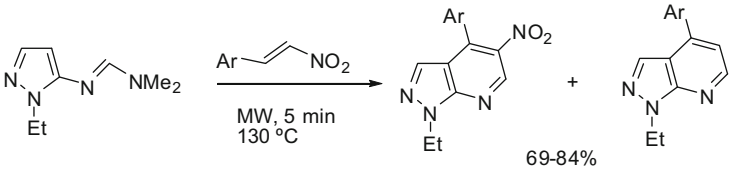

Scheme 3 Reaction of pyrazolylimines with nitroalkenes

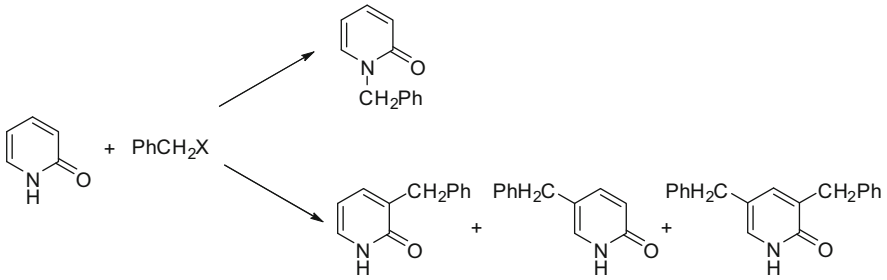

Scheme 4 Reaction of 2-pyridone with benzyl halides

changing the method of heating. Several modifications of selectivity have been observed under microwave irradiation but these effects are again more clearly shown in solvent-free conditions [23].

The reaction of 2-pyridone with benzyl bromide in the absence of base and under solvent-free conditions was one of the first reported examples in which a dramatic modification of selectivity under microwave irradiation was observed (Scheme 4) [24, 25].

Selectivity depended on the halide used (Table 3); using benzyl chloride only *N*-alkylation was observed regardless of the heating method; with benzyl iodide traces of *N*-alkylation were observed under conventional heating while exclusive *C*-benzylation is observed under microwaves. Finally, when using benzyl bromide the selectivity depended on the heating method. Under MW irradiation, it depended on the power used, i.e. the heating rate.

Computational calculations showed that modification on selectivity can be explained through thermal effects that lead to thermodynamic control under microwave irradiation. Results obtained when using benzyl chloride and benzyl iodide can be rationalized by considering the modifications expected in the mechanism according to the nature of the leaving group (chloride, S_N2 favorable, exclusive *N*-alkylation; iodide, S_N1 favorable, exclusive *C*-alkylation under microwave irradiation) (Fig. 2).

When using benzyl bromide, *N*-alkylation through an S_N2 mechanism is kinetically favored while *C*-alkylation, through an S_N1-type, mechanism is thermodynamically favored and is observed under microwave irradiation (S_Ni). The occurrence of *C*-alkylation under microwave irradiation is explained by the

Table 3 Selectivity in the reaction of 2-pyridone with benzyl halides

X	Conditions	*t* (min)	*T* (°C)	N/C
Cl	MW, 780 W	5	198	100:0
	CH	5	176	100:0
Br	MW, 150 W	5	81	100:0
	MW, 450 W	2.5	180	0:100
	CH	5	196	100:0
I	MW, 150 W	5	146	0:100
	CH	5	180	Traces: 0

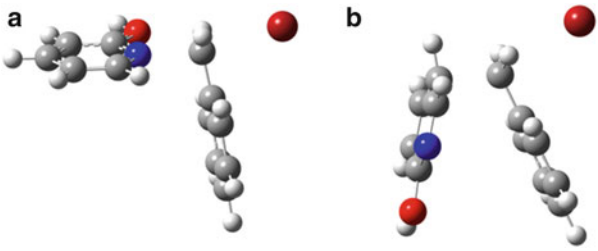

Fig. 2 Transition structures of *C*-alkylation (**a**) and *N*-alkylation (**b**) (S_N2) computed at PBE/6-31G* level

predominance of the thermodynamic control in these conditions. Microwave irradiation also induced a shift from *C*- to *N*-alkylation using an excess of benzyl bromide through an S_N1 type mechanism

3.4 Reproducibility

There is a plethora of interesting transformations reported in domestic microwave ovens. However, reactions performed in these kinds of instruments without appropriate temperature and pressure controls are generally considered as non-reproducible, limiting the application of such reactions [26, 27].

In recent years a number of reports have disclosed the reproducibility of results between monomode and multimode microwave instruments for solution chemistry [28–32].

The polarity of the solvent is the most important parameter to consider when microwave reactions are performed in solution. As stated above, polar solvents directly absorb the microwave radiation and the polarity of the substrate is relatively unimportant. When using non-polar solvents the microwave radiation is absorbed by the substrates, but the differences in absorption of the substrates are moderated by the solvent, especially in dilute solution. In both cases, the reaction temperature is limited by the solvent boiling point and microwave-assisted reactions in solution are easily controlled.

In neat reactions, microwave radiation is again absorbed by the substrates but there is no solvent to stabilize the temperature. In this situation the nature of the

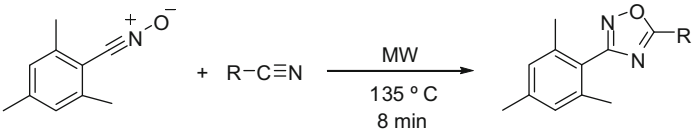

Scheme 5 Comparative results for **2a–h** in all different applications and isolated yields

substituents and the polarity of the substrates influence the absorption of microwave energy and, as a consequence, the yield.

We showed for the first time that solvent-free 1,3-dipolar cycloadditions of nitrile *N*-oxides with nitriles, when carried out in a domestic oven [33], can be reproduced in both monomode and multimode microwave instruments (Scheme 5). This allowed the reaction to be scaled up or performed in a parallel manner using a multi-well plate. The parallel approach required the use of a Weflon® multi-well plate to ensure that the absorption in individual vessels across the plate is minimized, in order to avoid temperature differences. The results obtained in all applications were comparable [33].

In an extension of this work we performed an experimental and computational study of a series of reactions that cover a wide range of chemical transformations and, in contrast to the aforementioned cycloaddition reaction, the polarity in the course of the process increases and, as a consequence, it could be more difficult to control [34]. The reactions selected were: *N*-alkylation of (1*H*)-benzotriazoles, condensation of anilines with urea (or thiourea), Beckmann rearrangement of ketoximes, and oxidation of benzylic bromides to aromatic aldehydes (Scheme 6).

Computational results were in complete agreement with the experimental ones. They showed that most solvent-free reactions previously performed in a domestic oven, without appropriate temperature control, can be reproduced in both monomode and multimode microwave instruments using temperature-controlled conditions, regardless of the polarity of the species and the evolution during the reaction.

However, some solvent-free reactions, such as the oxidation of benzylic bromides may not be reproducible in dedicated microwave reactors. When the polarity undergoes a dramatic increase during the course of the process, the reaction temperature cannot be controlled and reproducibility is impossible (Table 4).

These conclusions represent a useful contribution to microwave synthesis and green process research. They emphasize the advantages that modern microwave instrumentation offers to be applied to synthetic transformations that have previously been carried out in domestic ovens. Furthermore, these results provided a tool to predict the reproducibility of such reactions.

Scheme 6 Oxidation of benzylic bromides with pyridine *N*-oxide

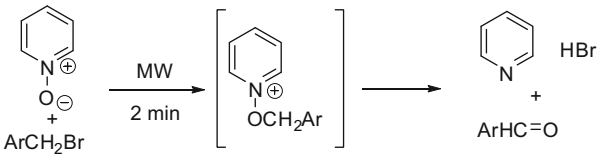

Table 4 Dipole Moments (Debyes) of all stationary points in the S_N1 and S_N2 mechanism in the oxidation of benzyl bromide with pyridine *N*-oxide

	Reactants	TS1	Int	TS2	Products
S_N2 Gas phase	3.60	15.6	–	9.02	3.92
S_N2 Solution (bromobenzene)	5.05	19.98	25.02	23.81	5.00
S_N1 Solution (bromobenzene)	5.55	22.74	52.04	24.88	5.43

3.5 Carbon Nanostructures

The interaction of microwaves with carbon nanotubes (CNTs) is an interesting topic for a variety of potential applications. Microwaves have been used for the purification of CNTs and for their chemical functionalization, providing a technique for simple, green, and large-scale protocols [35; and references therein].

When CNTs are exposed to microwaves, strong absorptions are observed, producing intense heating, outgassing, and light emission. Although the mechanism of CNT-microwave interaction remains incompletely understood, microwaves have been used for the purification of raw CNTs for their chemical functionalization.

One of the first demonstrations of microwave-assisted single-walled carbon nanotube (SWNT) purification was published by our group. It was based on the treatment of raw nanotubes in a microwave domestic oven, under air and in the absence of solvent. In these conditions, the selective burning of metal particles led to a strong depletion of the iron content in the soot [36]. Similar techniques were implemented after using monomode instruments [37].

The energy delivered in the strong interaction. Microwaves-CNT can be used to achieve sufficient functionalization of the CNT surface in short reaction time and to ensure easy processing, while avoiding significant degradation of the structure.

Microwave irradiation of CNTs reduces the reaction times and gives rise to products with higher degrees of functionalization than those obtained by conventional thermal methods.

Our group has described a green solvent-free technique combined with microwave irradiation. This methodology represents a different approach considering the chemistry of CNTs as microwave irradiation is absorbed directly by CNTs and it is possible to take complete advantage of the strong microwave absorption of CNTs. We have used this approach for the 1,3-dipolar cycloaddition of azomethine ylides derived from aziridines [38] (Scheme 7). Reactions were performed in a closed quartz tube and 1 h of irradiation.

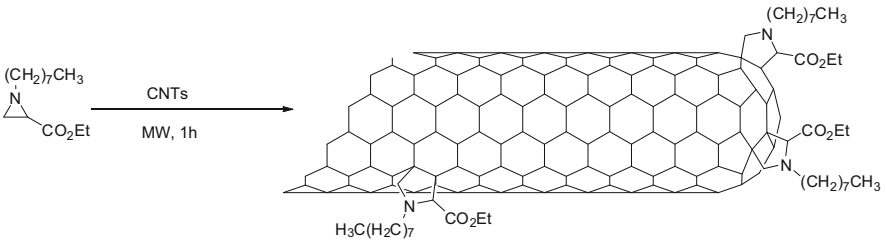

Scheme 7 Microwave-assisted reaction of CNTs with aziridines in solvent-free conditions

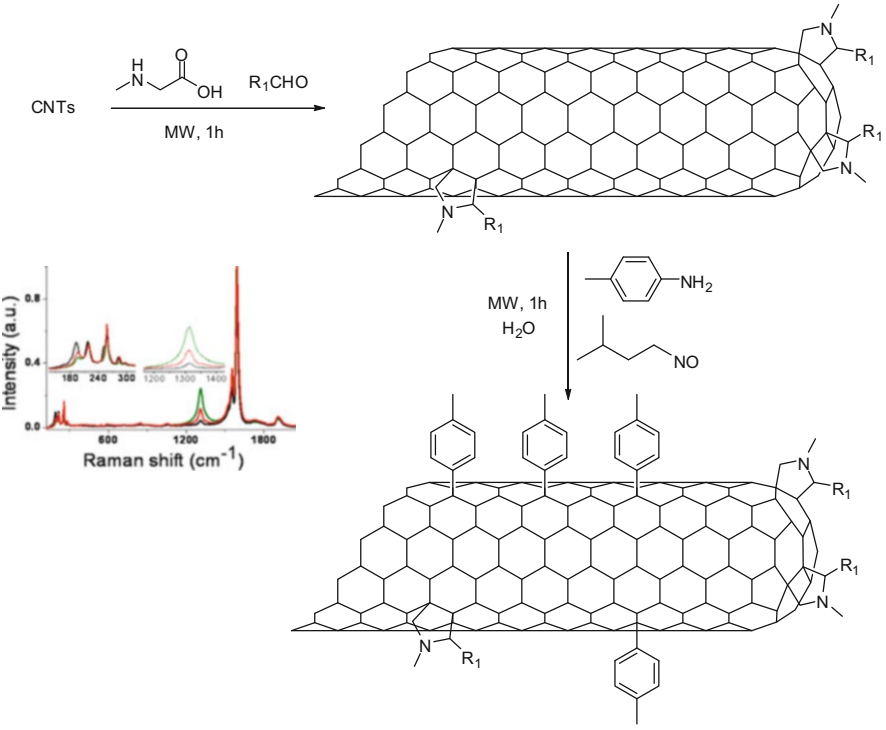

Scheme 8 Microwave-assisted double functionalization of SWNTs. Raman spectra (λ_{exc} 633 nm) of pristine SWNTs (*black line*), SWNTs functionalized by 1,3-dipolar cycloaddition (*red line*), and doubly functionalized SWNTs (*green line*)

Solvent-free conditions pave the way to large-scale functionalization and can be applied also to the multifunctionalization of carbon nanotubes using different reactions. This methodology has been applied to a combination of two different addition reactions: the 1,3-dipolar cycloaddition of azomethine ylides and the addition of diazonium salts, the first in solvent-free conditions and the second in water. In both reactions simple, fast, and environmentally friendly methods were used [39] (Scheme 8).

Reactions can be followed by Raman spectroscopy, which shows the increase of the D-band (1,300 cm^{-1}, sp^3 carbons) at the expense of the G-band (1,600 cm^{-1}, sp^2 carbons).

4 Reactions with Solid Supports

The use of heterogeneous catalysis is one of the keystones among the principles of green chemistry. In this regard, synergy of microwave irradiation, solvent-free conditions and solid catalyst is an excellent combination. Mineral oxides are often poor conductors of heat and conventional methods lead to non-homogeneous heating and also to overheating. Under microwave irradiation, the organic compounds absorbed on the surface of inorganic oxides absorb microwaves efficiently and homogeneously.

We have reviewed our contributions in this field [40] including the Pechman reaction, synthesis of 1,3,5-triazines, quinoxalines, alanine derivatives, and Diels–Alder reactions. In all cases the advantage of using microwave irradiation is not exclusively in the acceleration of the reaction. Indeed most compounds gave very low yields or did not react when the reactions were performed using classical methods under comparable reactions conditions.

Some interesting examples were found in the cycloaddition reactions of furans with a wide variety of dienophiles, using silica supported Lewis acids. As furan is an acid-sensitive reagent, the rapid heating induced by microwave irradiation led to the formation of the product under mild reaction conditions and in short reaction times. The catalysts used were obtained by treatment of silica with $ZnCl_2$ [Si(Zn)], Et_2AlCl [Si(Al)] or $TiCl_4$ [Si(Ti)].

We found that furan derivatives reacted with different alkenes as dienophiles under microwave irradiation in solvent-free conditions affording in one pot the aromatic products (Scheme 9). The use of classical heating under comparable reaction conditions leads to a dramatic decrease in the yield [41, 42].

Computational calculations were used to establish the reaction mechanism and the role of the Lewis acid. Hard Lewis acids such as Si(Al) make ring opening of the adduct easier and resulted in aromatic products [42].

Reactions with alkynes as dienophiles under solvent-free conditions using silica supported Lewis acid catalyst did not produce the expected bicyclic intermediate but the phenolic products in one step (Scheme 10) [43]. Ring opening is favored by the presence of the supported Lewis acid and especially when Si(Zn) was used. When 2,5-disubstituted furans were used, formation of the phenol implies also a rearrangement reaction. Cycloaddition and rearrangement occur with high regioselectivity giving always the most substituted product. This method represented a simple, general, regioselective, and useful alternative for the preparation of polysubstituted phenols (up to 5 substituents) whose synthesis is difficult by other methods.

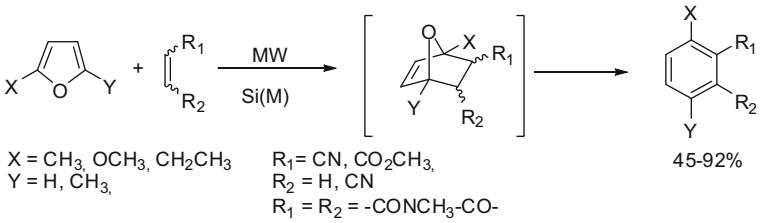

Scheme 9 Cycloaddition of furans with alkenes catalyzed by silica supported Lewis acids

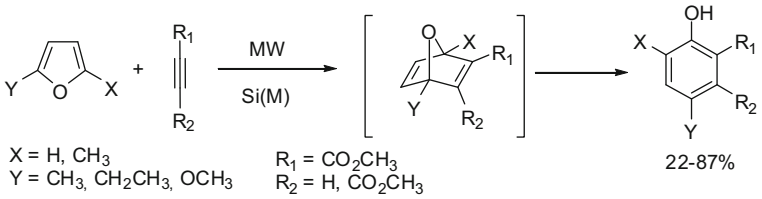

Scheme 10 Cycloaddition of furans with alkynes catalyzed by silica supported Lewis acids

5 Reactions in the Presence of Solvents

Because many organic compounds do not interact appreciably with MW radiation, many authors have described the use of a "susceptor," able to absorb, convert, and transfer energy provided by an MW source to the chemical reagents. An alternative is the use of an ionic liquid [44] even in a low ratio with an apolar solvent or other high polar solvent [45]. Microwave Organic Reaction Enhancement (MORE) Chemistry was described by Bose, the solvent of choice is one which absorbs microwave energy efficiently and is therefore heated rapidly under microwave irradiation and which has a boiling point that is at least 20–30 higher than the desired temperature. Reactions can be described as green since very high concentration is used, product may not be solubilized at room temperature and little heat of vaporization is involved since the solvent is kept below its boiling point.

We have used a similar approach in the preparation and reactivity of amino-1,3,5-triazines. These useful heterocyclic systems can be prepared by reaction of cyanuric chloride with amines by sequential substitution reaction. It is described that the first and the second substitutions can be performed easily at low temperatures while the third substitution requires harder conditions that depend on the reactivity and steric hindrance of the amine (Scheme 11).

In this third substitution microwave irradiation has proved to have a very positive influence, yields can be improved, and reaction times shortened. We have described the preparation of trispyrazolylphenylamino-1,3,5-triazines in solvent-free conditions in good yield in only 10 min [46] (Scheme 12).

However, when using less reactive, more hindered amines or in order to obtain a required selectivity, a different approach can be used. Addition of a small amount of

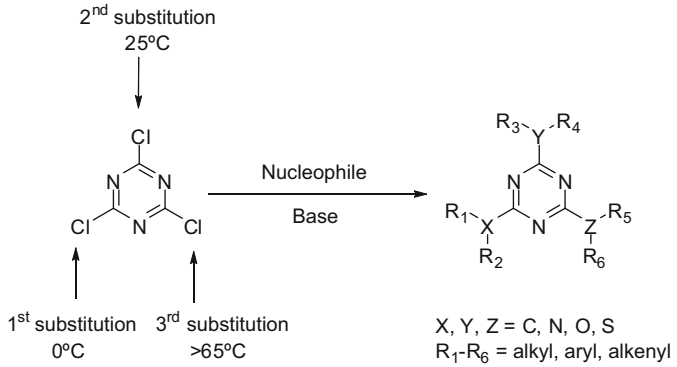

Scheme 11 Preparation of trisubstituted-triazines by selective substitution of chlorine atoms by nucleophiles

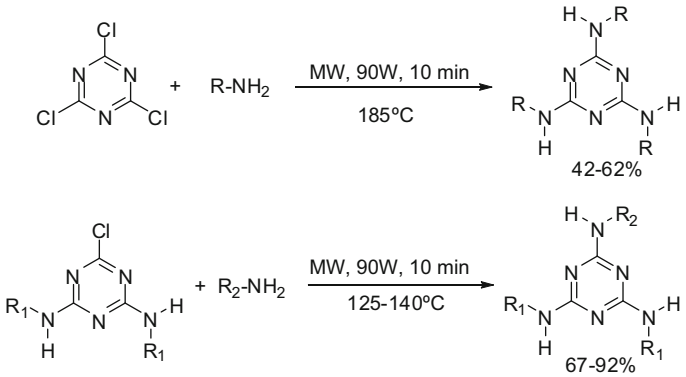

Scheme 12 Solvent-free preparation of trispyrazolylphenylamino-1,3,5-triazines

solvent 1 mL/mmol can be used to homogenize the sample, to control the temperature and to obtain the desired selectivity. Moreover, isolation of the pure product can be performed just by precipitation on cooling or by addition of a small amount of water.

In this regard, an apolar solvent can be used to homogenize the reaction mixture, to assure absorption of microwaves by the substrates and to control the temperature of the reaction and consequently the selectivity. On the contrary, a polar solvent can be used when using low absorbing compounds or when harsh conditions are required. As an example, reaction of diaminosubstituted chlorotriazines with *p*-aminobenzylamine can be performed selectively. Substitution with the more reactive benzylamine can be performed in toluene at 80°C, while the less reactive aniline requires the use of dimethyl sulfoxide (DMSO) and 140°C to obtain good yields of the required bistriazines (Scheme 13) [47].

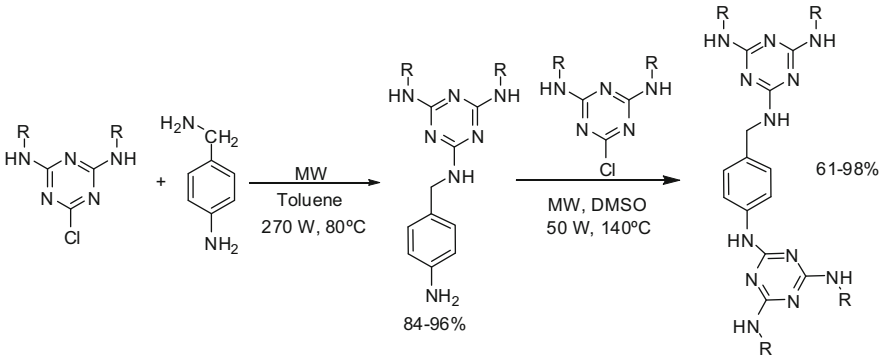

Scheme 13 Selective synthesis of mono and bistriazines

6 Predictive Models

Our research group has maintained an interest in the computational study of microwave-assisted reactions in order to understand and predict the effects of microwave irradiation in organic synthesis. We have studied the reaction improvements, the modifications in the regio- and stereoselectivity under microwave irradiation, and the occurrence of thermal and non-thermal effects through the determination of the thermodynamic and kinetic parameters of the reaction.

Our main interest was to develop a predictive model that permits with simple calculation to determine "a priori" if a given reaction will be improved under microwave irradiation.

6.1 Thermal Effects

The occurrence of thermal and non-thermal effects is a matter of controversy. Many reported effects have been contradicted and other problems in the experimental comparison. It is almost impossible to reproduce under microwaves identical reaction conditions that under conventional heating and to separate the effect of the electromagnetic radiation from the heating effects.

We think that computational calculations on microwave-assisted reactions are a good choice because thermal and non-thermal effect can be efficiently separated by calculation of the thermodynamic parameters and the polarity of the species implicated in the reaction.

We have performed a complete study of cycloaddition reactions where microwave effects were claimed that in order to explain the improvements obtained. Computational calculations demonstrated that thermal effects alone can account for the results obtained. Theoretical outcomes show that modification of selectivity in the reactions with isopolar transition states is a consequence of thermal microwave

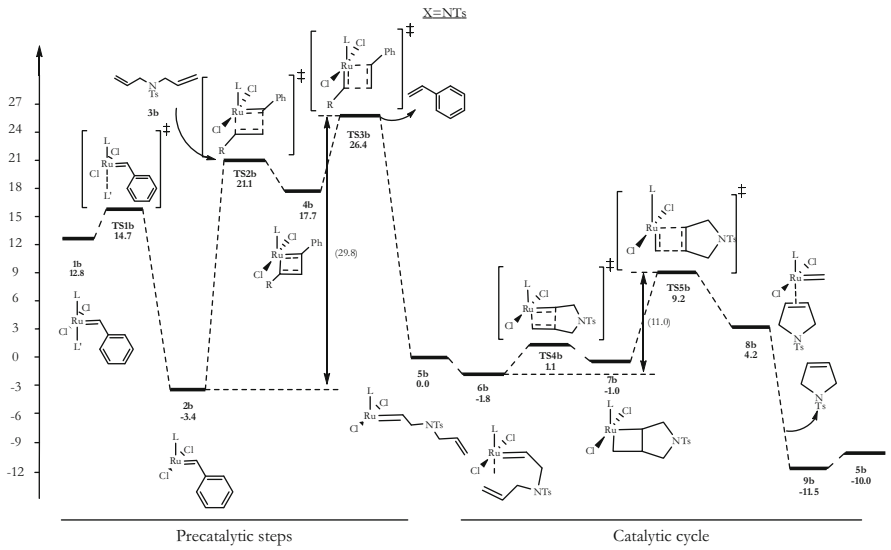

Scheme 14 Computed reaction pathway for the RCM of *N*,*N*-diallyl-*p*-toluenesulfonamide at the PCM-B3LYP/6-311+G(2*d*,*p*)//B3LYP/SDD theory level

effects [48, 49]. Non-thermal microwave effects could not be detected. In all the examples the thermodynamic product is favored under microwave irradiation.

Similar conclusions could be drawn in the study of Ring Closing Metathesis (RCM) of diallyl ether and *N*,*N*-diallyl-*p*-toluenesulfonamide catalyzed by a second-generation Grubbs-type ruthenium carbene complex [50]. In this paper we studied the issue of "molecular radiators." They are believed to be formed when a polar reactant is irradiated in a nonpolar medium. It has been suggested that 'molecular radiators' can directly couple microwave energy and thus create microscopic hot spots at the molecular level. However, this hypothesis is difficult to prove experimentally.

Our study demonstrated that microwave thermal effects affect the induction period of the catalytic kinetics, since the energy gap in the pre-catalytic steps amounts to ca. 30 kcal mol^{-1}. This will result in a shorter induction period by increasing the catalyst turnover and therefore an enhancement in the conversion rate of the reactants (Scheme 14). This energy could be reached due to the high polarity of the diene ($\mu = 7.2$ D) and other participating species.

The proposed 'molecular radiators' far from being a non-thermal effect or a selective absorption that creates microscopic 'hot spots' represent an example of the modification of the polarity of the reaction that improves the absorption of microwave radiation and may improve the reaction through a thermal effect. Dielectric properties are group properties and cannot be modelled by an interaction between the single dipole and the electric field. A group of dipoles interacting themselves could be considered.

Table 5 Conclusions on thermal effects

ΔEa (kcal mol^{-1})	ΔH	Conclusions
<20	<0	Not improved
	>0	Improved
20–30	<0	Improved
	>0	Improved
>30		Do not occur Improved with susceptors

On the basis of this and previous results [48–50] the following conclusions could be drawn regarding thermal effects:

- The presence of any component of high polarity allows a very effective interaction with microwaves through an ionic conduction mechanism.
- Reactions with activation energies below 20 kcal mol^{-1} occur easily by conventional heating and improvements are not expected under microwaves. Microwave irradiation may have a beneficial effect if these processes are endothermic.
- Reactions with activation energies from 20 to 30 kcal mol^{-1} can be improved under microwave irradiation without the use of harsh reaction conditions (e.g., high pressure, pyrolysis).
- Reactions with activation energies above 30 kcal mol^{-1} cannot be performed either under conventional heating or microwave irradiation. However, the use of microwave susceptors such as ionic liquids or highly polar solvents (microwave flash heating) can improve these processes.

The main conclusions of this study are summarized in Table 5 and, in consequence, we succeeded in the development of the predictive model to identify when a reaction can be improved under microwave irradiation.

6.2 Non-thermal Effects

The occurrence of non-thermal effects has not been proved. Many authors consider that "it is not necessary to invoke a non-thermal effect in order to justify microwave chemistry and that rather than claiming non-thermal effects it is better to claim a way or a tool to induce a specific thermal history" [51, 52].

In order to confirm or not the occurrence of non-thermal microwave effect by computational calculations, the contribution of the electromagnetic radiation on the energy should be essential. We have determined the polarity of the species implicated in the reaction as an indication of a possible non-thermal effect. In general only thermal effects have been found.

Only two of the studied examples gave a result that cannot be explained exclusively by thermal effects.

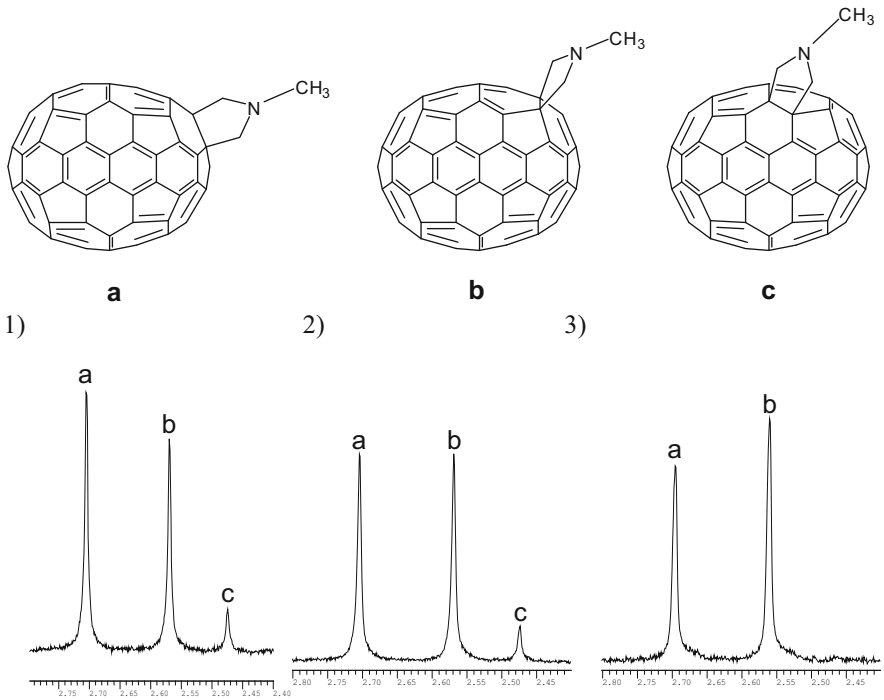

Fig. 3 Cycloaddition of C_{70} with azomethine ylides. Products of reaction and NMR spectra of the *N*-Methyl groups. (*1*) Conventional heating, Toluene. (*2*) Conventional heating, ODCB. (*3*) Microwaves, ODCB

The first one was the cycloaddition of azomethyne ylides with C_{70} [53]. C_{70} contains four different [6,6] bonds, but cycloaddition reactions take place at the 1–2 (**a**) and 5–6 (**b**) bonds and in a lower extent at the [5–19] bond (**c**) (Fig. 3).

There is a strong influence in the isomer distribution of the polarity of the solvent and of the heating technique used. The use of toluene does not lead to any significant differences, the major isomer is always isomer **a**; however with a polar solvent as ODCB significant changes were observed and the product ratio depends on the heating technique used. Under classical heating the ratio **a**:**b** changes to 1:1. Under microwave irradiation additional effects are observed, isomer **c** was not observed and ratio **a**:**b** could be modified by changing the incident power, with isomer **b** being predominant at higher power.

A computational study on the modes of cycloaddition between *N*-methylazomethine ylide and C_{70} revealed that reaction follows a stepwise mechanism. A second-order nucleophilic addition of the 1,3-dipole over the dipolarophile to yield a zwitterionic intermediate, whose ring closure leads to the corresponding cycloadduct. The results suggested that this modification of selectivity could be explained by considering that, under kinetic control, microwave irradiation favors the formation of the product corresponding to the hardest and least polarizable transition structure, **Tsb** (Table 6).

Table 6 Hardness (η, eV), and Free Energies (ΔG^{o}, kcal/mol) of Transition Structures **TSa-c**

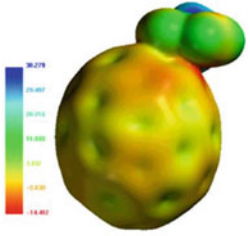

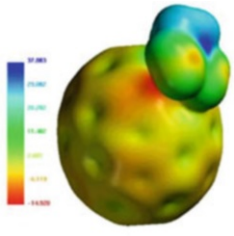

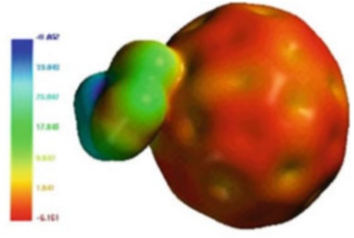

TS	η	ΔG^{o} 384 K	405 K	454 K
TSa (1–2)	2.492	855.70	850.95	838.00
TSb (5–6)	2.505	855.69	850.94	839.00
TSc (7–21)	2.488	858.41	853.75	842.00

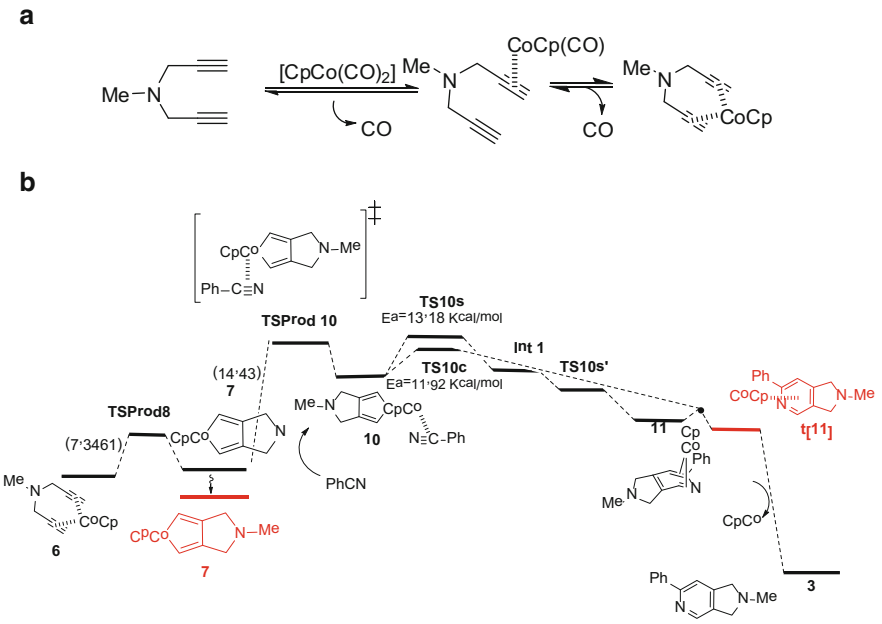

Scheme 15 Cyclotrimerization reaction. (**a**) Formation of the cobaltocyclopentadiene intermediate (precatalytic step) and (**b**) cyclotrimerization

It is remarkable that purely thermal effects, overheating, hot spots, etc. could be ruled out in this reaction since they predicted the preferential formation of isomer **a**, with a lower free energy of activation at higher temperatures (Table 6).

The second example corresponds to the cobalt-catalyzed [2+2+2] cyclotrimerization of diynes with benzonitrile. This reaction was described to be greatly improved under microwave irradiation [54].

We have completely elucidated the mechanism and determined the beneficial effect of microwave irradiation (Scheme 15). The energy requirement to the formation of the cobaltocyclopentadiene in the precatalytic step is 28.45 kcal/mol while the activation energy in the cyclotrimerization is 14.43 kcal/mol. In a first step coordination of the bispropargylamine to the Cobalt complex and spontaneous oxidative coupling gives the key intermediate **7**.

Cobaltacyclopentadiene **7** relaxes to the triplet ground state in a key step of the mechanism. This is a non-adiabatic mechanism with intersystem crossing (ISC) between the singlet and the triplet state. Intermediate **7** evolves by coordination of benzonitrile, intramolecular metal-assisted [4+2] cycloaddition, Intersystem Crossing to the triplet state, and dissociation to the final product.

We have found that an inversion of the dipolar moment vector in the ESP surface of both singlet and triplet species of product **7** occurs (Fig. 4). Considering previous results, microwave irradiation which is in resonance with the energy gaps between

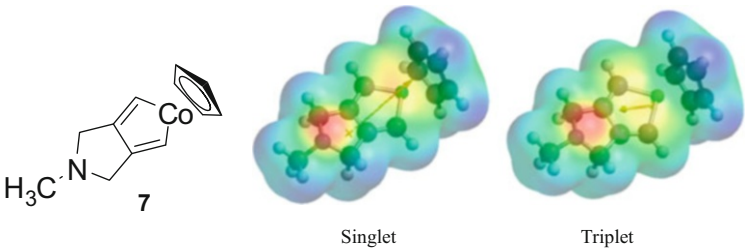

Fig. 4 Dipolar moment vector in the ESP surface of both singlet and triplet species of intermediate **7**

the triplet levels (Fig. 4) can stabilize this state [55]. On the other way as a polarizing field microwaves would favor the inversion of the dipolar moment and would promote Cobalt catalyzed [2+2+2] cyclotrimerizations.

7 Conclusions

In conclusion, microwave irradiation has proved to be a very useful and efficient tool in organic synthesis and green chemistry with improvements in yields and modifications in the selectivity.

Microwave irradiation is more efficient using substrates with high loss tangent (principle 6). The Green character of this methodology is further enhanced in solvent-free conditions (principle 5) and using heterogeneous catalysis (principle 9).

We have proved that almost any reaction can be performed under microwave irradiation and in this regard multi-step synthesis can be designed.

Solvent-free conditions make more evident the effect of microwaves since the radiation is directly absorbed by the substrates. This effect is very important in substrates that absorb microwaves efficiently like carbon nanostructures.

We have proved also that, in most cases, solvent-free conditions performed under microwaves can be reproduced across monomode and multimode instruments and also scaled up.

Addition of a small amount of solvent could be beneficial in order to homogenize the reaction mixture and to control heating (apolar solvent) or to assure a high temperature and a rapid conversion (polar solvent). In most cases reaction products can be easily isolated by precipitation.

Finally, we have used computational calculations to determine the characteristics of the reaction that can be improved under microwave irradiation by thermal effects. In this regard simple calculation of microwave-assisted reactions can be used as a predictive tool. The use of computational studies has become essential as these can be considered as the “greenest” experiments, allowing the selection of potentially interesting experiments.

Acknowledgement Financial support from the MINECO of Spain through project CTQ2011-22410 is gratefully acknowledged.

References

1. Anastas PT, Warner J (1998) Green Chemistry. Theory and practice. Oxford University Press, Oxford
2. Noyori R (2010) Insight: Green Chemistry: the key to our future. Tetrahedron 66:1028
3. Li C-J, Anastas PT eds (2012) Chem Soc Rev 41:4. Green Chemistry themed issue
4. Dunn PJ (2012) The importance of Green Chemistry in process research and development. Chem Soc Rev 41:1452–1461
5. Burmeister M, Rauch F, Eilks I (2012) Education for Sustainable Development (ESD) and chemistry education. Chem Educ Res Pract 13:59–68
6. Meyer DE, González MA (2014) The economics of green and sustainable chemistry. In: Marteel-Parrish AE, Abraham MA (eds) Green chemistry and engineering. A pathway to sustainability, AIChE-Wiley, Hoboken pp 287–324
7. Anastas PT, Zimmerman JB (2003) Design through the 12 principles of green engineering. Environ Sci Tech 37:94A–101A
8. Trost B (1991) The atom economy-a search for synthetic efficiency. Science 254:1471–1477
9. Sheldon RA (1992) Organic synthesis; past, present and future. Chem Ind 903–906
10. de la Hoz A, Loupy A (2012) Microwaves in organic synthesis, 3rd edn. Wiley, Weinheim
11. Kappe CO, Stadler A (2012) Microwaves in organic and medicinal chemistry, 2nd edn. Wiley, Weinheim
12. König B, NOP Project (2014) Sustainability in the organic chemistry lab course. http://www.oc-praktikum.de/nop/en-entry. Accessed 19 Feb 2014
13. Razzaq T, Kappe CO (2008) On the energy efficiency of microwave-assisted organic reactions. ChemSusChem 1:123–132
14. Moseley JD, Kappe CO (2011) A critical assessment of the greenness and energy efficiency of microwave-assisted organic synthesis. Green Chem 13:794–805
15. Schneider F, Szuppa T, Stolle A, Ondruschka B, Hopf H (2009) Energetic assessment of the Suzuki–Miyaura reaction: a curtate life cycle assessment as an easily understandable and applicable tool for reaction optimization. Green Chem 11:1894–1899
16. Benaskar F, Ben-Abdelmoumen A, Patil NG, Rebrov EV, Meuldijk J, Hulshof LA, Hessel V, Krtschil U, Schouten JC (2011) Cost analysis for a continuously operated fine chemicals production plant at 10 kg/day using a combination of microprocessing and microwave heating. J Flow Chem 2:74–89
17. Díez-Barra E, de la Hoz A, Díaz-Ortiz A, Prieto P (1991) Preparation of racemic and enantiomerically pure ketene acetals. Synth Commun 23:1935–1942
18. Díaz-Ortiz A, Díez-Barra E, de la Hoz A, Prieto, P, Moreno A (1994) Cycloadditions of ketene acetals under microwave irradiation in solvent-free conditions. J Chem Soc Perkin Trans 1:3595–3598
19. Díaz-Ortiz A, Díez-Barra E, de la Hoz A, Prieto P, Moreno A, Langa F, Prangé T, Neuman A (1995) Facial selectivity in cycloadditions of a chiral ketene acetal under microwave irradiation in solvent-free conditions. Configurational assignment by NOESY experiments and molecular mechanics calculations. J Org Chem 60:4160–4166
20. Díaz-Ortiz A, Carrillo JR, Gómez-Escalonilla MJ, de la Hoz A, Moreno, A, Prieto P (1998) First Diels–Alder reaction of pyrazolyl imines under microwave irradiation. Synlett 1069–1070

21. Díaz-Ortiz A, de la Hoz A, Langa F (2000) Microwave irradiation in solvent-free conditions: an eco-friendly methodology to prepare indazoles, pyrazolopyridines and bipyrazoles by cycloaddition reactions. Green Chem 2:165–172
22. Díaz-Ortiz A, Carrillo JR, Cossío FP, Gómez-Escalonilla MJ, de la Hoz A, Moreno A, Prieto P (2000) Synthesis of pyrazolo[3,4-b]pyridines by cycloaddition reactions under microwave irradiation. Tetrahedron 56:1569–1577
23. Díaz-Ortiz A, de la Hoz A, Carrillo JR, Herrero M (2012) Selectivity modifications under microwave irradiation. In: de la Hoz A, Loupy A (eds) Microwaves in Organic Synthesis, 3rd edn. Wiley, Weinheim, pp 209–244
24. Almena I, Díaz-Ortiz A, Díez-Barra E, de la Hoz A, Loupy A (1996) Solvent-free benzylations of 2-pyridone. Regiospecific N- or C-alkylation. Chem Lett 5:333–334
25. de la Hoz A, Prieto P, Rajzmann M, de Cózar A, Díaz-Ortiz A, Moreno A, Cossío FP (2008) Selectivity under microwave irradiation. Benzylation of 2-pyridone: an experimental and theoretical study. Tetrahedron 64:8169–8176
26. Nüchter M, Ondruschka B, Bonrath W, Gum A (2004) Microwave assisted synthesis – a critical technology overview. Green Chem 6:128–141
27. Nüchter M, Müller U, Ondruschka B, Tied A, Lautenschläger W (2003) Microwave-assisted chemical reactions. Chem Eng Technol 26:1207–1216
28. Stadler A, Yousefi BH, Dallinger D, Walla P, Van der Eycken E, Kaval N, Kappe CO (2003) Scalability of microwave assisted organic synthesis. From single-mode to multimode parallel batch reactors. Org Process Res Develop 7:707–716
29. Alcázar J, Diels G, Schoentjes B (2004) Reproducibility across microwave instruments: first example of genuine parallel scale up of compounds under microwave irradiation. QSAR Comb Sci 23:906–910
30. Alcázar J (2005) Reproducibility across microwave instruments: Preparation of a set of 24 compounds on a multiwell plate under temperature-controlled conditions. J Comb Chem 7:353–355
31. Loones KTJ, Maes BUW, Rombouts G, Hostyna S, Diels G (2005) Microwave-assisted organic synthesis: scale-up of palladium catalyzed aminations using single-mode and multi-mode microwave equipment. Tetrahedron 61:10338–10348
32. Murray JK, Gellman SH (2006) Microwave-assisted parallel synthesis of a 14-helical beta-peptide library. J Comb Chem 8:58–65
33. Alcázar J, de la Hoz A, Díaz-Ortiz A, Carrillo JR, Herrero MA (2007) Reproducibility and scalability of solvent-free microwave assisted reactions: from domestic ovens to controllable parallel applications. Comb Chem High Throughput Screen 10:163–169
34. Alcázar J, de la Hoz A, Díaz-Ortiz A, Carrillo JR, Herrero MA, Fontana A, Muñoz JM, Prieto P, de Cózar A (2011) Influence of polarity on the scalability and reproducibility of solvent-free reactions comb. Chem High Throughput Screen 14:109–116
35. Vázquez E, Prato M (2009) Carbon nanotubes and microwaves: interactions, responses, and applications. ACS Nano 2:3819–3824
36. Vázquez E, Georgakilas V, Prato M (2002) Microwave-assisted purification of HIPCO carbon nanotubes Chem. Commun. 2308–2309
37. Harutyunyan AR, Pradhan BK, Chang J, Chen G, Eklund PC (2002) Purification of single-wall carbon nanotubes by selective microwave heating of catalyst particles. J Phys Chem B 106:8671–8675
38. Brunetti FG, Herrero MA, Muñoz JM, Giordani S, Díaz-Ortiz A, Filippone S, Ruaro G, Meneghetti M, Prato P, Vázquez E (2007) Reversible microwave-assisted cycloaddition of aziridines to carbon nanotubes. J Am Chem Soc 129:14580–14581
39. Brunetti FG, Herrero MA, Muñoz JM, Díaz-Ortiz A, Alfonsi J, Meneghetti M, Prato M, Vázquez E (2008) Microwave-induced multiple functionalization of carbon nanotubes. J Am Chem Soc 130:8094–8100

40. Carrillo JR, Díaz-Ortiz A, de la Hoz A, Moreno A, Gómez MV, Prieto P, Sánchez-Migallón A, Vázquez E (2003) Application of microwave irradiation, solid supports and catalyst in environmentally benign heterocyclic chemistry. Targets Heterocyclic Chem 7:64–90
41. de la Hoz A, Díaz-Ortiz A, Fraile JM, Gómez MV, Mayoral JA, Moreno A, Saiz A, Vázquez E (2001) Synergy between heterogeneous catalysis and microwave irradiation in an efficient one-pot synthesis of benzene derivatives via ring-opening of Diels–Alder cycloadducts of substituted furans. Synlett 753–756
42. Fraile JM, García JI, Gómez MV, de la Hoz A, Mayoral JA, Moreno A, Prieto P, Salvatella L, Vázquez E (2001) Tandem Diels–Alder aromatization reactions of furans under unconventional reaction conditions – experimental and theoretical studies. Eur J Org Chem 2891–2899
43. Moreno A, Gómez MV, Vázquez E, de la Hoz A, Díaz-Ortiz A, Prieto P, Mayoral JA, Pires E (2004) An efficient one-pot synthesis of phenol derivatives by ring opening and rearrangement of Diels–Alder cycloadducts of substituted furans using heterogeneous catalysis and microwave irradiation. Synlett 1259–1263
44. Leadbeater NE, Torenius HM (2002) A study of the ionic liquid mediated microwave heating of organic solvents. J Org Chem 67:3145–3148
45. Bose AK, Manhas MS, Ganguly SN, Sharma AH, Banik BK (2002) MORE chemistry for less pollution: applications for process development. Synthesis 1578–1591
46. Díaz-Ortiz A, Elguero J, de la Hoz A, Jiménez A, Moreno A, Moreno S, Sánchez-Migallón A (2005) Microwave-assisted synthesis and dynamic behavior of N2, N4, N6-Tris (1H-pyrazolyl)-1,3,5-triazine-2,4,6-triamines. QSAR Comb Sci 24:649–659
47. Moral M, Ruiz A, Moreno A, Díaz-Ortiz A, López-Solera I, de la Hoz A, Sánchez-Migallón A (2010) Microwave-assisted synthesis of pyrazolyl bistriazines. Tetrahedron 66:121–127
48. de Cózar A, Millán MC, Cebrián C, Prieto P, Díaz-Ortiz A, de la Hoz A, Cossío FP (2010) Computational calculations in microwave-assisted organic synthesis (MAOS). Application to cycloaddition reactions. Org Biomol Chem 8:1000–1009
49. Rodriguez AM, Prieto P, de la Hoz A, Díaz-Ortiz A (2011) "In silico" mechanistic studies as predictive tools in microwave-assisted organic synthesis. Org Biomol Chem 9:2371–2377
50. Rodriguez AM, Prieto P, de la Hoz A, Díaz-Ortiz A, García JI (2014) The issue of 'molecular radiators' in microwave assisted reactions. Computational calculations on ring closing metathesis (RCM). Org Biomol Chem 12:2436–2445
51. Stuerga D, Pribetich P (2012) Key ingredients for mastery of chemical microwave processes. In: de la Hoz A, Loupy A (eds) Microwaves in organic synthesis, 3rd edn. Wiley, Weinheim, pp 105–126
52. Kappe CO, Pieber B, Dallinger D (2013) Microwave effects in organic synthesis: myth or reality? Angew Chem Int Ed 52:1088–1094
53. Langa F, de la Cruz P, de la Hoz A, Espíldora E, Cossío FP, Lecea B (2000) Modification of regioselectivity in cycloadditions to C_{70} under microwave irradiation. J Org Chem 65:2499–2507
54. Rodriguez AM, Cebrián C, Prieto P, García JI, de la Hoz A, Díaz-Ortiz A (2012) DFT studies on cobalt-catalyzed cyclotrimerization reactions: the mechanism and origin of reaction improvement under microwave irradiation. Chem Eur J 18:6217–6224
55. Miura T, Wasielewski MR (2011) Manipulating photogenerated radical ion pair lifetimes in wirelike molecules using microwave pulses: molecular spintronic gates. J Am Chem Soc 133:2844–2847

Index

E. Jiménez et al. (eds.), *Environment, Energy and Climate Change I: Environmental Chemistry of Pollutants and Wastes*, Hdb Env Chem (2015) 32: 429–432,
DOI 10.1007/698_2014,